VOLUME 113 NUMBER 3

THE ASTROPHYSICAL JOURNAL

MAY 1951

THE UNIVERSITY OF CHICAGO PRESS
CHICAGO, ILLINOIS, U.S.A.

May 1951 Vol. 113, No. 3

THE ASTROPHYSICAL JOURNAL

AN INTERNATIONAL REVIEW OF SPECTROSCOPY AND ASTRONOMICAL PHYSICS

The Astrophysical Journal is published bimonthly by the University of Chicago at the University of Chicago Press, 5750 Ellis Avenue, Chicago 37, Illinois, during July, September, November, January, March, and May. ¶Two volumes are published per year, one beginning with the January issue and the other beginning with the July issue. The subscription price is $6.00 per volume or $12.00 per year; the price of single copies is $3.00. (Orders for service of less than a volume will be charged at the single copy rate.) ¶Postage is prepaid by the publishers on all orders from the United States and its possessions. No extra charge is made for postage to countries in the Pan American Postal Union. ¶Postage is charged extra as follows: for Canada, 20 cents per volume, 40 cents per year (total $6.20 per volume, $12.40 per year); on single copies 5 cents (total $3.05); for all other countries in the Postal Union, 50 cents per volume, $1.00 per year (total $6.50 per volume, $13.00 per year), on single copies 20 cents (total $3.20). ¶Subscriptions are payable in advance. Please make all remittances payable to The University of Chicago Press, in United States currency or its equivalent by postal or express money orders or bank drafts.

The following is an authorized agent:

For the British Empire, except North America and Australasia: The Cambridge University Press, Bentley House, 200 Euston Road, London, N.W. 1, England. Prices of yearly subscriptions and of single copies may be had on application.

Claims for missing numbers should be made within the month following the regular month of publication. The publishers expect to supply missing numbers free only when losses have been sustained in transit, and when the reserve stock will permit.

Business correspondence should be addressed to The University of Chicago Press, Chicago 37, Illinois.

Communications for the editors and manuscripts should be addressed to: W. W. Morgan, Editor of THE ASTROPHYSICAL JOURNAL, Yerkes Observatory, Williams Bay, Wisconsin.

Line drawings and photographs should be made by the author, and all marginal notes such as co-ordinates, wave lengths, etc., should be included in the cuts. It will not be possible to set up such material in type.

One copy of the corrected galley proof should be returned as soon as possible to the editor, Yerkes Observatory, Williams Bay, Wisconsin. Authors should take notice that the manuscript will not be sent to them with the proof.

The cable address is "Observatory, Williamsbay, Wisconsin."

The articles in this journal are indexed in the *International Index to Periodicals*, New York, N.Y.

Applications for permission to quote from this journal should be addressed to The University of Chicago Press, and will be freely granted.

Microfilms of complete journal volumes are available to regular subscribers only and may be obtained at the end of the year. Orders and inquiries should be addressed to University Microfilms, 313 North First Street, Ann Arbor, Michigan.

Notice to subscribers: If you change your address, please notify us and your local postmaster immediately.

Entered as second-class matter, July 21, 1949, at the Post-Office at Chicago, Ill., under the Act of March 3, 1879.
Acceptance for mailing at special rate of postage provided for in United States Postal Act of October 3, 1917, Section 1103, amended February 28, 1925.

[*opposite* p. v of cover]

THE ASTROPHYSICAL JOURNAL

An International Review of Spectroscopy and Astronomical Physics

FOUNDED IN 1895 BY GEORGE E. HALE AND JAMES E. KEELER

VOLUME 113

JANUARY–MAY, 1951

THE UNIVERSITY OF CHICAGO PRESS
CHICAGO, ILLINOIS

CAMBRIDGE UNIVERSITY PRESS, LONDON

PUBLISHED JANUARY, MARCH, MAY, 1951

COMPOSED AND PRINTED BY THE UNIVERSITY OF CHICAGO PRESS
CHICAGO, ILLINOIS, U.S.A.

CONTENTS

NUMBER 1

NUMBER 2

NUMBER 3

THE ASTROPHYSICAL JOURNAL

AN INTERNATIONAL REVIEW OF SPECTROSCOPY AND ASTRONOMICAL PHYSICS

VOLUME 113 MAY 1951 NUMBER 3

THE DENSITY OF MOLECULES IN INTERSTELLAR SPACE

DAVID R. BATES* AND LYMAN SPITZER, JR.

University College, London, and Princeton University Observatory

Received January 22, 1951

ABSTRACT

Analysis of Adams' visual estimates indicates that the interstellar lines CH^+ λ 4232 and CH λ 4300 originate in two types of regions—in the normal obscuring clouds responsible for selective extinction and in circumstellar clouds near stars of late B types. In stars of types O and early B, the intensities of λ 4232 and λ 4300 are closely correlated with color excess, E_1; the mean particle densities of these molecules, averaged over the volume in and between the clouds, is about 10^{-3} cm^{-3}. Among stars of later B types, many unreddened stars ($E_1 \leqslant 0.05$) show strong molecular lines; the number of molecules per square centimeter in the line of sight averages about 3×10^{13} cm^{-2} for types B2–B5. Of fifteen unreddened stars showing the molecular lines, the velocity difference, interstellar minus stellar lines, is positive in all but one case.

A theoretical analysis shows that many of the rate coefficients affecting the equilibrium abundance of CH and CH^+ molecules have different values from those assumed hitherto. In particular, the formation of CH by radiative association is markedly slower than previously believed, and there is some possibility that dissociative recombination ($CH^+ + e \rightarrow C + H$) is very rapid. If best estimates are adopted for all the rate coefficients, the observed molecular densities can be explained only if the clouds are extremely concentrated, with a central density $n_0(H)$ of neutral H about 10^3 cm^{-3}. If, however, the f-value for CH λ 4300 is increased by a factor of 30 above the theoretical figure, an increase for which there is some observational evidence, agreement is obtained with $n_0(H)$ equal to about 80. Alternatively, the molecules may be formed at the surface of the grains.

The molecules observed in circumstellar clouds may originate from the sublimation of CH_4 from the grains, a process which should occur when the internal temperature of the grains rises much above some 25° K. The CH_4 molecules will dissociate, forming a hemispherical shell of CH^+ molecules on the side of the star from which the cloud is advancing. This hypothesis explains why the circumstellar molecular lines in an unreddened star show a greater radial velocity than do the stellar lines, and quantitative agreement with the number of observed CH^+ molecules is obtained with reasonable values for the unfortunately rather uncertain physical parameters. However, once again, agreement with the observed abundance of CH can be obtained only if the f-value for λ 4300 is taken to be 30 times that indicated by quantal calculation.

The existence of molecules in interstellar space is indicated by the presence of molecular absorption lines in the spectra of a number of stars; the identified lines are produced by the neutral molecules [1, 2, 3] CH and CN and by the ionized molecule CH^+.[4] A few

* Research associate at Princeton University during February, 1950, when this work was begun.

[1] P. Swings and L. Rosenfeld, *Ap. J.*, **86**, 483, 1937.

[2] A. McKellar, *Pub. A.S.P.*, **52**, 187, 1940; *Pub. Dom. Ap. Obs. Victoria*, **7**, No. 15, 251, 1941.

[3] W. S. Adams, *Ap. J.*, **93**, 11, 1941.

[4] A. E. Douglas and G. Herzberg, *Ap. J.*, **94**, 381, 1941.

equivalent widths for some of these lines have been obtained.[5] Recently an extensive set of visual estimates of molecular intensities in a considerable number of stars has been published by Adams.[6]

An analysis of the density of molecules in interstellar space should yield useful information on the physical conditions between the stars. Such analyses have been carried through by Swings[7] and by Kramers and ter Haar,[8] but they have been somewhat unsatisfactory; for example, they have failed to explain adequately the approximate equality in strength of the strongest lines of *CH* and CH^+. Moreover, the values which they assumed for the mean densities of molecules were too great by more than an order of magnitude, and the rate coefficients used in the equilibrium calculations were in some cases seriously incorrect.

Merrill has expressed some doubt[9] as to whether the molecular lines are interstellar at all. He suggests that they may be to some extent circumstellar, that is, formed by clouds of gas associated with a star whose light they are absorbing.

The extensive observational material obtained by Adams[6] and recent investigations on certain relevant atomic processes make it possible to undertake a further study of this problem. In Section I, prepared mainly by L. Spitzer, the observations are analyzed to determine the change of equivalent widths with color excess, distance, spectral type, etc. Section II, prepared mainly by D. R. Bates, analyzes the equilibrium density of *CH* and CH^+ molecules in interstellar space. Section III, prepared mainly by L. Spitzer, treats the increase of molecular density resulting from the sublimation of grains near a hot star.

I. OBSERVED EQUIVALENT WIDTHS OF INTERSTELLAR MOLECULAR LINES

Dunham[5] has determined the equivalent width W, of the line $CH(X^2\Pi - A^2\Delta)\lambda$ 4300.3 in six stars, and of the line $CN(X^2\Sigma^+ - B^2\Sigma^+)\lambda$ 3874.6 in three stars; for the former line his values range from 0.003 to 0.014 A, while for the latter they are all about 0.006A. In collaboration with King he has also carried out some preliminary laboratory measurements, from which it appeared that the oscillator strengths f associated with these lines are 0.06 and 0.07, respectively. It may readily be shown that, for a line on the linear part of the curve of growth, W, f, and N, the number of molecules per unit area in the line of sight, are related by the equation

$$N = \frac{m c^2 W}{\pi e^2 \lambda^2 f} = 1.13 \times 10^{20} \frac{W}{f\lambda^2} \text{ cm}^{-2}, \tag{1}$$

where the symbols have their usual significance and where the numerical factor has been calculated for W and λ expressed in Angstrom units. On substituting the data mentioned above in this equation and dividing the N thus derived by the stellar distance, a *mean* molecular density $\bar{n}$ of some 10^{-9} cm^{-3} is obtained. In his original paper Dunham gave values around 10^{-6} cm^{-3}; presumably a mistake was made in the computations.

The f-value quoted for *CH* λ 3874 is in fair agreement with some independent measurements by White[10] and with a quantal calculation[11] of the f-value for the corresponding line of the isoelectric system N_2^+. It is probably, therefore, approximately correct.

The situation regarding *CH* λ 4300 is different. During a spectroscopic study of low-

[5] T. Dunham, Jr., *Pub. A.A.S.*, **10**, 123, 1940.

[6] *Ap. J.*, **109**, 354, 1949.

[7] *Ap. J.*, **95**, 270, 1942.

[8] *B.A.N.*, **10**, 137, 1946.

[9] *Pub. A.S.P.*, **58**, 354, 1946.

[10] *J. Chem. Phys.*, **8**, 79 and 459, 1940.

[11] D. R. Bates, *Proc. R. Soc. London, A*, **196**, 562, 1949.

pressure flames, Gaydon and Wolfhard[12] made a determination of the Doppler widths of lines emitted from *CH*, $A^2\Delta$ and $B^2\Sigma^-$. They found that the temperature deduced from these widths was significantly higher than the true temperature. In their view the implication is that the radicals were given some excess translational energy during excitation which they did not have time to lose before radiating. On making an approximate estimate of the collision rate, Gaydon and Wolfhard then reached the conclusion that the spontaneous probabilities involved must be at least 5×10^6 sec^{-1}. This result is consistent with the *f*-value obtained by Dunham and King. But such indirect evidence must be treated with reserve, particularly as there are several peculiarities to be explained. It is surprising, for example, that the radicals apparently gained the same amount of translational energy in being raised either to $A^2\Delta$ or to $B^2\Sigma^-$, in spite of the fact that these two levels differ in energy by about 0.3 e.v. Again, the intensity distributions in the bands were found to correspond to the temperature of the flame, so it would seem that the excitation mechanism would have to have the somewhat unusual property of converting all the surplus energy into translation and none into rotation.

Since the *CH* ($X^2\Pi - A^2\Delta$) transition is of the ordinary sub-Rydberg type, it is not easy to believe that its *f*-value is almost as high as that of *CN* ($X^2\Sigma^+ - B^2\Sigma^+$), which is partially of the charge-transfer type. Instead, it seems better to assume that the measurement of Dunham and King is inaccurate (owing perhaps to an error in the determination of the *CH* concentration in their furnace), to ignore the rather complicated experiment of Gaydon and Wolfhard, and to take the *f*-value in question to be 2×10^{-3}, as recommended by Herzberg,[13] who obtained this estimate by applying a semi-empirical correction to a theoretical figure found by Lyddane, Rogers, and Roach.[14] In order to check this value a detailed quantal calculation will later be performed. It may be noted that the dipole strength *D*, corresponding to Herzberg's *f*-value, is 2.8×10^{-2} atomic units.

Two other transitions are of interest, namely, *CH*($X^2\Pi - B^2\Sigma^-$) λ 3886.4 and CH^+($X^1\Sigma^+ - A^1\Pi$) λ 4232.6. Direct information on them is lacking; but, involving, as they do, a $\sigma - \pi$ orbital jump, they are rather similar to *CH* λ 4300; and it is perhaps plausible to assume provisionally that they have approximately the same dipole strength, so that the *f*-value of the first is also 2×10^{-3} and the *f*-value of the second is 4×10^{-3}. (It may be noted that the orbital degeneracy factor appearing in the expression for the *f*-value is 1 for both *CH* λ 4300 and *CH* λ 3886; it is 2 for CH^+ λ 4232.)

If we adopt the revised *f*-value for *CH* λ 4300, but otherwise use the same data as before, it appears that $\bar{n}(CH)$ is about 3×10^{-8} cm^{-3}. As shown below, the equivalent width of CH^+ λ 4232 is about the same as that of the neutral line. With an *f*-value twice as large, a value of 1.5×10^{-8} cm^{-3} is obviously obtained for $\bar{n}(CH^+)$.

Before anything can be said about the *actual* densities (as distinct from the *mean* densities), it is necessary to know whether the molecules are uniformly distributed or whether they are concentrated in the obscuring clouds known to be present between the stars. A study of the interstellar *Na* lines[15] has shown that the *Na* atoms in interstellar space are mostly concentrated in the same clouds responsible for the observed general and selective extinction of starlight. One might expect such clouds also to contain an appreciable concentration of molecules, in which case the equivalent width of the molecular lines should show a marked correlation with color excess. To test this possibility, Adams' extensive visual estimates of interstellar line intensities were plotted against color excess for the two lines *CH* λ 4300 and CH^+ λ 4232. The results are shown in Figure 1.

[12] *Proc. R. Soc. London, A*, 199, 89, 1949.

[13] *Molecular Structure and Molecular Spectra—Diatomic Molecules* (2d ed.; New York: D. Van Nostrand Co., 1950).

[14] *Phys. Rev.*, 60, 281, 1941.

[15] L. Spitzer, Jr., *Ap. J.*, 108, 276, 1948.

Since the data indicated a pronounced difference between stars of different spectral types, separate plots are given for stars in three groups of spectral types, O5–B1, B2–B5, B6–B9. In each plot Adams' visual estimate is shown against values of the photoelectric color excess E_1, taken from the catalogue by Stebbins, Huffer, and Whitford.[16] Different symbols are used to denote stars at different distances, as follows: solid circles for stars with $m_0 - M$ equal to or greater than 10.0; crosses for stars with $m_0 - M$ between 8.0 and 10.0; and triangles for stars with $m_0 - M$ less than 8.0. Spectral types and distance moduli were taken mostly from the catalogue by Ramsey.[17] For the few stars not in Ramsey's catalogue these quantities were taken from the paper by Stebbins, Huffer, and Whitford. To preserve the homogeneity of the material, only those stars observed

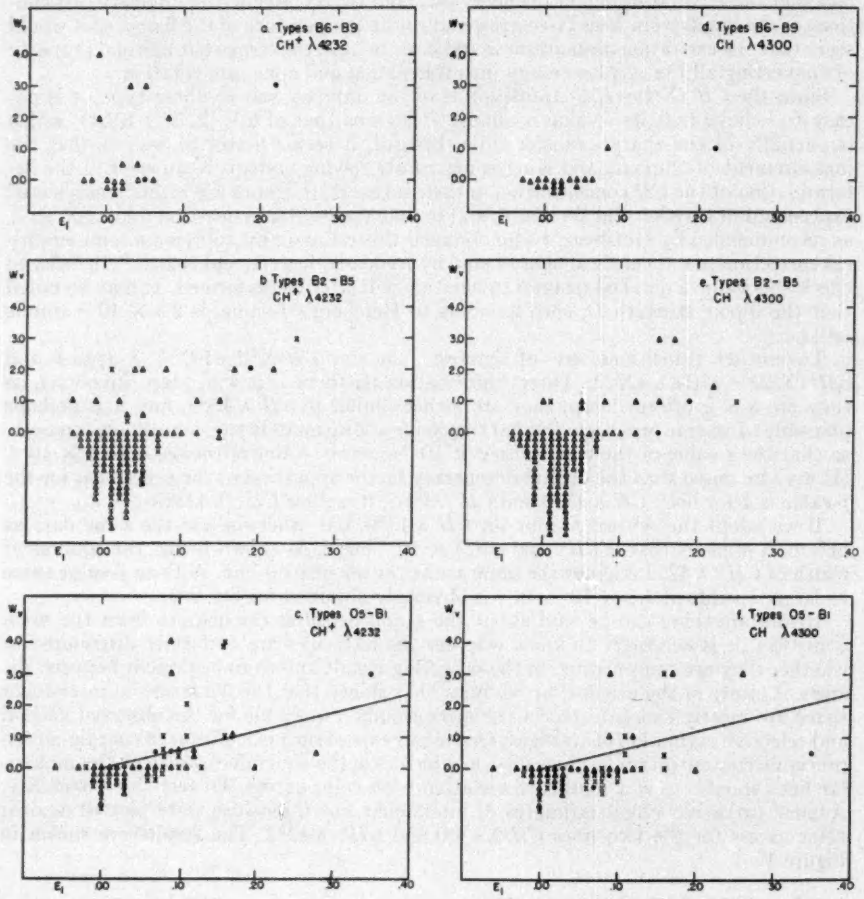

FIG. 1.—Correlation between strengths of interstellar molecular lines and color excess

[16] *Ap. J.*, 91, 20, 1940.

[17] *Ap. J.*, 111, 434, 1950.

with the 114-inch camera are included in these plots. A visual estimated intensity of ½ is attributed to lines marked "tr" ("trace") in Adams' list. Where there are many stars with the same color excess and with zero estimated intensity, some of these are plotted below the line $W_v = 0$.

It is evident from Figure 1, *c* and *f*, that in the stars of earliest spectral type the correlation of molecular line intensity with color excess is very marked, while distance seems to produce relatively little effect. In particular, no unreddened star ($E_1 \leqslant 0.05$) of type B1 or earlier shows either of the molecular lines, while in the fifteen highly reddened stars ($E_1 \geqslant 0.15$) of all types either or both of the molecular lines appear in all but two stars—3 Gem and θ^1 Orionis; it is perhaps significant that this latter star also shows anomalously weak and unsaturated interstellar D lines.[15]

It would appear that in the spectra of these stars of early type the concentration of molecules within the obscuring clouds is relatively high, even though considerable scatter is shown in Figure 1, *c* and *f*. It may be noted that some correlation of the equivalent widths of the molecular lines with distance, which has not as yet been found, would be expected to appear if stars at great distances and with correspondingly high color excesses, on the average, could be observed with the same high dispersion as can the closer stars.

For the CH^+ line λ 4232 a completely different picture is apparent for the stars of later spectral types. Because of observational selection, the stars of spectral types B6–B9 are practically all unreddened, but, in sharp contrast to the stars of earlier type, a substantial fraction of these stars show λ 4232. It may be noted that all the unreddened stars of types B6–B9 showing λ 4232 are in the Pleiades. The data for the stars of types B2–B5 indicate, however, that strong λ 4232 can occur in unreddened stars in all parts of the sky. While it is possible that the "unreddened" stars might be intrinsically bluer than the average, with, actually, considerable space reddening, it seems unlikely that this effect could account for all the "unreddened" stars with molecular lines plotted in Figure 1, *a* and *b*, especially in view of the radial-velocity data presented below.

We may therefore infer that there is some tendency for the CH^+ lines to appear in appreciable strength near a star of spectral type between B2 and B9, even if no relatively opaque obscuring clouds lie between the earth and the star. Following Merrill's terminology, we shall designate such lines as "circumstellar," since the dependence on spectral type indicates that the lines must originate in the neighborhood of the stars whose spectra are photographed. The use of the term is not meant to imply that the absorbing gases originate in the star. For the line *CH* λ 4300 the circumstellar component apparently disappears for the stars of types B6–B9, i.e., for the Pleiades. For the stars of types B2–B5 the effect is apparently weaker than for λ 4232, being limited to the two stars 2 Cyg and HD 212978 and two stars with color excess 0.05, all of spectral types B2 or B3.

The data in Figure 1 may be used to determine quantitatively the average interstellar densities of *CH* and CH^+. The straight lines in Figure 1, *c* and *f*, have been drawn to give approximately the best fit for the molecular lines in the stars of earliest spectral type and are represented by the equation

$$W_v = 6.0E_1 , \tag{2}$$

applicable to both λ 4232 and λ 4300. The correction to the zero point of the photoelectric color-excess scale is small and is neglected here; the quantity W_v represents Adams' visual estimate of the line intensity. Quantitative measurements of the equivalent width of the K and H lines[18] have yielded a calibration of Adams' visual scale, as indicated by the equation

$$W = 0.016W_v , \tag{3}$$

[18] L. Spitzer, I. Epstein, and Li Hen, *Ann. d'ap.*, 13, 147, 1950.

where W is again the equivalent width in Angstrom units. If equations (1), (2), and (3) are combined for the line CH λ 4300, with f set equal to 2×10^{-3}, we find

$$N(CH) = 2.9 \times 10^{14} E_1 . \tag{4}$$

where $N(CH)$ is the number of CH molecules per square centimeter in the line of sight. Since most H atoms are presumably also concentrated in the obscuring clouds, $N(H)$ is also directly proportional to E_1. If we assume that $\bar{n}(H)$, the average density of H in the galactic plane, is 1 cm^{-3} and that the average coefficient of selective extinction is 0.17 mag. per kiloparsec, then we find

$$N(H) = 1.8 \times 10^{22} E_1 . \tag{5}$$

From equations (4) and (5) at once we have

$$\frac{N(CH)}{N(H)} = \frac{\bar{n}(CH)}{\bar{n}(H)} = 1.6 \times 10^{-8}, \tag{6}$$

where, as before, $\bar{n}(CH)$ and $\bar{n}(H)$ represent the mean densities of CH and H along the line of sight. Similarly, we find

$$\frac{N(CH^+)}{N(H)} = \frac{\bar{n}(CH^+)}{\bar{n}(H)} = 8 \times 10^{-9}. \tag{7}$$

These results are clearly consistent with the deductions made from Dunham's data.

We are interested, however, not in the mean but in the *actual* densities throughout space. Denoting these by $n(CH)$, $n(CH^+)$, and $n(H)$ and assuming that

$$n(CH) \propto n(H)^{p_1}, \tag{8}$$

$$n(CH^+) \propto n(H)^{p_2}, \tag{9}$$

where p_1 and p_2 are small numbers, we readily see that, if the distribution in the clouds is approximately of the Gaussian type, then at the center of a cloud the densities $n_0(CH)$, $n_0(CH^+)$, and $n_0(H)$ are related by the equations

$$\frac{n_0(CH)}{n_0(H)} = 1.6 \times 10^{-8} (p_1)^{1/2}, \tag{10}$$

and

$$\frac{n_0(CH^+)}{n_0(H)} = 8 \times 10^{-9} (p_2)^{1/2}. \tag{11}$$

Next we consider the number of circumstellar molecules in the line of sight to the stars of later B types. The data in Figure 1, *a*, indicate that for 17 unreddened ($E_1 \leqslant 0.05$) stars the average value of W_v for CH^+ λ 4232 is 0.76, corresponding to an equivalent width W of 0.012 A. For the 97 unreddened stars in Figure 1, *b*, the average value of W_v for λ 4232 is 0.11, yielding an equivalent width of 0.0017 A; for λ 4300 the corresponding equivalent width is 0.00065 A. If these values are substituted in equation (1), with f again set equal to 2×10^{-3} and 4×10^{-3} for λ 4300 and λ 4232, respectively, we find

$$N(CH^+) = \begin{cases} 1.9 \times 10^{13} \text{ cm}^{-2} \text{ for types B6–B9}, \\ 2.7 \times 10^{12} \text{ cm}^{-2} \text{ for types B2–B5}; \end{cases} \tag{12}$$

$$N(CH) = 2.1 \times 10^{12} \text{ cm}^{-2} \text{ for types B2–B5}. \tag{13}$$

These averages are more reliable for the stars of types B2–B5 than for the later spectral types, since the values for the stars of types B6–B9 are entirely dependent on the inclusion of the Pleiades cluster.

Finally, we may consider the radial velocities of the clouds producing molecular lines. Adams[6] has shown that the difference between the velocities found from K and H and those found from the molecular lines is generally very small and is primarily due to observational errors. Since the former velocities are the more accurate, we shall use these for the molecular lines instead of the actual values measured for the molecular lines themselves. For each star showing the molecular lines, one may obtain a value of Δv, defined as the radial velocity of the interstellar lines minus the radial velocity of the star. Data for stellar radial velocities are given in Moore's catalogue.[19]

Information on the values of Δv found in this way is presented in Table 1. Evidently, the velocities behave quite differently in reddened and in unreddened stars. For the unreddened stars showing either of the molecular lines Δv is positive in all cases, with the

TABLE 1

VELOCITY DIFFERENCES, INTERSTELLAR MINUS STELLAR LINES

Stars	Spectral Types	No. of Positive Values of Δv	No. of Negative Values of Δv	Mean Δv (Km/Sec)
Unreddened..... $E_1 \leqslant 0.05$	O5–B1	0	0	.....
	B2–B5	9	1	+ 3
	B6–B9 (Pleiades)	6	0	+ 9
Reddened..... $E_1 > 0.05$	O5–B1	3	13	−16
	B2–B5	5	5	− 4
	B6–B9	0	2	− 4

sole exception of the star 31 Peg, in which Δv is −17 cm/sec, E_1 is 0.03, and λ 4232 appears as a "trace"; if this star is excluded, the average Δv for unreddened stars of types B2–B5 becomes 5 cm/sec. In sharp contrast Δv is preponderantly negative for the more reddened stars, especially for those of the earliest spectral types. These negative values are partly the result of differential galactic rotation, since the stars are about twice as far away, on the average, as the interstellar clouds, and the distribution of those stars over galactic longitudes is far from uniform. If, for each star, half the computed radial velocity due to galactic rotation is added to Δv, the average value of this corrected Δv is about 2 km/sec less negative than the mean values shown for reddened stars in Table 1. (The unreddened stars are so close that motions due to galactic rotation are quite negligible.) A large part of the remaining effect is presumably the familiar K effect. This evident difference in Δv between reddened and unreddened stars showing the molecular lines seems a clear indication that two different processes must be responsible for the molecules seen in the light of these two types of stars.

Theoretical explanations of two quite different processes which may form interstellar molecules are presented in the next two sections. Section II discusses theoretically the interstellar density of CH and CH^+ molecules given in equations (10) and (11), while a possible explanation for the number of circumstellar molecules given in equations (12) and (13) is presented in Section III.

[19] *Pub. Lick Obs.*, Vol. 18, 1932.

II. THEORETICAL INTERSTELLAR DENSITY OF CH AND CH^+ MOLECULES

The basic collision processes which might be expected to control the equilibrium interstellar densities of the molecules CH and CH^+ are listed in Table 2, together with the designations of the rate coefficients and their probable values. These have been calculated on the assumption that the radiation field corresponds to that from a 10,000° K black body diluted by a factor 3×10^{-15} at moderate energies (~ 4 e.v.), by a factor 1×10^{-14} at high energies (~ 10 e.v.), and by a factor 1×10^{-16} beyond the Lyman limit, and on the assumption that the gas kinetic temperature is 100° K. Essentially the same processes were considered some years ago by Swings[7] and by Kramers and ter Haar.[8] However, the values we attribute to many of the rate coefficients are very different from those adopted earlier. Our estimates will first be discussed in Section II*a*, and then in Section II*b* and *c* the equilibrium will be investigated.

TABLE 2

Process	Rate Coefficient	
	Designation	Value
a) $C+H \rightarrow CH+h\nu$	γ_1	$\begin{cases} 2\times10^{-18}\ \text{cm}^3/\text{sec}\ [\frac{1}{9}C(^3P_0+3^3P_1+5^3P_2)] \\ 6\times10^{-18}\ \text{cm}^3/\text{sec}\ [C(^3P_0)] \end{cases}$
b) $C^+ + H \rightarrow CH^+ + h\nu$	γ_2	$\begin{cases} 2\times10^{-18}\ \text{cm}^3/\text{sec}\ [\frac{1}{3}C^+(^2P_{1/2}+2^2P_{3/2})] \\ 0 \qquad\qquad [C^+(^2P_{1/2})] \end{cases}$
c) $CH+h\nu \rightarrow CH^+ + e$	β_1	$8\times10^{-12}\ \text{sec}^{-1}$
d) $CH^+ + e \rightarrow CH + h\nu$ *e*) $CH^+ + e \rightarrow CH' + h\nu$ $CH' \rightarrow$ (i) $CH+h\nu$; (ii) $C+H$	α_1	$7\times10^{-12}\ \text{cm}^3/\text{sec}$
f) $CH^+ + e \rightarrow C+H$	α_2	Unknown (probably small but conceivably large)
g) $CH+h\nu \rightarrow C+H$	β_2	$1.5\times10^{-11}\ \text{sec}^{-1}$
h) $CH+h\nu \rightarrow C^+ + H$	β_3	$5\times10^{-13}\ \text{sec}^{-1}$

a) RATE COEFFICIENTS

Radiative association.—A general treatment of radiative association has been carried through (by Bates) and will be published elsewhere. In its classical aspects this analysis differs significantly from the treatment of Kramers and ter Haar (which overestimates the influence which the interatomic field has in increasing the number of collisions by drawing the particles together), and at low temperatures it gives much smaller coefficients. Application of the formula that is developed indicates that under *normal laboratory conditions* γ_1 and γ_2, the coefficients concerned in the formation of CH and CH^+ through processes *a* and *b* (Table 2), are each about 2×10^{-18} cm^3/sec. It should be noted that the magnitudes of the coefficients depend upon the dipole strengths of the transitions $CH(B^2\Sigma^- - X^2\Pi)$ and $CH^+(A^1\Pi - X^1\Sigma^+)$ and hence are related to the *f*-values of the lines CH λ 3886 and CH^+ λ 4232. If future work shows that the figures adopted for these latter should be modified, a proportional change should be made in γ_1 and γ_2.

For the *conditions of interstellar space* an important correction must be introduced. There the effective excitation temperatures are extremely small, so that the carbon occurs almost entirely as $C(^3P_0)$ and $C^+(^2P_{1/2})$. This may greatly influence the chance that a hydrogen atom can approach along a curve from which a transition resulting in association can occur. If the approach is adiabatic, it appears probable that γ_1 is increased to 6×10^{-18} cm^3/sec and that γ_2 is reduced to zero. In the later analysis of the equilib-

rium both sets of results will be applied and both are displayed in the table. As the collisions may be partially nonadiabatic, the true coefficients may be of intermediate magnitude.

The values quoted are for 100° K. They are not very sensitive to the kinetic temperature.

Photoionization.—The $X^2\Pi$ term of *CH* has the configuration $(2p\sigma^2)\ (2p\pi)$. Clearly, the removal of the $(2p\pi)$ electron always yields $CH^+(2p\sigma^2)X^1\Sigma^+$, and the removal of either $(2p\sigma)$ electron yields $CH^+(2p\sigma)(2p\pi)\ a^3\Pi$ with a 3-in-4 chance.[20] The photoionization of *N* has been investigated theoretically, and it has been found that at the spectral head the cross-section is some 3×10^{-18} cm^2 *per outer electron*.[21] As the wave functions of *CH* are presumably more diffuse than those of the united atom, it is not unreasonable to suppose that the cross-section for the process

$$CH\ (X^2\Pi) + h\nu \rightarrow CH^+\ (X^1\Sigma^+) + e \tag{14}$$

is rather greater than this[22] and that the cross-section for the process

$$CH\ (X^2\Pi) + h\nu \rightarrow CH^+\ (a^3\Pi) + e \tag{15}$$

is rather greater than $2 \times \frac{3}{4} \times 3 \times 10^{-18}$ cm^2. Values of 4×10^{-18} cm^2 and 6×10^{-18} cm^2, respectively, will be adopted, and it will be assumed further that both cross-sections remain essentially constant over a considerable wave-length range beyond the spectral head (as is the case for *N*).[23]

Since the dissociation energy of *CH* is 3.47 e.v. and that of CH^+ is 3.61 e.v. and since the ionization energy of *C* is 11.26 e.v., it follows that the energy required for reaction (14) is 11.1 e.v.[24] The error is probably less than 0.3 e.v. $CH^+\ a^3\Pi$ would be expected[25] to lie about 1 e.v. above $CH^+X^1\Sigma^+$. Its exact location is not very important.

From the various figures given, it may be shown that β_1, the ionization rate due to the postulated radiation field, is 8×10^{-12} sec^{-1} per *CH* molecule. The true rate cannot be seriously different from this unless the radiation field assumed is grossly in error.

Recombination.—The rate coefficient for direct radiative recombination into the ground level of *CH* can be obtained from the cross-section of reaction (14) by means of Milne's well-known formula. Its value at 100° K was found to be 2×10^{-12} cm^3/sec. The temperature dependence is approximately a $T^{-1/2}$ power law.

Radiative recombination can also lead to excited *CH* molecules. Contrary to the belief of some earlier workers, the entry of the free electron into the very high orbits is particularly important. These orbits must be closely hydrogenic. The results of some calculations carried out by Bates, Buckingham, Massey, and Unwin[26] can thus be used. They give the rate coefficient at 100° K to be 5×10^{-12} cm^3/sec. In this case also a $T^{-1/2}$ power law is followed.

After an excited atom is formed, downward cascading takes place. It is probable that $CH(X^2\Pi)$ is usually the final product. There would, of course, be immediate dissociation into *C* and *H* if an unstable level were ever reached. But this is likely to be comparatively infrequent. Thus consider the unstable levels which are not associated with

[20] There is a 1 in 4 chance of $CH^+\ (2p\sigma)(2p\pi)A^1\Pi$ being formed. Greater energy must, of course, be provided.

[21] D. R. Bates and M. J. Seaton, *M.N.*, **109**, 698, 1950.

[22] The trend is exemplified by the ionization cross-sections of *N* and *C:* the value of the former is quoted in the text, that of the latter is about 5×10^{-18} cm^2 per outer electron.

[23] The much quoted λ^{-3} law is not applicable to such systems (cf. D. R. Bates, *M.N.*, **106**, 432, 1946).

[24] A. E. Douglas and G. Herzberg, *Canadian J. Res.*, **20**, 71, 1942.

[25] R. S. Mulliken, *Rev. Mod. Phys.*, **4**, 1, 1932.

[26] *Proc. R. Soc. London, A*, **170**, 322, 1939.

$C(2s^2)(2p^2)$, or $(2s)(2p^3)$, and $H(1s)$. Even at infinite nuclear separation they are not more than about 0.1 e.v. below the minimum of the CH^+ ($X^1\Sigma^+$) potential energy-curve, and so, at the equilibrium nuclear separation, they are probably *above* the relevant stable levels. Again consider the remaining unstable levels: $^4\Sigma^-$ and $^6\Sigma^-$ (leading to $C[^5S^0]$, $H[^2S]$), $^4\Pi$ (leading to $C[^3P]$, $H[^2S]$), $^2\Pi$ (leading to $C[^1D]$, $H[^2S]$), and $^2\Sigma^+$ (leading to $C[^1S]$, $H[^2S]$). With the exception of the last, they will generally be by-passed, since to reach them requires at least one double electron jump and, in the case of $^4\Sigma^-$, $^6\Sigma^-$, and $^4\Pi$, a change of multiplicity in addition. While the disruptive action of $^2\Sigma^+$ may have some influence on the sequence of events, it seems unlikely that this single level is entered after any considerable fraction of the recombinations. Hence α_1 can reasonably be taken to be the sum of two rate coefficients given, which at 100° K is 7×10^{-12} cm^3/sec; and the contribution to α_2 can be assumed to be small.

Dissociative recombination.—If the $CH^+(X^1\Sigma^+)$ potential energy-curve is crossed by a suitable repulsive potential energy-curve of CH, a radiationless transition can occur, leading to dissociative recombination. Recent work[27] has indicated that the rate of this type of process may be extremely high; for example, a coefficient of 10^{-7} cm^3/sec is not impossible in favorable circumstances. Unfortunately, the prediction of the actual coefficient for any particular system is scarcely feasible at present, as it necessitates a detailed and extensive knowledge of the potential energy-curves and of other factors. For CH–CH^+ the required crossing might conceivably be provided by the same $^2\Sigma^+$-curve mentioned in the previous paragraph. However, the chance of this is not high. In view of the uncertainty, the most judicious procedure is perhaps to treat the rate coefficient for the process as an unknown parameter, whose value may be either zero, moderate, or very large, and to regard the first contingency as the most, and the last as the least, probable.

Radiationless transitions involving attractive potential energy-curves are also possible. In this case the essential *stabilization* of the neutralization can take place only through the subsequent emission of a photon, which is an inefficient method.[27] Consequently, a marked augmentation of α_1 will not be produced.

Photodissociation.—Kramers and ter Haar assumed that photodissociation takes place only through a transition to a repulsive potential energy-curve. They considered the processes

$$CH\,(X^2\Pi) + h\nu \rightarrow C\,(^3P) + H\,(^2S)\,\{^2\Sigma^+\} \tag{16}$$

and

$$CH^+\,(X^1\Sigma^+) + h\nu \rightarrow C^+\,(^2P) + H\,(^2S)\,\{^3\Sigma^+\} \tag{17}$$

and estimated that the energies required are 10 and 14 e.v., that the f-values involved are 3×10^{-2} and 1×10^{-2}, and hence that the associated rate coefficients are 1×10^{-11} sec^{-1} per CH molecule and 1×10^{-15} sec^{-1} per CH^+ molecule. These values will be adopted here. Their reliability, unfortunately, is poor.

It should be noted, however, that transitions to attractive potential energy-curves cannot be neglected. Thus, as Herzberg[28] has pointed out, dissociation of CH might result from

$$CH\,(X^2\Pi) + h\nu \rightarrow C\,(^3P) + H\,(^2S)\,\{B^2\Sigma^-\} \tag{18}$$

or

$$CH\,(X^2\Pi) + h\nu \rightarrow C\,(^1D) + H\,(^2S)\,\{A^2\Delta,\ C^2\Sigma^+\}. \tag{19}$$

Similarly, photodissociation of CH^+ might result from

$$CH^+\,(X^1\Sigma^+) + h\nu \rightarrow C^+\,(^2P) + H\,(^2S)\,\{A^1\Pi\}. \tag{20}$$

[27] D. R. Bates, *Phys. Rev.*, **77**, 718, and **78**, 492, 1950.

[28] Private communication.

Figure 2 depicts the Morse[29] representations of the various potential energy-curves, calculated by means of the molecular constants recommended in Herzberg's recent book.[12] As can be seen, no serious violation of the Franck-Condon principle is incurred by the processes mentioned. A more quantitative appraisal of the situation can be gained by the inspection of Table 3, which for the ground levels gives r_e, the equilibrium internuclear separation, and for the excited levels gives r_d, the *inner* internuclear separation at which the potential passes through its asymptotic value.

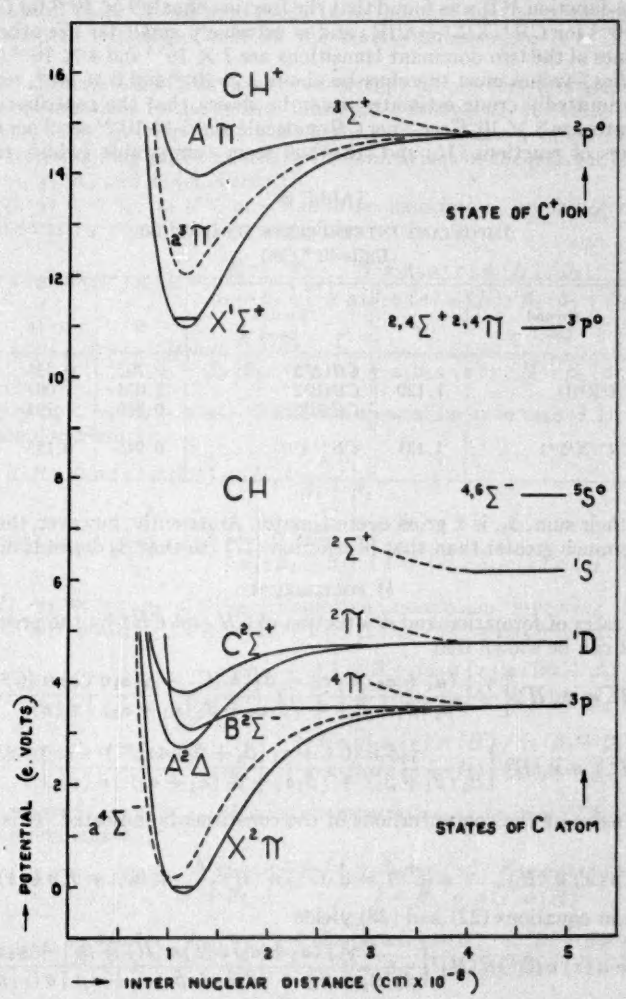

FIG. 2.—Morse potential energy-curves for *CH* and *CH*+. The full curves have been calculated from experimental data; the dashed curves refer to unobserved terms, and in sketching them the recommendations of Mulliken have been followed.

[29] P. Morse, *Phys. Rev.*, **34**, 57, 1929.

For any transition the fraction of the oscillator strength that is involved in dissociation is approximately

$$\left| \int_0^{r_d} S_i(r)\, S_f(r)\, dr \right|^2, \tag{21}$$

where $rS_i(r)$ and $rS_f(r)$ are the normalized initial and final nuclear wave functions. The evaluation of the integral was performed numerically, taking for $S_i(r)$ the solution for the Morse form of the potential (a simple analytical expression), and for $S_f(r)$ the Winans-Stueckelberg δ-function.[30] It was found that the fraction equals 9×10^{-2} for CH ($X^2\Pi \rightarrow B^2\Sigma^-$); 5×10^{-3} for $CH^+(X^1\Sigma^+ \rightarrow A^1\Pi)$; and is extremely small for the other cases. If the *total* f-values of the two dominant transitions are 2×10^{-3} and 4×10^{-3} (cf. Sec. I), their *dissociative* f-values must therefore be about 2×10^{-4} and 2×10^{-5}, respectively. From these admittedly crude estimates it can be shown that the contributions to the dissociation rates are 5×10^{-12} sec^{-1} per CH molecule and 5×10^{-13} sec^{-1} per CH^+ molecule. The rates of reactions (16) and (18) thus seem comparable (which reduces the

TABLE 3

IMPORTANT INTERNUCLEAR SEPARATIONS
(Units 10^{-8} Cm)

Ground Level	r_e	Excited Level	r_d	$r_e - r_d$
$CH(X^2\Pi)$	1.120	$CH(A^2\Delta)$	0.792	0.328
		$CH(B^2\Sigma^-)$	1.033	.087
		$CH(C^2\Sigma^+)$	0.826	.294
$CH^+(X^1\Sigma^+)$	1.131	$CH^+(A^1\Pi)$	0.945	0.185

chance that their sum, β_2, is a gross overestimate). Apparently, however, the rate of reaction (20) is much greater than that of reaction (17) (so that β_3 depends on it alone).

b) EQUILIBRIUM

From the rates of formation and destruction of CH and CH^+ by the processes listed in Table 2, it can be shown that

$$n(CH) = n(H)\left[\frac{\gamma_1\{(\alpha_1+\alpha_2)\, n(e) + \beta_3\}\, n(C) + \gamma_2\alpha_1 n(e)\, n(C^+)}{\beta_3(\beta_1+\beta_2) + \{\beta_1\alpha_2 + \beta_2(\alpha_1+\alpha_2)\}\, n(e)}\right], \tag{22}$$

$$n(CH^+) = n(H)\left[\frac{\gamma_1\beta_1 n(C) + \gamma_2(\beta_1+\beta_2)\, n(C^+)}{\beta_3(\beta_1+\beta_2) + \{\beta_1\alpha_2 + \beta_2(\alpha_1+\alpha_2)\}\, n(e)}\right], \tag{23}$$

where the n's denote the concentrations of the constituents indicated. It is convenient to write

$$n(e) = a(e)\, n(H), \qquad n(C^+) = a(C^+)\, n(H), \qquad n(C) = K n(e)\, n(C^+). \tag{24}$$

Substitution in equations (22) and (23) yields

$$n(CH) = a(e)\, a(C^+)\, n(H)^2\left[\frac{K\gamma_1\{(\alpha_1+\alpha_2)\, a(e)\, n(H) + \beta_3\} + \gamma_2\alpha_1}{\beta_3(\beta_1+\beta_2) + \{\beta_1\alpha_2 + \beta_2(\alpha_1+\alpha_2)\}\, a(e)\, n(H)}\right], \tag{25}$$

$$n(CH^+) = a(C^+)\, n(H)^2\left[\frac{K\gamma_1\beta_1 a(e)\, n(H) + \gamma_2(\beta_1+\beta_2)}{\beta_3(\beta_1+\beta_2) + \{\beta_1\alpha_2 + \beta_2(\alpha_1+\alpha_2)\}\, a(e)\, n(H)}\right]. \tag{26}$$

[30] J. G. Winans and E. C. G. Stueckelberg, *Proc. Nat. Acad. Amer.*, **14**, 867, 1928; see also A. S. Coolidge, H. M. James, and R. D. Present, *J. Chem. Phys.*, **4**, 193, 1936.

According to the present estimates of the relative cosmic abundances of the elements, $a(e)$ and $a(C^+)$ would appear to be about 1/2000 and 1/3000, respectively. Quantal calculations[21, 26] have been performed on the rates of the processes

$$C + h\nu \rightarrow C^+ + e \tag{27}$$

and

$$C^+ + e \rightarrow C' + h\nu\,. \tag{28}$$

By making use of these, K has been found to be 0.6 cm^3 for the standard interstellar conditions adopted. Its dependence on the kinetic temperature is as $T^{-1/2}$ approximately.

To gain an appreciation of what are the controlling parameters, it is useful to note the following approximations to the general formulae. Throughout, the term in brackets is of the order of unity, provided that $n(H)$ has not too extreme a value. Four cases are considered, corresponding to the alternative combinations of the possible choices of the coefficients γ_1, γ_2, α_1, and α_2 (cf. Table 2).

Case (1.1) $\gamma_2 << \gamma_1$; $\alpha_2 << \alpha_1$.—Radiative association involving only $C(^3P_0)$, $C^+(^2P_{1/2})$; dissociative recombination negligible:

$$n(CH) \simeq a(e)\, a(C^+)\, n(H)^2 \frac{K\gamma_1}{\beta_1+\beta_2}\left[\frac{1+\alpha_1 a(e)\, n(H)/\beta_3}{1+\alpha_1\beta_2 a(e)\, n(H)/\beta_3(\beta_1+\beta_2)}\right], \tag{29}$$

$$n(CH^+) \simeq a(e)\, a(C^+)\, n(H)^2 \frac{K\gamma_1\beta_1}{\beta_3(\beta_1+\beta_2)}\left[\frac{1}{1+\alpha_1\beta_2 a(e)\, n(H)/\beta_3(\beta_1+\beta_2)}\right]. \tag{30}$$

Case (1.2) $\gamma_2 << \gamma_1$; $\alpha_2 >> \alpha_1$.—Radiative association as in case (1.1); dissociative recombination dominant:

$$n(CH) \simeq a(e)\, a(C^+)\, n(H)^2 \frac{K\gamma_1}{\beta_1+\beta_2}, \tag{31}$$

$$n(CH^+) \simeq a(C^+)\, n(H)^2 \frac{K\gamma_1\beta_1}{\alpha_2(\beta_1+\beta_2)}\left[\frac{1}{1+\{\beta_3/\alpha_2 a(e)\, n(H)\}}\right]. \tag{32}$$

Case (2.1) $\gamma_2 \simeq \gamma_1$; $\alpha_2 << \alpha_1$.—Radiative association involving $\frac{1}{9}\{C(^3P_0) + 3C(^3P_1) + 5C(^3P_2)\}$ and $\frac{1}{3}\{C^+(^2P_{1/2}) + 2C^+(^2P_{3/2})\}$; dissociative recombination negligible:

$$n(CH) \simeq a(e)\, a(C^+)\, n(H)^2 \frac{\gamma_2\alpha_1}{\beta_3(\beta_1+\beta_2)}\left[\frac{1+K\gamma_1(\alpha_1 a(e)\, n(H)+\beta_3)/\gamma_2\alpha_1}{1+\alpha_1\beta_2 a(e)\, n(H)/\beta_3(\beta_1+\beta_2)}\right], \tag{33}$$

$$n(CH^+) \simeq a(C^+)\, n(H)^2 \frac{\gamma_2}{\beta_3}\left[\frac{1+K\gamma_1\beta_1 a(e)\, n(H)/\gamma_2(\beta_1+\beta_2)}{1+\alpha_1\beta_2 a(e)\, n(H)/\beta_3(\beta_1+\beta_2)}\right]. \tag{34}$$

Case (2.2) $\gamma_2 \simeq \gamma_1$, $\alpha_2 >> \alpha_1$.—Radiative association as in case (2.1); dissociative recombination dominant:

$$n(CH) \simeq a(e)\, a(C^+)\, n(H)^2 \frac{K\gamma_1}{\beta_1+\beta_2}\left[\frac{1+(K\gamma_1\beta_3+\alpha_1\gamma_2)/K\gamma_1\alpha_2 a(e)\, n(H)}{1+\beta_3/\alpha_2 a(e)\, n(H)}\right], \tag{35}$$

$$n(CH^+) \simeq \frac{a(C^+)}{a(e)}\, n(H)\, \frac{\gamma_2}{\alpha_2}\left[\frac{1+K\gamma_1\beta_1 a(e)\, n(H)/\gamma_2(\beta_1+\beta_2)}{1+\beta_3/\alpha_2 a(e)\, n(H)}\right]. \tag{36}$$

The data and formulae given above were used to examine the equilibrium in the center of a cloud. Calculations were performed on the values of $n_0(CH)$ and $n_0(CH^+)$ associated with a selected set of values of $n_0(H)$ covering a range intended to include and, indeed, extend beyond, the greatest density Strömgren considers likely to be encountered. The results for cases (1.1) and (1.2) are displayed in Tables 4 and 5, which

TABLE 4

EQUILIBRIUM DENSITIES, CASE (1.1)

$n_0(H)$	$n_0(CH)_{calc}$	$n_0(CH^+)_{calc}$	$n_0(CH)_{calc}/n_0(CH)_{obs}$	$n_0(CH^+)_{calc}/n_0(CH^+)_{obs}$
10 cm^{-3}	3×10^{-11} cm^{-3}	4×10^{-10} cm^{-3}	1×10^{-4}	3×10^{-3}
20	2×10^{-10}	3×10^{-9}	4×10^{-4}	1×10^{-2}
40	2×10^{-9}	2×10^{-8}	2×10^{-3}	4×10^{-2}
80	2×10^{-8}	2×10^{-7}	7×10^{-3}	1×10^{-1}
280	7×10^{-7}	4×10^{-6}	1×10^{-1}	1
870	2×10^{-5}	5×10^{-5}	1	4

TABLE 5

EQUILIBRIUM DENSITIES, CASE (1.2)

$n_0(H)$	$n_0(CH)_{calc}$	$n_0(CH^+)_{calc}$	$n_{0\,calc}/n_{0\,obs}$ for CH, CH^+	Assumed a_2
10 cm^{-3}	3×10^{-11} cm^{-3}	1×10^{-11} cm^{-3}	1×10^{-4}	4×10^{-9} cm^3/sec
20	2×10^{-10}	9×10^{-11}	4×10^{-4}	2×10^{-9}
40	2×10^{-9}	7×10^{-10}	2×10^{-3}	1×10^{-9}
80	1×10^{-8}	6×10^{-9}	6×10^{-3}	5×10^{-10}
1000	3×10^{-5}	1×10^{-5}	1	4×10^{-11}

TABLE 6

EQUILIBRIUM DENSITIES, CASE (2.1)

$n_0(H)$	$n_0(CH)_{calc}$	$n_0(CH^+)_{calc}$	$n_0(CH)_{calc}/n_0(CH)_{obs}$	$n_0(CH^+)_{calc}/n_0(CH^+)_{obs}$
10 cm^{-3}	$2\times10^{-10}/cm^3$	$1\times10^{-7}/cm^3$	8×10^{-4}	1
20	2×10^{-9}	5×10^{-7}	3×10^{-3}	2
40	1×10^{-8}	2×10^{-6}	1×10^{-2}	4
80	8×10^{-8}	6×10^{-6}	4×10^{-2}	7
10	2×10^{-10}	1×10^{-7}	8×10^{-4}	1
650	2×10^{-5}	1×10^{-4}	1	20

TABLE 7

EQUILIBRIUM DENSITIES, CASE (2.2)

$n_0(H)$	$n_0(CH)_{calc}$	$n_0(CH^+)_{calc}$	$n_{0\,calc}/n_{0\,obs}$ for CH, CH^+	Assumed a_2
10 cm^{-3}	9×10^{-12} cm^{-3}	3×10^{-12} cm^{-3}	3×10^{-5}	5×10^{-6} cm^3/sec
20	7×10^{-11}	2×10^{-11}	1×10^{-4}	1×10^{-6}
40	6×10^{-10}	2×10^{-10}	5×10^{-4}	3×10^{-7}
80	4×10^{-9}	1×10^{-9}	2×10^{-3}	8×10^{-8}
1700	4×10^{-5}	1×10^{-5}	1	2×10^{-10}

also show (1) the ratios of the calculated densities of CH and CH^+ to the so-called observed densities obtained from equations (10) and (11) on taking the numbers p_1 and p_2 to be as indicated by the preceding analysis; (2) the values of $n_0(H)$ required to make the ratios for CH unity and the values required to make the ratios for CH^+ unity; (3) the magnitudes of the corresponding ratios for CH^+ and CH at these densities; and (4) the coefficients α_2 used in case (1.2)—these were arbitrarily chosen to make the calculated and observed CH and CH^+ ratios equal.

If Strömgren's view[21] that $n_0(H)$ rarely exceeds 20 cm^{-3} is accepted, there is clearly a grievous discrepancy between calculation and observation. Thus the former yields much smaller values of $n_0(CH)$ and $n_0(CH^+)$ than are suggested by the latter. Further, in case (1.1) (but not, of course, in case [1.2]) the predicted magnitude of the ratio $n_0(CH)/n_0(CH^+)$ is apparently too low. To be sure, the basic parameters used may be appreciably in error, and it might be argued that the combination of a number of minor inaccuracies might be the cause of the difficulties. For example, the *supposition* might be made that the dipole moments—and hence γ_1 and the f-values—are actually three times greater than has been supposed, so that the calculated densities should be raised by this amount and the densities deduced from the observations should be similarly reduced. A further consequence would be that β_2 and β_3 should be increased. Possibly some adjustment to the radiation field might be *postulated* which would cancel the vexing increase in the former, would not alter the welcome increase in the latter, and would cause β_1 to become three times smaller. And yet another factor of 3 in the desired direction might be gained by *assuming* that $a(e)$ and $a(C^+)$ have been underestimated. On referring to the approximate formulae, it can be seen that the improbable combination of all these artificial changes would multiply $n_0(CH)_{calc}/n_0(CH)_{obs}$ by a little over 30 and would multiply $n_0(CH^+)_{calc}/n_0(CH^+)_{obs}$ (in case [1.1])[22] by about 3, so that, when $n_0(H)$ is 20 cm^{-3}, these ratios would still be only 1×10^{-2} and 3×10^{-2}, respectively. The suspicion is therefore aroused that the explanation of the discrepancy is much more fundamental: either that the density or radiation field in clouds is very different from what is generally thought or that there is a grave defect or omission in the equilibrium theory presented. Appeal to the first alternative is scarcely warranted at present; but the second must be subjected to the closest scrutiny.

It is natural to inquire whether matters would be improved if nonadiabatic collisions were so probable that the adoption of cases (2.1) and (2.2) could be justified. Tables 6 and 7 show the results of calculations based on them. As can be seen, case (2.1) does indeed lead to an increase in the values of $n_0(CH)_{calc}/n_0(CH)_{obs}$ and $n_0(CH^+)_{calc}/n_0(CH^+)_{obs}$; but it also greatly magnifies the difference between these ratios and, in consequence, is quite unacceptable. Case (2.2) fails utterly; for the value of α_2 required to make the two vital ratios equal is improbably high, and the ratios themselves are even smaller than before.

Evidently, all four cases considered require densities of about 10^3 H atoms/cm^3 to produce agreement between theory and observation. The most direct information on the density in the average H I cloud is provided by the analysis of Strömgren,[21] which shows that $n_0(e) \times n_0(Na^+)$ must average about 10^{-7} cm^{-6}. If we assume that the electrons come from C, then, in terms of the relative abundances a defined in equation (24), we see that $n_0(H)$ is about $3 \times 10^{-4}/\{a^{1/2}(C^+)a^{1/2}(Na^+)\}$. A decrease in $a(C^+)$ would require even higher H densities in Tables 4–7, and we are therefore free to change only $a(Na^+)$. The value of $a(Na^+)$ assumed by Strömgren and typical of stellar matter generally is 4×10^{-6}. To obtain a value of 10^3 for $n_0(H)$, we must decrease $a(Na^+)$ by a factor of 10^4 (to 4×10^{-10}). The possibility that so large a fraction of the sodium is

[21] *Ap. J.*, **108**, 242, 1948.

[22] In case (1.2) this ratio can always be forced to equal unity by assigning a suitable value to α_2, which is, of course, unknown. The procedure of keeping it equal to $n_0(CH)_{calc}/n_0(CH)_{obs}$ seems more satisfactory.

locked up in the grains cannot be excluded, but it seems implausible in view of the observed correlation[15] between the interstellar D lines and the color excess.

It will be recalled (cf. Sec. I) that there is a wide difference between the f-values obtained by quantal calculations and those indicated by such laboratory measurements as have been performed. The former have been employed throughout, since it is believed that they are the more reliable. Nevertheless, the possibility cannot be altogether ignored that it is, in fact, the latter which are correct. It is of interest, therefore, to see whether their use would bring about agreement between prediction and observation. Instead of adopting any specific f-values, it is instructive to assume that the true f-values of CH are λ_1 times the calculated, that those of CH^+ are λ_2 times the calculated, and to determine what these correcting factors must be if their introduction is to remove the discrepancy.

Several of the rate coefficients depend on the f-values and hence have to be modified. If the symbols in Table 2 are defined as being the original rate coefficients, then the new

TABLE 8

CHANGES IN RATE COEFFICIENTS REQUIRED IF $n_0(H)$ IS 20 CM^{-3}

MODEL	$M(CH)$*	$M(CH^+)$	CONDITIONS TO BE SATISFIED BY λ_1, λ_2, AND μ	
			(i) To Yield $[n_0(CH)_{calc}/n_0(CH)_{obs}]=1$	(ii) To Yield $[n_0(CH^+)_{calc}/n_0(CH^+)_{obs}]=1$
Case (1.1).....	$\lambda_1^2 B$	$\lambda_1 B$	$\lambda_1=5\times10^2$	(No positive λ_1 satisfactory)
Case (1.2).....	$\lambda_1^2 B$	$(\lambda_1\lambda_2/\mu)B$	$\lambda_1=5\times10^2$	$\lambda_2=5\times10^2\mu$
Case (2.1).....	$\lambda_1 BC$	λ_2	$\lambda_1=2\times10^3$	$\lambda_2=5\times10^{-1}$
Case (2.2).....	$\lambda_1^2 B$	(λ_2^2/μ)	$\lambda_1=2\times10^3$	$\lambda_2=8\times10^3\mu$

* The values for B and C are as follows:

$$B=\frac{\beta_1+\beta_2}{\beta_1+\beta_2'+\lambda_1\beta_2''}=\frac{2.3}{1.8+0.5\lambda_1},$$

$$C=1+\frac{K\gamma_1\beta_3\lambda_1}{\gamma_2\alpha_1}=1+4\times10^{-2}\lambda_1.$$

rate coefficient of process a is $\lambda_1\gamma_1$, that of b is $\lambda_2\gamma_2$, that of g is $\beta_2'+\lambda_1\beta_2''$ (where β_2' is the contribution arising from the transition to the repulsive curve and β_2'' is the contribution arising from the transition to the attractive curve [cf. Sec. IIa]), and that of h is $\lambda_2\beta_3$. The optimum rate coefficient for the combination of processes e (ii) and f may, of course, also be changed; it will be denoted by $\mu\alpha_2$, where μ is another factor to be determined. Table 8 gives the expressions for the approximate multiplying factors $M(CH)$ and $M(CH^+)$ that should be applied to the original $n_0(CH)_{calc}/n_0(CH)_{obs}$ and $n_0(CH^+)_{calc}/n_0(CH^+)_{obs}$ ratios (contained in Tables 4, 5, 6, and 7), together with the conditions that λ_1, λ_2, and μ must satisfy in order that, when $n_0(H)$ is 20 cm^{-3}, the new ratios should equal unity. It is apparent that the demands on λ_1 are impossible to accept, since they would clearly lead to a violation of the f-sum rule.

If $n_0(H)$ is indeed no greater than 20 cm^{-3}, then the only way of bringing the ratios to unity without incurring such a violation is to make the additional arbitrary assumptions either that β_2'' has been grossly overestimated or that there are a number of rela-

tively minor errors in the various parameters (as discussed earlier). However, it must be admitted that, if $n_0(H)$ were actually as much as 80 cm^{-3}, good agreement would be obtained by the use of the laboratory f-values. With this value of $n_0(H)$ the supposition that λ_1 is 30 leads to the results in Table 9. It would clearly be unwise to discount completely the f-values indicated by experiment. However, in view of the difficulty of reconciling them with Herzberg's theoretical estimates, it would seem most judicious merely to note that they offer a possible solution and to continue the search for an alternative.

What appears to be required is some new mechanism leading to the formation of CH or CH^+ or, less important, to the conversion of CH^+ into CH. There is a very limited

TABLE 9

EQUILIBRIUM DENSITIES IF $n_0(H)$ IS 80 CM^{-3} AND f FOR CH λ4300 IS THIRTY TIMES THE THEORETICAL VALUE

Model	$n_0(CH)_{calc}/n_0(CH)_{obs}$	$n_0(CH^+)_{calc}/n_0(CH^+)_{obs}$	Value Assumed for λ_2
Case (1.1).....	1	0.6	.....
Case (1.2).....	1	1	μ
Case (2.1).....	0.3	0.7	0.1
Case (2.2).....	0.3	0.3	μ

number of such atomic or molecular processes, and none of them seems to be at all effective under interstellar conditions. Thus

$$H_2+C\rightarrow H+CH\,, \tag{37}$$

$$H_2+C^+\rightarrow H+CH^+\,, \tag{38}$$

and

$$CH^+ + H\rightarrow CH+H^+ \tag{39}$$

are endothermic and can therefore be ignored. Negative ions of hydrogen might be suggested as possible reactants. Using the results of quantal calculations,[33] it may be shown that, in interstellar space,

$$n\,(H^-) \doteq 10^{-9} n\,(H)\, n\,(e)\,, \tag{40}$$

provided that the kinetic temperature is about 100° K. The very low density indicated by this relation enables the process

$$C+H^-\rightarrow CH+e \tag{41}$$

to be dismissed at once. Because of the extremely large collecting action of a Coulomb field,

$$C^+ + H^-\rightarrow CH^+ + e \tag{42}$$

and

$$C^+ + H^-\rightarrow CH+h\nu \tag{43}$$

might seem to merit some consideration. However, it would seem that neither can, in fact, occur; for, as regards reaction (42), it is likely that the potential curves of the C^+–H^- system and of CH^+ do not intersect; and, as regards reaction (43), the kinetic energy gained by the approaching ions would be so great that stabilization probably could not be effected by the emission of a photon. It may be remarked also that

$$CH^+ + H^-\rightarrow CH+H \tag{44}$$

[33] S. Chandrasekhar, *Ap. J.*, **102**, 395, 1945.

would not be important compared with radiative electron recombination, even if it took place on almost every collision. Other conceivable atomic and molecular processes were listed as systematically as possible. All obviously proceeded at utterly negligible rates.

c) POSSIBLE INFLUENCE OF GRAINS

In view of the difficulty of explaining the observed CH and CH^+ densities by purely atomic or molecular reactions, it is natural to ask whether some reaction involving the grains could be responsible; and, if this were the case, whether it would be necessary to abandon the view that CH and CH^+ are the nuclei from which the grains are formed. Unfortunately, there are too many unknown factors for such an inquiry to be pursued with any assurance. All that can be attempted at present is a tentative preliminary exploration.

One obvious possibility is that a fraction F of the carbon impinging on the grains ultimately evaporates as a neutral hydride. Clearly, the whole position regarding the equilibrium would be greatly eased if this evaporation should proceed some 10^3 times faster than the calculated rate of formation of CH by radiative association. The yield E due to this evaporation may be expressed as follows:

$$E = \lambda_0 Q v \{ n_0(C) + n_0(C^+) \} F, \tag{45}$$

where λ_0 is the factor by which the cross-section of the grains per unit volume at the center of a cloud exceeds the corresponding cross-section averaged over all interstellar space; Q is this mean cross-section; and v is the velocity of approach of a carbon atom or ion. Taking Q to be 3×10^{-22} cm^{-1} and v to be 4×10^4 cm/sec and writing $n_0(C)$ and $n_0(C^+)$ in terms of $n_0(H)$ gives

$$E = 4 \times 10^{-21} \lambda_0 n_0(H) F \text{ cm}^{-3}/\text{sec}. \tag{46}$$

It may readily be verified that this yield satisfies the condition specified above if

$$F > 0.15 \frac{n_0(H)^2}{\lambda_0}. \tag{47}$$

As it is not unlikely that $n_0(H)^2$ is comparable with λ_0, the requirement concerning F is thus not severe. Whether or not it is actually met cannot be decided with certainty.

Even if the absolute densities can be raised in this way, the problem of the $n_0(CH)/n_0(CH^+)$ ratio remains to be considered. By an obvious modification of the equilibrium formulae it can easily be seen that this ratio equals either β_3/β_1 or $a(e)n_0(H)\alpha_2/\beta_1$, according as dissociative recombination is negligible or is important. The value of β_3/β_1 is only 0.06, which is much too small; but it must be remembered that β_3 is ill determined. By suitable choice of α_2 the value of $a(e)n_0(H)\alpha_2/\beta_1$ can be adjusted at will, without changing condition (47) on F.

The theory of the growth of the grains is still very qualitative, particularly as regards the initial stages. Though the CH and CH^+ densities provided by atomic and molecular reactions alone are very low, it is possible that they may be sufficient to allow the condensation to commence.

d) CONCLUSION

Purely atomic and molecular reactions do not appear to account for the observed CH–CH^+ equilibrium in interstellar clouds, if the conditions in these clouds are as generally believed and if the quantal calculations are correct. It seems necessary to postulate either that the conditions are more favorable (i.e., that the density is much higher or that the radiation field is much less intense) or that reactions involving the grains are operative.

III. MOLECULES NEAR EARLY-TYPE STARS

We have seen in Section I that stars of late B types tend to be surrounded by clouds of CH^+ gas. It seems very improbable that such clouds are actually ejected by these stars. In the first place, Adams[6] has shown that in the Pleiades, for example, the radial velocities of the CH^+ lines are closely equal to the radial velocities found for K and H and are quite different from the velocities of the stars themselves. In the second place, we have seen that for almost all molecular lines appearing in the spectra of unreddened stars the velocity difference, cloud minus star, is positive. Thus, if these clouds are assumed to originate in the stars, we must conclude that they are now contracting toward the stars rather than expanding from them. In the third place, it is very difficult to see how the equilibrium abundance of CH^+ in a rarefied cloud of gas near a B-type star can be as high as observed. Examination of equation (23) and a consideration of the changes in the rate coefficients from normal interstellar clouds to heated circumstellar clouds indicate that the equilibrium value of $n(CH^+)/n(H)$ is less in a circumstellar cloud than in an interstellar cloud of the same density, while the observations require a greater value of this ratio. While the circumstellar cloud might have relatively high density, the effect of this change on the equilibrium abundance of CH^+ is probably offset by the almost complete ionization of H.

One is therefore led to consider the possibility that nonequilibrium processes may be responsible for the large number of CH^+ molecules observed near these B stars of late spectral types. The most obvious reservoir of CH^+ molecules lies within the grains themselves, and it is possible that the observed results may be explained on the assumption that the sublimation of CH_4 near stars of late B types may produce a high abundance of CH^+ molecules. The present section is devoted to a detailed discussion of this proposed mechanism.

As a grain approaches an early-type star, its internal temperature T_g will be gradually increased. At a certain critical distance, which we shall denote by r_S, the CH_4 will start to sublime at a substantial rate. The melting point of CH_4 is 90° K, substantially less than for the other abundant constituents of a grain, and sublimation will occur before T_g reaches this value. At a distance slightly less than r_S, all the CH_4 within a grain will have sublimed, since the vapor pressure increases very rapidly with the grain temperature and the radiation incident on the grain is sufficient for sublimation of the CH_4 in a few days, once the temperature is sufficiently high. The individual CH_4 molecules will then gradually become dissociated into their component atoms, with ionization probable en route. Since one H atom is likely to be knocked off at a time and since single ionization is more likely than double ionization, a large fraction of CH_4 molecules will go through a CH^+ stage before they finally dissociate completely.

We again let β_3 represent the probability of dissociation of CH^+ by radiation, evaluated at the distance r_S from the star. An individual CH^+ molecule will last, on the average, $1/\beta_3$ seconds before it dissociates; in a reference frame in which the star is at rest, a CH^+ molecule will travel a distance V/β_3 during its life, where $\mathbf{V}$ is the vector cloud velocity relative to the star, and V is the scalar magnitude of $\mathbf{V}$. Thus a hemispherical shell of CH^+ molecules will form, of thickness V/β_3 (measured parallel to $\mathbf{V}$) and centered at the star.

Naturally, this mechanism presupposes that a cloud of grains is passing sufficiently near the star or, rather, that the star is passing through an absorbing cloud. Stars not passing through such a cloud should show no circumstellar lines. However, a single small or tenuous cloud, with not enough grains to produce marked obscuration, may yet contain a sufficient density of grains to yield measurable circumstellar lines. Since the color excess produced by a single small cloud averages about 0.03 mag., a star passing through one such cloud is essentially unreddened.

We proceed now to a quantitative evaluation of these processes. First, we consider the value of r_S, the distance from a star at which the CH_4 in a grain will sublime. The

rate of sublimation may be computed from the vapor pressure of solid CH_4, measured in the range from 76°.9 to 87°.2 K by Karwat.[34] If the formula which Karwat uses to fit his data is extrapolated to lower temperatures, one finds that, at a temperature of about 24° K, the CH_4 in a grain will all sublime in about 10^4 years. Since this extrapolation may be considerably in error, this sublimation temperature is somewhat uncertain but probably lies within the range from 20° to 30° K.

Values of T_g, the internal temperature of a grain, have been considered by van de Hulst.[35] Unfortunately, the results are rather uncertain, and, while the most probable temperature is apparently between 10° and 20° K, the possibility is not altogether excluded that T_g in equilibrium may be great enough so that CH_4 could not form an equilibrium constituent of the grains. The same uncertainty appearing in T_g for an average interstellar grain is also present in the value of T_g for a grain near a hot star. In view of these uncertainties, we shall introduce as an unknown parameter the quantity X, defined as the ratio of the energy density at the critical distance r_S to the mean density of radiation in interstellar space, which, following Dunham,[36] we shall set equal to 5.2×10^{-13} erg/cm^3. In other words, we assume that the CH_4 sublimes rapidly at a distance r_S from the star, such that the energy density $u(r_S)$ of radiation from the star is given by

$$u(r_S) = 5 \times 10^{-13} X \text{ erg/cm}^3 . \tag{48}$$

If a grain radiated and absorbed like a black body and the temperature of sublimation were twice the mean temperature of an interstellar grain, X would equal 2^4 or 16. If the optical properties of the grain are considered, one will see that the ultraviolet radiation from an early-type star must be more effective in heating a grain than is the average interstellar radiation. The extinction cross-section of the grain is certainly higher in the ultraviolet than in the visible, and the albedo is likely to be considerably less, especially in the far ultraviolet, where the material in the grain is likely to show strong absorption bands. Hence a value of X in the general neighborhood of 1 is not unreasonable.

We may now proceed with the determination of r_S, the value of r at which equation (48) holds. If L is the bolometric luminosity of the star in erg/sec, then we have, in general,

$$u(r) = \frac{L}{4\pi c r^2} . \tag{49}$$

If we adopt the effective temperatures and resultant bolometric corrections given by Kuiper[37] and take absolute magnitudes from Stebbins, Huffer, and Whitford,[16] we obtain the values of r_S given in Table 10.

The values of β_3, the probability of dissociation of CH^+ by radiation, are readily obtained from the results in Section II, by the use of the general formula for the rate of a radiative process in a dilute Planck radiation field,

$$\beta = 4.35 \times 10^7 \Omega f E^2 10^{-E\theta} , \tag{50}$$

where Ω is the dilution, f the oscillator strength, E the energy in electron volts, and θ the reciprocal absolute temperature, $5040°/T$. We find that β_3 is given by the formula

$$\beta_3 = \Omega\{1.1 \times 10^{4-3.61\theta} + 8.5 \times 10^{7-14\theta}\} . \tag{51}$$

[34] *Zs. f. phys. Chem.*, **112**, 488, 1924.

[35] *Rech. Astr. Obs. Utrecht*, Vol. **11**, Part I, 1946.

[36] *Proc. Amer. Phil. Soc.*, **81**, 277, 1939.

[37] *Ap. J.*, **88**, 429, 1939.

Since the energy density equals the dilution Ω times aT^4, Ω at the distance r_S may be obtained by the use of equation (48). The resultant equation is

$$\Omega = 1.0 \times 10^{-13} X \theta^4 . \tag{52}$$

Since the distance l_D traveled by a CH^+ ion before dissociation is given by the relationship

$$l_D = \frac{V}{\beta_3}, \tag{53}$$

equations (50)–(53) may be combined to give the final values for l_D. These values, computed with V set equal to 10 km/sec, are also listed in Table 10.

To obtain the total number of CH^+ molecules, we must also compute the density of CH_4 molecules resulting from the sublimation of all the CH_4 within the grains. The

TABLE 10

COMPUTED NUMBER OF CH^+ MOLECULES IN LINE OF SIGHT

Spectral Type	T_e (° K)	M_{bol} (Mag.)	$r_S X^{1/2}$ (Parsecs)	$l_D X$ (Parsecs)	$N(CH^+)$ [$Cm^{-2}(X=1.6)$]	$N(CH^+)$ (Observed)
O5	80,000	−10.1	39	0.017	1.0×10^{12}	.....
O7	50,000	− 8.8	21	.010	5.9×10^{11}	.....
O9	32,000	− 7.7	13	.010	5.9×10^{11}	.....
B0	25,000	− 6.6	7.6	.015	9.0×10^{11}	.....
B1	23,000	− 6.1	6.0	.019	1.2×10^{12}	.....
B2	20,500	− 5.2	3.6	.028	1.7×10^{12}	.....
B3	18,700	− 4.2	2.5	.039	2.4×10^{12}	2.7×10^{12}
B4	17,000	− 3.7	2.2	.066	4.0×10^{12}	.....
B5	15,500	− 3.2	1.6	.090	5.5×10^{12}	.....
B6	14,500	− 2.8	0.4	.13	8.0×10^{12}	.....
B8	12,300	− 1.9	0.87	.22	1.3×10^{13}	1.9×10^{13}
A0	10,700	− 0.7	0.44	.27	1.6×10^{13}	.....
A2	9700	+ 0.1	0.35	.31	1.8×10^{13}	.....
A5	8500	+ 1.0	0.22	0.32	1.9×10^{13}	.....

mean value of this density, averaged over clouds and intercloud regions as well, we shall denote by $\bar{n}(CH_4)_S$; we have

$$\bar{n}\,(CH_4)_S = \frac{\bar{\rho}_g \zeta_M}{m_M} = 7.8 \times 10^{-5}\ \mathrm{cm}^{-3}, \tag{54}$$

where $\bar{\rho}_g$ is the average smoothed density of grains in interstellar space, ζ_M is the fraction of CH_4 by mass within the grains, and m_M is the mass of a CH_4 molecule in grams. The numerical value in equation (54) has been obtained with the assumption that $\bar{\rho}_g$ equals 1.4×10^{-26} gm/cm^3, the average value found within about 1000 parsecs from the sun by van de Hulst,[38] and that ζ_M is 0.15, the value found from the composition given by Kuiper,[39] with the assumption that all the elements other than H, He, and Ne are present in the grains, combined with H whenever possible.

We may now compute $N(CH^+)$, the number of CH^+ molecules per square centimeter in the line of sight to the star. Three particular assumptions will be made: (*a*) that each CH_4 molecule becomes a CH^+ molecule before complete dissociation; (*b*) that the distance traveled by any molecule before it loses an electron or H atom by photon

[38] *Rech. Astr. Obs. Utrecht*, Vol. 11, Part II, 1950.

[39] *The Atmospheres of the Earth and Planets* (Chicago: University of Chicago Press, 1949).

capture is small compared with r_S; and (*c*) that a CH^+ molecule will, on the average, be dissociated by radiation before it is neutralized or dissociated by electron capture. Assumption *a* would seem to be closely correct; even if the molecule is not ionized by the time that three *H* atoms have been removed, *CH* is about as likely to be ionized, forming CH^+, as to be dissociated (see Sec. II). Assumption *b* is certainly valid in stars of sufficiently early spectral type; for example, Table 10 indicates that, if X exceeds unity, l_D is less than r_S for stars of type A2 or earlier, and similar results may be expected to hold for the disruption of other molecules. From Section II it may be shown that assumption *c* is correct (i.e., $\beta_3 > [a_1 + a_2]n[e]$) if a_2 is small and the electron density $n(e)$ is less than $17X$, a reasonable upper limit in most *H* II regions. With these assumptions, we may readily find $N(CH^+)$ for a line of sight directed toward the advancing cloud and parallel to the relative velocity between cloud and star. We have, simply,

$$N(CH^+) = n(CH_4)_S l_D . \tag{55}$$

To obtain the mean value of $N(CH^+)$, we must use the average value of $n(CH_4)_S$ given in equation (54). In addition, we must average over all directions of the cloud velocity **V** relative to the star. Let θ be the angle between the line of sight (from earth to star) and the relative cloud velocity **V**. Then, for θ greater than $\pi/2$, the shell of CH^+ molecules is on the far side of the star from the earth and $N(CH_4)$ vanishes. For lesser values of θ, $N(CH_4)$ varies as $\sin\theta$. Averaging over all θ, we obtain an additional factor of $\pi/8$, which must be included in $N(CH^+)$. Then we have

$$N(CH^+) = \frac{\pi \bar{\rho}_g \zeta_M l_D}{8 m_M} = 3.1 \times 10^{-5} l_D . \tag{56}$$

The values of $N(CH^+)$ listed in Table 10 have been computed from this equation, with l_D computed for X equal to 1.6; this value was chosen to give good agreement between the computed values of $N(CH^+)$ and those observed, also listed in Table 10.

One would expect X to increase somewhat as the stellar temperature diminishes and the fraction of energy in the ultraviolet decreases to more nearly its average value in interstellar space. This effect will presumably give a maximum value of $N(CH^+)$ for stars of some particular type. Since the precise value of X is difficult to estimate, changes of X with spectral type have not been considered in detail here but should certainly be taken into account in a more complete theory.

While the present hypothesis can scarcely be said to allow a quantitative test, it seems consistent with all known facts as far as CH^+ is concerned. In particular, it provides a reasonable theoretical explanation for the observed fact that Δv, the velocity difference, cloud minus star, is positive for all unreddened stars showing molecular lines, with but one exception. The photoelectric color index of the exceptional star (31 Peg) is 0.03 mag., and the very weak λ 4232 in this star may be produced by a single dense cloud in the line of sight, not necessarily close to the star.

However, the presence of *CH* λ 4300 in a few unreddened stars of types B2–B5 does not find a ready explanation in terms of the present theory. The radiative dissociation and ionization of *CH* near a star of surface temperature 20,000° should be considerably more rapid than the corresponding rates for CH^+. In fact, from the data given in Section II we see that β_1 and β_2 exceed β_3 by factors of about 18 and 15, respectively, when the color temperature of the radiation is 20,000°. Hence $N(CH)$ should be less than $N(CH^+)$ by about an order of magnitude. According to Figure 1, *b*, there are four unreddened stars showing appreciable intensities for λ 4300. Two of these have color indices of 0.05 mag., and the molecular lines may not be circumstellar. In the two stars 2 Cyg and HD 212978, however, the color indices are 0.00 and 0.02, respectively, and it seems improbable that the line of sight to these stars passes through any very dense

obscuring cloud. Certainly, Figure 1, *c* and *f*, does not suggest that such relatively transparent clouds can produce detectable molecular lines. Unless these two stars are intrinsically bluer by at least 0.05 mag. than is assumed,[16] the presence of λ 4300 in the spectra of these two stars appears discordant with the present theory.

This discrepancy would disappear if the *f*-value for this transition were greater than assumed. A value of 30 for λ_1, yielding an *f*-value of 0.06 for λ 4300, would increase β_2 by only about 2 for stars of types B2–B3 and would give good agreement between observation and theory for these circumstellar lines, provided that an *f*-value of 0.002 is retained for λ 4232 (λ_2 equal to unity). Since this increased *f*-value for λ 4300 is supported by other observational evidence (see Sec. I), it may be correct; until more definitive information on these *f*-values is obtained, however, this possibility must be regarded with some reserve in view of the type of transition involved (see Sec. I).

Two other ways for diminishing this discrepancy between the theoretical and observed values of $N(CH)$ may be noted. If the values of β_1 and β_2 were much less, the observations could be explained, but Section II indicates that such small values for these quantities are improbable. Also, if α_2 were large, the ratio of $N(CH)$ to $N(CH^+)$ would again be near unity, but the number of each type of molecule in the line of sight would be smaller than observed, unless implausibly small values of X were assumed.

We conclude that the sublimation and subsequent dissociation and ionization of CH_4 from interstellar grains can apparently explain the presence of CH^+ λ 4232 in the spectra of unreddened B stars, but there is some question whether the presence of CH λ 4300 in 2 Cyg and HD 212978 can be explained on this basis. Evidently, further work is required to yield a complete understanding of the processes which are responsible for the presence of molecules in interstellar space.

A COMET MODEL. II. PHYSICAL RELATIONS FOR COMETS AND METEORS*

FRED L. WHIPPLE
Harvard College Observatory
Received October 22, 1950

ABSTRACT

It has been shown previously that the icy conglomerate model for comets explains the anomalous accelerations of certain comets and also possible reductions in the effective attraction by the sun. These effects depend upon a moderate loss of matter, $\Delta M/M$ per period. This loss measures the loss of radius, $\Delta R/R$, while the solar radiation determines the maximum loss of radius by sublimation. By this means an upper limit of radius for seven comets has been determined. Numerical values in kilometers are: Encke, 4; Pons-Winnecke, 82; Biela, 1.7; D'Arrest, 1.4; Brooks, 1.2; Wolf I, 19; and 1905 III, 0.2. The smaller values are the most significant and are generally greater than the expected values derived from the reflected light at great solar distances.

The model predicts a large excess of unobserved hydrides, H_2O, NH_2, and CH_4 molecules, as compared to the observed CO^+, C_2, and CN. For Halley's Comet, using Wurm's calculations for the rate of loss of CO^+ and C_2 and using the total loss of ices calculated from solar radiation for a nucleus of radius 10 km, the relative abundances of CO^+ and C_2 to the combined hydrides are 10^{-6} and 10^{-3}, respectively. These abundances are roughly consistent with certain of ter Haar's calculations for molecules formed from interstellar atoms. Calculations show that the predicted excess of hydrides will produce no appreciable Rayleigh scattering in comets and also little electron scattering, should all atoms become singly ionized by photoionization. Little visible radiation from the hydrides of C, N, and O would be expected.

The comet model requires that a large cometary nucleus eject visual or photographic meteoroids with greater velocities than a small nucleus at the same perihelion distance (velocity proportional to the square root of the radius). Hence the meteor streams from the greater comets should generally be more dispersed and more uniform from year to year than streams from lesser comets with comparable orbits. Confirming examples of streams from greater comets are the Perseids and the Orionids and Eta Aquarids, if the latter streams arise from Halley's Comet; the Leonids and Bielids represent debris from dying comets. Qualitatively, the model predicts well for the meteor streams from known comets.

A. INTRODUCTION

In Paper I[1] a new comet model was described. The model consists of a conglomerate made up of *ices*, such as H_2O, NH_2, and other molecules volatile at normal temperature, mixed with meteoritic materials. The model is shown to be capable of accounting for the abnormal accelerations in mean motion and eccentricity observed for periodic Comets Encke, D'Arrest, and Wolf I, discussed previously, without requiring an excessive rate of mass loss. The acceleration is postulated to occur by a time lag in sublimation of the ices in a rotating cometary nucleus.

Some previous results of the theory applied to these three comets are summarized in Table 1 of the present paper, along with corresponding new calculations for periodic Comets Pons-Winnecke, Biela, and Brooks. The entries of the first eight lines of Table 1 are self-explanatory. The quantity $\Delta\mu/\mu$ (obs.) is the observed relative acceleration per period in the mean daily motion. Averaged values of orbital elements are used. The quantity r_0 represents the solar distance within which acceleration is assumed to act. The quantity (mean) $r^{-1/4}$ is an adopted value used to avoid the numerical integration of

* An investigation carried out under NOrd Contract No. 10449-05512 of the Naval Bureau of Ordnance.

[1] F. L. Whipple, *Ap. J.*, 111, 375, 1950.

the integrals I_a, I_e, and I_ϖ of equations (33_1), (33_2), and (33_3) of Paper I. These integrals and their approximations are

$$I_a = \int_0^{v_0} r^{-5/4} d v_1 \cong \frac{v_0 + e \sin v_0}{r^{1/4} p}, \tag{1a}$$

$$I_e = \int_0^{v_0} r^{-5/4} (a p - r^2) d v_1, \tag{1b}$$

$$I_e r^{1/4} \cong a (v_0 + e \sin v_0) + \frac{p}{\sqrt{(1-e^2)}} \left\{ \sin^{-1} \left(\frac{e + \cos v_0}{1 + e \cos v_0} \right) - \frac{\pi}{2} \right\} \tag{1c}$$

and

$$I_\varpi = \int_0^{v_0} r^{-1/4} \cos v_1 d v_1 \cong r^{-1/4} \sin v_0, \tag{1d}$$

where v_1 is the true anomaly and v_0 its value at r_0. The integrations have been made numerically only for Comet Encke. The quantity r_m (A.U.) in Table 1 is the solar distance

TABLE 1

SECULAR CHANGES IN COMETARY ORBITS

Periodic Comet	Encke	Encke	Pons-Winnecke	Biela	D'Arrest	Brooks	Brooks	Wolf I	1905 III
Interval	<1865	>1865	.....	<1847	.....	<1922	>1922	>1920	.....
No. returns	13	20	5	3	6	3	3	4	0
Period (years)	3.30	3.30	6.04	6.65	6.67	7.10	6.94	8.28	297
e	0.847	0.847	0.686	0.751	0.627	0.470	0.486	0.405	0.975
q (A.U.)	0.34	0.34	1.04	0.88	1.32	1.96	1.87	2.43	1.12
$\Delta\mu/\mu$ (obs.)$\times 10^{+5}$	+9.7	+4.2	−0.16	+10	− 6.4	+ 5.6	+ 3.8	−0.30	*
Direction of rotation	Retr.	Retr.	Direct	Retr.	Direct	Retr.	Retr.	Direct	.....
r_0 (A.U.)	2.0	2.0	2.0	2.0	2.0	3.0	3.0	3.0	.....
(Mean) $r^{-1/4}$ (A.U.)	.....	.....	0.94	0.97	0.89	0.82	0.82	0.78	0.91
r_m (A.U.)	3.0	3.0	3.0	3.0	3.0	3.0	3.0	3.0	3.0
I_a (A.U.)$^{-5/4}$	5.8	5.8	1.30	1.64	0.86	0.61	0.65	0.46	.....
I_e (A.U.)$^{3/4}$	6.2	6.2	5.4	6.8	4.6	3.3	3.4	3.0	.....
I_ϖ (A.U.)	0.87	0.87	0.92	0.92	0.88	0.82	0.81	0.78	.....
v_m (rad.)	2.8	2.8	1.81	1.89	2.04	1.66	1.72	1.45	1.86
$\Delta M/M$ (calc.)$\times 10^{+3}$	4.8	2.0	0.09	4.7	5.2	4.4	2.9	0.23	40
Δe (obs.)$\times 10^{+6}$	−9.4	−4	−1.5	−10.2	+17	.....	.....	.....	.....
Δe (q=const.)$\times 10^{+6}$	−9.8	−4.3	+0.3	−16.5	+16	−20	−13	+1.2	.....
Δe (calc.)$\times 10^{+6}$	−8.3	−3.6	+0.3	−15	+15	−16	−11	+1.0	.....
$\Delta\varpi$ (calc.)	−2".1	−0".9	−0".14	− 5".8	− 8".2	−12".0	− 7".4	−0".85	.....

* Based on $\Delta k^2/k^2 = -9\ (\pm 3) \times 10^{-5}$; see Paper I, p. 393.

within which the loss of cometary material from the nucleus is assumed to be essentially complete. The true anomaly v_m corresponds to r_m.

The loss of material per period by the cometary nucleus, $\Delta M/M$, has been calculated from $\Delta\mu/\mu$ on the assumption that the dimensionless force component, γ, in the orbital plane normal to the radius vector, is 0.1 as contrasted to its maximum value $\frac{1}{2}$. This assumption is quite arbitrary. The tabulated quantity $\Delta M/M$ should be multiplied by $0.1/\gamma$ to give its value for another chosen value of γ. The sign of γ is positive for direct rotation of the cometary nucleus and negative for retrograde rotation, as assumed in the ninth line of Table 1.

The observed value of Δe per period can be compared in Table 1 with its value, Δe (q=const.), calculated on the assumption that the observed acceleration in mean daily

motion arises from a tangential impulse at the instant of perihelion. It can also be compared with its value, calculated by the present theory, Δe (calc.), from the observed acceleration in mean daily motion, on the assumption that the acceleration on the nucleus occurs only at solar distances less than r_0.

The change in the direction of perihelion passage per period, $\Delta\varpi$, is calculated from the ratio of equations (33_3) and (33_1) of Paper I, viz.,

$$\Delta\varpi = \frac{1}{3ae}\frac{I_\varpi}{I_a}\frac{\zeta}{\gamma}\frac{\Delta\mu}{\mu}. \tag{2}$$

The quantity ζ is the dimensionless component of the force acting on the cometary nucleus along the radius vector away from the sun. The ratio ζ/γ has been adopted arbitrarily as ± 4, on the assumption that γ is finite but that the radial component generally exceeds the normal component.

The motion of perihelion is essentially zero if the cometary nucleus be assumed to lose matter proportionately to the solar flux entirely around the orbit and if a negative correction be applied to the gravitational constant. In the calculation of secular accelerations in the elements of periodic comets, possible variations in ϖ tend to be absorbed in a correction to the mean anomaly and hence to the period. The order of magnitude of the calculated values of $\Delta\varpi$ are of general interest, and the writer hopes that a special search may be made for a secular effect in ϖ. An empirical determination of the ratio ζ/γ would be invaluable. The expected changes in i and Ω from similar forces perpendicular to the orbital plane are below detectability.

The source data for the observed values of $\Delta\mu/\mu$ and Δe have been given in Paper I for Comets Encke, D'Arrest, and Wolf I. The values for Comets Pons-Winnecke and Brooks were adopted from the recent investigation by A. D. Dubiago.[2] The value for Comet Biela up to the discovery of its duplicity in 1845 is based on the results of J. von Hepperger.[3] From Hepperger's and J. S. Hubbard's[4] work, it appears that no secular acceleration of the mean position of the two components is required in the period from 1846 to 1852. On the other hand, the difference in the mean motions of the two components had become considerably greater than the previous secular change per period.

The writer obtains a somewhat larger value of the accelerations in μ for Comet Biela than was obtained by Dubiago (30 per cent difference) even after correcting his values by the usual factor of 2 required to obtain agreement for Comets Encke and Wolf I. Apparently his definition of the secular change in μ differs from the present one by a factor of 2. No difference appears in Δe. The values of $\Delta\mu$ for Comets Pons-Winnecke and Brooks used here were taken from the *Bulletin of the Committee for Distribution of Astronomical Literature* rather than from the original source, making possible an uncertainty in terminology. Dubiago questions his value of Δe for Comet Pons-Winnecke, and we note that the predicted value is of opposite sign. Similarly, the predicted value of Δe for Comet Brooks is quite sizable, though Dubiago found no measurable value.

For the other comets, however, the calculated values of Δe are in good agreement with the observed values, while the calculated losses of mass in Table 1 are sufficiently small to permit considerable lifetimes for the comets. Note, however, that the calculated rate of mass loss for Comet Biela just prior to its bifurcation and disappearance is about the same as that for Comet Encke during the first half of the nineteenth century. There is no assurance of cometary longevity in a small value of $\Delta M/M$!

In evaluating the reality of the secular accelerations given in Table 1, the writer is of the opinion that the acceleration is unquestionably real for Comet Encke and is well

[2] *A.J. Soviet Union*, **25**, No. 6, 361, 1948.

[3] *Sitz-ber. Akad. Wiss. Wien*, Abt. IIa, **109**, 299, 623, 1900; **112**, 1329, 1903.

[4] *A.J.*, **4**, 1, 1854; **6**, 137, 1860.

determined for Comets Biela and D'Arrest. The check in Δe is especially satisfactory for these three comets. For the other comets the writer has had less opportunity to study the basis of the determination. Further checks on the validity of the proposed comet model will be presented in the following sections of this paper, particularly with regard to the physical nature of comets and their relationships with meteor streams.

B. DETERMINATION OF THE RADII OF COMETS

A knowledge of the proportion of mass lost per period by a spherical cometary nucleus and of the solar heat falling upon it determines the radius of the comet in terms of certain physical characteristics of the cometary material. A comparison with other determinations of the cometary radius provides a check on the comet model or a determination of the physical characteristics, as one chooses.

We have concluded previously that the rate of absorption of solar heat by the model nucleus becomes relatively small at a solar distance of 1.5–2.0 A.U. and essentially negligible at 3 A.U. or more. Comets with perihelion distances greater than these values must be quite large or else covered with an exceedingly thin layer of meteoric material to show much activity. Hence the solar flux, F/r^2, may be ignored at true anomalies from $+v_m$ to $-v_m$. The effective time, f, of solar heating equivalent to the solar constant ($F = 0.032$ cal cm^{-2} sec^{-1} at 1 A.U.) is obtained from the averaged time integral of F_0/r^2 from $-v_m$ to $+v_m$. The result is

$$f = \frac{v_m}{\pi\sqrt{p}} \text{ years} = 1.01 \times 10^7 \frac{v_m}{\sqrt{p}} \text{ sec}, \tag{3}$$

where p (in A.U.) is the parameter of the orbit.

Suppose that the cometary ices utilize a fraction, $1/n$, of the solar radiation for sublimation; that the nucleus is spherical, of radius R_c and density ρ_c; and that the mean heat of sublimation for the ices is H calories per gram. Then the total mass of the ices, ΔM, sublimated in one orbital period, is given by:

$$\Delta M = \frac{\pi R_c^2 f F}{nH}. \tag{4}$$

The corresponding loss of radius, ΔR_c, if we neglect the meteoric material, then becomes

$$\Delta R_c = \frac{fF}{4nH\rho_c}. \tag{5}$$

But the differential losses in mass and radius for a sphere are related by the equation

$$\frac{\Delta M}{M} = 3\frac{\Delta R_c}{R_c}. \tag{6}$$

Hence the radius of the comet is given by

$$R_c = \frac{M}{\Delta M}\frac{3fF}{4nH\rho_c}. \tag{7}$$

If $\Delta M/M$ is accepted for the comets in Table 1, we have only three physical constants to evaluate in equation (7). The quantity n may be taken as unity to give a maximum value of the calculated radius. A later discussion will show that $H = 450$ cal/gm and $\rho_c = 1.0$ are reasonable values and that the neglect of the meteoric materials in computing ρ_c and the mass loss is probably not serious. With these adopted values of the physical quantities, we find the maximum radii of the six comets as given in the fourth column of Table 2. The table entries are self-explanatory after reference to Table 1 and

equations (3) and (7). For Comet 1905 III (Giacobinid) the value of $\Delta M/M$ is adopted from the effective decrease in the Gaussian constant (Paper I).

In Table 2 the smaller values of the maximum radius should be considered as more significant, since they are based generally on the more reliable values of $\Delta\mu/\mu$ and hence $\Delta M/M$. Included implicitly in the calculated values of R_c (max.) is the arbitrarily adopted quantity γ, taken as 0.1. The calculated radii can be increased as much as the factor 0.444/0.1 by increasing γ, but they may be reduced indefinitely as γ is taken nearer to zero. An increase in n will reduce the calculated values proportionately.

Vorontsov-Velyaminov[5] concluded that a solid spherical nucleus for Halley's Comet cannot exceed a radius of 30 km and most probably is about 15 km in radius. Now Halley's Comet is some 5 mag. brighter intrinsically than the average comets of Table 2. Hence we see that the order of magnitude of the agreement is good if we except the large limiting radii for Comets Pons-Winnecke and Wolf I.

Comet Encke, the most reliable example in Table 2, was observed by H. M. Jeffers[6] as magnitude 18 on September 3, 1937. Reducing to the standard distance of 1 A.U. from

TABLE 2

MAXIMUM RADII OF COMETS

Comet	$\Delta M/M$ (Per Period)	f (Sec $\times 10^{-7}$)	R_c (max.) (Km)	Comet	$\Delta M/M$ (Per Period)	f (Sec $\times 10^{-7}$)	R_c (max.) (Km)
Encke (<1865)....	0.0048	3.5	4.0	Brooks (<1922)..	0.0044	1.0	1.2
Encke (>1865)....	.0020	3.5	9.2	Brooks (>1922)..	.0029	1.0	1.8
Pons-Winnecke....	.0001	1.4	82	Wolf I (>1920)..	.0002	0.8	19
Biela.....	.0047	1.5	1.7	1905 III.....	0.04*	1.3	0.2
D'Arrest.....	0.0052	1.4	1.4				

* Derived from $\Delta k^2/k^2 = -0.00009$.

both the earth and the sun by the ephemeris of the *B.A.A. Handbook*, one finds that the corresponding absolute magnitude was 16. If the albedo of the nucleus were not less than that of the moon, the nucleus of Comet Encke could not have exceeded 1 km in radius. Probably the nucleus was considerably smaller, as the comet then showed a coma-tail with a radius of some thousands of kilometers. One must conclude, therefore, by comparison with Table 2, that for Comet Encke the heating efficiency factor, $1/n$, is of the order of 0.1 or that the projection factor, γ, is of the order of 0.01 instead of 0.1.

The calculated maximum radius for Comet Biela is 1.7 km at a time just prior to its bifurcation and the rapid disappearance (if not disintegration) of its two components. It is probable, as for Comet Encke, that the actual dimensions of the nucleus were much smaller and that $(1/n) < 1$ or $\gamma < 0.1$.

The radius calculated for Comet 1905 III appears excessively small and may, of course, lack significance in case the observed value of $\Delta k^2/k^2$ arises from other causes. On the other hand, the comet at perihelion was diffuse and relatively faint, with a nucleus of 12.5 mag. on April 6, 1905, according to K. Graff.[7] We may conclude generally that the proposed comet model predicts maximum radii of cometary nuclei that are consistent with other independent data. For purposes of comparison in terms of mass, a sphere of radius 1 km and density 1 contains a mass of 4.2×10^{15} gm.

[5] *Ap. J.*, **104**, 226, 1946.

[6] *Harvard Announcement Card*, No. 433, 1937.

[7] *A.N.*, **173**, 377, 1907.

C. ORIGIN AND NATURE OF THE COMETARY CONGLOMERATE

The writer does not wish to speculate at this time on the detailed theories for the origin of comets. Nevertheless, the subject can hardly be completely avoided in making estimates of the relative abundances of the various materials. Furthermore, the basic assumptions for the comet model demand certain limitations in the conditions under which comets can come into existence. The most critical condition is that the temperature be very low. Presumably, in addition, the atoms (or molecules) must combine from the gaseous state, and the solid particles coalesce by encounter at relatively small velocities. One seems justified in assuming that the relative abundance of the elements in comets should be typical of the universe at large, with the limitation that elements not freezing or forming compounds should be rare or absent.

Reference to estimates of the cosmic abundances of elements—for example, those essentially by J. L. Greenstein, as tabulated by G. P. Kuiper[8]—shows that, on the basis of unity for O, the major contributions are 100 by H, 0.3 by C, 0.35 by N, and 0.8 by the sum of the major heavier contributors through Ni. Helium is, of course, omitted above. Since solid H_2 is unlikely to form in the interstellar space of the galaxy, H can occur only in compounds in small bodies like comets. Hence the contribution of H to the cometary masses will be small. The great abundance of H, however, leads one to expect that most of the C, N, and O will combine with H rather than with one another or with other elements.

On the basis of the above discussion, then, the meteoric materials should constitute about one-third or less the mass of cometary nuclei, the other two-thirds being made up largely of hydrides of C, N, and O. Estimates of the distribution of the chemical and physical structures of the meteoric materials must be made from studies of comets, meteors, and micrometeorites.[9] Determinations of these quantities can then lead to quantitative understanding of the physical conditions under which comets developed. This general problem constitutes one of the challenges in solar-system astronomy.

An example of this type of reasoning concerns the appearance of sodium (and other metals) in cometary spectra. Bobrovnikoff[10] points out that for certain comets the Na lines are extremely strong, even though the equilibrium temperature with sunlight could scarcely exceed the melting point of water. Neither vapor pressure from the solid state nor desorption would be likely to produce so much Na vapor from solid particles. On the other hand, if Na atoms or molecules of sodium compounds were imbedded in the ices of the present model, sublimation of the ices or sublimation plus dissociation of the molecules could release the Na atoms observed. The existence of such phenomena helps describe the conditions under which comets were formed.

Lacking, at present, sufficient information to estimate the frequency distribution of the various molecules of H, C, N, and O, the writer has arbitrarily assumed that the major mass is in the form of CH_4, NH_3, and H_2O.[11] The heat required to sublimate the above-assumed proportions of these compounds to the average surface temperatures at cometary nuclei is of the order of 450 cal/gm, as assumed in previous calculations.

The assumed high abundance of H_2O ice is the basis for expecting it to play a major part in reducing the efficiency of sublimation of cometary ices at fairly large solar distances.

If, indeed, a third of the mass of the comet is in the form of meteoric material (21 per cent, according to Harrison Brown), then the calculations of $\Delta M/M$ made previously

[8] *The Atmospheres of the Earth and Planets* (Chicago: University of Chicago Press, 1949), p. 309.

[9] Small meteoric particles that can pass through the atmosphere undamaged (see *Proc. Nat. Acad. Sci.*, 36, 687, 1951.

[10] *Rev. Mod. Phys.*, 14, 164, 1942.

[11] This assumption is in agreement with that made by Harrison Brown in his postulated composition of the preplanetary medium. I am indebted to Dr. Brown for a discussion of this point.

must be increased appropriately to allow for the macroscopic material carried along at low velocities by the hydrides of C, N, and O. This correction will not affect the calculated values of Δe and $\Delta\varpi$ in Table 1 but will reduce proportionately the calculated maximum radii of comets in Table 2. A low density of $\rho_c = 1.0$ has been chosen to allow for spaces between finite particles.

Of vital interest in interpreting the spectra of comets are the expected or observed percentages of the C-N-O material in the forms of compounds such as C_2, CN, C_2N_2, CO, CO_2, N_2, and NO. K. Wurm,[12] for example, has corrected the earlier estimates by Schwarzschild and Kron[13] for the mass of CO^+ lost by Halley's Comet near perihelion. He obtains a rate of loss of 1500 gm/sec, approximately ten times the previous value and about this same factor greater than was obtained by Vorontsov-Velyaminov.[14] Wurm also estimates that some 1.5×10^{32} C_2 molecules are required to produce the C_2 radiation observed for Halley's Comet near perihelion. If we accept Wurm's value of a lifetime of 10 hours for the C_2 molecule between $r = 0.5$ and $r = 1$ A.U., the rate of loss of C_2 becomes 2×10^5 gm/sec. Again his numerical results exceed the corresponding value obtained by Vorontsov-Velyaminov by about one order of magnitude.

We can now estimate the relative abundances of CO^+ and C_2 to the hydrides if we adopt a radius and heating efficiency factor for Halley's Comet. Suppose the radius to be 10 km (probably a generous estimate) and half the solar heat to be effective in sublimating the ices. Then the loss of matter from Halley's Comet at $r = 0.6$ A.U. becomes 3×10^5 gm/sec, yielding a relative abundance by mass of about 5×10^{-6} for CO^+ and 7×10^{-4} for C_2.

As an illustration of the type of argument that is applicable, without defending any implied conclusions, we note that D. ter Haar,[15] in an extension of the C. F. von Weizsäcker[16] theory of planetary formation, has calculated the relative abundances of various molecules from a medium at a temperature of a few hundred degrees K and a density of 10^{16} atom/cm^3. His calculated ratio of CO to H_2O is numerically 10^{-2} and of C_2 to CH and CH_4, 10^{-4}. Other such ratios are given by ter Haar. The agreement of the values for C_2 is excellent, and we note that C_2 might remain mixed with the ices rather than be derived from C_2N_2. Indeed, ter Haar would predict a relatively low abundance of C_2N_2. On the other hand, CO^+ must be derived from some parent-compound, such as CO or CO_2, by photoionization. Losses would be expected in the secondary processes. The abundance ratio of CO_2 to H_2O is 10^{-5}, as predicted by ter Haar, more in keeping with the observed-theoretical ratio for comets if CO^+ is derived from CO_2.

Before continuing with the abundance problem, we note that certain general restrictions on the origin of the solar system may be set by the present comet model. Three possibilities may be mentioned briefly.

a) If the comets were acquired by the system since its origin, possibly in the manner suggested by R. A. Lyttleton,[17] no implications concerning the origin of the system would be involved. In this case the material of the comets should typify interstellar solids, possibly somewhat modified. J. Oort's suggestion[18] that the comets were derived from asteroidal material is, of course, incompatible with the proposed comet model.

b) If the comets were formed with the planets *and* with the sun, limits on the physical surroundings of the protosun become established. Unless the radiation from the con-

[12] *Mitt. Hamburger Sternw., Bergedorf*, No. 51, p. 57, 1943.

[13] *Ap. J.*, **34**, 342, 1911. [14] *Op. cit.*, p. 231.

[15] *Det. Kgl. dansk. Vid. Selsk., Mat.-fys. Medd.*, Vol. **25**, No. 3, 1948.

[16] *Zs. f. Ap.*, **22**, 319, 1944.

[17] *M.N.*, **108**, 465, 1948. It can easily be shown, however, that planetary perturbations destroy the precise convergence of particles required by Lyttleton's theory and render the process inoperative.

[18] *B.A.N.*, **11**, 91, 1950.

densing (or disrupting) system was surprisingly small, the comets must have formed at very large solar distances, as would follow, for example, from the writer's dust-cloud hypothesis of the origin of the system.[19]

c) If the comets and planets formed in a ring of matter revolving about the sun after the sun was formed, as is most commonly assumed, much depends upon the solar radiation at the time, the density of the ring, and whether solid CH_4 is actually present in cometary nuclei. At low gas pressures solid CH_4 can scarcely condense at gas temperatures above 50° K and possibly not above 30° K (ter Haar). These stringent temperature limitations almost demand that solid CH_4 be condensed in HI regions of space within large quiescent dust clouds. Whether CH_4 might condense at higher temperatures on finite particles of H_2O or meteoritic material requires further investigation, as do the general problems of physical chemistry in interstellar space.

The absence of H_2O, NH_3, and CH_4 in observed cometary spectra sets no particular limit on the relative abundances of these substances in cometary nuclei. These gases are poor radiators in the photographic, the visual, and even the far red regions of the spectra. Little is known about the detailed processes of their photodissociation. A simple calculation shows that Rayleigh scattering by these molecules is negligible compared to the direct reflection of sunlight from the cometary nucleus at the rates of sublimation assumed in the present paper. A similar calculation of electron scattering, on the assumption that each atom produces one electron immediately on its escape from the cometary nucleus, shows that the scattering by electrons near perihelion could be comparable only to the direct reflection of sunlight from the nucleus. Hence electron scattering, even with such a generous assumption, appears ineligible to account for much cometary radiation. The haze of fine particles surrounding and escaping from the nucleus would be expected to outshine the nucleus itself.

D. THE EJECTION OF METEORITIC MATERIAL

Meteoritic material near the model cometary nucleus will be forced away from the surface against gravity by momentum transfer from the outgoing gases. Very near the surface the law of force will be complicated and the actual force increased by the "multiple reflection" of outgoing gases between the surface of the nucleus and the particle. Furthermore, for a rotating nucleus, the rate of gas output will vary with time and in all cases will depend upon the position on the nucleus.

Let us consider only the meteoritic material that is already carried an appreciable distance from the nucleus and let us assume that escape is sufficiently rapid with respect to the rotation of the nucleus so that we need consider only the gases escaping from the sunlit hemisphere (perhaps somewhat rotated from the sun's direction by the heat-transfer lag). Although various solutions are possible, the following appears sufficiently representative for our present needs: similarly to equation (4), the mass of gas lost per second by the nucleus at a distance r (A.U.) from the sun is $(\pi F R_c^2)/(nr^2H)$. At a distance R ($\gg R_c$) from the nucleus we assume that this gas escapes over the hemisphere $2\pi R^2$ with an outward velocity $\bar{v}$ (eq. [28], Paper I). Hence the momentum transferred per square centimeter per second at distance R is $(\bar{v}FR_c^2)/(2nr^2HR^2)$.

The meteoritic particles must be exceedingly irregular and rough, thus acting with a large accommodation coefficient for gaseous encounters. For simplicity let us assume that the accommodation coefficient is unity and that the particles are spherical, of radius s and density ρ_s. If the cometary gas of very low density is momentarily stopped by the particles and re-emitted immediately with thermal velocities, the drag coefficient is approximately 2 $(1 + \frac{4}{9})$, the case of free molecular flow. Hence the outward force on a

[19] *Centennial Symposia* (Cambridge: Harvard College Observatory, 1948), p. 126.

slowly moving particle is given by $(13\pi\bar{v}s^2FR_c^2)/(18nr^2HR^2)$. The total force will be reduced by gravity so that the net outward acceleration becomes

$$\frac{d^2R}{dt^2} = \frac{(C_1 - C\,R_c)R_c^2}{R^2}, \tag{8a}$$

where

$$C_1 = \frac{39\,\bar{v}F}{72n\,r^2\,s\,\rho_s H} \tag{8b}$$

and

$$C_2 = 4\pi\rho_c\,\frac{G}{3}. \tag{8c}$$

The relative velocity, V_∞, of the particle at infinity with respect to the cometary nucleus, then, is

$$V_\infty^2 = 2C_1R_c - 2C_2R_c^2\,. \tag{9a}$$

We may evaluate $\bar{v}$ numerically from equation (28), Paper I, and express equation (9*a*) numerically from solar-system data as previously for a cometary density of $\rho_c = 1$ gm cm^{-3} and a particle density of $\rho_s = 4$ gm cm^{-3}. If the particle radius s is expressed in centimeters, the cometary radius R_c in kilometers, and the solar distance r in A.U., then we find the velocity of ejection for meteoritic particles to be

$$V_\infty = \left(\frac{1}{n\,s\,r^{9/4}} - 0.052R_c\right)^{1/2} R_c^{1/2} \times 328 \text{ cm sec}^{-1}. \tag{9b}$$

It must be noted that equations (9*a*) and (9*b*) apply to the case when the velocity of ejection of the particle is *small* compared to the velocity of the outgoing gas. The upper limit to the particle velocity for very small particles is obviously near the gas velocity given by equation (28) of Paper I.

Since $1/n$ represents the efficiency of solar radiation in sublimating cometary gases, we see that a new comet (with $n = 1$) of radius 1 km at 1 A.U. from the sun would eject meteoritic particles of radius 1 cm and density 4 gm cm^{-3} with a velocity of about 3 meters per second. A bright photographic meteor of geocentric velocity 30 km sec^{-1} arises from a meteoroid of about this dimension.[20] For particles of this size or smaller, the velocity of ejection theoretically varies directly as the square root of the cometary radius and the efficiency factor, inversely as the square root of the particle radius, and approximately inversely as the solar distance.

Hence the ejection of the meteoritic particles from comets should be more violent as well as more frequent near perihelion. Also, larger comets should eject particles with greater velocities than smaller comets of comparable $1/n$. Observational evidence to test these conclusions must come from detailed studies of meteor showers. Certain data concerning the major meteor showers are given in Table 3. The column headings are self-explanatory. Data have been taken largely from F. G. Watson[21] and C. P. Olivier.[22] The durations of the showers are only approximate. The strength of the photographic showers are based on Harvard photographic meteors of this century and are of average values, neglecting the unusual displays from Comet Giacobini-Zinner in 1933 and 1946, which could not be photographed in Massachusetts. The showers that are most widely

[20] See, e.g., F. L. Whipple, *Proc. Amer. Phil. Soc.*, **79**, 499, 1938.

[21] *Between the Planets* (Philadelphia: Blakiston Co., 1941), chap. vii.

[22] *Meteors* (Baltimore: Williams & Wilkins Co., 1925), chaps. iv–viii.

dispersed and associated with known comets are the Perseids, the Taurids, and the *two* showers from Halley's Comet, if these last two associations are admitted. All arise from very bright comets, since Encke's Comet must originally have been massive to have persisted so long in a short-period orbit.

S. Hamid[23] finds for the Perseid meteor shower that its long persistence and the random deviations in radiants for the photographic meteors[24] can be explained adequately by planetary perturbations, particularly Jupiter's, if the shower has endured for about two hundred revolutions of the parent-comet. Initial ejection velocities as given by equation (9) are sufficient. Greater initial velocities for smaller particles probably will account for the larger spread in radiants of the faint visual Perseids, but precise data from the Super-Schmidt meteor cameras are required to prove this possibility.

If the case of Comet Encke we have an old, but not too faint, comet providing a widely spread shower. The Harvard photographic data[24] coupled with secular-perturbation theory by S. Hamid and the writer[25] indicate clearly that the dispersion among the

TABLE 3

METEOR STREAM CHARACTERISTICS

Meteor Shower	Geocentric Velocity (Km/Sec)	Associated Comet	Comet Brightness	q (A.U.)	Shower Length (Days)	Photographic Shower
Perseids*	60	1862 III	Bright	0.97	30	Strong
Leonids*	72	1866 I	Lost	0.98	5	Medium
Lyrids*	51?	1861 I	Bright	0.92	4	Weak
Androminids*	16?	Biela	Lost	0.86	5	Weak
Geminids	35	.....	.....	0.14	4	Strong
Eta Aquarids	66?	Halley?	Bright	0.59	6	Weak
Orionids	66	Halley?	Bright	0.59	10	Medium
Giacobinids*	23	1933 III	Faint	1.00	1	Weak?
Taurids	27	Encke	Medium	0.39	40	Strong
Delta Aquarids	50?	.....	.....	0.04	10	Strong
Quadrantids	46?	.....	.....	0.99	2	Weak

* Have presented outstanding displays.

Taurid orbits must arise from ejection in the asteroid belt rather than at perihelion. Presumably, collisions with asteroidal material are responsible for the dispersions in these orbits of low inclination and short period.

In contrast to the widely spread Perseid and Halley-Comet showers from bright comets, we find that the faint comets—Giacobini-Zinner, Biela, and the lost Leonid parent-comet—have produced showers of marked concentration. However, in the past, both the Perseid and the Lyrid showers from bright comets have also provided remarkable displays. Although the evidence from meteor showers is by no means conclusive, it is generally consistent with the conclusions from equations (9). The most extensive and widely spread showers tend to arise from large comets; although some large comets have produced concentrated showers, *all* the faint comets responsible for showers in Table 3 have done so.

A solution of equations (8) and (9) for the maximum radius, s_{max}, of ejected meteoritic

[23] "The Formation and Evolution of the Perseid Meteor Stream" (doctoral thesis; Harvard, 1950).

[24] *Technical Report No. 6* ("Harvard Rept. Ser.," No. II-35 [1950]).

[25] *A.J.*, **55**, 185, 1950 (abstr.).

particles yields the following numerical result on the basis of the assumptions made above:

$$s_{\max} = \frac{19 \text{ cm}}{n\, r^{9/4} R_c}, \tag{10}$$

where R_c is expressed in kilometers and r in A.U.

One notices that the maximum radius is quite sensitive to the perihelion distance of the comet and, for small perihelion distances, corresponds to extremely bright fireballs. Table 3 contains three perihelion distances less than 0.5 A.U. All the associated showers are strong photographically, indicating the presence of relatively large meteoric particles. Although the Perseid shower is also strong photographically, the ratio of photographic to visual strength would be smaller than for most of the other showers in Table 3. A perusal of the fireball catalogue by G. von Niessl and C. Hoffmeister[26] leads to similar conclusions. A rough identification ($\pm 40°$ in radiant within the shower interval) of possible fireballs associated with the various showers indicates perhaps 50 Taurids, 12 Geminids, 12 Delta Aquarids, 7 Perseids, and 3 or less representatives of other showers in Table 3. Hence meteor showers with small perihelion distances tend definitely to show more unusually bright members.

Although the evidence of the above several paragraphs is preliminary in character and subject to alternative explanations, the writer feels that, in totality, the comet-meteor data tend to support the comet model in associating comets and meteor streams by a physical process. Much more precise testing of the theory is possible and will be carried out as the photographic and radar observations of meteors become more extensive.

A forthcoming Paper III will present a quantitative relationship associating the loss of particles by comets with the maintenance of the Fraunhofer corona and the zodiacal light via the Poynting-Robertson effect.

[26] *Denkschriften Akad. Wiss. Wien*, **100**, 1, 1926.

THE PHYSICAL THEORY OF METEORS. I. A REACTION-RATE APPROACH TO THE RATE OF MASS LOSS IN METEORS

M. A. Cook, H. Eyring, and R. N. Thomas
University of Utah
Received December 9, 1950

ABSTRACT

The generalized reaction-rate theory is applied to the rate of mass loss in meteors. Temperatures around 3100° K are found for meteor *surfaces* near the point of maximum luminosity. An additional resistance term arises owing to this mass loss, with a v^3 dependence, which doubles the resistance computed from the usual expression at velocities about 60 km/sec. Some comment on the mechanism of flaring is offered.

From the ordinary telescopic observations of meteors, two kinds of data result: measures of position and measures of luminosity. The position measures describe the kinematics of the meteor's motion. The luminosity measures, on the one hand, characterize the mass of the meteor and hence combine with the kinematic results to describe the dynamics of the meteor's motion. From this aspect of the problem we obtain the density structure of the upper atmosphere. On the other hand, the procedure whereby we infer the meteor mass from the meteor luminosity characterizes the physics of the heat-transfer and radiation processes. These processes contain the details of the meteor interaction with the atmosphere. We consider here the details of the heat-transfer process.

I. THE RATE OF MASS LOSS FROM THE METEOR

Current ideas on heat transfer in meteors follow Whipple's analysis.[1] In brief, the heat transfer is expressed in terms of that for the Newtonian putty-ball model, viz.,

$$\text{Heat transfer} = H_T = \tfrac{1}{2}\Lambda \rho_a v^3 \mathfrak{A} , \tag{1}$$

where ρ_a is air density; v the meteor velocity; $\mathfrak{A}$ the meteor projected area perpendicular to v; and Λ the heat-transfer coefficient. The meteor analysis assumes Λ to be constant. The mass loss is then taken to be

$$\frac{dm}{dt} = \frac{H_T}{\zeta} , \tag{2}$$

where ζ is the energy required to vaporize 1 gm of meteoric material from the initial temperature of the meteor and is also assumed constant.

It is a priori evident that, while Λ may be a slowly varying function, particularly in regions where the incident gas atoms have energy nearly equal to the vaporization energy for the meteor atoms, the region over which equation (1) may be used with constant Λ is limited. For the case of small velocity, the expression for the heat transfer must involve the temperature difference between gas and solid. This region is that of the conventional aerodynamic heat-transfer calculations.[2] The second paper in this series will consider the boundary of this region and that region where equation (1) is preferable. On the other hand, for very large velocity the incident gas atoms interact with the solid essentially as though it were a collection of free atoms, and each meteor atom acquires an energy considerably in excess of the vaporization energy. Consequently, the use of

[1] *Rev. Mod. Phys.*, **15**, 246, 1943.

[2] E. R. G. Eckert, *Introduction to Transfer of Heat and Mass* (New York: McGraw-Hill Book Co., Inc., 1950), p. 88.

equations (1) and (2) with constant Λ/ζ would lead to an overestimate of dm/dt. We consider, then, the problem of a more suitable assumption than constancy of Λ/ζ.

One approach would be the microscopic one, where the details of the interaction between incident gas atom and solid lattice are investigated. For energies smaller than the binding energy in the lattice, the incident gas atom essentially interacts with the lattice as a whole. The problem is that of the accommodation coefficient—how much of the energy of the incident gas atom goes into the solid. For energies high with respect to the binding energy, the incident gas atom penetrates the solid, essentially interacts individually with the atoms of the solid, and loses all its energy. The first of these problems has not been treated theoretically; the last has been considered for energies considerably greater than those occurring in meteors in the various treatments of the absorption of fast particles in matter. A theoretical treatment covering the meteoric range of energies presents some complexity.

A thermodynamic treatment suggests itself. The heat transfer to the meteor is sufficiently great that the outer layers, where the interaction with gas atoms takes place, vaporize before any significant heat transfer to the interior occurs. A reasonably satisfactory picture of the meteor should therefore be one with a "hot" surface layer, from which vaporization occurs, and an undisturbed interior. The thickness of this hot layer would, for sufficiently energetic gas atoms, be fixed by the energy per gas atom. Hence, until the meteor slows down appreciably—only over the last small fraction of its visible path—the hot layer is probably of essentially constant thickness. We should therefore be able to regard the hot layer as a "reaction zone," with the reaction being

$$\text{Bound meteor atom} \rightleftharpoons \text{Free meteor atom} + \text{kinetic energy}.$$

If we assign a temperature T to this hot layer, the standard reaction-rate theory[3] gives, for the rate at which atoms leave unit area, with N atom/cm^2 on the surface,

$$\text{Rate} = \frac{kT}{h} N e^{-\Delta F^*/kT}, \tag{3}$$

where ΔF^* is the difference in Gibbs free energy of the bound atom and of the atom in the activated state. Alternatively, in terms of partition functions, we have

$$\text{Rate} = \frac{kT}{h} \frac{f^*}{f} e^{-\epsilon/kT}, \tag{4}$$

where f^* is the partition function of the activated atom (with the contribution along the direction of the reaction co-ordinate factored out), f that of the bound atom, and ϵ the activation energy at 0° K, i.e., the energy to vaporize the atom at 0° K. Hence the rate of vaporization from the meteor surface becomes

$$\frac{dm}{dt} = \frac{f^*}{f} \frac{kT}{h} e^{-\epsilon/kT} \left(\frac{\rho_s}{\mu_s m_H}\right)^{2/3} \mathcal{S} \mu_s m_H, \tag{5}$$

where $\mathcal{S}$ is the surface area of the meteor, ρ_s the density of the meteor, and μ_s the molecular weight of the meteor. Since the vaporization occurs only from the leading surface of the meteor, $\mathcal{S}$ is this area rather than that of the meteor as a whole.

In our first considerations,[4] we took for T a constant value at the boiling point of the meteor (assumed to be 3000° K) and f^*/f to be 1. So long as the available energy given by equation (1) exceeded that required by equation (5), we assumed that equation (5) gave

[3] E.g., Eyring, Glasstone, and Laidler, *Theory of Rate Processes* (New York: McGraw-Hill Book Co., Inc., 1941).

[4] M. A. Cook and R. N. Thomas, *A.J.*, **55**, 167, 1950 (abstr.).

the mass loss. There would therefore be a point along the meteor trail at which the right side of equation (5) equaled the right side of equation (2)—and here should be the point of maximum light for the meteor. Thereafter the light decreased with $\mathcal{S}$. This theory required a constant value of $\rho_a v^3$ at maximum light for meteors of the same composition. The observed values of $\rho_a v^3$ at maximum light showed a variation of about a factor of 4, with the observed values of $(\rho v^3)_{\max}$ lying between the predicted values for pure iron and pure stone meteors. This assumed constant value for T clearly has the same limitation as the assumed constancy of Λ/ζ when equation (2) is used and has the further limitation that it requires a diversion, by some means, of some of the available energy given by equation (1) into other processes than disintegrating the meteor (because of the independence of eq. [5] of gas density ρ_a).

We can modify this earlier theory to remove these objections by recognizing that T may exceed the boiling point, in which case T is a variable parameter and measures the velocity with which the meteor atoms leave the meteor surface. (Also, then, a knowledge of T suffices to calculate the momentum transfer to the meteor surface by the meteor atoms that leave it—the reverse-rocket action that is probably responsible for the indications[5] from meteor observations of a v^3 resistance law.) That is, if we take ΔH as the energy of reaction per atom and determine T by the condition that the available energy all be used, then (cf. eqs. [1] and [5])

$$\frac{f^*}{f}\frac{kT}{h}e^{-\epsilon/kT}\left(\frac{\rho_s}{\mu_s m_H}\right)^{2/3}\mathcal{S}\Delta H=\tfrac{1}{2}\Lambda\rho_a v^3\mathfrak{A}\,, \tag{6}$$

where Λ now is a direct measure of the accommodation coefficient—all the energy given to the surface goes toward heating it. The result differs from the standard meteor theory (2) in the use of ΔH as temperature-dependent and in actually fixing the temperature of the meteor surface with the temperature determined by equation (6), in which Λ or its equivalent, the accommodation coefficient, is the only free parameter. We have, for the temperature dependence of H,

$$H=E+PV=kT^2\frac{\partial}{\partial T}\ln f+PV\,. \tag{7}$$

We note now that ΔH refers to the difference in H calculated for the original meteoric material—at essentially the temperature T_i of the meteor before entering the earth's atmosphere—and for the final "meteor gas" at temperature T. Hence[6]

$$\begin{aligned}\Delta H&=kT^2\frac{\partial}{\partial T}\ln\left[\frac{(2\pi mkT)^{3/2}V}{h^3}\right]-kT_i^2\frac{\partial}{\partial T_i}\ln\left[(1-e^{-3\Theta_s/4T_i})^{-3}e^{\epsilon/kT_i}\right]\\&\qquad+PV_g-PV_s \qquad (8)\\&=\tfrac{3}{2}kT-3\left(\tfrac{3}{4}k\Theta_s\right)(1-e^{-3\Theta_s/4T_i})^{-1}+\epsilon+kT\,,\end{aligned}$$

since V_s is negligible compared with V_g. We note now that T_i is, at maximum, some 300° K, hence $T_i\sim\frac{3}{4}\Theta_s$ for iron. Hence the (constant) second term is less than 1 per cent of the (constant) third term and may be safely neglected. Hence we use

$$\Delta H=\epsilon+\tfrac{5}{2}kT\,. \tag{8.1}$$

The value of the partition function ratio is not obvious, since f refers to the atom in the solid at temperature T_i and f^* to the "activated atom," with the contribution from

[5] Private communication from F. L. Whipple.

[6] Alternatively, we can use the activated state for the final state instead of the meteor gas, and then we have in the partition function two vibrational and one translational degrees of freedom. The V term refers, then, to the solid and is thus negligible. Hence the value of ΔH remains the same. The two approaches are, of course, completely equivalent.

the reaction co-ordinate factored out. As the atom becomes completely free of the surface, its partition function increases drastically and becomes that for the free gas. However, f^* does not refer to that state. It would seem that f^*/f lies between unity and a value fixed by taking three degrees of vibrational freedom for f and two for f^*, since the reaction degree of freedom has been factored out of f^*. It might be argued that f^* corresponds to the atom just free of the lattice, hence with lesser binding and greater vibrational freedom and therefore characterized by a lesser Debye characteristic frequency. We have, therefore, for this approximation,

$$\frac{f^*}{f} = \frac{(1 - e^{-3\Theta^*/4T})^3}{(1 - e^{-3\Theta_s/4T})^3} \sim \frac{4}{3}\frac{T}{\Theta_s}\left(\frac{\Theta^*}{\Theta_s}\right)^2, \tag{9}$$

where Θ is the Debye characteristic frequency and $\Theta^* < \Theta_s$, while for iron, for example, Θ_s is 453.[7] Thus f^*/f has a value somewhere between $4T/3\Theta_s$ and 1, with the favored value somewhat closer to the former. It might be possible to decide between the two

TABLE 1

SURFACE TEMPERATURE OF METEORS

METEOR NO.	s		$-\log \tau$		$T(^\circ K)^*$		Σ
	i	m	i	m	i	m	
642	3.19	3.02	5.62	4.12	2635	3130	4.8
670	2.46	2.33	4.20	3.89	2980	3080	38
689	6.47	6.12	6.32	5.25	2700	3040	1.9
710	3.15	2.92	5.90	3.92	2550	3190	5.0
736	3.66	3.60	5.50	4.38	2720	3120	1.7

* We may comment here on the effect of the uncertainty in the value of f^*/f remarked in the discussion of eq. (9). In the change from solid to liquid state, Θ decreases by about a factor of 1.5. At the average T at maximum luminosity, $4T/3\Theta_s$ has the value 9.1. It would seem, then, that $(\Theta^*/\Theta_s)^2$ should be greater than about $\frac{1}{2}$. If we use the value $\frac{1}{2}$ and make this numerical change in eq. (12), a value of πr^3 that gave $T = 3100°$ for $\Theta^*/\Theta_s = 1$ now gives $T = 3370°$ K. Thus the effect of the uncertainty in f^*/f is not great on the value of T and hence is not great on the rate of vaporization (since T enters through ΔH only) or on the additional air-resistance term in Sec. II (since $T^{1/3}$ is the main temperature-dependent term).

extreme values experimentally, using materials of varying Θ_s. The difficulty here is to obtain observations on known bodies at sufficiently high velocities. Observations on lined-shaped charges might settle the point, when we obtain a satisfactory theory of the luminous efficiency of the meteor vapor. For the present, we note only the uncertainty in f^*/f and proceed to use expression (9) with $\Theta^* = \Theta_s$. The correct value of f^*/f thus is something less than the value used. We will indicate the effect of the uncertainty in the numerical calculations (cf. Table 1).

The ratio $\mathfrak{A}/\mathfrak{H}$ is the remaining unknown in equation (6). We shall simply use for this ratio its upper limit 1. Then equation (6) becomes

$$\frac{kT^2}{\Theta_s h} e^{-\epsilon/kT}\left[\epsilon + \tfrac{5}{2}kT\right]\left(\frac{\rho_s}{\mu_s m_H}\right)^{2/3} = \tfrac{1}{2}\Lambda \rho_a v^2. \tag{10}$$

From equation (10) we determine T and hence the rate of mass loss by the meteor. Making the substitution

$$\tau = \frac{\epsilon}{kT}, \tag{11}$$

[7] Slater, *Chemical Physics* (New York: McGraw-Hill Book Co., Inc., 1939), p. 454. Fowler and Guggenheim, *Statistical Thermodynamics* (Cambridge: At the University Press, 1939), p. 145.

we may rewrite equation (10) in a form suitable for numerical computation:

$$(1+0.4\tau)\,\tau^{-3}e^{-\tau} = 10^{-6.91}\,r\,s^3\Lambda\,, \tag{12}$$

where r is the ratio of density to the sea-level value, $1.2 \cdot 10^{-3}$ gm/cm^3, and s is the meteor velocity in units of 10 km/sec. We have considered an iron meteor and have used the values[7] 4.22 e.v./atom for ϵ and 453° for Θ_s. We set Λ equal to 1. As typical numerical values we have computed T for several meteors observed by Whipple[1] and have tabulated the values in Table 1 for the beginning point, i, of the meteor trail and for the point, m, of maximum light. We have chosen meteors with not too great a range in integrated luminosity divided by v^3. (Meteor 670 is the exception, but a low-velocity meteor was desired.) According to the current theory,[1] this quantity measures the meteor mass. In the last column of Table 1, Σ is proportional to this quantity.

II. INCREASED DRAG DUE TO VAPORIZATION

Ascribing a temperature T to the meteoric material leaving the meteor surface implies a certain momentum transfer to the meteor. Hence, to the usual retardation law that neglects the contribution of the vaporized material,

$$\text{Drag} = -\Gamma\rho_a v^2 \mathfrak{A}\,, \tag{13}$$

we add the quantity

$$-\left(\frac{kT}{2\pi\mu_e m_H}\right)^{1/2}\frac{dn}{dt}\,\mu_e m_H\,. \tag{14}$$

The first term is the mean thermal velocity in one direction; the second term, the rate of meteor atoms leaving the surface; and the last terms, the mass per meteor atom. Substituting for the second term from equation (6), we have, for the total drag,

$$\text{Drag} = -\Gamma\rho_a v^2\mathfrak{A}\left[1+\frac{\Lambda}{\Gamma}\frac{v}{2}\left(\frac{kT\mu_e m_H}{2\pi}\right)^{1/2}(\epsilon+\tfrac{5}{2}kT)^{-1}\right]. \tag{15}$$

We thus see the possibility of obtaining a v^3 resistance law for fast meteors. From Table 1 we see that, near maximum light, T is very close to 3100° K. Since the principal temperature-dependent term in equation (15) varies as $T^{1/2}$ and Table 1 shows T not to vary a great deal anyway, the use of the 3100° K value will introduce less error than the uncertainty in Γ above. Thus we obtain

$$\text{Drag} = -\Gamma\rho_a v^2\mathfrak{A}\left[1+0.16\,s\,\frac{\Lambda}{\Gamma}\right]. \tag{16}$$

Thus, for meteor velocities of 30 km/sec, we increase the drag by 50 per cent; and, for 60 km/sec, we double the drag. (Our assumption of Λ equal to 1 implies also that we take Γ equal to 1.)

The physical picture of this "reverse-rocket" action was described to us by Dr. F. L. Whipple, of the Harvard Observatory, prior to our present work and served as a stimulus to us in constructing this model; for, as seen from equation (15), the coefficient of the v^3 term depends upon the surface temperature of the meteor, a quantity heretofore only estimated. Dr. Whipple tells us that the possibility of the existence of the added resistance term from the vaporizing material arose in a discussion between himself and Dr. Ernst Öpik, of the Dublin Observatory. Clearly, expression (15) is strictly valid only under conditions such that the free path of the meteor atoms is comparable with the meteor dimension. For shorter free path, the additional resistance term must still arise, but its numerical value requires a more detailed discussion than the present indication of the limiting case. Here we are concerned only with presenting this reaction-rate approach to the physical model of the meteor and include this brief comment on the added re-

sistance term as an obvious corollary of the treatment. In a forthcoming paper a more detailed consideration of this resistance term will be presented by Dr. Whipple and one of us.

III. PENETRATION OF ATMOSPHERIC ATOMS INTO THE METEOR AND METEOR "FLARES"

As it stands, equation (10) is not strictly accurate for the case in which the incident gas atoms penetrate the meteor surface; for the atmospheric atoms will form oxides and nitrides with the meteor atoms and liberate a certain amount of energy in these exothermic reactions. Thus we should add to the right side of equation (10) a term,

$$\Delta E_c = \Lambda \frac{\rho_a v}{\mu_a m_H} \mathfrak{A} Q , \tag{17}$$

where Q is the heat of reaction per atmospheric atom. For an iron meteor, Q is about 2.8 e.v. for the oxides and somewhat less for the nitrides. The kinetic energy of an oxygen atom for a meteor moving 10 km/sec is 8.3 e.v. Thus, for the typical meteor moving 30 km/sec or more, the additional term (17) is something less than 4 per cent of the right-hand side of equation (10) and hence is negligible. For slow meteors the term should perhaps be included; but for slow meteors Λ presumably has a value less than 1, i.e., only a fraction of the incident atoms actually penetrate the meteor surface. Until we have a theory for Λ, we might approximate the situation by ignoring equation (17) and choosing a constant value of Λ near unity. The variation of Λ and the effect of equation (17) act, then, in a compensating direction.

We note, however, a difference between the character of the energy supply (17) and that from the kinetic energy of the incident air atoms. The energy (17) becomes available only in those regions where the gas atom energy has dropped low enough to allow the oxidation reaction to take place. As a crude estimate, the kinetic energy should probably drop to about the reaction energy of some 3 e.v., corresponding to about 6 km/sec for the incident oxygen atom. At this relatively low velocity the oxygen atom loses roughly half its energy at each collision with the iron atoms. Hence the geometric region in which the energy is low enough to permit the oxidation reaction is not large, perhaps a few lattice spacings thick, and in it the oxygen atoms lose their remaining kinetic energy and, in addition, the energy term (17). Thus near the end of the "reaction zone" discussed in Section I we expect a localized rise in the energy liberation. For a great enough rise and shallow enough reaction zone, we might suggest the possibility of "explosions" that would blow off the whole reaction zone at once rather than vaporizing it layer by layer. We note that the possibility of such an explosion is favored by a decrease in depth of reaction zone—i.e., decrease in meteor velocity—and by an increase in energy supply—i.e., increasing air density. Thus on both accounts we should expect such "explosions," if they occur, to favor the slow meteors, which, because of the ρv^3 term in the mass loss, disintegrate lower in the atmosphere. For fast meteors we should expect such explosions only near the end of the path. The explosions should, of course, be observed as momentary increases in luminosity of the meteor due to the increase in vaporized meteor material.

It is then suggestive to recall Jacchia's statistics[8] on meteor "flares" and periodic luminosity variation. For initial velocities around 20 km/sec, flares begin to occur as early as 0.4 of the way along the path. As the initial velocity increases, the range within which flares occur is compressed more and more toward the end of the trail; and meteors with velocities >60 km/sec usually have flares only in the last quarter of the visible path. Further, low-velocity meteors may have any number of flares, while the fastest meteors, as a rule, have only one flare, if any. We note thus that the qualitative features

[8] *Harvard Meteor Program* (Tech. Rept. No. 3 [1949]).

of flares are very similar to those predicted for our explosions. It has, of course, long since been suggested that flares came from sudden fragmenting of the meteor, but the initiating mechanism has never been specified. It is tempting to see in our explosions such a mechanism.

A quantitative analogy presents a somewhat greater problem. Our mechanism would make flaring a continual, periodic event, once conditions were ripe for its start, with a period comparable to the time required to vaporize a reaction-zone width. Using the rate equation (4) and some kind of reasonable estimate of the energy lost per collision, we conclude that the reaction zone should be no more than 50 atoms thick (for a velocity $\sim$20 km/sec), and hence the explosion period should be $<$0.001 second. While the data from Jacchia[8] are meager, it seems that the interval between flares is $>$0.01 second. Thus the physics of our explosions and the data on flares and other periodic luminosity changes must be investigated in more detail before the suggestions of this section can be considered well founded. We do, however, consider suggestive the similarity with regard to dependence on meteor velocity between the predicted behavior of our explosions and the observed behavior of flares.

NOTE ADDED IN PROOF.—The calculations in this paper balance the heat transfer to the meteor by impacting atmospheric atoms against energy dissipated by vaporization of material from the meteor surface. Energy loss by radiation of the meteor surface has been neglected. It can be shown[9] that the energy loss by radiation equals that by mass loss at 2260° K; but for higher surface temperatures the mass-loss term predominates and the relative importance of the radiation term decreases as $\tau\epsilon^{-\tau}$.

[9] Work supported by the U.S. Naval Ordnance Test Station.

TRANSFER OF RADIATION. II. RADIATIVE TRANSFER IN ABSORPTION LINES*

DONALD H. MENZEL AND HARI K. SEN
Harvard College Observatory
Received December 26, 1950

ABSTRACT

The equation of the formation of absorption lines in the Milne-Eddington model of a stellar atmosphere has been solved by an extension of the method previously described (*Ap. J.* **110**, 1, 1949). The equation of transfer in the standard case is

$$\mu \frac{\partial}{\partial \tau} I_\nu(\tau, \mu) = I_\nu(\tau, \mu) - \tfrac{1}{2}(1-\lambda) \int_{-1}^{1} I_\nu(\tau, \mu)\, d\mu - \lambda(a + b\tau),$$

where τ is the optical depth in the total (line and continuous) absorption, λ is the ratio of the continuous to the total absorption coefficient, and a and b are the first two coefficients of the Taylor expansion of the Planck function in powers of τ.

The authors assume an expansion of the "source function,"

$$J_\nu(\tau) = \tfrac{1}{2}(1-\lambda) \int_{-1}^{1} I_\nu(\tau, \mu)\, d\mu + \lambda(a + b\tau),$$

of the form

$$J(\tau) = a + b\tau + c e^{-m\tau} + \sum_0^\infty A_j K_{j+2}(\tau),$$

where m is the positive root of the equation

$$m = (1-\lambda) \tanh^{-1} m,$$

and $K_n(\tau)$ is the exponential integral of the nth order, defined by

$$K_n(\tau) = \int_1^\infty \frac{e^{-x\tau}}{x^n}\, dx.$$

The A_j's and c in $J(\tau)$ are constants which are found to be the solutions of a set of n simultaneous linear equations in the nth order. Finally, the quantities r and R, defined as the ratios of the emergent intensities and fluxes in the line and continuum respectively, are obtained as functions of λ, ν (frequency), c, and the A_j's.

The equations have been solved for a four-term expansion of $J(\tau)$, and the values of R and r obtained have been tabulated for the standard value of $\lambda = 0.2$ and various values of the parameter x, which is a function of the frequency ν. They are more accurate than the values obtained by Chandrasekhar (*Ap. J.*, **100**, 355, 1944) in the third approximation by Gaussian quadrature and comparable in accuracy to the values obtained by him (*Ap. J.*, **106**, 145, 1947) from the $H(\mu)$ function and its moments.

A special feature of the method is that it is not restricted to the atmospheric surface but enables one to evaluate the "source function" $J(\tau)$ for any τ.

We have applied the method previously described[1] to solve the equation of the formation of absorption lines in the Milne-Eddington model of a solar or stellar atmosphere. The equation of transfer in the standard case reduces to the form[2]

$$\mu \frac{\partial}{\partial \tau} I_\nu(\tau, \mu) = I_\nu(\tau, \mu) - \tfrac{1}{2}(1-\lambda) \int_{-1}^{1} I_\nu(\tau, \mu)\, d\mu - \lambda(a + b\tau), \qquad (1)$$

* The research reported in this paper has been made possible through sponsorship extended by the Geophysical Research Directorate of Air Force Cambridge Research Laboratories under Contract No. W19-122 ac-17.

[1] Menzel and Sen, *Ap. J.*, **110**, 1, 1949; hereafter called "Paper I."

[2] Chandrasekhar, *Ap. J.*, **100**, 355, 1944.

where τ is the optical depth in the total (line and continuous) absorption and λ is the ratio of the continuous to the total absorption coefficient.

In equation (1) we have retained only the first two terms of the Taylor expansion in τ of the Planck function:

$$B_\nu = \frac{2h\nu^3}{c^2}\frac{1}{e^{h\nu/kT}-1}. \tag{2}$$

The Taylor expansion is obtained from Milne's standard formula

$$T^4 = T_0^4(1+\tfrac{3}{2}\tau). \tag{3}$$

We can easily derive from equations (2) and (3)

$$\frac{b}{a} = \left(\frac{1}{B_\nu}\frac{dB_\nu}{d\tau}\right)_{\tau=\tau_0} = \frac{3\lambda}{8x}, \tag{4}$$

where

$$x = \frac{1}{u}\frac{e^u-1}{e^u} \tag{5}$$

and

$$u = \frac{h\nu}{kT_0}. \tag{6}$$

We find that the method of averaging through the atmospheric depth enables us to evaluate, fairly simply and at the same time with high accuracy, the residual fluxes and intensities in an absorption line. The residual intensity in a line is defined by

$$r = \frac{I_\nu(0,\mu)}{I_c(0,\mu)}, \tag{7}$$

that is, by the ratio of the emergent intensities in the line and continuum, respectively. Similarly, the residual flux is defined by

$$R = \frac{F_\nu(0)}{F_c(0)}, \tag{8}$$

that is, by the ratio of the emergent fluxes in the line and continuum, respectively.

For the continuum, $\lambda = 1$. In this case τ denotes the opacity in the continuum, and the corresponding Taylor expansion of the Planck function will be $a + b_0\tau$, where

$$b_0 = \frac{b}{\lambda}. \tag{9}$$

For the continuum, equation (1) can be immediately integrated to give[2]

$$F_c(0) = a + \tfrac{2}{3}b_0. \tag{10}$$

From equations (7)-(10), we have

$$r = \frac{3\lambda}{8x+3\mu}\frac{I^+(0,\mu)}{b} \tag{11}$$

and

$$R = \frac{3\lambda}{2(1+4x)}\frac{F_\nu(0)}{b}. \tag{12}$$

Now we can write equation (1) as

$$\mu \frac{\partial}{\partial \tau} I(\tau, \mu) = I(\tau, \mu) - J(\tau), \tag{13}$$

where the "source function" is

$$J(\tau) = \tfrac{1}{2}(1-\lambda) \int_{-1}^{1} I(\tau, \mu)\, d\mu + \lambda(a + b\tau). \tag{14}$$

We have omitted the suffix ν for convenience.

The "source function" $J(\tau)$ determines both the emergent intensity and the flux:

$$I^{+}(0, \mu) = \int_0^{\infty} J(\tau)\, e^{-\tau/\mu} \frac{d\tau}{\mu} \tag{15}$$

and

$$F(0) = 2 \int_0^{\infty} J(\tau)\, K_2(\tau)\, d\tau, \tag{16}$$

where $K_n(\tau)$ is the exponential integral of the nth order, defined by

$$K_n(\tau) = \int_1^{\infty} \frac{e^{-x\tau}}{x^n}\, dx = \int_0^1 e^{-\tau/x} x^{n-2} dx. \tag{17}$$

We may also note that $J(\tau)$ satisfies the following integral equation,[3] which is equivalent to equation (1):

$$J(\tau) = \lambda(a + b\tau) + \tfrac{1}{2}(1-\lambda) \int_0^{\infty} J(x)\, K(|\tau - x|)\, dx. \tag{18}$$

The quantity $J(\tau)$ in equation (18) has the following asymptotic form[4] ($\tau \to \infty$):

$$J(\tau) = a + b\tau + c e^{-m\tau}, \tag{19}$$

where a, b, and c are constants and m is the positive root of the equation

$$m = (1-\lambda) \tanh^{-1} m. \tag{20}$$

We take the positive root of equation (20) to avoid exponential divergence of equation (19).

Substitution of equation (19) in equation (18) gives terms in the exponential integrals $K_n(\tau)$ defined by equation (17).[5] We therefore assume the following expansion for $J(\tau)$:

$$J(\tau) = a + b\tau + c e^{-m\tau} + \sum_0^{\infty} A_j K_{j+2}(\tau), \tag{21}$$

where the a, b, c, and A_j's are constants and m is the positive root of equation (20).

[3] Unsöld, *Physik der Sternatmosphären* (Berlin: J. Springer, 1938), p. 251.

[4] $J(\tau)$ in eq. (19) satisfies the integral equation for an *infinite* atmosphere, viz. (cf. eq. [18]),

$$J(\tau) = \lambda(a + b\tau) + \tfrac{1}{2}(1-\lambda) \int_{-\infty}^{\infty} J(x)\, K(|\tau - x|)\, dx.$$

[5] There are residual terms besides the exponential integrals (cf. C. Mark, *Phys. Rev.*, **72**, 558, 1947). Consideration of these terms may lead to a higher order of accuracy than is attained in this paper.

Assumption (21) is equivalent to the following:

$$J(\tau) = a + b\tau + ce^{-m\tau} + \int_0^1 e^{-\tau/y}\phi(y)\,dy, \tag{22}$$

where

$$\phi(y) = \sum_0^\infty A_j y^j. \tag{23}$$

Substitution[6] of equation (22) in equation (18) yields the following equation in $\phi(y)$:

$$Q(0) \equiv \int_0^1\int_0^1\left[-1+\frac{1-\lambda}{2}\left(\frac{y}{y+\mu}+\frac{y}{y-\mu}\right)\right]e^{-\tau/y}\phi(y)\,dy\,d\mu - \tfrac{1}{2}(1-\lambda)$$
$$\times\int_0^1\int_0^1\frac{y}{y-\mu}\,e^{-\tau/\mu}\phi(y)\,dy\,d\mu - \tfrac{1}{2}(1-\lambda)\int_0^1 e^{-\tau/\mu}\left(a-b\mu+\frac{c}{1-m\mu}\right)d\mu = 0. \tag{24}$$

Integrating equation (24) n times successively with respect to τ, we obtain

$$(-1)^n Q(n) \equiv \frac{1}{D^n}Q(0)$$
$$\equiv \int_0^1\int_0^1\left[-1+\frac{1-\lambda}{2}\left(\frac{y}{y+\mu}+\frac{y}{y-\mu}\right)\right]e^{-\tau/y}y^n\phi(y)\,dy\,d\mu$$
$$-\tfrac{1}{2}(1-\lambda)\int_0^1\int_0^1\frac{y}{y-\mu}\,e^{-\tau/\mu}\mu^n\phi(y)\,dy\,d\mu$$
$$-\tfrac{1}{2}(1-\lambda)\int_0^1 e^{-\tau/\mu}\mu^n\left(a-b\mu+\frac{c}{1-m\mu}\right)d\mu = 0, \tag{25}$$

since $Q(0) = 0$, and the $Q(n)$'s all vanish at $\tau \to \infty$, because of the exponential factor.

Equation (25) is valid for all τ and n. Adopting a set of weighted mean values through the layers, we multiply equation (25) by $\tau^k d\tau$, and we integrate from 0 to ∞. The resulting equations agree with that obtained from equation (25) when we set $\tau = 0$ and replace n by $n + k + 1$.

Thus, if we can determine $\phi(y)$ to satisfy the equation

$$\int_0^1\int_0^1\left[-1+\frac{1-\lambda}{2}\left(\frac{y}{y+\mu}+\frac{y}{y-\mu}\right)\right]y^n\phi(y)\,dy\,d\mu - \tfrac{1}{2}(1-\lambda)\int_0^1\int_0^1\frac{y}{y-\mu}$$
$$\times\mu^n\phi(y)\,dy\,d\mu - \tfrac{1}{2}(1-\lambda)\int_0^1\mu^n\left(a-b\mu+\frac{c}{1-m\mu}\right)d\mu = 0, \tag{26}$$

for all n, we shall have the correct solution.

[6] We are indebted to Mrs. Harold Jeffreys and Dr. V. Kourganoff for independent confirmation of a part of the following analysis. The method adopted in this paper of starting from the Milne integral equation is a departure from the operational method of the first part of Paper I. The latter analysis has recently been criticized by Miss Busbridge (*Ap. J.*, 111, 654, 1950). Our analysis is purely heuristic and does not lay any claim to mathematical rigor. As Miss Busbridge remarks, we "do not make any use of the explicit form" of the function $\phi(y)$ obtained by our operational method. We believe, however, that the singularities mentioned by Miss Busbridge cancel out so that the final form of the result is correct. We did not attempt a detailed justification, since the correct form of the function $\phi(y)$ is known anyway (Mark, *loc. cit.*). The method adopted in Paper I of averaging through the atmospheric depth, which is not "artificial" but has a definite physical meaning (see V. Kourganoff, *Ap. J.*, 111, 443, 1950), has been retained in the present paper. We submit that Miss Busbridge's statement in her abstract that "the mathematics of the paper by Menzel and Sen is examined and shown to be unsound, the results being correct only in form," is unfair to the authors and misleading to the readers, especially in view of the fact that the results, as Miss Busbridge herself admits, are correct.

Integrating equation (26) with respect to μ, we obtain

$$\int_0^1 \left(-y^n + \frac{1-\lambda}{2} y^{n+1} \ln \frac{1+y}{y} + \frac{1-\lambda}{2} \sum_{k=1}^{n} \frac{y^{n-k+1}}{k} \right) \phi(y)\, dy \tag{27}$$

$$- \tfrac{1}{2}(1-\lambda) \left[\frac{a}{n+1} - \frac{b}{n+2} - \frac{c}{m} \left\{ \sum_{j=0}^{n-1} \frac{1}{n-j} \frac{1}{m^j} + \frac{\ln|1-m|}{m^n} \right\} \right] = 0 .$$

Set equation (23) in equation (27) and obtain the equation

$$\sum_0^\infty C_{nj} A_j = \frac{a}{n+1} - \frac{b}{n+2} - \frac{c}{m} \left\{ \sum_{j=0}^{n-1} \frac{1}{n-j} \frac{1}{m^j} + \frac{\ln|1-m|}{m^n} \right\}, \tag{28}$$

where the coefficients C_{nj} are given by

$$C_{nj} = \frac{2\ln 2 - \sum_1^{n+j+1} \frac{(-1)^{k-1}}{k} + \sum_1^{n+j+1} \frac{1}{k} - \sum_1^{j+1} \frac{1}{k} + \sum_1^{n} \frac{1}{k}}{n+j+2} - \frac{2}{1-\lambda} \frac{1}{n+j+1}, \tag{29}$$

for $n+j$ odd, and

$$C_{nj} = \frac{\sum_1^{n+j+1} \frac{(-1)^{k-1}}{k} + \sum_1^{n} \frac{1}{k} + \sum_1^{n+j+1} \frac{1}{k} - \sum_1^{j+1} \frac{1}{k}}{n+j+2} - \frac{2}{1-\lambda} \frac{1}{n+j+1}, \tag{30}$$

for $n+j$ even.

Note that the coefficients C_{nj} given by equations (29) and (30) are related to the coefficients C'_{nj} of Paper I as follows:

$$C_{nj} = C'^{j}_{n} - \frac{2\lambda}{1-\lambda} \frac{1}{n+j+1}. \tag{31}$$

From a given λ, the C_{nj}'s can therefore be easily computed from Table 1 of Paper I. The coefficients A_j/b and the constant c/b can be calculated from equation (28) as a function of λ and x defined by equation (4). The function J/b can now be calculated from equation (21) to any degree of approximation. Finally, the residual intensity and flux, r and R, are to be obtained from equations (11), (12), (15), and (16).

More explicitly, from equations (12), (16), and (21), we have

$$R = \frac{3\lambda}{1+4x} \left[\frac{4x}{3\lambda} + \frac{1}{3} + \frac{c}{v} \left\{ \frac{1}{m} - \frac{\ln(1+m)}{m^2} \right\} + \sum_0^\infty \frac{A_j}{b} \int_0^\infty E_2(\tau) E_{j+2}(\tau)\, d\tau \right]. \tag{32}$$

As for equation (32), note that

$$\int_0^\infty E_2(\tau)\, d\tau = E_3(0) = \tfrac{1}{2}, \tag{33}$$

$$\int_0^\infty \tau E_2(\tau)\, d\tau = \tfrac{1}{3}, \tag{34}$$

and[7]

$$\int_0^\infty E_n(\tau) E_2(\tau)\, d\tau = \frac{1}{n} - \frac{1}{n+1} \left[1 - \tfrac{1}{2} + \tfrac{1}{3} - \tfrac{1}{4} + \ldots + \frac{1}{n} \right], \tag{35}$$

[7] Cf. Kourganoff, *Ann. d'ap.*, **10**, 331, 1947.

for n odd and

$$\int_0^\infty E_n(\tau)E_2(\tau)\,d\tau = \frac{1}{n} - \frac{1}{n+1}\left[2\ln 2 - \left(1 - \tfrac{1}{2} + \tfrac{1}{3} - \tfrac{1}{4} + \ldots - \frac{1}{n}\right)\right], \tag{36}$$

for n even.

Again, from equations (11), (15), and (21) we obtain

$$r = \frac{3\lambda}{8x+3\mu}\,\frac{I^+(0,\mu)}{b}, \tag{37}$$

where

$$I^+(0,\mu) = \left(a + A_0 + \frac{A_1}{2} + \frac{A_2}{3} + \frac{A_3}{4}\right) + \left(b - A_1 - \frac{A_2}{2} - \frac{A_3}{3}\right)\mu$$
$$+\left(A_2 + \frac{A_3}{2}\right)\mu^2 - A_3\mu^3 - (A_0\mu - A_1\mu^2 + A_2\mu^3 - A_3\mu^4)\ln\frac{\mu+1}{\mu} + \frac{c}{m\mu+1}. \tag{38}$$

We have numerically evaluated R and r in this paper for the standard value of $\lambda = 0.2$, considered by Eddington,[8] and for various values of x. For $\lambda = 0.2$, equation (20) reduces to

$$m = 0.8\,\tanh^{-1} m\,. \tag{39}$$

We have solved equation (39) by interpolation in a table of inverse hyperbolic tangents[9] and found the positive root

$$m = 0.7104117843\,. \tag{40}$$

Table 1 gives the constants A_j and c as a function of x and in units of the constant b.[10] Table 2 gives the values of R defined by equation (8). We have also quoted for com-

TABLE 1

x	0.1	$\frac{1}{3}$	0.25	$\frac{1}{2}$	0.35
A_0.....	−0.3491244710	−0.5067439162	−0.7037682066	−0.9007923698	−0.9401973184
A_1.....	+ .5694156921	+0.7827654562	+1.049452730	+1.316138042	+1.369476673
A_2.....	− .7259012116	−1.122333696	−1.617874733	−2.113410137	−2.212521435
A_3.....	+ .4559637213	+0.7473637130	+1.111614114	+1.475860403	+1.548711262
C.....	−0.250330694	−0.6314569722	−1.107864821	−1.584272667	−1.679554238

TABLE 2

x	0.1	$\frac{1}{3}$	0.25	$\frac{1}{2}$	0.35
Present method	0.377303	0.422236	0.461552	0.489635	0.494316
Gaussian quadrature (3d approximation)..	.3794	.4248	.4645	.4928	.4976
$H(\mu)$ function.....	0.377298	0.422231	0.461547	0.489630	0.494310

[8] *M.N.*, **89**, 620, 1929.

[9] *Tables of Inverse Hyperbolic Functions* (Cambridge: Harvard University Press, 1949).

[10] For a given λ, the A_j's and c are linear in x. We owe this remark to Dr. Kourganoff, although the relation is implicit in the linearity of eq. (28). It suffices, therefore, to solve these equations for two values of x.

parison Chandrasekhar's values obtained from Gaussian quadrature[2] and by the $H(\mu)$ function and its moments.[11]

We may obtain an estimate of the rapidity of convergence of our method from Table 3, which gives the values of R for $x = \frac{1}{3}$, obtained from solving successively two through

TABLE 3

Approximation	R	Approximation	R
C, A_0	0.4884913	$C, A_0A_1A_2$	0.4896284
C, A_0A_1	0.4896233	$C, A_0A_1A_2A_3$	0.4896352

five simultaneous equations. Note that even our first approximation is more accurate than the third approximation of Gaussian quadrature and that the accuracy of the second approximation is already comparable to that of the $H(\mu)$ function.

Table 4 gives the values of the residual intensity r (see eq. [7]), obtained from the

TABLE 4

μ	x				
	0.10	$\frac{1}{8}$	0.25	$\frac{1}{3}$	0.35
0	0.667957	0.579660	0.535512	0.513437	0.510284
0.1	.580990	.557583	.543587	.535882	.534739
0.2	.516055	.525273	.531477	.535149	.535710
0.3	.470403	.496968	.516434	.528622	.530533
0.4	.436704	.472914	.501202	.519736	.522702
0.5	.410787	.452433	.486642	.509904	.513691
0.6	.390217	.434876	.473070	.499864	.504290
0.7	.373435	.419599	.460414	.489813	.494733
0.8	.359494	.406258	.448771	.480096	.485397
0.9	.347706	.394486	.438030	.470756	.476349
1.0	0.337605	0.384018	0.428115	0.461836	0.467656

TABLE 5

μ	x				
	0.10	$\frac{1}{8}$	0.25	$\frac{1}{3}$	0.35
0	0.667956	0.579659	0.535511	0.513436	0.510283
0.1	.580993	.557578	.543581	.535874	.534731
0.2	.516039	.525255	.531458	.535129	.535690
0.3	.470407	.496971	.516437	.528625	.530536
0.4	.436706	.472916	.501205	.519739	.522704
0.5	.410767	.452412	.486619	.509881	.513667
0.6	.390205	.434848	.473030	.499814	.504240
0.7	.373424	.419587	.460402	.489800	.494719
0.8	.359486	.406250	.448762	.480087	.485388
0.9	.347696	.394474	.438017	.470743	.476336
1.0	0.337596	0.384013	0.428110	0.461830	0.467644

[11] Chandrasekhar, *Ap. J.*, **106**, 145, 1947.

solution of five simultaneous equations by the operational method, as a function of x and μ. We have also computed in Table 5, for comparison, the corresponding values from Chandrasekhar's formula in terms of the $H(\mu)$ function and its moments.[12]

As there exists no exact solution of the present problem, it is difficult to give a rigorous estimate of the accuracy obtained. Nevertheless, it is evident from Tables 2, 4, and 5 that the accuracy attained by our method is at least equal to that reached by Chandrasekhar by means of his functional equation. According to Chandrasekhar's estimate,[12] his values are correct to five significant figures. Our method, moreover, is not restricted to the atmospheric surface and enables us to evaluate the "source function" $J(\tau)$ for any τ, to a high degree of accuracy.

We should like to thank Mr. John G. Wolbach and Dr. Edith M. Janssen for having helped us with the numerical work in this paper. We also wish to acknowledge several stimulating discussions with Dr. V. Kourganoff, whose interest has encouraged us to develop this method more fully.

[12] *Ibid.*, p. 144.

TRANSFER OF RADIATION. III. REFLECTION EFFECT IN ECLIPSING BINARIES*

DONALD H. MENZEL AND HARI K. SEN
Harvard College Observatory
Received December 26, 1950

ABSTRACT

We have applied the method described in *Ap. J.*, **110**, 1, 1949 (hereafter called "Paper I") to solve the Milne integrodifferential equation for diffuse radiation (I) in the plane-parallel atmosphere of a reflecting star:

$$\mu \frac{\partial}{\partial \tau} I(\tau, \mu) = I(\tau, \mu) - B(\tau),$$

where

$$B(\tau) = \frac{1}{2} \int_{-1}^{1} I(\tau, \mu)\, d\mu + \tfrac{1}{4} F e^{-\tau \sec \beta}.$$

The reflecting star is exposed to a parallel beam of radiation of flux πF per unit area normal to itself and incident at an angle β normal to the boundary of the atmosphere.

We have assumed the following expansion for $B(\tau)$:

$$B(\tau) = a + \sum_{0}^{\infty} A_j K_{j+2}(\tau) + \tfrac{1}{4} \gamma F e^{-\tau \sec \beta}$$

where $K_n(\tau)$ is the exponential integral of the nth order, defined by

$$K_n(\tau) = \int_1^{\infty} \frac{e^{-x\tau}}{x^n}\, dx$$

and

$$\gamma = \frac{1}{1 + \cos \beta \ln (\tan \beta / 2)}.$$

The coefficients A_j can be evaluated from a system of linear equations involving the C_{nj}'s tabulated in Paper I. We have calculated the emergent intensity corresponding to the solution of four simultaneous equations and have compared our values with those obtained from the Chandrasekhar-Hopf formula (*Ap. J.*, **106**, 143, 1947):

$$I(\mu, \mu_0) = \tfrac{1}{4} F \frac{\mu_0}{\mu_0 + \mu} H(\mu) H(\mu_0),$$

where $H(\mu)$ is the solution of the functional equation

$$H(\mu) = 1 + \tfrac{1}{2} \mu H(\mu) \int_0^1 \frac{H(\mu')\, d\mu'}{\mu + \mu'}$$

and

$$\mu_0 = \cos \beta.$$

The two sets of values of the emergent intensity agree to within one part in a thousand, on the average, and somewhat less for $\beta = 0°$, on account of a singularity in the solution.

The solution of more equations does not consistently improve the agreement. We believe that for higher accuracy we need to improve the trial function for $B(\tau)$.

* The research reported in this paper has been made possible through sponsorship extended by the Geophysical Research Directorate of Air Force Cambridge Research Laboratories under Contract No. W19-122 ac-17.

Milne[1] first derived the following integrodifferential equation for the *diffuse* radiation (I) in the semi-infinite plane-parallel atmosphere of a reflecting star:

$$\mu \frac{\partial}{\partial \tau} I(\tau, \mu) = I(\tau, \mu) - B(\tau), \tag{1}$$

where

$$B(\tau) = \frac{1}{2} \int_{-1}^{1} I(\tau, \mu)\, d\mu + \tfrac{1}{4} F e^{-\tau \sec\beta}, \tag{2}$$

β is the angle of incidence on the boundary of the atmosphere of the reflecting star of a parallel beam of radiation of flux πF per unit area normal to itself, and the other symbols have their usual meanings. Milne also gave the integral equation corresponding to equation (1) for the "source function" $B(\tau)$:

$$B(\tau) = \frac{1}{2} \int_{0}^{\infty} B(t)\, K(|\tau - t|)\, dt + \tfrac{1}{4} F e^{-\tau \sec\beta}, \tag{3}$$

where $K_n(\tau)$ is the exponential integral of the nth order, defined by

$$K_n(\tau) = \int_{1}^{\infty} \frac{e^{-x\tau}}{x^n}\, dx = \int_{0}^{1} e^{-\tau/x} x^{n-2} dx. \tag{4}$$

We have applied the averaging method previously described[2] to obtain an approximate solution of the transfer equation (1).

Integrating equation (1) with respect to μ between the limits 1 and -1, we have

$$\frac{d}{d\tau}\left[\int_{-1}^{1} I(\tau, \mu)\, \mu\, d\mu\right] = -\tfrac{1}{2} F e^{-\tau \sec\beta}. \tag{5}$$

Equation (5) gives, on integration, the diffuse flux πF at depth τ:

$$\pi F = 2\pi \int_{-1}^{1} I(\tau, \mu)\, \mu\, d\mu = \pi F \cos\beta\, e^{-\tau \sec\beta}. \tag{6}$$

The constant of integration in equation (6) vanishes, as the *net* flux is zero, the reflecting star acting as a perfect reflector with albedo unity.[3]

The quantity $B(\tau)$ in equation (3) has the following asymptotic form[4] ($\tau \to \infty$):

$$B(\tau) = a + b\tau + \tfrac{1}{4} \gamma F e^{-\tau \sec\beta}, \tag{7}$$

where a and b are constants and γ is a function of β:

$$\gamma = \frac{1}{1 + (\cos\beta) \ln(\tan \beta/2)}. \tag{8}$$

The constant b in equation (7) is proportional[5] to the asymptotic diffuse flux and vanishes with it (see eq. [6]). Substitution of equation (7) in equation (3) gives terms in

[1] *M.N.*, **87**, 43, 1926.

[2] Menzel and Sen, *Ap. J.*, **110**, 1, 1949; hereafter called "Paper I."

[3] Eddington, *M.N.*, **86**, 320, 1926.

[4] $B(\tau)$ in eq. (7) satisfies the integral equation for an *infinite* atmosphere, viz. (cf. eq. [3]):

$$B(\tau) = \frac{1}{2} \int_{-\infty}^{\infty} B(t)\, K(|\tau - t|)\, dt + \tfrac{1}{4} F e^{-\tau \sec\beta}.$$

[5] The proof is as in the standard case of no incident radiation.

the exponential integrals $K_n(\tau)$ defined by equation (4).[6] We therefore assume the following expansion for $B(\tau)$:

$$B(\tau) = a + \sum_0^\infty A_j K_{j+2}(\tau) + \tfrac{1}{4}\gamma F e^{-\tau \sec\beta}, \tag{9}$$

where a and the A_j's are constants and γ is a function of β given by equation (8).

Assumption (9) is equivalent to the following:

$$B(\tau) = a + \int_0^1 e^{-\tau/y}\phi(y)\,dy + \tfrac{1}{4}\gamma F e^{-\tau \sec\beta}, \tag{10}$$

where

$$\phi(y) = \sum_0^\infty A_j y^j. \tag{11}$$

Set equation (10) back in equation (3) and obtain

$$\begin{aligned} Q(0) \equiv \int_0^1\int_0^1 \left[-2 + \frac{y}{y+\mu} + \frac{y}{y-\mu}\right] e^{-\tau/y}\phi(y)\,dy\,d\mu - \int_0^1\int_0^1 e^{-\tau/\mu}\frac{y}{y-\mu} \\ \times \phi(y)\,dy\,d\mu - \int_0^1 e^{-\tau/\mu}\left(a + \frac{\frac{1}{4}\gamma F}{1-\mu\sec\beta}\right)d\mu = 0. \end{aligned} \tag{12}$$

Integrating equation (12) n times with respect to τ, we have

$$\begin{aligned} (-1)^n Q(n) &\equiv \frac{1}{D^n} Q(0) \\ &\equiv \int_0^1\int_0^1 \left[-2 + \frac{y}{y+\mu} + \frac{y}{y-\mu}\right] e^{-\tau/y} y^n \phi(y)\,dy\,d\mu - \int_0^1\int_0^1 e^{-\tau/\mu} \\ &\quad \times \frac{y}{y-\mu}\mu^n\phi(y)\,dy\,d\mu - \int_0^1 e^{-\tau/\mu}\mu^n\left(a + \frac{\frac{1}{4}\gamma F}{1-\mu\sec\beta}\right)d\mu = 0, \end{aligned} \tag{13}$$

since $Q(0) = 0$, and the $Q(n)$'s all vanish at $\tau \to \infty$, because of the exponential factor.

Equation (13) is valid for all τ and n. Adopting a set of weighted mean values through the layers, we multiply equation (13) by $\tau^k d\tau$ and integrate from 0 to ∞. The resulting equations agree with those obtained from equation (13) when we set $\tau = 0$ and replace n by $n + k + 1$. Thus, if we can determine $\phi(y)$ to satisfy the equation

$$\begin{aligned} \int_0^1\int_0^1 \left[-2 + \frac{y}{y+\mu} + \frac{y}{y-\mu}\right] y^n\phi(y)\,dy\,d\mu - \int_0^1\int_0^1 \frac{y}{y-\mu}\mu^n\phi(y)\,dy\,d\mu \\ - \int_0^1 \mu^n\left(a + \frac{\frac{1}{4}\gamma F}{1-\mu\sec\beta}\right)d\mu = 0 \end{aligned} \tag{14}$$

for all n, we shall have the correct solution.

[6] There are residual terms neglected in the present paper. Consideration of these terms would presumably lead to a higher order of accuracy than is attained herein.

Perform the integration with respect to μ in equation (14) and obtain finally the equation that $\phi(y)$ in equation (10) must satisfy:

$$\int_0^1 \left(-2y^n + y^{n+1} \ln \frac{1+y}{y} + \sum_{k=1}^{n} \frac{y^{n-k+1}}{k} \right) \phi(y)\, dy - \frac{a}{n+1} + \tfrac{1}{4}\gamma F \cos\beta \times \left[\sum_{0}^{n-1} \frac{1}{n-k} \cos^k \beta + \cos^n \beta \ln(\sec\beta - 1) \right] = 0. \tag{15}$$

Set equation (11) in equation (15) and obtain the equation

$$\sum_0^\infty C_{nj} A_j = \frac{a}{n+1} - \tfrac{1}{4}\gamma F \cos\beta \left[\sum_0^{n-1} \frac{1}{n-k} \cos^k \beta + \cos^n \beta \ln(\sec\beta - 1) \right], \tag{16}$$

where the coefficients C_{nj} are given by

$$C_{nj} = \frac{2\ln 2 - \sum_1^{n+j+1} \frac{(-1)^{k-1}}{k} + \sum_1^{n+j+1} \frac{1}{k} - \sum_1^{j+1} \frac{1}{k} + \sum_1^{n} \frac{1}{k}}{n+j+2} - \frac{2}{n+j+1} \tag{17}$$

for $n+j$ odd, and

$$C_{nj} = \frac{\sum_1^{n+j+1} \frac{(-1)^{k-1}}{k} + \sum_1^{n} \frac{1}{k} + \sum_1^{n+j+1} \frac{1}{k} - \sum_1^{j+1} \frac{1}{k}}{n+j+2} - \frac{2}{n+j+1} \tag{18}$$

for $n+j$ even. The C_{nj}'s are the same as those in Paper I and have already been tabulated there.

Note that a singularity occurs in equation (8) for $\beta \to 0$, as $\gamma \to 0$ in this case. A corresponding singularity exis's in equation (16), as

$$\operatorname*{Lt}_{\beta \to 0} \ln(\sec\beta - 1) = -\infty.$$

Hence for $\beta \to 0$ we have to evaluate the last term in the right-hand side of equation (16) as a limit, which is easily found to equal $\frac{1}{2}F$. Equation (16) therefore holds for $\beta \neq 0$, and the equation corresponding to equation (16) for $\beta = 0$ is

$$\sum_0^\infty C_{nj} A_j = \frac{a}{n+1} - \tfrac{1}{2}F. \tag{16'}$$

The quantity $B(\tau)$ may now be computed from equation (9) after we have solved the simultaneous equation (16) or (16').

From equation (9) we easily derive the following formula for the emergent reflected intensity (as far as terms in A_2):

$$I^+(0,\mu) = \left(a + A_0 + \frac{A_1}{2} + \frac{A_2}{3}\right) - \left(A_1 + \frac{A_2}{2}\right)\mu + A_2\mu^2 - (A_0\mu - A_1\mu^2 + A_2\mu^3) \ln\frac{\mu+1}{\mu} + \frac{1}{4}\gamma \frac{F}{1+\mu\sec\beta}. \tag{19}$$

The last term in equation (19) will vanish when $\beta = 0$.

In order to test the efficacy of our method, we have considered in this paper two values of β: viz., 0° and 60°. We have solved four simultaneous equations in equations (16) and (16′) and have evaluated $I^+(0, \mu)/F$ from formula (19). Table 1 gives a comparison of our values with those obtained from the Chandrasekhar-Hopf formula:[7]

$$I(\mu, \mu_0) = \tfrac{1}{4}F \frac{\mu_0}{\mu_0 + \mu} H(\mu) H(\mu_0), \tag{20}$$

where $H(\mu)$ is the solution of the functional equation

$$H(\mu) = 1 + \tfrac{1}{2}\mu H(\mu) \int_0^1 \frac{H(\mu')\, d\mu'}{\mu + \mu'}, \tag{21}$$

and

$$\mu_0 = \cos \beta . \tag{22}$$

The two sets of values of the emergent intensity agree to within one part in a thousand, on the average. The agreement is less good for $\beta = 0°$, on account of a singularity in the solution to which we have already drawn attention.[8]

TABLE 1

μ	$I^+(0, \mu)/F$			
	$\beta = 0°$		$\beta = 60°$	
	Computed (Formula [19])	Chandrasekhar (Formula [20])	Computed (Formula [19])	Chandrasekhar (Formula [20])
0.0	0.727457	0.726950	0.503209	0.503200
0.1	0.829197	0.824361	.523120	.523076
0.2	0.881379	0.878580	.521698	.521279
0.3	0.919899	0.918473	.516913	.516566
0.4	0.950439	0.949864	.511596	.511391
0.5	0.975541	0.975467	.506511	.506420
0.6	0.996657	0.996876	.501863	.501851
0.7	1.014724	1.051643	.497681	.497749
0.8	1.030387	1.030936	.493937	.494046
0.9	1.044117	1.044742	.490583	.490728
1.0	1.056250	1.056913	0.487572	0.487735

Solution of more equations does not consistently improve the agreement. We believe that for higher accuracy we need to improve the trial function (9). The last term in equation (9) is a particular solution of the integral equation (3) only in the first approximation.[6] In fact, γ in that term cannot be a constant for an accurate solution. We may note in this connection that Chandrasekhar's solution[9] of the present problem by Gaussian quadrature has singularities at an enumerable set of values of β. His particular solution is

$$B(\tau) = \tfrac{1}{4}\gamma F e^{-\tau \sec \beta}, \tag{23}$$

[7] Chandrasekhar, *Ap. J.*, **106**, 143, 1947.

[8] See eq. (16′).

[9] *Ap. J.*, **101**, 348, 1945.

where

$$\gamma = \frac{1}{1 - \sum_{j=1}^{n} \frac{a_j}{1 - \mu_j^2 \sec^2 \beta}}. \tag{24}$$

The μ_j's are the roots for the vanishing of the Legendre polynomial $P_{2j}(\mu)$, and the a_j's are certain weight factors.

The constant γ in equation (24) $\rightarrow \infty$ when

$$\sec \beta = k_a, \tag{25}$$

where k_a is a root of Chandrasekhar's indicial equation

$$1 = \sum_{j=1}^{n} \frac{a_j}{1 - \mu_j^2 k^2}. \tag{26}$$

Equation (25) is valid as $k_a > 1$. The same conclusion follows from equation (48) of Chandrasekhar's paper.[10]

We should like to thank Mr. John G. Wolbach for having helped us with the numerical work in this paper.

[10] *Ibid.*

THE PROPAGATION OF SHOCK WAVES IN A STELLAR MODEL WITH CONTINUOUS DENSITY DISTRIBUTION*

PIERRE A. CARRUS, PHYLLIS A. FOX, FELIX HAAS, AND ZDENĚK KOPAL
Massachusetts Institute of Technology
Received November 30, 1950

ABSTRACT

The aim of the present paper has been to investigate the properties of progressing waves which arise if a compressible-gas configuration, in which the density ρ_0 diminishes with increasing distance r from the center, as $\rho_0 \sim r^{-5/2}$ is disturbed from its state of equilibrium by an instantaneous central explosion. It is shown that, if this explosion has been sufficiently energetic for the outgoing disturbance to possess the characteristics of a shock wave, the central part of our configuration will be effectively evacuated by the explosion up to a certain distance from the center, depending on the amount of energy liberated by the initial explosion. If the release has been instantaneous (and, in consequence, the total energy of the wave motion is independent of the time t), the inner boundary of our flow (inclosing the empty core) becomes, by definition, a surface of contact discontinuity.

In order to study the properties of the actual flow of gas trapped between the shock wave and the contact discontinuity, which is of the nature of a progressing wave, the fundamental system of partial differential equations of our problem has been converted to ordinary differential equations with $\xi = r^{-5}t^4$ as the sole independent variable and has been integrated numerically for 8 cases corresponding to different strengths (i.e., the Mach numbers) of the head wave and to the ratio of specific heats $\gamma = \frac{5}{3}$. The physical properties of our flow—such as the velocity, pressure, and density at any point of the disturbed medium—remain the same along the lines ξ = Constant. In particular, the radii of both boundaries limiting our expanding regime increase as $t^{4/5}$; and as for the generalized Roche model, the thickness (ξ-wise) of the shell between them is found to increase with the increasing Mach number of the head wave.

Table 1 contains the numerical data describing the details of the individual solutions in terms of nondimensional parameters, which can be easily converted into absolute units by a suitable choice of the initial parameters. Table 2 summarizes the physical properties of the respective shock waves and indicates, in particular, the fractional amount of energy necessary to give rise to the computed phenomena.

Finally, the appendix contains a proof of the uniqueness of the solutions of the form of progressing blast waves investigated in Sections II–V. It demonstrates that, if the dependent variables U, P, and Ω of our fundamental system of partial differential equations are to be expressible in terms of an equivalent system of ordinary differential equations with $\xi(r, t)$ as the sole independent variable, $\xi(r, t)$ must necessarily be of the form $\phi(r)\psi(t)$, where $\phi(r)$ is a power of r alone, while $\psi(t)$ may be either a power or an exponential of t. The product of the powers of both r and t represents, moreover, the only possible form of ξ which will render the total energy of the corresponding wave motion independent of the time. If, ultimately, the expanding field of flow is to be headed by a shock front characterized by a constant Mach number (i.e., if both sides of the Rankine-Hugoniot conditions are to be functions of ξ alone), the structure of the undisturbed configuration becomes uniquely specified.

I. INTRODUCTION

In a previous communication[1] we investigated the propagation of shock waves in the envelope of a generalized Roche model, caused by a sudden expansion of its core. As is well known, a generalized Roche model (GRM) is characterized by a discontinuity in density across the interface of the core and its envelope, and for this reason it may not (except possibly under very special circumstances) come very close to stellar models of real astrophysical importance. In the present paper we shall, naturally enough, aim at removing this special feature of our previous work and shall attempt to extend it by considering the propagation of intense spherical disturbances in gaseous configurations in which the density remains a continuous function of radial distance from the center to the surface. In doing so, we shall find our problem to be considerably less tractable for an obvious reason. In a GRM practically the whole mass of the configuration was supposed

* An investigation supported by Contract N5ori-07843 with the Office of Naval Research.

[1] *Ap. J.*, 113, 193, 1951. This paper will hereafter be referred to as "Paper I."

to be confined to its core, so that the gravitational acceleration throughout the envelope varied simply as the inverse square of the distance from the center. If, however, the density is to be a continuous function of the radius r, the mass $m(r)$ interior to any arbitrary radius will likewise vary with r; as a result, the field of force in which the shock waves are to propagate will no longer be of the simple inverse-square type, but its intensity will respond to any fluctuation in density caused by the passage of any disturbance. In mathematical language the mass $m(r)$ contained within a sphere of radius r becomes an additional dependent variable of our problem, and its presence will increase the order of the system of differential equations by one.

The aim of the present paper will be to investigate, in the light of such equations, the events which will follow if the center of our compressible-gas configuration is disturbed by a radially symmetrical explosion. In doing so, we shall again consider the central explosion to be instantaneous—an assumption which necessitates the total energy of the wave motion being independent of the time—and, as in Paper I, we shall limit our present contribution to an analysis of the "progressing blast waves"—i.e., to such motions for which the velocity, pressure, and density of the disturbed field of flow can be made to depend on a sole variable $\xi = r^{\phi}t^{\psi}$, where r denotes the radial distance, t the time, and ϕ and ψ are suitably chosen constants. The form of the fundamental equations of the problem, together with the requirement that the total energy carried off by the wave motion be independent of t, will uniquely specify the values of ϕ and ψ; while the requirement that the expanding regime be limited on the outside by a shock wave will again impose a certain definite variation of the undisturbed density in front of the shock. Conversely, should the actual exploding configuration possess a different equilibrium structure, the fundamental system of partial differential equations describing, implicitly, the effects of explosion in terms of the independent variables r and t will not be reducible to ordinary differential equations with ξ as the sole independent variable. In reality—as represented by the phenomenon of nova outbursts—the equilibrium structure of the prenovae (which is being explored concurrently with these investigations) may not come very close to the one postulated later in this paper; at any rate, it should be understood that the reasons which have led us to adopt the latter have been prompted by mathematical convenience rather than by its physical reasonableness We do not believe, however, that this attitude calls for any apology, for the strategy inherent in our approach is obvious. Unlike the numerical solutions of partial differential equations (which are, besides, much more difficult and laborious), the cases in which such equations can be made to depend on a single variable ξ are capable of furnishing solutions which hold good without any limit of time. In point of fact, the progressing waves—like the periodic orbits of dynamical astronomy—represent, to use the words of Henri Poincaré, "la seule brèche par où nous puissions essayer de pénétrer dans une place jusqu'ici réputée inabordable."[2] It is therefore only logical that an exploration of solutions of the fundamental equations of the problem should begin with waves of the progressing type; and this constitutes the task which will be dealt with in the present paper. The main conclusions arrived at in the course of this investigation are summarized in the abstract.

II. EQUATIONS OF THE PROBLEM

As in Paper I, let u, p, and ρ denote the radial velocity, pressure, and density at any point of a compressible-gas configuration at a distance r from the center and at a time t. If, moreover, $m \equiv m(r, t)$ denotes the mass interior to r, γ the ratio of specific heats of the constituent gas, and G the gravitation constant, the Eulerian hydrodynamical equations of motion reduce to

$$\frac{\partial u}{\partial t} + u\frac{\partial u}{\partial r} + \frac{1}{\rho}\frac{\partial p}{\partial r} + \frac{Gm}{r^2} = 0\,, \tag{1}$$

[2] *Les Méthodes nouvelles de la mécanique céleste* (Paris: Gauthier-Villars et fils, 1892), 1, 82.

where now

$$\frac{\partial m}{\partial r} = 4\pi \rho r^2; \tag{2}$$

the equation of continuity can be written as

$$\frac{\partial \rho}{\partial t} + u \frac{\partial \rho}{\partial r} + \rho \left\{ \frac{\partial u}{\partial r} + \frac{2u}{r} \right\} = 0, \tag{3}$$

while the energy equation appropriate for polytropic gas assumes the form

$$\frac{\partial}{\partial t}(p\rho^{-\gamma}) + u \frac{\partial}{\partial r}(p\rho^{-\gamma}) = 0. \tag{4}$$

As in Paper I, the outer boundary conditions of our problem are given, by hypothesis, over a moving surface (the shock wave); but, since we do not postulate a priori the existence of any discrete core inside the configuration, the inner boundary conditions merely imply that the center is a point of no displacement. In what follows, let the subscript 0 again denote the undisturbed values of pressure, density, etc., in front of the shock wave (where they are functions of r alone), while the subscript 1 will denote the values of the respective quantities immediately behind the shock. If, moreover, V stands for the velocity of propagation of the shock front, the Rankine-Hugoniot shock-wave conditions

$$\frac{\rho_1}{\rho_0} = \frac{\gamma - 1 + (\gamma + 1) y}{\gamma + 1 + (\gamma - 1) y}, \tag{5}$$

$$\frac{V - u_1}{V} = \frac{\rho_0}{\rho_1}, \tag{6}$$

and

$$\rho_0 V u_1 = p_1 - p_0 = (y - 1) p_0, \tag{7}$$

where we have abbreviated $y = p_1/p_0$ expressing the continuity of energy, mass, and momentum across the shock wave, permit us to express u_1, p_1, and ρ_1 in terms of undisturbed values of these quantities by means of the equations

$$u_1 = \frac{2V}{\gamma + 1} - \frac{2\gamma p_0}{(\gamma + 1)\rho_0 V}, \tag{8}$$

$$p_1 = \frac{2\rho_0 V^2 - (\gamma - 1) p_0}{\gamma + 1}, \tag{9}$$

$$\rho_1 = \frac{(\gamma + 1)\rho_0^2 V^2}{(\gamma - 1)\rho_0 V^2 + 2\gamma p_0}. \tag{10}$$

In addition, it is easy to see that

$$m_1 = 4\pi \int_0^R \rho r^2 dr = 4\pi \int_0^R \rho_0 r^2 dr, \tag{11}$$

where $R \equiv R(t)$ denotes the radius of the shock front. Equation (6) makes it evident that, under any circumstances, the mass particles behind the shock move with velocities inferior to that of the shock itself; hence the mass interior to the shock front at any time must be equal to that contained within a sphere of radius R in the undisturbed state; none could have escaped outside.

The system of partial differential equations (1)–(4) is one of fourth order and of second

degree, in two independent variables, with initial conditions defined over a moving boundary. As in Paper I, our augmented system of equations cannot be linearized by any transformation of the variables, and any attempt to eliminate the nonlinear terms would leave us with an approximation in which the essential features of our problem would be completely lost. On the other hand, a retention of the nonlinear terms precludes the construction of an analytical solution, so that numerical integrations appear to offer the only avenue of approach. Before embarking upon them, however, we propose again to investigate, first, the conditions for which the fundamental system (1)–(4) of partial differential equations may be reducible to one of ordinary differential equations which can be solved—numerically or otherwise—with much less difficulty.

In more specific terms we propose to seek such solutions of the basic equations as will make u, p, ρ, or m depend on r and t only through the product

$$\xi = r^{\phi} t^{\psi}, \tag{12}$$

where ϕ and ψ are suitably chosen constants. Accordingly, as in Paper I, we shall assume that

$$u = \frac{r}{t} U(\xi), \tag{13}$$

$$p = r^{\kappa+2} t^{\lambda-2} P(\xi), \tag{14}$$

$$\rho = r^{\kappa} t^{\lambda} \Omega(\xi), \tag{15}$$

and likewise that the local velocity of sound,

$$C^2 = \gamma \frac{p}{\rho} = \left(\frac{r}{t}\right)^2 C^2(\xi), \tag{16}$$

where $U(\xi)$, $P(\xi)$, and $\Omega(\xi)$ are new functions defined by the foregoing relations and the parameters κ, λ, ϕ, and ψ are to be determined by physical considerations.

The first such condition is imposed by the requirement that, when the new variable ξ, as defined by equation (12), is introduced, together with equations (13)–(15), into equations (1)–(4), the exponents of the remaining powers of r and t will vanish. The reader can easily verify that this will be the case, provided that

$$\lambda + 2 - \kappa \frac{\psi}{\phi} = 0. \tag{17}$$

On the other hand, the total energy E of the configuration we are considering will be given by

$$E = 4\pi \int_a^R \left\{ \frac{1}{2} \rho u^2 + \frac{p}{\gamma - 1} - G \frac{m\rho}{r} \right\} r^2 dr, \tag{18}$$

where a denotes a radius (so far arbitrary) at which the explosion is supposed to take place.[3] Now if this explosion is to be instantaneous, the foregoing expression for E must obviously be independent of the time. Consistent with equation (12), we may write

$$R(t) = \xi_0^{1/\phi} t^{-\psi/\phi} \tag{19}$$

and

$$a(t) = \xi_1^{1/\phi} t^{-\psi/\phi}, \tag{20}$$

[3] For a justification of this assertion cf. Sec. IV of this paper.

where ξ_0 and ξ_1 are the values which our new independent variable ξ will assume at the shock front and the locus of explosion, respectively. Inserting equations (19) and (20) together with (13)–(15) into equation (18), we find that the kinetic and thermal energies carried by the wave motion will be independent of the time, provided that

$$\lambda - 2 - (\kappa + 5)\frac{\psi}{\phi} = 0, \tag{21}$$

while the gravitational energy will be time-independent if

$$2\lambda - (2\kappa + 5)\frac{\psi}{\phi} = 0. \tag{22}$$

Equations (17) and (21)–(22) constitute the conditions which bear on the determination of κ, λ, and ψ/ϕ. It is instructive to compare these conditions with the corresponding equations of Paper I. In discussing the GRM, we were dealing with a nonhomogeneous system of differential equations of third order. The nonhomogeneity of the Eulerian equation of motion at once imposed the ratio $\psi/\phi = -\frac{2}{3}$ if ξ was to replace r and t throughout as the independent variable. The required constancy of the kinetic and thermal energies with time then led to a relation between κ and λ (as represented by eq. [16] of Paper I) which automatically insured the constancy of the gravitational contribution to the total energy as well; and this left us with a (trivial) multiplicity of solutions corresponding to the same ratio of ψ/ϕ. In the present case, when dealing with a homogeneous system (1)–(4) of fourth order, our system does not, by itself, yield the value of ψ/ϕ directly but furnishes only relation (17) between the four parameters involved. In order to specify these parameters, it is again necessary to enforce the constancy of the total energy of our wave motion. The constancy of its kinetic and thermal constituents furnishes us with equation (21), which, together with equation (17), yields

$$\frac{\psi}{\phi} = -\frac{4}{5} \quad \text{and} \quad \lambda + 2 = -\frac{4}{5}\kappa. \tag{23}$$

It is noteworthy that, as in Paper I, these are precisely the values which also satisfy equation (22) and thus automatically render constant the gravitational energy of the disturbed field of flow. As in Paper I, the foregoing equations do not specify our parameters uniquely, but provide only two relations between them. These relations are obviously satisfied by

$$\kappa = 0; \quad \lambda = -2; \quad \psi = 4; \quad \text{and} \quad \phi = -5, \tag{24}$$

the values which we shall hereafter adopt. It can be easily shown that no generality has been lost by this choice; for all other combinations of the four parameters consistent with equations (23) will lead to no new solutions.[4]

Having done so, we may now proceed to rewrite our fundamental equations (1)–(4) in terms of our new independent variable $\xi = r^{-5}t^4$. If we abbreviate, for the sake of simplicity,

$$5U(\xi) - 4 = \Xi(\xi) \tag{25}$$

and

$$C^2(\xi) = S(\xi) \tag{26}$$

[4] In general, the first one of eqs. (23) permits us to assert that $\psi = 4n$ and $\phi = -5n$, where n may denote any number (positive or negative). It is, however, evident that no generality can be lost by setting $n = 1$; for any solution with $n \neq 1$ would merely correspond to the choice of a new variable $\eta = \xi^n$.

and eliminate m from equation (1) by means of equation (2) by differentiation, then after some transformation we establish that our original system (1)–(4) is equivalent to the following three simultaneous ordinary differential equations of the form

$$\frac{1}{P}\frac{dP}{d\xi}=\frac{-5\gamma\xi\Xi'+(3\gamma+2)\Xi+12(\gamma-1)}{5\xi\Xi}, \tag{27}$$

$$\frac{1}{S}\frac{dS}{d\xi}=\frac{-5(\gamma-1)\xi\Xi'+(3\gamma-1)\Xi+12\gamma-14}{5\xi\Xi}, \tag{28}$$

and

$$\frac{d^2\Xi}{d\xi^2}=\{\xi^2\Xi(25\gamma S-\gamma\Xi^2)\}^{-1}\Big\{5\xi\Xi^2\frac{P'}{P}(2S+5\xi S')+4\pi G\gamma^2\Xi^2\frac{P}{S}$$

$$-\Xi^2[10\xi S'+(15\gamma+4)S]+5S[5\gamma\xi^2\Xi'^2-12(\gamma-1)\xi\Xi'-12(\gamma-1)\Xi] \tag{29}$$

$$+\gamma\frac{\Xi^2}{5}[5\xi^2\Xi'^2-3\xi\Xi'+\tfrac{3}{5}(\Xi+4)(\Xi-1)]\Big\},$$

where primes denote differentiation with respect to ξ and where, consistent with equations (16) and (26),

$$S(\xi)=\gamma\frac{P(\xi)}{\Omega(\xi)}. \tag{30}$$

These are the equations governing the propagation of blast waves of the progressing type in the configurations which we are considering.

III. SOLUTION OF THE EQUATIONS

Having reduced the differential equations of our problem to tractable forms, it remains for us to specify the initial conditions which determine the nature of their solution. Consider, first, the boundary conditions at the shock front. On the passage through the shock, the velocity, pressure, and density are known to undergo discontinuous changes expressed by equations (8)–(10), where, consistent with the assumptions of the preceding section,

$$V=\frac{dR}{dt}=\frac{4}{5}\frac{R}{t}. \tag{31}$$

Moreover, if the values of u_1, p_1, and ρ_1 immediately behind the shock wave, as given by equations (8)–(10), are to be consistent with equations (13)–(15) in which we have set $\xi=\xi_0$ and inserted from equation (24), it follows that p_0 and ρ_0 in equations (8)–(10) cannot be arbitrary functions of r but must be such as to render both sides of the equations dimensionally correct at all times. This is found to be true if, in front of the shock wave,

$$\rho_0=\beta r^{-5/2}, \tag{32}$$

which, by equation (2), leads to

$$m_0=4\pi\int_0^r\rho_0 r^2dr=8\pi\beta\sqrt{r}, \tag{33}$$

and if, consistent with the equation (1) in the state of equilibrium,

$$p_0=\frac{8\pi\beta^2G}{3r^8}, \tag{34}$$

where β is an arbitrary constant.[5] The equilibrium structure of our configuration is thus specified by a polytropic equation of state,

$$p_0 = K\rho_0^{6/5}, \tag{35}$$

where

$$K = \tfrac{6}{5}\pi G\beta^{4/5}. \tag{36}$$

The radius of our configuration is thus infinite, and so is its total mass. These facts do not, however, give rise to any complications in this connection; in point of fact, the infiniteness of the radius will absolve us from having to consider the reflection of a shock wave from a finite spherical boundary.

Let us now proceed to insert the foregoing equations (32) and (34) into equations (8)–(10). If, furthermore, we replace in the latter the values of u_1, p_1, and ρ_1 by expressions (13)–(15), which are supposed to hold good from the shock inward, we find that, immediately behind the shock front, when $\xi = \xi_0$,

$$U(\xi_0) = \frac{8(1-x)}{5(\gamma+1)}, \tag{37}$$

$$P(\xi_0) = \frac{16\beta(\gamma-1)\xi_0^{1/2}}{25\gamma(\gamma+1)}\left\{\frac{2\gamma}{\gamma-1} - x\right\}, \tag{38}$$

$$\Omega(\xi_0) = \frac{(\gamma+1)\beta\xi_0^{1/2}}{\gamma-1+2x}, \tag{39}$$

and, therefore,

$$S(\xi_0) = \frac{16(\gamma-1+2x)[2\gamma-(\gamma-1)x]}{25(\gamma+1)^2}, \tag{40}$$

where we have abbreviated

$$x = \tfrac{25}{6}\pi\beta G\gamma\xi_0^{1/2}. \tag{41}$$

The fundamental system of differential equations (27)–(29) is one of fourth order; therefore, in order to be able to integrate it from the shock inward, one more initial condition at $\xi = \xi_0$ remains yet to be ascertained. This remaining boundary condition should be the value of $\Xi'(\xi_0)$ or—which is the same thing—of $U'(\xi_0)$, where primes denote differentiation with respect to ξ. It can be evaluated from the initial differential equations (1), (3), and (4), rewritten in terms of ξ in place of r and t, in which we set $\xi = \xi_0$ and, by virtue of equations (11), (19), and (32),

$$m(R) = 8\pi\beta\sqrt{R(t)} = 8\pi\beta\xi_0^{-1/10}t^{2/5}. \tag{42}$$

These equations assume the explicit form

$$(4-5U)\Omega\xi_0U' - 5\xi_0P' = U(1-U)\Omega - 2P - 8\pi\beta G\xi_0^{1/2}\Omega, \tag{43}$$

$$5\xi_0\Omega U' - (4-5U)\xi_0\Omega' = (3U-2)\Omega, \tag{44}$$

$$(4-5U)\xi_0\Omega P' - \gamma(4-5U)\xi_0P\Omega' = 2(2-\gamma-U)P\Omega. \tag{45}$$

[5] The law of density (and pressure) in the form in which we take it leads to an infinite density (and pressure) at the center. This singularity presents us, however, with a mathematical, rather than a physical, difficulty; for we may imagine that the law (32) holds only to a very small distance from the center, within which the density remains finite. This avoids the physical difficulty, without appreciably altering either the mass within any significant radius or the values of the gravity and pressure.

If, in these equations, we insert values for U, P, and Ω from equations (37)–(39), we can solve the foregoing simultaneous system for U', P', and Ω', any one of which is sufficient to complete the requisite number of initial conditions of our problem. The reader should notice that, unlike in Paper I, the pressure P occurs in equation (29) not only through its logarithmic derivative but also explicitly. It follows, therefore, that the requisite solutions of the system (27)–(29) will also depend, apart from γ, x, and ξ_0, on the absolute value of β. Of these four, a choice of ξ_0 determines the position of the shock at a given time t_0 and depends, therefore, on our choice of the units of length and time. In what follows, we shall, for simplicity's sake, set $\xi_0 = 1$, a convention which obviously entails no loss of generality. The ratio γ of specific heats depends, in turn, on the properties and composition of the gas constituting our configuration; so that, once a fixed value of γ has been adopted, either one of the constants x or β, related by equation (41), remains as the only arbitrary nondimensional parameter characterizing our solutions. It is easy to show that, as in Paper I, the parameter x is again intimately related with the strength (i.e., the Mach number M) of the respective shock wave. Let us define, as usual,

$$M = \frac{V}{c_0}, \tag{46}$$

where c_0 denotes the Laplacean velocity of sound in the undisturbed medium in front of the shock wave. Now, in our present case, V is given by equation (31), while

$$c_0^2 = \gamma \frac{p_0}{\rho_0} = \frac{8\pi\beta\gamma G}{3\sqrt{r}} \tag{47}$$

by equations (32) and (34). Hence, it transpires immediately that

$$M^2 = \frac{1}{x}, \tag{48}$$

which discloses that, if the expanding regime we are considering is to possess a shock wave on its head, we must have

$$0 \leqslant x < 1\,, \tag{49}$$

the strength of the shock being greater, the smaller the value of x.

Suppose, now, that a proper value of x has been chosen and an integration of equations (27)–(29) started from the initial conditions as represented by equations (37), (38), (40), and (43)–(45) from $\xi_0 = 1$ in the direction of increasing ξ, which, for fixed t, corresponds to an inward march toward the center, where $\xi = \infty$. Such integrations can be continued until, for each value of x, a point $\xi = \xi_1$ has been reached at which $\Xi(\xi_1)$ vanishes. The place at which $\Xi(\xi_1) = 0$ again turns out to be a singular point of our solution; and our equations readily disclose what happens at this point. The mass $m(\xi)$ contained within a shell between two concentric spheres of radii ξ_0 and ξ at time t is obviously given by

$$m(\xi, t) = \frac{4\pi}{3} t^{2/5} M(\xi)\,, \qquad \text{where} \qquad M(\xi) = \frac{3}{5}\int_{\xi_0}^{\xi} \gamma \frac{P}{c^2}\, \xi^{-8/5} d\xi$$

$$= \frac{3}{5}\int_{\xi_0}^{\xi} \Omega(\xi)\, \xi^{-8/5} d\xi \tag{50}$$

and can be integrated simultaneously with the solution of our fundamental system (27)–(29). When we arrive at a point $\xi = \xi_1$ at which $\Xi(\xi_1) = 0$, we find that the mass $m(\xi_1)$, as defined by the above equation (50), becomes numerically equal to the mass

$m(R)$ of the whole configuration inside the shock wave of radius R, which has already been expressed by equation (42). In order to describe the situation in terms of physical language, we may say that, by having produced a requisite condensation behind the postulated shock wave, we have depleted the available supply of mass in the interior of our model to such an extent that none is left near the center, all mass interior to (ξ_1) being swept clean and driven outward by the initial explosion at time $t = 0$.

By having assumed the initial explosion to be instantaneous, we have, moreover, compelled the sphere characterized by the radius ξ_1 to become a surface of contact discontinuity (i.e., one across which there is no flow of mass or energy for $t > 0$). The pressure must be continuous across this surface, and its gradient must therefore remain finite; since, moreover, there is no mass inside ξ_1, the pressure must be zero at either side of the interface. Accordingly, the logarithmic derivative P'/P should become infinite at $\Xi = 0$, as it indeed does in accordance with equation (27). Numerical integrations of the system (27)–(29) disclose, however, that the ratio $S = \gamma P/\Omega$ vanishes as $\xi \to \xi_1$; hence P must approach zero faster than Ω and, if P' is to be (by definition of a contact discontinuity) finite at $\xi = \xi_1$, $\Omega'(\xi_1)$ must become infinite. Therefore, we meet essentially the same situation as in the problem of a GRM of Paper I. In either case the density derivative is infinite at $\xi = \xi_1$. In the case of the Roche model, this singularity marked the boundary of the inner core whose mass was assumed to be infinite in comparison with the mass of its envelope. The actual distribution of this mass within the core is wholly irrelevant; as long as spherical symmetry is preserved, its gravitational attraction will be the same if it is distributed uniformly through the volume or confined to an infinitesimally thin hollow shell. The fact that the mass within this shell should be infinite in comparison with that of the surrounding envelope discloses that, in the case of a generalized Roche model, the singularity in the density distribution at $\xi = \xi_1$ is a nonintegrable one—in contrast to the present problem, which is characterized by an integrable density distribution for $\xi \leqslant \xi_1$.

The reader may notice that, as long as ξ_1 remains finite,[6] there exists one possibility for the logarithmic derivatives P'/P or Ω'/Ω to assume finite values (or possibly even to vanish) at $\xi = \xi_1$. Of the density derivative this will be true if

$$\Xi'(\xi) \to \frac{12(\gamma-1)}{5\gamma\xi}, \tag{51}$$

as $\xi \to \xi_1$ in such a way that

$$\lim_{\xi \to \xi_1} \left\{ \Xi'(\xi) - \frac{12(\gamma-1)}{5\gamma\xi} \right\} = B\Xi^n(\xi), \tag{52}$$

where $n \geqslant 1$ and B is an arbitrary constant. If, in particular, $n = 1$ and $B = (2 + 3\gamma)/5\xi_1$, it is evident that

$$\lim_{\xi \to \xi_1} \frac{P'}{P} = 0. \tag{53}$$

The logarithmic derivative of Ω will, in turn, remain finite at $\xi = \xi_1$ if, as $\xi \to \xi_1$,

$$\Xi'(\xi) \to \frac{2}{5\xi} \tag{54}$$

in such a way that

$$\lim_{\xi \to \xi_1} \left\{ \Xi'(\xi) - \frac{2}{5\xi} \right\} = D\Xi^n(\xi), \tag{55}$$

[6] It will be shown below that $\xi_1 = \infty$ only if $\gamma = \frac{4}{3}$.

where $n \geqslant 1$ and D is a constant; if, in particular, $n = 1$ and $D = (3\gamma - 1)/5\xi_1$, we again find that

$$\lim_{\xi \to \xi_1} \frac{\Omega'}{\Omega} = 0 . \tag{56}$$

The reader may observe that equations (51) and (54) are compatible only if $\gamma = 1.2$;[7] for any other value of γ, only one of these relations can be satisfied.

It is easy to show by the same argument invoked in Paper I that, for $\gamma \neq \frac{4}{3}$, the value of ξ for which $\Xi(\xi)$ vanishes is always finite. Consider the total energy of the configuration in its undisturbed state inclosed between the surfaces of radii R and a; it is given by

$$\begin{aligned} H &= 4\pi \int_a^R \left\{ \frac{1}{\gamma - 1} \frac{p_0}{\rho_0} - \frac{G m_0}{r} \right\} \rho_0 r^2 dr \\ &= \frac{32\,(4 - 3\gamma)}{3\,(\gamma - 1)} \pi^2 G \beta^2 \log \frac{R}{a} \end{aligned} \tag{57}$$

by virtue of equations (32)–(34). For $\gamma \neq \frac{4}{3}$, this latter expression evidently remains finite only if $a > 0$, i.e., if the density distribution (32) in the undisturbed state breaks down at a finite distance from the center. The distance at which this occurs corresponds to the singular point ξ_1 of our solution. Since this singular point again specifies the location of a contact discontinuity across which there is no flow of matter or heat, the regimes at either side of the discontinuity do not communicate and can be investigated separately. For our present purpose the actual structure of the inner core between $0 \leqslant r \leqslant a$ is wholly irrelevant—except that its mass and energy contents should be negligible in comparison with those outside in the concentric shell between $a < r < R$. It is this requirement which distinguishes our present problem from that discussed in Paper I, where the converse assumption was made.

If we now revert from r to ξ, equations (19) and (20) disclose that $R/a = (\xi_1/\xi_0)^{1/5}$. With the value of this ratio determined from a solution of the system (27)–(29) for any particular value of x, equation (57) can be used to determine the absolute value of our arbitrary constant β if the total energy H of our configuration in its equilibrium state is known—or, conversely, to determine H from a given value of β.

IV. NUMERICAL INTEGRATIONS

Equations (27)–(29) as they stand are too involved to admit of an analytical solution; so that, in order to investigate the properties of an expanding gas flow governed by such equations, recourse must be had to numerical integration. We have performed, altogether, eight such integrations, corresponding to $\gamma = \frac{5}{3}$ (monatomic gas) and Mach numbers M ranging from $M^2 = 5$ to $M^2 = \infty$. The outcome of the integrations is presented in Table 1, the successive columns of which are self-explanatory. Each solution is given from $\xi_0 = 1$ (corresponding to the assumed position of the shock wave) to ξ_1, where the inner contact discontinuity sets in. Table 2 summarizes the characteristic properties of the medium immediately behind the shock wave, for various values of the strength of the shock. As many decimals are retained in both tables as are considered significant. The normalized values of the successive variables permit the evaluation of the actual absolute properties of the respective expanding regime of gas flow by choosing the appropriate absolute values of β and ξ_0. Figures 1, 2, and 3 give the profiles of the velocity, pressure, and density, respectively, at a given time $t = 1$, extending from the shock wave ($r = 1$) inward to the core. In this manner, these figures can be regarded as instantaneous

[7] I.e. (cf. Sec. IV), if the medium in front of the shock wave is isentropic.

TABLE I

Physical Properties of the Expanding Field of Flow behind Shock Waves of different Strength

ξ	U	C	P/β	Ω/β	M	$\left(\frac{P}{\beta\sqrt{2}}\right)^{\gamma}\left(\frac{\Omega}{\beta\sqrt{2}}\right)^{-\gamma}$	F
		$\gamma = \frac{5}{3}$			$M^2 = 3$		
1.00	0.4000	0.6110	0.4480	2.0000	0.0000	0.1411	0.0000
1.02	0.3994	0.6119	0.4523	2.0139	0.0237	0.1419	0.0065
1.04	0.3988	0.6128	0.4565	2.0258	0.0468	0.1426	0.0130
1.06	0.3983	0.6137	0.4607	2.0398	0.0694	0.1435	0.0171
1.08	0.3978	0.6146	0.4649	2.0512	0.0914	0.1440	0.0215
1.10	0.3973	0.6155	0.4691	2.0637	0.1129	0.1448	0.0265
1.12	0.3968	0.6164	0.4733	2.0761	0.1339	0.1455	0.0290
1.14	0.3963	0.6173	0.4776	2.0885	0.1545	0.1462	0.0320
1.16	0.3958	0.6182	0.4817	2.1008	0.1746	0.1469	0.0346
1.16	0.3958	0.6182	0.4817	2.1008	0.1746	0.1469	0.0346
1.20	0.3950	0.6199	0.4900	2.1252	0.2135	0.1482	0.0386
1.24	0.3942	0.6216	0.4982	2.1492	0.2508	0.1495	0.0412
1.28	0.3934	0.6233	0.5065	2.1733	0.2867	0.1508	0.0436
1.32	0.3927	0.6249	0.5147	2.1963	0.3211	0.1521	0.0429
1.36	0.3921	0.6265	0.5228	2.2195	0.3543	0.1534	0.0423
1.40	0.3915	0.6282	0.5310	2.2424	0.3863	0.1546	0.0408
1.44	0.3910	0.6298	0.5391	2.2651	0.4171	0.1558	0.0384
1.48	0.3906	0.6314	0.5472	2.2878	0.4470	0.1570	0.0367
1.52	0.3900	0.6330	0.5553	2.3098	0.4758	0.1582	0.0325
1.56	0.3896	0.6345	0.5633	2.3318	0.5037	0.1595	0.0293
1.60	0.3892	0.6361	0.5714	2.3537	0.5308	0.1604	0.0239
1.64	0.3889	0.6376	0.5794	2.3754	0.5570	0.1616	0.0190
1.68	0.3886	0.6391	0.5874	2.3969	0.5824	0.1627	0.0139
1.72	0.3883	0.6406	0.5954	2.4182	0.6072	0.1637	0.0083
1.76	0.3880	0.6420	0.6033	2.4394	0.6312	0.1648	0.0026
1.80	0.3878	0.6435	0.6113	2.4604	0.6546	0.1658	-0.0035
1.8	0.3878	0.6435	0.6113	2.4604	0.6546	0.1658	-0.0035
1.9	0.3873	0.6471	0.6311	2.5122	0.7105	0.1683	-0.0194
2.0	0.3870	0.6506	0.6508	2.5631	0.7627	0.1708	-0.0364
2.1	0.3868	0.6539	0.6705	2.6132	0.8119	0.1732	-0.0542
2.2	0.3866	0.6572	0.6901	2.6627	0.8584	0.1755	-0.0725
2.3	0.3868	0.6604	0.7096	2.7114	0.9025	0.1777	-0.0911
2.4	0.3869	0.6636	0.7291	2.7595	0.9443	0.1798	-0.1099
2.5	0.3871	0.6667	0.7485	2.8069	0.9842	0.1819	-0.1289
2.6	0.3874	0.6697	0.7679	2.8539	1.0221	0.1839	-0.1479
2.7	0.3877	0.6726	0.7872	2.9001	1.0584	0.1859	-0.1669
2.8	0.3881	0.6755	0.8065	2.9459	1.0932	0.1878	-0.1859
2.9	0.3885	0.6783	0.8258	2.9912	1.1265	0.1896	-0.2047
3.0	0.3890	0.6811	0.8450	3.0363	1.1586	0.1914	-0.2234
3.1	0.3895	0.6838	0.8642	3.0809	1.1894	0.1932	-0.2419
3.2	0.3900	0.6864	0.8833	3.1247	1.2191	0.1949	-0.2602
3.3	0.3908	0.6890	0.9024	3.1684	1.2477	0.1966	-0.2784
3.4	0.3912	0.6915	0.9215	3.2116	1.2754	0.1983	-0.2963
3.5	0.3918	0.6940	0.9405	3.2545	1.3021	0.1998	-0.3140
3.6	0.3925	0.6965	0.9596	3.2970	1.3280	0.2014	-0.3315
3.7	0.3932	0.6989	0.9786	3.3392	1.3531	0.2029	-0.3488
3.8	0.3939	0.7012	0.9975	3.3810	1.3774	0.2044	-0.3659
3.9	0.3946	0.7035	1.0164	3.4226	1.4010	0.2058	-0.3827
4.0	0.3953	0.7058	1.0354	3.4639	1.4240	0.2072	-0.3993
4.1	0.3961	0.7081	1.0542	3.5048	1.4463	0.2086	-0.4157
4.2	0.3968	0.7102	1.0731	3.5455	1.4680	0.2100	-0.4319
4.3	0.3976	0.7124	1.0919	3.5859	1.4891	0.2114	-0.4478
4.4	0.3983	0.7145	1.1107	3.6260	1.5097	0.2127	-0.4635
4.5	0.3991	0.7166	1.1295	3.6658	1.5296	0.2140	-0.4791
4.6	0.3999	0.7187	1.1483	3.7054	1.5494	0.2152	-0.4944
4.7	0.4007	0.7207	1.1670	3.7448	1.5686	0.2165	-0.5095
4.8	0.4015	0.7227	1.1857	3.7840	1.5872	0.2177	-0.5244
4.9	0.4023	0.7246	1.2044	3.8229	1.6054	0.2189	-0.5392
5.0	0.4031	0.7266	1.2231	3.8616	1.6232	0.2200	-0.5537
5.1	0.4039	0.7286	1.2418	3.9001	1.6407	0.2212	-0.5680
5.2	0.4047	0.7305	1.2604	3.9384	1.6578	0.2223	-0.5822
5.3	0.4055	0.7323	1.2790	3.9766	1.6745	0.2234	-0.5961
5.4	0.4063	0.7340	1.2976	4.0145	1.6909	0.2245	-0.6099
5.5	0.4072	0.7358	1.3162	4.0522	1.7069	0.2256	-0.6236
5.6	0.4080	0.7376	1.3348	4.0897	1.7227	0.2266	-0.6370
5.7	0.4088	0.7393	1.3533	4.1270	1.7381	0.2277	-0.6503
5.8	0.4096	0.7410	1.3719	4.1642	1.7533	0.2287	-0.6634
5.9	0.4104	0.7427	1.3904	4.2012	1.7681	0.2297	-0.6764
6.0	0.4113	0.7444	1.4089	4.2380	1.7827	0.2307	-0.6892
6.0	0.4113	0.7444	1.4089	4.2380	1.7827	0.2307	-0.6892
6.2	0.4129	0.7476	1.4459	4.3112	1.8111	0.2326	-0.7143
6.4	0.4145	0.7508	1.4828	4.3829	1.8386	0.2344	-0.7389
6.6	0.4162	0.7539	1.5196	4.4559	1.8651	0.2362	-0.7629
6.8	0.4178	0.7569	1.5564	4.5274	1.8908	0.2380	-0.7864
7.0	0.4194	0.7599	1.5931	4.5984	1.9157	0.2397	-0.8094
7.2	0.4210	0.7628	1.6298	4.6686	1.9399	0.2413	-0.8319
7.4	0.4226	0.7656	1.6665	4.7388	1.9634	0.2429	-0.8539
7.6	0.4242	0.7683	1.7031	4.8084	1.9862	0.2444	-0.8755
7.8	0.4258	0.7710	1.7396	4.8775	2.0083	0.2459	-0.8966
8.0	0.4274	0.7736	1.7761	4.9461	2.0299	0.2474	-0.9173
8.0	0.4274	0.7736	1.7761	4.9461	2.0299	0.2474	-0.9173
8.4	0.4305	0.7787	1.8490	5.0822	2.0715	0.2502	-0.9578
8.8	0.4335	0.7835	1.9217	5.2168	2.1110	0.2528	-0.9963
9.2	0.4366	0.7882	1.9943	5.3500	2.1487	0.2553	-1.0327
9.6	0.4396	0.7927	2.0667	5.4820	2.1847	0.2577	-1.0672
10.0	0.4425	0.7970	2.1391	5.6128	2.2193	0.2600	-1.1047
10.4	0.4454	0.8011	2.2112	5.7425	2.2525	0.2621	-1.1298
10.8	0.4482	0.8051	2.2833	5.8710	2.2844	0.2642	-1.1713
11.2	0.4510	0.8090	2.3553	5.9986	2.3151	0.2661	-1.2031
11.6	0.4538	0.8127	2.4272	6.1250	2.3447	0.2680	-1.2340
12.0	0.4565	0.8163	2.4990	6.2507	2.3734	0.2697	-1.2639
12.4	0.4592	0.8197	2.5707	6.3759	2.4011	0.2714	-1.2931
12.8	0.4618	0.8231	2.6423	6.5004	2.4279	0.2730	-1.3215
13.2	0.4644	0.8263	2.7138	6.6243	2.4539	0.2745	-1.3492
13.6	0.4670	0.8294	2.7853	6.7476	2.4791	0.2759	-1.3762
14.0	0.4695	0.8325	2.8567	6.8701	2.5037	0.2773	-1.4025

ξ	U	C	P/β	Ω/β	M	$\left(\frac{P}{\beta\sqrt{2}}\right)^{\gamma}\left(\frac{\Omega}{\beta\sqrt{2}}\right)^{-\gamma}$	F
		$\gamma = \frac{5}{3}$			$M^2 = 3$		
14.4	0.4720	0.8354	2.9280	6.9923	2.5276	0.2786	-1.4282
14.8	0.4745	0.8383	2.9993	7.1139	2.5507	0.2798	-1.4533
15.2	0.4769	0.8410	3.0706	7.2350	2.5733	0.2810	-1.4779
15.6	0.4793	0.8437	3.1417	7.3556	2.5954	0.2821	-1.5019
16.0	0.4816	0.8463	3.2129	7.4762	2.6169	0.2832	-1.5254
16.0	0.4816	0.8463	3.2129	7.476	2.6169	0.2832	-1.5254
17.2	0.4886	0.8536	3.4260	7.836	2.6784	0.2861	-1.5930
18.4	0.4951	0.8604	3.6368	8.192	2.7360	0.2886	-1.6548
19.6	0.5015	0.8668	3.8513	8.547	2.7902	0.2906	-1.7178
20.8	0.5077	0.8728	4.0638	8.900	2.8415	0.2924	-1.7746
22.0	0.5137	0.8778	4.2767	9.249	2.8902	0.2940	-1.8293
22.0	0.5137	0.8778	4.2767	9.249	2.8902	0.2940	-1.8293
24.4	0.5251	0.8872	4.6995	9.951	2.9805	0.2961	-1.9314
26.8	0.5359	0.8952	5.1220	10.654	3.0635	0.2972	-2.0252
29.2	0.5459	0.9021	5.5466	11.361	3.1401	0.2976	-2.1122
31.6	0.5554	0.9080	5.9708	12.071	3.2117	0.2972	-2.1955
34.0	0.5646	0.9129	6.3942	12.789	3.2790	0.2962	-2.2699
36.4	0.5735	0.9170	6.8187	13.516	3.3426	0.2947	-2.3417
38.8	0.5819	0.9205	7.2427	14.254	3.4029	0.2927	-2.4100
41.2	0.5900	0.9230	7.6665	15.003	3.4605	0.2902	-2.4749
43.6	0.5978	0.9251	8.0910	15.767	3.5157	0.2873	-2.5367
46.0	0.6052	0.9266	8.5154	16.547	3.5688	0.2842	-2.5958
48.4	0.6125	0.9275	8.9518	17.345	3.6200	0.2807	-2.6524
50.8	0.6195	0.9279	9.3812	18.160	3.6696	0.2769	-2.7069
53.2	0.6262	0.9278	9.8115	18.995	3.7176	0.2729	-2.7598
55.6	0.6328	0.9273	10.245	19.853	3.7643	0.2686	-2.8103
58.0	0.6391	0.9265	10.676	20.737	3.8097	0.2640	-2.8594
60.4	0.6453	0.9249	11.109	21.648	3.8541	0.2592	-2.9069
62.8	0.6513	0.9230	11.546	22.587	3.8977	0.2543	-2.9530
65.2	0.6572	0.9207	11.986	23.558	3.9406	0.2491	-2.9978
67.6	0.6629	0.9180	12.421	24.567	3.9827	0.2437	-3.0414
70.0	0.6685	0.9149	12.862	25.610	4.0242	0.2382	-3.0839
72.4	0.6739	0.9114	13.304	26.695	4.0652	0.2325	-3.1253
74.8	0.6792	0.9076	13.747	27.822	4.1058	0.2267	-3.1657
77.2	0.6844	0.9031	14.192	29.002	4.1458	0.2207	-3.2052
79.6	0.6895	0.8983	14.639	30.233	4.1856	0.2146	-3.2438
82.0	0.6945	0.8931	15.088	31.523	4.2251	0.2084	-3.2816
82.0	0.6945	0.8931	15.088	31.523	4.2251	0.2084	-3.2816
86.8	0.7041	0.8815	15.993	34.305	4.3035	0.1956	-3.3550
91.6	0.7133	0.8690	16.907	37.392	4.3818	0.1822	-3.4256
96.4	0.7222	0.8555	17.830	40.861	4.4603	0.1685	-3.4942
101.2	0.7308	0.8347	18.761	44.873	4.5397	0.1543	-3.5604
106.0	0.7391	0.8144	19.700	49.505	4.6205	0.1397	-3.6250
110.8	0.7471	0.7913	20.645	55.010	4.7043	0.1247	-3.6861
115.6	0.7549	0.7646	21.595	61.660	4.7912	0.1094	-3.7498
120.4	0.7624	0.7356	22.625	70.056	4.8827	0.0938	-3.8100
125.2	0.7695	0.6970	23.654	81.023	4.9811	0.0778	-3.8699
130.0	0.7767	0.6525	24.666	96.555	5.0898	0.0615	-3.9292
134.8	0.7836	0.5961	25.730	120.697	5.2142	0.0448	-3.9816
139.6	0.7902	0.5178	26.832	166.800	5.3682	0.0276	-4.0334
144.4	0.7967	0.3738	27.962	334.194	5.6079	0.0097	-4.0704
146.92	0.8000						
		$\gamma = \frac{5}{3}$			$M^2 = 10$		
1.00	0.5400	0.5048	0.4704	3.0770	0.0000	0.0723	0.0000
1.02	0.5402	0.5044	0.4727	3.0976	0.0366	0.0723	0.2726
1.04	0.5405	0.5039	0.4750	3.1179	0.0720	0.0723	0.5355
1.06	0.5407	0.5034	0.4772	3.1383	0.1068	0.0723	0.7893
1.08	0.5410	0.5030	0.4796	3.1586	0.1407	0.0723	1.0344
1.10	0.5412	0.5025	0.4817	3.1787	0.1738	0.0724	1.2713
1.12	0.5415	0.5022	0.4839	3.1985	0.2062	0.0724	1.5004
1.14	0.5417	0.5017	0.4861	3.2181	0.2378	0.0724	1.7221
1.16	0.5420	0.5013	0.4882	3.2376	0.2688	0.0724	1.9367
1.18	0.5422	0.5008	0.4904	3.2569	0.2991	0.0724	2.1448
1.20	0.5425	0.5006	0.4925	3.2760	0.3288	0.0724	2.3461
1.22	0.5428	0.5002	0.4946	3.2951	0.3579	0.0724	2.5415
1.24	0.5430	0.4998	0.4967	3.3140	0.3865	0.0724	2.7311
1.26	0.5433	0.4994	0.4988	3.3327	0.4142	0.0725	2.9152
1.28	0.5436	0.4991	0.5008	3.3513	0.4416	0.0724	3.0941
1.30	0.5438	0.4987	0.5029	3.3697	0.4684	0.0725	3.2678
1.3	0.5439	0.4987	0.5029	3.3697	0.4684	0.0725	3.268
1.4	0.5452	0.4970	0.5139	3.4604	0.5983	0.0725	4.068
1.5	0.5466	0.4955	0.5257	3.5484	0.7114	0.0725	4.770
1.6	0.5480	0.4940	0.5382	3.6342	0.8184	0.0725	5.392
1.7	0.5494	0.4926	0.5414	3.7181	0.9174	0.0724	5.947
1.8	0.5508	0.4913	0.5504	3.8003	1.0098	0.0723	6.448
1.9	0.5523	0.4900	0.5598	3.8809	1.0957	0.0723	6.907
2.0	0.5538	0.4889	0.5679	3.9600	1.1765	0.0722	7.307
2.1	0.5553	0.4878	0.5764	4.0378	1.2526	0.0721	7.662
2.2	0.5568	0.4867	0.5848	4.1145	1.3245	0.0720	8.027
2.3	0.5584	0.4857	0.5931	4.1903	1.3926	0.0719	8.345
2.4	0.5599	0.4847	0.6012	4.2656	1.4573	0.0717	8.640
2.4	0.5599	0.4847	0.6012	4.2656	1.4573	0.0717	8.640
2.6	0.5630	0.4828	0.6171	4.4132	1.5776	0.0715	9.169
2.8	0.5660	0.4810	0.6327	4.5586	1.6875	0.0712	9.631
3.0	0.5691	0.4793	0.6479	4.7018	1.7887	0.0708	10.039
3.2	0.5722	0.4778	0.6628	4.8436	1.8834	0.0704	10.405
3.4	0.5753	0.4760	0.6774	4.9843	1.9728	0.0700	10.731
3.6	0.5784	0.4744	0.6918	5.1237	2.0575	0.0696	11.028
3.8	0.5814	0.4729	0.7060	5.2624	2.1384	0.0692	11.299

TABLE I

Physical Properties of the Expanding Field of Flow behind Shock Waves of different Strength

ξ	U	C	P/β	Ω/β	M	$\left(\frac{P}{\beta\sqrt{\xi}}\right)\left(\frac{\Omega}{\beta\sqrt{\xi}}\right)^{\gamma}$	F
			$\gamma = 5/3$		$M^2 = 10$		
4.0	0.5845	0.4714	0.7200	5.4005	2.2222	0.0698	11.548
4.2	0.5675	0.4699	0.7339	5.5363	2.2868	0.0663	11.777
4.4	0.5906	0.4685	0.7474	5.6719	2.3348	0.0678	11.999
4.6	0.5825	0.4671	0.7608	5.8134	2.3970	0.0673	12.196
4.8	0.5945	0.4657	0.7741	5.9510	2.4563	0.0668	12.370
5.0	0.5994	0.4642	0.7872	6.0869	2.5131	0.0663	12.543
5.2	0.6024	0.4629	0.8002	6.2270	2.5676	0.0656	12.706
5.2	0.6024	0.4629	0.8002	6.227	2.5676	0.0656	12.706
5.4	0.6061	0.4600	0.8256	6.505	2.6706	0.0647	13.005
6.0	0.6138	0.4571	0.8506	6.786	2.7964	0.0626	13.270
6.4	0.6194	0.4543	0.8754	7.070	2.8562	0.0624	13.513
6.8	0.6249	0.4514	0.8998	7.356	2.9407	0.0612	13.726
7.2	0.6305	0.4485	0.9234	7.652	3.0208	0.0600	13.940
7.6	0.6356	0.4455	0.9467	7.950	3.0970	0.0588	14.131
8.0	0.6409	0.4425	0.9696	8.256	3.1696	0.0576	14.309
8.4	0.6459	0.4394	0.9923	8.566	3.2393	0.0563	14.476
8.8	0.6509	0.4363	1.0145	8.884	3.3062	0.0550	14.633
9.2	0.6558	0.4331	1.0365	9.211	3.3708	0.0537	14.782
9.6	0.6607	0.4298	1.0581	9.547	3.4332	0.0523	14.924
10.0	0.6655	0.4264	1.0794	9.892	3.4936	0.0510	15.060
10.4	0.6702	0.4230	1.1003	10.248	3.5526	0.0497	15.190
10.8	0.6748	0.4195	1.1208	10.616	3.6099	0.0483	15.315
11.2	0.6794	0.4159	1.1412	10.997	3.6659	0.0470	15.434
11.6	0.6839	0.4122	1.1614	11.392	3.7205	0.0456	15.548
12.0	0.6883	0.4084	1.1811	11.802	3.7741	0.0442	15.657
12.0	0.6883	0.4084	1.1811	11.80	3.7741	0.0442	15.657
12.8	0.6969	0.4005	1.2197	12.67	3.8787	0.0414	15.866
13.6	0.7053	0.3922	1.2570	13.62	3.9803	0.0386	16.066
14.4	0.7135	0.3834	1.2931	14.66	4.0797	0.0358	16.259
15.2	0.7215	0.3740	1.3279	15.83	4.1778	0.0330	16.457
16.0	0.7293	0.3638	1.3612	17.14	4.2753	0.0301	16.663
16.8	0.7369	0.3530	1.3931	18.64	4.3729	0.0272	16.889
17.6	0.7441	0.3412	1.4233	20.38	4.4716	0.0244	17.096
18.4	0.7513	0.3284	1.4517	22.44	4.5722	0.0215	17.297
19.2	0.7583	0.3142	1.4779	24.96	4.6760	0.0186	17.496
20.0	0.7652	0.2983	1.5014	28.15	4.7847	0.0157	17.715
20.0	0.7652	0.2983	1.5014	28.13	4.7847	0.0157	17.715
20.4	0.7686	0.2895	1.5120	30.07	4.8417	0.0142	17.831
20.8	0.7720	0.2801	1.5216	32.25	4.9008	0.0128	17.952
21.2	0.7753	0.2699	1.5301	35.02	4.9627	0.0113	18.079
21.6	0.7786	0.2586	1.5372	38.30	5.0280	0.0098	18.214
22.0	0.7819	0.2460	1.5426	42.40	5.0973	0.0084	18.360
22.4	0.7851	0.2322	1.5461	47.61	5.1735	0.0069	18.519
22.4	0.7851	0.2322	1.5461	47.61	5.1735	0.0069	18.52
22.8	0.7867	0.2243	1.5470	51.22	5.2143	0.0062	18.61
23.2	0.7883	0.2158	1.5472	55.34	5.2575	0.0055	18.70
23.6	0.7899	0.2065	1.5469	60.41	5.3037	0.0047	18.80
23.2	0.7915	0.1961	1.5435	66.86	5.3539	0.0040	18.91
23.4	0.7931	0.1843	1.5390	75.48	5.4091	0.0033	19.03
23.6	0.7946	0.1705	1.5325	87.66	5.4716	0.0025	19.17
23.8	0.7962	0.1535	1.5219	107.65	5.5452	0.0018	19.34
24.0	0.7976	0.1306	1.5048	147.09	5.6362	0.0011	19.59
24.2	0.7994	0.0894	1.4675	306.07	5.7921	0.0005	20.23
24.263	0.8000						
			$\gamma = 5/3$		$M^2 = 20$		
1.00	0.5700	0.4772	0.4752	3.4783	0.0000	0.0595	0.000
1.02	0.5704	0.4763	0.4767	3.5020	0.0412	0.0594	0.735
1.04	0.5709	0.4754	0.4782	3.5255	0.0814	0.0593	1.445
1.06	0.5712	0.4746	0.4797	3.5488	0.1207	0.0592	2.131
1.08	0.5717	0.4738	0.4811	3.5719	0.1591	0.0591	2.794
1.10	0.5721	0.4730	0.4826	3.5948	0.1966	0.0590	3.436
1.12	0.5725	0.4722	0.4840	3.6176	0.2332	0.0589	4.057
1.14	0.5729	0.4714	0.4854	3.6399	0.2690	0.0588	4.659
1.16	0.5733	0.4707	0.4867	3.6622	0.3040	0.0588	5.242
1.18	0.5737	0.4699	0.4881	3.6843	0.3383	0.0587	5.808
1.20	0.5741	0.4691	0.4894	3.7065	0.3719	0.0586	6.357
1.20	0.5741	0.4691	0.4894	3.7065	0.3719	0.0586	6.357
1.25	0.5751	0.4673	0.4927	3.7605	0.4528	0.0584	7.681
1.30	0.5761	0.4656	0.4958	3.8133	0.5298	0.0581	8.876
1.35	0.5771	0.4638	0.4989	3.8653	0.6032	0.0579	10.011
1.40	0.5781	0.4622	0.5019	3.9165	0.6735	0.0577	11.074
1.45	0.5791	0.4606	0.5048	3.9669	0.7404	0.0575	12.072
1.50	0.5801	0.4590	0.5076	4.0167	0.8047	0.0572	13.011
1.5	0.5801	0.4590	0.5076	4.0167	0.8047	0.0572	13.011
1.6	0.5820	0.4560	0.5131	4.1142	0.9257	0.0568	14.733
1.7	0.5839	0.4531	0.5184	4.2092	1.0378	0.0564	16.277
1.8	0.5858	0.4503	0.5234	4.3021	1.1421	0.0559	17.671
1.9	0.5877	0.4477	0.5283	4.3932	1.2394	0.0555	18.950
2.0	0.5895	0.4451	0.5330	4.4827	1.3311	0.0551	20.091
2.1	0.5914	0.4427	0.5376	4.5707	1.4172	0.0547	21.151
2.2	0.5932	0.4404	0.5419	4.6573	1.4985	0.0543	22.128
2.3	0.5950	0.4381	0.5461	4.7426	1.5755	0.0539	23.032
2.4	0.5968	0.4359	0.5503	4.8275	1.6487	0.0534	23.872
2.4	0.5968	0.4359	0.5503	4.8276	1.6487	0.0534	23.872
2.8	0.6044	0.4317	0.5662	4.9942	1.7848	0.0526	25.386
2.9	0.6059	0.4276	0.5692	5.1581	1.9092	0.0518	26.717
3.0	0.6074	0.4237	0.5732	5.2200	2.0237	0.0510	27.889

ξ	U	C	P/β	Ω/β	M	$\left(\frac{P}{\beta\sqrt{\xi}}\right)\left(\frac{\Omega}{\beta\sqrt{\xi}}\right)^{\gamma}$	F
			$\gamma = 5/3$		$M^2 = 20$		
3.2	0.6109	0.4200	0.5802	5.4803	2.1298	0.0502	29.959
3.4	0.6142	0.4165	0.5869	5.6092	2.2256	0.0494	29.917
3.6	0.6176	0.4131	0.5934	5.7374	2.3211	0.0486	30.769
3.8	0.6209	0.4097	0.5997	5.8652	2.4061	0.0478	31.568
4.0	0.6242	0.4064	0.6058	6.1128	2.4922	0.0471	32.321
4.2	0.6274	0.4032	0.6118	6.2707	2.5680	0.0463	33.031
4.4	0.6306	0.4001	0.6176	6.4280	2.6419	0.0455	33.698
4.6	0.6338	0.3970	0.6231	6.5850	2.7125	0.0448	34.323
4.8	0.6369	0.3940	0.6286	6.7478	2.7796	0.0440	34.776
5.0	0.6400	0.3911	0.6339	6.9083	2.8441	0.0432	35.296
5.0	0.6400	0.3911	0.6339	6.908	2.8441	0.0432	35.296
5.5	0.6477	0.3838	0.6465	7.316	2.9949	0.0414	36.473
6.0	0.6551	0.3767	0.6584	7.734	3.1324	0.0395	37.508
6.5	0.6624	0.3697	0.6695	8.166	3.2596	0.0377	38.433
7.0	0.6696	0.3627	0.6799	8.614	3.3781	0.0358	39.270
7.5	0.6766	0.3558	0.6896	9.081	3.4896	0.0339	40.035
8.0	0.6834	0.3488	0.6987	9.571	3.5958	0.0319	40.742
8.5	0.6901	0.3418	0.7071	10.088	3.6961	0.0299	41.401
9.0	0.6966	0.3347	0.7148	10.630	3.7928	0.0280	42.021
9.5	0.7030	0.3275	0.7219	11.217	3.8861	0.0278	42.608
10.0	0.7093	0.3201	0.7282	11.841	3.9765	0.0235	43.168
10.5	0.7155	0.3126	0.7339	12.515	4.0647	0.0238	43.706
11.0	0.7216	0.3049	0.7389	13.247	4.1512	0.0221	44.225
11.5	0.7275	0.2969	0.7432	14.047	4.2364	0.0205	44.730
12.0	0.7334	0.2886	0.7471	14.930	4.3208	0.0189	45.224
12.5	0.7392	0.2800	0.7484	15.914	4.4048	0.0172	45.711
13.0	0.7449	0.2709	0.7496	17.025	4.4889	0.0156	46.194
13.5	0.7505	0.2614	0.7500	18.296	4.5737	0.0141	46.677
14.0	0.7560	0.2513	0.7489	19.772	4.6598	0.0125	47.164
14.5	0.7614	0.2404	0.7464	21.525	4.7480	0.0110	47.659
15.0	0.7668	0.2287	0.7423	23.652	4.8392	0.0094	48.169
15.5	0.7721	0.2156	0.7356	26.336	4.9347	0.0079	48.701
16.0	0.7773	0.2014	0.7263	29.676	5.0356	0.0064	49.267
16.5	0.7825	0.1848	0.7142	34.065	5.1427	0.0049	49.884
17.0	0.7876	0.1648	0.6983	42.743	5.2767	0.0034	50.586
17.5	0.7927	0.1386	0.6690	58.077	5.4317	0.0020	51.447
18.0	0.7978	0.0944	0.6174	115.490	5.6769	0.0006	52.509
18.212	0.8000						
			$\gamma = 5/3$		$M^2 = 50$		
1.00	0.5880	0.4695	0.4781	3.7732	0.0000	0.0523	0.00
1.02	0.5884	0.4684	0.4790	3.7951	0.0447	0.0521	2.19
1.04	0.5890	0.4676	0.4799	3.8248	0.0883	0.0520	4.30
1.06	0.5896	0.4662	0.4808	3.8503	0.1309	0.0518	6.34
1.08	0.5901	0.4651	0.4816	3.8756	0.1725	0.0517	8.32
1.10	0.5906	0.4641	0.4825	3.9006	0.2132	0.0515	10.23
1.12	0.5911	0.4630	0.4833	3.9254	0.2528	0.0514	12.08
1.14	0.5916	0.4620	0.4841	3.9501	0.2916	0.0512	13.89
1.16	0.5921	0.4609	0.4849	3.9745	0.3297	0.0511	15.62
1.18	0.5926	0.4599	0.4856	3.9987	0.3669	0.0509	17.31
1.20	0.5931	0.4589	0.4864	4.0227	0.4033	0.0508	18.96
1.20	0.5931	0.4589	0.4864	4.0227	0.4033	0.0508	18.95
1.25	0.5943	0.4565	0.4882	4.0818	0.4912	0.0504	22.84
1.30	0.5955	0.4541	0.4899	4.1396	0.5746	0.0501	26.48
1.35	0.5967	0.4518	0.4915	4.1967	0.6545	0.0497	29.88
1.40	0.5978	0.4496	0.4930	4.2525	0.7306	0.0494	33.07
1.45	0.5990	0.4474	0.4945	4.3074	0.8034	0.0491	36.06
1.50	0.6001	0.4453	0.4958	4.3615	0.8732	0.0487	38.88
1.55	0.6013	0.4432	0.4972	4.4147	0.9402	0.0484	41.54
1.60	0.6024	0.4312	0.4984	4.4672	1.0046	0.0481	44.06
1.6	0.6024	0.4312	0.4984	4.4672	1.0046	0.0481	44.06
1.7	0.6046	0.4275	0.5008	4.5703	1.1283	0.0475	48.70
1.8	0.6067	0.4239	0.5029	4.6710	1.2396	0.0469	52.90
1.9	0.6088	0.4203	0.5049	4.7695	1.3403	0.0463	56.72
2.0	0.6109	0.4168	0.5067	4.8662	1.4446	0.0457	60.21
2.1	0.6129	0.4135	0.5084	4.9611	1.5381	0.0451	63.41
2.2	0.6149	0.4102	0.5099	5.0546	1.6284	0.0445	66.36
2.3	0.6169	0.4069	0.5113	5.1465	1.7160	0.0440	69.10
2.4	0.6188	0.4039	0.5126	5.2372	1.7994	0.0434	71.64
2.4	0.6188	0.4039	0.5126	5.2372	1.7994	0.0434	71.64
2.7	0.6245	0.3941	0.5150	5.4160	1.8570	0.0418	78.52
2.8	0.6265	0.3908	0.5170	5.5011	2.0719	0.0414	80.98
3.0	0.6299	0.3874	0.5188	5.7036	2.1960	0.0404	85.66
3.2	0.6335	0.3823	0.5205	5.9345	2.3109	0.0394	87.07
3.4	0.6370	0.3774	0.5216	6.1040	2.4179	0.0386	89.98
3.6	0.6404	0.3727	0.5226	6.2725	2.5180	0.0377	92.63
3.8	0.6438	0.3681	0.5235	6.4405	2.6120	0.0368	95.06
4.0	0.6471	0.3638	0.5242	6.6077	2.7007	0.0358	97.30
4.2	0.6504	0.3596	0.5248	6.7752	2.7847	0.0349	99.37
4.4	0.6536	0.3555	0.5252	6.9428	2.8646	0.0340	101.29
4.6	0.6568	0.3519	0.5255	7.1128	2.9406	0.0332	103.06
4.8	0.6599	0.3488	0.5256	7.2830	3.0131	0.0324	104.76
5.0	0.6630	0.3428	0.5257	7.4545	3.0827	0.0316	106.34
5.0	0.6630	0.3428	0.5257	7.454	3.0827	0.0316	106.34
5.5	0.6706	0.3331	0.5253	7.880	3.2448	0.0297	109.92
6.0	0.6779	0.3237	0.5242	8.297	3.3980	0.0278	113.07
6.5	0.6851	0.3145	0.5224	8.704	3.5300	0.0260	115.88
7.0	0.6921	0.3054	0.5201	9.092	3.6570	0.0242	118.43
7.5	0.6989	0.2964	0.5171	9.507	3.7783	0.0225	120.76

TABLE I

Physical Properties of the Expanding Field of Flow behind Shock Waves of different Strength

ξ	U	C	P/β	Ω/β	M	$\left(\frac{P}{\beta\sqrt{\xi}}\right)\left(\frac{\Omega}{\beta\sqrt{\xi}}\right)^{-\gamma}$	F
		$\gamma = 5/3$			$M^2 = 50$		
8.0	0.7056	0.2975	0.5135	10.353	3.6925	0.0209	122.91
8.5	0.7121	0.2785	0.5092	10.937	4.0016	0.0193	124.92
9.0	0.7185	0.2695	0.5042	11.547	4.1082	0.0177	126.81
9.5	0.7248	0.2604	0.4995	12.253	4.2081	0.0162	128.60
10.0	0.7310	0.2511	0.4920	13.006	4.3071	0.0147	130.31
10.5	0.7371	0.2418	0.4847	13.829	4.4043	0.0133	131.96
11.0	0.7430	0.2318	0.4765	14.774	4.5004	0.0119	133.57
11.5	0.7489	0.2217	0.4672	15.842	4.5960	0.0106	135.15
12.0	0.7547	0.2111	0.4567	17.076	4.6917	0.0092	136.71
12.5	0.7604	0.2000	0.4448	18.530	4.7885	0.0080	138.29
12.8	0.7661	0.1881	0.4314	20.300	4.8876	0.0067	139.89
13.0	0.7716	0.1753	0.4156	22.562	4.9903	0.0055	141.52
13.5	0.7770	0.1611	0.3977	25.545	5.0998	0.0043	143.22
14.0	0.7772	0.1611	0.3977	25.545	5.0998	0.0043	143.22
14.2	0.7794	0.1549	0.3892	27.098	5.1445	0.0039	143.93
14.4	0.7815	0.1494	0.3804	28.792	5.1919	0.0034	144.66
14.6	0.7837	0.1415	0.3709	30.866	5.2415	0.0030	145.42
14.8	0.7859	0.1340	0.3603	33.455	5.2938	0.0025	146.22
15.0	0.7881	0.1258	0.3487	36.708	5.3496	0.0021	147.07
15.2	0.7902	0.1168	0.3355	41.027	5.4100	0.0017	147.99
15.4	0.7924	0.1064	0.3203	47.165	5.4770	0.0013	149.01
15.6	0.7946	0.0941	0.3021	56.650	5.5542	0.0009	150.17
15.8	0.7968	0.0783	0.2786	75.798	5.650	0.0006	151.60
16.0	0.7990	0.0523	0.2409	146.908	5.800	0.0002	153.77
16.086	0.8000						
		$\gamma = 5/3$			$M^2 = 100$		
1.00	0.5940	0.4534	0.4790	3.9656	0.0000	0.0499	0.00
1.02	0.5946	0.4522	0.4797	3.9126	0.0460	0.0497	9.39
1.04	0.5951	0.4510	0.4804	3.9272	0.0909	0.0496	18.55
1.06	0.5957	0.4498	0.4811	3.9637	0.1348	0.0494	26.91
1.08	0.5962	0.4486	0.4817	3.9699	0.1778	0.0492	35.29
1.10	0.5968	0.4474	0.4824	4.0158	0.2195	0.0491	43.41
1.12	0.5973	0.4463	0.4830	4.0414	0.2604	0.0489	51.27
1.14	0.5978	0.4452	0.4836	4.0668	0.3004	0.0487	58.89
1.16	0.5984	0.4440	0.4841	4.0920	0.3396	0.0486	66.28
1.18	0.5989	0.4429	0.4846	4.1169	0.3778	0.0484	73.45
1.20	0.5994	0.4419	0.4852	4.1415	0.4154	0.0483	80.41
1.20	0.5994	0.4419	0.4852	4.1415	0.4154	0.0483	80.41
1.25	0.6007	0.4392	0.4864	4.2024	0.5068	0.0479	98.69
1.30	0.6020	0.4368	0.4876	4.2621	0.5919	0.0475	98.40
1.35	0.6032	0.4341	0.4888	4.3208	0.6740	0.0471	103.62
1.40	0.6044	0.4317	0.4899	4.3784	0.7524	0.0467	110.39
1.45	0.6056	0.4293	0.4905	4.4351	0.8274	0.0464	116.75
1.50	0.6068	0.4270	0.4913	4.4910	0.8994	0.0460	122.74
1.5	0.6068	0.4270	0.4913	4.4910	0.8994	0.0460	122.74
1.6	0.6091	0.4226	0.4928	4.6000	1.0347	0.0453	133.74
1.7	0.6114	0.4184	0.4941	4.7060	1.1601	0.0446	143.61
1.8	0.6136	0.4143	0.4952	4.8095	1.2767	0.0440	152.53
1.9	0.6158	0.4104	0.4961	4.9107	1.3856	0.0433	160.64
2.0	0.6179	0.4065	0.4969	5.0098	1.4880	0.0427	168.06
2.1	0.6200	0.4029	0.4975	5.1070	1.5843	0.0421	174.87
2.2	0.6221	0.3994	0.4980	5.2025	1.6752	0.0414	181.15
2.3	0.6241	0.3960	0.4984	5.2965	1.7613	0.0409	186.97
2.4	0.6261	0.3927	0.4986	5.3893	1.8430	0.0403	192.38
2.5	0.6280	0.3895	0.4988	5.4810	1.9206	0.0397	197.42
2.6	0.6299	0.3865	0.4989	5.5716	1.9949	0.0392	202.14
2.7	0.6318	0.3835	0.4990	5.6612	2.0659	0.0387	206.56
2.8	0.6337	0.3805	0.4990	5.7500	2.1337	0.0381	210.72
2.9	0.6356	0.3774	0.4989	5.8381	2.1988	0.0376	214.64
3.0	0.6374	0.3745	0.4987	5.9257	2.2613	0.0371	218.35
3.1	0.6392	0.3717	0.4985	6.0127	2.3214	0.0366	221.86
3.2	0.6410	0.3690	0.4982	6.0991	2.3794	0.0361	225.19
3.3	0.6427	0.3663	0.4979	6.1851	2.4353	0.0356	228.35
3.4	0.6444	0.3637	0.4975	6.2708	2.4892	0.0351	231.36
3.5	0.6462	0.3611	0.4971	6.3562	2.5416	0.0346	234.24
3.6	0.6479	0.3586	0.4967	6.4414	2.5920	0.0341	236.99
3.7	0.6496	0.3560	0.4962	6.5263	2.6410	0.0337	239.62
3.8	0.6512	0.3535	0.4956	6.6110	2.6886	0.0332	242.14
3.9	0.6529	0.3510	0.4950	6.6957	2.7348	0.0328	244.56
4.0	0.6545	0.3486	0.4944	6.7804	2.7797	0.0323	246.88
4.1	0.6562	0.3462	0.4938	6.8651	2.8234	0.0319	249.11
4.2	0.6578	0.3439	0.4931	6.9498	2.8659	0.0314	251.26
4.3	0.6594	0.3416	0.4924	7.0344	2.9073	0.0310	253.33
4.4	0.6610	0.3393	0.4917	7.1192	2.9477	0.0306	255.33
4.5	0.6625	0.3370	0.4909	7.2042	2.9871	0.0302	257.26
4.6	0.6641	0.3348	0.4901	7.2895	3.0256	0.0298	259.13
4.7	0.6656	0.3325	0.4893	7.3745	3.0633	0.0293	260.94
4.8	0.6672	0.3303	0.4884	7.4600	3.1001	0.0289	262.69
4.9	0.6687	0.3281	0.4876	7.5460	3.1363	0.0285	264.39
5.0	0.6702	0.3260	0.4866	7.6327	3.1718	0.0281	266.04
5.0	0.6702	0.3260	0.4866	7.6327	3.1718	0.0281	266.04
5.2	0.6732	0.3217	0.4847	7.8066	3.2394	0.0273	269.19
5.4	0.6762	0.3175	0.4827	7.9821	3.3054	0.0266	272.17
5.6	0.6791	0.3133	0.4806	8.1595	3.3687	0.0258	275.00
5.8	0.6820	0.3092	0.4784	8.3391	3.4298	0.0251	277.69
6.0	0.6849	0.3052	0.4761	8.5212	3.4889	0.0245	280.25
6.2	0.6877	0.3012	0.4737	8.7058	3.5462	0.0238	282.69
6.4	0.6905	0.2972	0.4713	8.8931	3.6018	0.0232	285.03
6.6	0.6932	0.2933	0.4688	9.0837	3.6557	0.0222	287.27

ξ	U	C	P/β	Ω/β	M	$\left(\frac{P}{\beta\sqrt{\xi}}\right)\left(\frac{\Omega}{\beta\sqrt{\xi}}\right)^{-\gamma}$	F
		$\gamma = 5/3$			$M^2 = 100$		
6.8	0.6960	0.2894	0.4662	9.2761	3.7083	0.0216	289.43
7.0	0.6987	0.2855	0.4634	9.4764	3.7594	0.0209	291.51
7.2	0.7014	0.2817	0.4606	9.6799	3.8094	0.0202	293.51
7.4	0.7040	0.2778	0.4577	9.8855	3.8582	0.0195	295.45
7.6	0.7066	0.2740	0.4547	10.0970	3.9059	0.0189	297.32
7.8	0.7092	0.2702	0.4516	10.3140	3.9526	0.0183	299.14
8.0	0.7118	0.2663	0.4484	10.5372	3.9984	0.0177	300.90
8.0	0.7118	0.2663	0.4484	10.54	3.9984	0.0177	300.90
8.4	0.7169	0.2587	0.4418	11.00	4.0876	0.0165	304.28
8.8	0.7219	0.2511	0.4347	11.49	4.1739	0.0153	307.49
9.2	0.7268	0.2434	0.4272	12.02	4.2578	0.0142	310.56
9.6	0.7317	0.2357	0.4193	12.58	4.3396	0.0131	313.51
10.0	0.7365	0.2278	0.4109	13.19	4.4198	0.0120	316.32
10.4	0.7412	0.2196	0.4020	13.86	4.4988	0.0110	319.12
10.8	0.7458	0.2117	0.3926	14.59	4.5769	0.0100	321.82
11.2	0.7504	0.2034	0.3824	15.41	4.6545	0.0090	324.47
11.6	0.7549	0.1948	0.3715	16.32	4.7320	0.0080	327.08
12.0	0.7594	0.1859	0.3599	17.35	4.8098	0.0071	329.67
12.4	0.7638	0.1767	0.3474	18.55	4.8884	0.0062	332.26
12.8	0.7682	0.1670	0.3339	19.96	4.9685	0.0053	334.87
13.2	0.7725	0.1567	0.3191	21.66	5.0508	0.0045	337.53
13.6	0.7768	0.1456	0.3027	23.79	5.1365	0.0037	340.27
14.0	0.7811	0.1336	0.2844	26.57	5.2269	0.0029	343.14
14.0	0.7811	0.1336	0.2844	26.57	5.2269	0.0029	343.14
14.2	0.7832	0.1270	0.2743	28.33	5.2746	0.0025	344.66
14.4	0.7854	0.1201	0.2635	30.45	5.3245	0.0022	346.22
14.6	0.7875	0.1126	0.2517	33.10	5.3775	0.0018	347.87
14.8	0.7896	0.1044	0.2386	36.52	5.4338	0.0015	349.63
15.0	0.7917	0.0952	0.2240	41.20	5.4955	0.0011	351.55
15.2	0.7938	0.0844	0.2070	48.19	5.5648	0.0008	353.70
15.4	0.7960	0.0717	0.1863	60.42	5.6466	0.0005	356.24
15.6	0.7981	0.0538	0.1580	109.50	5.7566	0.0002	360.01
15.766	0.8000						
		$\gamma = 5/3$			$M^2 = 200$		
1.00	0.5970	0.4803	0.4796	3.9408	0.0000	0.0498	0.00
1.02	0.5976	0.4791	0.4801	3.9662	0.0467	0.0496	9.56
1.04	0.5982	0.4778	0.4807	3.9952	0.0925	0.0494	18.77
1.06	0.5987	0.4766	0.4812	4.0220	0.1369	0.0492	27.69
1.08	0.5993	0.4753	0.4817	4.0485	0.1803	0.0490	36.32
1.10	0.5998	0.4741	0.4822	4.0747	0.2228	0.0479	44.66
1.12	0.6004	0.4729	0.4827	4.1007	0.2643	0.0477	52.73
1.14	0.6009	0.4718	0.4832	4.1266	0.3049	0.0475	60.53
1.16	0.6015	0.4706	0.4836	4.1520	0.3446	0.0473	68.24
1.18	0.6020	0.4695	0.4840	4.1773	0.3835	0.0472	75.62
1.20	0.6026	0.4683	0.4844	4.2023	0.4216	0.0470	82.79
1.20	0.6026	0.4683	0.4844	4.2023	0.4216	0.0470	82.79
1.25	0.6039	0.4656	0.4854	4.2648	0.5134	0.0466	99.83
1.30	0.6052	0.4629	0.4863	4.3249	0.6007	0.0462	115.72
1.35	0.6065	0.4605	0.4870	4.3843	0.6839	0.0458	130.58
1.40	0.6077	0.4578	0.4877	4.4428	0.7634	0.0454	144.52
1.45	0.6089	0.4553	0.4884	4.5003	0.8395	0.0451	157.62
1.50	0.6102	0.4529	0.4889	4.5569	0.9125	0.0447	169.98
1.55	0.6114	0.4505	0.4894	4.6127	0.9825	0.0443	181.61
1.60	0.6125	0.4482	0.4899	4.6677	1.0498	0.0440	192.62
1.6	0.6125	0.4482	0.4899	4.6677	1.0498	0.0440	192.62
1.7	0.6148	0.4438	0.4906	4.7752	1.1770	0.0432	212.97
1.8	0.6171	0.4396	0.4911	4.8800	1.2953	0.0425	231.37
1.9	0.6193	0.4355	0.4915	4.9824	1.4059	0.0418	248.09
2.0	0.6215	0.4315	0.4917	5.0828	1.5097	0.0412	263.38
2.1	0.6236	0.4277	0.4918	5.1815	1.6074	0.0406	277.42
2.2	0.6257	0.4240	0.4917	5.2785	1.6996	0.0400	290.37
2.3	0.6277	0.4205	0.4916	5.3735	1.7869	0.0394	302.36
2.4	0.6297	0.4170	0.4914	5.4675	1.8698	0.0388	313.50
2.4	0.6297	0.4170	0.4914	5.4675	1.8698	0.0388	313.5
2.6	0.6336	0.4104	0.4908	5.6518	2.0259	0.0376	333.6
2.8	0.6374	0.4041	0.4898	5.8322	2.1646	0.0365	351.3
3.0	0.6410	0.3980	0.4885	6.0093	2.2940	0.0354	367.0
3.2	0.6446	0.3922	0.4869	6.1840	2.4158	0.0344	381.1
3.4	0.6481	0.3866	0.4851	6.3568	2.5323	0.0334	393.8
3.6	0.6515	0.3812	0.4832	6.5280	2.6296	0.0325	405.4
3.8	0.6549	0.3760	0.4812	6.6985	2.7274	0.0316	416.0
4.0	0.6582	0.3709	0.4791	6.8682	2.8197	0.0308	425.8
4.2	0.6614	0.3660	0.4769	7.0376	2.9070	0.0299	434.8
4.4	0.6646	0.3612	0.4744	7.2071	2.9896	0.0289	443.2
4.6	0.6677	0.3565	0.4719	7.3772	3.0687	0.0281	451.0
4.8	0.6707	0.3519	0.4693	7.5479	3.1440	0.0273	458.3
5.0	0.6737	0.3474	0.4668	7.7197	3.2160	0.0266	465.2
5.0	0.6737	0.3474	0.4668	7.720	3.2160	0.0266	465.2
5.4	0.6796	0.3386	0.4609	8.067	3.3518	0.0249	477.8
5.8	0.6853	0.3300	0.4548	8.422	3.4776	0.0234	489.1
6.2	0.6909	0.3217	0.4484	8.786	3.5948	0.0220	499.3
6.6	0.6964	0.3135	0.4417	9.161	3.7052	0.0206	508.7
7.0	0.7018	0.2754	0.4346	9.549	3.8097	0.0193	517.4
7.4	0.7070	0.2976	0.4273	9.953	3.9091	0.0181	525.4
7.8	0.7121	0.2896	0.4195	10.376	4.0042	0.0169	532.9
8.2	0.7171	0.2818	0.4115	10.820	4.0955	0.0157	540.0

TABLE I

Physical Properties of the Expanding Field of Flow behind Shock Waves of different Strength

ξ	U	C	P/β	Ω/β	M	$\left(\frac{P}{\beta\sqrt{\xi}}\right)\left(\frac{\Omega}{\beta\sqrt{\xi}}\right)^{\gamma}$	F
		$\gamma = 5/3$			$M^2 = 200$		
8.6	0.7220	0.2440	0.4031	11.290	4.1636	0.0145	546.7
9.0	0.7268	0.2361	0.3943	11.789	4.2689	0.0134	553.1
9.4	0.7316	0.2282	0.3851	12.292	4.3810	0.0124	559.2
9.8	0.7365	0.2203	0.3754	12.795	4.4980	0.0113	565.1
10.2	0.7409	0.2123	0.3653	13.315	4.6126	0.0103	570.8
10.6	0.7455	0.2041	0.3547	14.193	4.8910	0.0094	576.3
11.0	0.7500	0.1958	0.3436	14.942	4.9686	0.0084	581.7
11.4	0.7544	0.1872	0.3318	15.776	4.7456	0.0075	587.0
11.8	0.7587	0.1784	0.3198	16.713	4.8220	0.0066	592.2
12.2	0.7630	0.1694	0.3060	17.765	4.9006	0.0056	597.4
12.6	0.7673	0.1599	0.2919	19.032	4.9792	0.0050	602.6
13.0	0.7715	0.1499	0.2766	20.508	5.0594	0.0042	607.9
13.4	0.7757	0.1395	0.2601	22.320	5.1421	0.0035	613.3
13.8	0.7796	0.1290	0.2419	24.627	5.2284	0.0029	618.8
13.8	0.7796	0.1290	0.2419	24.63	5.2284	0.00278	618.8
14.0	0.7819	0.1219	0.2290	26.04	5.2735	0.00245	621.7
14.2	0.7839	0.1155	0.2216	27.70	5.3202	0.00212	624.7
14.4	0.7860	0.1096	0.2104	29.72	5.3690	0.00180	627.8
14.6	0.7880	0.1013	0.1963	32.21	5.4204	0.00149	631.0
14.8	0.7900	0.0934	0.1851	35.40	5.4753	0.00118	634.4
15.0	0.7921	0.0845	0.1704	39.75	5.5350	0.00091	638.1
15.2	0.7941	0.0743	0.1535	46.22	5.6017	0.00064	642.3
15.4	0.7962	0.0622	0.1328	57.18	5.6800	0.00039	647.2
15.6	0.7982	0.0453	0.1054	85.40	5.7835	0.00016	653.6
15.784	0.8000						
		$\gamma = 5/3$			$M^2 = 500$		
1.00	0.5988	0.4485	0.4798	3.9762	0.0000	0.0481	0.00
1.02	0.5994	0.4472	0.4803	4.0037	0.0471	0.0479	24.29
1.04	0.6000	0.4459	0.4808	4.0310	0.0931	0.0477	47.78
1.06	0.6006	0.4446	0.4813	4.0580	0.1380	0.0476	70.45
1.08	0.6011	0.4433	0.4817	4.0848	0.1818	0.0473	92.40
1.10	0.6017	0.4421	0.4822	4.1114	0.2246	0.0472	113.65
1.12	0.6023	0.4409	0.4828	4.1378	0.2665	0.0470	134.24
1.14	0.6028	0.4397	0.4830	4.1638	0.3076	0.0468	154.20
1.16	0.6034	0.4385	0.4833	4.1896	0.3478	0.0466	173.56
1.18	0.6039	0.4373	0.4837	4.2152	0.3868	0.0464	192.34
1.20	0.6045	0.4362	0.4840	4.2406	0.4252	0.0463	210.56
1.20	0.6045	0.4362	0.4840	4.2406	0.4252	0.0463	210.56
1.25	0.6059	0.4334	0.4846	4.3031	0.5178	0.0459	255.93
1.30	0.6071	0.4306	0.4855	4.3643	0.6060	0.0455	294.37
1.35	0.6084	0.4279	0.4861	4.4243	0.6901	0.0451	332.20
1.40	0.6097	0.4253	0.4868	4.4832	0.7704	0.0447	367.67
1.45	0.6109	0.4228	0.4871	4.5410	0.8472	0.0443	401.01
1.50	0.6122	0.4204	0.4876	4.5982	0.9208	0.0439	432.42
1.5	0.6122	0.4204	0.4876	4.5982	0.9208	0.0439	432.4
1.6	0.6146	0.4156	0.4890	4.7098	1.0594	0.0431	490.1
1.7	0.6169	0.4109	0.4894	4.8185	1.1877	0.0424	541.9
1.8	0.6192	0.4067	0.4898	4.9240	1.3071	0.0417	588.7
1.9	0.6214	0.4025	0.4898	5.0272	1.4187	0.0410	631.3
2.0	0.6236	0.3985	0.4905	5.1282	1.5234	0.0404	670.2
2.1	0.6257	0.3946	0.4903	5.2273	1.6219	0.0397	705.9
2.2	0.6278	0.3908	0.4898	5.3246	1.7149	0.0391	738.9
2.3	0.6299	0.3871	0.4874	5.4203	1.8030	0.0385	769.4
2.4	0.6319	0.3836	0.4868	5.5147	1.8868	0.0379	797.8
2.5	0.6338	0.3802	0.4862	5.6080	1.9662	0.0373	824.3
2.6	0.6358	0.3768	0.4855	5.7001	2.0421	0.0367	849.0
2.7	0.6377	0.3735	0.4847	5.7911	2.1146	0.0361	872.2
2.8	0.6396	0.3703	0.4838	5.8811	2.1840	0.0356	894.0
2.9	0.6414	0.3672	0.4829	5.9703	2.2506	0.0350	914.6
3.0	0.6433	0.3641	0.4819	6.0586	2.3145	0.0345	934.0
3.0	0.6433	0.3641	0.4819	6.0586	2.3145	0.0345	934.
3.2	0.6468	0.3581	0.4798	6.2327	2.4362	0.0335	1292.
3.4	0.6503	0.3524	0.4776	6.4070	2.5475	0.0325	1616.
3.6	0.6537	0.3469	0.4750	6.5799	2.6525	0.0315	1910.
3.8	0.6570	0.3415	0.4724	6.7496	2.7511	0.0306	2179.
4.0	0.6603	0.3363	0.4696	6.9194	2.8441	0.0297	2427.
4.2	0.6635	0.3312	0.4667	7.0887	2.9321	0.0288	2656.
4.4	0.6667	0.3263	0.4638	7.2578	3.0156	0.0279	2869.
4.6	0.6698	0.3215	0.4607	7.4272	3.0950	0.0271	3067.
4.8	0.6728	0.3168	0.4575	7.5973	3.1708	0.0263	3252.
5.0	0.6758	0.3122	0.4542	7.7682	3.2433	0.0255	3426.
5.2	0.6787	0.3078	0.4508	7.9402	3.3128	0.0247	3590.
5.4	0.6816	0.3033	0.4473	8.1136	3.3796	0.0239	3745.
5.6	0.6845	0.2987	0.4438	8.2887	3.4439	0.0232	3892.
5.8	0.6873	0.2944	0.4402	8.4658	3.5060	0.0225	4032.
6.0	0.6900	0.2901	0.4366	8.6452	3.5660	0.0218	4165.
6.0	0.6900	0.2901	0.4366	8.645	3.5660	0.0218	4165.
6.5	0.6968	0.2796	0.4270	9.104	3.7079	0.0201	4226.
7.0	0.7034	0.2693	0.4169	9.581	3.8400	0.0184	4281.
7.5	0.7096	0.2592	0.4064	10.082	3.9640	0.0169	4331.
8.0	0.7160	0.2492	0.3954	10.611	4.0812	0.0154	4377.
8.5	0.7221	0.2393	0.3839	11.174	4.1928	0.0140	4420.
9.0	0.7281	0.2294	0.3718	11.777	4.2998	0.0127	4460.
9.5	0.7339	0.2194	0.3592	12.430	4.4031	0.0114	4498.
10.0	0.7396	0.2094	0.3459	13.144	4.5034	0.0102	4534.
10.5	0.7452	0.1993	0.3319	13.934	4.6014	0.0090	4569.
11.0	0.7506	0.1889	0.3171	14.818	4.6978	0.0079	4603.
11.5	0.7560	0.1782	0.3015	15.825	4.7933	0.0068	4636.
12.0	0.7613	0.1671	0.2848	16.998	4.8887	0.0058	4668.
12.5	0.7666	0.1554	0.2668	18.392	4.9849	0.0049	4700.
13.0	0.7716	0.1435	0.2474	20.040	5.0827	0.0039	4732.
13.5	0.7766	0.1304	0.2262	22.165	5.1839	0.0030	4765.
14.0	0.7816	0.1162	0.2026	25.010	5.2903	0.0022	4799.
14.5	0.7865	0.1002	0.1755	29.198	5.4064	0.0015	4835.
15.0	0.7914	0.0811	0.1431	35.847	5.5362	0.0006	4876.
15.5	0.7962	0.0568	0.0997	53.923	5.7050	0.0000	4926.
15.888	0.8000						
		$\gamma = 5/3$			$M^2 = \infty$		
1.00	0.6000	0.4472	0.4800	4.0000	0.0000	0.0476	
1.02	0.6006	0.4459	0.4805	4.0279	0.0474	0.0474	
1.04	0.6012	0.4446	0.4809	4.0555	0.0937	0.0472	
1.06	0.6018	0.4433	0.4813	4.0828	0.1388	0.0470	
1.08	0.6024	0.4420	0.4817	4.1098	0.1829	0.0468	
1.10	0.6029	0.4407	0.4821	4.1365	0.2261	0.0467	
1.12	0.6035	0.4396	0.4825	4.1630	0.2682	0.0465	
1.14	0.6041	0.4383	0.4828	4.1892	0.3094	0.0463	
1.16	0.6046	0.4371	0.4832	4.2153	0.3497	0.0462	
1.18	0.6052	0.4359	0.4835	4.2411	0.3892	0.0460	
1.20	0.6057	0.4347	0.4838	4.2665	0.4279	0.0458	
1.20	0.6057	0.4347	0.4838	4.2665	0.4279	0.0458	
1.25	0.6071	0.4318	0.4844	4.3294	0.5211	0.0454	
1.30	0.6084	0.4290	0.4850	4.3910	0.6098	0.0449	
1.35	0.6097	0.4263	0.4855	4.4515	0.6943	0.0445	
1.40	0.6110	0.4237	0.4859	4.5108	0.7751	0.0441	
1.45	0.6123	0.4211	0.4862	4.5691	0.8524	0.0437	
1.50	0.6135	0.4186	0.4865	4.6264	0.9265	0.0433	
1.55	0.6147	0.4162	0.4867	4.6829	0.9976	0.0430	
1.60	0.6159	0.4138	0.4868	4.7386	1.0659	0.0426	
1.65	0.6171	0.4115	0.4869	4.7936	1.1317	0.0422	
1.70	0.6183	0.4092	0.4870	4.8479	1.1950	0.0418	
1.75	0.6195	0.4069	0.4870	4.9015	1.2562	0.0415	
1.80	0.6206	0.4047	0.4869	4.9544	1.3152	0.0411	
1.8	0.6206	0.4047	0.4869	4.9544	1.3152	0.0411	
1.9	0.6228	0.4005	0.4867	5.0585	1.4275	0.0404	
2.0	0.6250	0.3964	0.4864	5.1600	1.5328	0.0398	
2.1	0.6272	0.3924	0.4859	5.2597	1.6320	0.0391	
2.2	0.6293	0.3886	0.4853	5.3577	1.7256	0.0385	
2.3	0.6313	0.3848	0.4846	5.4541	1.8142	0.0378	
2.4	0.6333	0.3812	0.4839	5.5490	1.8984	0.0372	
2.5	0.6353	0.3777	0.4830	5.642	1.9785	0.0366	
2.6	0.6372	0.3743	0.4820	5.734	2.0548	0.0361	
2.7	0.6392	0.3710	0.4810	5.824	2.1277	0.0355	
2.8	0.6410	0.3677	0.4799	5.917	2.1976	0.0349	
2.9	0.6429	0.3645	0.4788	6.008	2.2645	0.0344	
3.0	0.6447	0.3614	0.4776	6.098	2.3286	0.0339	
3.1	0.6465	0.3585	0.4764	6.188	2.3907	0.0333	
3.2	0.6483	0.3553	0.4751	6.277	2.4503	0.0328	
3.3	0.6501	0.3524	0.4737	6.366	2.5076	0.0323	
3.4	0.6518	0.3495	0.4723	6.444	2.5633	0.0318	
3.5	0.6535	0.3467	0.4709	6.530	2.6170	0.0313	
3.6	0.6552	0.3439	0.4695	6.615	2.6690	0.0309	
3.7	0.6569	0.3412	0.4680	6.701	2.7192	0.0304	
3.8	0.6585	0.3385	0.4664	6.786	2.7681	0.0299	
3.9	0.6601	0.3358	0.4649	6.871	2.8155	0.0294	
4.0	0.6618	0.3332	0.4633	6.955	2.8615	0.0290	
4.0	0.6618	0.3332	0.4633	6.955	2.8615	0.0290	
4.2	0.6650	0.3281	0.4600	7.125	2.9499	0.0281	
4.4	0.6681	0.3230	0.4567	7.294	3.0336	0.0272	
4.6	0.6712	0.3181	0.4532	7.463	3.1139	0.0264	
4.8	0.6742	0.3133	0.4496	7.633	3.1898	0.0256	
5.0	0.6771	0.3086	0.4460	7.803	3.2628	0.0248	
5.2	0.6801	0.3040	0.4423	7.975	3.3325	0.0240	
5.4	0.6829	0.2996	0.4384	8.148	3.3996	0.0232	
5.6	0.6858	0.2950	0.4346	8.322	3.4642	0.0226	
5.8	0.6885	0.2906	0.4305	8.497	3.5265	0.0219	
6.0	0.6913	0.2862	0.4265	8.675	3.5867	0.0212	
6.2	0.6940	0.2819	0.4224	8.855	3.6450	0.0205	
6.4	0.6967	0.2777	0.4182	9.038	3.7015	0.0199	
6.6	0.6993	0.2735	0.4140	9.224	3.7563	0.0191	
6.8	0.7020	0.2693	0.4096	9.411	3.8096	0.0185	
7.0	0.7045	0.2652	0.4052	9.600	3.8615	0.0179	
7.0	0.7045	0.2652	0.4052	9.600	3.8615	0.0179	
7.4	0.7096	0.2570	0.3962	9.997	3.9614	0.0165	
7.8	0.7146	0.2489	0.3869	10.406	4.0568	0.0153	
8.2	0.7194	0.2409	0.3773	10.836	4.1488	0.0143	
8.6	0.7242	0.2329	0.3674	11.287	4.2382	0.0132	
9.0	0.7289	0.2249	0.3571	11.765	4.3217	0.0122	
9.4	0.7335	0.2169	0.3465	12.272	4.4045	0.0112	
9.8	0.7380	0.2089	0.3356	12.814	4.4852	0.0102	
10.2	0.7424	0.2008	0.3241	13.398	4.5642	0.0093	
10.6	0.7468	0.1926	0.3123	14.032	4.6418	0.0084	
11.0	0.7511	0.1843	0.3000	14.726	4.7184	0.0075	
11.4	0.7553	0.1758	0.2871	15.490	4.7943	0.0067	
11.8	0.7595	0.1671	0.2736	16.341	4.8700	0.0059	
12.2	0.7636	0.1581	0.2595	17.300	4.9457	0.0052	
12.6	0.7676	0.1486	0.2446	18.404	5.0219	0.0044	
13.0	0.7716	0.1391	0.2288	19.694	5.0992	0.0037	

TABLE I

Physical Properties of the Expanding Field Flow behind Shock Waves of different Strength

ξ	U	C	P/β	Ω/β	M	$\left(\frac{P}{\beta\sqrt{\xi}}\right)\left(\frac{\Omega}{\beta\sqrt{\xi}}\right)^{-\gamma}$	F
		$\gamma = \frac{5}{3}$			$M^2 = \infty$		
13.4	0.7758	0.1290	0.2119	21.286	5.1782		0.0031
13.8	0.7794	0.1181	0.1937	23.123	5.2598		0.0025
14.2	0.7832	0.1065	0.1739	25.547	5.3453		0.0019
14.6	0.7870	0.0936	0.1518	28.841	5.4364		0.0014
15.0	0.7907	0.0790	0.1266	33.795	5.5366		0.0009
15.0	0.7907	0.0790	0.1265	33.80	5.5368		0.00088
15.2	0.7926	0.0708	0.1122	37.47	5.5920		0.00066
15.4	0.7944	0.0612	0.0951	42.72	5.6529		0.00046
15.6	0.7962	0.0502	0.0774	51.20	5.7225		0.00027
15.60	0.7962	0.0502	0.0774	51.20	5.7225		0.00027
15.65	0.7967	0.0470	0.0721	54.40	5.7420		0.00023
15.70	0.7972	0.0427	0.0655	59.04	5.7628		0.00019
15.75	0.7976	0.0401	0.0605	62.61	5.7846		0.00015
15.80	0.7980	0.0362	0.0539	68.59	5.8084		0.00012
15.85	0.7985	0.0316	0.0466	77.30	5.8347		0.00009
15.90	0.7990	0.0265	0.0382	91.00	5.8649		0.00006
15.90	0.7990	0.0265	0.0382	91.0	5.8649		0.00006
15.91	0.7991	0.0253	0.0364	94.7	5.8716		0.00005
15.92	0.7991	0.0241	0.0344	98.9	5.8795		0.00004
15.93	0.7992	0.0228	0.0324	105.8	5.8858		0.00003
15.94	0.7993	0.0215	0.0302	109.5	5.8934		0.00003
15.95	0.7994	0.0200	0.0280	116.5	5.9015		0.00002
15.96	0.7995	0.0184	0.0256	125.0	5.9101		0.00002
15.97	0.7996	0.0167	0.0228	136.0	5.9194		0.00001
15.98	0.7997	0.0148	0.0199	150.8	5.9296		0.00001
15.99	0.7998	0.0127	0.0165	172.4	5.9410		0.00000
16.00	0.7999	0.0098	0.0125	219.3	5.9547		0.00000
16.01	0.8000	0.0055	0.0068	368.3	5.9747		0.00000
16.015	0.8000						

representation of the behavior of the particles inside the shock wave at a given time. The interchangeability of r and t in the variable ξ also permits us to interpret these figures—with a proper reversal and change of scale—as the velocity, pressure, and density which prevail at a given fixed radius $r = 1$, as time increases from that of the passage of the shock to that of the arrival of the core. The arbitrary choice of the numbers $r = 1$ and $t = 1$ for which the figures are drawn is justified by the latent arbitrariness of the units in which these quantities are expressed.

A comparison of Table 2 with the corresponding table of Paper I discloses the equality of the columns p_1/p_0, ρ_1/ρ_0, and, consequently, T_1/T_0 and K_1/K_0, at corresponding γ's and Mach numbers. This follows immediately from the fact that the Rankine-Hugoniot

TABLE 2

SUMMARY OF THE PHYSICAL PROPERTIES OF THE SHOCK WAVE

($\gamma = \frac{5}{3}$)

M^2	a/R	p_1/p_0	ρ_1/ρ_0	$(l/r)_{x_1}$	$(l/r)_{c_1}$	T_1/T_0	K_1/K_0	ξ_0/ξ_1	$\lvert E-H\rvert/\lvert H\rvert$
3.....	0.3686	3.500	2.000	0.4000	0.6110	1.75	1.102	0.00681	0.4600
10.....	.5284	12.25	3.077	.5400	.5048	3.98	1.882	.04118	7.098
20.....	.5596	24.75	3.479	.5700	.4772	7.11	3.099	.05491	18.69
50.....	.5737	62.25	3.773	.5880	.4595	16.50	6.810	.06217	54.81
100.....	.5760	124.75	3.884	.5940	.4534	32.13	13.001	.06343	127.9
200.....	.5760	249.75	3.942	.5970	.4503	63.36	25.372	.06344	231.3
500.....	.5752	624.75	3.976	.5988	.4485	157.13	62.606	.06294	1734
∞.....	0.5742	∞	4.000	0.6000	0.4472	∞	∞	0.06244	∞

conditions for pressure and density across the shock front of progressing waves can be written as follows:

$$\frac{p_1}{p_0} = f(M^2, \gamma), \qquad \frac{\rho_1}{\rho_0} = g(M^2, \gamma).$$

The field of flow considered in this investigation is not isentropic. As is well known, the mere existence of the shock front is bound to bring about a discontinuous increase of the entropy of gas streaming through it; and, as will be shown below, the

entropy continues to increase thereafter as $\xi \to \infty$. Let $s(\xi)$, in what follows, denote the entropy at any point within the shock wave, and s_0 that of the undisturbed medium in front of the shock. As is well known,

$$s(\xi) - s_0 = \frac{\Re}{\gamma - 1} \log \frac{K}{K_0}, \tag{58}$$

where $\Re$ denotes the gas constant and K_0 and K are the values of the adiabatic constants in front of and behind the shock wave. Now, in front of the shock,

$$K_0 = p_0 \rho_0^{-\gamma} = \tfrac{8}{3}\pi G \beta^{2-\gamma} r^{5/2(\gamma-3)} \tag{59}$$

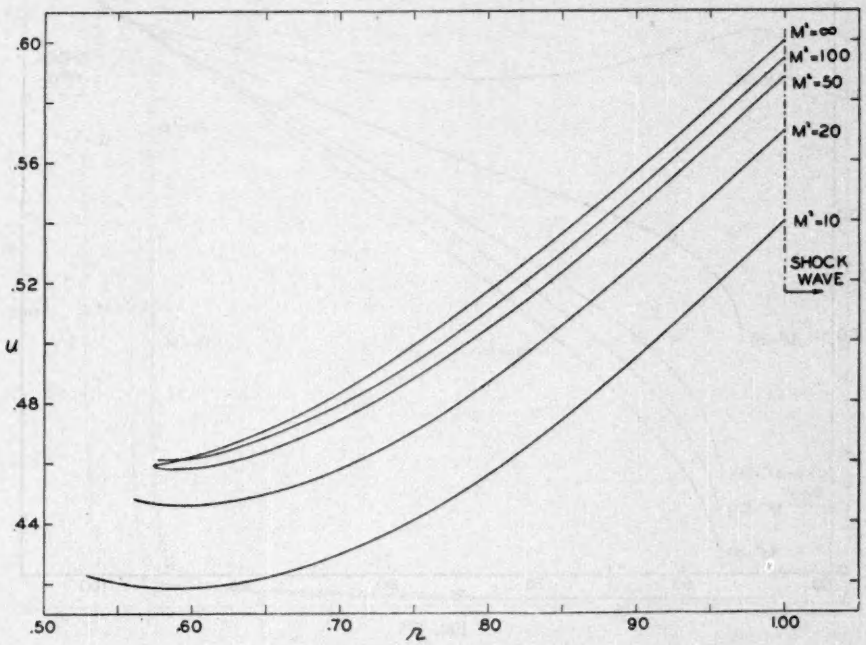

FIG. 1

by virtue of equations (32) and (34), while, behind the shock,

$$K = p\rho^{-\gamma} = r^2 t^{2\gamma-4} P \Omega^{-\gamma} \tag{60}$$

by equations (14) and (15). These equations disclose that the undisturbed medium itself will not be isentropic unless $\gamma = 1.2$; and the medium behind the shock wave will not be so, even if the entropy in front of the wave is constant. In general, we find that

$$\frac{K}{K_0} = \frac{3\beta^{\gamma-2}}{8\pi G} \frac{P\Omega^{-\gamma}}{\xi^{1-\gamma/2}} = \frac{25\gamma}{16x} \left(\frac{\xi_0}{\xi}\right)^{1/2} \left(\frac{P}{\beta\sqrt{\xi}}\right) \left(\frac{\Omega}{\beta\sqrt{\xi}}\right)^{-\gamma}; \tag{61}$$

and, in particular, if K_1 denotes the value of the adiabatic constant immediately behind the shock, an appeal to equations (38) and (39) discloses that

$$\frac{K_1}{K_0} = \frac{2\gamma - \gamma x + x}{x(\gamma+1)^{1+\gamma}(\gamma - 1 + 2x)^{-\gamma}}, \tag{62}$$

which, for $x = 1$ (i.e., the Mach number $M = 1$), indeed reduces to 1. In this case there is no entropy change across the incipient shock. The reader should note that the foregoing equation turns out to be identical with equation (53) of Paper I, which discloses that the ratio K_1/K_0 (and so the difference in entropy $s_1 - s_0$) across a shock wave of the same strength in both the GRM and the present model turns out to be the same. The penultimate column of Table 1 lists the auxiliary quantity $(P/\beta\sqrt{\xi})(\Omega/\beta\sqrt{\xi})^{-\gamma}$ as a function of ξ, which should facilitate the computation of the entropy at any point of the field of flow under investigation.

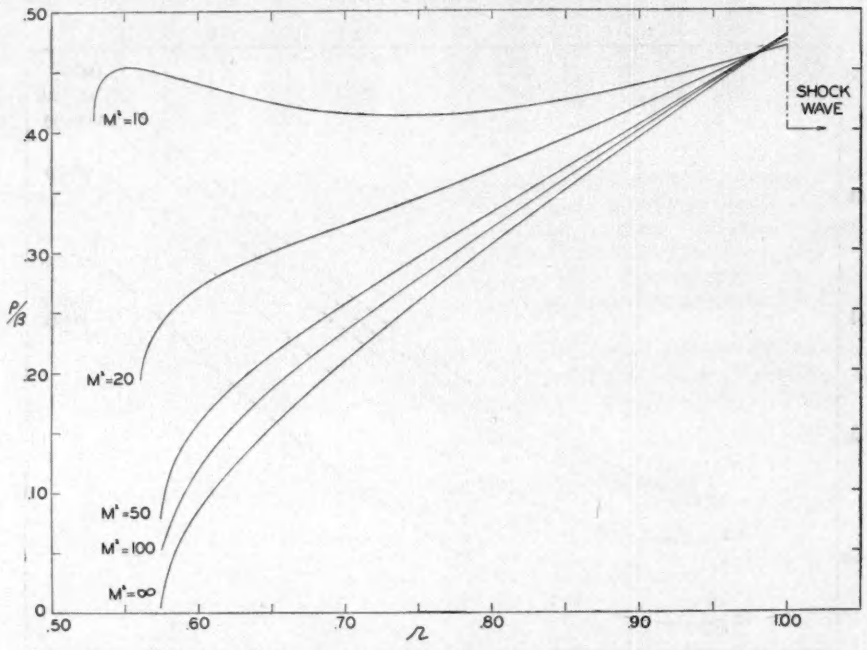

FIG. 2

The last column of Table 1 contains the values of the integral

$$F(\xi) = \int_{\xi_0}^{\xi} \left\{ \frac{25\gamma}{24x} \left[\frac{U^2\Omega}{2\beta} + \frac{P}{\beta(\gamma-1)} \right] - \frac{\xi^{3/5}\Omega}{5\beta} \int_{\xi}^{\xi_1} \frac{\Omega d\xi}{\beta\xi^{8/5}} \right\} \frac{d\xi}{\xi^2}, \tag{63}$$

which is related with the total energy $E(\xi)$ contained, at any time, within a concentric shell extending from ξ_0 to ξ by means of

$$E(\xi) = \tfrac{16}{5}\pi^2 G\beta^2 F(\xi). \tag{64}$$

In particular, the total energy contained in our model can be obtained from equation (64) by setting, in the latter, $\xi = \xi_1$.

A knowledge of $E(\xi_1)$ puts us, in turn, in a position to determine the amount of energy which must be released by the instantaneous initial explosion in order to produce a

shock wave of requisite strength. A sum H of the thermal and gravitational energy originally stored in the envelope has already been given by equation (57), where, by virtue of equations (19) and (20), we are now entitled to set $R/a = (\xi_1/\xi_0)^{1/5}$. The difference $|E(\xi_1) - H(\xi_1)|$ therefore furnishes the absolute amount of energy whose instantaneous release was adequate to produce the computed phenomena, and the ratio $|E - H|/|H|$ expresses this amount in terms of the original contents of energy of our model.

The numerical values of the quantity $|E - H|/|H|$ corresponding to each one of our solutions can be found in the last column of Table 2, which summarizes the main physical characteristics of our solutions.

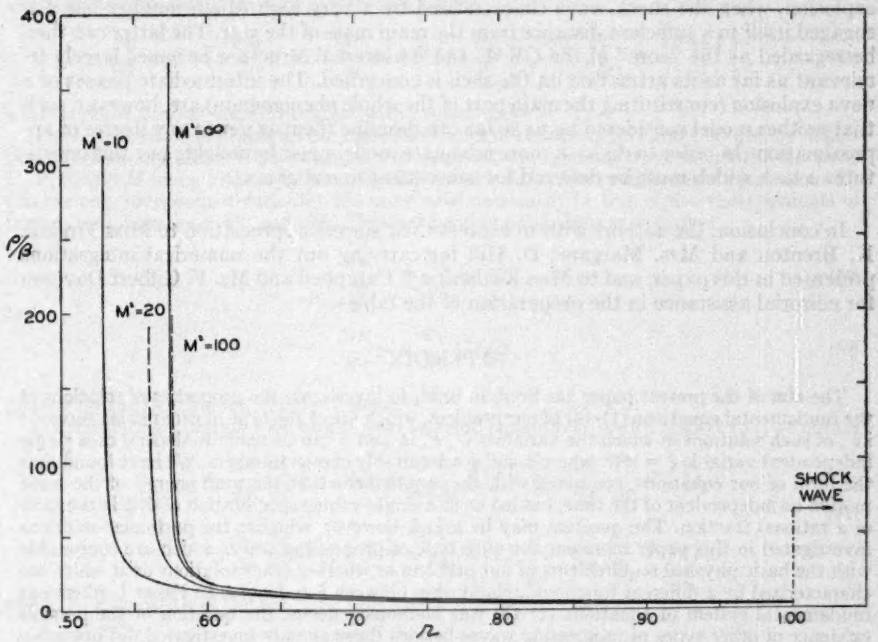

FIG. 3

V. DISCUSSION OF THE RESULTS

In conclusion, the bearing of the results obtained in the preceding sections and in Paper I on the dynamics of the nova phenomenon may be briefly discussed. The models at the basis of our investigations—the GRM of Paper I and that of the present contribution—differ widely in their assumed internal structure. A decrease in density with increasing radial distance in the layers through which our flow propagates is not so different in either case—with ρ_0 varying as r^{-2} in the envelope of a GRM, and as $r^{-2.5}$ in the model considered in the present paper—but, whereas the total mass contained in the envelope of a GRM is assumed to be negligible in comparison with the mass of its core, the model considered in this paper possessed no massive core (or, at least, the volume within which the law $\rho_0 \sim r^{-5/2}$ could be expected to break down was considered to be small enough for the mass inclosed within it to be negligible).

This fact has one important consequence, namely, whereas in the GRM the total energy of the model is effectively stored in its core, this will not be true of our second model. Now it is a well-known fact that the energy lost by a nova in the course of its explosion represents but a minute fraction (10^{-5}–10^{-6}) of the total energy stored inside the star. Since a glance at Table 2 discloses that the values of $|E - H|/|H|$ listed in its last column for our second model are incomparably larger than those permissible by the astrophysical evidence, it follows that this model may come close to reality only in the initial phases of the explosion, when the radius R of the corresponding shock wave includes but a small fraction of the total volume of a prenova and the "bubble" created by the initial explosion at the center still continues to grow. On the other hand, the GRM may possibly offer an approximation to the actual phenomenon in advanced stages of the explosion, when the shock wave characterized by a very high Mach number has disengaged itself to a sufficient distance from the main mass of the star. The latter can then be regarded as the "core" of the GRM, and its internal structure becomes largely irrelevant as far as its attraction on the shell is concerned. The intermediate phases of a nova explosion (constituting the main part of the whole phenomenon) are, however, such that neither model considered by us so far can describe them as yet to any degree of approximation. In order to do so, a more adequate model must be sought; but this constitutes a task which must be deferred for subsequent investigation.

In conclusion, the authors wish to express their sincere appreciation to Miss Virginia K. Brenton and Mrs. Margaret D. Hill for carrying out the numerical integrations presented in this paper, and to Miss Katherine J. Campbell and Mr. F. Gilbert Davoren for editorial assistance in the preparation of the tables.

APPENDIX

The aim of the present paper has been, in brief, to investigate the properties of solutions of the fundamental equations (1)–(4) of our problem, which are of the type of progressing waves—i.e., of such solutions in which the variables U, P, Ω, and S can be made to depend on a single independent variable $\xi = r^{\phi}t^{\psi}$, where ϕ and ψ are suitably chosen numbers. We have found that the form of our equations, combined with the requirement that the total energy of the wave motion be independent of the time, has led us to a single-valued specification of ψ/ϕ in the form of a rational fraction. The question may be asked, however, whether the particular solutions investigated in this paper represent the only type of progressing waves which are compatible with the basic physical requirements of our problem or whether other solutions exist which are characterized by a different functional relationship between ξ and r or t. In Paper I, where our fundamental system of equations (1)–(3) was nonhomogeneous, the question of the possible existence of other types of progressing waves besides those already investigated did not arise; for the gravity term in the Eulerian equation of motion by itself precluded the functional dependence of ξ on r and t in any other way than through a product of their powers, characterized by a fixed ratio $\psi/\phi = -\frac{2}{3}$. In the present case of a variable mass, where our fundamental system of equations (1)–(4) is homogeneous in the dependent variables, the possibility of other types of progressing waves besides those already investigated cannot, however, be a priori ruled out. The aim of this appendix will be to examine this specific question and to demonstrate *that if the dependent variables U, P, and Ω of our fundamental system of partial differential equations are to be expressible in terms of an equivalent system of ordinary differential equations with $\xi(r, t)$ as the sole independent variable, $\xi(r, t)$ must necessarily be of the form $\phi(r)\psi(t)$, where $\phi(r)$ is a power of r alone, and $\psi(t)$ may be either a power or an exponential of t. A product of the powers of both r and t represents, moreover, the only admissible form of ξ which may render the total energy of the corresponding wave motion independent of the time.*

In order to prove these assertions, let us assume that

$$\xi = \xi(r, t) \tag{65}$$

and seek the solution of equations (1)–(4) in terms of

$$u = \bar{u}(r, t)\, U(\xi), \qquad p = \bar{p}(r, t)\, P(\xi), \qquad \rho = \bar{\rho}(r, t)\, \Omega(\xi), \qquad m = \bar{m}(r, t)\, M(\xi). \tag{66}$$

Consider, now, one set of the seven partial derivatives involved in the system (1)–(4)—say, those of u. Differentiating the first one of the foregoing equations (66) with respect to r, we find that

$$\frac{\partial u}{\partial r} = U(\xi)\frac{\partial \bar{u}}{\partial r} + \bar{u}U'\frac{\partial \xi}{\partial r} = \bar{u}U(\xi)\frac{\partial \xi}{\partial r}\left\{\frac{\partial \bar{u}/\partial r}{\bar{u}(\partial \xi/\partial r)} + \frac{U'(\xi)}{U(\xi)}\right\}; \tag{67}$$

and a similar differentiation with respect to t yields

$$\frac{\partial u}{\partial t} = U(\xi)\frac{\partial \bar{u}}{\partial t} + \bar{u}U'\frac{\partial \xi}{\partial t} = \bar{u}U(\xi)\frac{\partial \xi}{\partial t}\left\{\frac{\partial \bar{u}/\partial t}{\bar{u}(\partial \xi/\partial t)} + \frac{U'(\xi)}{U(\xi)}\right\}, \tag{68}$$

where a prime denotes a differentiation with respect to ξ.[8]

The second terms in braces on the right-hand sides of equations (67) and (68) are, by definition, functions of ξ alone. If our solution is to represent a progressing wave (i.e., if the functions U, P, Ω, and M in eq. [66] are to be expressible in terms of ordinary differential equations with ξ as the only independent variable), the same must necessarily be true of the whole contents of the braces in equations (67) and (68). This fact permits us to assert at once that

$$\frac{\partial \bar{u}}{\partial t} = \bar{u}\frac{\partial \xi}{\partial t}F(\xi) \tag{69}$$

and

$$\frac{\partial \bar{u}}{\partial r} = \bar{u}\frac{\partial \xi}{\partial r}G(\xi), \tag{70}$$

where $F(\xi)$ and $G(\xi)$ are functions of ξ alone.

Differentiating equation (69) with respect to r and equation (70) with respect to t, we obtain

$$\begin{aligned}\frac{\partial^2 \bar{u}}{\partial r\,\partial t} &= \frac{\partial \bar{u}}{\partial r}\frac{\partial \xi}{\partial t}F(\xi) + \bar{u}\frac{\partial^2 \xi}{\partial r\,\partial t}F(\xi) + \bar{u}\frac{\partial \xi}{\partial r}\frac{\partial \xi}{\partial t}F'(\xi)\\ &= \frac{\partial \bar{u}}{\partial t}\frac{\partial \xi}{\partial r}G(\xi) + \bar{u}\frac{\partial^2 \xi}{\partial r\,\partial t}G(\xi) + \bar{u}\frac{\partial \xi}{\partial r}\frac{\partial \xi}{\partial t}G'(\xi),\end{aligned} \tag{71}$$

which, by elimination of the left-hand side, yields

$$\{F(\xi) - G(\xi)\}\frac{\partial^2 \xi}{\partial r\,\partial t} + \{F'(\xi) - G'(\xi)\}\frac{\partial \xi}{\partial r}\frac{\partial \xi}{\partial t} = 0, \tag{72}$$

as the partial differential equation determining ξ. This equation admits immediately of the following integrals:

$$\frac{\partial \xi}{\partial r} = \frac{f(r)}{F(\xi) - G(\xi)} \tag{73}$$

and

$$\frac{\partial \xi}{\partial t} = \frac{g(t)}{F(\xi) - G(\xi)}, \tag{74}$$

where $f(r)$ and $g(t)$ are, so far, arbitrary functions of their parameters.

[8] Primes will, as before, be used to denote differentiation whenever a function depends on a single variable only.

Consider, now, the last two terms of equation (3) of continuity. In accordance with equations (66), we find that

$$\frac{\partial u}{\partial r}+\frac{2u}{r}=U(\xi)\frac{\partial \bar{u}}{\partial r}+\bar{u}U'(\xi)\frac{\partial \xi}{\partial r}+\frac{2\bar{u}U(\xi)}{r}$$
$$=\frac{\bar{u}U'(\xi)}{r}\left\{\frac{2U(\xi)}{U'(\xi)}+r\frac{\partial \xi}{\partial r}\right\}+U\frac{\partial \bar{u}}{\partial r}. \tag{75}$$

By the same argument as that used before, if $U(\xi)/U'(\xi)$ is a function of ξ alone, so also must be $r(\partial\xi/\partial r)$, which permits us to assert that

$$r\frac{\partial \xi}{\partial r}=H_1(\xi) \tag{76}$$

and, likewise, that

$$r\frac{\partial \bar{u}}{\partial r}=\bar{u}H_2(\xi), \tag{77}$$

where $H_1(\xi)$ and $H_2(\xi)$ are again arbitrary functions of ξ. A comparison of equations (73) and (76) discloses that, of necessity,

$$f(r)=r^{-1}, \qquad H_1(\xi)=[F(\xi)-G(\xi)]^{-1}, \tag{78}$$

by virtue of which, equations (73) and (74) can be combined to yield

$$r\frac{\partial \xi}{\partial r}-\frac{1}{g(t)}\frac{\partial \xi}{\partial t}=0 \tag{79}$$

as the necessary and sufficient condition for the function $\xi(r, t)$ to reduce our system of partial differential equations for $U(\xi)$, $P(\xi)$, and $\Omega(\xi)$ into ordinary differential equations.

The function $g(t)$ in equation (79), moreover, is not arbitrary, and its explicit form can be determined as follows. The Lagrangian derivative of u in equation (1) can be rewritten by means of equations (67) and (68) as

$$\frac{\partial u}{\partial t}+u\frac{\partial u}{d r}=U\frac{\partial \bar{u}}{\partial t}+\bar{u}U'\frac{\partial \xi}{\partial t}+\bar{u}U^2\frac{\partial \bar{u}}{\partial r}+\bar{u}^2UU'\frac{\partial \xi}{\partial r}$$
$$=\bar{u}U\frac{\partial \bar{u}}{\partial r}\left\{U+\frac{\partial \bar{u}/\partial t}{\bar{u}(\partial \bar{u}/\partial r)}\right\}+\bar{u}^2U'\frac{\partial \xi}{\partial r}\left\{U+\frac{\partial \xi/\partial t}{\bar{u}(\partial \xi/\partial r)}\right\}, \tag{80}$$

from which it follows that

$$\bar{u}\frac{\partial \bar{u}}{\partial r}\div\frac{\partial \bar{u}}{\partial t}=K_1(\xi) \tag{81}$$

and

$$\bar{u}\frac{\partial \xi}{\partial r}\div\frac{\partial \xi}{\partial t}=K_2(\xi), \tag{82}$$

where $K_1(\xi)$ and $K_2(\xi)$ again denote arbitrary functions of ξ. A comparison of equations (79) and (82) indicates that

$$\bar{u}=\left\{\frac{\partial \xi}{\partial t}\div\frac{\partial \xi}{\partial r}\right\}K_2(\xi)=rg(t)K_2(\xi). \tag{83}$$

Differentiating this equation, we obtain

$$\frac{\partial \bar{u}}{\partial r}=g(t)K_2(\xi)+rg(t)K_2'(\xi)\frac{\partial \xi}{\partial r} \tag{84}$$

and

$$\frac{\partial \bar{u}}{\partial t}=rg'(t)K_2(\xi)+rg(t)K_2'(\xi)\frac{\partial \xi}{\partial t}, \tag{85}$$

respectively; and a division of these equations yields

$$\frac{\partial \bar{u}}{\partial t} \div \frac{\partial \bar{u}}{\partial r} = \frac{(g'[t])/(g[t]) + (K_2'[\xi])/(K_2[\xi])(\partial \xi)/(\partial t)}{1/r + (K_2'[\xi])/(K_2[\xi])(\partial \xi)/(\partial r)}. \tag{86}$$

On the other hand, from equations (69) and (70) it follows that

$$\frac{\partial \bar{u}}{\partial t} \div \frac{\partial \bar{u}}{\partial r} = \frac{F(\xi)}{G(\xi)} \left\{ \frac{\partial \xi}{\partial t} \div \frac{\partial \xi}{\partial r} \right\} = \frac{F(\xi)}{G(\xi)} \, r g(t) \tag{87}$$

by equations (73), (74), and (78). By equating the right-hand sides of equations (86) and (87), we find that the differential equation governing the function $g(t)$ is of the form

$$\frac{1}{g^2(t)} \frac{dg(t)}{dt} = \left\{ \frac{K_2'(\xi)}{K_2(\xi)} + F(\xi) \right\} \frac{1}{G(\xi)}. \tag{88}$$

Now the left-hand side of this equation is a function of t alone, while the right-hand side depends only on ξ. Since, by equation (65), ξ is assumed to depend on both r and t, it follows that the foregoing equation can be satisfied only if both its sides are zero or both equal to a constant, (say) $-\lambda^{-1}$. If so, the equation for $g(t)$ takes the neat form

$$\frac{g'}{g^2} + \frac{1}{\lambda} = 0, \tag{89}$$

which can be readily integrated.

In doing so we encounter two possibilities, depending on whether or not the ratio g'/g^2 is equal to, or different from, zero. Let us assume λ to be finite, in which case equation (89) integrates into

$$g(t) = \frac{\lambda}{t + \mu}, \tag{90}$$

where μ denotes an arbitrary constant. The value of this constant depends on the origin from which the time is reckoned and, without loss of generality, may be set equal to zero. Let us now insert (putting $\mu = 0$) the foregoing equation (90) into equation (79) and, furthermore, let $t^{-\lambda} = \tau$. If so, equation (79), governing the function $\xi(r, t)$, readily takes the form

$$r \frac{\partial \xi}{\partial r} + \tau \frac{\partial \xi}{\partial t} = 0, \tag{91}$$

which, by Euler's theorem, constitutes the necessary and sufficient condition for $\xi(r, \tau)$ to be a homogeneous function of r and $\tau = t^{-\lambda}$ of zero degree. In consequence, it follows that

$$\xi(r, t) = f(rt^{\lambda}); \tag{92}$$

and, without loss of generality, we may put $\xi \sim rt^{\lambda}$, since any other functional relationship between ξ and rt^{λ}, introduced into the fundamental equations (1)–(4), would not lead to any new solutions.

In order to complete our discussion, let us consider the case which arises if both sides of equation (88) vanish. If this happens, equation

$$\frac{1}{g^2} \frac{dg}{dt} = 0 \tag{93}$$

integrates readily into

$$g(t) = \text{Constant} \quad (\text{say, } \mu \neq 0). \tag{94}$$

In this case, equation (79) ceases to express Euler's theorem on homogeneous functions, and ξ is, therefore, no longer required to be a homogeneous function of its arguments. In order to

establish the explicit form of this function, let us introduce $f(r) = r^{-1}$ and $g(t) = \mu$ in equations (73) and (74); integrating the former along a line t = Constant, we find that

$$\log cr = \int \{F(\xi) - G(\xi)\}\, d\xi = A(\xi), \tag{95}$$

where c is independent of r but may be a function of t. In order to establish its form, let us differentiate equation (95) with respect to t, and we obtain

$$A'(\xi)\frac{\partial \xi}{\partial t} = \frac{c'(t)}{c(t)}. \tag{96}$$

By equation (95), however, $A'(\xi) = F(\xi) - G(\xi)$, and an appeal to equations (74) and (94) discloses that

$$\frac{c'(t)}{c(t)} = \mu. \tag{97}$$

This equation can be immediately integrated to yield

$$c(t) = \nu e^{\mu t}, \tag{98}$$

where the integration constant ν is immaterial, as it can again be absorbed in the choice of our origin of the time. Inserting equation (98) into equation (95), we establish that

$$e^{A(\xi)} = \nu r e^{\mu t}, \tag{99}$$

which discloses that, in the present case,

$$\xi(r, t) = f(re^{\mu t}); \tag{100}$$

and, without loss of generality, we can again set $\xi \sim re^{\mu t}$.

The foregoing discussion demonstrates that, if our fundamental system (1)–(4) of partial differential equations is to be reducible to ordinary differential equations with ξ as the sole independent variable, the latter must be of the form

$$\xi = rt^{\lambda} \tag{101}$$

or

$$\xi = re^{\mu t}, \tag{102}$$

where the constants λ and μ must be determined by supplementary physical conditions of the problem under investigation. In particular, the reader can easily verify that the alternative form of ξ as represented by equation (102) is incompatible with a requirement that the total energy of the wave motion (or even a sum of the kinetic and thermal energies) be independent of the time (which is a definition of the blast wave). As we have seen in Section II of this paper, the form of ξ as represented by equation (101) can be reconciled with the assumption of a blast wave, provided that $\lambda = -\frac{4}{5}$. Thus, as long as the functions $U(\xi)$, $P(\xi)$, or $\Omega(\xi)$ are to be expressible in terms of ordinary differential equations, *the solutions of our fundamental system (1)–(4) investigated earlier in this paper represent the only possible type of progressing blast waves of our problem;* and, in addition, if the expanding field of flow is to be headed by a shock front characterized by a constant Mach number throughout all time, the structure of the undisturbed configuration is uniquely specified by equations (32) and (34).

THE ERUPTIVE PROMINENCE OF AUGUST 7, 1950*

HELEN W. DODSON AND ROBERT W. DONSELMAN
McMath-Hulbert Observatory, University of Michigan
Received January 8, 1951

ABSTRACT

The eruptive prominence of August 7, 1950, is shown to be associated with an active sunspot group and plage area. Spectra of the prominence indicate that the large opening in the prominence prior to and during the eruption was due to the absence of $H\alpha$ radiation and was not a result of wave-length displacement caused by high radial velocity. The velocities of the measured features varied in a similar way with time and ranged from 10 km/sec to an average maximum of 155 km/sec. A burst of 200 Mc solar radio noise occurred when the ascending prominence reached a height of 285,000 km.

I. ASSOCIATED DISK PHENOMENA

The eruption of the large arch that extended between latitudes 24° N. and 45° N. on the east limb of the sun on August 7, 1950, was of especial interest because of the repetitive aspect of the phenomenon and its association with an active sunspot area. Intercomparison of the cross-motions of the prominence with simultaneous radial velocities indicates that the prominence was not parallel to the limb of the sun but extended across the limb from the southeast to the northwest. The northern tip of the prominence was projected against the solar disk; the southern tip apparently emerged from behind the limb. This orientation, coupled with the details of $H\alpha$ spectroheliograms secured between August 7 and 17, indicates that on August 7 the eruptive prominence extended northwestward from a well-formed spot group which was just behind the limb. This spot group and its surrounding bright flocculus or plage area were centered in latitude 14° N. and crossed the central meridian early on August 16.

Relative positions of prominence and plage are shown on the composite map reproduced in Figure 1. The northern and southern tips of either a re-formed prominence or remnants of the old one can be seen on successive days as small dark filaments. The prominence material associated with the spot area again was active between August $15^d13^h50^m$ U.T. and August $16^d12^h15^m$ U.T., since the dark filaments corresponding to both the southern and the northern tips of the prominence had completely disappeared between spectroheliograms taken at these two times. The southern tip had re-formed by the seventeenth.

Examination of spectroheliograms taken during the preceding solar rotation reveals an earlier instance of activity in the neighborhood of the same plage area. Between July 18 and 19 a filament just north of the region disappeared. There were traces of its re-formation on July 21. The disappearance and re-formation of filaments in approximately the same location form an interesting, but not extremely rare, phenomenon.[1] It is here suggested that the eruptive prominence of August 7 was the limb manifestation of one of the repeated disappearances of the filament associated with this active solar region. A flare of importance 2, which was observed[2] in the spot group under consideration, occurred on August $15^d17^h45^m$ U.T., during the period in which the filament disappeared. In this connection it can be noted that the great flares of July 25, 1946, and May 10, 1949, were each followed in a matter of some hours by the disappearance of large, well-formed fila-

* Work supported in part by contract N6-onr-232-V with the Office of Naval Research.

[1] L. d'Azambuja, *Ann. Obs. Paris, Meudon*, 6, Part 7, 104, 1948.

[2] Observed at the High Altitude Observatory, Boulder, Colorado. CRPL-F75, 43, 1950. The flare was known to us only by telegraphic communication prior to the now included reference.

ments in their close, but not immediate, neighborhoods.[3] On the other hand, there is no evidence for significant flare activity before, or for magnetic disturbances after, the disappearance of the long filament on September 7, 1948.[4]

The spot group associated with the eruptive prominence of August 7, 1950, and with the repeatedly disappearing filaments in its neighborhood was located within the last large, bright plage area to cross the central meridian prior to the onset of the spectacular aurora and "very great" magnetic storm of August 19, 1950. This storm did not have a "sudden commencement."[5] It may therefore have been one of those geomagnetic disturbances thought to be associated with a stream of particles ejected more or less continuously from the sun.

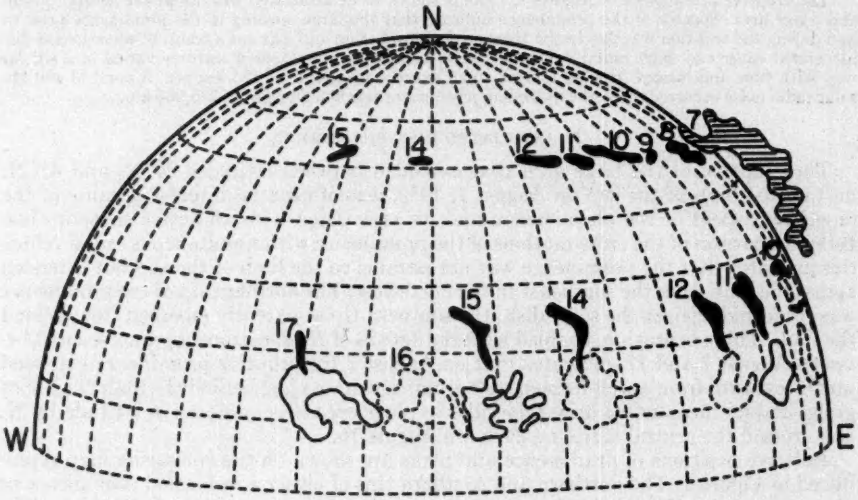

FIG. 1.—Composite map of northern hemisphere of sun, showing relative positions of eruptive prominence and associated dark filaments and bright plage area, August 7–17, 1950 (no observations for Aug. 13).

II. PRIMARY MOTIONS, RADIAL VELOCITIES, AND SPECTRA

More than 450 spectroheliograms and 225 series of *Hα* spectra were taken of the eruptive prominence of August 7, 1950, with the 50-foot solar tower and the Stone spectroheliograph of the McMath-Hulbert Observatory. The prominence first appeared as a well-defined continuous arch lying between latitude 24° and 45° N., with faint streamers extending as far north as latitude 60° (see Fig. 2). By 16^h00^m U.T. a crescent-shaped opening, which penetrated almost halfway through the prominence, had developed in latitude 35°. *Hα* spectra of the prominence taken at this time and later show clearly that this apparent break in the prominence was not an instrumental effect due to velocity displacements. The spectra indicate that *Hα* radiation had become very weak or was entirely absent in this part of the prominence (see spectroheliogram and spectra for 17^h59^m U.T. in Fig. 3).

[3] R. Servajean and G. Olivieri, *Bull. Soc. Astr. France*, **60**, 215, 1946; H. W. Dodson, *Ap. J.*, **110**, 382, 1947.

[4] H. W. Dodson and R. R. McMath, *Pub. A.S.P.*, **60**, 366, 1948.

[5] Information regarding magnetic storm was made available through CRPL of National Bureau of Standards.

The prominence began to rise very slowly. The motion was detectable as early as 1630 U.T. but remained less than 10 km/sec until 1730 U.T. The "opening" or break increased in size until it effectively divided the arch into two parts—a northern and a southern branch. The southern branch rose slightly ahead of the northern one and its lower portion faded rapidly. The upper part remained relatively bright and was measured to a height of 300,000 km. The radial velocity of this ascending southern branch was negative. At 1732 U.T. it ranged in value from −40 km/sec near the chromosphere to −5 km/sec or 0 km/sec near the top of the arch. At 1842 U.T. the radial velocity of feature *B* had increased to −50 km/sec.

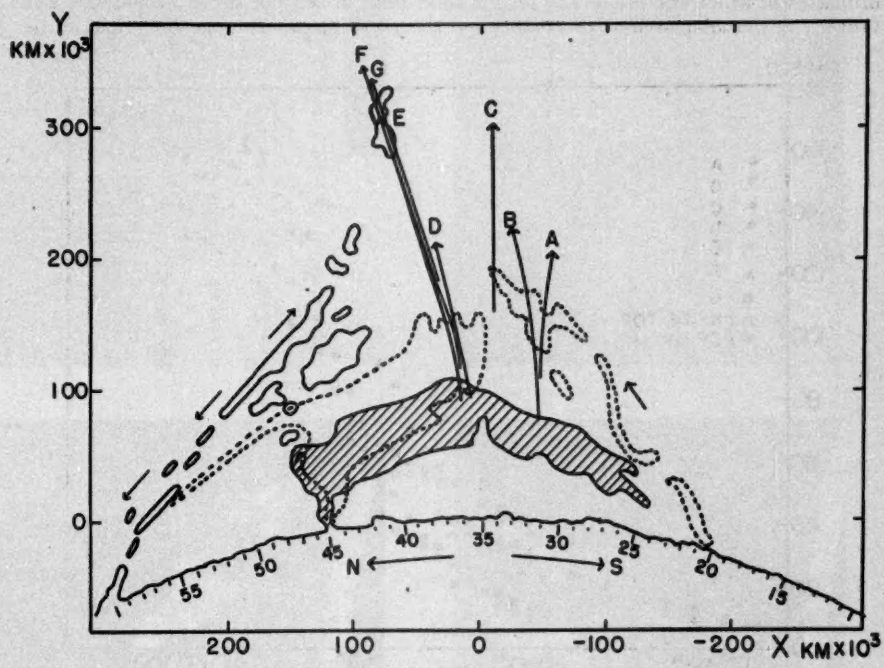

FIG. 2.—Schematic drawing of prominence and trajectories of measured features for 1554 U.T. (*shaded*), 1818 U.T. (*dotted*), and 1854 U.T. (*full line*).

The motion of the northern branch of the prominence was more complex. Within the portion of this branch lying south of latitude 45° N., the motion was principally one of ascent, with large positive radial velocities which at times, and in certain regions, exceeded +80 km/sec. Spectra taken with tangential slits of this part of the prominence showed tilted lines (see spectra for 18^h42^m in Fig. 4). North of latitude 45° the motion of the prominence was principally downward into a region in 60° N. latitude. In this part of the northern branch, the radial velocity was negative, with values of the order of −40 km/sec.

The effect of radial-velocity displacements on the apparent form and intensity of the prominence can be detected in the northern branch through comparison of the spectra and spectroheliograms for 18^h42^m in Figure 4. The large positive radial velocities present at this time on the northern border produced an apparent cut-off well within the con-

fines of the prominence as determined by the extent of the spectrum lines. This emphasizes the fact that, even with slits or filters of wide band pass, there is danger of a false intensity distribution on the spectroheliogram.

III. CROSS-MOTIONS

Near the center of the arch and at the tips of the two ascending branches, the radial velocities were relatively small. Therefore, for these regions, the cross-motions shown by the spectroheliograms can be considered as representative of the space motions of the gases. Measurements of such motions have been made in a system of rectanguiar coordinates in which the origin was on the solar limb in latitude 35° N., the x-axis was tangent to the solar limb at this point, and the y-axis passed through the origin in the

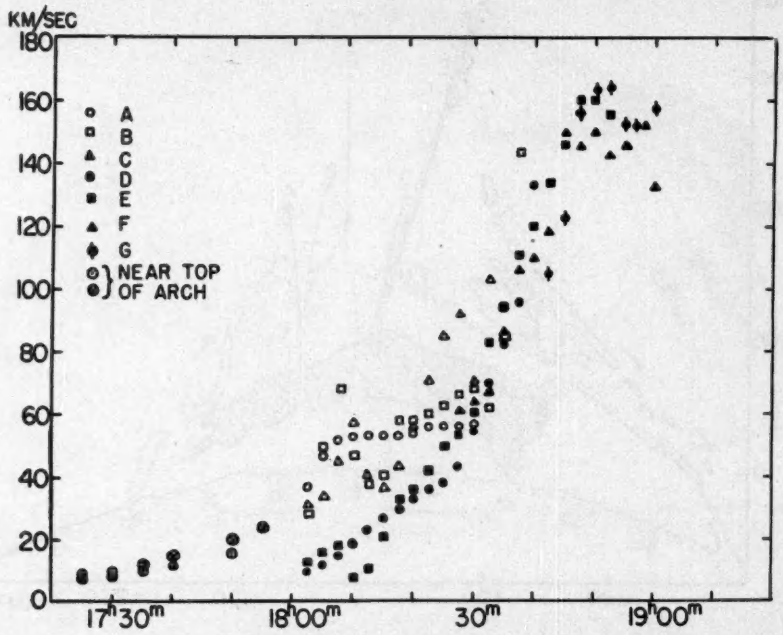

FIG. 3.—Plot of velocity versus time for measured features of eruptive prominence of August 7, 1950

direction of the radius of the apparent solar disk. Seven features were measured, three in the southern and four in the northern branch. The tip of the southern branch rose almost radially along an essentially linear trajectory. For the tip of the northern branch, the initial rise was nearly radial and later became a linear path inclined about 20° from the radial direction.

In general, the spectroheliograms were taken at intervals of 30 seconds. The x- and y-co-ordinates were measured for each feature on each spectroheliogram and were plotted versus time. Velocities in the x- and y-directions, V_x and V_y, were determined at intervals of 2½ minutes from slopes of curves drawn through the mean of the plotted points. The values so determined are recorded in Table 1. Velocities in the xy-plane, V_{xy}, were computed for the corresponding times and are recorded in Table 1 and plotted in Figure 3.

Between 17^h30^m and 18^h00^m the arch was rising with a velocity that increased from 10 km/sec to slightly more than 20 km/sec. At about 18^h00^m, nodule A in the southern branch began to move rapidly and by 18^h10^m had a velocity of 53 km/sec. Motions in

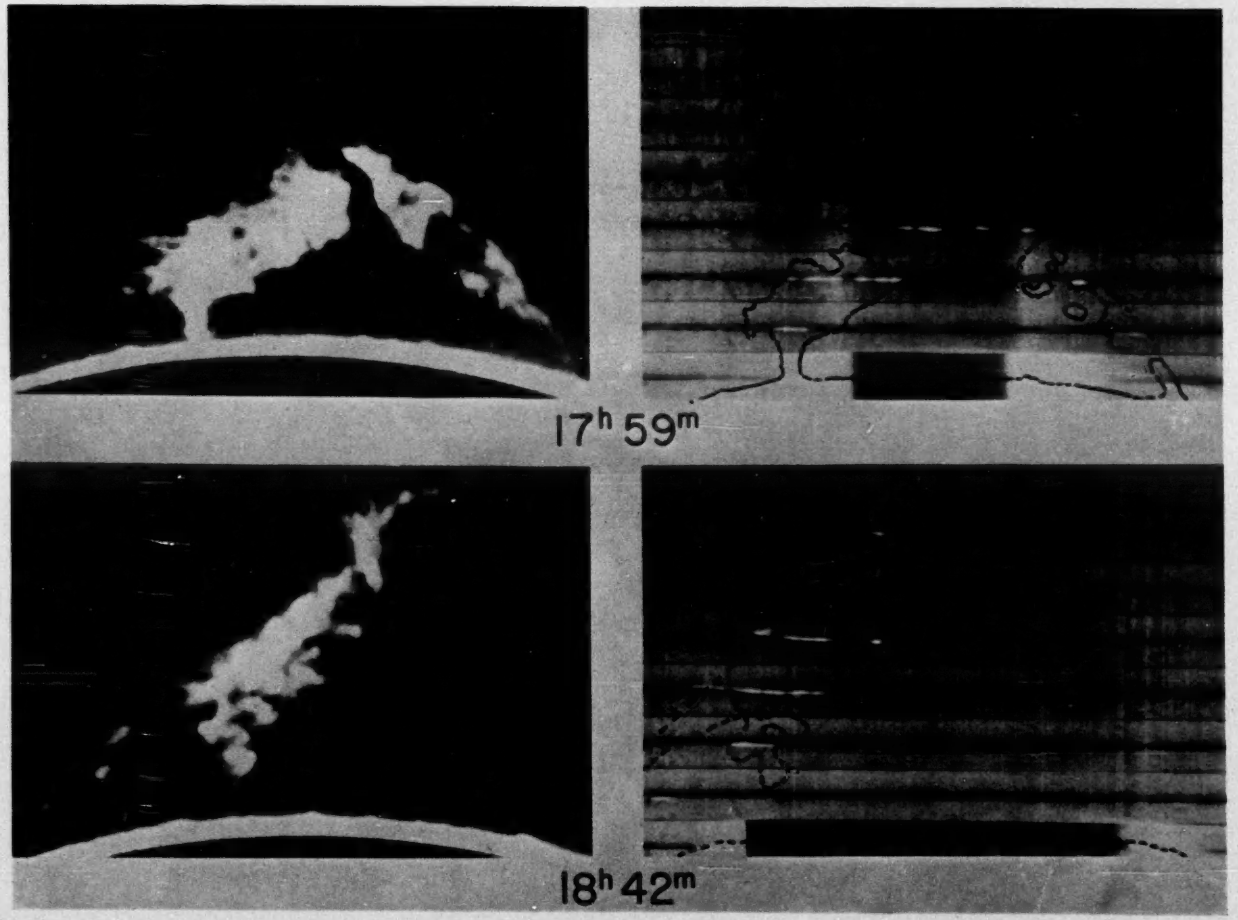

FIG. 4.—Spectroheliograms and concomitant series of $H\alpha$ spectra for the eruptive prominence of August 7, 1950

TABLE 1

POSITION AND VELOCITY FOR MEASURED FEATURES OF PROMINENCE

TIME U.T.	X (KM×10³)	Y (KM×10³)	V_x (KM/SEC)	V_y (KM/SEC)	V_{xy} (KM/SEC)	X (KM×10³)	Y (KM×10³)	V_x (KM/SEC)	V_y (KM/SEC)	V_{xy} (KM/SEC)	X (KM×10³)	Y (KM×10³)	V_x (KM/SEC)	V_y (KM/SEC)	V_{xy} (KM/SEC)
	A					*B*					*C*				
18ʰ02ᵐ5	−47	107	0	37	37	−45	81	5	30	30	−12*	159	0	31	31
05	−47	113	0	47	47	−44	88	5	48	48	−12	164	0	34	34
07.5	−47	121	0	52	52	−43	99	4	68	68	−12	170	0	45	45
10	−48	129	0	53	53	−43	110	5	47	47	−12	178	0	57	57
12.5	−48	137	0	53	53	−42	116	5	38	38	−12	185	0	40	40
15	−48	145	0	52	52	−41	122	5	40	40	−12	191	0	37	37
17.5	−48	153	0	53	53	−41	131	5	58	58	−12	197	0	43	43
20	−48	161	−11	53	54	−40	140	5	56	56	−12	204	0	56	56
22.5	−50	169	−14	54	56	−39	150	5	60	60	−12	214	0	71	71
25	−52	177	−14	54	56	−39	159	5	63	63	−12	226	0	85	85
27.5	−54	185	−14	54	56	−38	169	5	66	66	−12	240	0	92	92
30	−56	194	−14	56	57	−37	180	11	68	69	−12	253	0	70	70
32.5	.....		.....			−34	189	19	58	61	−12	266	0	103	103
35	.....		.....			−30	198	32	79	85	−12	286	.....		
37.5	.....		.....			−23	222	73	124	144	.....		.....		
	D					*E*									
02.5	10	96	0	10	10	16	90	0	12	12					
05	10	98	1	12	12	16	92	0	16	16					
07.5	10	100	1	14	15	16	95	0	17	17					
10	11	102	2	19	19	16	97	1	8	8					
12.5	11	105	2	22	23	16	98	2	10	11					
15	11	109	4	26	27	17	100	4	20	21					
17.5	12	113	4	30	30	17	104	5	31	32					
20	12	118	5	33	34	18	109	5	36	36					
22.5	13	123	6	36	36	20	115	15	39	42					
25	14	128	7	38	38	23	121	22	45	50					
27.5	15	134	8	42	43	26	128	21	49	54	*F*				
30	17	142	10	55	56	29	136	7	60	61	19	118	0	61	61
32.5	18	151	15	68	70	29	148	2	82	83	19	128	0	64	64
35	21	162	22	78	82	31	161	29	89	94	19	138	1	67	67
37.5	26	175	36	89	96	35	175	29	107	111	22	148	40	75	85
40	32	191	48	124	133	40	193	31	116	120	29	161	43	96	106
	G										35	176	40	103	110
42.5	38	184	38	98	105	45	212	37	129	134	41	193	33	114	119
45	44	200	39	116	123	51	231	46	139	146	46	215	41	144	150
47.5	50	220	42	150	156	59	254	53	150	160	55	235	64	131	146
50	56	243	43	157	163	67	277	58	150	161	65	256	57	139	150
52.5	63	267	47	157	164	76	301	60	144	156	71	276	43	136	143
55	71	290	52	144	153	.....		.....			78	298	46	139	146
57.5	79	311	61	139	152	.....		.....			85	319	46	144	152
19 00	89	332	75	139	158	.....		.....			91	339	47	124	133

* Feature *C* was the top of the ascending southern branch. The x-co-ordinate was poorly defined. It did not change systematically or significantly throughout the period of measurement.

the northern branch were still low but were beginning to increase. By 18^h30^m velocities in both branches had increased to about 60 km/sec, and in the following 20-minute interval they rose to an average of 155 km/sec. During the last 10 minutes for which the features were considered measurable on our records (1850–1900 U.T.) velocities either remained constant at this maximum value or decreased slightly.

IV. ACCELERATIONS

Figure 3 shows that, in general, the velocities of all the measured features varied in a similar way with time and that the slope of a curve drawn through their mean values would give an indication of the magnitude of the acceleration along the trajectory. Throughout the early part of the activity of the prominence, the accelerations were small and increased slowly. Between 1830 and 1850 U.T. the changes in velocity indicated a constant acceleration outward along the trajectory of the order of 0.08 km/sec^2, a value which is slightly less than one-third the magnitude of solar gravity. Since the trajectories during this period were essentially linear and the radial velocities small, the above values of "acceleration along the trajectory" in the xy-plane should be approximately equal to

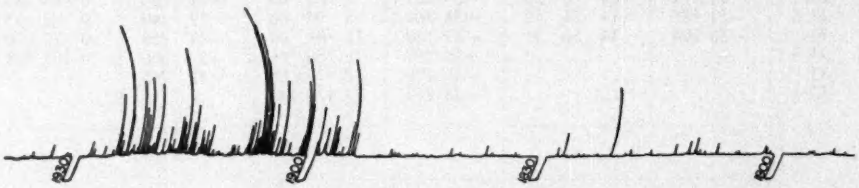

FIG. 5.—Copy of portion of 200-Mc radio-noise tracing for August 7, 1950, secured by School of Electrical Engineering, Cornell University.

the magnitude of the space acceleration. The similarity in the values of the velocities and accelerations for this eruptive prominence to those of feature E, which was similarly placed in the eruptive prominence of September 27, 1948, should be noted.[6] After 1850 U.T. the accelerations of the measured features were either zero or negative.

V. SOLAR RADIO OBSERVATIONS

During recent months it has been our privilege at the McMath-Hulbert Observatory to examine a number of the continuous records of 200 Mc solar radio noise secured by the School of Electrical Engineering at Cornell University. Theoretical studies indicate that these long-wave-length radiations cannot escape from the sun unless they originate from heights far above the chromosphere. It was therefore of interest to note the occurrence of a well-defined series of bursts beginning at 1854 U.T. on the 200 Mc record for August 7, 1950 (see Fig. 5). It was at this time that the principal ascending material of the eruptive prominence had reached a height of the order of 285,000 km and the velocity of ascent had begun to diminish. This coincidence of the onset of the radio bursts with the arrival of moving prominence material at a height of 0.4 solar radii above the chromosphere is here pointed out, since it may be of interest in this field in which concurrent solar observations are all too few.

The writers wish to acknowledge with gratitude the assistance of all members of the staff of the McMath-Hulbert Observatory. It is only through their co-operation that studies of this nature are possible. They also wish to thank McGregor Fund of Detroit for their continued support of the work of the Observatory.

[6] H. W. Dodson and E. Weston, "A Study of the Eruptive Prominence of 1948 September 27," *M.N.*, 110, 15, 1950.

THE SOLAR CURVE OF GROWTH FOR LINES OF *Cr* I

ALLAN R. SANDAGE AND ARMIN J. HILL
MOUNT WILSON AND PALOMAR OBSERVATORIES
CARNEGIE INSTITUTION OF WASHINGTON
CALIFORNIA INSTITUTE OF TECHNOLOGY
Received December 5, 1950

ABSTRACT

Curves of growth for solar *Cr* I lines have been constructed from laboratory *gf*-values. The displacements of these curves as a function of excitation potential give an unexpectedly low excitation temperature of 3790° ± 20° K. The final composite curve of growth agrees well with Wrubel's theoretical curve. A fit to the theoretical curve gives a total velocity of 2.3 km/sec, a turbulent velocity of 1.9 km/sec, and a damping factor of $\Gamma/\gamma_{el} = 12.6$. Evidence from *Cr* I lines whose lower state is of odd parity suggests that the parity effect found in *Fe* is due to selective pressure broadening. Adopting Estabrook's absolute *f*-values to calibrate Hill's relative scale, we find 10^{16} *Cr* I atoms per gram of solar matter. Correction for the degree of ionization gives, for the total number of *Cr* atoms per gram of material, $\log N_t = 17.24$. A comparison with Brown's meteoritic abundances is made.

I. OBSERVATIONS

This investigation is concerned with the solar curve of growth for lines of *Cr* I. The relative gf_r-values for *Cr* I have been reported by A. J. Hill in a recent paper.[1] Equivalent widths for approximately two hundred lines were measured in the Utrecht *Photometric Atlas of the Solar Spectrum* between wave lengths λ 3430 and λ 5409. No pronounced systematic difference between our measurements and those of C. W. Allen[2] was found; the mean of the two equivalent-width determinations was therefore adopted.

II. COMPOSITE CURVE-OF-GROWTH AND TEMPERATURE DETERMINATION

The lines were separated into nine groups having excitation potentials of 0.00, 0.937, 0.980, 2.530, 2.700, 2.880, 3.000, 3.100, and 3.400 volts. A curve of growth was obtained for each group by plotting $\log W/\lambda$ against $\log \eta_f + (5040/T)\chi$, where

$$\log \eta_f + \frac{5040}{T}\chi = \log gf_r\lambda + \log \bar{\kappa}/\kappa_\nu + \Delta \log \eta_0 \,. \qquad (1)$$

The factor $\bar{\kappa}/\kappa_\nu$, which corrects for the wave-length variation of the continuous absorption coefficient, was taken from G. Münch's observational determination.[3] To reduce all lines to a single curve, a further correction, $\Delta \log \eta_0$, is required. This correction has been tabulated for the Milne-Eddington model by M. H. Wrubel.[4] All lines were reduced to a single curve whose darkening coefficient was $B^0/B^1 = \frac{2}{3}$.

Each separate curve of growth, corresponding to a given excitation potential, was displaced horizontally until the best possible fit to a composite curve was obtained. In all cases the displacement $\Delta \log \eta_f$, given in Table 1, was well determined.

The plot of $\Delta \log \eta_f$ against excitation potential is shown in Figure 1. The straight line was fitted to the points by least squares. Since $\Delta \log \eta_f = (5040/T)\chi$, the slope of 1.331 corresponds to a mean temperature of 3790° ± 20° K. There is a slight indication that the excitation temperature increases with excitation potential. This effect would be

[1] *J. Opt. Soc. America*, in press.

[2] *Mem. Commonwealth Solar Obs.*, Vol. 1, No. 5, 1934; Vol. 2, No. 6, 1938.

[3] *Ap. J.*, **102**, 385, 1945. [4] *Ap. J.*, **111**, 157, 1950.

expected if the lines of higher excitation potential were preferentially formed deeper in the solar atmosphere. The very low temperature of 3790° is rather surprising. The solar temperature determined from the relative gf_r-values depends directly upon the temperature, T_f, of the electric furnace in which the gf_r-values were determined. The error introduced into the solar temperature by an error, ΔT_f, in the furnace is

$$\Delta T_\odot = -\left(\frac{T_\odot}{T_f}\right)^2 \Delta T_f , \tag{2}$$

where ΔT in each case is the correction to be applied to the observed temperature to obtain the true temperature.

TABLE 1

DISPLACEMENT OF CURVES OF GROWTH FOR LINES OF DIFFERENT EXCITATION POTENTIAL

E.P.	Δ log ηf	No. Lines	E.P.	Δ log ηf	No. Lines	E.P.	Δ log ηf	No. Lines
0.000.....	0.10	7	2.530.....	3.54	52	3.000....	4.16	18
0.937.....	1.31	11	2.700.....	3.82	16	3.100....	4.22	18
0.980.....	1.40	40	2.880.....	3.95	26	3.400....	4.46	8

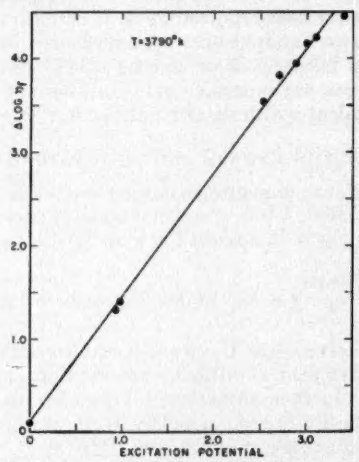

FIG. 1.—Displacements of the curve-of-growth segments as a function of excitation potential

To explain an error of the order of 1000° K in the solar temperature, a systematic error of nearly 400° K in the furnace temperature is required. So large an error is very unlikely. It is therefore probable that the explanation of the apparent low temperature lies in the solar atmosphere. The excitation temperature is a parameter which tells how the various excited atomic energy levels are populated. Only in strict thermodynamic equilibrium is it expected that this parameter should correspond to the radiation temperature. The low temperature of 3790° could be explained if some mechanism were found which would prevent the *Cr* I atom from populating its upper states at a rate cor-

responding to the radiation temperature or which would overpopulate the lower states. The excitation temperatures from *Ti* and *Fe* are also lower than those expected from equilibrium considerations, although not to such an extent as is exhibited by *Cr*. Thus any mechanism proposed must work for *Ti* and *Fe* as well as for *Cr*. The mechanism must also explain why the excitation temperature from *V* I agrees with that expected from a model solar atmosphere.[5] The suggestion of A. Unsöld and O. Struve[6] that turbulence could explain the temperature anomaly appears not to be applicable here, since there is no evidence that the turbulence is a function of excitation potential in *Cr* I.

A composite curve of growth was constructed by shifting the individual segments horizontally by an amount $\Delta \log \eta_f = (5040/3790)\chi$. Figure 2 shows the resulting curve, using only the fifty best lines with wave lengths greater than 4000 A and with gf_r-values of weight *Ar*, *A*, *Br*, or *B*. This group comprises slightly less than 30 per cent of the available data. When the remaining hundred and fifty lines are plotted, the general shape

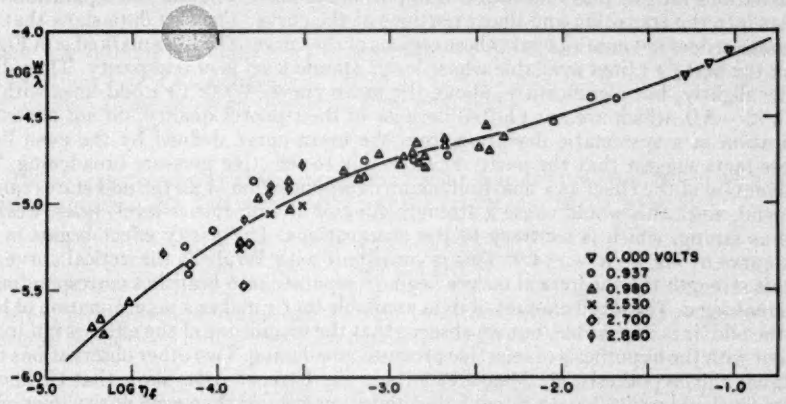

FIG. 2.—The composite curve of growth for *Cr* I. Only the best unblended lines with gf_r-values o high weight are plotted.

of the curve is preserved, but the scatter becomes greater, especially below $\log W/\lambda = -5.0$. This increased scatter is due (1) to the poorer quality of the gf_r-values of weight *C*, *D*, and *W* and (2) to the greater percentage of inaccuracy in the solar equivalent widths of weak lines. The solid curve drawn in Figure 2 is Wrubel's theoretical Milne-Eddington curve for $B^0/B^1 = \frac{2}{3}$ and with the log of the ratio of the damping to Doppler half-widths of $\log a = -1.7$. The agreement is quite satisfactory, with the possible exception of the lines marked ϕ situated near $\log W/\lambda = -4.9$. These lines will be discussed in the following section. The best fit to the theoretical curve was obtained with the following parameters:

$$\log a = -1.7 , \tag{3}$$

$$\log \frac{W}{b} - \log \frac{W}{\lambda} = 5.12 \pm 0.02 , \tag{4}$$

$$\log \eta_0 - \log \eta_f = 4.12 . \tag{5}$$

This value of $\log a$ corresponds to a damping factor, $\Gamma/\nu = 2.0 \times 10^{-4}$, which is slightly less than that found by K. O. Wright[7] (Γ is expressed in circular frequency units

[5] A. R. Sandage, *Ap. J.*, 111, 575, 1950.

[6] *Ap. J.*, 110, 455, 1949.

[7] *Ap. J.*, 99, 249, 1944.

and is the total half-intensity width of the collisional plus radiation damping coefficient). This value of log a gives $\Gamma/\gamma_{el} = 12.6$, while equation (4) gives $V = 2.3$ km/sec for the total random velocity. If we adopt a kinetic temperature of 5000° K, we find a turbulent velocity of 1.9 km/sec, in general agreement with the value found by others. There is no evidence for a change of turbulent velocity with excitation potential.

III. THE PARITY EFFECT

The connection between the present *Cr* I data and the parity effect, first reported by W. W. Carter[8] for *Fe* I, will be discussed in this section. Carter found that certain lines whose lower atomic state was of odd parity were stronger in the sun than lines from lower even levels of the same gf-value. His data show the separation of the odd and even lines that lie on the damping portion of the *Fe* curve of growth. To choose between possible explanations for this phenomenon, it is important to know whether the separation continues into the transition and linear portions of the curve. The *Cr* I data show that the separation does not continue into these regions of the curve. The lines marked ϕ in Figure 2 are the best *Cr* I lines available whose lower atomic level is of odd parity. These lines do lie slightly, but significantly, above the mean curve. Weak *Cr* I odd lines with log $W/\lambda < -5.0$, which are not plotted because of their poorer quality, do not show any indication of a systematic deviation from the mean curve defined by the even lines. These facts suggest that the parity effect is due to selective pressure broadening. The explanation of the effect as a non-Boltzmann overpopulation of all the odd states cannot be valid, since this would cause a strengthening of all odd (lower-level) lines, weak as well as strong, which is contrary to the observations. The parity effect begins in the *Cr* I curve at log $W/\lambda = -4.9$. This is consistent with Wrubel's theoretical curve, for at this strength the theoretical curves begin to separate into branches corresponding to different log a. The small amount of data available for *Cr* makes a determination of log a for the odd lines impossible, but we observe that the magnitude of the effect is not inconsistent with the hypothesis of selective pressure broadening. Two other observations tend to favor this hypothesis. (1) Measurements in the Utrecht *Atlas* show that *Cr* lines of lower-level odd parity have a larger half-intensity width (h) than even parity lines of the same excitation potential. This is especially true for the lines arising from the z^7P° lower level, where, in the mean, $h/\lambda = (237 \pm 8) \times 10^{-7}$ (9 lines). For even parity lines arising from the a^3P and a^3H levels, $h/\lambda = (210 \pm 3) \times 10^{-7}$ (20 lines). (2) The distribution of the odd and even lines among the pressure classes given in the revision of Rowland's table of solar wave lengths[9] again suggests the selective-broadening explanation for the parity effect. These pressure classifications were assigned by early workers on the basis of the degree of asymmetry and pressure shifts exhibited by the lines under laboratory conditions. The larger pressure effects occur in the later pressure classes. The correlation between the pressure class and the parity of the lower state of the line is good. All *Cr* I lines listed in the Revised Multiplet Table[10] with known pressure class were used. For the even lower-level lines between 2.5 and 3.5 volts E.P., 2 per cent are of class a, 75 per cent class b, and 23 per cent class d. For odd-level lines of nearly the same excitation (E.P. = 2.9–3.4 volts) there are no class a lines, 22 per cent class b, and 78 per cent class d. Between 3.8 and 4.8 volts excitation, even (lower) levels are distributed, with 2 per cent class a, 42 per cent class b, 56 per cent class d, while odd levels in the excitation range 3.8–4.2 volts show no class a, 22 per cent class b, and 78 per cent class d. If the laboratory pressure classification is significant, this pressure-class distribution suggests that even atomic levels are more susceptible to pressure broadening. The even

[8] *Phys. Rev.*, **76**, 962, 1949.

[9] C. E. St. John *et al.*, *Pub. Carnegie Inst. Washington*, No. 396, 1928.

[10] C. E. Moore, *Contr. Princeton U. Obs.*, No. 20, 1945.

levels must have the larger collisional cross-section, since it is the upper level of a line which is important in the broadening process.

It is possible to estimate roughly the ratio of the collisional cross-section of the upper-even to upper-odd states of the same excitation potential from Carter's *Fe* curve of growth with the assumption that the collisional broadening is in the upper state only. A fit of Wrubel's theoretical curve to the odd (lower) *Fe* I lines gives $\log a \sim 1.5$, which corresponds to $\Gamma/\gamma_{cl} = 20.0$. Even lines give $\log a = -1.7$. We denote the mean-square radius of the atom in the upper state of the broadened line by $\overline{R^2}$, and the radius of the effective cross-section for broadening collisions by σ. With Weisskopf's approximate quantum-mechanical theory for the cross-section, it can be shown[11] that

$$\frac{\sigma_e}{\sigma_o} = \left[\frac{\overline{R_e^2}}{\overline{R_o^2}}\right]^{1/5} = \left[\frac{\Gamma_e - \gamma_{cl}}{\Gamma_o - \gamma_{cl}}\right]^{1/2}, \tag{6}$$

where the subscripts o and e refer to the parity of the upper state. With the observed value of $\log a$ for *Fe* I, equation (6) gives $\sigma_e/\sigma_o = 1.3$ and $\overline{R_e^2}/\overline{R_o^2} = 3.4$. These are not impossible values, although they seem somewhat high.

IV. ABUNDANCE

The abundance of *Cr* I atoms per gram of solar matter may be obtained with the results of equation (5). The optical depth at the center of a line is given by

$$\eta_0 = \frac{\sqrt{\pi}e^2 g f_A \lambda N_0 10^{-(5040/T)\chi}}{m c \kappa_\nu b(T) V}, \tag{7}$$

where f_A is the absolute f-value and N_0 is the total number of *Cr* I atoms per gram of solar material. Equation (1) together with equation (7) gives

$$\log \frac{N_0}{\bar{\kappa}} = \log \eta_0 - \log \eta_f - \log \frac{\sqrt{\pi}e^2}{mc} + \log \frac{f_R}{f_A} + \log V b(T). \tag{8}$$

We have disregarded the $\Delta \log \eta_0$ correction term in equation (1), since this merely corrects individual lines to a single curve of growth so that a fit to the theoretical curve is possible. The partition function based on our excitation temperature of 3800° is 8.5. F. B. Estabrook[12] has determined experimentally the absolute f-values for three *Cr* I resonance lines—λλ 4290, 4275, and 4254—by the method of total absorption. This required a knowledge of the vapor pressure of *Cr* I. Uncertainties in the vapor-pressure data are so serious that the ratio f_R/f_A is rather poorly determined. The best value which Estabrook suggests is $\log f_R/f_A = 4.07$. Adopting this value together with equation (5) permits the evaluation of equation (8) to give

$$\log \frac{N_0}{\bar{\kappa}} = 16.30. \tag{9}$$

The total number of *Cr* atoms per gram is now obtained by applying the Saha equation to equation (9) with the known values of the ionization temperature and electron pressure. Strömgren's[13] model solar-atmosphere tables give p_e and T at several optical depths for various values of A (H to metal ratio). Strömgren's model atmosphere was adopted in preference to Münch's[14] more accurate model because we wish to compare our *Cr*

[11] Cf. B. Strömgren, *Pub. Copenhagen Obs.*, No. 127, eqs. (16)–(19),

[12] Thesis, California Institute of Technology, 1950.

[13] *Pub. Copenhagen Obs.*, No. 138. [14] *Ap. J.*, **106**, 217, 1947.

abundance with Strömgren's values for the *Ca*, *K*, *Mg*, and *Na* abundances (Table 2) which were obtained with his atmospheric model. The N_t so derived is independent of A and the electron pressure. It depends only upon the ionization temperature. This is because, by the Saha equation, $N_1/N_0 = (1/p_e)f(T)$. However, we know $N_0/\bar{\kappa}$ from the curve of growth (eq. [9]). (In the present case $N_t \sim N_1$.) Hence $N_t \sim (N_0/\bar{\kappa})(\bar{\kappa}/p_e)f(T)$. But $\bar{\kappa}/p_e$ is independent of A, since $\bar{\kappa} \sim p_e$ and hence $\bar{\kappa}/p_e$ is a constant. Therefore, N_t is independent of the abundance ratio of H to the metals and of the electron pressure adopted.

From other considerations it has been found that a representative point of $\tau = 0.25$ well represents the mean pressure, temperature, and opacity relevant to the production of weak lines of the neutral metals, with excitation potential of 0–3 volts. From Strömgren's model atmosphere at $\tau = 0.25$ we find, by application of the Saha equation to equation (9), that

$$\log N_t = 17.24 . \tag{10}$$

We denote by ζ the abundance ratio (by number) of H to *Cr*. Adopting the H to *He* ratio of 10 to 1 reported by Mrs. Harrison[15] gives a mean molecular weight in the solar

TABLE 2

SOLAR ABUNDANCE RATIOS COMPARED TO METEORITES

Element	log N_t Solar	*Cr*/Metal Solar	*Cr*/Metal Meteorites	Element	log N_t Solar	*Cr*/Metal Solar	*Cr*/Metal Meteorites
Cr	17.24	1	1	*Ca*	18.0	0.17	0.14
Na	17.7	0.35	0.2	*Mg*	19.3	0.009	0.011
K	17.1	1.4	1.4				

atmosphere of $\bar{\mu} = 1.26$. The log of the number of H atoms per gram of material, then, is $\log 1/\mu m_H = 23.68$. Hence the H to *Cr* ratio is $\log \zeta = 6.44$ (if we adopt Münch's model atmosphere, the values are: $\log N_t = 17.41$ and $\log \zeta = 6.27$).

To compare the *Cr* abundance with other cosmic abundance data, it is convenient to obtain the ratios of *Cr* to other metals from solar data. Strömgren[11] has obtained solar abundances for *Na*, *K*, *Ca*, and *Mg*. Table 2 gives his values, together with the abundance ratios with *Cr*. Harrison Brown[16] has compiled the most recent data on the abundance of nuclear species, obtained mostly from meteoritic sources. The meteoritic abundance ratios of these same metals from Brown's compilation are also given in Table 2. The solar and meteoritic abundances all agree within a factor of 2.

There are two uncertainties in the *Cr* abundance data derived in this investigation: (1) Estabrook's absolute calibration of the f-values is of low weight because of vapor-pressure uncertainties, and (2) the representative point of $\tau = 0.25$ at which to choose the ionization temperature may be incorrect. However, the close agreement of the *Cr* abundances with meteoritic data indicates, if the assumption of uniform cosmic abundance is accepted, that these sources of error are small.

We wish to thank Dr. J. L. Greenstein and Dr. R. B. King for offering helpful suggestions during this investigation.

[15] *Ap. J.*, **108**, 310, 1948.

[16] *Rev. Mod. Phys.*, **21**, 625, Table 3, 1949.

A SEARCH FOR He^3 IN THE SUN

JESSE L. GREENSTEIN
MOUNT WILSON AND PALOMAR OBSERVATORIES
CARNEGIE INSTITUTION OF WASHINGTON
CALIFORNIA INSTITUTE OF TECHNOLOGY
Received January 3, 1951

ABSTRACT

Nuclear processes in the sun might produce an appreciable abundance of the He^3 isotope if the proton-proton reaction ended at He^3. The chromospheric wave lengths, observed at eclipses, and accurate wave lengths of a few lines observed without eclipse or in absorption are compared in Table 2 with the isotope shifts measured at the Argonne National Laboratory. No evidence is found for the existence of He^3. The ratio determined from the shifts and from the absence of certain lines is $He^3/He^4 \approx 0.02 \pm 0.03$.

NUCLEAR PROCESSES INVOLVING He^3

Recent theoretical investigation has suggested that the proton-proton reaction may be an important source of nuclear energy in the sun. The p-p reaction has recently been studied by L. H. Aller in the late dwarfs[1] and, after a suggestion by Bethe and Salpeter, it was reinvestigated by W. A. Fowler and B. Strömgren. Numerical calculations of the rate of the p-p reaction in the sun have been made by I. Epstein.[2] He finds that the p-p reaction produces more energy than the carbon cycle in solar models which have been computed on the basis of the carbon cycle. If more detailed computations show that the p-p reaction is the dominant one, an appreciable concentration of He^3 might be predicted. The cycle of successive proton captures is

$$H^1 + H^1 \rightarrow D^2 + e^+ + \nu\,, \tag{1}$$

$$D^2 + H^1 \rightarrow He^3 + \gamma\,. \tag{2}$$

In these equations, the symbol ν represents a neutrino and γ a quantum. Two possible steps then exist:

$$He^3 + H^1 \rightarrow He^4 + e^+ + \nu\,, \tag{3}$$

$$He^3 + He^3 \rightarrow He^4 + 2H^1\,. \tag{4}$$

A different type of process is

$$He^3 + He^4 \rightarrow Be^7 + \gamma\,, \tag{5}$$

with subsequent decay to Li^7 and then

$$Li^7 + H^1 \rightarrow 2He^4\,. \tag{6}$$

Process (1) is very slow and (3) may be nearly as slow. Processes (2) and (6) are very fast. Process (5) is slow because both nuclei carry two charges and the barrier penetration is small; it would operate only at high temperatures. Thus, unless processes (3) and (4) go rapidly, the concentration of He^3 in equilibrium with protons could be high. Since (3) is a beta-decay process, He^3 will have a life comparable to H^1. This investigation was made because approximate computation of process (3) by Dr. W. A. Fowler, of the California Institute of Technology, indicated that the abundance of He^3 might lie between 7 and 20 per cent of that of He^4. More recently the importance of reaction (4), $He^3 + He^3$, has

[1] *Ap. J.*, 111, 173, 1950. [2] *Ap. J.*, 112, 207, 1950.

been emphasized by Lauritsen and Fowler. It involves particle ejection, which occurs with high probability during collision. Lauritsen and Fowler predict that the ratio He^3/H is 4×10^{-5} by number of atoms. Since He/H is about 0.1, He^3/He^4 is 4×10^{-4}, and He^3 should be rare in the solar interior.

HELIUM LINES IN THE CHROMOSPHERE

The deviation from thermodynamic equilibrium increases in the outer layers of the sun and results in the appearance of some *He* I absorption lines and in strong *He* I (and some *He* II) emission lines in the chromosphere. Some of the *He* I emission lines can be observed without eclipse under favorable conditions. Babcock and Moore[3] have observed the strong infrared line λ 10830 and two weak components of λ 7065 in absorption. The intensity (about 5 NN) of λ 10830 is variable and is greatest at times near sunspots. Babcock and Moore also consider the possibility (their n. 55) that the strong solar line at λ 10123.90, intensity 8, may be *He* II. They doubt this identification because of the sharpness of the line, weakness near sunspots, and absence from the chromosphere. Chromospheric emission wave lengths have been measured during many eclipses by D. H. Menzel,[4] S. A. Mitchell,[5] and Davidson and Stratton.[6] Dispersions used range from 6 to 10 A/mm in the blue to 80 A/mm in the red. These measures were reduced by the

TABLE 1

NEW WAVE LENGTHS OF *He* I IN THE CHROMOSPHERE MEASURED BY H. W. AND H. D. BABCOCK

λ(⊙)	λ (Lab.)	Remarks
5875.69±0.03.....	75.618 (5) 75.650 (3) 75.989 (1)	Components of unresolved triplet
6678.20±0.05.....	78.149	Singlet
7065.22±0.04.....	65.188	Two components of unresolved triplet

various authors to the International System. An intercomparison of the published data reveals small systematic trends and accidental errors greater than ±0.05 A. Taken as a group, the eclipse measures provide about twenty wave lengths of helium emission lines in the chromosphere. With great kindness, Mr. H. D. Babcock and Dr. H. W. Babcock have measured and permit me to quote accurate wave lengths of three strong emissions observed without eclipse. The 150-foot tower gave spectra with dispersion 0.71 A/mm; the emission lines of the chromosphere are superposed on the continuum and absorption lines of the scattered sunlight, which provide the wave length scale. Table 1 gives their measured wave lengths. For λ 5875, I include the predicted relative intensities of the components. Table 2 contains a résumé of the data on *He* I lines. The first two columns give the mean measured wave length and the total weight of the measurement. Eclipse observations were given equal unit weight; the absorption lines and the lines in Table 1 were given weight 5; one or two units of weight were subtracted if the lines were blended. Blending is indicated by the symbol "b." The third column gives Δλ in units of 10^{-2} A, observed minus He^4 laboratory wave length. The fourth column gives the isotope shifts $\Delta\lambda_I$, He^3 minus He^4, in the same units. The fifth column gives the multiplet designation in abbreviated form; e.g., ^{3}SP is $2^3S-n^3P^o$.

[3] *Pub. Carnegie Inst. Washington*, No. 579, 1947.

[4] *Pub. Lick Obs.*, Vol. 17, Part I, 1931.

[5] *Ap. J.*, **105**, 1, 1947.

[6] *Mem. R. Astr. Soc.*, **64**, 105, 1927.

The eclipse wave lengths have been adjusted by the observers to be on the International scale, and the Einstein shift has been automatically removed in this process. The same is true of the observations of the chromosphere without eclipse. The absorption wave lengths, however, were measured with respect to the neon laboratory standard and were corrected only for radial velocity. The Einstein shift has been eliminated from the absorption wave lengths for use in Table 2.

I am deeply indebted to Dr. Mark Fred, of the Argonne National Laboratory, for communicating the isotope shifts before publication. They were measured by Fred,

TABLE 2

SOLAR WAVE LENGTHS AND ISOTOPE SHIFTS OF HELIUM LINES
(Unit = 0.01 A)

λ	Wt.*	Δλ	$\Delta\lambda_I$	Series	Notes
3187.71	(2) b	−03	+ 16	^{3}SP	
3354.49	(1)	−06	+ 16	^{1}SP	
3554.36	(1)	−05	+ 08	^{3}PD	
3587.32	(1)	+05	+ 08	^{3}PD	
3613.61	(1)	−03	+ 17	^{1}SP	
3634.24	(1) b	−01	+ 08	^{3}PD	
3704.98	(2) b	−04	+ 08	^{3}PD	
3819.70	(2) b	+08	+ 08	^{3}PD	
3867.59	(1) b	+10	+ 08	^{3}PS	
3964.72	(2) b	−01	+ 18	^{1}SP	
4009.27	(3)	00	+ 25	^{1}PD	
4026.26	(3)	+05	+ 08	^{3}PD	
4120.80	(1) b	−03	+ 07	^{3}PS	
4143.83	(1) b	+07	+ 26	^{1}PD	
4169.05	(1)	+08	+ 27	^{1}PS	
4387.91	(2) b	−02	+ 28	^{1}PD	
4471.51	(2)	+01	+ 07	^{3}PD	
4713.11	(2)	−05	+ 07	^{3}PS	
4922.03	(2)	+10	+ 33	^{1}PD	
5015.59	(1) b	−09	+ 21	^{1}SP	
5047.71	(1)	00	+ 34	^{1}PS	
5875.68	(6)	+04	+ 04	^{3}PD	
6678.18	(5) b	+03	+ 50	^{1}PD	
7065.22	(11)	+03	00	^{3}PS	1
7065.72	(5)	00	00	^{3}PS	2
7281.35	(1)	00	+ 55	^{1}PS	
10830.36	(5)	+05	+138	^{3}SP	3
		He II			
3203.32	(1) b	+16	+ 14	^{2}DF	4
4685.89	(2)	+11	+ 21	^{2}DF	
10123.87	(5)	+15	+ 45	^{2}FG	5

NOTES TO TABLE 2

* "b" indicates some blending.

1. Absorption line in disk. Emission in chromosphere.
2. Absorption line.
3. Absorption line; isotope shift so large that no wave-length shift to be expected in He^4 component.
4. Probably not *He* II. Blended strongly.
5. Absorption line. Probably not *He* II.

Tomkins, Brody, and Hamermesh[7] with a Fabry-Perot etalon. The sources contained the pure separated isotopes of He^3 and He^4 in an electrodeless discharge cooled to 80° K. The observed shifts range from +1.38 A for λ 10830 to moderate values for the singlet series (+0.55 to +0.16 A) and small values for most of the triplets (+0.08 to 0.00 A). The triplets, although complicated by blending, are included to permit discussion of a probable systematic shift of all *He* wave lengths in the sun. The laboratory wave lengths of He^4 are based on the *Revised Multiplet Table*.[8] Some of these have been measured interferometrically, including λ 10830. The mean wave lengths of unresolved triplets were predicted by weighting each component by the factor $(2J + 1)$. The partially resolved triplet at λ 7065 is simple; the infrared triplet includes the two components at λ 10830.34 and λ 10830.25, but probably not that at λ 10829.08. This satellite was seen resolved when λ 10830 was very strong.[9] *He* II exists in the chromosphere, but the chromospheric observations are inadequate. Absorption by λ 10124 of *He* II seems improbable in view of the 50.8-volt excitation required. Only λ 4686 emission seems certain and unblended; its wave length is given as 4685.83 A by Mitchell and 4685.95 A by Menzel. A large positive shift of +0.11 A exists if we adopt the blended normal wave length as 4685.78 A. This and the other adopted wave lengths of *He* II are predicted values; they have been kindly communicated by Mrs. Sitterly and are based on J. E. Mack's recomputation of the fine structure. The isotope shifts are computed from the change in the Rydberg constant. For λ 4686, $\Delta\lambda/\Delta\lambda_I \approx 0.5$; thus $\Delta\lambda$ is much too large to be explained as an isotope shift, and the shift may be due to pressure or Stark effects in disturbed regions of the chromosphere.

DISCUSSION

If the abundance ratio He^3/He^4 equals R and if the lines of the two isotopes blend without self-absorption or saturation, then

$$\Delta\lambda = \frac{R}{1+R}\,\Delta\lambda_I . \tag{7}$$

The *He* II lines and λ 10830 are omitted from the following discussion. It is obvious from Table 2 that $\Delta\lambda$ and $\Delta\lambda_I$ are only slightly correlated. Since $\Delta\lambda_I$ is accurately determined, the correct procedure is to make a least-squares solution and determine the probable error of the coefficients. This has been done, including the weight factors given in Table 2, with the result that

$$\begin{aligned} \Delta\lambda = {} & +0.013 && +0.016\Delta\lambda_I \\ & \pm 0.006\ \text{(p.e.)} && \pm 0.026\ \text{(p.e.)} . \end{aligned} \tag{8}$$

The He^3/He^4 ratio R is less than 2 per cent, and the uncertainty of this ratio is itself about 3 per cent. The observed degree of dependence of $\Delta\lambda$ on $\Delta\lambda_I$ would be found in a random uncorrelated sample.

Solution (8) gives a zero-point shift near +0.013 A in *He* lines of zero isotope shift. This can be directly confirmed by the lines of small isotope shift. Lines with $\Delta\lambda_I \leqslant 0.09$ A. give a mean $\Delta\lambda = +0.018$ A, with a mean $\Delta\lambda_I = +0.053$. In hydrogen the isotope shifts are negative and near −1.0 A; the eclipse wave lengths of twenty lines (λλ 3656–4101) give a mean $\Delta\lambda = +0.027$ A ± 0.010. We must investigate the dependability of the scale of eclipse wave lengths. For this purpose the mean wave lengths of 90 ionized metallic lines, substantially unblended in the chromosphere and distributed from λ 3500 to λ 5200, have been obtained from the same lists[4, 5, 6] as those used for *He* I. The mean difference—sun minus laboratory—is +0.005 A ± 0.002 A. Thus the *He* and *H* lines show, just outside the limits of statistical fluctuations, a larger positive residual than do the metallic lines. It is important to decide whether the positive shift of *He* I wave lengths is real. If we may not use a constant term in equation (8), the weighted mean of $\Delta\lambda$ is

[7] *Phys. Rev.*, **82**, 406, 1951; also **75**, 1772, 1949. [8] C. E. Moore, *Contr. Princeton U. Obs.*, No. 20, 1945.

[9] D'Azambuja and D'Azambuja, *Bull. Astr.*, **11**, 349, 1938.

+0.016 A and that of $\Delta\lambda_I$ is +0.14 A, i.e., an apparent isotope ratio of 11 per cent. The existence of shifts in lines with small $\Delta\lambda_I$ as well as the positive shift of the hydrogen lines strongly suggest that some physical mechanism is at work. Laboratory pressure shifts of *He* I wave lengths are generally positive when the broadening and shift are due to *He*; the theoretical computation of the *He* I shifts caused by proton collision[10] also predicts mainly positive displacements. However, the density of the *He* emitting layers of the chromosphere is low, perhaps 0.002 that of the reversing layer of τ Sco, in which pressure shifts do not surpass 0.2 A; hence the chromospheric shifts would be expected to be quite small. If self-absorption occurs in hydrogen or helium lines in a moving atmosphere, there could be a positive shift in the limb spectrum. A further possibility is that the type of electric discharge occurs which has been suggested in solar flares. In the flare spectrum, *Hα* is widened asymmetrically. I will adopt the hypothesis that some physical mechanism displaces the *He* I lines by +0.013 A and that the value of R is correctly determined by equation (8).

The line at λ 10830 provides an independent method of estimating the He^3 abundance. Its wave length is accurately determined in the sun and in the laboratory. The two strong components of the triplet in He^3 lie at λ 10831.69, and would be completely resolved from the He^4 line; they are within 0.43 A of a strong atmospheric line and are partially obscured by its wings. However, no line of variable intensity longward of λ 10830 has ever been reported. The He^3 blend is probably always weaker than the shortward He^4 satellite, even when the latter is at maximum intensity. We may estimate the intensity I of λ 10831.69 as −3 or less, when λ 10830.36 is at intensity 5 NN. This provides a rough estimate of its equivalent width. For diffuse lines, Babcock and Moore give the equivalent width, W, in milliangstroms thus:

$$\log W = \frac{I+16}{11.33}. \qquad (9)$$

For He^4 and He^3, respectively, W = 71 mA and less than 17 mA. If the helium lines are on the straight-line portion of the curve of growth, $R \leqslant 0.24$. However, the He^4 line is at least partially saturated, and, if it lies on the normal solar curve of growth, $He^3/He^4 \leqslant 0.14$. In the infrared the central absorption, A_c, of strong lines is quite low; if we estimate it to be 50 per cent, we may use the normal curve of growth but determine the number of absorbing atoms from $W/(\lambda A_c)$ rather than from W/λ. This method gives $He^3/He^4 \leqslant 0.11$.

A few remarks should be made about the possible existence of He^3 in other stellar spectra. Late-type dwarfs almost certainly derive their energy from the proton-proton cycle. Accurate wave lengths of the *He* I emission sometimes found in K or M dwarfs would be valuable. In the B stars, pressure and Stark effects prove a serious observational complication. In τ Sco[11] Merrill and Adams found that the displacements of individual *He* I lines depended on the multiplicity and quantum number of the upper state. The principal singlets have displacements of from −2 to −7 km/sec, while the triplets range from +1 to +8 km/sec. Such effects are so large that the isotope shifts would be unobservable. The interpretation of measures in shell stars with sharp *He* lines would probably be adversely affected by P Cygni absorption and differential velocity shifts.

I am indebted to Dr. Mark Fred and his colleagues, of the Argonne National Laboratory, for their kindness in communicating the measured isotope shifts in advance of publication; to Dr. W. A. Fowler, of the California Institute of Technology, for his discussion of the nuclear reactions involved; and to Dr. H. W. and Mr. H. D. Babcock for providing the new chromospheric wave lengths of several *He* I lines.

[10] M. K. Krogdahl, *Ap. J.*, **102**, 64, 1945; **105**, 327, 1947.

[11] *Mt. W. Contr.*, No. 672; *Ap. J.*, **97**, 98, 1943.

LITHIUM AND THE INTERNAL CIRCULATION OF THE SUN

JESSE L. GREENSTEIN AND ROBERT S. RICHARDSON
MOUNT WILSON AND PALOMAR OBSERVATORIES
CARNEGIE INSTITUTION OF WASHINGTON
CALIFORNIA INSTITUTE OF TECHNOLOGY
Received November 22, 1950

ABSTRACT

The profiles and intensity of the *Li* resonance doublet at λ 6708 have been measured on the solar disk and in the spot penumbra, with dispersion 0.7 A/mm. A special technique was required, since the lines have a central absorption less than 3 per cent. The isotope ratio Li^6/Li^7 is less than 0.25 and may be the same as on the earth, 0.08. From the equivalent width the abundance of *Li* I has been found to be 6.7×10^9 atom/gm. Two different methods of analysis yield the abundance ratio H/Li as 1.4×10^{11} or 0.6×10^{11}. The ratio Li/Ca is 7×10^{-6}. Compared to the other metals, *Li* is only one one-hundredth as abundant as on earth.

Analysis of the nuclear cross-sections for proton capture shows that in equilibrium with protons the ratio Li^6/Li^7 should be small, in agreement with observation. The lifetime of *Li* is short at $T > 3 \times 10^6$ degrees. The deficiency of *Li* in the sun may arise from a very slow circulation down to at least half the solar radius with period near 7×10^8 years. If the circulation is more rapid, all *Li* should have been destroyed. Accretion from interstellar matter can maintain the observed *Li* abundance only if the space density is improbably high.

Lithium, although the third element in the periodic table, is among the rarest on earth as well as in the sun and most stars. It takes part in rapid thermonuclear reactions at the mean temperature of the solar interior. Two isotopes occur on the earth with a rather high ratio $R = Li^6/Li^7 = 0.08$. We have attempted to evaluate R and also the abundance ratio Li/H in the sun.

The resonance doublet, $2^2S - 2^2P^\circ$ is at λ 6708; it has a total *f*-value near unity and lies in a relatively clear region of the solar spectrum. The ionization potential of *Li* I is 5.37 volts; hence *Li* is highly ionized. A blended line of Rowland intensity −3 is observed in the disk; it is enormously strengthened in sunspots and broadened by the Zeeman splitting in the spot magnetic field. The line is slightly strengthened at the limb. After some investigation it was found that the penumbra of large spots showed the line double and of moderate intensity only slightly widened by Zeeman effect. We have obtained spectra of several spots near the center of the disk, using the 150-foot tower with the Michelson grating in the first order, at a dispersion of 0.7 A/mm. The high contrast IV-F plates used were developed to a high gamma. An oscillating triangular slit provided calibration, and the plates were analyzed in the Babcock direct-intensity microphotometer. A slit-width of 0.125 mm, equivalent to 0.087 A, gives ample resolution because of the large Doppler breadth of the lines. On these plates the line is just visible on the disk and is clearly seen as a blended double in the penumbra; its intensity and width increase toward the umbra. The length of our analyzing slit on the plate was less than 1 mm, which corresponds to less than 3280 km on the sun.

The line is so shallow that even with fine-grain plates measurement of its profile is quite difficult. On the tracings 1 mm = 0.01142 A; the central depth of the line was near 3 mm and the over-all width near 60 mm. To eliminate errors introduced by smoothing of the tracing, it was found best to adopt a completely objective procedure. A millimeter réseau was superposed, and readings taken at every millimeter of $A(x)$, the absorption in millimeters, with an accuracy of $\frac{1}{4}$ mm in $A(x)$. This rather laborious process was carried through on seven tracings of sections of four different plates of both disk and penumbra. The zero points of $A(x)$ were then adjusted from the measures in the con-

tinuum, and final mean values of $A(x)$ were formed. The observed mean absorptions are plotted without any smoothing in Figure 1. Most of the erratic fluctuation is caused by emulsion imperfections rather than by plate grain. The unit of $A(x)$ was 1 mm = 0.97 per cent absorption, determined from the measured equivalent widths of ten stronger lines which could be measured on the tracings of the disk and in the Utrecht *Photometric Atlas*.

ANALYSIS OF THE LITHIUM LINES

The wave lengths of the lines have been measured in an atomic beam,[1] with the results given in Table 1. The relative intensities are predicted from the isotope ratio R. The stronger component of Li^6 nearly coincides with the weaker Li^7 component, and there

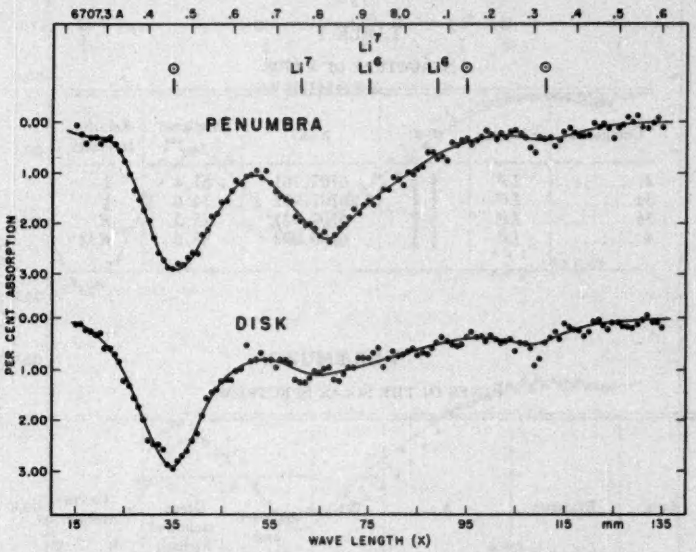

FIG. 1.—Mean observed smoothed profiles of *Li* I in the sunspot penumbra and on the disk. Plotted points are the mean of seven measurements on unsmoothed tracings. The laboratory wave lengths of the *Li* components and the measured wave lengths of unidentified solar lines are shown at the top.

is no possibility of resolving the two. However, strong Li^6 would produce an anomalous doublet ratio and asymmetry on the longward side, and it is this asymmetry which we must use. In the solar spectrum several interloping lines complicate the structure. We use the infrared measures of Babcock and Moore[2] as a guide. In Table 2 the measured wave lengths and corresponding x-co-ordinates are given according to Babcock and Moore and the x-co-ordinates which we finally adopted. We combine the components *3a* and *3b* as 3 in Table 2. The last column gives the relative central absorption for each line. We shall analyze the observations to obtain a probable upper limit for R. The wave lengths of solar and laboratory lines do not always agree. The Evershed effect and motions near sunspots, together with pressure shifts, might produce relative shifts between lines of 1 or 2 km/sec, i.e., 2–4 mm on our scale. Since we cannot expect exact wave-length co-

[1] K. W. Meissner, L. G. Mundie, and P. H. Stelson, *Phys. Rev.*, **74**, 932, 1948.

[2] *Pub. Carnegie Inst. Washington*, No. 579, 1947.

incidence, we may be permitted to introduce a small shift of the *Li* components and, in fact, are forced to do so. The isotope ratio derived depends on the size of these shifts.[2a]

Let us assume that the finite slit-width and the Doppler and magnetic broadening in the sun combine to give line profiles which are approximately Gaussian. Since all the lines are shallow and unsaturated, we should be able to represent the observed line absorption by the sum of six Gaussian curves, thus

$$A(x) = \sum_{i=1}^{6} a_i \exp\left[-\left(\frac{x - x_i}{\Delta x}\right)^2\right]. \qquad (1)$$

The central absorption is a_i and the wave length x_i for each line; Δx is the effective-width parameter. The solution of equation (1) was obtained by trial and error. The value

TABLE 1

STRUCTURE OF λ 6708

Component	Element	J–J'	λ (A)	Predicted x_{mm}	Relative Intensity
2.....	Li^7	$\frac{1}{2}$–$\frac{3}{2}$	6707.761	61.4	1
3*a*.....	Li^7	$\frac{3}{2}$–$\frac{3}{2}$	6707.912	74.6	$\frac{1}{2}$
3*b*.....	Li^6	$\frac{3}{2}$–$\frac{3}{2}$	6707.921	75.3	R
4.....	Li^6	$\frac{1}{2}$–$\frac{3}{2}$	6708.072	88.6	$R/2$

TABLE 2

LINES IN THE SOLAR SPECTRUM

Line	Element	λ	Int.	x_{mm}		Central Absorption
				Babcock and Moore	Greenstein and Richardson	
1.....	⊙	6707.449R	−2	34.1	35	a_1
2.....	Li^7	6707.76	−3	61.4	61	a_2
3.....	Li^7, Li^6	6707.98	−3	80.7	75	$a_3 = a_2(R+\frac{1}{2})$
4.....	Li^6				89	$a_4 = a_2 R/2$
5.....	⊙ (Atm?)	6708.14	−3	94.6	95	a_5
6.....	⊙	6708.32	−3	110.3	111	a_6

of $\Delta x = 10$ mm was obtained from the shortward wing of line No. 1. It corresponds to 114 mA and gives a blurring pattern whose total width at half-intensity is 190 mA. The Doppler broadening for *Li*, 135 mA, and the slit-width, 87 mA, make this value of Δx quite reasonable as a lower limit, without Zeeman effects. It is certainly too low for *Li* in the penumbra, since the Zeeman pattern is broader for *Li* than for line No. 1. If we adopt a larger $\Delta x = 12$ mm for the *Li* components, we depress the high points near λ 6707.6

[2a] Dr. A. S. King studied the *Li* I lines in the arc, furnace, and sunspot (*Mt. W. Contr.*, No. 122; *Ap. J.*, **44**, 169, 1916). He pointed out that different laboratory conditions of excitation produced asymmetric central reversal and longward wave-length shifts. It is possible that the lines are sensitive to pressure.

and obtain a better fit. The value of $\Delta x = 10$ mm was adopted, however, for simplicity. The solution of equation (1) involves adopting the four independent values of a_1, a_2, a_5, and a_6 and computing a_3 and a_4 for the adopted trial ratio R. It was soon found that for small R no adequate representation of the observed profile was possible unless wavelength shifts of about +0.03 A could be made in the Li components. If no shift is permitted, a large value of R is required, but the fit to the shortward wing is then very poor.

Figures 2 and 3 show the results of the solution. Each solution given was judged the best possible, after several trials, given the assumed value of R. The smoothed observed

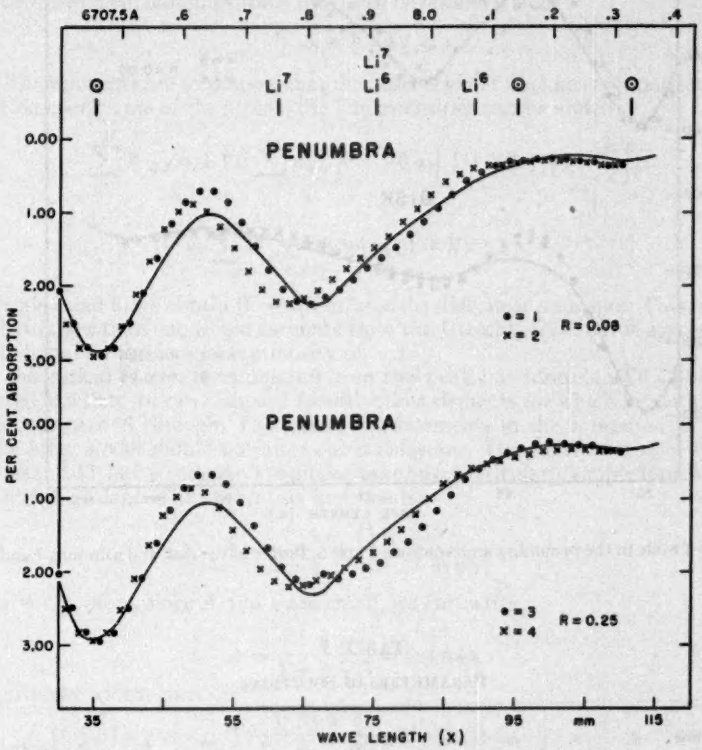

FIG. 2.—The profiles of the *Li* I lines in the penumbra traced from Fig. 1, together with computed points from solutions 1–4, for the isotope ratio R.

curves are traced from Figure 1; the plotted points result from equation (1). Table 3 contains the adopted values of a_i and x_i, as well as R for each trial. It can be seen that a fit is possible or good for $R = 0.00$ or $R = 0.08$, the terrestrial value. In our judgment a value of $R = 0.25$ is the maximum compatible with the observations but does not give so good a fit as does $R = 0.08$. In summary, one might say that Li^6, if present at all, is probably less than three times as abundant, with respect to Li^7, as it is on earth. Solutions 1–6 are for the penumbra; 7 and 8 for the disk. The observations for the disk are poorer, since the line is very shallow. Note in Figure 3 that on the disk the central absorption is only 1 per cent!

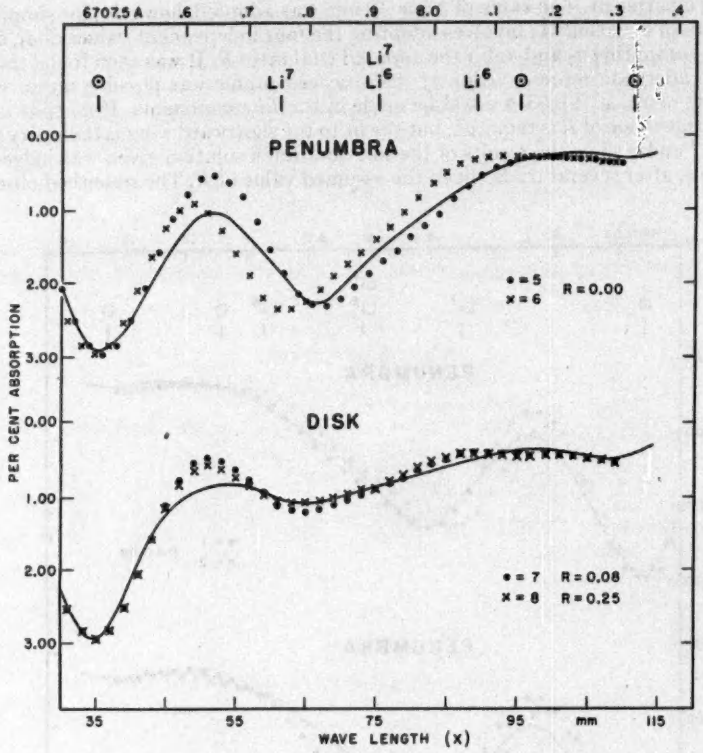

FIG. 3.—Profile in the penumbra and solutions 5 and 6. Profile in the disk and solutions 7 and 8

TABLE 3

PARAMETERS OF SOLUTIONS

Solution	R	a_1	a_2	a_5	a_6	x_1	x_2	x_3	x_4	x_5	x_6
1.....	0.08	3.05	2.10	0.15	0.36	36	64	78	92	96	111
2.....	.08	3.05	2.10	.25	.36	35	61	75	89	95	111
3.....	.25	3.05	2.00	.15	.36	36	64	78	92	96	111
4.....	.25	3.05	2.00	.25	.36	35	61	75	89	95	111
5.....	.00	3.05	2.20	.20	.36	36	66	80	.....	96	111
6.....	.00	3.05	2.25	.25	.36	35	61	75	.....	95	111
7.....	.08	3.05	1.15	.35	.55	35	63	77	91	95	111
8.....	0.25	3.05	1.00	0.35	0.55	35	61	75	89	95	111

THE ABUNDANCE OF LITHIUM IN THE SUN

From the fit to the measures on the solar disk we obtain the equivalent width of the blend of all *Li* components. At a distance δx from the center of each line,

$$A(\delta x) = a e^{-(\delta x/\Delta x)^2}. \tag{2}$$

Also

$$W = \int_{-\infty}^{+\infty} A(\delta x)\, d(\delta x) = \pi^{1/2} a \Delta x. \tag{3}$$

Equivalent widths in milliangstroms (mA) can be obtained from

$$W_{\mathrm{mA}} = 1.96 a_{\mathrm{mm}}. \tag{4}$$

Since all components are so shallow that the absorption in the line is proportional to the absorption coefficients of the atoms, the line intensities can be added:

$$\sum_{i=2}^{4} W_{\mathrm{mA}} = 1.96 \sum_{i=2}^{4} a_{\mathrm{mm}} = 1.96 a_2 \left[1 + (R + \tfrac{1}{2}) + \frac{R}{2}\right], \tag{5}$$

$$\overline{W} = \sum_{i=2}^{4} W_{\mathrm{mA}} = 2.94 a_2 (1 + R). \tag{6}$$

From trials 7 and 8, we obtain $\overline{W} = 3.7$ mA for the disk, near a sunspot. This is perhaps somewhat larger than one would estimate from the Utrecht *Atlas*, but it agrees with an estimate based on the Rowland intensity of -3.

The theoretical $\overline{W}$ can be computed from the weak-line formula. We will follow B. Strömgren,[3] so that we can compare *Li* with other elements for which his detailed solar analysis was carried through. The recent improvements in the computed H^- opacity or in the solar model should not alter our conclusions. The parameter x_0/n should, in fact, be near 0.33, but Strömgren's formulae take on a particularly simple form for $x_0/n = 0.25$, which we adopt. The absorption in a line is

$$A = \frac{1 - (1+\eta)^{-1}}{1 + \frac{2}{3}\sqrt{[3/(1+\eta)]}}, \tag{7}$$

where $\eta = l/k$. Now, since A and η are small, we can write

$$A = \frac{\eta}{1 + \frac{2}{3}\sqrt{3}} = 0.464\eta. \tag{8}$$

The equivalent width, then, is

$$W = \frac{0.464}{k_r} \frac{\pi e^2}{m c^2} \lambda^2 N f, \tag{9}$$

which, at λ 6708, yields

$$N = 5.45 \times 10^9 \frac{k_r W_{\mathrm{mA}}}{f}. \tag{10}$$

Since our measured $\overline{W}$ is for both isotopes, N represents the total number of atoms of both isotopes of *Li* I per gram of solar material. The amount of neutral lithium and of H^- are both proportional to the electron pressure P_e; thus the ratio l/k is independent of P_e and only a slow function of T; the use of the Milne-Eddington model, which leads to equation (7), is justified. For the same reason the abundance of *Li* II, in which form most solar lithium exists, will not be sensitive to the optical depth at which we assume the line to be formed. Trials also showed that it is not sensitive to A, the ratio hydrogen/

[3] *Pub. Copenhagen Obs.*, No. 127, 1940.

metals, over a range log $A = 3.0$ to log $A = 4.2$. Strömgren found that weak lines like λ 3303 of *Na* I or λ 6573 of *Ca* I are formed near $\tau_0 = 0.25$; at this point his solar model gives $\theta = 0.963$, log $P_e = 0.87$, log $\bar{k} = -0.67$. From the analysis of the solar continuum,[4] $k(\lambda\,6708)/\bar{k} = 1.10$. The total *f*-value for the sum of the four *Li* components should be about $(1 + R)$ times the sum of the *f*'s of the Li^7 lines. The *f*-value has been computed by B. Trumpy[5] and by J. Hargreaves[6] as $f \approx 0.72$. Equation (10) then gives $N(Li\ \text{I}) = 6.7 \times 10^9$ atom/gm. The ionization equilibrium computed at τ_0 gives $(Li\ \text{I} + Li\ \text{II})/Li\ \text{I} = 616$, so that the total abundance of *Li*, $N_t(Li) = 4.1 \times 10^{12}$ atom/gm. Since, in Strömgren's analysis, helium was neglected, the number of *H* atom/gm is nearly $1/m_H$, and $H/Li = 1.45 \times 10^{11}$, based on the theoretical $\bar{k}(H)$. (If we let $H/He = 10$, the mean atomic weight is 14/11, and $H/Li = 1.14 \times 10^{11}$.) If the empirically required increase of $\bar{k}(\odot) = 1.4\bar{k}(H^-)$ should require an increase of $k(\lambda\,6708)$ by a similar factor, then Strömgren's model would also have to be changed, and it is not advisable to complicate the situation now.

Assumptions about the opacity are not needed if we determine the ratio of *Li* to *Ca*, which can be compared to terrestrial values. If we use Strömgren's evaluation of *Ca* to the metals and of *A*, the ratio of hydrogen to the metals, we can get an independent determination of H/Li. The line λ 6573 of *Ca* I has $W = 32$ mA; it is on the transition part of the curve of growth. We use J. L. Greenstein's[7] redetermination of the solar curve of growth, which is based on a relation very similar to equation (7). We find log $W/\lambda = -0.17$, which gives $\eta_0 = 1.35$. Then, using the mean velocity $V = 2.2$ km/sec, we obtain from

$$N = \frac{\eta_0 k_\nu V m c}{\lambda f \pi^{1/2} e^2} \tag{11}$$

the value $N(Ca\ \text{I}) = 7.8 \times 10^{14}$. Note that any errors in k_ν will disappear in a comparison of λ 6708 and λ 6573. The *f*-value of λ 6573 used is 7×10^{-5}. From the ionization equilibrium, $N_t(Ca)/N(Ca\ \text{I}) = 500$. Trial shows that several different choices of τ_0 or *A* do not affect the ratio $Li/Ca = 1.05 \times 10^{-5}$. Adopting Strömgren's H/Ca ratio of 6.3×10^5, we now find $H/Li = 6 \times 10^{10}$ as against 14×10^{10} by the first method. The difference may arise from *A*, which would have to correspond to log $A = 4.2$ to make the two methods agree, or from an error of $\bar{k}$. It should be pointed out that the *f*-value of λ 6573 is probably too high; this will not affect our H/Li ratio but does affect the Li/Ca ratio. W. Prokofjew[8] found $f(4227)/f(6573) = 33{,}000$. D. R. Hartree[9] computed from quantum mechanics $f(4227) = 2.26$, which seems rather high. The sum rule predicts $f(4227) < 2$, and the resonance absorption continuum of *Ca* I must contribute appreciably to the *f*-sum. Thus we can estimate $f(4227)$ near 1.5, which increases the *Ca* I abundance by a factor of 1.5. Then $Li/Ca = 7 \times 10^{-6}$ appears to be the best value. This ratio is remarkably close to H. N. Russell's estimate that $Li/Ca = 20 \times 10^{-6}$.

NUCLEAR PROCESSES AND THE CIRCULATION IN THE SUN

The compilation of abundances in meteorites and on the earth by Harrison Brown[10] gives a ratio $Li/Ca = 1.7 \times 10^{-4}$. This is about twenty-five times the best solar estimate.

[4] S. Chandrasekhar and G. Münch, *Ap. J.*, **104**, 446, 1946; see also Chandrasekhar, *Radiative Transfer* (Oxford: Clarendon Press, 1950), p. 310. The latter discussion indicates that perhaps we should take $\bar{k} = 1.4\bar{k}(H^-)$. However, this would make the comparison with Strömgren's other results quite difficult.

[5] *Zs. f. Phys.*, **57**, 787, 1929.

[6] *Proc. Cambridge Phil. Soc.*, **25**, 75, 1929.

[7] *Ap. J.*, **107**, 168, 1948.

[8] *Zs. f. Phys.*, **50**, 701, 1928.

[9] *Proc. R. Soc. London, A*, **164**, 167, 1938.

[10] *Rev. Mod. Phys.*, **21**, 625, 1949. In a private communication Dr. Brown kindly informs us that the ratio $Li/K = 1/400$ is well determined in the earth's crust. If we combine this with the ratio $K/Ca = 1/10$ in meteorites, $Li/Ca = 2.5 \times 10^{-4}$. His new determination is considerably more certain than Noddack's estimates and is thirty-six times larger than the solar value.

Noddack's work on meteorites gives an even larger Li/Ca ratio. From a résumé of the older work on abundances, Von Kluber[11] gives $Li/Ca = 5 \times 10^{-3}$ for the earth and about 1.5×10^{-3} in meteorites. Such figures indicate that Li is about four hundred times more abundant in the earth and meteorites than in the sun. Similarly, if we take the general run of abundances of the metals to Li in the sun and the earth, we find that Li is about one hundred times less abundant in the sun than on earth. While this deficiency ratio may be uncertain by a factor of 2, we are faced with the problem as to why there is any Li in the sun at all. Since the thermonuclear disintegration of Li at temperatures greater than 3×10^6 degrees is very rapid, any mixing of the atmosphere of the sun with the interior will rapidly deplete the Li in the atmosphere.

The following approach to the study of the circulation in the solar envelope developed from a conversation with Dr. Bengt Strömgren. Let us assume that mixing or circulations exist which, in a time t_0, bring $1/e$ of the matter to the surface from a depth at which the temperature T is sufficient to destroy Li. Then, after an interval t, the concentration of Li as compared to other metals will be decreased from its initial value by

$$\frac{n(t)}{n(0)} = e^{-t/t_0}. \tag{12}$$

A deficiency by a factor of 100 means that $t = 4.6\,t_0$; if we identify the terrestrial concentration with $n(0)$ and set $t = 3 \times 10^9$ years, $t_0 = 7 \times 10^8$ years. If the circulation is more rapid in the outer envelope of the sun, all Li should long ago have disappeared, except for material accreted from interplanetary or interstellar space.

The nuclear processes involved are simple, and both isotopes suffer rapid disintegration on proton capture. Soon after the Li^7 disintegration was first observed, E. McMillan[12] predicted that Li^7 would be rapidly destroyed in the sun and searched without success for Li^6 in the sunspot spectrum. It was later found that the Li^7 reaction is a relatively slow one and that Li^6 would also be destroyed. We are indebted to Dr. W. A. Fowler, of the Kellogg Laboratory of the California Institute of Technology, for extensive discussions and for new data on the Li reactions. We need consider only

$$Li^7 + H^1 \rightarrow 2He^4; \qquad \sigma = 1.75 \times 10^{-27}\ \text{cm}^2 \quad \text{at} \quad 300\ \text{KEV};^{13}$$

$$Li^6 + H^1 \rightarrow He^3 + He^4; \qquad \sigma = 5.2 \times 10^{-26}\ \text{cm}^2 \quad \text{at} \quad 300\ \text{KEV}.^{14}$$

The extrapolation of the Li^7 process to low energies is abnormal for Li^7, since, according to the parity selection rules, only p-wave protons can react with Li^7 to form two alpha particles, which obey the Bose-Einstein statistics. The theoretical dependence on energy of the penetration factors in the cross-section has been given by Christy and Latter.[15] The standard Gamow-Teller formula predicts that the cross-sections of Li^6 and Li^7 would be in a nearly constant ratio. However, for very low energies, Fowler represents the cross-sections approximately by the formula

$$\frac{\sigma(Li^6)}{\sigma(Li^7)} \approx \frac{16}{E + 0.223}, \tag{13}$$

[11] *Vorkommen der chemischen Elemente im Kosmos* (Leipzig, 1931), p. 29.

[12] *Phys. Rev.*, **44**, 240, 1933.

[13] L. J. Howarth and L. D. P. King, *Phys. Rev.*, **54**, 38, 1938; R. G. Herb, D. B. Parkinson, and D. W. Kerst, *Phys. Rev.*, **48**, 118, 1935.

[14] A. V. Tollestrup, W. A. Fowler, and C. C. Lauritsen, *Phys. Rev.*, **76**, 428, 1949, and unpublished data.

[15] *Rev. Mod. Phys.*, **20**, 185, 1948.

with E the proton energy in MEV. This interpolation formula is obtained by considering the ratio of s-wave to p-wave captures and adjusting the constants at 0.3 MEV. If the Li reached equilibrium with protons of energy E, then the isotope ratio, $1/R = Li^7/Li^6 = \sigma(Li^6)/\sigma(Li^7)$, is given by equation (13). The terrestrial ratio $1/R = 12$ corresponds to $E = 1.1$ MEV, which is much too high for any Li to survive. At the solar energies, which do not exceed 0.014 MEV, there should be almost no Li^6 present. This is in agreement with our observations that $R < 0.25$.

We wish to know the lifetime of Li at solar temperatures. The Gamow-Teller formula, with H. Bethe's definitions,[16] will suffice if we extrapolate to the low solar energies from observations of the cross-section at the lowest possible laboratory energies. We will consider Li^7 only, since it is the more stable isotope, and estimate its lifetime. Adopt the hydrogen abundance $X = 0.7$. Then $1/P\rho X$ will be the lifetime, and Bethe shows that

$$\text{Lifetime} = \frac{1}{P\rho X} = \frac{1.6 \times 10^{-3} e^{\tau}}{\tau^2 \Gamma\phi \rho X}, \tag{14}$$

where

$$\tau = 85 \left(\frac{T}{10^6}\right)^{-1/3}. \tag{15}$$

The evaluation of $\Gamma(Li^7)$ and ϕ from the observational data, using the correction expressed roughly in equation (13), leads to

$$\Gamma\phi = 1.7 \times 10^4 \text{ from data at } 100 \text{ KEV},$$

$$\Gamma\phi = 1.3 \times 10^4 \text{ from data at } 36 \text{ KEV}.$$

The agreement shows that the one-level formula should work sufficiently well down to 10 KEV. For Li^6 we derive $\Gamma\phi = 10^6$, a value much higher than those given for Li^7. The difference originates, presumably, in the limitation of Li^7 processes to p-wave collisions. At the low energies in the solar envelope, the isotope ratio predicted is $1/R \approx 1/70$ if Li^6 and Li^7 are in equilibrium with protons. Finally, we obtain for Li^7

$$\frac{1}{P\rho X} = 1.8 \times 10^{-7} \frac{e^{\tau}}{\rho \tau^2}. \tag{16}$$

We can apply equation (16) to determine the depth in the sun at which Li^7 will be rapidly destroyed; at the center, $T_c = 17 \times 10^6$, $\rho_c = 120$, gives a lifetime of only about 300 seconds. Thus Li will persist only if the circulation is very slow or does not reach the core. Let us find a point at which the lifetime is of the order of, or less than, the circulation period $t_0 = 7 \times 10^8$ years. Under what values of T_0 and ρ_0 in the sun does the Li^7 in fact have a lifetime of 0.1 t_0, i.e., 2×10^{15} seconds? All lithium carried downward from the atmosphere and envelope to this region will be substantially destroyed, and the exponential decrease of concentration given in equation (12) will hold. Inspection showed that T_0 and ρ_0 are actually encountered in the envelope of the sun. They can be obtained from recent standard solar models and prove to be $\tau = 57.6$, i.e., $T_0 = 3.2 \times 10^6$ degrees, and $\rho_0 = 0.36$ gm/cm^3. This point is 0.55 $R\odot$ distant from the center, and about 0.04 $M\odot$ lies exterior to it. Therefore, the circulation we imagine affects only 4 per cent of the mass and need not reach the convective core. It may do so, but the results of a deeper circulation would be indistinguishable from those of a shallow one.

Another possible interpretation of the mixing has been suggested by Dr. Martin Schwarzschild. If the outer envelope of the sun is in convective equilibrium, the mixing

[16] *Phys. Rev.*, **55**, 434, 1938.

may be complete and very rapid; all matter in the envelope would spend an appreciable period, say 3×10^{16} seconds, at a high temperature, T_0. A reduction of *Li* abundance by a factor of 100 requires that the lifetime at T_0 be 6×10^{15} seconds. Solution of equation (16) gives $T_0 \approx 3.1 \times 10^6$, i.e., very slightly nearer the surface than on our previous hypothesis. If the hydrogen convective zone extends deep into the sun, T_0 would represent the temperature at its lower boundary.

ACCRETION

Much more rapid circulation would be compatible with the presence of *Li* in the atmosphere only if fresh material is brought in from space. If the period t_0 is short, it is necessary for the sun to receive by accretion enough *Li* to maintain a steady state. The rate of loss is

$$\frac{dM\,(Li)}{dt} = -\frac{M\,(\text{envelope})\,n\,(\odot)}{t_0}, \tag{17}$$

where $n(\odot)$ is the surface concentration. The accreted material may bring in a higher concentration, say $n(0)$; based on the terrestrial abundance, $n(0)/n(\odot)$ may be 10^2. It cannot be much richer in *Li*, from L. Spitzer's negative results in a search for λ 6708 in interstellar space.[17] The accretion formula, neglecting radiation pressure and collisions, is

$$\frac{dM\,(Li)}{dt} = +\frac{2\pi GMR\rho\,n\,(0)}{V}. \tag{18}$$

The required density of interstellar matter, ρ, is

$$\rho = \frac{V}{2\pi GRt_0}\,\frac{n\,(\odot)}{n\,(0)}\,\frac{M\,(\text{envelope})}{M}. \tag{19}$$

With $V = 10^6$ cm/sec, $n(\odot)/n(0) = 10^{-2}$, and the circulation confined to the outer $0.04\,M\odot$, i.e., about $0.5\,R\odot$,

$$\rho = \frac{0.014}{t_0}\ \text{gm/cm}^3. \tag{20}$$

If $t_0 = 7 \times 10^8$ years, a density of 7×10^{-19} gm/cm^3 would appreciably affect the surface composition of the sun. If t_0 is shorter—say, 10^7 years—a density of 5×10^{-17} gm/cm^3 is required (at such high densities, if V is small, the use of eq. [18] is probably incorrect, and the Hoyle-Lyttleton formula might be used). If the circulation were to penetrate to the core, the last term in equation (19) is unity, and the densities must be multiplied by a factor of 25. But in any case the mean densities of interstellar matter required are so high that it seems improbable that accretion plays any role in maintaining the surface abundance of *Li*. The presence of *Li* in the atmosphere of the sun indicates that only a very slow interchange of matter takes place with points at half a solar radius. Thus evidence exists against complete mixing of the solar atmosphere and the interior.

RED GIANT STARS

Strong *Li* I absorption was found in WZ Cas by A. McKellar.[18] McKellar and R. F. Sanford[19] suggest that the abundance of *Li* with respect to *Na* and *K* may differ from one N star to another. The absolute visual magnitude of an N star is near −2; if the effective

[17] *Ap. J.*, **109**, 548, 1949.

[18] *Pub. A.S.P.*, **52**, 407, 1940; *Observatory*, **64**, 4, 1941.

[19] *Ap. J.*, **111**, 270, 1950.

temperature is 2500°, the bolometric magnitude is -6 and $L = 1700\odot$. The radius is then $700\odot$ and the mass roughly $18\odot$. If the red giants are homologous with the sun, the central temperature, T_c, of an N star would be only 500,000°—too low to maintain any thermonuclear reaction. A more centrally condensed model than that of the sun must be found. While the noise-zone model[20] may not be correct, it displays some features which a model for the red giants must retain. The ratio of T_c to the mean temperature is very high, and the region where T is high is very small. Case 6 computed by Richardson and Schwarzschild has physical properties not very different from those of an N star. The temperature greater than 3,000,000° necessary to destroy *Li* is reached at a distance of only $10^{-3}R$ from the center of case 6; the mass interior to this point is only $0.067M$.

Let us assume that the N stars initially had an abundance ratio *Li/Na* similar to that on the earth, i.e., about one hundred times the ratio now found in the sun. Those N stars with very complete mixing throughout their entire volume would reduce the *Li/Na* ratio to the solar value. If the circulation did not penetrate to the small inner zone, however, the *Li/Na* ratio would retain the terrestrial value. For strong lines like *Li* and *Na* the equivalent widths would be proportional to the square root of the abundances. Thus a variation by a factor of 10 in W could occur from one N star to the other. In his Table 7, R. F. Sanford gives values of W from 1 A to 10 A in the N stars with strong D lines.

[20] R. S. Richardson and M. Schwarzschild, *Ap. J.*, **108**, 373, 1948.

TEMPERATURE GRADIENT IN THE SUN'S ATMOSPHERE MEASURED AT RADIO FREQUENCIES*

JOHN P. HAGEN
Naval Research Laboratory
Received March 29, 1950

ABSTRACT

The intensity of the radiation from the quiet sun varies with radio wave length. The purpose of this paper is to discuss this radiation and to show that it may be treated as thermal radiation originating in the corona and chromosphere. New measurements at the short-wave-length end of the radio spectrum are reported. An analysis of these measurements in conjunction with measurements of others at longer wave lengths is made, and from the analysis, with the assumption that previously determined values of the electron concentration in the sun's atmosphere are correct, the temperatures of the inner corona and of the chromosphere are determined. It will be shown that the temperature is fairly uniform at less than 10,000° K to a height of 10,000 km and then rises steeply to a temperature of 1,000,000° K at a height of 25,000 km.

Since the discovery of radio waves arriving at the earth from an outside source, two components have been identified—galactic radiation and solar radiation. Much recent work has been done on the measurement of solar radiation and on the correlation of variations in the radio intensity with solar activity as observed by other means. The results of this work have shown that over a wide range of wave lengths the radiation from the sun is extremely variable, the variation being greater at the longer wave lengths. In each wave-length region, however, the radio intensity falls occasionally to some minimum value, below which it never seems to go. It is assumed that this minimum radiation is thermal radiation due to the quiet or undisturbed sun and that the variations which appear as increases in the intensity above the minimum are due to disturbed conditions in the sun's atmosphere.

The precise measurement of the intensity of the thermal radiation from the sun in the radio-frequency spectrum requires the use of a directive antenna and a sensitive and stable radio receiver. The thermal radiation from the sun and the galaxy is essentially white noise; that is, there are components in the radiation at all random phases and amplitudes, and the average amplitude distribution with frequency is described by Planck's law. Thermal noise generated in the first circuits and antenna of a radio receiver is also white noise. Thus, when a receiver is pointed at the sun, both the solar noise and the locally generated receiver noise are amplified and appear in the output as a current or voltage, which may be measured. Since there is no distinguishing difference between the receiver noise and solar radiation, an accurate measurement of the intensity of the solar radiation necessitates great stability in the gain of the receiver and requires that the inherent receiver noise be reduced to a minimum.

The antennas used in the experimental work reported here are parabolic reflectors of small F/D ratio. The same principles apply to the parabolic reflector as apply to the telescope objective. The beam width is proportional to λ/D, where D is the diameter of the opening, λ the wave length, and the power gain is proportional to $(D/\lambda)^2$. As an example, the 10-foot parabola used here at 8.5-mm wave length has a beam width of 0°.2 and a calculated power gain of 8.3×10^5.

The radiation from the sun may be considered as though it were black-body radiation emanating from a body of the same dimensions as the sun and at an equivalent tempera-

* Thesis, Georgetown University, and Naval Research Laboratory Report, No. 3504.

ture T_ν. By the use of the Rayleigh-Jeans approximation to Planck's law, the intensity of the radiation is related to the equivalent temperature thus:

$$I_\nu d\nu = \frac{2kT_\nu \nu^2}{c^2} d\nu \text{ erg/sec/cm}^{-2}\text{/unit solid angle}, \tag{1}$$

where I_ν is the intensity at the frequency ν, k is Boltzmann's constant, and c is the velocity of light. Throughout this paper we are concerned only with monochromatic radiation. The subscript ν will be dropped and used only where it is required for clarity. As will appear later, the receivers are calibrated in terms of temperature, and so it is a convenience to measure the intensity of the radiation in temperature units, related to the intensity by equation (1).

If the beam width of the antenna is sufficiently narrow that the entire radiation pattern is included in a cone whose diameter is less than that of the sun, then the power received is independent of the gain of the antenna. It is as though the antenna were within an inclosure whose walls are at the temperature of the sun. Under those conditions the available power at the input terminals of the receiver is

$$P = kT_\nu d\nu, \tag{2}$$

where T is the temperature in ° K. This is the condition which holds in the experiment reported here. If, on the other hand, the beam width of the antenna is sufficiently greater than the angle subtended by the sun that there is little variation in antenna gain across the surface of the sun, then the power at the input terminals of the receiver will be proportional to the gain of the antenna,

$$P = \frac{G}{4} kT_\nu d\nu \frac{r^2}{R^2}, \tag{3}$$

where G is the gain of the antenna, r is the radius of the sun, and R is the distance of the earth from the sun. The intermediate case, where the beam width is comparable to the angle subtended by the sun and where the gain of the antenna varies across the surface of the sun, is much more complex to analyze and awkward to use. Since the condition can be avoided experimentally, it is not discussed here.

The measurement of solar radiation has been extended into the millimeter wavelength region, and, since this part of the measurement program is new, it will be briefly discussed here. The antenna consists of a 10-foot diameter paraboloidal cast-aluminum reflector, having a beam width at 8.5-mm wave length of 0°.2. The surface of the reflector is machined so that it varies from a true parabola by less than ± 0.003 inch and is thus usable through most of the millimeter wave-length region. The mirror has an F/D ratio of 0.3. The antenna is on a polar mount and can be pointed to the sun by means of hand cranks, which adjust the armature of selsyn units, which are part of an electromechanical system for controlling the position of the antenna. The antenna can also be made to follow the sun through the day by means of a synchronous motor drive.

The receiver is of the superheterodyne type, with a silicon point-contact rectifier as the first detector, since at these wave lengths there are no vacuum tubes available for this purpose. The local oscillator is a klystron tube especially made to operate at this wave length. The *i-f* amplifier has a center frequency of 30 mc and a band width of 1 mc. The *i-f* amplifier is followed by a second detector, and it is the rectified current of this second detector which is brought out to a meter and is proportional to the power at the input terminals of the receiver. Great care was taken in the design of the receiver to minimize noise, both thermal and tube-generated, in the early circuits. To obtain the required stability, all the voltages applied to the receiver were carefully stabilized. The 8.5-mm receiver has a sensitivity referred to a perfect receiver of 20 decibels and represents the best that can be obtained with present-day techniques.

The receiver is connected to the antenna by means of a wave-guide. If a properly tapered block of carbon or other suitable material is inserted in the wave-guide at the input to the receiver in place of the antenna, the carbon block can be made to terminate the line properly with a voltage standing-wave ratio less than 1.01; in other words, it acts as a black body at these wave lengths. The carbon radiates thermal noise according to the equation $P = kTdv$ and serves as an absolute calibration device.

The figure of merit or noise figure of a radio receiver is defined[1] as the ratio of the available noise-to-signal ratio at the output terminals to the noise-to-signal ratio at the input terminals:

$$F = \frac{N/S}{n/s}, \tag{4}$$

where F is the noise figure, N is the output noise power when the receiver network and the input termination are at ambient temperature T_0, S is the output signal power, n is the available noise power at the input terminals, and s is the available signal power at the input terminals. It can be seen that the better receiver has less locally generated noise.

If a superheterodyne receiver using both the signal and the image channel is employed, then it can be shown that the output noise power when the input termination to the receiver is at any temperature T, while the remainder of the receiver is held constant at ambient temperature, may be obtained from the equation

$$F = 2\frac{T - T_0}{T_0}\frac{N}{N_T - N}, \tag{5}$$

where N_T is the output noise power when the input termination is at T. To obtain the equivalent temperature of the sun, the procedure followed was first to point the antenna beam at the sun and observe the output noise power N_s, then to point the antenna at the sky and again observe the output noise power N_{sk}. After this, the carbon block wave-guide termination was connected to the input terminals of the receiver. The termination was inclosed in a small oven and a thermocouple attached to the block. The temperature of the block was then raised from ambient to about 800° K and the output noise power measured as a function of the temperature of the input termination. Such a calibration for the 8.5-mm receiver is shown in Figure 1. It can then be demonstrated that

$$T_s = \frac{N_s - N_{sk}}{N}\frac{N}{N_L - N}(T_L - T_0) = \frac{N_s - N_{sk}}{N_L - N}(T_L - T_0). \tag{6}$$

This procedure gives the temperature of the sun above sky temperature. While the sky temperature has not been accurately measured at 8.5 mm, it has been measured at 3.14 cm and found to be less than 50° K. It is reasonable to assume that at 8.5 mm the value will not be greater than this and will perhaps be less. Two factors contribute to the sky temperature: thermal radiation by our atmosphere and galactic radiation. Since the attenuation through the entire atmosphere for this wave length is about 0.5 decibels, which corresponds to a reduction in signal of 11 per cent, then if it is assumed that the absorption takes place where the temperature is approximately 300° K, the atmosphere should have an effective temperature as a radiator of about 30° K. The intensity of galactic radiation decreases with wave length.[2] The effective temperature of this radiation is not over 20° at the 3-cm wave length. Thus the sum of galactic radiation and thermal radiation from our atmosphere at 8.5 mm will not be over 50° K.

The signal from the sun will be attenuated in the portion of the wave-guide going from the focal point of the parabola to the input terminals of the receiver. This attenua-

[1] H. T. Friis, *Proc. I.R.E.*, **32**, 419, 1944.

[2] Jack W. Herbstreit, "Cosmic Radio Noise," in *Advances in Electronics* (New York: Academic Press, 1948), **1**, 347–80.

tion has been measured as 2.05 decibels, which corresponds to a power ratio of 1.603. The average of many readings of the equivalent temperature of the sun at 8.5-mm wave length, corrected for atmospheric absorption, for sky noise, and for attenuation in the wave-guide, is 6740° K ± 10 per cent. There is a small variation in this temperature from day to day, but the variation is quite small compared with that experienced at 3-cm and longer wave lengths.

The resolution of this equipment is such that some detail can be observed across the disk of the sun, and, for a while, daily contour maps of the intensity of the radiation from the sun were drawn. As yet, no good correlation between the observed variations in intensity and some index of solar activity has been found. However, during the week of September 17, 1948, the passage of a large sunspot group across the sun was accompanied

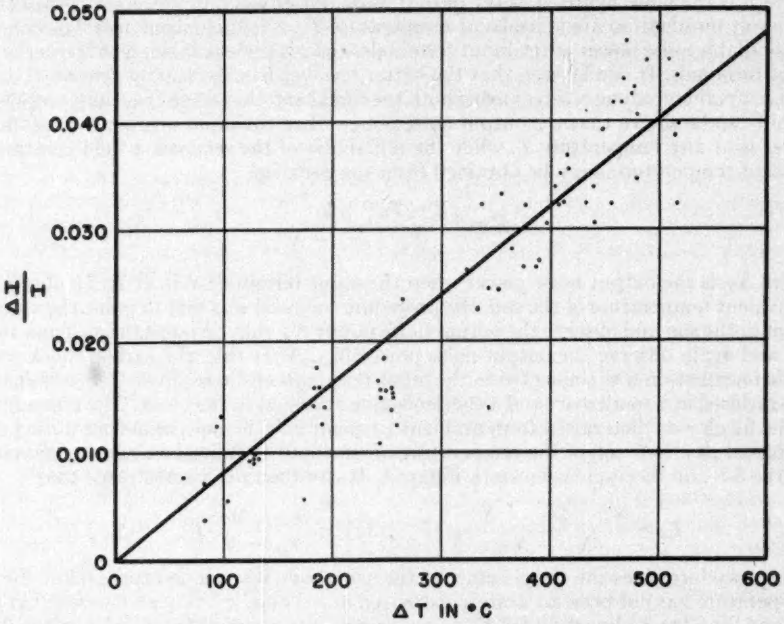

FIG. 1.—Calibration of the 8.5-mm receiver, using a hot load. ΔI is the increment in output current of the receiver. I is the output current when the load is at ambient temperature.

by a localized increase in intensity, which corresponded in position to the position of the spot all during its passage. This is shown in Figure 2. Assuming that the disturbed area responsible for the increased radio emission at 8.5-mm wave length was the area of the spot group, then the equivalent temperature of that area would be 100,000° K. An attempt is being made to correlate the observed variations with other indices of solar activity.

All the available published data on the equivalent temperature at radio wave lengths of the quiet sun have been collected and are shown in Figure 3 and Table 1. It is seen that the equivalent temperature varies between the rough limits 7000° and 1,000,000° K through the range of wave lengths 8 mm to 300 cm. It is the purpose of this paper to show that a consistent picture is obtained if it is assumed that the radiation from the quiet sun is thermal in origin, the millimeter radiation originating in the middle chromo-

sphere and the longer-wave-length radiation originating in the higher levels of the chromosphere and corona. It is a further purpose to show that, if an electron distribution is assumed, then the radio data can be made to yield the kinetic temperature of the various layers of the sun's atmosphere, and it will be shown that the temperature is fairly uniform at less than 10,000° K to a height of 10,000 km and then rises steeply to a temperature of 1,000,000° K at a height of 25,000 km. This region of steep rise in temperature may be considered to be the boundary between the chromosphere and the corona.

In order for an electromagnetic wave to propagate through an ionized medium, it is necessary that the concentration of electrons not exceed a certain critical value. This

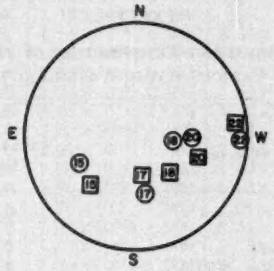

FIG. 2.—Relative positions on the sun of radio disturbances and an associated spot group. September 15-22, 1948. Circles indicate measured position of radio disturbance. Date shown in center. Squares indicate position of spot group, with date in center.

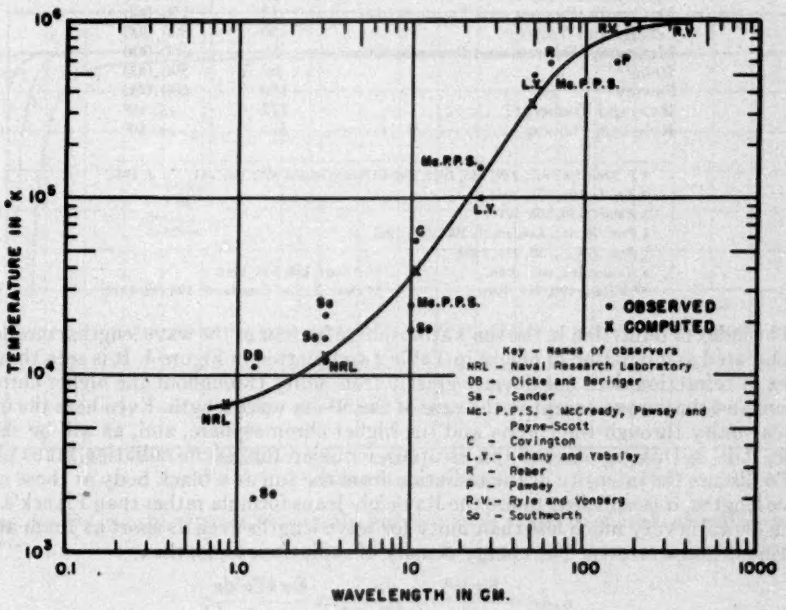

FIG. 3.—The equivalent temperature as a function of wave length

value is that which causes the index of refraction of the medium for the wave length of the wave considered to approach zero. The index of refraction in an ionized medium may be determined by the equation[3]

$$\mu^2 = 1 - \frac{4\pi n_1 e^2}{m(\omega^2 + f_c^2)} \simeq 1 - \frac{4\pi n_1 e^2}{m\omega^2} = 1 - \frac{\lambda^2 n_1 e^2}{m\pi c^2} \quad \text{if} \quad f_c^2 \ll \omega^2, \tag{7}$$

where μ is the index of refraction, n_1 the number density of electrons, e the electronic charge and m the mass of the electron, ω the angular frequency ($\omega = 2\pi\nu$), f_c the collision frequency, c the velocity of light, and λ the wave length.

TABLE 1

OBSERVED EQUIVALENT TEMPERATURE OF THE QUIET SUN AT VARIOUS RADIO WAVE LENGTHS

Observer	Wave Length (Cm)	Effective Temperature in ° K
Hagen	0.85	6,740
Southworth*	1.25	2,000
Dicke and Beringer†	1.25	11,000
Haddock and Decker, NRL	3.15	12,000
Southworth	3.2	16,000
Sander‡	3.2	22,000
McCready, Pawsey, and Payne-Scott§	10	25,000
Southworth	10	18,000
Covington‖	10.6	58,000
Lehany and Yabsley#	25	100,000
McCready, Pawsey, and Payne-Scott	25	150,000
Lehany and Yabsley	50	500,000
McCready, Pawsey, and Payne-Scott	50	500,000
Reber**	62.5	590,000
Pawsey††	150	600,000
Ryle and Vonberg‡‡	172	*ca.* 10^6
Ryle and Vonberg	375	*ca.* 10^6

* *J. Franklin Inst.*, **239**, 285, 1945, and Erratum issued with Vol. **241**, No. 3, 1946.
† *Ap. J.*, **103**, 375, 1946.
‡ *Nature*, **159**, 506, 1947.
§ *Proc. R. Soc. London, A*, **190**, 357, 1947.
‖ *Proc. I.R.E.*, **36**, 454, 1948.
Nature, **161**, 645, 1948.
** *Nature*, **158**, 945, 1946.
†† *Nature*, **158**, 633, 1946.
‡‡ *Proc. R. Soc. London, A*, **193**, 98, 1948.

The index of refraction in the sun's atmosphere for four of the wave lengths considered is tabulated as a function of height in Table 2 and plotted in Figure 4. It is seen that the index of refraction does not deviate greatly from unity throughout the higher chromosphere and the corona except in the case of the 50-cm wave length. Even here the index is near unity through the corona and the higher chromosphere, and, as will be shown later, it is in this region that the escaping emission for 50-cm radiation takes place.

To discuss the intensity of the radiation from the sun as a black body at these radio wave lengths, it is sufficient to use the Rayleigh-Jeans formula rather than Planck's law, since $h\nu/kT$ is very much less than unity for wave lengths even as short as 1 mm at the pertinent temperatures. The energy density of radiation, ψ_ν, is, then,

$$\psi_\nu d\nu = \frac{8\pi h\nu^3}{c^3} \frac{d\nu}{e^{h\nu/kT} - 1} \simeq \frac{8\pi kT\nu^2 d\nu}{c^3}; \tag{8}$$

[3] Many authors. See William G. Baker and Chester W. Rice, *J. Amer. Inst. Elect. Eng.*, **45**, 302, 1926.

TABLE 2

VARIATION OF INDEX OF REFRACTION, μ, AND $1 - \mu^2$ WITH WAVE LENGTH AND HEIGHT ABOVE THE PHOTOSPHERE

h (Km)	8.5 Mm		3.14 Cm		10.6 Cm		50 Cm	
	$1-\mu^2$	μ	$1-\mu^2$	μ	$1-\mu^2$	μ	$1-\mu^2$	μ
500.....	1.12×10^{-2}	0.994	1.53×10^{-1}	0.910	.....	.....	.....	.....
1,000.....	8.72×10^{-3}	0.996	1.19×10^{-1}	0.939	.....	.....	.....	.....
2,000.....	5.5×10^{-3}	0.997	7.51×10^{-2}	0.962	8.55×10^{-1}	0.371	.....	.....
4,000.....	2.34×10^{-3}	0.999	3.19×10^{-2}	0.984	3.64×10^{-1}	0.797	.....	.....
6,000.....	9.75×10^{-4}	1.000	1.33×10^{-2}	0.993	1.52×10^{-1}	0.911	.....	.....
10,000.....	1.64×10^{-4}	1.000	2.24×10^{-3}	0.999	2.55×10^{-2}	0.987	5.67×10^{-1}	0.803
20,000.....	2.38×10^{-5}	1.000	3.25×10^{-4}	1.000	3.70×10^{-3}	0.998	8.23×10^{-2}	0.958
28,000.....	1.70×10^{-5}	1.000	2.32×10^{-4}	1.000	2.64×10^{-3}	0.999	5.88×10^{-2}	0.970
30,000.....	1.63×10^{-5}	1.000	2.22×10^{-4}	1.000	2.53×10^{-3}	0.999	5.63×10^{-2}	0.971
70,000.....	9.56×10^{-6}	1.000	1.30×10^{-4}	1.000	1.49×10^{-3}	0.999	3.30×10^{-2}	0.983
139,000.....	4.20×10^{-6}	1.000	5.73×10^{-5}	1.000	6.53×10^{-4}	1.000	1.45×10^{-2}	0.993
278,000.....	1.29×10^{-6}	1.000	1.76×10^{-5}	1.000	2.01×10^{-4}	1.000	4.46×10^{-3}	0.998
417,000.....	5.49×10^{-7}	1.000	7.49×10^{-6}	1.000	8.54×10^{-5}	1.000	1.90×10^{-3}	0.999
695,000.....	1.42×10^{-7}	1.000	1.94×10^{-6}	1.000	2.75×10^{-5}	1.000	4.91×10^{-4}	1.000
1,390,000.....	1.36×10^{-8}	1.000	1.86×10^{-7}	1.000	2.11×10^{-6}	1.000	4.70×10^{-5}	1.000

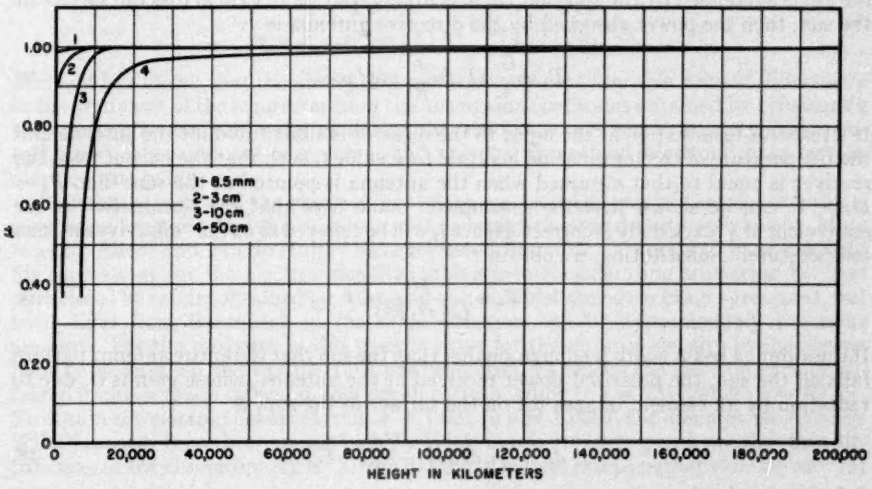

FIG. 4.—The index of refraction at four radio wave lengths as a function of height above the photosphere.

but the energy density is related to the specific intensity, i_ν, thus:

$$\frac{4\pi i_\nu d\nu}{c} = \psi_\nu d\nu . \tag{9}$$

The intensity of the radiation may then be written

$$i_\nu d\nu = \frac{2kT\nu^2 d\nu}{c^2} \text{ erg/sec/cm}^2\text{/unit solid angle} . \tag{10}$$

The polarized flux at the earth due to radiation from the sun of intensity i_ν is

$$F_s = \tfrac{1}{2} i_\nu d\nu \pi r^2 \frac{1}{R^2} , \tag{11}$$

where r is the radius of the sun and R is the average distance from the earth to the sun. The power absorbed by an isotropic radiator of equivalent area $\lambda^2/4\pi = c^2/4\pi\nu^2$ is, then,

$$P_s = \tfrac{1}{2} i_\nu d\nu \pi r^2 \frac{c^2/4\pi\nu^2}{R^2} . \tag{12}$$

Substituting for i_ν, the power absorbed by an isotropic radiator becomes:

$$P_s = \tfrac{1}{4} kT_\nu d\nu \frac{r^2}{R^2} , \tag{13}$$

where T_ν is the equivalent temperature of the sun. If a directive antenna having a gain G over an isotropic radiator is used and if the antenna beam width is enough greater than the angle subtended by the sun that there is little variation in gain across the surface of the sun, then the power absorbed by the directive antenna is

$$P_s = \frac{G}{4} kT_\nu d\nu \frac{r^2}{R^2} \text{ erg/sec} . \tag{3}$$

If a resistive termination at the input to the receiver is substituted for the antenna and the temperature of the termination is raised to a value t_s such that the output from the receiver is equal to that obtained when the antenna is pointed at the sun, then $P_s = kt_s d\nu$. It can be shown that the assumption made here that the termination is the equivalent of a black body is correct. Hence t_s will be referred to as the "effective antenna temperature." Substituting, we obtain

$$T_\nu = \frac{4t_s}{G(r^2/R^2)} . \tag{14}$$

If the antenna beam width is enough smaller than the sun that the entire antenna pattern falls on the sun, the polarized power received at the antenna, whose gain is G, due to radiation by an element of area dA on the surface of the sun, is

$$dP = \tfrac{1}{2} i_\nu d\nu dA \frac{c^2/4\pi\nu^2}{R^2} G . \tag{15}$$

Substituting for i_ν, we have

$$dP = \frac{1}{4\pi} kT_\nu d\nu G \frac{dA}{R^2} ; \tag{16}$$

but

$$\frac{dA}{R^2} = d\omega ,$$

where ω is here the solid angle. When equation (16) is integrated over all space, the relation cited earlier is obtained:

$$P_e = kT_e dv\,, \tag{2}$$

since

$$\int G d\omega = 4\pi\,.$$

Equations (2) and (3) are sufficient to describe the majority of cases that occur in making these measurements.

The coefficient of absorption of an electromagnetic wave in an ionized gas is[3]

$$\kappa = \frac{f_c}{c}\frac{1-\mu^2}{\mu}\,, \tag{17}$$

where f_c is the number of collisions suffered by an electron per second. Chapman[4] and Cowling[5] have discussed the collision frequency in a binary gas such as that encountered in the atmosphere of the sun. Using Cowling's expression for the collision frequency, the coefficient of absorption may be written

$$\kappa = \frac{2\sqrt{2}\, n_1^2 e^6}{3\sqrt{\pi}\, c\mu\nu^2 (mkT)^{3/2}} \log_e \left[1 + \left(\frac{4dkT}{e^2}\right)^2\right], \tag{18}$$

where m is the mass of the electron and d is the average distance between molecules in the gas. Hence $d \simeq n^{-1/3}$, and, for an electrically neutral binary gas, $d \simeq (2n_1)^{-1/3}$. For the conditions in the chromosphere and corona the argument of the logarithm in equation (18) is much greater than unity. The formula may then be simplified as follows:

$$\kappa = \frac{2\sqrt{2}\, n_1^2 e^6}{3\sqrt{\pi}\, c\mu\nu^2 (mkT)^{3/2}} \log_e \left[\frac{4kT}{e^2 (2n_1)^{1/3}}\right]^2. \tag{19}$$

Martyn[6] has shown that the absorption coefficient obtained by this method differs only in the argument of the logarithm from the absorption coefficient obtained by considering the energy absorbed and radiated during the free-free transitions in an electrically neutral binary gas composed of electrons and protons. Smerd and Westfold[7] have further clarified this point.

Baumbach[8] reviewed the observational data on the brightness of the corona and arrived at an expression for the variation of the average electron density with height. More recently Allen[9] and van de Hulst[10] have reviewed Baumbach's work and have modified his expressions for the electron density, taking into consideration scattering by dust particles. The results obtained by Allen and van de Hulst are not in exact agreement, but both differ from Baumbach in the same direction and by approximately the same amounts. For the purposes of this work a value for the electron density in the corona lying between Allen and van de Hulst has been used. Values for the electron density obtained in this way are carried in to a depth corresponding to $\rho = 1.03$, where $\rho = R/R_\odot$. To obtain the electron densities from $\rho = 1.021$ to $\rho = 1.0007$, the assumption made by Wildt[11] is used. It has been pointed out by Wildt in private correspondence that this distribution in the chromosphere is "somewhat hypothetical except perhaps the density (or

[4] S. Chapman and T. G. Cowling, *The Mathematical Theory of Non-uniform Gases* (Cambridge: At the University Press, 1939).

[5] *Proc. R. Soc. London, A*, **183**, 453, 1945.

[6] *Proc. R. Soc. London, A*, **193**, 44, 1948.

[7] *Phil. Mag.*, **40**, 831, 1949.

[8] *A.N.*, **263**, 121, 1937.

[9] *M.N.*, **107**, 426, 1947.

[10] *Ap. J.*, **105**, 471, 1947.

[11] *Ap. J.*, **105**, 36, 1947.

rather upper limit to the density) of 1.74×10^{11} electrons per cubic centimeter at elevation H = 500 kilometers." At $\rho = 1.021$, n_1, the number of electrons per cubic centimeter, is taken as 3.55×10^8, and at the base of the chromosphere the value $n_1 = 1.74 \times 10^{11}$ adopted. In the intervening region the electron pressure is assumed to follow the law

$$\frac{d \log p_e}{dh} = -0.20 \times 10^{-8} \text{ cm}^{-1},$$

where p_e is the electron pressure and h the height above the photosphere. To obtain the distribution used in this paper, these two distributions are smoothly joined in the region $\rho = 1.015$ to $\rho = 1.05$. The data are shown in Figure 5 and tabulated in Table 3.

The absorption coefficient calculated as a function of height above the photosphere for the wave length 8.5 mm, using the electron distribution of Table 3 and the final approximation to the temperature distribution, is given in Table 4 and plotted in Figures

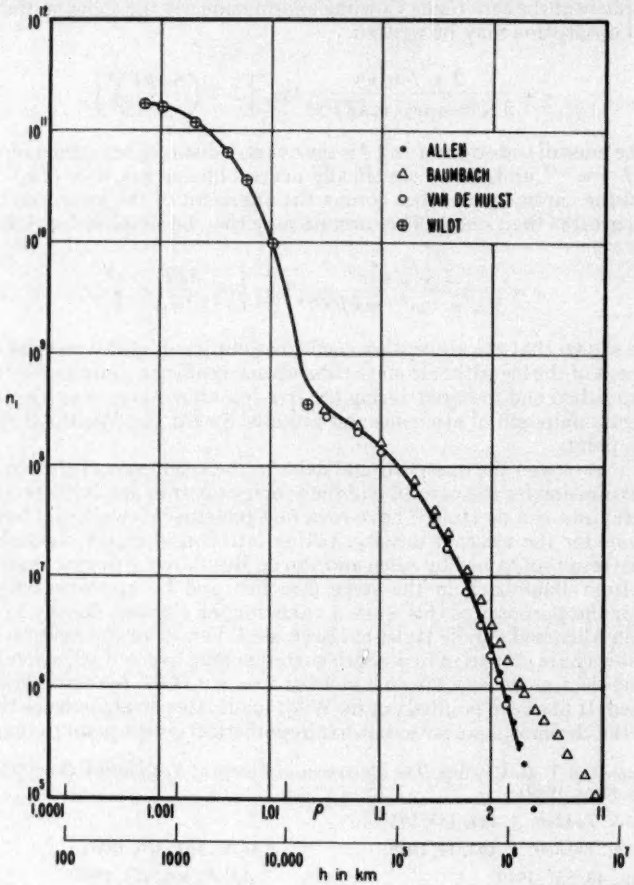

FIG. 5.—The assumed electron distribution in the sun's atmosphere

TABLE 3

CORRECTED ELECTRON DENSITIES
(n_1—Electrons per Cc$\times 10^{-6}$)

ρ	Baumbach	Van de Hulst	Allen	Wildt	Final Smooth Values
1.0	458	430	454	.....	.....
1.0007	.....	.....	.....	174,000	174,000
1.001	.....	.....	.....	.....	162,000
1.003	.....	.....	.....	.....	86,000
1.006	.....	.....	.....	.....	33,300
1.01	.....	.....	.....	.....	9,800
1.02	.....	.....	.....	.....	615
1.021	.....	.....	.....	355	.....
1.03	311	290	.....	.....	355
1.06	229	210	.....	.....	210
1.10	156	137	154	.....	148
1.20	70.4	58	68.5	.....	65
1.30	38.4	30	36.6	.....	33
1.40	23.8	18	22.0	.....	20
1.60	11.1	7.5	9.3	.....	8.5
1.80	6.13	3.8	4.57	.....	4.0
2.00	3.73	2.0	2.42	.....	2.2
3.00	0.913	0.19	0.213	.....	0.21

TABLE 4

COLLISION FREQUENCY AND ABSORPTION COEFFICIENT AS A FUNCTION OF HEIGHT ABOVE THE PHOTOSPHERE

h (Km)	n_1 (Per Cc)	T (° K)	$A_1(2)$	Collisions/ Sec/Molecule	$\kappa_{4.5}$ (Per Cm)
500	1.73×10^{11}	5.07×10^{3}	14.92	1.30×10^{7}	4.82×10^{-6}
1,000	1.35×10^{11}	5.13×10^{3}	15.11	1.01×10^{7}	2.94×10^{-6}
2,000	8.52×10^{10}	5.24×10^{3}	15.46	6.29×10^{6}	1.15×10^{-6}
4,000	3.63×10^{10}	5.75×10^{3}	16.21	2.45×10^{6}	1.91×10^{-7}
6,000	1.51×10^{10}	6.14×10^{3}	16.93	9.58×10^{5}	3.11×10^{-8}
10,000	2.54×10^{9}	8.32×10^{3}	18.90	1.14×10^{5}	6.26×10^{-10}
13,900	6.20×10^{8}	2.88×10^{4}	22.13	5.10×10^{3}	6.88×10^{-12}
20,000	3.68×10^{8}	1.80×10^{5}	26.76	2.34×10^{3}	1.86×10^{-13}
28,000	2.63×10^{8}	8.40×10^{5}	29.46	1.83×10^{1}	1.04×10^{-14}
34,750	2.30×10^{8}	8.40×10^{5}	29.56	1.60×10^{1}	7.94×10^{-15}
70,000	1.48×10^{8}	8.40×10^{5}	29.85	1.04×10^{1}	3.31×10^{-15}
139,000	6.50×10^{7}	8.40×10^{5}	30.39	4.65×10^{0}	6.51×10^{-16}
278,000	2.00×10^{7}	8.10×10^{5}	31.10	1.54×10^{0}	6.62×10^{-17}
417,000	8.5×10^{6}	7.30×10^{5}	31.47	7.82×10^{-1}	1.43×10^{-17}
695,000	2.2×10^{6}	6.70×10^{5}	32.19	2.33×10^{-1}	1.10×10^{-18}
1,390,000	2.1×10^{5}	5.60×10^{5}	33.42	3.03×10^{-2}	1.37×10^{-20}

6 and 7. Also tabulated are the logarithmic term in the absorption coefficient, $A_1(2)$, and the collision frequency f_c, where

$$A_1(2) = \log_e \left[1 + \left(\frac{4dkT}{e^2}\right)^2\right]$$

and

$$f_c = \frac{2\sqrt{2\pi}\, n_1 e^4}{3m^{1/2}(kT)^{3/2}} A_1(2).$$

It is seen that $A_1(2)$ is a slowly varying function of the height. It is at the four wave lengths for which κ is computed that the best values of the equivalent temperature of the quiet sun have been obtained by experiment. The results of the measurements to date of the intensity of radiation from the quiet sun over the wave-length range 8 mm to 275 meters are shown in Figure 3. Over this wave-length range the equivalent temperature of the quiet sun is seen to vary from 7000° to 10^6° K. In considering these data, it should be borne in mind that the accuracy with which the equivalent temperature can be assigned is, in nearly all cases, quite low. In order to locate this curve precisely, most of these measurements should be repeated, using recent improvements in the techniques of measurement and calibration.

The absorption coefficient κ is such that

$$I = I_0 e^{-\kappa h}, \tag{20}$$

where I_0 is the intensity of radiation entering a uniformly absorbent slab of thickness h, and I is the intensity of the emergent radiation. The absorption coefficient is related to the optical depth through the equation $d\tau = \kappa dh$. If κ is constant over the path of the integration, then $\tau = \kappa h$. Thus (in eq. [20]), with the restriction that κ be constant over the interval considered, $I = I_0 e^{-\tau}$. The power absorbed in the medium is

$$I_0 - I = I_0(1 - e^{-\kappa h}) = aI_0, \tag{21}$$

where a is the fractional absorption and varies from 0 to 1.

The variation in κ through the sun's atmosphere cannot be described by a simple analytical expression, so it is convenient to obtain a solution to the transfer equation by a summation process. Figure 8 represents the path of a ray traveling to the right. The path is broken up into elemental units, each Δh long. The elements are numbered successively from 1 through n, starting at the left. Let $I_{r,s}$ be the intensity of the radiation emitted by the rth element measured at the point where it leaves the sth element, where $s > r$. Then

$$I_{1,2} = I_1 e^{-\kappa_2 \Delta h_2}$$

and

$$I_{r,n} = I_r \exp\left[-\sum_{s=r+1}^{n} \kappa_s \Delta h_s\right].$$

If I is written as the sum of the intensities of the emergent radiation from all elements after passing through the nth element, then I is the intensity of the emergent radiation,

$$I = \sum_{r=1}^{n} I_r \exp\left[-\sum_{s=r+1}^{n} \kappa_s \Delta h_s\right]. \tag{22}$$

For each of the elements considered, the absorption, a, has the value $1 - e^{-\kappa_r \Delta h_r}$, and so the intensity of the emission from the rth element is

$$I_r = a_r i_r = (1 - e^{-\kappa_r \Delta h_r}) \frac{2kT_r \nu^2}{c^2}. \tag{23}$$

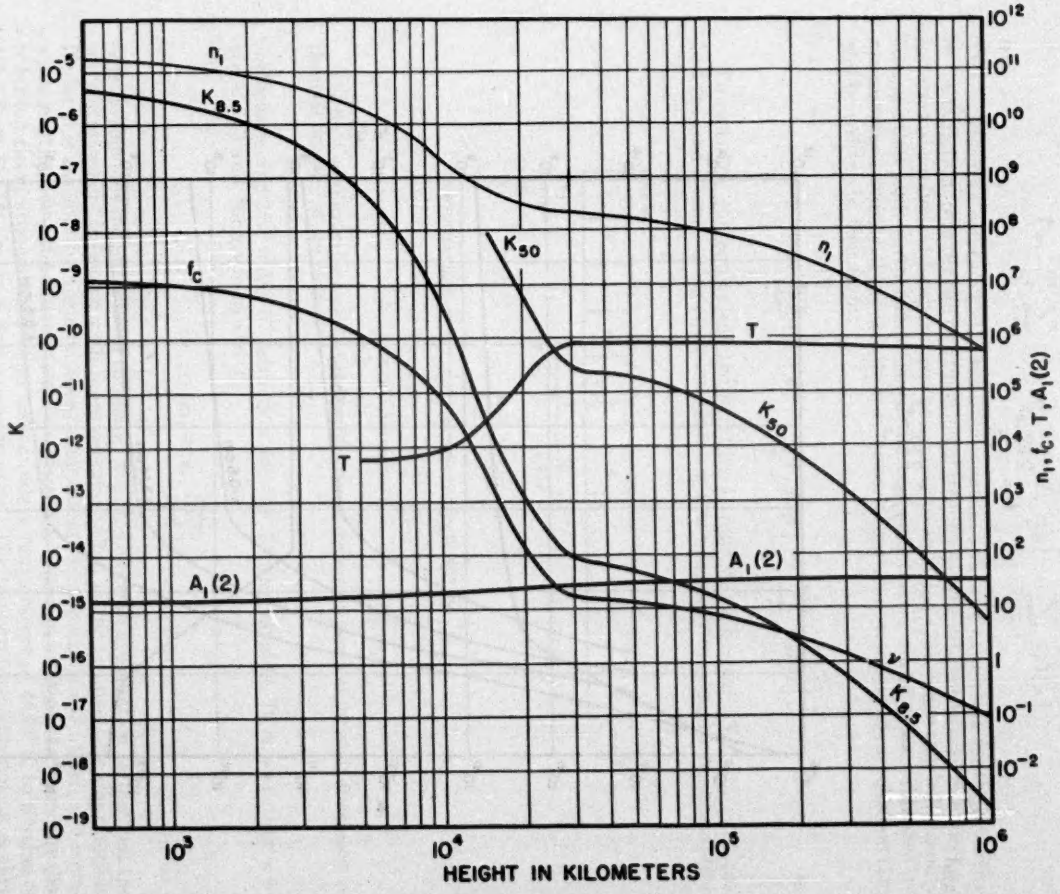

FIG. 6.—The variation with height above the photosphere of the electron distribution, collision frequency, temperature, absorption coefficient for 8.5 mm and 50 cm, and the factor A_1 (2).

If the equivalent temperature T_r is defined as the temperature of the equivalent black body radiating with the intensity I, then

$$I = \frac{2kT_r\nu^2}{c^2} \tag{24}$$

and

$$I_r = \frac{2kT_{r_r}\nu^2}{c^2}.$$

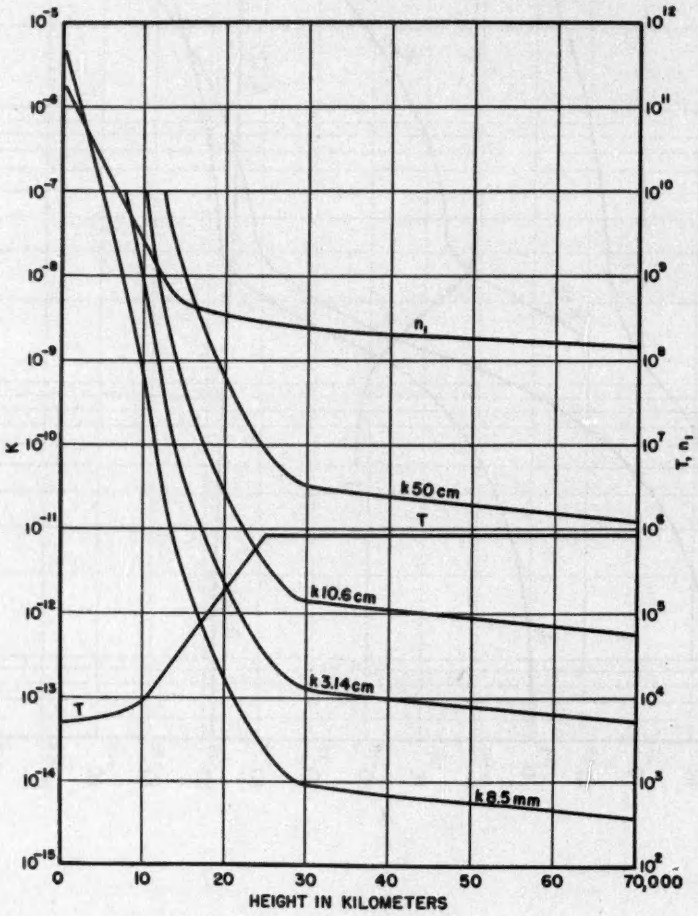

FIG. 7.—The absorption coefficients for 8.5 mm, 3.14 cm, 10.6 cm, and 50 cm. The assumed electron distribution and the calculated temperature distribution as a function of height.

Equation (22) becomes, upon substitution from equation (23),

$$I = \frac{2kv^2}{c^2} \sum_{r=1}^{n} (1 - e^{-\kappa_r \Delta h_r}) T_r \exp\left[- \sum_{s=r+1}^{n} \kappa_s \Delta h_s \right]. \tag{25}$$

This represents a solution to the transfer equation and is an expression for the intensity of the radiation from the sun as a function of frequency. The intensities may be expressed in terms of equivalent temperatures according to equation (24). Since this will simplify computation and, furthermore, since the equipment is in many cases calibrated to measure the intensity of the radiation in terms of equivalent temperatures, equation (25) will be written in that form:

$$T_r = \sum_{r=1}^{n} (1 - e^{-\kappa_r \Delta h_r}) T_r \exp\left[- \sum_{s=r+1}^{n} \kappa_s \Delta h_s \right]. \tag{26}$$

To calculate the equivalent temperature at four wave lengths—8.5 mm, 3.14 cm, 10.6 cm, and 50 cm—using equation (26), it is first necessary to compute the absorption

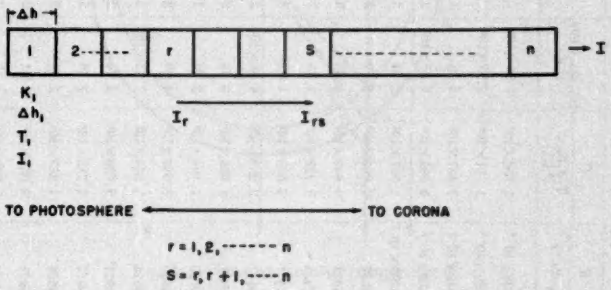

FIG. 8.—Construction for analyzing the contribution of the various layers of the sun's atmosphere to the total intensity of the radiation.

coefficients and the index of refraction for the various heights. It is seen that $\kappa = \kappa(\nu, n_1, T)$ and, for given n_1 and T,

$$\kappa_{\nu_2} = \kappa_{\nu_1} \frac{\mu_1 \nu_1^2}{\mu_2 \nu_2^2}.$$

It is assumed for the purposes of this paper that the electron distribution throughout the sun's atmosphere is known with more certainty than is the temperature distribution. Under this assumption the equivalent temperature of the sun is calculated at several wave lengths, using the assumed electron distribution and an arbitrary temperature distribution rising exponentially from the boundary temperature of 4830° K to a value of 10^6 ° K at 50,000 km as a first approximation. The temperature distribution is then modified until the calculated equivalent temperature at each wave length agrees with that obtained by experiment. It is assumed throughout that the sun's atmosphere has spherical symmetry, is electrically neutral, and is composed of completely ionized hydrogen. This last assumption should lead to no significant error, since the least height from which emission escapes is 5000 km at a wave length of 8.5 mm. It is at these heights, though, that neutral hydrogen becomes abundant; and, if very much shorter wave

TABLE 5

CALCULATION OF THE EFFECTIVE TEMPERATURE FOR $\rho = 0$ AND $\rho = 1$ AT 8.5 MM WAVE LENGTH

				$\rho=0$							$\rho=1$					
r	h (Km)	T (° K)	κ (Cm)	h (Cm)	$\kappa\Delta h$	A $1-e^{-\kappa\Delta h}$	$\Sigma\kappa\Delta h$	B $e^{-\Sigma\kappa\Delta h}$	C $T_rA_rB_{r+1}$ (° K)	$(C_r/h_{km})1000$ (° K)	h' (Cm)	$\kappa\Delta h'$	D $1-e^{-\kappa\Delta h'}$	$\Sigma\kappa\Delta h'$	E $e^{-\Sigma\kappa\Delta h'}$	$T_rD_rE_{r+1}$ (° K)
1	5000	5.92×10^{2}	6.55×10^{-8}	5×10^{7}	3.275	0.9622	9.1082	1.108 ± 10^{-4}	1.668×10^{0}	3.34×10^{0}	.....	.....	.....	.....	.....	.....
2	5500	6.01	4.24	5×10^{7}	2.120	.8800	5.8332	2.929×10^{-4}	1.291×10^{2}	2.58×10^{2}	.....	.....	.....	.....	.....	.....
3	6000	6.14	2.75	5×10^{7}	1.375	.7472	3.7132	2.440×10^{-2}	4.427×10^{2}	8.85	3.75×10^{8}	10.312	1.000	26.451	3.254×10^{-12}	6.013×10^{-4}
4	6500	6.24	1.88	5×10^{7}	0.9400	.6094	2.3382	9.650×10^{-2}	9.395×10^{2}	1.88×10^{3}	3.61	6.787	0.9989	16.139	9.793×10^{-8}	5.407×10^{-1}
5	7000	6.38	1.13	5×10^{7}	0.5650	.4316	1.3982	2.4705×10^{-1}	1.197×10^{3}	2.39	3.49	3.944	0.9806	9.352	8.679×10^{-5}	2.805×10^{1}
6	7500	6.51	6.37×10^{-9}	5×10^{7}	0.3185	.2728	0.8332	0.4347	1.062×10^{3}	2.12	3.37	2.147	0.8832	5.408	4.481×10^{-3}	2.205×10^{2}
7	8000	6.64	4.36	5×10^{7}	0.2180	.1959	0.5147	0.5977	9.669×10^{2}	1.93	3.28	1.430	0.7607	3.261	3.835×10^{-2}	8.097×10^{2}
8	8500	6.92	2.63	5×10^{7}	0.1315	.1232	0.2967	0.7433	7.227×10^{2}	1.45	3.18	0.8363	0.5667	1.8310	1.603×10^{-1}	1.450×10^{2}
9	9000	7.60	1.52	5×10^{7}	0.0760	.0732	0.1652	0.8477	5.088×10^{2}	1.02	3.09	0.4697	0.3748	0.9947	0.36983	1.685×10^{2}
10	9500	8.10	8.66×10^{-10}	5×10^{7}	0.0433	.0424	0.08918	0.9147	3.280×10^{2}	6.56×10^{2}	3.02	0.2615	0.2301	0.5250	0.59156	1.432×10^{2}
11	10,000	9.20	4.49	5×10^{7}	0.02245	.0222	0.04588	0.9551	1.995×10^{2}	3.99	2.94	0.1320	0.1237	0.2635	0.7684	9.978×10^{2}
12	10,500	1.07×10^{4}	2.27	5×10^{7}	0.01135	0.0113	0.02343	0.9769	1.194×10^{2}	2.39	2.88	0.06538	0.0633	0.1315	0.8768	6.339×10^{2}
13	11,000	1.29	1.09	5×10^{7}	0.005450	.....	0.01208	0.9880	6.984×10^{1}	1.40	2.81	0.03063	0.03010	0.06617	0.9359	3.747×10^{2}
14	11,500	1.45	5.49×10^{-11}	5×10^{7}	0.002745	.....	0.006630	0.9934	3.964×10^{1}	7.93×10^{1}	2.76	0.01515	0.01515	0.03554	0.9651	2.153×10^{2}
15	12,000	1.70	3.09	5×10^{7}	0.001545	.....	0.003885	0.9961	2.620×10^{1}	5.24	2.69	0.008212	0.008312	0.02039	0.9798	1.396×10^{2}
16	12,500	1.95	1.83	5×10^{7}	0.000915	.....	0.002340	0.9977	1.782×10^{1}	3.56	2.65	0.004850	0.004850	0.01208	0.9880	9.390×10^{2}
17	13,000	2.29	1.09	5×10^{7}	0.000545	.....	0.001425	0.9986	1.247×10^{1}	2.49	2.60	0.002834	.....	0.007228	0.9928	6.461×10^{2}
18	13,500	2.73	6.62×10^{-12}	5×10^{7}	0.000331	.....	0.000880	0.9991	9.031×10^{0}	1.81	2.55	0.001688	.....	0.004394	0.9956	4.596×10^{2}
19	14,000	3.16	4.28	5×10^{7}	0.000214	.....	0.000549	0.9995	6.760×10^{0}	1.35	2.51	0.001074	.....	0.002706	0.9973	3.389×10^{1}
20	14,500	3.71	2.93	5×10^{7}	0.000146	.....	0.000335	0.9997	5.416×10^{0}	1.08	2.46	0.0007208	.....	0.001632	0.9984	2.672×10^{1}
21	15,000	4.68	1.89	1×10^{8}	0.000189	.....	0.000189	0.9998	.....	.....	4.82	0.000910	.....	0.000911	0.9991	.....
	16,000								$\Sigma_{\rho=0}=6800°$ K							$\Sigma_{\rho=1}=8250°$ K

lengths, where penetrations would be deeper, were discussed, then it would be necessary to consider the effect of the neutral hydrogen on the collision frequency and consequently upon the absorption coefficient. For this work it is assumed that neutral hydrogen is not present in sufficient amount to modify seriously the absorption coefficient.

The computation of the equivalent temperature at 8.5 mm for the central ray and the ray emerging at the limb is given in Table 5, where the summation is continued to the point where $e^{-\Sigma\kappa\Delta h}$ becomes $\ll 1$ and the contribution to the equivalent temperature is negligible. Similar calculations for other values of ρ were made for 8.5 mm and for the other three wave lengths. The path length for the ray emerging at any distance ρ from

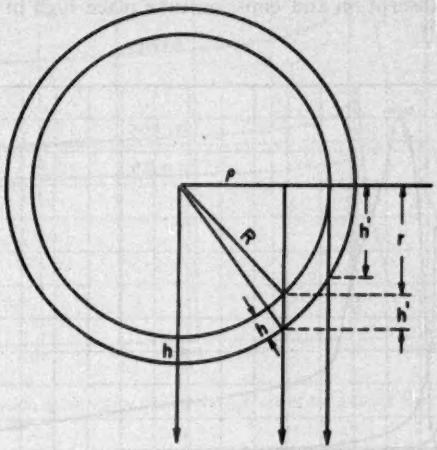

FIG. 9.—Construction for computing h'

TABLE 6

CALCULATED MEAN EQUIVALENT TEMPERATURE OF THE SUN AT FOUR RADIO WAVE LENGTHS AND THE DISTRIBUTION ACROSS THE DISK

(Equivalent Temperature $[T_\nu]$ in ° K)

Wave Length	$\rho=0$	$\rho=0.79$	$\rho=0.935$	$\rho=1.0$	$\rho=1.015$	$\rho=1.02$	$\rho=1.03$	$\rho=1.04$	$\rho=1.10$	$\rho=1.20$	Mean
8.5 mm	6800	7070	7470	8250	9330	1540	.....	.....	.....	.....	7400
3.14 cm	10,000	11,400	12,700	15,600	18,500	16,300	.....	.....	.....	.....	12,700
10.6 cm	26,000	32,500	40,200	53,480	61,800	.....	98,800	.....	18,600	4920	43,000
50 cm	217,000	284,000	352,000	437,000	468,000	.....	.....	634,500	334,000	101,000	420,000

the center is h', and, as is seen in Figure 9, it is related to the radial thickness of the layer by the equation $h' = -r + \sqrt{r^2 + 2R_\odot h + h^2}$.

The net equivalent temperature lies somewhere between that for the center and that for the limb, its value being determined by the amount of limb brightening present. The computed mean equivalent temperatures from Table 6 are plotted in Figure 3, along with the observed data.

The eleventh column of Table 5 contains the normalized contribution of the various

layers to the emergent intensity of the radiation. The dependence of this contribution upon height for the four wave lengths is shown in Figure 10, where it is seen that, especially for the shorter-wave-length radiation, the effective emitting region is rather sharply defined. This is due to the fact that the absorption coefficient varies rapidly with height. Thus a fairly well-defined temperature variation is required to obtain agreement between the computed and measured equivalent temperature.

The distribution in intensity across the surface of the sun for the four wave lengths is shown in Figure 11 and Table 6. In every case there is limb brightening, since the temperature increases with height. The limb brightening is greatest at 10 cm and becomes nearly negligible at 8.5 mm. Others have shown[6,12] that for the very long wave lengths, where the principal absorption and emission take place high in the corona, the limb brightening disappears.

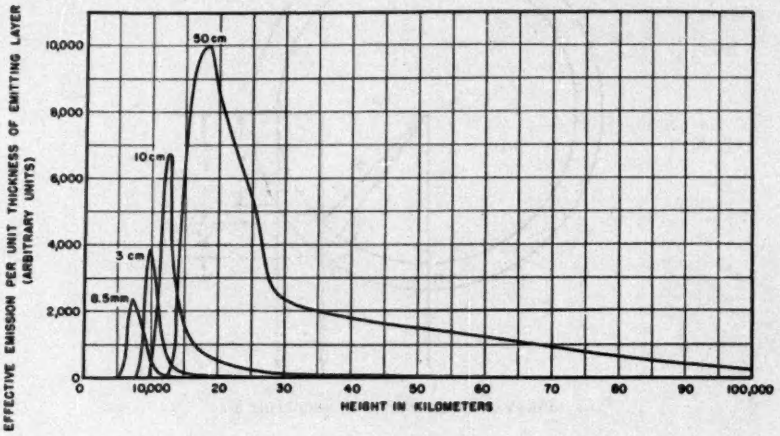

FIG. 10.—The contribution of the various layers of the sun's atmosphere, at indicated heights above the photosphere, to the emission from the center of the sun for the four wave lengths 8.5 mm, 3.14 cm, 10.6 cm, and 50 cm.

The resulting temperature distribution for the sun's atmosphere from Table 4 is given in Figure 12. The present analysis deals only with heights greater than about 7000 km. It is reasonable to assume that the temperatures in the lower chromosphere might be represented by the dotted curve representing a smooth variation out of the photosphere through the chromosphere. Redman's determination[13] of a temperature of 30,000° K at a height as low as 1500 km does not fit this temperature distribution. To obtain agreement with Redman's value at 1500 km, it is necessary to decrease the absorption coefficients so that the principal absorption for the shorter wave lengths will occur at much lower heights. Since the absorption coefficient varies with the square of the electron concentration and inversely with $T^{3/2}$, either an increase in the assigned temperature of the chromosphere, a decrease in the electron density, or some combination of these two is indicated. Detailed calculations show that, in order to satisfy simultaneously the conditions that a kinetic temperature of 30,000° exists at a height of 1500 km and that the equivalent temperature of the sun at the various radio wave lengths is as shown

[12] M. Waldmeier and H. Müller, *Zurich Pub.*, No. 155, 1948.

[13] *M.N.*, **102**, 140, 1942.

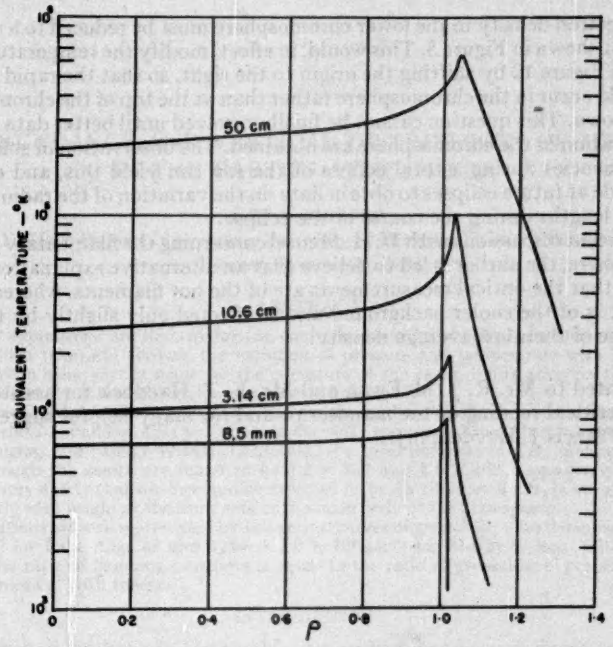

FIG. 11.—The distribution in intensity across the surface of the sun for the four wave lengths, 8.5 mm, 3.14 cm, 10.6 cm, and 50 cm.

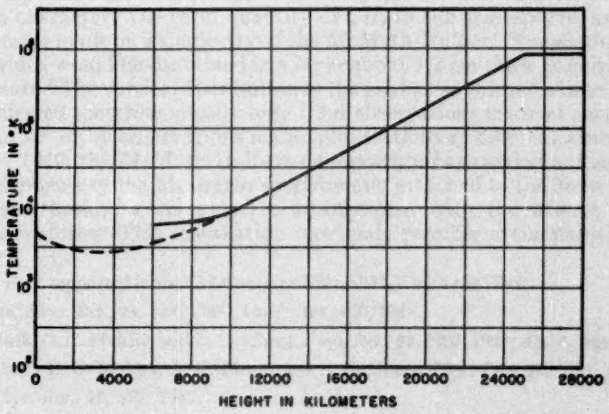

FIG. 12.—The calculated temperature for the lower atmosphere. The full line indicates the distribution used in the report; the dotted line a possible temperature distribution.

earlier, the electron density in the lower chromosphere must be reduced to a value about one-tenth that shown in Figure 5. This would, in effect, modify the temperature distribution shown in Figure 12 by shifting the origin to the right, so that the rapid rise in temperature would occur in the chromosphere rather than at the top of the chromosphere, as previously shown. This question cannot be finally resolved until better data on the electron concentration in the chromosphere are obtained. The observation of solar radiation at radio frequencies during a total eclipse of the sun can yield this, and every effort should be made at future eclipses to obtain data on the variation of the radio emission at several wave lengths during the course of the eclipse.

Through recent discussions with D. H. Menzel concerning the filamentary structure of the chromosphere, the author is led to believe that an alternative explanation of the disagreement is that the optical measurements are of the hot filaments, whereas the radio measurement is of the cooler background and is affected only slightly by the hot filaments because of their low average density.

I am indebted to Mr. R. J. McEwan and Mr. F. T. Haddock for assistance in this work. For a critical reading of the manuscript and for many helpful suggestions I am indebted to Francis J. Heyden, S.J.

THE ABUNDANCE AND VERTICAL DISTRIBUTION OF METHANE IN THE EARTH'S ATMOSPHERE*

LEO GOLDBERG
McMath-Hulbert Observatory, University of Michigan, Pontiac, Michigan
Received December 20, 1950

ABSTRACT

Theoretical expressions are derived for the equivalent widths of CH_4 lines formed in the earth's atmosphere which take into account the variation of pressure and temperature with altitude in the atmosphere. When allowance is made for the curvature of the earth, information on the vertical distribution of CH_4 can be obtained from low-sun observations.

The theoretical formulae have been employed for the analysis of observations of the 0–1, 5–6, and 10–11 lines in the 2 ν_3 band of CH_4 at 1.666 μ in the solar spectrum. From observations made at Lake Angelus, Michigan, and Mount Wilson, California, the total numbers of CH_4 molecules per square centimeter through the zenith are found to be 3.2×10^{19} and 2.6×10^{19}, respectively. The ratio of abundances is very nearly that which would be expected if the distribution of CH_4 is world-wide and falls off exponentially with height at the same rate as the main body of the atmosphere.

The observations are well represented by theoretical curves of growth for pure damping, with $\gamma/4\pi = 1.2 \times 10^9$ sec^{-1} for Lake Angelus and $\gamma/4\pi = 1.0 \times 10^9$ sec^{-1} for Mount Wilson. Within the experimental error the ratio of damping constants is equal to the ratio of ground-level pressures at the two stations, in agreement with theory.

INTRODUCTION

The presence of methane in the earth's atmosphere has been deduced from observations of the infrared solar spectrum at six widely separated points on the earth's surface, namely, at Columbus, Ohio;[1] at Lake Angelus, Michigan;[2] at Mount Wilson, California;[3] at Flagstaff, Arizona;[4] at Baltimore, Maryland;[5] and on the Jungfraujoch, Switzerland.[6] Since the observations referred to have extended over a period of ten years, it appears that CH_4 is a permanent constituent of the atmosphere and that its distribution is world-wide in character. The total quantity of CH_4 in the atmosphere, as determined from observations made on a single day at the McMath-Hulbert Observatory, is equivalent to that which would be contained in a layer about 1.2 cm thick at normal temperature and pressure.[7] The vertical distribution of the gas has not hitherto been investigated and can be inferred spectroscopically only from observations made at solar zenith distances close to 90° or by observations made from stations at different altitudes.

Since May, 1949, the McMath-Hulbert Observatory has carried out solar observations with a duplicate of the McGregor spectrometer attached to the Snow telescope on Mount Wilson, through a co-operative arrangement with the Mount Wilson and Palomar Observatories. This installation has made possible a comparative study of

* Report on work supported in part by Contract N6onr-232-V with the ONR.

[1] M. Migeotte, *Phys. Rev.*, **73**, 519, 1948; *Ap. J.*, **107**, 400, 1948.

[2] R. R. McMath, O. C. Mohler, and L. Goldberg, *Phys. Rev.*, **73**, 1203, 1948; *Ap. J.*, **109**, 17, 1949.

[3] R. R. McMath, O. C. Mohler, A. K. Pierce, and L. Goldberg, *Phys. Rev.*, **76**, 1533, 1949.

[4] A. Adel, *Phys. Rev.*, **75**, 322, 1949.

[5] W. Benesch, T. Elder, and J. Strong, *Progress Report on Spectrum of the Lower Atmosphere from 2.5 to 4.0 Microns* (ONR Contract N5ori-166-V, September 15, 1950).

[6] M. Migeotte, reported at Ohio State symposium, June, 1950.

[7] R. R. McMath and L. Goldberg, *Proc. Amer. Phil. Soc.*, **93**, 362, 1949.

telluric absorption bands from two different altitudes (Lake Angelus, 296 meters; Mount Wilson, 1742 meters). Furthermore, observations with the sun close to the horizon are made more conveniently from Mount Wilson. The present paper deals with the analysis of the intensities of the 0–1, 5–6, and 10–11 lines of the positive branch of the $2\nu_3$ band of CH_4, as observed both from Lake Angelus and from Mount Wilson. The chief purpose of the investigation was to determine the abundance of CH_4 and to infer the vertical distribution of the gas both from comparison of its abundance over Lake Angelus and Mount Wilson and from the observed variation of line intensity with solar altitude near the horizon.

Inasmuch as the resolving power of near infrared spectrometers is not yet sufficient to record the true profiles of all but the very widest absorption lines, the theoretical discussion will be confined to the derivation of expressions for the equivalent widths of telluric absorption lines. The problem is complicated by the nonhomogeneity of the earth's atmosphere, i.e., the density, pressure, temperature, and therefore the absorption coefficient vary with height. W. H. J. Childs,[8] C. W. Allen,[9] and H. C. van de Hulst[10] have shown, however, that the calculation of equivalent widths can be accomplished in a straightforward fashion by the adoption of a suitable model atmosphere. Their results are generally applicable to diatomic and linear polyatomic molecules, for which the partition function depends linearly on the temperature. For CH_4, however, the partition function is proportional to the three-halves power of the temperature, and new formulae for the line intensities must therefore be derived.

In an isothermal atmosphere of constant pressure the relation between the equivalent widths of a telluric line and the secant of the sun's zenith distance defines the so-called "curve of growth" of the absorption line. This relation is valid, of course, only for the case of a plane-parallel atmosphere or, in the case of the spherical earth, for values of $\sec z <$ about 10. Allen's investigation showed that the equivalent width of an absorption line produced in the nonhomogeneous earth's atmosphere closely approximates that which would be formed in a homogeneous atmosphere in which the density is equal to that at ground level and the damping constant is half the ground value. In short, the curve-of-growth relationship holds for the nonhomogeneous atmosphere, provided that suitable values of the parameters are chosen. Allen's theoretical curve of growth, which allows for the combined effects of Doppler and collisional broadening, differs inappreciably from that for pure damping.

Van de Hulst's treatment of the problem is more detailed and exact. By taking account of the dependence of the damping constant on the square root of the temperature, he shows that the effective damping constant increases with excitation potential, E, from a value 0.48 γ_0 for $E = 0$, to 0.73 γ_0 for $E = 2000$ cm^{-1}, where γ_0 is the damping at ground level. He also finds that the total numbers of molecules in the various excited states, integrated through the atmosphere, cannot be represented by a Boltzmann distribution. However, two asymptotic effective temperatures appear to be valid for $E = 0$, namely, $T_0/T_e = 1.20$ for weak lines on the linear branch of the curve of growth and $T_0/T_e = 1.09$ for strong lines on the square-root branch, where T_0 and T_e are the ground and effective temperatures, respectively. The physical meaning of the two temperatures is not clear, inasmuch as the effective temperature is defined by the distribution of molecules in the various excited states. The "temperature" may vary with excitation potential but should be independent of the line intensity. It will be shown in the next section that a single asymptotic effective temperature is valid for all lines, although both the effective te nperature and the effective damping constant depend on the excitation potential.

[8] *Ap. J.*, **77**, 212, 1933.

[9] *Ap. J.*, **85**, 156, 1937.

[10] *Ann. d'ap.*, **8**, 1, 12, 1945.

THEORY

Van de Hulst[11] has given the following expressions for the equivalent widths of absorption lines formed in a nonhomogeneous atmosphere:

$$W_{\mathrm{I}} = \int_0^L S\,dl; \tag{1}$$

$$W_{\mathrm{II}}^2 = \frac{1}{\pi}\int_0^L S\gamma\,dl, \tag{2}$$

where the integration is to be taken over the entire length of the absorbing column. In equations (1) and (2), W_{I} and W_{II} are the equivalent widths, in frequency units, of lines on the linear and square-root branches of the curve of growth, respectively. It is assumed that the lines are formed by pure absorption and that they are widened solely by collisions between molecules. The absorption coefficient per unit volume at any point is assumed to be given by the Lorentz-Weisskopf formula for collisional broadening, viz.,

$$s_\nu = S\,\frac{\gamma/4\pi^2}{(\nu-\nu_0)^2+(\gamma/4\pi)^2}, \tag{3}$$

where γ is the damping constant. Therefore, S is the line-absorption coefficient per unit volume, integrated over all frequencies, thus:

$$S = \int_0^\infty s_\nu\,d_\nu = \frac{\pi e^2}{m\,c}\,f_{JJ'}n_J. \tag{4}$$

In equation (4) $f_{JJ'}$ is the f-value for a transition between lower-level J and upper-level J', and n_J is the number of molecules per unit volume in level J. The geometry of the absorbing column is shown in Figure 1. The angle z is the sun's zenith distance, x is the height in the atmosphere measured upward from ground level, l is the distance along the absorbing column, and R is the radius of the earth. The element of path length, dl, is given by

$$dl = \frac{(1+x/R)}{(\cos^2 z + 2x/R + x^2/R^2)^{1/2}}\,dx. \tag{5}$$

The ratio x/R is very small compared with unity throughout the region where absorption is appreciable. For example, when $x = 100$ km, $x/R \backsim 1/64$. It will therefore be sufficient to neglect x/R as compared with unity and to write, for equation (5),

$$dl = \frac{dx}{(\cos^2 z + 2x/R)^{1/2}}. \tag{6}$$

In the plane-parallel approximation, $R \to \infty$, and we obtain the familiar secant law,

$$dl = dx \cdot \sec z. \tag{7}$$

In equations (1) and (2), both S and γ depend upon the density and temperature; they are therefore functions of the altitude x. To evaluate the integrals, we must adopt a suitable model atmosphere. Following Allen,[12] we shall assume that the density of the molecules considered decreases exponentially with altitude. Let n_x denote the total number of molecules of a particular kind per unit volume; then

$$n_x = n_0 e^{-ax}, \tag{8}$$

[11] *Op. cit.* [12] *Op. cit.*

where the subscript zero refers to the value of n_x at ground level. The total number of molecules per unit cross-section through the atmosphere, then, is n_0/a. We shall also employ Allen's expression for the temperature gradient, namely,

$$T = \frac{T_0}{(1 + x/\beta)}, \tag{9}$$

where T_0 is the ground temperature and β is a constant equal to 5.3×10^6 cm. Equation (9) does not take account of the isothermal region between 10 and 20 km or of the reversal in temperature gradient above 20 km, but it is sufficient for our purpose, in view of the assumed exponential decrease in density.

WEAK LINES

We shall proceed, first, to calculate the equivalent widths of molecular lines on the linear branch of the curve of growth. For simplicity, we have confined the observations

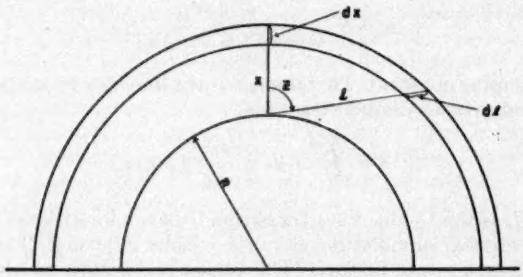

FIG. 1.—Geometry of the earth's atmosphere

of the weak lines of CH_4 to the range of solar altitudes for which the plane-parallel approximation is valid. Hence we may use equation (7) for dl and write, for equation (1),

$$W_I = \frac{\pi e^2}{m c} f_{JJ'} \sec z \int_0^\infty n_J dx, \tag{10}$$

where

$$N_J = \int_0^\infty n_J dx \tag{11}$$

is the total number of molecules per unit cross-section through the zenith in level J. If we make use of the Boltzmann formula and equation (8), we have

$$n_J = \frac{n_0 e^{-ax}}{b(T)} g_J e^{-E_J/kT}, \tag{12}$$

where E_J is the energy, g_J the statistical weight of level J, and $b(T)$ the partition function. For diatomic and linear polyatomic molecules (O_2, CO_2, N_2O, etc.),[13]

$$b(T) = 0.695 \frac{T}{B}, \tag{13}$$

[13]G. Herzberg, *Infrared and Raman Spectra* (New York: D. van Nostrand Co., 1946), p. 505.

where B is the average half-spacing of the band lines in cm^{-1}. For spherical top molecules (CH_4),[14]

$$b(T) = 1.027\left(\frac{T}{B}\right)^{3/2}. \tag{14}$$

Since T varies with height in the atmosphere, the equivalent widths must be calculated separately for each type of molecule. We give in detail here the calculation for CH_4. Let b_0 be the value of the partition function for $T = T_0$, i.e., at ground level. Then, from equations (9) and (14), we have

$$b(T) = b_0\left(1+\frac{x}{\beta}\right)^{-3/2}. \tag{15}$$

If we now substitute expression (12) for n_J in equation (11) and write $T = T(x)$, we obtain

$$N_J = g_J\frac{n_0}{b_0}e^{-E_J/kT_0}\int_0^\infty\left(1+\frac{x}{\beta}\right)^{3/2}e^{-(a+E_J/\beta kT_0)x}dx. \tag{16}$$

Make the following substitution:

$$y = y_0\left(1+\frac{x}{\beta}\right)^{1/2}, \tag{17}$$

where

$$y_0 = (A_1\beta)^{1/2} \tag{18}$$

and

$$A_1 = a+\frac{E_J}{\beta kT_0}. \tag{19}$$

Then the integral in equation (16) reduces to

$$\frac{1}{A_1}\frac{e^{y_0^2}}{y_0^3}\int_{y_0}^\infty y^3e^{-y^2}dy^2 = \frac{1}{A_1}\left(1+\tfrac{3}{2}\frac{1}{y_0^2}+\tfrac{3}{2}\frac{e^{y_0^2}}{y_0^3}\int_{y_0}^\infty e^{-y^2}dy\right). \tag{20}$$

With $a = 1.10\times10^{-6}\ cm^{-1}$ and $\beta = 5.3\times10^6$ cm, the minimum value of y_0 is about 2.4. It is therefore permissible to substitute for the error function in equation (20) the first term of its asymptotic expansion, namely,

$$\int_{y_0}^\infty e^{-y^2}dy \sim \frac{e^{-y_0^2}}{2y_0}. \tag{21}$$

The final expression for N_J becomes

$$N_J = \frac{n_0}{b_0}g_Je^{-E_J/kT_0}\frac{1}{A_1}\left(1+\tfrac{3}{2}\frac{1}{A_1\beta}+\tfrac{3}{4}\frac{1}{A_1^2\beta^2}\right). \tag{22}$$

Inasmuch as A_1 is a function of the excitation potential, it is clear that a single effective temperature will not represent exactly the populations of all the rotational levels. To a good approximation, when E_J is small, however,

$$\frac{1}{A_1} = \left[\frac{1}{a}\left(1+\frac{E_J}{a\beta kT_0}\right)^{-1}\right] \sim \frac{1}{a}e^{-E_J/a\beta kT_0} \tag{23}$$

and

$$1+\tfrac{3}{2}\frac{1}{A_1\beta}+\tfrac{3}{4}\frac{1}{A_1^2\beta^2} \sim \left[1+\frac{1}{A_1\beta}\right]^{3/2} \sim \left[1+\frac{1}{a\beta}\right]^{3/2}. \tag{24}$$

[14] *Ibid.*, p. 506.

Hence

$$N_J\,(\text{effective}) = \frac{n_0}{a}\left[\frac{g_J}{b_0}\left(1+\frac{1}{a\beta}\right)^{3/2}\right] e^{-(E_J/k)\,(1/[T_0(1+1/a\beta)^{-1}])} \tag{25}$$

$$= \frac{n_0}{a}\left[\frac{g_J}{b\,(T_e)}\right] e^{-E_J/kT_e},$$

where

$$T_e = \frac{T_0}{1+1/a\beta}. \tag{26}$$

Within the limits of approximations (23) and (24), therefore, the total numbers of molecules in the various J levels are identical with those that would be found in an equivalent homogeneous atmosphere at the temperature T_e given by equation (26).

Recalling that

$$T = \frac{T_0}{1+x/\beta}, \tag{9}$$

we note that the effective temperature is that occurring at an altitude $x = 1/a \sim 9$ km. The observed effective temperature may be slightly higher than the predicted one, since the latter does not take account of the isothermal stratosphere.

TABLE 1

POPULATIONS OF ROTATIONAL LEVELS OF CH_4 AS COMPARED WITH BOLTZMANN DISTRIBUTION AT EFFECTIVE TEMPERATURE T_e

J	N_J/N_J (eff.)	J	N_J/N_J (eff.)	J	N_J/N_J (eff.)
0	1.009	4	0.993	8	0.993
1	1.007	5	.989	9	1.004
2	1.003	6	.987	10	1.021
3	0.998	7	0.988		

The extent to which the ratio $N_J(\text{eff.})/N_J$ departs from unity measures the validity of approximation (25). The ratio is given by

$$\frac{N_J}{N_J\,(\text{eff.})} = \frac{a}{A_1}\,\frac{1+\frac{3}{2}\,(1/A_1\beta)+\frac{3}{4}\,(1/A_1^2\beta^2)}{(1+1/a\beta)^{3/2}}\; e^{E_J/a\beta kT_0}. \tag{27}$$

As a numerical example, we adopt $a = 1.10 \times 10^{-6}$ cm^{-1}, $\beta = 5.3 \times 10^6$ cm, and $T_0 = 288°$ K. The energies of the rotational levels of CH_4 in the lowest vibrational state are

$$E_J = Bhc\,J\,(J+1), \tag{28}$$

with $B = 5.163$ cm^{-1}. The results of the calculation of N_J/N_J(eff.) for the levels $J = 0$ to $J = 10$ are shown in Table 1. We conclude that the Boltzmann formula with effective temperature given by equation (9) represents with high accuracy the populations of the levels up to $J = 10$, the practical limit of observation for the $2\nu_3$ band of CH_4.

STRONG LINES

We next employ equation (2) and our adopted model atmosphere to derive an expression for the equivalent widths of the strong lines of CH_4. We assume that the damping

constant, γ, is proportional to the density and to the square root of the temperature. Hence

$$\gamma = \gamma_0 e^{-ax}\left(1+\frac{x}{\beta}\right)^{-1/2}, \tag{29}$$

where γ_0 is the damping at ground level. For dl we use equation (6) and thereby validate the theory for low solar altitudes. After the indicated substitutions are performed, equation (2) becomes

$$W_{II}^2 = \frac{1}{\pi}\frac{\pi e^2}{mc} f_{JJ'}\frac{n_0}{b_0} g_J \gamma_0 e^{-E_J/kT_0}\int_0^\infty \frac{[(1+x/\beta)\, e^{-(2a+E_J/\beta k T_0)x}]}{(\cos^2 z + 2x/R)^{1/2}}\, dx. \tag{30}$$

Let

$$A_2 = 2a + \frac{E_J}{\beta k T_0}, \tag{31}$$

and make the substitution

$$y^2 = y_0^2 + Ax, \tag{32}$$

where

$$y_0^2 = \frac{A_2 R}{2}\cos^2 z. \tag{33}$$

Then the integral in equation (30) reduces to

$$\frac{2y_0 e^{y_0^2}}{A_2^2\beta}\sec z\int_{y_0}^\infty (y^2 - y_0^2 + A_2\beta)\, e^{-y^2} dy \tag{34}$$

$$= \frac{y_0 \sec z}{A_2^2\beta}\left[y_0 + (1 + 2A_2\beta - 2y_0^2)\, e^{y_0^2}\int_{y_0}^\infty e^{-y^2} dy\right]. \tag{35}$$

The solution of equation (2), taking into account the curvature of the earth's atmosphere, is given in calculable form by equations (30) and (35). The physical significance of the solution is more readily apparent from the plane-parallel approximation, which is obtained from equation (35) when y_0 is large enough that

$$e^{y_0^2}\int_{y_0}^\infty e^{-y^2} dy = \frac{1}{2y_0}\left(1 - \frac{1}{2y_0^2}\right). \tag{36}$$

The solution of equation (30) is then simply

$$W_{II}^2 = \frac{1}{\pi}\frac{\pi e^2}{mc} f_{JJ'}\frac{n_0}{b_0} g_J \gamma_0 e^{-E_J/kT_0}\sec z\left[\frac{(1+1/A_2\beta)}{A_2}\right]. \tag{37}$$

Equation (37) may also be written in the form

$$W_{II}^2 = \frac{1}{\pi}\frac{\pi e^2}{mc} f_{JJ'} N_J \sec z\, \gamma_e, \tag{38}$$

with N_J given by equation (22). The effective damping constant is therefore

$$\gamma_e = \frac{A_1}{A_2}\frac{(1/A_2 + 1/\beta A_2)}{[1 + \frac{3}{2}(1/A_1\beta) + \frac{3}{4}(1/A_1^2\beta^2)]}\,\gamma_0. \tag{39}$$

Numerical values of the ratio γ_e/γ_0 for CH_4 are shown in Table 2. The ratio of the effective damping constant to that at ground level increases slowly with excitation potential from a value of 0.42 for $E_J = 0$ to a value of 0.54 for $E_J = 570$ cm^{-1}.

Expressions similar to those obtained above for CH_4 may also be derived for other molecules by suitable choice of partition functions. For diatomic and linear polyatomic molecules the partition function $b(T)$ varies linearly with temperature:

$$b(T) = b_0\left(1+\frac{x}{\beta}\right)^{-1}. \tag{40}$$

The total number of molecules, N_J, then, is

$$N_J = \left[g_J \frac{n_0}{b_0} \sec z\, e^{-E_J/kT_0}\right]\left[\frac{1}{A_1}\left(1+\frac{1}{A_1\beta}\right)\right]. \tag{41}$$

The effective temperature for small values of J can be shown to be identical with that found for CH_4, namely,

$$T_e = \frac{T_0}{1+1/a\beta}. \tag{26}$$

The effective damping constant is

$$\gamma_e = \frac{A_1}{A_2}\frac{(1+1/2A_2\beta)}{(1+1/A_1\beta)}\gamma_0. \tag{42}$$

TABLE 2

RATIO OF EFFECTIVE DAMPING γ_e TO DAMPING AT GROUND LEVEL γ_0 FOR LINES OF CH_4

J	γ_e/γ_0	J	γ_e/γ_0	J	γ_e/γ_0
0	0.42	4	0.45	8	0.50
1	.43	5	.46	9	.52
2	.43	6	.47	10	0.54
3	0.44	7	0.49		

ANALYSIS OF $2\nu_3$ BANDS

In the preceding section we found that the equivalent widths of both weak and strong telluric lines of CH_4 could be reproduced accurately by an atmosphere of uniform density with suitably chosen effective temperature and damping. The appropriate expressions, in wave-length units, are, for weak lines,

$$\frac{W}{\lambda} = \frac{\lambda}{c}\frac{\pi\epsilon^2}{mc} f_{JJ'} N_J \sec z \tag{43}$$

and, for strong lines,

$$\frac{W}{\lambda} = \frac{\lambda}{c}\left[\frac{1}{\pi}\frac{\pi\epsilon^2}{mc} f_{JJ'}\gamma_e N_J \sec z\right]^{1/2}, \tag{44}$$

where N_J is given by the Boltzmann formula;

$$N_J = \frac{n_0}{a}\left[\frac{g_J}{b(T_e)}\right] e^{-E_J/kT_e}. \tag{45}$$

For convenience, we make the substitutions

$$\tau_0 = \frac{4}{\gamma_e}\frac{\pi\epsilon^2}{mc} f_{JJ'} N_J \tag{46}$$

and

$$\delta_e = \frac{\lambda \gamma_e}{4c}. \tag{47}$$

Then equations (43) and (44) become, respectively,

$$\frac{W}{\lambda} = \delta_e \tau_0 \sec z \tag{48}$$

and

$$\frac{W}{\lambda} = 2\left(\frac{\delta_e}{\pi}\right)^{1/2} (\delta_e \tau_0)^{1/2} (\sec z)^{1/2}. \tag{49}$$

Equations (47) and (48) represent the asymptotes of the curve of growth for $\tau_0 \ll 1$ and $\tau_0 \gg 1$, respectively. For intermediate values of τ_0, the equivalent widths may be determined by numerical or graphical integration of the computed line profiles. Observational curves of growth may be derived either by holding sec z constant and plotting log W/λ against relative values of log $\delta_e \tau_0$ for the various band lines or by keeping $\delta_e \tau_0$ constant and varying sec z for each line separately. In theory the latter method is preferable, since it makes possible the construction of a separate curve of growth for each line, without advance knowledge of the excitation temperature. Practically, however, it is impossible to define the complete curve of growth from observations of a single line because the path length is proportional to sec z only for values of sec z less than about 10.

The advantages of both methods may be combined, however, if we construct curves of growth by the sec z method for, say, three lines of different intensity and combine the curves by displacing them along the sec z axis. Also, if the lines cover a wide range of excitation potential, they may be employed for the determination of the effective temperature.

The lines selected for observation were the 0–1, 5–6, and 10–11 members of the $2\nu_3$ band of CH_4. The values of log W/λ, observed at Lake Angelus and at Mount Wilson, are plotted against log sec z in Figures 2–7, inclusive. The 0–1 and 10–11 lines fall mainly on the linear branch of the curve of growth, whereas the 5–6 line defines the intermediate and square-root branches. The observations show little evidence, within the errors of measurement, for a seasonal variation in the abundance of CH_4. It is to be expected that temperature variations will produce small seasonal changes in the line intensities. For example, an increase of 10° K in the effective temperature would decrease log N_J for the $J = 0$ and $J = 5$ levels by 0.03 and 0.01, respectively. For the $J = 10$ level, a similar increase in T_e would increase log N_J by 0.03. The resulting changes in intensity would probably be too small to be detected. The noonday ground temperatures for the dates of observation are given in Table 3. It is clear that fluctuations in temperature do not contribute appreciably to the scatter of points in Figures 2–7.

Two observations of the 5–6 line at Mount Wilson were made with the sun close to the horizon, at values of sec z equal to about 25 and 60, after correction for refraction. The straight line at the left of Figure 6 has a slope of $\frac{1}{2}$ and represents the square-root branch of the curve of growth. Deviation from the square-root law sets in at about sec $z = 10$, and for larger values the equivalent widths are determined by the vertical distribution of the absorbing gas. Curve *a* was calculated from equation (30), on the assumption that the density of CH_4 decreases exponentially with altitude. Curves *b* and *c* represent the calculated variation of equivalent width in the case where the gas is concentrated in a thin homogeneous layer at altitudes of 5 and 10 km, respectively. The intensities are difficult to measure when the sun is 1° or 2° above the horizon, owing chiefly to uncertainties in the location of the continuous background. Additional observations of the 5–6 line are being secured to define more accurately the intensity variation near the horizon. The two observations shown in Figure 6 suggest, however, that CH_4 in the earth's atmosphere is not concentrated at high altitudes but is located mainly in the troposphere.

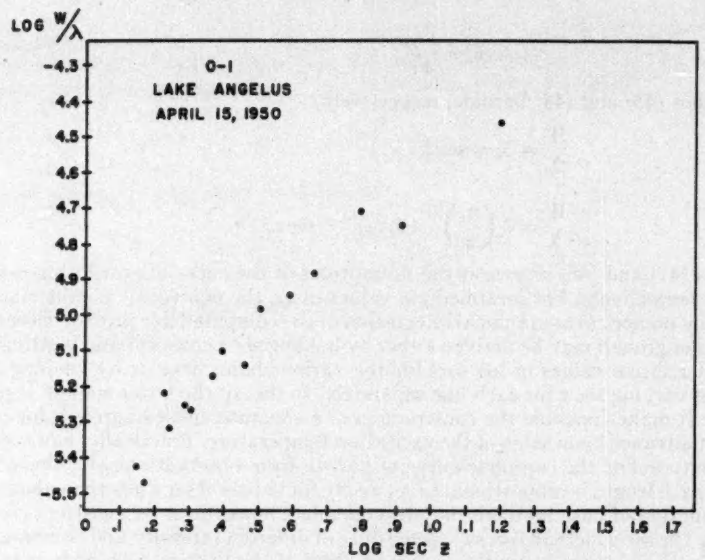

FIG. 2.—Observed curve of growth, 0–1 line, Lake Angelus

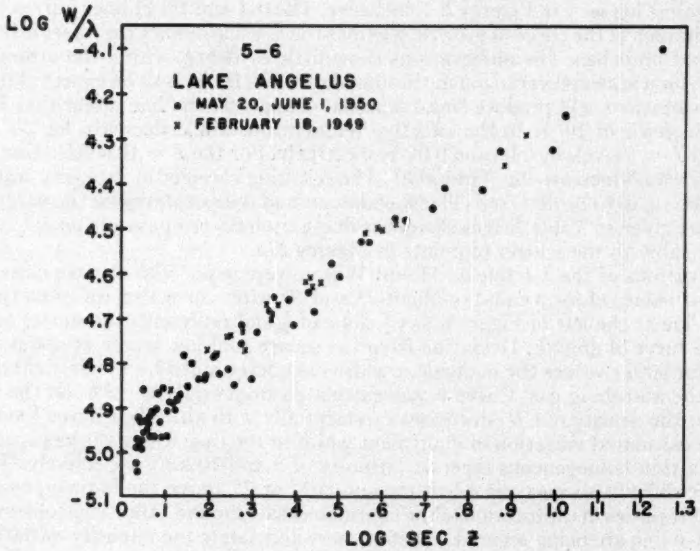

FIG. 3.—Observed curve of growth, 5–6 line, Lake Angelus

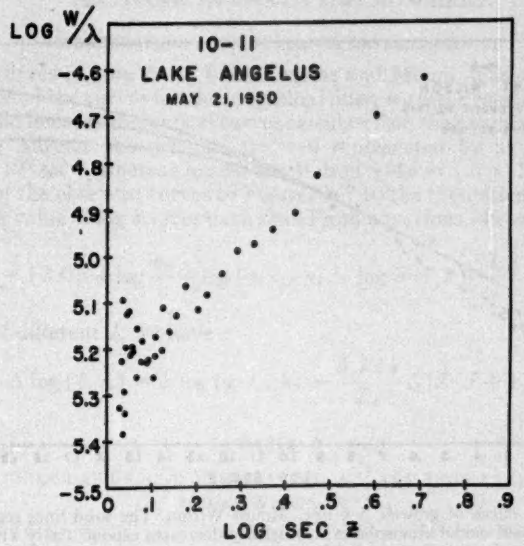

FIG. 4.—Observed curve of growth, 10–11 line, Lake Angelus

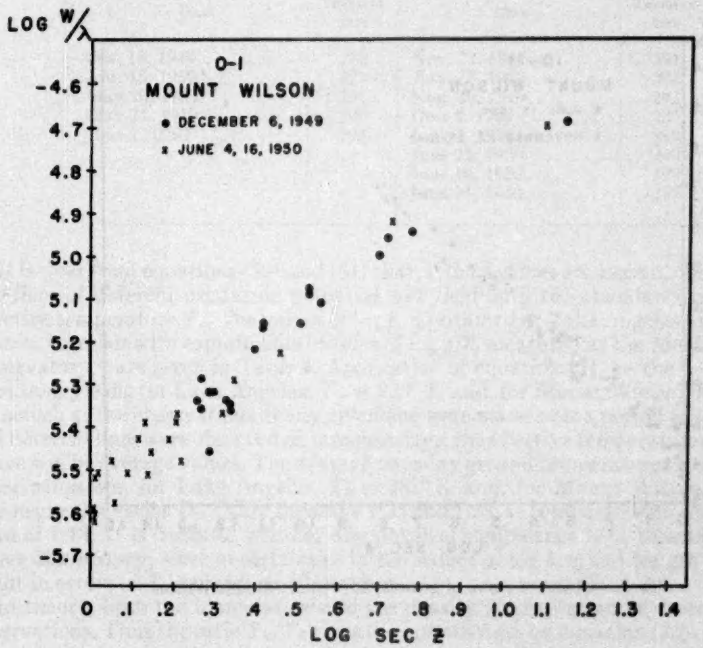

FIG. 5.—Observed curve of growth, 0–1 line, Mount Wilson

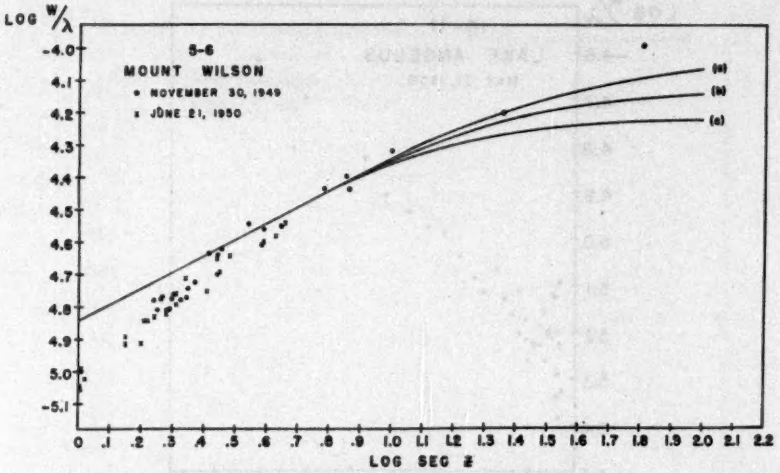

FIG. 6.—Observed curve of growth, 5–6 line, Mount Wilson. The solid lines represent theoretical curves for three assumed model atmospheres: (*a*) density decreases exponentially with height; (*b*) thin layer at height of 5 km; (*c*) thin layer at height of 10 km.

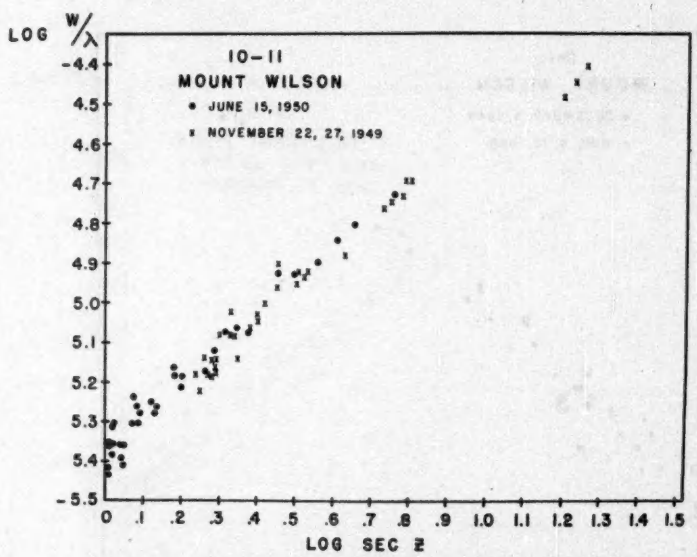

FIG. 7.—Observed curve of growth, 10–11 line, Mount Wilson

TEMPERATURE AND ABUNDANCE DETERMINATIONS

Composite curves of growth for Lake Angelus and Mount Wilson were constructed by superposition of the curves for the individual lines, with the results shown in Figures 8 and 9. The solid lines are theoretical curves calculated on the assumption of pure damping. The Lake Angelus observations are well represented by a damping constant, $\gamma/4\pi = 1.2 \times 10^9$ sec^{-1}, whereas for Mount Wilson $\gamma/4\pi = 1.0 \times 10^9$ sec^{-1}.

The fitting of the observed curves of Figures 2–7 to the theoretical curves of Figures 8 and 9 yields a value of log $\delta_e\tau_0$ for each line. From equations (46) and (47), we obtain

$$\log \delta_e \tau_0 = -12.05 + \log \frac{n_0}{a} + \log (g_J f_{JJ'} \lambda) - \log b(T_e) - \frac{3.224 J(J+1)}{T_e}. \quad (50)$$

For two lines of different J, we have

$$\Delta \log (\delta_e \tau_0) = \Delta \log (g_J f_{JJ'} \lambda) - \frac{3.224}{T_e} \Delta [J(J+1)]. \quad (51)$$

TABLE 3

NOONDAY GROUND TEMPERATURES AT LAKE ANGELUS AND MOUNT WILSON IN ° K

Lake Angelus		Mount Wilson	
Date	Temperature	Date	Temperature
Feb. 18, 1949	282	Nov. 22, 1949	291
Apr. 15, 1950	277	Nov. 27, 1949	292
May 20, 1950	291	Nov. 30, 1949	292
May 21, 1950	296	Dec. 6, 1949	285
June 1, 1950	293	June 4, 1950	299
		June 15, 1950	290
		June 16, 1950	290
		June 21, 1950	295

It is clear from equations (50) and (51) that, if the f-values are known, observations of two lines of different excitation potential will yield both the abundance n_0/a and the effective temperature T_e. The values of log $\delta_e\tau_0$ obtained at Lake Angelus and at Mount Wilson, together with experimental values of log $gf\lambda$, measured at the McMath-Hulbert Observatory,[15] are given in Table 4. Application of equation (51) to the 0–1 and 10–11 lines then yields, for Lake Angelus, $T_e = 229°$ K and, for Mount Wilson, $T_e = 227°$ K. Inasmuch as the observations of any given line were made over a period of several hours and different lines were observed on separate days, the effective temperatures determined above will be average values. The average noonday ground temperatures for the dates of observation are, for Lake Angelus, $T_0 = 287°$ K and, for Mount Wilson, $T_0 = 291°$. The respective ratios T_0/T_e are therefore 1.25 and 1.28, as compared with the theoretical ratio of 1.18. It is doubtful whether any physical significance is to be attached to the above discrepancy, since uncertainties in the values of log $\delta_e\tau_0$ and log $gf\lambda$ could easily result in errors in T_e as large as 10 per cent.

In theory, both the temperature and the density gradients can be derived from the observations. Thus the ratio T_e/T_0 gives the quantity $a\beta$, by equation (26). Further, the

[15] To be published elsewhere at a later date.

density gradient a can be obtained from a comparison of the abundances over Lake Angelus and Mount Wilson. In practice, however, a 10 per cent error in the effective temperature will introduce a 50 per cent error in the determination of $a\beta$. The method is therefore practicable only when applied to line intensities of the highest precision.

Once the effective temperatures are known, the abundance n_0/a may be found from equation (50). The results are tabulated in Table 4. The mean values of log (n_0/a) are, for Lake Angelus, 19.51 and, for Mount Wilson, 19.42. The corresponding numbers of molecules are 3.2×10^{19} cm^{-2} and 2.6×10^{19} cm^{-2}, respectively, the ratio of abundances

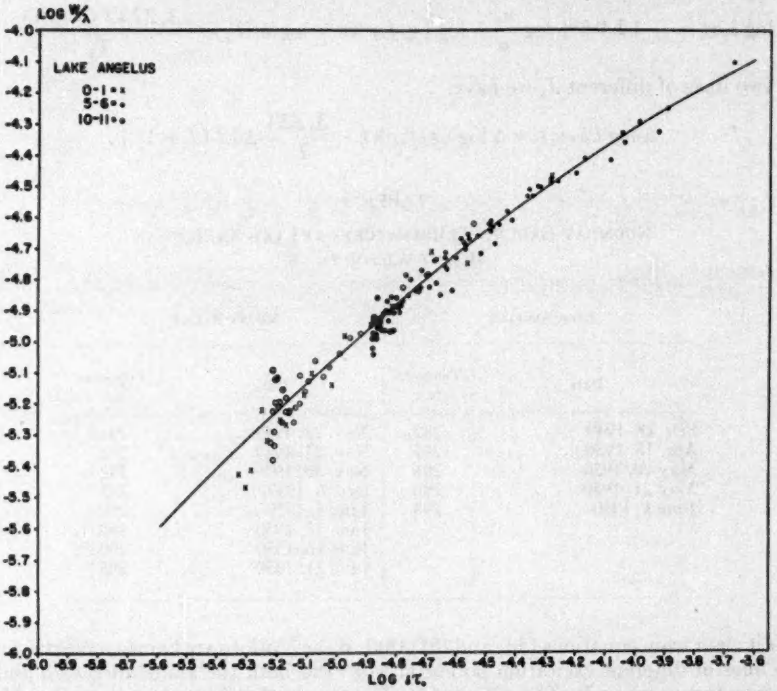

FIG. 8.—Composite curve of growth, Lake Angelus. The solid line is a theoretical curve for pure damping, with $\gamma/4\pi = 1.2 \times 10^9$ sec^{-1}.

TABLE 4

VALUES OF LOG $gf\lambda$, LOG $\delta_\tau\tau_0$ AND LOG n_0/a

LINE	LOG $gf\lambda$	LOG $\delta_\tau\tau_0$		LOG n_0/a	
		Lake Angelus	Mt. Wilson	Lake Angelus	Mt. Wilson
0–1	−10.51	−5.48	−5.61	19.56	19.43
5–6	− 9.38	−4.92	−4.95	19.41	19.39
10–11	− 8.73	−5.25	−5.39	19.56	19.43

being 1.23. In an atmosphere in hydrostatic equilibrium with $a = 1.10 \times 10^{-6}$ cm^{-1}, the ratio would be

$$e^{a \times \Delta h} = e^{1.10 \times 10^{-6} \times 1.45 \times 10^{5}} = 1.17 ,$$

where Δh is the altitude difference in centimeters. We may conclude that the observed relative abundance of CH_4 over Lake Angelus and Mount Wilson is consistent with the idea that the gas is evenly distributed around the earth and that its density falls off exponentially with height at about the same rate as the main body of the atmosphere. The abundance of CH_4 over Lake Angelus is equivalent to that which would be contained in a layer 1.25 cm thick at atmospheric pressure and at a temperature of 288° K.

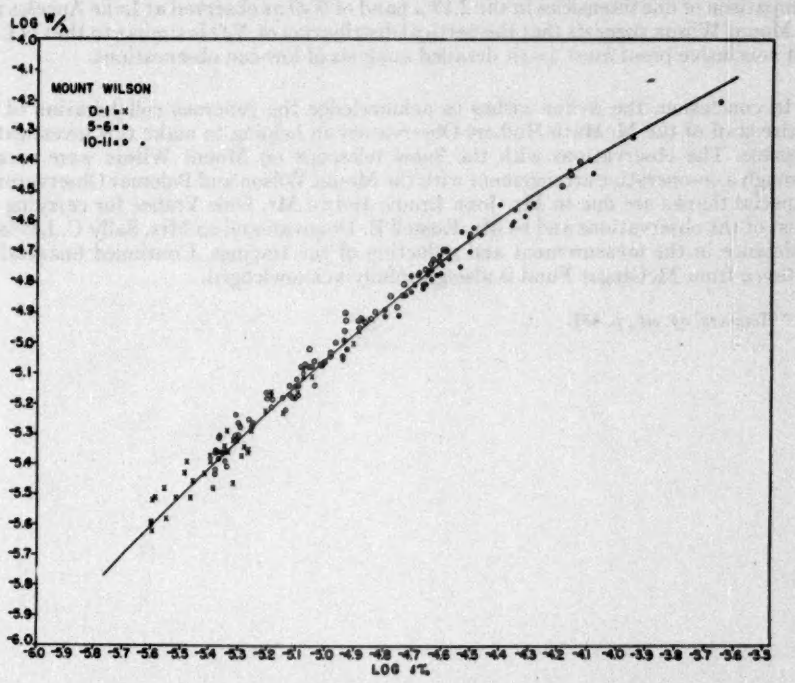

FIG. 9.—Composite curve of growth, Mount Wilson. The solid line is a theoretical curve for pure damping, with $\gamma/4\pi = 1.0 \times 10^{9}$ sec^{-1}.

DAMPING CONSTANTS

The observational curves of growth in Figures 8 and 9 are well represented by theoretical curves with $\gamma_e/4\pi = 1.2 \times 10^{9}$ sec^{-1} (Lake Angelus) and $\gamma_e/4\pi = 1.0 \times 10^{9}$ sec^{-1} (Mount Wilson). According to Table 2, the effective damping constant for the 5–6 line is 0.46 times the value at ground level. Hence the ground-level values, $\gamma_0/4\pi$, at Lake Angelus and at Mount Wilson are 2.6×10^{9} sec^{-1} and 2.2×10^{9} sec^{-1}, respectively. The Lorentz formula for the collisional damping constant is

$$\frac{\gamma}{4\pi} = N\sigma^2\left[\frac{2RT}{\pi}\left(\frac{1}{\mu_1}+\frac{1}{\mu_2}\right)\right]^{1/2}, \qquad (52)$$

where N is the total number of perturbing molecules per cubic centimeter, σ is the collision diameter, R is the gas constant, T is the absolute temperature, and μ_1 and μ_2 are the molecular weights of the colliding molecules. We adopt $N = 2.5 \times 10^{19}$, $T = 288°$ K, $\mu_1 = 29.2$, and $\mu_2 = 16$. With $\gamma/4\pi = 2.6 \times 10^9$, $\sigma^2 = 2.7 \times 10^{-15}$, or $\sigma = 5.2$ A. Similarly, both Allen and van de Hulst obtained $\sigma = 4.1$ A from their analyses of the A and B bands of O_2.

The relatively large collision diameter found for CH_4 can probably be ascribed to the Coriolis splitting[16] of the CH_4 lines, which is conspicuous in the high series members of the $2\nu_3$ band. In the 5–6 line the splitting is unresolved, but the line broadening is undoubtedly increased by the effect.

Studies similar to the above are also being carried out for CO_2 and N_2O. A preliminary comparison of line intensities in the 2.13 μ band of N_2O as observed at Lake Angelus and at Mount Wilson suggests that the vertical distribution of N_2O is similar to that of CH_4, but conclusive proof must await detailed analysis of low-sun observations.

In conclusion, the writer wishes to acknowledge the generous collaboration of the entire staff of the McMath-Hulbert Observatory in helping to make this investigation possible. The observations with the Snow telescope on Mount Wilson were secured through a co-operative arrangement with the Mount Wilson and Palomar Observatories. Especial thanks are due to Mr. John Brodie and to Mr. Dale Vrabec for carrying out most of the observations and to Mr. Russell E. Donovan and to Mrs. Sally C. Lewis for assistance in the measurement and reduction of the tracings. Continued financial assistance from McGregor Fund is also gratefully acknowledged.

[16] Herzberg, *op. cit.*, p. 451.

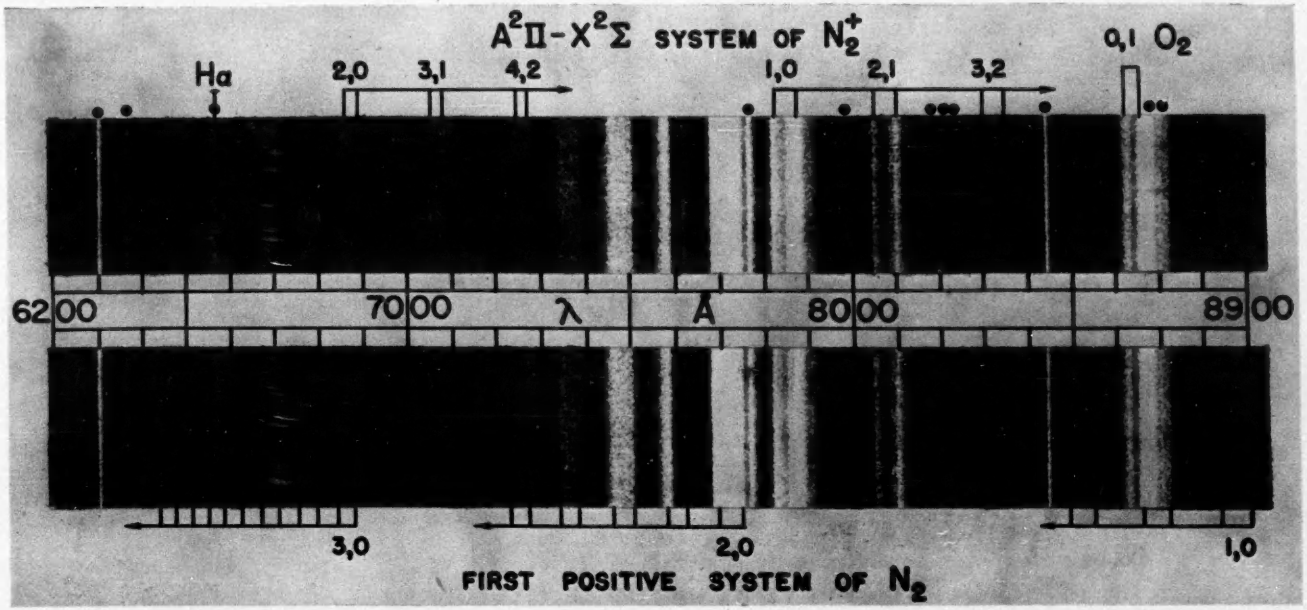

FIG. 1.—The auroral spectrum between 6200 and 8900 A. Exposure 1½ hours, Eastman I-N (hypersensitized), August 19, 1950

THE AURORAL SPECTRUM FROM 6200 TO 8900 A*

A. B. MEINEL
Yerkes Observatory
Received December 27, 1950

ABSTRACT

The infrared region of the auroral spectrum is rich in molecular and atomic emissions. The molecular bands are due to a new system of N_2^+, the first positive system of N_2, and the atmospheric system of O_2. Several permitted atomic lines of N I and O I, as well as $H\alpha$, are present. A table of wave lengths and intensities has been prepared.

The intense auroral storm of August 18 and 19, 1950, presented the opportunity to obtain exposures of varying duration covering the infrared spectrum as far as 8900 A. A brief description of the spectrograph used for these observations has been published.[1] The spectrum reproduced in Figure 1 shows the auroral spectrum as obtained with an exposure of 1½ hours on a hypersensitized Eastman I-N emulsion. Figures 2 and 3 are microphotometer tracings of this auroral spectrum. The two superimposed tracings are from the same plate, with tracing *a* from an effective zenith distance of 35° (N.) and tracing *b* from 55° (N.). It is interesting to note that $H\alpha$ in tracing *a* is shifted visibly to the violet of tracing *b*. The difference in air-path lengths between *a* and *b* is evident for the A-band absorption.

MOLECULAR BANDS

The most striking feature of the auroral spectrum in this region is the presence of a new band system, identified by the author[2] as being due to the $A^2\Pi - X^2\Sigma$ transition of N_2^+. The typical doublet appearance of these bands is readily seen. The tentative numbering of the bands is indicated in Figure 1. The observed intensities, however, would not exclude increasing the numbering of the upper vibrational levels by one or two numbers. Since both ω_e and $\omega_e x_e$ have been determined, the value of ν_e can readily be determined after the numbering is known.

The transition probability for the $A^2\Pi - X^2\Sigma$ bands must be small, since these bands have never been observed in the laboratory, although the transition is entirely permitted. On the other hand, the $B^2\Sigma - X^2\Sigma$ negative bands of N_2^+ have a high transition probability. In laboratory sources the $A^2\Pi - X^2\Sigma$ bands of N_2^+ are weaker than the negative bands of N_2^+ by a factor greater than 10. In the past the large transition probability of the negative bands has led to the conclusion that a small number of N_2^+ molecules would be sufficient to produce the auroral emissions. The great intensity of these new bands, however, requires a large upward revision of the number of N_2^+ molecules in the aurora. The excitation process must be such that a large number of excitations occurs to the $A^2\Pi$ level (1.35 e.v.) for each excitation to the $B^2\Sigma$ level (3.15 e.v.). This supposition then strongly indicates that the excitations of N_2^+ occur from the $X^2\Sigma$ level of N_2^+ rather than from the $X^1\Sigma$ state of the normal N_2 molecule, as is generally advocated. If the excitations were from the $X^1\Sigma$ state of N_2, then the populations in the $A^2\Pi$ and $B^2\Sigma$ states would depend on the relative ionization probabilities from the $X^1\Sigma$ state. Since N_2^+ in laboratory sources must largely arise from the $X^1\Sigma$ state because of the brief existence of the N_2^+ ions, the laboratory intensities then should not be appreciably dif-

* The investigation was supported in part by a grant from the Office of Naval Research.

[1] A. B. Meinel, *Ap. J.*, 111, 555, 1950.

[2] A. B. Meinel, *C.R.*, 231, 1049, 1950; *Ap. J.*, 112, 562, 1950.

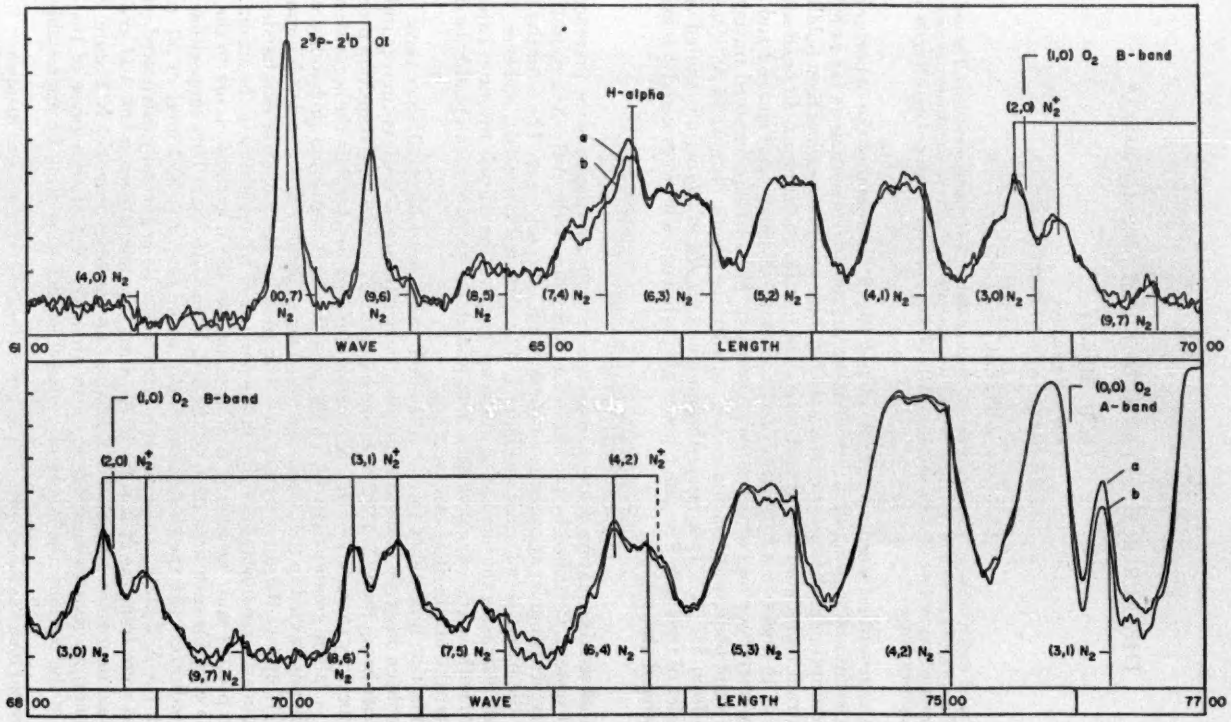

FIG. 2.—Microphotometer tracings of the auroral spectrum from 6100 to 7700 A

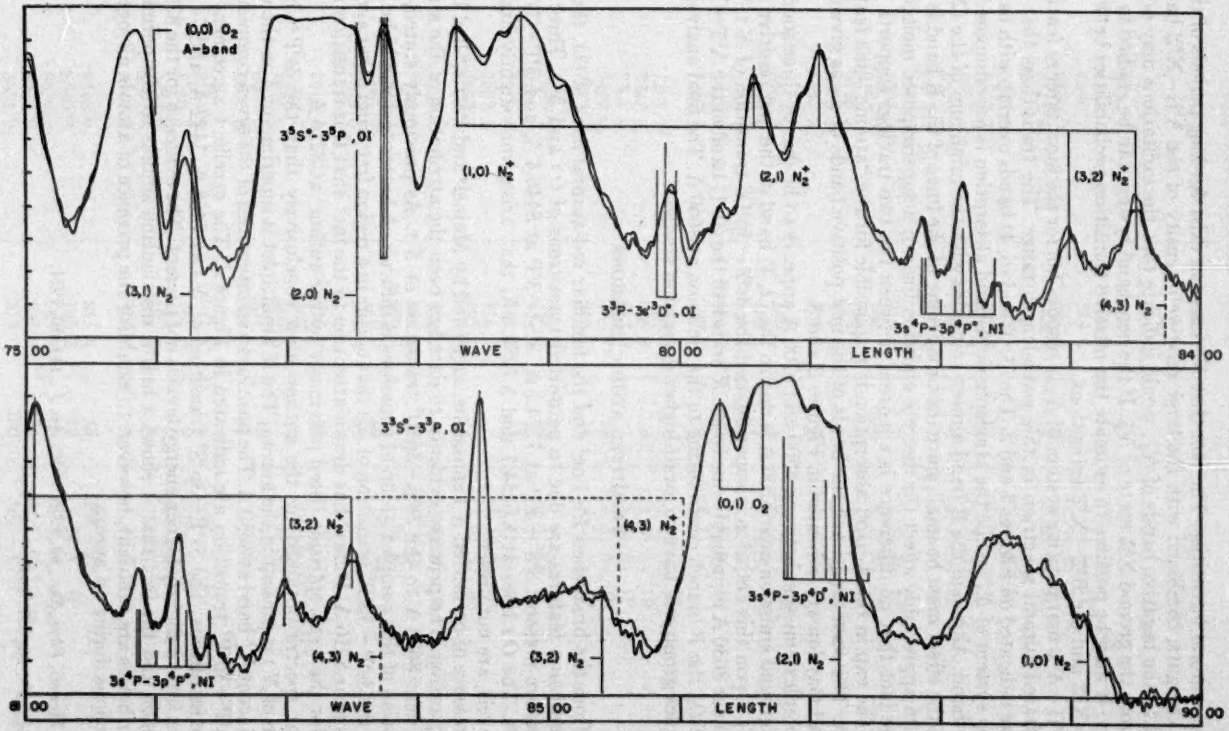

FIG. 3.—Microphotometer tracings of the auroral spectrum from 7500 to 9000 A

ferent from auroral intensities. The fact that N_2^+ ions can exist for long periods of time at auroral heights, combined with the large relative intensity of the $A^2\Pi-X^2\Sigma$ bands compared to the negative bands of N_2^+, would indicate that the excitations may occur directly from the ground $X^2\Sigma$ state of N_2^+. If the new band system can be studied in the laboratory, it may be possible to estimate the relative transition probabilities between the $A^2\Pi-X^2\Sigma$ and the $B^2\Sigma-X^2\Sigma$ transitions.

The $B^3\Pi-A^3\Sigma$ first positive system of N_2 is responsible for the most intense features of the infrared auroral spectrum in this wave-length range. The transitions that are present are indicated on Figures 1 and 2. The (3, 0) and (6, 4) bands overlap with bands of the new system of N_2^+, while the atmospheric A-band absorption is superimposed on the (3, 1) band. Although the B band almost coincides with the minimum of the (2, 0) N_2^+ band, the effect must be small, since the broadening of the lines of the B band is not sufficient to appreciably affect the discrete emission lines of a superimposed molecular band. The fact that no difference is apparent between the two tracings supports this opinion. The gap in the A-band absorption is responsible for the "atomic"-line feature at 7622 A. The wave lengths of the heads of the first positive bands of N_2 as given by Pearse and Gaydon are indicated in Figures 2 and 3.

The complex emission between 8600 and 8700 A appears to be due to three sources. The background emission near 8700 A is due to the (2, 1) band of the first positive system of N_2. Upon this emission is superimposed the $3s^4P-3p^4D^\circ$ transition of N I. The emission near 8630 A is probably due to the *R* branch of the (0, 1) band of the $A^1\Sigma-X^3\Sigma$ system of O_2, the *P* branch contributing to the emission at 8660 A. The final analysis of this complex group will have to await higher-dispersion studies.

PERMITTED ATOMIC EMISSIONS

Aside from the broadened *Hα* line[3] and the familiar red auroral lines of O I, the remaining emission features are due to permitted transitions of O I and N I. Three O I transitions are present: $3^5S^\circ-3^5P$ at 7774.7 A, $3^3S^\circ-3^3P$ at 8446.4 A, and $3^3P-3s'^3D^\circ$ at 7987 A. The O I lines at λ 6454.7 and λ 7254.5 A, that arise from slightly higher-energy levels, are not present.

The presence of permitted N I emissions, suggested by Meinel[4] and Petrie,[5] had been open to question. The primary evidence to date has been the attribution of the strong emission near 8680 A to the $3s^4p-3p^4D^\circ$ transition of N I. As previously stated, the identification of this complex group of emissions is difficult. A better test would be provided by the $3s^4P-3p^4P^\circ$ transition of N I that occurs in a region free from other auroral emissions near 8216 A. Dufay[6] has drawn attention to the fact that this transition may account for the weak emission listed previously by the author[4] at 8216 A.

Current spectra obtained by the author show conclusively that the $3s^4P-3p^4P^\circ$ transition of N I is present in the aurora. The N I multiplet is superimposed on the wing of the adjacent N_2^+ band at 8050 A. The positions and intensities of the seven components of the $3s^4P-3p^4P^\circ$ transition are indicated in Figure 3. The excellent agreement can hardly be fortuitous. The $3s^4P-3p^4S^\circ$ transition of N I at 7468 A, 7442 A, and 7423 A that arises from a slightly higher-energy level is not present. The evidence for the 8216 A N I emission and the fact that it shows a height distribution similar to the permitted molecular bands are sufficient, however, to establish the presence of atomic nitrogen at low elevations during an aurora.

[3] A. B. Meinel, *Phys. Rev.*, **80**, 1096, 1950; *Ap. J.*, **113**, 50, 1951.

[4] *Pub. A.S.P.*, **60**, 357, 1948.

[5] *J. Geophys. Res.*, **55**, No. 2, 143, 1950.

[6] *C.R.*, **228**, 496, 1949.

TABLE 1

AURORAL WAVE LENGTHS IN THE INFRARED

Wave Length (Air) A	Wave Number (Vac.) (Cm^{-1})	Intensity	Identification
6300.2	15868.2	43	2^3P-2^1D [O I]
6363.7	709.9	12	2^3P-2^1D [O I]
6390.2	644.6	1	(9, 6) N_2 IP*
6480.0	427.8	2	(8, 5) N_2 IP
6515.6	343.5	4	(7, 4) N_2 IP
6544.6	275.5	5	(7, 4) N_2 IP
6563.2	232.3	10	$H\alpha$
6591.8	166.2	7	(6, 3) N_2 IP
6619.5	102.8	6	(6, 3) N_2 IP
6671.5	14985.1	7	(5, 2) N_2 IP
6702.3	916.2	7	(5, 2) N_2 IP
6755.2	799.5	6	(4, 1) N_2 IP
6784.3	736.0	6	(4, 1) N_2 IP
6858.2†	577.0	7	(2, 0) N_2^+; (3, 0) N_2 IP
6892.2	505.2	4	(2, 0) N_2^+
6962.2	359.4	1	(9, 7) N_2 IP
7049.9	180.8	5	(3, 1) N_2^+
7085.1	110.3	5	(3, 1) N_2^+
7148.9	13984.2	2	(7, 5) N_2 IP
7249.5	790.2	6	(4, 2) N_2^+
7281.1†	730.4	5	(4, 2) N_2^+; (6, 4) N_2 IP
7347.8	605.8	8	(5, 3) N_2 IP
7381.9	543.0	7	(5, 3) N_2 IP
7467.0	388.7	25	(4, 2) N_2 IP
7479.3	366.7	24	(4, 2) N_2 IP
7489.1	349.2	25	(4, 2) N_2 IP
7501.6	326.9	22	(4, 2) N_2 IP
7583.6	182.7	32	(3, 1) N_2 IP
7622.1	116.1	7	(3, 1) N_2 IP
7693.1	12995.1	57	(2, 0) N_2 IP
7748.6	902.1	41	(2, 0) N_2 IP
7773.6	860.6	39	$3^5S^\circ-3^5P$ O I
7828.2	770.7	42	(1, 0) N_2^+
7861.9	716.0	39	(1, 0) N_2^+
7879.6	687.4	63	(1, 0) N_2^+
7912.2	635.2	19	(1, 0) N_2^+
7991.7	509.5	6	$3^3P-3s'^3D^\circ$ O I
8056.8	408.5	27	(2, 1) N_2^+
8094.0	351.5	13	(2, 1) N_2^+
8107.0	331.7	31	(2, 1) N_2^+
8186.6	211.8	6	$3s^4P-3p^4p^\circ$ N I
8216.3	167.5	9	$3s^4P-3p^4P^\circ$ N I
8243.0	128.1	2	$3s^4P-3p^4p^\circ$ N I
8297.6	048.3	5	(3, 2) N_2^+
8349.2	11973.9	8	(3, 2) N_2^+
8446.9	835.4	58	$3^3S^\circ-3^3P$ O I
8540.9	705.2	12	(3, 2) N_2 IP
8629.2	585.3	108	(0, 1) O_2 Atm
8664.9	537.6	150	(0, 1) O_2 Atm
8681.9	515.0	280	$3s^4P-3p^4D^\circ$ N I
8703.8	486.1	150	$3s^4P-3p^4D^\circ$ N I
8718.8	466.3	120	(2, 1) N_2 IP
8908.5	222.2	300	(1, 0) N_2 IP

*"IP" indicates first positive system.

† N_2 IP maxima obscured by infrared N_2^+ bands.

AURORAL EMISSION WAVE LENGTHS

The wave lengths and relative intensities for all emissions in the region from 6200 to 8900 A are given in Table 1. The wave lengths of molecular features refer to the positions of the maxima. Where possible, the wave length of the first and last maximum is given. For some bands, however, the observed detail has warranted detailed measurements. The intensities are corrected for the variation of sensitivity with wave length. The intensities for the molecular features refer to the specific intensity at the tabulated wave length and not to the integrated band intensity.

THE VELOCITY-CURVE OF 12 LACERTAE*

OTTO STRUVE
Berkeley Astronomical Department, University of California
Received December 30, 1950

ABSTRACT

Measurements of 259 spectrograms indicate that the velocity-curve and the curve of variation in line contour agree in period (P_3). Both are variable, and an average interval of $P_4 = 39$ days has been tentatively derived from the observations made in 1950. The absorption lines are double at maximum and minimum radial velocity, but this effect is measurable only when the amplitude, K_2, is exceptionally large. Nevertheless, it is the alternation of sharp and broad line components that results in the measurements of variable radial velocity. The velocity changes are attributable to this effect of line doubling. But there is some indication that there is still another velocity variation, with small K_1 and unknown P_1. This oscillation would be analogous to the principal oscillation of β Canis Majoris. Because of the relative insignificance of K_1 in 12 Lacertae, this star shows no beat period that would correspond to P_3 in β Canis Majoris. And while in the latter the changes of K_2 and P_2 are small and slow, they are large and rapid in 12 Lacertae.

The spectroscopic binary 12 Lacertae was discovered by W. S. Adams[1] in 1912 from measurements of four Mount Wilson 60-inch spectrograms, which gave a range of 49 km/sec. A period of $4\frac{1}{2}$ hours was established by R. K. Young[2] in 1915. The same observer, in 1918, found that the "amplitude of the radial velocity curve varies from night to night, being as small as 15 or 20 km/sec at some times and as large as 70 at others."[3] In 1925 W. H. Christie[4] published the results obtained from 152 Victoria spectrograms, and in 1927 he[5] discussed 127 additional measures. There is no record of any spectrographic observations since 1926.

In the meantime, J. Stebbins had found that 12 Lacertae varies in brightness.[6] It was independently observed with a photoelectric photometer by P. Guthnick[7] and photographically by W. H. Christie.[8] The most recent photoelectric observations were obtained by E. A. Fath.[9] In his 1938 paper Fath confirmed the conclusions of Stebbins, Guthnick, and Christie that the principal photometric period coincides with Young's spectrographic period. In addition, he announced that the amplitude of the light-curve varies with a period of 7.5 days. He found some evidence that this beat period also represents the 11 radial-velocity-curves obtained by Young and Christie between 1918 and 1924. No attempt was apparently made to apply the 7.5-day period to Christie's spectrographic measurements in 1925 and 1926, which would have yielded five additional values of the velocity amplitude.

Fath's second paper is a short abstract and contains only a summary of his results.

* This investigation was made possible by a co-operative arrangement with the Mount Wilson, Lick, and McDonald Observatories. The author is grateful to the directors and staffs of these institutions for permission to use their instruments and for assistance in carrying out the observations. He is also indebted to Dr. D. McNamara, who obtained for him the McDonald spectrograms, and to Miss A. Johnson, who measured many plates.

[1] *Ap. J.*, **35**, 179, 1912. [2] *Pub. Dom. Obs. Ottawa*, **3**, No. 3, 87, 1915.

[3] *Pub. Dom. Ap. Obs., Victoria*, Vol. 1, No. 2, 1918.

[4] *Pub. Dom. Ap. Obs. Victoria*, Vol. 3, No. 9, 1925.

[5] *Ibid.*, Vol. 4, No. 5, 1927. [6] *Pub. A.A.S.*, **3**, 318, 1917; *Pop. Astr.*, **25**, 657, 1917.

[7] *A.N.*, **208**, 219, 1919; for additional references see M. Güssow and P. Guthnick, *Kl. Veröff. Sternw. Berlin-Babelsberg*, No. 8, p. 53, 1930.

[8] *Pub. Dom. Ap. Obs. Victoria*, Vol. 4, No. 5, 1927.

[9] *Pop. Astr.*, **46**, 241, 1938; *A.J.*, **52**, 123, 1947.

From 63 maxima of the light-curve obtained by various observers, the mean light-curve is found to have a mean period:

$$P_1 = 0.19308902 \text{ day}, \quad \text{with} \quad \Delta_1 \text{ mag.} = 0.082 \text{ mag.}$$

There is a second period:

$$P_2 = 0.164850 \text{ day}, \quad \Delta_2 \text{ mag.} = 0.031 \text{ mag.};$$

and a third:

$$P_3 = 0.1316 \text{ day}, \quad \Delta_3 \text{ mag.} = 0.017 \text{ mag.}$$

These periods are not consistent with the earlier beat period of 7.5 days which Fath had announced in 1938, and, in the absence of a more complete discussion of his observations, we must assume that, despite the convincing character of the two curves—for the amplitudes in brightness and velocity—which had led Fath to announce the 7.5-day period, he later found it necessary to discard it.

It might be mentioned that Christie had, in 1927, suggested that "as a preliminary value 0.89 day appears fairly satisfactory" as the beat period, or the period of the variation in velocity amplitude. This value does not agree with any of the beat periods resulting from the three periods of Fath. If we combine P_1 and P_2, we find

$$\frac{1}{P_{\text{beat}}} = \frac{1}{0.1649} - \frac{1}{0.1931} = \frac{1}{1.1}.$$

Similarly, P_2 and P_3 give

$$\frac{1}{P_{\text{beat}}} = \frac{1}{0.1316} - \frac{1}{0.1649} = \frac{1}{1.5}.$$

The latest results by Fath have been adopted in the 1948 *General Catalogue of Variable Stars* by B. V. Kukarkin and P. P. Parenago. The star is now designated as "DD Lacertae" and is classified as a β Cephei or β Canis Majoris variable.

During the interval from July 16 to September 24, 1950, twenty nights of observing were devoted to the study of 12 Lacertae. During these nights 259 spectrograms were secured. Of these, 63 were obtained with the Mills three-prism spectrograph of the Lick Observatory, 124 with the 32-inch camera of the coudé spectrograph at the 100-inch telescope, 55 with the Cassegrain spectrograph of the Mount Wilson 60-inch reflector, and 17 with the quartz Cassegrain spectrograph of the McDonald Observatory. The dispersions of the first two instruments were approximately the same—about 10 A/mm—but the resolving power of the Mount Wilson coudé was about twice that of the Lick Mills spectrograph. The McDonald and Mount Wilson Cassegrain spectrographs also were of about the same dispersion—approximately 50 A/mm—but the resolving power of the McDonald instrument was somewhat greater. For the high-dispersion spectrograms, Eastman emulsion II*a*-O was used; for the small-dispersion work, Eastman Process plates were used.

The character of the spectrum undergoes marked variations. With the high resolving power of the coudé spectrograph it was possible to show that the absorption lines become double near maximum and minimum of the velocity-curve. The two components are approximately of the same spectral type, but the lines of one are sharp and narrow, those of the other diffuse and broad. At maximum velocity the sharp component is displaced toward the red, at minimum it is displaced toward the violet. In fact, the measurements of the blended lines yield essentially the radial velocity of the sharp component. The center of gravity of the two components is also variable, and the observed variation may have two periods, one of which coincides or nearly coincides with the period of the line duplicities, while the other may be different.[10]

The line duplicities are seen clearly only when the amplitude of the velocity-curve, as inferred from the blended lines, is large. Table 1 gives the results for these blended lines,

[10] For a preliminary description of the lines of 12 Lacertae see O. Struve, *Pub. A.S.P.*, **62**, 263, 1950.

TABLE 1

RADIAL VELOCITIES OF 12 LACERTAE

Plate*	Date 1950	U.T.	JD 2433+	Phase (Days)	No. of Cycles	Vel. (Km/Sec)
L 33516	July 16	8:42	478.862	0.051	−155	−14.8
33517	16	9:22	478.890	.079	.....	−18.3
33518	16	10:12	478.925	.114	.....	−21.2
33519	16	10:52	478.953	.142	.....	−11.5
33520	16	11:48	478.992	.181	.....	+ 0.3
33539	24	6:41	486.778	.050	−114	− 8.3
33540	24	7:20	486.806	.078	.....	−15.0
33541	24	7:58	486.832	.104	.....	−15.8
33542	24	8:37	486.859	.131	.....	− 7.9
33543	24	9:15	486.885	.157	.....	− 1.6
33544	24	9:52	486.911	.183	.....	− 3.7
33545	24	10:27	486.935	.014	−113	−16.1
33546	24	11:28	486.978	.057	.....	−16.9
33547	24	12:05	487.003	.082	.....	−12.8
33584	31	5:29	493.728	.049	− 78	−20.8
33585	31	6:05	493.73	.074	.....	−23.0
33586	31	6:41	493.778	.099	.....	−21.2
33587	31	7:12	493.800	.121	.....	−27.6
33588	31	7:53	493.828	.149	.....	−21.9
33589	31	8:29	493.853	.174	.....	−16.3
33590	31	9:07	493.880	.003	− 77	−14.2
33591	31	9:44	493.906	.034	.....	− 9.5
33592	31	10:40	493.944	.072	.....	−18.2
33593	31	11:16	493.969	.097	.....	−25.3
33594	31	11:53	493.995	.123	.....	−23.9
33623	Aug. 7	5:30	500.729	.099	− 42	−36.9
33624	7	6:06	500.754	.124	.....	−30.2
33625	7	6:42	500.779	.149	.....	−14.9
33626	7	7:22	500.807	.177	.....	0.0
33627	7	7:58	500.832	.009	− 41	+ 3.6
33628	7	8:34	500.857	.034	.....	+ 4.2
33628	7	9:10	500.882	.059	.....	−19.7
33630	7	10:06	500.921	.098	.....	−31.8
33631	7	10:42	500.946	.123	.....	−34.5
33632	7	11:19	500.972	.149	.....	−22.8
33633	7	11:56	500.997	.174	.....	− 0.7
33634	7	12:28	501.019	.003	− 40	+ 8.0
33650	14	4:48	507.700	.119	− 6	−31.9
33651	14	5:25	507.726	.145	.....	−18.8
33652	14	6:06	507.754	.173	.....	− 3.0?
33653	14	6:46	507.782	.007	− 5	+16.7
33654	14	7:25	507.809	.034	.....	+10.3
33655	14	8:04	507.836	.061	.....	− 6.6
33656	14	8:42	507.862	.087	.....	−37.9
33657	14	9:38	507.901	.126	.....	−32.5
33658	14	10:15	507.927	.152	.....	−13.8
33659	14	10:51	507.952	.177	− 5	+ 6.7
33660	14	11:27	507.977	.009	− 4	+19.4
33661	14	12:04	508.003	.035	.....	+ 9.9
33666	15	4:38	508.693	.146	− 1	− 3.9
33667	15	5:25	508.726	.179	.....	+21.1
33668	15	6:03	508.752	.012	0	+30.5
33669	15	6:40	508.778	.038	.....	− 4.5
33670	15	7:16	508.803	.063	.....	−37.7
33671	15	7:52	508.828	.088	.....	−55.8
33672	15	8:28	508.853	.113	.....	−39.3
33673	15	9:04	508.878	0.138	.....	−21.0

*The Lick three-prism plates are indicated by "L"; the Mount Wilson 100-inch coudé plates are marked "Ce," and the 60-inch Cassegrain plates, "γ." The McDonald Cassegrain plates are designated "CQ."

TABLE 1—*Continued*

Plate*	Date 1950	U.T.	JD 2433+	Phase (Days)	No. of Cycles	Vel. (Km/Sec)
L 33674	Aug. 15	9:56	508.914	0.174	.....	+12.0
33675	15	10:32	508.939	.006	+ 1	+11.3
33676	15	11:08	508.964	.031	.....	− 5.6
33677	15	11:44	508.989	.086	.....	−31.2
33678	15	12:21	509.015	.082	.....	−42.6
Ce 6452a	23	10:22	516.932	.082	+ 42	−37.8
b	23	10:40	516.944	.094	.....	−37.6
c	23	10:58	516.957	.107	.....	−38.9
d	23	11:16	516.969	.119	.....	−31.1
e	23	11:33	516.981	.131	.....	−24.2
f	23	11:50	516.993	.143	.....	−13.5
g	23	12:07	517.005	.155	.....	− 3.4
h	23	12:24	517.017	.167	.....	+ 6.6
i	23	12:42	517.029	.179	.....	+11.0
6454a	24	6:59	517.791	.169	+ 46	+ 1.6
b	24	7:21	517.806	.184	.....	+ 8.1
c	24	7:40	517.819	.004	+ 47	+10.1
d	24	7:59	517.833	.018	.....	− 0.2
e	24	8:19	517.847	.032	.....	−12.8
f	24	8:39	517.860	.045	.....	−13.3
g	24	8:59	517.874	.059	.....	−10.6
h	24	9:19	517.888	.073	.....	−23.6
6455a	24	9:45	517.906	.091	.....	−44.6
b	24	10:05	517.920	.115	.....	−42.4
c	24	10:25	517.934	.119	.....	−32.3
d	24	10:49	517.951	.136	.....	−22.0
e	24	11:12	517.967	.152	.....	− 7.5
f	24	11:32	517.981	.166	.....	+ 0.1
6459a	25	7:02	518.793	.012	+ 52	+ 4.3
b	25	7:21	518.806	.025	.....	− 2.2
c	25	7:45	518.823	.042	.....	− 2.9
d	25	8:05	518.837	.056	.....	−10.9
e	25	8:23	518.849	.068	.....	−16.9
f	25	8:41	518.862	.081	.....	−30.1
g	25	8:59	518.874	.093	.....	−35.6
h	25	9:16	518.886	.105	.....	−32.9
i	25	9:32	518.897	.116	.....	−30.7
6460a	25	9:56	518.914	.133	+ 52	−19.4
b	25	10:14	518.926	.145	.....	−12.9
c	25	10:29	518.937	.156	.....	− 5.1
d	25	10:46	518.949	.168	.....	− 2.1
e	25	11:05	518.962	.181	.....	+10.8
f	25	11:24	518.975	.001	+ 53	+ 8.0
g	25	11:43	518.988	.014	.....	− 2.1
h	25	12:05	519.003	.029	.....	−11.4
6465a	26	4:49	519.701	.148	+ 56	−21.5
b	26	5:08	519.714	.161	.....	−16.1
c	26	5:28	519.728	.175	.....	−12.5
d	26	5:50	519.743	.190	.....	− 6.2
e	26	6:09	519.756	.010	+ 57	+ 0.5
f	26	6:29	519.770	.024	.....	+ 7.6
6466a	26	6:56	519.789	.043	.....	+ 3.6
b	26	7:20	519.806	.060	.....	0.0
c	26	7:43	519.822	.076	.....	−13.3
d	26	8:04	519.836	.090	.....	−30.2
e	26	8:28	519.853	.107	.....	−36.7
f	26	8:58	519.874	.128	.....	−36.4
g	26	9:22	519.890	.144	.....	−29.1
6467a	26	9:49	519.909	.163	.....	−20.6
b	26	10:08	519.922	.176	.....	−14.9
c	26	10:26	519.935	0.189	.....	− 5.2

TABLE 1—*Continued*

Plate*	Date 1950	U.T.	JD 2433+	Phase (Days)	No. of Cycles	Vel. (Km/Sec)
Ce 6467d	Aug. 26	10:46	519.949	0.010	+ 58	− 4.4
e	26	11:09	519.965	.026	+ 58	+ 4.3
f	26	11:31	519.980	.041	.....	− 0.7
g	26	11:55	519.997	.058	.....	− 4.6
h	26	12:21	520.015	.076	.....	−18.8
γ 31665	27	4:09	520.673	.155	+ 61	− 9.1
γ 31666	27	5:05	520.712	.000	+ 62	− 0.4
γ 31667	27	5:40	520.736	.024	.....	− 6.3
γ 31668a	27	6:16	520.761	.049	.....	+ 8.5
b	27	6:41	520.778	.066	.....	−11.2
c	27	7:26	520.810	.098	.....	−35.1
d	27	8:00	520.833	.121	.....	−30.4
e	27	8:34	520.857	.145	.....	−24.7
γ 31669a	27	9:08	520.881	.169	.....	−17.9
b	27	9:42	520.904	.192	.....	− 2.2
e	27	10:16	520.928	.023	+ 63	+ 8.0
d	27	10:50	520.951	.046	.....	+ 0.8
e	27	11:24	520.975	.070	.....	−18.0
γ 31670a	27	11:58	520.999	.094	.....	−32.1
b	27	12:32	521.022	.117	.....	−34.9
γ 31671b	28	3:58	521.665	.181	+ 66	− 3.3
c	28	4:32	521.689	.012	+ 67	+14.7
d	28	5:06	521.712	.035	.....	− 0.7
e	28	5:41	521.737	.060	.....	−14.4
f	28	6:15	521.760	.083	+ 67	−29.2
g	28	6:49	521.784	.107	.....	−32.9
h	28	7:22	521.807	.130	.....	−23.6
CQ 8537	28	8:31	521.855	.178	.....	+ 4.8
8538	28	9:31	521.897	.027	+ 68	+ 4.2
8539	28	10:04	521.919	.049	.....	−16.1
8540	28	10:31	521.938	.068	.....	−29.9
8541	28	10:55	521.955	.085	.....	−34.8
γ 31673	28	12:30	522.021	.151	.....	−12.4
γ 31674a	29	3:21	522.640	.191	+ 71	+11.0
b	29	3:56	522.644	.022	+ 72	− 0.3
c	29	4:30	522.688	.046	.....	−17.2
d	29	5:04	522.711	.069	.....	−22.8
e	29	5:38	522.735	.093	.....	−29.0
f	29	6:12	522.758	.116	.....	−19.0
g	29	6:46	522.782	.140	.....	− 7.4
h	29	7:26	522.810	.168	.....	+ 3.7
i	29	7:53	522.828	.186	.....	+ 4.0
γ 31675a	29	8:27	522.852	.017	+ 73	−12.4
b	29	9:01	522.876	.041	.....	−20.9
c	29	9:35	522.899	.064	.....	−25.9
d	29	10:09	522.923	.088	.....	−21.5
e	29	10:43	522.947	.112	.....	−25.2
f	29	11:16	522.969	.134	.....	−10.4
g	29	11:49	522.992	.157	.....	− 2.9
h	29	12:23	523.016	.181	.....	+ 5.4
γ 31676a	30	3:18	523.637	.029	+ 77	−15.2
b	30	3:54	523.662	.054	.....	−24.4
c	30	4:30	523.687	.079	.....	−21.7
d	30	5:03	523.710	.102	.....	−27.8
e	30	5:38	523.735	.127	.....	−16.4
f	30	6:12	523.758	.150	.....	− 2.1
g	30	6:45	523.781	.173	.....	+ 5.3
h	30	7:20	523.806	.005	+ 78	− 4.3
i	30	7:54	523.829	.028	.....	−15.5
γ 31677a	30	8:29	523.853	.052	.....	−23.8
b	30	9:02	523.876	0.075	.....	−24.5

TABLE 1—*Continued*

Plate*	Date 1950	U.T.	JD 2433+	Phase (Days)	No. of Cycles	Vel. (Km/Sec)
γ 31677c	Aug. 30	9:35	523.899	0.098	.....	−32.7
d	30	10:09	523.923	.122	.....	−22.2
e	30	10:46	523.949	.148	.....	−12.0
f	30	11:20	523.972	.171	.....	− 4.8
CQ 8565	31	7:05	524.795	.029	+ 83	−16.7
8566	31	7:39	524.819	.053	.....	−19.8
8567	31	8:13	524.842	.076	.....	−33.9
8568	31	8:51	524.869	.103	.....	−31.7
8569	31	9:59	524.916	.150	.....	− 0.8
8570	31	10:37	524.942	.176	.....	+ 5.0
8571	31	11:11	524.966	.007	+ 84	− 1.7
8572	Sept. 1	6:23	525.766	.034	+ 88	−13.0
8573	1	6:58	525.790	.058	.....	−13.3
8574	1	7:31	525.813	.081	.....	−35.2
8575	1	8:06	525.838	.106	.....	−33.8
8576	1	8:29	525.853	.121	.....	−22.8
Ce 6517a	21	3:10	545.632	.012	+191	+ 0.7
b	21	3:32	545.647	.027	.....	+ 7.0
c	21	3:54	545.662	.042	.....	+ 4.0
d	21	4:16	545.678	.058	.....	− 1.0
6518	21	4:48	545.700	.080	.....	−23.6
6519a	21	5:19	545.722	.102	.....	−38.2
b	21	5:41	545.737	.117	.....	−35.8
c	21	6:04	545.753	.133	.....	−33.8
d	21	6:26	545.768	.148	.....	−21.1
e	21	6:48	545.783	.163	.....	−12.8
f	21	7:11	545.799	.179	.....	− 2.8
g	21	7:38	545.818	.005	+192	+ 5.4
h	21	8:12	545.842	.029	.....	+ 9.7
i	21	8:44	545.864	.051	.....	+ 2.7
j	21	9:12	545.883	.070	.....	−10.5
6520a	21	9:50	545.910	.097	.....	−41.4
b	21	10:20	545.931	.118	.....	−42.6
c	21	10:54	545.954	.141	.....	−29.0
d	21	11:26	545.976	.163	.....	− 9.1
6522a	22	2:50	546.618	.033	+196	+14.8
b	22	3:13	546.634	.049	.....	+ 2.3
c	22	3:35	546.649	.064	.....	−13.7
d	22	3:58	546.665	.080	.....	−33.6
e	22	4:22	546.682	.097	.....	−47.2
f	22	4:44	546.697	.112	.....	−41.9
g	22	5:07	546.713	.128	.....	−39.9
h	22	5:30	546.729	.144	.....	−29.4
i	22	5:51	546.744	.159	.....	−19.3
j	22	6:13	546.759	.174	.....	− 8.6
6523a	22	6:40	546.778	.193	.....	+ 7.5
b	22	7:04	546.794	.015	+197	+16.2
c	22	7:27	546.810	.031	.....	+13.3
d	22	7:54	546.829	.050	.....	+ 2.3
e	22	8:23	546.849	.070	.....	−28.2
f	22	8:52	546.869	.090	.....	−46.0
g	22	9:18	546.888	.109	.....	−46.5
h	22	9:46	546.907	.128	.....	−37.8
6528a	23	6:12	547.758	.014	+202	+ 4.5
b	23	6:31	547.772	.028	.....	−14.9
c	23	6:48	547.783	.039	.....	−23.8
d	23	7:09	547.798	.054	.....	−28.0
e	23	7:28	547.811	.067	.....	−29.7
f	23	7:50	547.826	.082	.....	−37.9
g	23	8:10	547.840	.096	.....	−38.9
h	23	8:32	547.856	0.112	+202	−35.0

TABLE 1—*Continued*

Plate*	Date 1950	U.T.	JD 2433+	Phase (Days)	No. of Cycles	Vel. (Km/Sec)
Ce 6528i	Sept. 23	8:51	547.869	0.125	.....	−23.3
j	23	9:14	547.885	.141	.....	−14.9
k	23	9:38	547.901	.157	.....	− 9.3
l	23	10:07	547.922	.178	.....	− 0.7
6535a	24	3:44	548.656	.140	+206	−18.0
b	24	4:05	548.670	.154	.....	−11.8
c	24	4:26	548.685	.169	.....	− 6.0
d	24	4:47	548.699	.183	.....	− 1.3
e	24	5:08	548.714	.005	+207	− 0.9
f	24	5:29	548.728	.019	.....	− 8.0
g	24	5:51	548.744	.035	.....	−15.5
h	24	6:10	548.757	.048	.....	−18.0
6536a	24	6:36	548.775	.066	.....	−19.8
b	24	6:58	548.790	.081	.....	−18.4
c	24	7:20	548.806	.097	.....	−21.3
d	24	7:43	548.822	.113	.....	−24.8
e	24	8:05	548.837	.128	.....	−22.1
f	24	8:27	548.852	0.143	.....	−10.8

and Figures 1 and 2 show the individual velocity-curves. The amplitudes of these curves change between about 15 km/sec on July 31 and 74 km/sec on August 15. Table 2 lists the velocities and epochs of the maxima and minima of the individual curves, the range in velocity, and the epochs at which the lines were sharpest and most diffuse. The last column of Table 2 gives, in arbitrary units, the range of variation of line contour. This variation, according to our present view, represents the difference in the contours of the sharp and diffuse components. Zero indicates that there was no change, 10 that the change was large. There is a strong correlation between these estimates and the ranges of the velocity-curves: when the amplitude in radial velocity is large, the change in line contour is also pronounced.

In Table 3 the cycles are counted both forward and backward from August 15. We have then computed the phases of these same epochs on other dates and have listed the residuals "observed epoch minus computed epoch." The first half of the table was computed with Young's period (which we shall designate "P_2" in order to facilitate comparison with β Canis Majoris),

$$P_2 = 0.193089 \text{ day} .$$

The second half was computed with a period

$$P_2 = 0.193175 \text{ day} ,$$

which results from the two maxima of the velocity-curves on August 15 and September 22, which were well observed and had large amplitudes. This revised period is definitely preferable in representing the observations between August 15 and September 24 but is slightly less satisfactory than Young's original period in representing the observations between July 16 and August 15.

The earlier observations of 12 Lacertae leave no doubt that the mean period is close to that found by Young, Christie, and Fath. This period leads to large positive residuals in September. Hence we must conclude that this period itself is slightly variable.

In Figures 1 and 2 we have shown the *computed* epochs of maximum velocity (*vertical line*), minimum velocity (*dotted line*), sharpest line contour (X), and broadest line contour (+). In this computation Young's period was used. It will be seen that on many

dates the observed times of maximum and minimum velocity are not consistent with the computed epochs. As a rule, on these same dates the computed epochs of the sharpest and broadest contours depart by similar amounts from the observed epochs (see Table 3). There is a weak correlation between the four sets of residuals computed with $P_2 = 0.193089$ day, and a similar correlation exists in the case of $P_2 = 0.193175$ day. This is shown in Figure 3. At the top is a plot of the velocity amplitudes as a function of time. This is followed by a plot of the range in line contour. Next, we have the means of the residuals from the third and fourth columns of Table 3 (representing the shift of the observed velocity-curve from the computed curve). At the bottom we have plotted, in a similar manner, the means of the residuals from the fifth and sixth columns of Table 3.

We notice that there is a systematic tendency of both curves at the bottom to favor positive values. This is an error of zero point and can be attributed to a small error in the adopted epochs for August 15. Thus the mean of the residuals of the middle drawing is about + 0.005 day, while that of the bottom drawing is + 0.010 day.

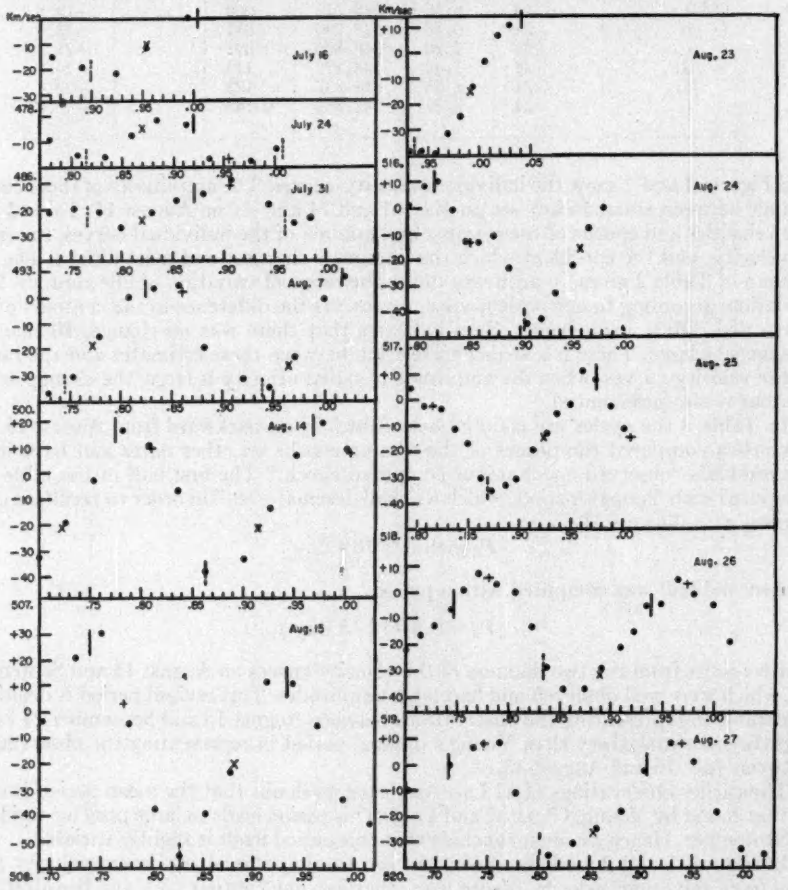

FIG. 1.—Radial-velocity-curves of 12 Lacertae

If we draw horizontal lines through these new zero-point values, we find the following correlation: 14 points of each curve agree in sign; 3 points disagree in sign. We can probably conclude that the velocity-curve and the curve of variation in line contour agree in having the same period P_2 and the same irregular departures from this period, which may at times add up to an accumulated shift in phase of the order of 0.02 days, or 0.1 P_2.

The curve at the top of Figure 3 shows a fairly strong correlation with the curve of estimated range in change of line contours. The latter is shown just below the curve of velocity amplitudes, and the corresponding scale is indicated on the left-hand margin. If we consider that these estimates were made on spectrograms of different dispersions and different emulsions, the agreement is fair. But there is no noticeable correlation be-

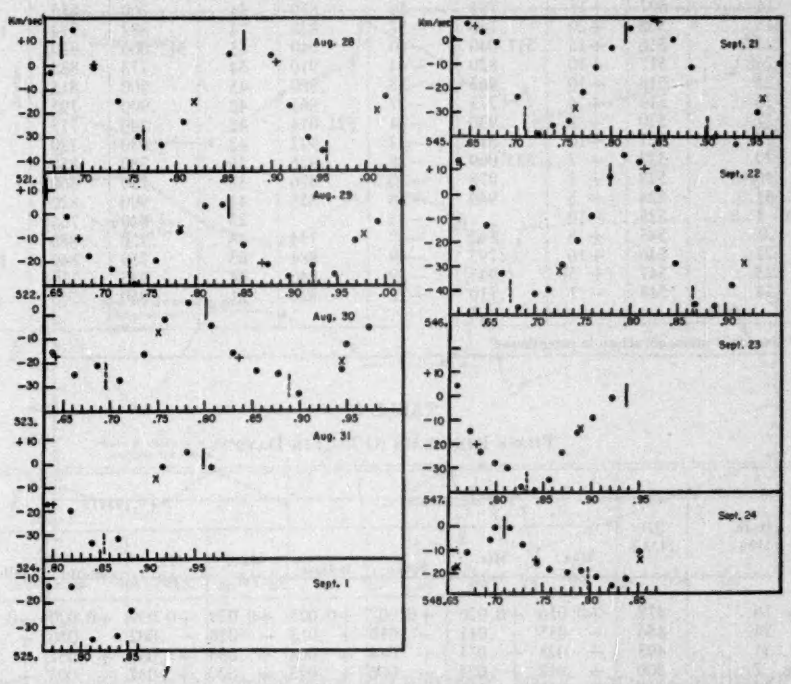

FIG. 2.—Radial-velocity-curves of 12 Lacertae

tween these two curves and the two curves of phase residuals. The velocity-curve has a large amplitude when the change in line contour is pronounced. This is understandable because it is the visual contrast between the sharp and the diffuse components that produces most of the observed velocity variation. Thus, when the two components are similar in intensity and width, we measure the center of the blend, but when they are different, we set the microscope wire upon the sharper component.

The curve of velocity amplitudes at the top of Figure 3 shows no definite periodicity. The beat periods found by Fath in the light-curve are probably not present. There are two pronounced maxima, at JD 509 and JD 547. The interval, 38 or 39 days, is perhaps real in the sense that there is a tendency for the large amplitudes to recur at intervals of about 39 days. But the steep decline in the curve from JD 547 to JD 549 is different from the slow decline between JD 516 and JD 526. On the other hand, if we regard the

TABLE 2

Observed Epochs

Date 1950	JD 2433+	Maximum		Minimum		Range in Vel. (Km/Sec)	Epoch (JD)		Range of Variation (Arb. Units)
		Vel. (Km/Sec)	Epoch (JD)	Vel. (Km/Sec)	Epoch (JD)		Sharp	Neb.	
July 16	478	(+10)*	(479.020)	−21	.925	31	.960	.870	10
24	486	− 1	.885	−18	.804	17	.860	.775	10
31	493	−11	.900	−26	.798	15	.865	.910	5
Aug. 7	500	+ 4	.840	−36	.945	40	.766	.880	3
14	507	+18	.785	−36	.870	54	.760	.855	8
15	508	+20	.740	−54	.828	74	.882	.774	10
23	516	+15	517.040	−40	.940	55	517.000	(.920)	7
24	517	+10	.820	−44	.910	54	.773	.885	5
25	518	+10	.965	−35	.880	45	.900	.815	6
26	519	+ 6	.773	−37	.865	42	.900	.795	3
27	520	+ 8	.930	−34	521.014	42	.880	.775	4
28	521	+10	.878	−32	.972	42	(.830)	.720	5
29	522	+ 7	523.009	−28	.926	35	.780	.850	2
30	523	+ 5	.978	−30	.876	35	.750	.860	2
31	524	+ 5	.940	−36	.855	41	.900	.820	5
Sept. 1	525	−10	.....	−35	.....	25	(.840)	(.766)	.....
21	545	+ 8	.842	−40	.734	48	.770	.880	6
22	546	+16	.795	−49	.884	65	.750	.840	10
23	547	(+ 5)	(.945)	−39	.840	44	.935	(.770)	9
24	548	− 1	.710	−22	.820	21	.850	.765	4

* Uncertain values are shown in parentheses.

TABLE 3

Phase Residuals (O − C) in Days

Date 1950	JD 2433+	$P = 0.193089$				$P = 0.193175$			
		Max. Vel.	Min. Vel.	Sharp	Diffuse	Max. Vel.	Min. Vel.	Sharp	Diffuse
July 16	478	+0.016	+0.026	+0.007	+0.025	+0.029	+0.039	+0.020	+0.038
24	486	− .035	− .011	− .010	+ .013	− .026	− .002	.000	+ .023
31	493	+ .028	+ .031	+ .044	+ .004	+ .035	+ .038	+ .051	+ .010
Aug. 7	500	+ .017	+ .034	− .006	+ .023	+ .020	+ .037	− .003	+ .026
14	507	+ .010	+ .007	+ .037	+ .046	+ .008	+ .008	+ .037	+ .047
15	508	.000	.000	.000	.000	.000	.000	.000	.000
23	516	− .002	+ .003	+ .008	+ .037	− .006	− .001	+ .005	+ .033
24	517	+ .005	+ .007	+ .009	+ .036	+ .001	+ .003	+ .005	+ .032
25	518	− .009	+ .011	− .023	.000	− .013	+ .007	− .027	− .004
26	519	+ .027	+ .031	+ .012	+ .015	+ .023	+ .026	+ .007	+ .011
27	520	+ .025	+ .022	+ .026	+ .029	+ .020	+ .016	+ .021	+ .024
28	521	+ .008	+ .014	+ .011	+ .009	+ .002	+ .008	+ .005	+ .003
29	522	− .019	+ .003	− .004	− .020	− .026	− .004	− .011	− .026
30	523	− .016	− .012	.000	+ .025	− .023	− .020	− .007	+ .018
31	524	− .019	+ .001	− .008	+ .020	− .027	− .007	− .016	+ .012
Sept. 1	525	.....	.....	− .034	.000	.....	.....	− .041	− .007
21	545	+ .029	+ .026	+ .008	+ .033	+ .012	+ .010	− .008	+ .016
22	546	+ .016	+ .017	+ .023	+ .029	.000	+ .001	+ .006	+ .013
23	547	+ .008	+ .008	+ .049	.000	− .009	− .009	+ .032	− .017
24	548	+0.001	(+0.053)	−0.001	+0.022	−0.017	+0.035	−0.019	+0.004

steep rise between JD 545 and JD 547 as a repetition of the similar rise between JD 508 and JD 509, then a beat period much shorter than 39 would be required. A period of about 7.6 days (5 cycles) would be consistent with Fath's 1938 conclusions but would be ruled out by the smooth run of the curve from JD 516 to JD 526. A period close to 1 day is ruled out by the long series secured on several of the nights when two complete cycles were observed. We can only conclude that the variation in amplitude is irregular, perhaps in the nature of outbursts, which at times cause the two components of the absorption lines to be of very different shape.

As a rule, two successive cycles of the velocity-curve agree within the errors of observation, but on August 15 the first maximum is much higher than the second. The three-

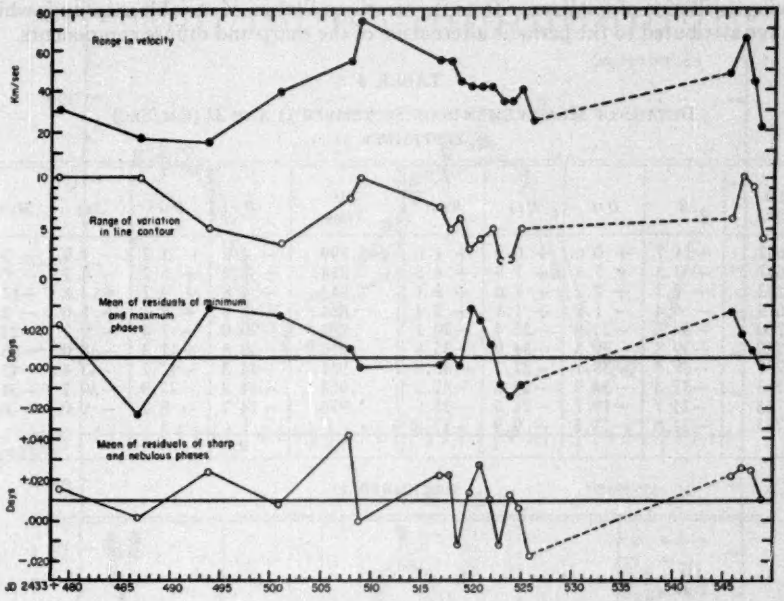

FIG. 3

prism Lick spectrograms clearly show this difference, and it cannot be attributed to errors of measurement (or of the instrument). We almost certainly have irregular and very sudden changes in amplitude, reminiscent of some observed long ago by Christie. Perhaps these sudden changes are related to the outbursts in light which Eggen has observed in several β Cephei stars.

Although on most of our plates we were able to measure only single (blended) lines, the evidence in favor of the observed duplicities is so strong that we can unreservedly accept it as a fundamental characteristic of the spectrum of 12 Lacertae. The two sets of absorption lines—sharp and diffuse—are of similar spectral type. Yet the lines are not equally affected by the changes in line contours: *Si* III shows them best, next follow *Mg* II, *O* II, and *He* I; and the changes are least pronounced in the *H* lines. Table 4 gives the details of the measurements for September 21 and 22. On the latter date, when the velocity amplitude was especially large, the *Si* III lines were measured as close doubles. For the other lines, only the stronger and sharper component was measured. These re-

sults are plotted in Figure 4. On September 21 there was no pronounced difference between the different atoms. But on September 22, *H* gave the smallest amplitude, followed by *He* I, *O* II, *Mg* II, and *Si* III. The difference manifested itself especially at the maximum of the velocity-curve.

The broad components, measured when the lines are double, have a smaller amplitude (30 km/sec) than the sharp components (70 km/sec). Moreover, the gamma velocity of the sharp components is − 10 km/sec, while that of the diffuse components is − 15 km/sec. This suggests that the observed velocity-curve on September 22 may have consisted of two harmonic components, which were approximately in phase with the sharper component and out of phase with the broader component. But, even if this conclusion should be confirmed by future observations, it would be difficult to reconstruct the underlying oscillation of small range from the erratic oscillation of variable amplitude which we have attributed to the periodic alternation of the sharp and diffuse components.

TABLE 4

DETAILS OF MEASUREMENTS ON SEPTEMBER 21 AND 22 (KM/SEC)

SEPTEMBER 21

JD Time	*H*	*O* II	*He* I	*Mg* II	JD Time	*H*	*O* II	*He* I	*Mg* II
545.632...	−14.7	+ 0.6	+ 6.9	+ 4.6	545.799...	− 4.0	− 3.2	− 1.9	− 0.5
.647...	+ 2.5	+ 7.8	+ 7.9	+ 4.5	.818...	+ 2.2	+ 6.7	− 6.2	− 0.5
.662...	+ 5.3	+ 2.7	+ 7.6	+ 3.1	.842...	+ 4.8	+ 9.2	+12.8	+12.1
.678...	− 4.4	− 1.7	+ 1.1	+ 2.4	.864...	+ 4.8	+ 3.7	+ 1.0	− 2.0
.700...	−34.2	−25.8	−22.4	−29.1	.883...	−20.0	− 7.4	− 9.2	−22.1
.722...	−39.8	−39.5	−34.9	−35.8	.910...	−40.8	−41.3	−38.0	−48.9
.737...	−39.8	−38.1	−27.1	−35.8	.931...	−44.3	−42.2	−43.4	−42.2
.753...	−32.3	−34.9	−29.6	−37.2	.954...	−31.2	−27.9	−30.2	−31.5
.768...	−24.7	−19.7	−21.5	−25.9	.976...	−14.7	− 8.7	− 9.0	− 6.2
.783...	−22.6	−11.3	− 9.9	−17.8					

SEPTEMBER 22

JD Time	*H*	*O* II	*He* I	*Mg* II	*Si* III	
					I	II
546.618.....	+ 3.6	+15.8	+13.3	+23.6	+22.9	−31.2
.634.....	−11.0	+11.5	− 3.3	−10.6	+23.6	−20.7
.649.....	−15.1	−13.0	−10.7	−22.6	.....	.....
.665.....	−30.4	−32.8	−32.5	−44.1	−41.1	+ 1.1
.682.....	−49.0	−47.2	−44.6	−49.4	−46.8	− 1.0
.697.....	−47.0	−40.6	−43.7	−40.8	−43.7	.....
.713.....	−45.0	−41.1	−36.0	−35.5	.....	.....
.729.....	−30.5	−28.3	−28.9	−36.2	.....	.....
.744.....	−20.1	−20.2	−16.3	−18.8	.....	.....
.759.....	−10.7	− 8.2	− 8.6	− 8.9	.....	.....
.778.....	− 0.9	+ 8.9	+ 6.6	+ 9.2	+15.4	−37.4
.794.....	+ 5.3	+16.3	+17.7	+23.9	+24.8	−30.1
.810.....	+ 2.5	+15.7	+14.6	+ 7.8	+37.4	−26.8
.829.....	− 5.1	+ 4.3	+ 2.4	− 0.3	.....	.....
.849.....	−14.8	−29.4	−24.3	−41.8	.....	.....
.869.....	−41.1	−45.6	−40.4	−58.1	−47.3	− 2.4
.888.....	−46.7	−46.9	−43.1	−50.6	−45.9	.....
.907.....	−37.8	−38.2	−35.0	−40.6	.....	.....

It is of interest to compare 12 Lacertae with β Canis Majoris.[11] Both stars have short periods, 4½ hours for 12 Lacertae and 6 hours for β Canis Majoris. Both are variable in light and in line contours. The latter are resolved into double lines in 12 Lacertae. In β Canis Majoris the lines are sometimes unsymmetrical, and there is little doubt that they, too, would be resolved into two components if the amplitude of the velocity-curve were as large as in 12 Lacertae.

The velocity-curve of β Canis Majoris shows four periods, of which the fourth is incompletely known. The first, $P_1 = 0.2500$ day, has a semiamplitude $K_1 = 5.8$ km/sec and has been constant over the entire interval of 40 years covered by the observations. The second, $P_2 = 0.2513$ day, has varied slightly during the 40 years and has had a

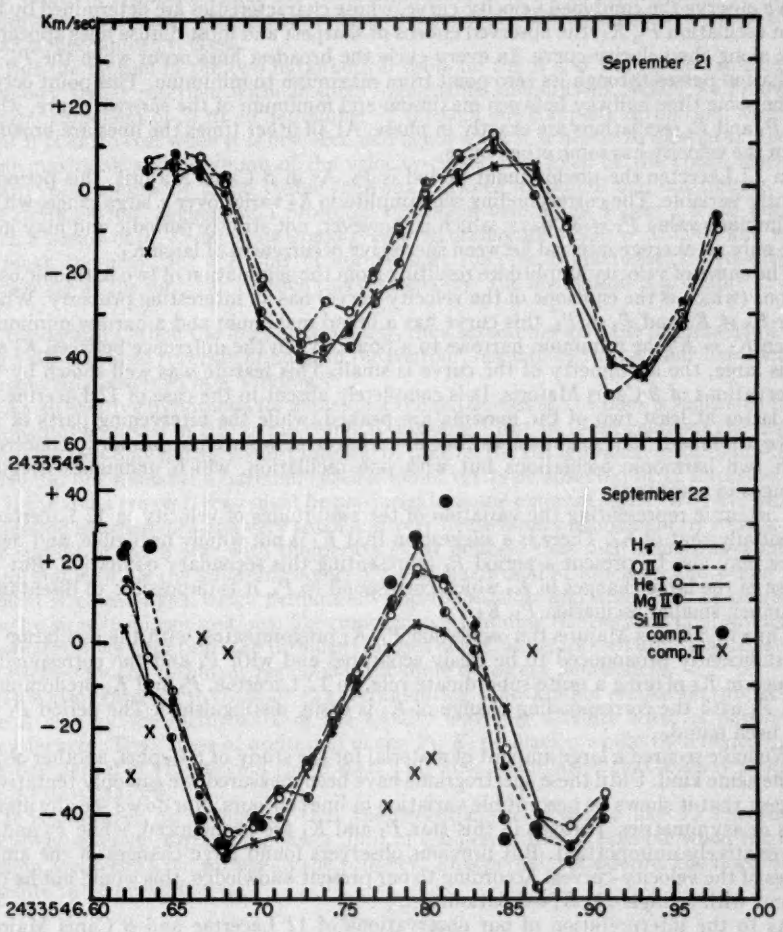

FIG. 4.—Radial-velocity-curves of 12 Lacertae

[11] O. Struve, *Ap. J.*, 112, 520, 1950.

variable amplitude; $K_2 = 4.2$ km/sec and $K_2 = 2.0$ km/sec. The period P_4 (if there is one) of the variation in K_2 is not known, but is probably long—of the order of several years. The period P_2 represents the variation in the line contours. This variation becomes smaller when K_2 decreases.

The periods P_1 and P_2 combine to give a beat period $P_3 = 49$ days, which represents the curve of the variation in the observed amplitude of the velocity-curve. Since K_2 is variable while K_1 is constant, the shape of this curve also undergoes slow changes which may have a period P_4. Similarly, P_2 changes while P_1 remains constant. Hence the beat period, P_3, also changes. The curve of the velocity amplitudes, whose period is P_3, agrees within the errors of observations with the shape predicted from the addition of two simple harmonic oscillations corresponding to P_1 and P_2, respectively.

We observe the combined velocity-curve, whose characteristics are determined by the main oscillation P_1, K_1; the observed epochs of sharpest and most diffuse lines appear to slide along the velocity-curve. In every cycle the broadest lines occur when the P_2, K_2 oscillation passes through its zero point from maximum to minimum. This point occurs at the same time halfway between maximum and minimum of the *observed* curve, when the P_1 and P_2 oscillations are exactly in phase. At all other times the lines are broadest when the velocity has some other value.

In 12 Lacertae the predominant period is P_2. As in β Canis Majoris, this period is slightly variable. The corresponding semiamplitude K_2 varies over a large range, with a preliminary value $P_4 = 39$ days, which is, however, not strictly periodic and may indicate only an average interval between successive occurrences of large K_2.

The curve of velocity amplitudes resulting from the summation of two harmonic oscillations (which is the envelope of the velocity-curve) has an interesting property. Whenever $K_1 \neq K_2$ and $P_1 \neq P_2$, this curve has a broad maximum and a narrow minimum. When $K_1 = K_2$ the minimum narrows to a point. When the difference between K_1 and K_2 is large, the asymmetry of the curve is small. This feature was well shown by the observations of β Canis Majoris. It is completely absent in the case of 12 Lacertae. In the latter at least two of the maxima are peaked, while the intervening parts of the curve are broad. This again shows that in 12 Lacertae we are not primarily concerned with two harmonic oscillations but with one oscillation, which undergoes irregular changes in amplitude.

The curve representing the variation of the amplitudes of velocity in 12 Lacertae is essentially that of K_2. There is a suggestion that K_1 is not wholly negligible, and hence there may also be present a period P_1 representing this secondary oscillation. But because of the large changes in K_2 which correspond to P_4, it is impossible to disentangle the much smaller oscillation P_1, K_2.

Thus in β Canis Majoris the oscillation P_1, K_1 predominates, with the oscillation P_2, K_2 sufficiently pronounced to be easily separated and with P_4 and the corresponding change in K_2 playing a quite subordinate role. In 12 Lacertae, P_2 and K_2 predominate, and P_4 with the corresponding change of K_2 is easily distinguished. The period P_1 has not been found.

We have secured a large amount of material for the study of β Cephei, another object of the same kind. Until these spectrograms have been measured, we can only tentatively suggest that it shows no perceptible variation in line contours. Nor do we see any duplicities or asymmetries. Perhaps in this star P_1 and K_1 are pronounced, while P_2 and K_2 are relatively unimportant. But previous observers found large changes in the amplitudes of the velocity-curves. According to our present knowledge, this would not be consistent with a single P_1, K_1 oscillation.

As to the interpretation of our observations of 12 Lacertae and β Canis Majoris, there is not much that we can add to our previous hypothesis.[12] The two components of the absorption lines cannot come from two stars because (*a*) there is not enough room

[12] O. Struve, *Pub. A.S.P.*, **62**, 263, 1950.

in the system to accommodate two ordinary B-type stars of nearly the same luminosity and (*b*) the erratic variation of K_2, corresponding to the interval P_4, eliminates binary motion of two B-type stars.

Hence the two lines must originate in a single star. Yet their periodic change in relative position, which resembles that of a double-lined binary, strongly suggests some kind of rotation. This led to the hypothesis of two spots traveling along the equator of the single B-type star—one of considerable area, in which the gases are turbulent, and another, diametrically opposite, in which they are quiescent. This interpretation agrees with some of the observations: it accounts for the fact that the maximum of the light-curve, which follows P_2, falls near the epoch of broadest lines; it can easily explain the difference in the values of K_2 obtained for the two components of *Si* III on September 22; and it is more attractive in the light of the peculiar changes of K_2, which suggest a physical, rather than a mechanical, process.

But the motion of the two hypothetical spots on the B star cannot be explained by ordinary stellar rotation, without some improbable assumptions. When we follow the sharp component of *Si* III on September 22 through one complete revolution, we notice that it is narrowest when it is first seen and again when it is about to disappear, that is, near maximum and minimum of the velocity-curve. But, even at the epoch when the sharp components are alone visible (halfway between minimum and maximum), they are quite narrow, suggesting a projected rotational velocity of $V_0 \sin i = 20$ km/sec; with a period of 0.193 day, this would give a circumference of $2\pi r = 325{,}000$ km, which is much too small for a B star of normal spectroscopic characteristics. No effect of darkening at the limb can remove this discrepancy; the inclination is probably close to 90°.

Incidentally, when the lines are broadest, they sometimes give the impression of having a slight central reversal, or bulge in the contour, resembling the peculiar line contours occasionally observed in α Virginis.[13]

An alternative hypothesis for explaining the duplicities of the lines is suggested in the duplicities observed in RR Lyrae,[14] and W Virginis.[15] But in these cepheids the duplicities were seen only during a short interval of time on the rising branch of the light-curve. They did not resemble a harmonic oscillation of the type observed in 12 Lacertae.

If the spots are real, they must be produced by some external agent. We have already suggested the existence of a very small and very dense binary component, revolving near the surface of the B star with the period P_2. It is likely that such a satellite would be quite stable, while the adjoining layers of the B star would be unstable, and would form violent streams of gas, which perhaps envelop the satellite and which may be characterized by large turbulent motions. The companion might drag this network of prominences, or whatever we might call the turbulent masses of gas, along its own orbit and thus show us alternately the turbulent region and the more quiescent hemisphere.

It is also tempting to think of P_1 as representing some kind of oscillation produced in the B star by the disturbance of the rapidly traveling satellite with its network of prominences. The degree of excitation of the P_1, K_1 oscillation would then depend upon the free period of vibration of the B star. This idea is similar to that already proposed for β Canis Majoris.

It is, however, to be noticed that the probable size of a star like 12 Lacertae or β Cephei severely restricts the lower limit of the period that is possible when the companion revolves at the surface of the primary. This period, considering the mass of the satellite to be negligible, is

$$P = \frac{2\pi a^{3/2}}{g\sqrt{M}}.$$

[13] O. Struve, *Ap. J.*, **108**, 154, 1948.

[14] O. Struve, *Pub. A.S.P.*, **59**, 192, 1947; *A.J.*, **54**, 50, 1948; R. F. Sanford, *Ap. J.*, **109**, 208, 1949.

[15] R. F. Sanford, *Pub. A.S.P.*, **61**, 135, 1949.

With $P = 0.19$ day and $M = 20M\odot$, we find

$$a = 3 \times 10^6 \text{ km} = 4R_\odot .$$

Thus the radius of the B-type star in 12 Lacertae would have to be not larger than $4\,R\odot$ in order to accommodate a satellite. It is true that 12 Lacertae is not a very luminous B star, and β Cephei is probably underluminous—it has strong forbidden lines of *He* I and resembles in this respect the dwarfs τ Scorpii and γ Pegasi. But β Canis Majoris, with its 6-hour period, has some giant characteristics in the spectrum.

Thus it is not possible to regard our suggestion as more than an intriguing working hypothesis that was primarily inspired by the inadequacy of the pulsation hypothesis when applied to the complicated phenomena of the β Cephei variables.[16] What we need is more observations!

[16] This hypothesis is similar to the revival of the double-star theory of cepheid variables which started with the work of Jeans (*M.N.*, **85**, 797, 1925). The latter was open to the objection that the rotational velocities of all known cepheids are small. A modified theory proposed by Hoyle and Lyttleton (*M.N.*, **103**, 21, 1943) avoided this difficulty by assuming that the binary is surrounded by a common envelope whose rotation is slowed down by the accretion of interstellar matter. A somewhat similar idea has been advanced by Menzel (private communication), who believes that "the Cepheids may well be shell stars in the extended sense of the word, wherein the shell is sufficiently opaque to become a photosphere, but a photosphere surrounding two rather than one star." The rotational difficulty would not be serious in this case because conservation of angular momentum would prevent the shell from rotating rapidly.

THE SPECTRUM OF BD+11°4673 DURING THE YEARS 1942–1950

PAUL W. MERRILL
MOUNT WILSON AND PALOMAR OBSERVATORIES
CARNEGIE INSTITUTION OF WASHINGTON
CALIFORNIA INSTITUTE OF TECHNOLOGY
Received January 2, 1951

ABSTRACT

The complex spectrum of BD+11°4673 has been extensively studied with low dispersion in previous years. The present article is based chiefly on spectrograms with dispersion 10 A/mm taken at Mount Wilson from 1943 to 1950. Table 2 lists 450 lines, mostly in emission, measured in the spectrum at various times.

Lines from various elements and from various ions of the same element exhibit remarkable differences in behavior. Bright lines of neutral and ionized metals are narrow; other lines are wide and diffuse. Velocity-curves derived from the following groups of bright lines have been compared: *H*, *He* I, *He* II, *N* III, *Si* IV, and neutral and singly ionized metals. These various curves probably have a common period of 800 days, but they exhibit numerous differences in phase, mean velocity, and amplitude. Lines of neutral and singly ionized metals have much smaller amplitudes than other lines. The mean velocity derived from singlet lines of *He* I is algebraically less than that from triplet lines, as has been found in other symbiotic stars. Certain changes in the velocity-curves have occurred since 1926. Differences in phase between various curves are less than in 1926. The hydrogen lines are narrowest on the rising branch of the velocity-curve, and the sharp metallic lines are most intense at the same phases. The persistent 800-day period probably corresponds to some kind of an oscillation in an extended atmosphere. Absorption lines of neutral metals (M-type spectrum) measured in the red on a few plates show little change in velocity.

Since 1922 the spectrum has gradually been developing features characteristic of symbiotic stars. Since 1941 the resemblance has become more pronounced. Certain progressive changes have been accelerated in 1949 and 1950. Bright lines of *He* II, *N* III, *N* IV, [*Ne* III], and [*O* III] are now more intense than in previous years. Velocities outward from the photosphere, as indicated by displaced absorption lines, have been increasing since 1915.

The spectrum of BD+11°4673[1] seems to have become progressively more complex since the discovery of bright hydrogen lines at the Harvard College Observatory in 1893. It was a fairly normal Be spectrum in 1915 and 1919, with bright lines of *H*, *Fe* II, *Si* I, *Si* II, and with dark lines of *He* I. Bright *He* I lines appeared in 1920 and became strong in 1921. This outburst was accompanied by an increase in the intensities of bright lines of several other elements. Beginning about 1922, the spectrum has gradually been developing features characteristic of combination or symbiotic stars; an M-type spectrum with dark lines of neutral metals and weak *TiO* bands has grown stronger, as have certain emission lines requiring high excitation, notably λ 4686 *He* II. The nebular lines of [*O* III] appeared faintly about 1942 and were well marked in 1950. Superposed on these progressive changes have been fluctuations in the positions and intensities of most of the lines. These fall in a well-marked cycle of 800 days but exhibit many irregularities of amplitude, mean velocity, and phase. In addition, there have recently been rapid variations in an unknown pattern in the displaced absorption-line components of the *He* I lines, especially of λ 3888.

This article is my fifth report on the spectrum of BD+11°4673. The last one,[2] printed in 1942, includes references to my earlier work and to that of other observers. Since that report, spectrograms have been obtained in 1942–1943 by Swings and Struve[3, 4] at the

[1] AG Pegasi, HD 207757; 1900 R.A. 21h46m2; Dec. +12°9′; mag. 7.6; spec. Bep.

[2] *Mt. W. Contr.*, No. 659; *Ap. J.*, **95**, 386, 1942.

[3] Swings and Struve, *Ap. J.*, **97**, 194, 1943.

[4] O. Struve, *Ap. J.*, **99**, 205, 1944.

McDonald Observatory and in 1946–1948 by Tcheng Mao-Lin[5] at the Observatoire de Haute Provence.

RECENT MOUNT WILSON SPECTROGRAMS

During 1942, two one-prism spectrograms of the blue-violet region, dispersion at $H\gamma$ 35 A/mm, were taken at Mount Wilson. From 1943 to 1950, one or more grating spectrograms of the region λλ 3600–5000, dispersion 10 A/mm, have been obtained each year. These were supplemented by a few of the red region, dispersion 15 or 20 A/mm. All are listed in Table 1. The appearance of the spectrum and the number of lines measurable varies greatly during the 800-day cycle, as illustrated by Figures 1–4.

A fairly complete list of lines measured at various phases of the 800-day cycle and over an interval of many years (Table 2) will be convenient for reference. All lines are

TABLE 1

SPECTROGRAMS OF BD+11°4673

Plate	Date	JD 243+	Quant. No. Last *H*	No. M II	Radial Velocity (Km/Sec)				
					H	*He* I		*He* II λ 4686	M II
						Sing.	Trip.		
γ 24221	1942 June 24	0535	12	18	− 9	+12	+16	+10	−14.4
γ 24657	Nov. 1	0665	9	8	+ 3	− 4	(+22)	+12	−10.1
Ce 3082	1943 June 23	0899	11	13	−30	−19	−18	.....	−20.1
3503	1944 July 9	1281	38	104	−17	−11	− 6	+ 2	−16.9
3531	Aug. 3	1306	35	66	−13	− 5	+ 3	+ 1	−15.3
3567	Sept. 7	1341	36	75	−11	+ 2	+ 5	+ 9	−14.6
3606	Oct. 6	1370	37	63	−13	− 4	+10	+ 6	−15.0
3989	1945 Sept. 25	1724	23	13	−21	−19	−19	.....	−17.9
4034*	Oct. 24	1753	3	2	(−41)	(−29)	(−16)	.....	(−20.0)
4038*	25	1754	3	3	(−27)	(−23)	(−11)	.....	(−20.0)
4323	1946 July 13	2015	36	64	−14	−17	− 4	−11	−17.4
4419	Sept. 14	2078	36	70	−11	− 8	+ 4	−13	−16.3
4459	Oct. 12	2106	34	56	−13	−10	+10	−16	−16.6
4737	1947 July 1	2368	22	11	+ 2	− 5	+ 7	.....	−19.4
4807	Aug. 25	2423	23	4	+10	0	+ 8	.....	−18.5
4810	26	2424	22	6	+ 6	+ 3	+12	.....	−16.2
4932	Oct. 25	2484	22	1	−23	−22	−25	.....	(−18.8)
5202*	1948 June 16	2719	3	9	(−20)	(−15)	(−23)	.....	−23.6
5208	17	2720	31	47	−25	−16	−10	−24	−23.0
5312	Sept. 11	2806	35	57	−15	−14	− 9	−18	−17.2
5318*	12	2807	3	7	(−12)	.....	(− 4)	.....	−15.2
5681	1949 June 11	3079	29	31	−14	− 5	+17	+ 3	−15.2
5808	Aug. 3	3132	17	16	+18	.....	+20	+12	−15.9
6024	Nov. 12	3233	(7)	0	(+ 4)	.....	(+ 6)	0	.....
6027*	13	3234	3	0	(−14)	.....	(− 3)	.....	.....
6245	1950 May 25	3427	12	12	−45	(−44)	−24	−24	−23.8
6337	June 29	3462	20	37	−29	−29	−21	−17	−21.4
6355	July 2	3465	.....	28	−36	.....	.....	− 9	−19.5
6429	Aug. 4	3498	31	42	−26	−30	−31	−25	−18.2
6435	5	3499	31	48	−26	−26	−19	−21	−18.8
6444	7	3501	33	42	−27	−30	−22	−17	−19.5
6445*	7	3501	4	(14)	(−17)	(−25)	(− 6)	.....	−20.3
6540	Sept. 24	3549	30	39	−22	−19	−24	−32	−16.0

* Region *Hβ* to *Hε*.

[5] *Ann. d'ap.*, **13**, 51, 1950.

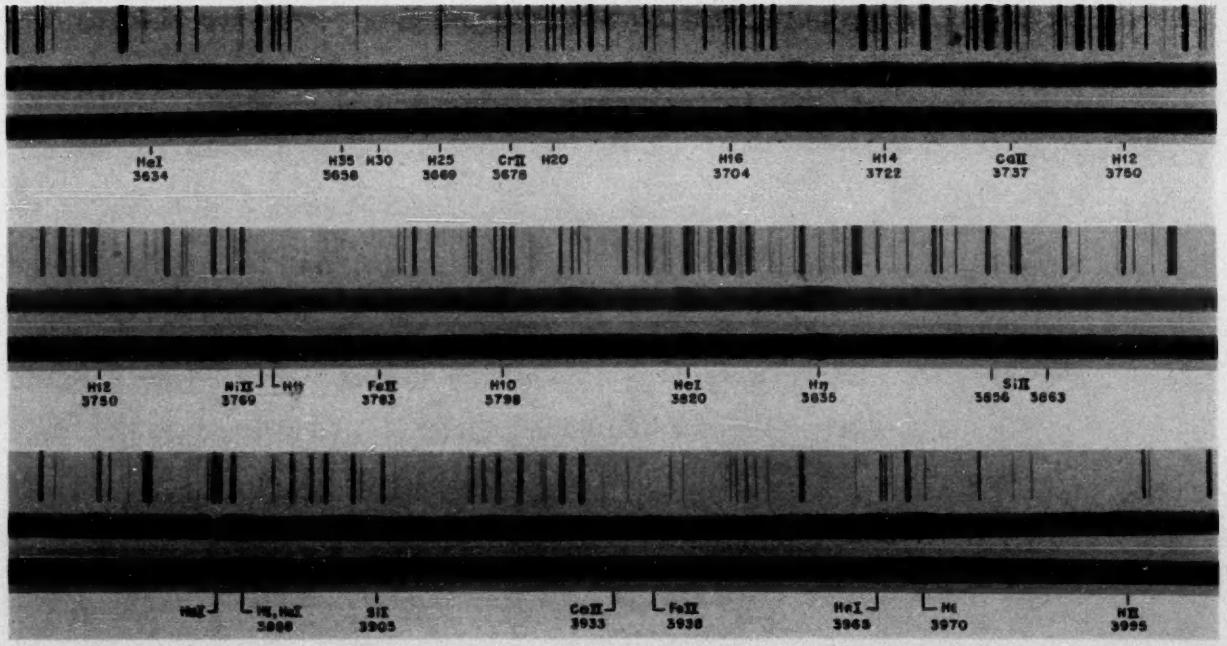

FIG. 1.—The spectrum of BD+11°4673, λλ 3620–4000. The lower spectrum in each strip is from plate Ce 3503, the upper from Ce 4810. See Table 1

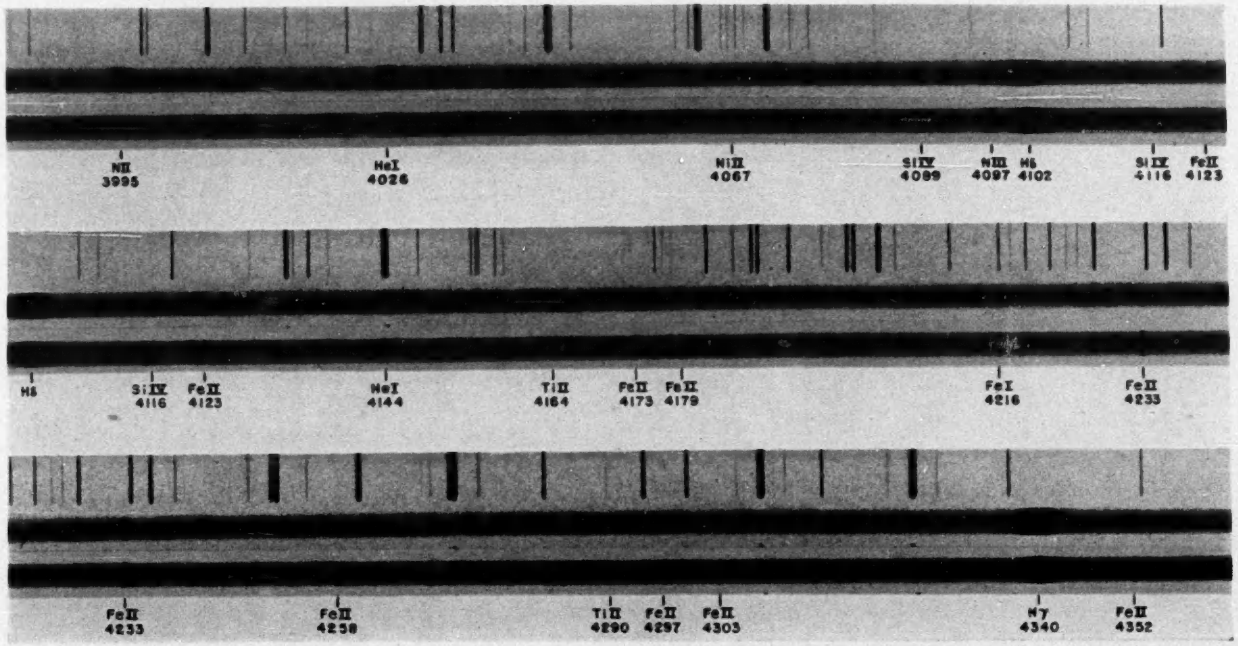

FIG. 2.—The spectrum of BD+11°4673, λλ 3990–4360. The lower spectrum in each strip is from plate Ce 3503, the upper from Ce 4810. See Table 1

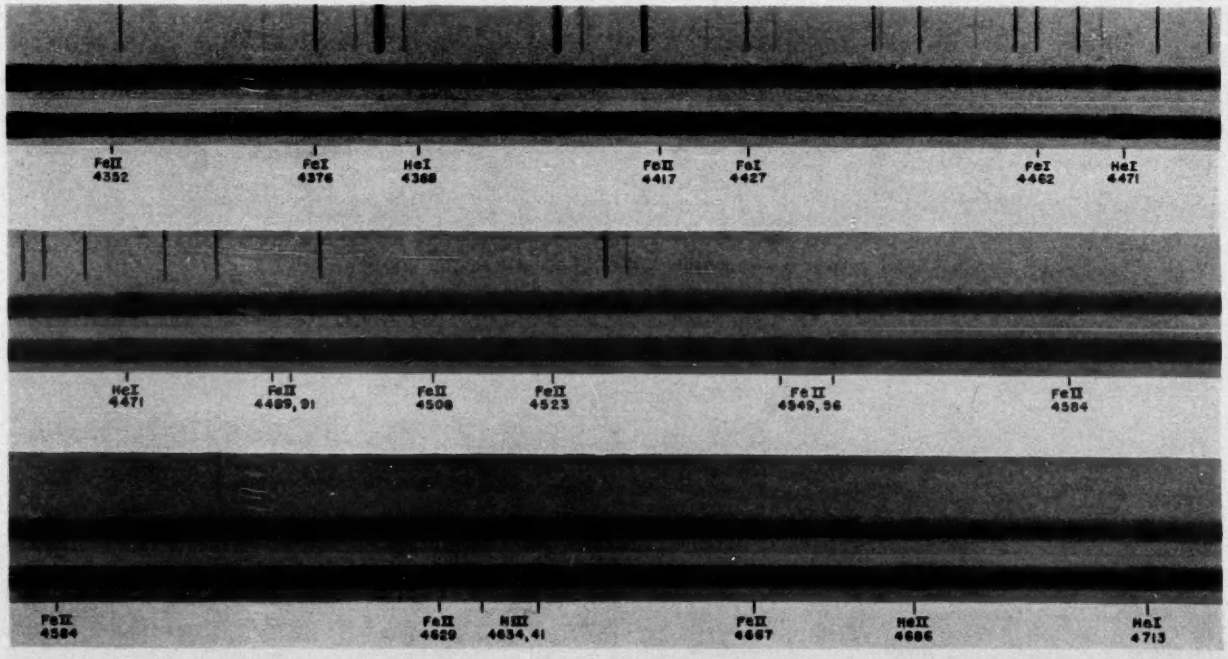

FIG. 3.—The spectrum of BD+11°4673, λλ 4340–4720. The lower spectrum in each strip is from plate Ce 3503, the upper from Ce 4810. See Table 1

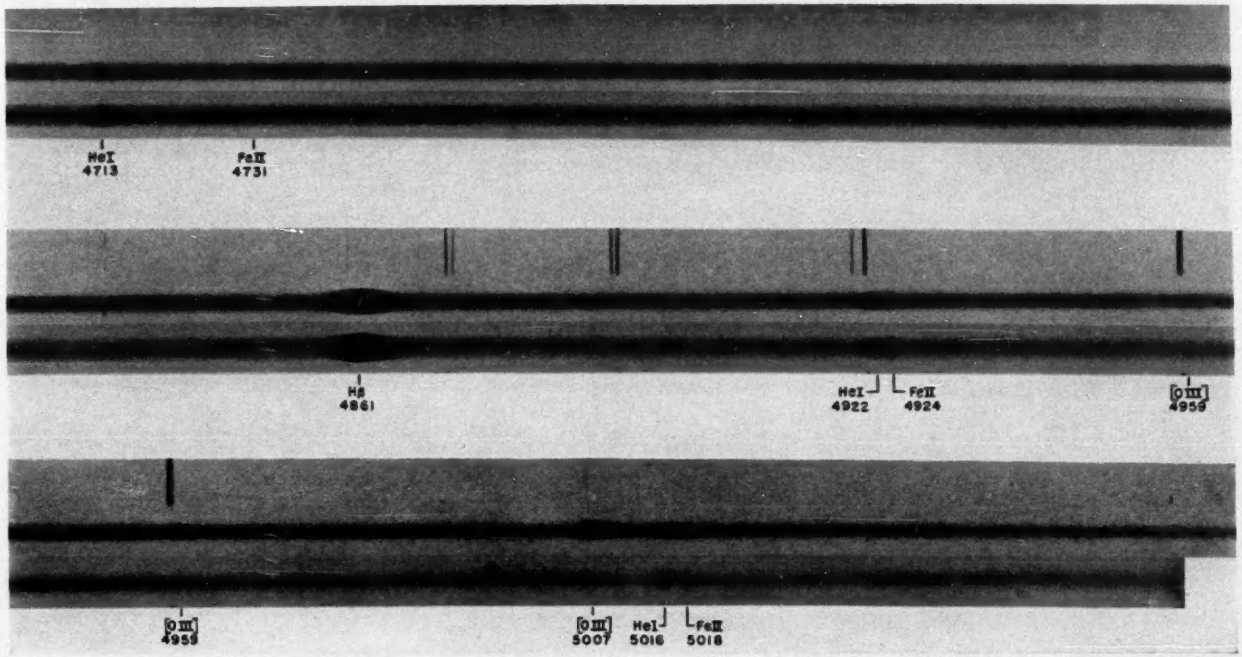

FIG. 4.—The spectrum of BD+11°4673, λλ 4700–5080. The lower spectrum in each strip is from plate Ce 3503, the upper from Ce 5808. See Table 1

TABLE 2

LINES IN THE SPECTRUM OF BD+11°4673

I.A.*	Element	Multiplet No.	Int.	I.A.*	Element	Multiplet No.	Int.
3255.88	*Fe* II	1	2	3679.36	*H* 21	4	5
3264.76	*Fe* II	1	tr	3682.81	*H* 20	4	5
3277.35	*Fe* II	1	3	3684.25	*Cr* II	145	tr
3281.29	*Fe* II	1	2	3685.19	*Ti* II	14	1
3285.42	*Fe* II	1	tr	3686.83†	*H* 19	4	6 n
3295.81	*Fe* II	1	1	3691.56†	*H* 18	4	6 n
3302.86	*Fe* II	1	1	3694.00	*Fe* I	394	tr
3303.47	*Fe* II	1	1	3697.15†	*H* 17	3	6 n
3314.00	*Fe* II	1	tr	3703.86†	*H* 16	3	6 n
3329.46	*Ti* II	7	tr	3705.00†	*He* I	25	3 n
3354.55†	*He* I	8	tr n‡	3706.03	*Ca* II	3	2
3367.36	*N* III	5	tr n	3711.97†	*H* 15	3	7 n
3374.06	*N* III	5	tr n	3712.99	*Cr* II	12	1
3403.32	*Cr* II	3	tr	3715.45	*Cr* II	145	tr
3408.76	*Cr* II	3	tr	3719.94	*Fe* I	5	1
3421.20	*Cr* II	3	tr	3721.94†	*H* 14	3	7 n
3422.74	*Cr* II	3	tr	3734.37†	*H* 13	3	7 n
3433.30	*Cr* II	3	tr	3736.90	*Ca* II	3	3
3438.98	*Mn* II	1	tr	3738.38	*Cr* II	20	tr
3441.98	*Mn* II	3	1	3741.63	*Ti* II	72	1
3447.59†	*He* I	7	tr	3743.36	*Fe* I	21	tr
3460.31	*Mn* II	3	1	3745.69	*Fe* I	5	1
3474.08	*Mn* II	3	tr	3746.56	*Fe* II	14	tr
3475.74	*Fe* II	4	tr	3748.49	*Fe* II	154	tr
3487.99	*Fe* II	4	tr	3750.15†	*H* 12	2	8 n
3488.68	*Mn* II	3	tr	3754.59	*Cr* II	20	tr
3494.67	*Fe* II	16	tr	3759.29	*Ti* II	13	tr
3497.54	*Mn* II	3	tr	3761.83	*Cr* II	11	tr
3503.47	*Fe* II	4	tr	3761.87	*Ti* II	107	
3511.84	*Cr* II	2	tr				
3513.93	*Ni* II	1	tr	3763.79	*Fe* I	21	tr
3530.49†	*He* I	36	tr n	3764.09	*Fe* II	29	
3554.45†	*He* I	34	1 n	3769.46	*Ni* II	4	2
3587.30†	*He* I	31	1 n	3770.63†	*H* 11	2	8 n
3590.46	*Si* III	7	1 n	3779.58	*Fe* II	23	tr
3601.62	*Al* III	1	2 n	3783.35	*Fe* II	14	3
3612.35	*Al* III	1	1 n	3786.37	*Fe* II	15	tr
3613.64†	*He* I	6	tr n	3787.88	*Fe* I	21	tr
3634.28†	*He* I	28	2 n	3791.41	*Si* III	5	1 n
3656.14	*H* 38	7	tr	3796.11	*Si* III	5	10 n
3656.67	*H* 37	7	tr	3797.90†	*H* 10	2	
3657.27	*H* 36	7	1	3806.56	*Si* III	5	3 n
3657.93	*H* 35	7	1	3819.61†	*He* I	22	4 n
3658.64	*H* 34	7	1	3820.43	*Fe* I	20	tr
3659.42	*H* 33	6	2	3824.44	*Fe* I	4	tr
3660.28	*H* 32	6	2	3824.91	*Fe* II	29	1
3661.22	*H* 31	6	3	3827.82	*Fe* I	45	tr
3662.26	*H* 30	6	3	3829.35	*Mg* I	3	1
3663.41	*H* 29	6	3	3832.30	*Mg* I	3	1
3664.68	*H* 28	6	4	3835.39†	*Hη*	2	10 n
3666.10	*H* 27	5	4	3838.29	*Mg* I	3	1
3667.68	*H* 26	5	4	3848.24	*Mg* II	5	1
3669.47	*H* 25	5	4	3849.58	*Ni* II	11	tr
3671.48	*H* 24	5	4	3850.40	*Mg* II	5	tr
3673.76	*H* 23	5	5	3852.57	*Fe* I	73	tr
3676.36	*H* 22	4	5	3853.66	*Si* II	1	tr
3677.82	*Cr* II	12	2	3856.02	*Si* II	1	3

* Lines bright unless otherwise indicated.

† Accompanied by dark component on the shortward side.

‡ n, diffuse.

TABLE 2—*Continued*

I.A.*	Element	Multiplet No.	Int.	I.A.*	Element	Multiplet No.	Int.
3859.91.....	*Fe* I	4	1	4053.81.....	*Ti* II	87	tr
3862.59.....	*Si* II	1	2	4057.80.....	*N* IV	3?	1 n
3863.81.....	*V* II	33	tr	4063.60.....	*Fe* I	43	tr
3867.54†.....	*He* I	20	2 n	4067.05.....	*Ni* II	11	2
3868.77.....	[*Ne* III]	1F		4088.86†.....	*Si* IV	1	3 n
3872.76.....	*Fe* II	29	tr	4097.31†.....	*N* III	1	2 n
3878.18.....	*He* I	59	tr n	4101.74†.....	*Hδ*	1	20 n
3882.28.....	*Ti* II	34?	tr	4102.93.....	*Si* I	2	1
3888.65†.....	*He* I	2	15 n	4103.37.....	*N* III	1	? n
3889.05†.....	*Hζ*	2		4116.10†.....	*Si* IV	1	3 n
				4120.81†.....	*He* I	16	3 n
3896.11.....	*Fe* II	23	tr	4122.64.....	*Fe* II	28	2
3896.16.....	*V* II	10		4124.79.....	*Fe* II	22	tr
3898.01.....	*Fe* I	20?	tr	4128.05.....	*Si* II	3	1
3899.14.....	*V* II	33	tr	4128.74.....	*Fe* II	27	tr
3899.71.....	*Fe* I	4	tr	4130.88.....	*Si* II	3	tr
3900.55.....	*Ti* II	34	2	4143.76†.....	*He* I	53	3 n
(3900.68)§.....	*Al* II	1		(4149.98).....	*Al* III	5	tr
3905.53.....	*Si* I	3	5	4161.52.....	*Ti* II	21	tr
3913.46.....	*Ti* II	34	1	4163.64.....	*Ti* II	105	2
3914.48.....	*Fe* II	3	2	4171.90.....	*Ti* II	105	1
3916.42.....	*V* II	10	tr	4173.45.....	*Fe* II	27	5
3919.00.....	*N* II	17	1 n	4177.70.....	*Fe* II	21?	2
3922.91.....	*Fe* I	4	tr	4178.86.....	*Fe* II	28	6
3926.53.....	*He* I	58	tr n	4181.76.....	*Fe* I	354	tr
3930.31.....	*Fe* II	3	2	4187.80.....	*Fe* I	152	tr
3932.01.....	*Ti* II	34	tr	4195.70.....	*N* III	6	tr n
3933.66†.....	*Ca* II	1	2	4200.02.....	*N* III	6	1 n
3934.41.....	*N* III	8	tr n	(4202.1).....	.....	.....	tr
3935.94.....	*Fe* II	173	tr	4216.19.....	*Fe* I	3	1
3938.29.....	*Fe* II	3	5	4226.73.....	*Ca* I	2	tr
3938.52.....	*N* III	8	tr n	4227.43.....	*Fe* I	693	tr
3944.01.....	*Al* I	1	tr	4233.17.....	*Fe* II	27	8
3945.21.....	*Fe* II	3	2	(4236.98).....	*N* II	48	tr
3949.95.....	*Fe* I	72	tr	(4238.6).....	.....	.....	tr
3951.16.....	*Fe* I	661?	tr	4238.82.....	*Fe* I	693	tr
3951.97.....	*V* II	10	1	(4241.79).....	*N* II	47, 48	tr
3955.85.....	*N* II	6	tr n	4242.38.....	*Cr* II	31	1
3956.46.....	*Fe* I	604	tr	4243.98.....	[*Fe* II]	21F	2
3956.68.....	*Fe* I	278		4244.81.....	[*Fe* II]	21F	tr
3961.52.....	*Al* I	1	tr	(4246.83).....	*Sc* II	7	tr
3964.73†.....	*He* I	5	4 n	4258.16.....	*Fe* II	28	2
3968.47†.....	*Ca* II	1	1?	4261.92.....	*Cr* II	31	tr
3970.07†.....	*He*	1	15 n	(4267.15).....	*C* II	6	tr
3974.16.....	*Fe* II	29	1	4271.76.....	*Fe* I	42	tr
3977.74.....	*Fe* I	72	tr	4273.32.....	*Fe* II	27	2
3981.61.....	*Fe* II	3	1	4275.57.....	*Cr* II	31	tr
3982.00.....	*Ti* II	11	tr	(4276.83).....	[*Fe* II]	21F	1
3987.63.....	*Ti* II	11	tr	4278.13.....	*Fe* II	32	1
3995.00†.....	*N* II	12	4 n	(4282.1).....	.....	.....	tr
4002.07.....	*Fe* II	29	tr	4287.40.....	[*Fe* II]	7F	3
4009.27†.....	*He* I	55	1 n	4287.89.....	*Ti* II	20	tr
4012.37.....	*Ti* II	11	1	4290.22.....	*Ti* II	41	1
4024.55.....	*Fe* II	127	tr?	4294.10.....	*Ti* II	20	1
4025.14.....	*Ti* II	11?	tr	4294.13.....	*Fe* I	41	
4026.19†.....	*He* I	18	6 n	4296.57.....	*Fe* II	28	4
4028.33.....	*Ti* II	87	tr	4299.24.....	*Fe* I	152	tr
4032.95.....	*Fe* II	126	tr	4300.05.....	*Ti* II	41	2
4035.54.....	*Fe* II	22?	1	4301.93.....	*Ti* II	41	2
4045.82.....	*Fe* I	43	tr	4303.17.....	*Fe* II	27	4

§ Parentheses indicate observed in *Mt. W. Contr.*, No. 381, 1919–1928, but not observed in present series.

TABLE 2—*Continued*

I.A.*	Element	Multiplet No.	Int.	I.A.*	Element	Multiplet No.	Int.
4307.90	*Ti* II	41	2	(4488.75)	[*Fe* II]	6F	1
4312.86	*Ti* II	41	2	4489.18	*Fe* II	37	3
4314.08	*Sc* II	15	1	4491.40	*Fe* II	37	4
4314.29	*Fe* II	32		4494.57	*Fe* I	68	tr
4314.98	*Ti* II	41	tr	4501.27	*Ti* II	31	tr
4316.81	*Ti* II	94?	tr	4508.28	*Fe* II	38	3
(4317.52)			tr	4510.92	*N* III	3	2 n
(4319.62)	[*Fe* II]	21F?	tr	(4512.54)	*Al* III	3	1
4320.74	*Sc* II	15	tr	4514.89	*N* III	3	1 n
4325.01	*Sc* II	15	tr	4515.34	*Fe* II	37	4
4337.92	*Ti* II	20	tr	4518.18	*N* III	3	tr n
4340.47†	*Hγ*	1	30 n	4520.22	*Fe* II	37	3
(4345‖)			tr	4522.63	*Fe* II	38	3
(4349.96)			tr	4523.60	*N* III	3	tr
4351.76	*Fe* II	27	6	4528.62	*Fe* I	68	tr
(4352.78)	[*Fe* II]	21F	tr	(4529.18)	*Al* III	3	2
(4358.38)	[*Fe* II]	21F	tr	4529.46	*Ti* II	82	tr
(4359.34)	[*Fe* II]	7F	2	(4532.5)			1
4363.21	[*O* III]	2F	2 n	4533.97	*Ti* II	50	2
4367.66	*Ti* II	104	tr	4534.17	*Fe* II	37	
4369.40	*Fe* II	28	1	4534.57	*N* III	3	tr n
(4372.43)	[*Fe* II]	21F?	tr	(4538.5)			tr
(4374.46)	*Sc* II	14?	tr	4541.52	*Fe* II	38	2
4375.93	*Fe* I	2	2	4549.47	*Fe* II	38	8
4379.09	*N* III	17	1 n	4549.62	*Ti* II	82	
4384.33	*Fe* II	32	3	4552.65†	*Si* III	2	2 n
4384.64	*Mg* II	10	tr	4555.89	*Fe* II	37	6
4385.38	*Fe* II	27	4	4558.66	*Cr* II	44	1
4387.93†	*He* I	51	4 n	4563.76	*Ti* II	50	tr
4390.58	*Mg* II	10	tr	4567.87†	*Si* III	2	2 n
4390.98	*Ti* II	61	tr	4571.10	*Mg* I	1	1
4394.06	*Ti* II	51	1	(4571.97)	*Ti* II	82	tr
4395.03	*Ti* II	19	tr	4574.78†	*Si* III	2	tr n
4395.85	*Ti* II	61	tr	4576.33	*Fe* II	38	3
4398.31	*Ti* II	61	tr	4580.06	*Fe* II	26?	1
4399.77	*Ti* II	51	1	4582.84	*Fe* II	37	2
4404.75	*Fe* I	41	tr	4583.83	*Fe* II	38	10
4413.60	*Fe* II	32	tr	(4595.68)	*Fe* II	38?	tr
(4413.78)	[*Fe* II]	7F	2	4601.34	*Fe* II	43?	tr
(4416.27)	[*Fe* II]	6F	2	4601.48†	*N* II	5	1 n
4416.82	*Fe* II	27	4	(4607.15†)	*N* II	5	tr n
(4419.59†)	*Fe* III	5?	tr	(4613.87†)	*N* II	5	tr n
4427.31	*Fe* I	2	2	4620.51	*Fe* II	38	2
(4427.59)	*N* II	55, 56	tr	(4621.39†)	*N* II	5	tr
(4430.94†)	*Fe* III	5?	tr	4629.34	*Fe* II	37	8
(4432.74)	*N* II	55	1	(4630.54)	*N* II	5	1
4437.55†	*He* I	50	tr n	4634.16	*N* III	2	5 n
(4438.7)			tr	4640.64	*N* III	2	7 n
(4441.99)	*N* II	55	tr	4641.90	*N* III	2	
4447.03	*N* II	15	2 n	(4643.09†)	*N* II	5	1
4447.72	*Fe* I	68	tr	(4649.3†)			tr
4452.11	[*Fe* II]	7F	1	4656.97	*Fe* II	43	tr
(4457.95)	[*Fe* II]	6F	tr	(4658.05)	[*Fe* III]	3F	1
4461.65	*Fe* I	2	2	(4663.05)	*Al* II	2	1
(4464.4)			tr	4666.75	*Fe* II	37	2
4471.48†	*He* I	14	10 n	4670.17	*Fe* II	25	1
4472.92	*Fe* II	37	tr	4685.68	*He* II	1	6 n
4474.19	*Fe* II	171?	tr	4713.14†	*He* I	12	4 n
4481.23	*Mg* II	4	tr	(4728.09)	[*Fe* II]	4F	tr
4482.17	*Fe* I	2	1	4731.44	*Fe* II	43	3

‖ Dark only.

TABLE 2—*Continued*

I.A.*	Element	Multiplet No.	Int.	I.A.*	Element	Multiplet No.	Int.
(4735.0)	.....	.....	tr	6021.80‖	*Mn* I	27	1
(4774.74)	[*Fe* II]	20F	tr	6064.63‖	*Ti* I	69	1
(4788.13)	*N* II	20	tr	6065.49	*Fe* I	207	1
(4803.27)	*N* II	20	tr	6081.42	*V* I	34	1
(4814.55)	[*Fe* II]	20F	1	6085.23	*Ti* I	69	1
4861.33†	*Hβ*	1	50 n	6090.18	*V* I	34	tr
4867.18	*N* III	9	tr n	6102.72‖	*Ca* I	3	2
(4889.63)	[*Fe* II]	4F	tr	6111.62	*V* I	34	1
(4895.20)	*N* II	1	tr	6119.50	*V* I	34	tr
4921.93†	*He* I	48	5 n	6122.22‖	*Ca* I	3	1
4923.92	*Fe* II	42	8	6141.72‖	*Ba* II	2	2
4958.91	[*O* III]	1F	2 n	(6147.74)	*Fe* II	74	tr
(4994.36)	*N* II	24, 64	tr	6154.22‖	*Na* I	5	tr
(5001.3)	*N* II	19	tr	6162.17‖	*Ca* I	3	2
(5006.)	*N* II	19, 24, 64	tr	6238.38	*Fe* II	74	tr
5006.84	[*O* III]	1F	4 n	6247.56	*Fe* II	74	1
5015.68†	*He* I	4	5 n	6248.92	*Fe* II	.....	tr
5018.43	*Fe* II	42	8	6292.86‖	*V* I	19	1
(5056.02)	*Si* II	5	1	6296.52‖	*V* I	19	tr
(5158.00)	[*Fe* II]	18F	tr	6305.67‖	*Sc* I	2	2
5169.03	*Fe* II	42	1	6317.98	*Fe* II	.....	3
5197.57	*Fe* II	49	1	6347.09	*Si* II	2	2
(5202.51)	*Si* II	—?	tr	(6371.36)	*Si* II	2?	1
5234.62	*Fe* II	49	2	6383.75	*Fe* II	.....	2
5264.80	*Fe* II	48	1	6385.47	*Fe* II	.....	1
5275.99	*Fe* II	49	2	6393.60‖	*Fe* I	168	1
5284.09	*Fe* II	41	tr	6400.01‖	*Fe* I	816	2
5316.61	*Fe* II	49	6	(6407.3)	.....	.....	tr
5316.78	*Fe* II	48		6408.03‖	*Fe* I	816	2
5325.56	*Fe* II	49	1	6411.66‖	*Fe* I	816	1
5362.86	*Fe* II	48	2	6413.35‖	*Sc* I	1	1
5397.13‖	*Fe* I	15	4	(6416.90)	*Fe* II	74	tr
5405.78‖	*Fe* I	15	2	6421.36‖	*Fe* I	111	2
5420.36‖	*Mn* I	4	1	6430.85‖	*Fe* I	62	2
5425.27	*Fe* II	49	2	6432.65	*Fe* II	40	2
5432.55‖	*Mn* I	1	tr	6439.07‖	*Ca* I	18	2
5434.53	*Fe* I	15	1	(6442.97)	*Fe* II	.....	1
5446.92	*Fe* I	15	3	6449.81‖	*Ca* I	19	2
5497.52‖	*Fe* I	15	2	6456.38	*Fe* II	74	2
5506.78‖	*Fe* I	15	1	6462.57‖	*Ca* I	18	3
5514.22‖	*Sc* I	15	1	6471.66‖	*Ca* I	18	1
5520.50‖	*Sc* I	15	3	6491.28	*Fe* II	.....	1
5534.86	*Fe* II	55	3	6493.05	*Fe* II	.....	1
5688.20‖	*Na* I	6	1	6496.90‖	*Ba* II	2	2
(5754.8)	[*N* II]	3F	tr	6516.05	*Fe* II	40	2
5875.63†	*He* I	11	15 n	6546.24‖	*Fe* I	268?	tr
5889.95‖	*Na* I	1	5	6548.06	[*N* II]	1F	1
5895.92‖	*Na* I	1	3	6562.82	*Hα*	1	100 n
(5957.61)	*Si* II	4	1	6583.43	[*N* II]	1F	3
(5978.97)	*Si* II	4	2	6599.11‖	*Ti* I	49?	2
5991.38	*Fe* II	46	2	6678.15	*He* I	46	5 n

in emission except those marked with superior parallel lines ([11]), which are in absorption only. Emission lines accompanied by an absorption component on the shortward side are marked with a dagger. Lines observed in the first Mount Wilson investigation,[6] 1919–1928, but not measured on the present series of plates, presumably because they have become less intense, are inclosed in parentheses. For the identified lines the wave lengths are laboratory values; for a few unidentified lines, measured stellar wave lengths reduced to zero velocity are given.

HYDROGEN LINES

Throughout the interval 1942–1950 the bright hydrogen lines have been strong, their shortward dark components weak and at times absent (Figs. 1–4). The displacements (Table 1 and Fig. 5), with small deviations, have maintained the previously observed period of 800 days, but there has been a slow progressive decrease in the mean velocity from +11.5 km/sec in 1926 to about −10 km/sec in 1949. Moreover, the semiamplitude of the velocity-curve has varied in a peculiar manner. Between 1920 and 1929 it increased from about 12 km/sec to 25 km/sec, but in 1939 it had resumed the smaller value of 12 km/sec; since then it has increased somewhat, the value in 1949 being about 20 km/sec (not well defined). The very strong *Hα* line yields about the same velocity as do the other hydrogen emission lines (see Table 7).

On three plates—Ce 4932, 5681, and 6245—the hydrogen velocities have large negative residuals, which seem to represent abrupt and anomalous disturbances. The residuals in Table 3 show that the anomalies are not shared by the lines of all elements. The lines of ionized metals appear not to be disturbed at all, but on plate Ce 4932 the helium residuals are similar to those of hydrogen.

Obvious changes occur in the widths of the bright hydrogen lines. These changes are especially noticeable in the ultraviolet toward the limit of the series because the lines fuse together into the Balmer continuum before they become too weak to measure (Fig. 1). Thus the quantum number of the upper level (*Hα* = 3, *Hβ* = 4, etc.) of the last line measured (Table 1) is an index of the sharpness of the lines. A plot of these numbers for the various coudé plates (Fig. 5) indicates an 800-day cycle, with maxima at times which fall on the rising branch of the velocity-curve. The lines appear to be strongest at these same times. The same relationship of intensity to displacement was found during the years 1922 to 1928 (see Fig. 1 and n. 6, above). Curiously enough, it was then thought that the lines were slightly wider when most intense. The apparent discrepancy may arise from the fact that the earlier discussion was based on low-dispersion plates and referred largely to the lines *Hγ* and *Hδ*.

On most plates the bright hydrogen lines are nearly symmetrical, with no pronounced structure. But on the three plates Ce 4932, 5681, and 6245, on which the hydrogen lines have large negative velocity residuals, a peculiar maximum appears near the shortward edge of the broad emission line. On Ce 4932 the absorption borders appear stronger than usual (see tracings in Fig. 7).

The explanation of the peculiar negative velocities may lie in phenomena somewhat similar to those in eruptive prominences in which upward motions occur at irregular intervals in regions so close above the photosphere that they are observable only over that half of the star which faces the earth. Corresponding positive velocities (on the other half) are not seen.

HELIUM LINES

He I emission.—The lines of *He* I are complex, having both bright and dark components (see Figs. 1–4). Velocities derived from the bright lines (Table 1 and Fig. 6) exhibit well-marked 800-day fluctuations whose phases slightly precede the corresponding phases of the hydrogen velocities. This differs from the behavior in 1926, when the curve for *He* I

[6] P. W. Merrill, *Mt. W. Contr.*, No. 381; *Ap. J.*, 69, 330, 1929.

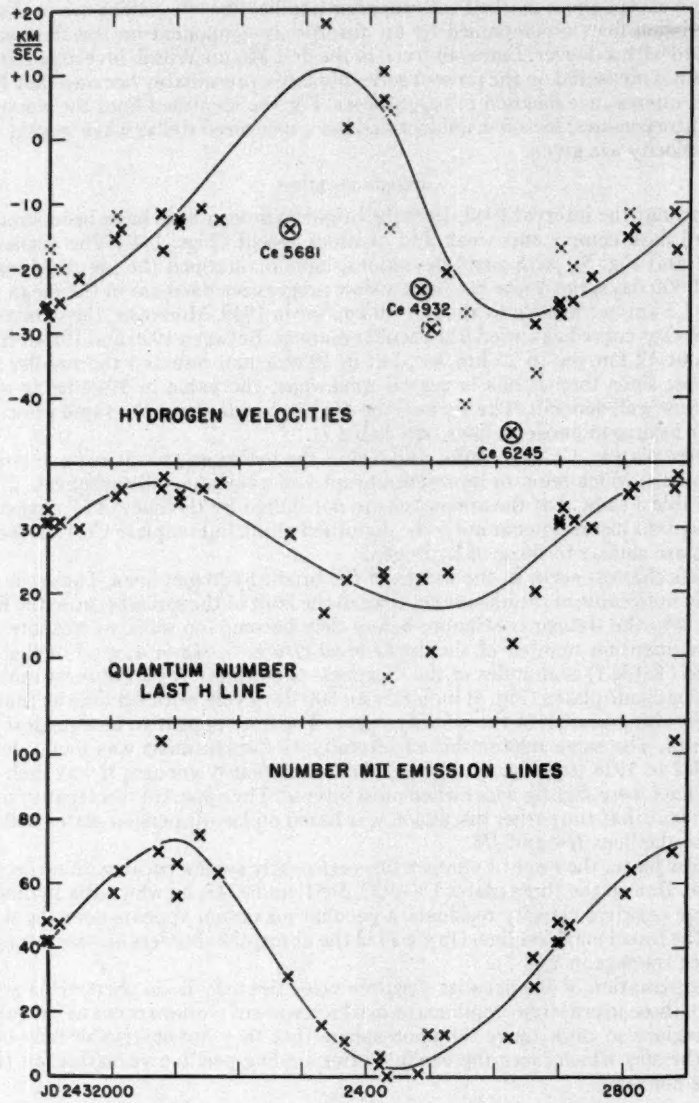

FIG. 5.—Periodic behavior of lines of hydrogen and of ionized metals (M II), reduced to one 800-day cycle.

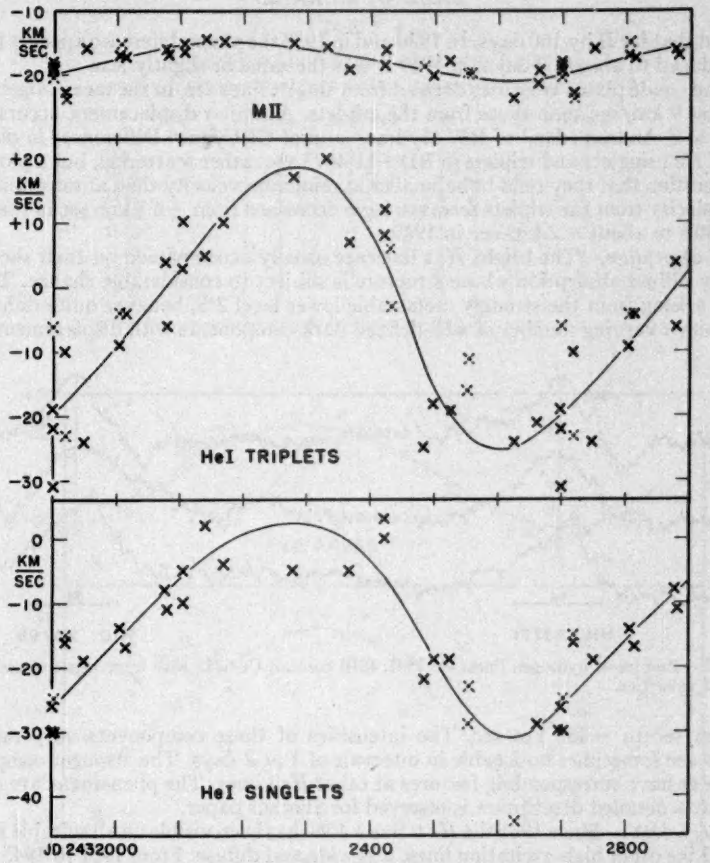

FIG. 6.—Radial velocities of lines of neutral helium and of ionized metals (M II), reduced to one 800-day cycle.

TABLE 3

ANOMALOUS RESIDUALS FROM VELOCITY-CURVES
(OBSERVED MINUS EXPECTED)
(Km/Sec)

Element	Ce 4932	Ce 5681	Ce 6245
H	−23	−21	−16
He sing.	− 4	− 4	(−12)
He trip.	−13	− 1	+ 1
M II	(0)	− 1	− 1

preceded that for *H* by 160 days. In 1930 and in 1938 the phase difference appears to have been reduced to about 60 days; in 1949 it was the same or slightly less.

On the coudé plates velocities derived from singlet lines are, in the mean, algebraically less by 9 km/sec than those from the triplets. A similar displacement occurs in the spectra of Z Andromedae,[7] of RW Hydrae,[8] and of CI Cygni.[8] Differences in displacement of *He* I singlets and triplets in BD+11°4673 are rather scattering, but a plot offers the suggestion that they tend to be smaller at minimum velocity than at maximum. The mean velocity from the triplets seems to have decreased from +6.5 km/sec in the 1920's and 1930's to about −2 km/sec in 1949.

He I absorption.—The bright *He* I lines are usually accompanied on their shortward edges by diffuse absorption whose structure is subject to considerable change. The line λ 3888, arising from the strongly metastable lower level 2^3S, behaves quite differently. It exhibits a varying number of well-defined dark components with displacements from

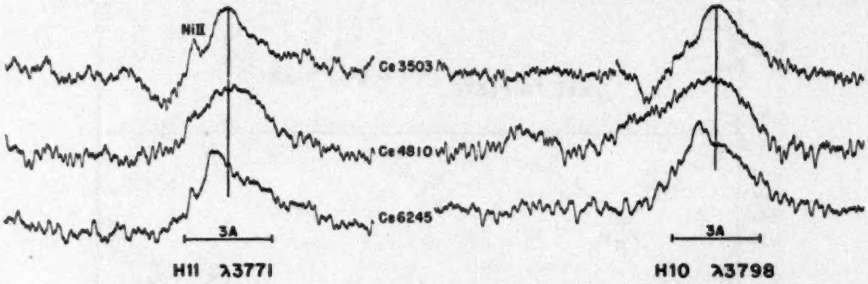

FIG. 7.—Profiles of hydrogen lines: Ce 3503, 4810 normal; Ce 6245 with large negative residuals in measured velocities.

−70 km/sec to −450 km/sec. The intensities of these components vary radically; changes are sometimes noticeable in intervals of 1 or 2 days. The stronger components sometimes have corresponding features at other *He* I lines. The phenomena are so complex that a detailed description is reserved for another paper.

He II, λ 4686.—Since 1931 the *He* II line λ 4686 has been visible on all suitable spectrograms. Like other high-excitation lines, it is wide and diffuse. From 1931 to 1945 it grew gradually stronger; in 1946 and 1947 it weakened considerably; but in 1949 and 1950 it has been stronger than ever before (see Table 4). The measured displacements (Table 1) yield a curve (Fig. 8) agreeing approximately with the mean curve for *He* I.

NITROGEN LINES

Lines of N II.—The triplet lines of multiplet (5) of the revised *Multiplet Table*[9] near λ 4600 previously observed are no longer recognizable. The singlet lines have become progressively weaker since 1921; through 1948 the line λ 3995, multiplet (12) appeared as a weak diffuse emission line with a mean displacement of −20 km/sec.

Lines of N III.—From 1915 to 1931, lines of *N* III were absent or so weak that their presence was doubtful. In 1937 they were decidedly stronger; on the present series of plates, λ 4097 is well marked, while λ 4634 and the blend at λ 4641 are conspicuous. They exhibit decided changes in intensity from year to year (see Table 4). A diffuse emis-

[7] P. W. Merrill, *Mt. W. Contr.*, No. 744; *Ap. J.*, **107**, 317, 1948.

[8] P. W. Merrill, *Mt. W. and P. Obs. Reprint*, No. 22; *Ap. J.*, **111**, 484, 1950.

[9] Charlotte E. Moore, *A Multiplet Table of Astrophysical Interest, Revised Edition* (*Princeton U. Obs. Contr.*, No. 20, 1945).

TABLE 4

INTENSITIES OF VARIOUS GROUPS OF LINES

Year	*He* II	*He* II/*He* I	*N* III	*N* IV	[*O* III]
1943	2	1.2	4	0	1
1944	2	1.6	4	tr	1
1945	2	1.6	4	0	1
1946	2	0.6	2	0	0
1947	1	0.7	3	0	0
1948	1	1.2	3	0	0
1949	3	4	6	tr	4
1950	4	5	8	1	5

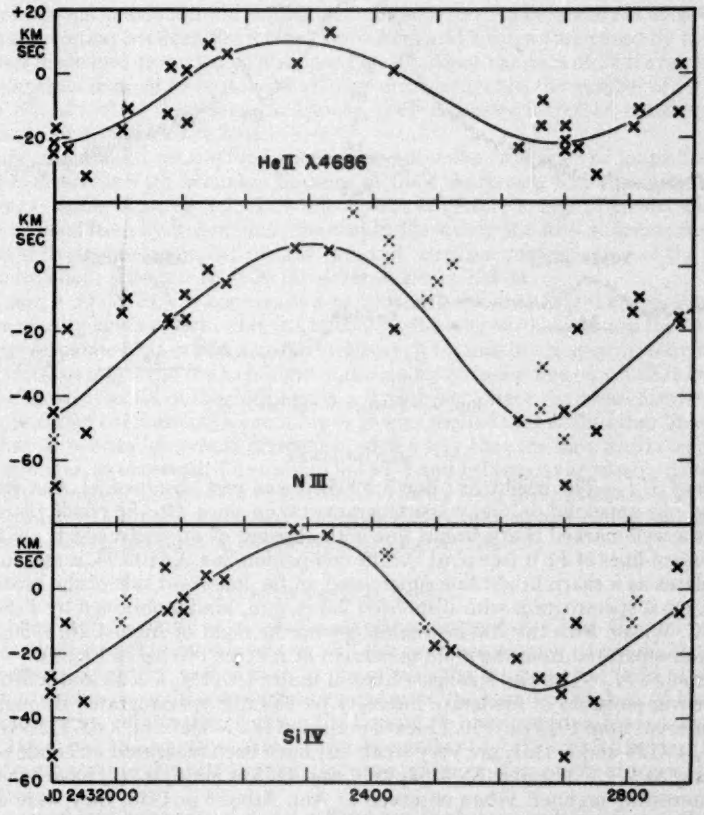

FIG. 8.—Radial velocities of various lines, reduced to one 800-day cycle

sion line near λ 4058, possibly *N* IV λ 4057.80, has appeared in increasing intensity on recent plates.

ALUMINUM LINES

The bright lines of *Al* II and *Al* III previously observed have practically disappeared from the spectrum. The strong *Al* III lines λ 3601 and λ 3613 (outside the spectral range previously observed) can be recognized as weak diffuse emission lines on some of the coudé plates. The weakening of *Al* III is particularly interesting because the general excitation of the emitting atmosphere seems to have been increasing. Possibly it has become high enough to change a considerable proportion of the *Al* III atoms, I.P. 28.4 volts, into *Al* IV. This would be in line with the shift from *N* II, I.P. 29.5 volts, to *N* III.

The lines of *Al* I are seen on the coudé plates for the first time, but they are narrow and very weak, and their visibility is probably due to the higher dispersion rather than to an increase in intensity.

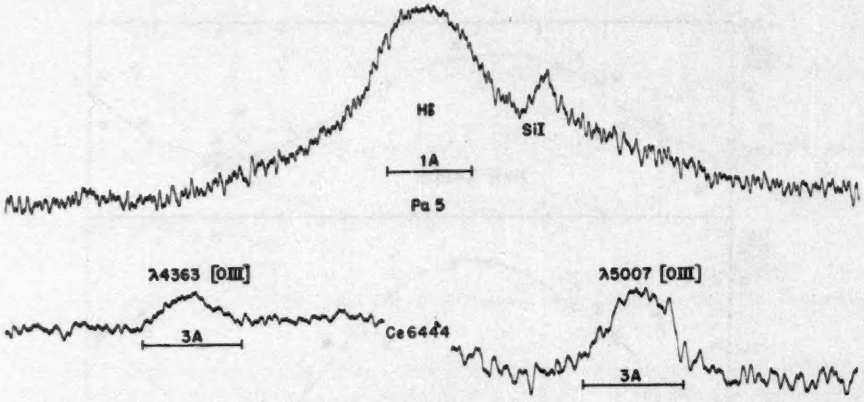

FIG. 9.—Profiles of various lines

SILICON LINES

Lines of Si I.—The bright *Si* I line λ 3905.53 was first observed at Ann Arbor[10] in 1915 and has appeared on many spectrograms taken since. On the coudé plates it appears as a well-marked sharp bright line with changes of intensity which are in phase with those of lines of *Fe* II (see p. 617). The companion line, λ 4102.93, is measurable on many plates as a sharp bright line superposed on the longward side of the broad bright *Hδ* line. On a spectrogram with dispersion 2.3 A/mm, kindly obtained by I. S. Bowen and O. C. Wilson with the 200-inch telescope on the night of August 26, 1950, the *Si* I line is well separated from the main maximum of *Hδ* (see tracing in Fig. 9).

Lines of Si II.—The two strongest lines of multiplet (11), λ 3856 and λ 3862, have been seen in emission in moderate intensity on suitable spectrograms throughout the whole interval from 1915 to 1950. Lines of multiplet (2), λ 6347 and λ 6371, and of multiplet (3), λ 4128 and λ 4131, are very weak but have been measured on coudé plates.

Lines of Si III.—The lines λλ 4553, 4568, and 4575 of multiplet (2) have behaved in a most interesting manner. When observed at Ann Arbor[10] in 1915, they were dark. On Mount Wilson plates taken from 1919 to 1931, they were dark, with weak bright edges on the longward side. From 1937 to 1941 they were well-developed bright lines, the absorption components being inconspicuous. In the present series the bright lines are weaker

[10] *Pub. Obs. U. Michigan*, 2, 71, 1916.

and of variable intensity, being visible on one or two plates only. The dark components are not seen.

Lines of Si IV.—The lines λ 4089 and λ 4116 of *Si* IV also have behaved in an interesting way. In 1915 and from 1919 to 1931 they were present in absorption, apparently in varying intensity. From 1937 to 1950 they were well-marked bright lines with weak dark borders shortward. On the coudé plates, 1943–1950, the lines are diffuse and ill defined. Since 1948 the dark components have been very weak or absent.

LINES OF IONIZED METALS

Narrow bright lines of *Fe* II, *Ti* II, *Cr* II, *Ni* II, *V* II, *Mn* II, and *Si* II occur in the spectrum, those of *Fe* II and *Ti* II being most numerous. They vary greatly in intensity in the 800-day cycle, being strongest (and most numerous) when the ultraviolet hydrogen lines are sharpest. This behavior is shown by the spectra in Figures 1–4 and by the plots in Figures 5, 6, and 10.

Lines of various metals seem to exhibit a common pattern of behavior; at least there is a distinct correlation between the intensities of *Fe* II and *Ti* II, as indicated by the numbers of lines measured on various plates (see Fig. 10). Since the lines of *Ti* II are considerably weaker than those of *Fe* II, none at all were measured when the number of *Fe* II lines fell below 35; but, after they begin to appear, their intensity increased more or less in proportion to that of the *Fe* II lines.

Although superposed on a strong continuous spectrum, the lines of ionized metals, M II, are measurable with accuracy because of their sharpness. The displacements of various lines (Table 5) agree well. The velocity-curve (Table 1, Fig. 6) is very different from that derived from hydrogen lines; the amplitude is only one-fifth as great; the mean velocity is −18 km/sec instead of −8 km/sec; and the phase precedes that of the hydrogen-curve by about 90 days. In 1926 the difference was 320 days.

The K line, λ 3933, of *Ca* II appears as a narrow dark line with bright edges, the shortward edge usually being several times as intense as the longward. Although the dark line appears to vary somewhat in position and intensity, it is probably largely interstellar; the apparent changes may arise from changes in the stellar emission line on which it is superposed. The mean velocity of the dark line is −9.3 km/sec. Since the mean displacement of the bright stellar calcium line is probably −18 km/sec like that of the other M II lines, the dark line at −9 km/sec would divide it in such a way that the shortward component would be stronger, as observed. The sodium lines D1 and D2 appear as narrow dark lines, considerably stronger than K of *Ca* II; the mean velocity from three plates is −9 km/sec. They are probably largely interstellar, although their displacements differ but slightly from those of absorption lines of the M-type spectrum (Table 7).

LINES OF NEUTRAL METALS

Bright lines of *Si* I occur on practically all plates, lines of *Fe* I and *Mg* I on most of them, lines of *Al* I weakly on one or two. All the lines are narrow, those of *Fe* I being especially sharp. Their intensities vary in phase with the intensities of lines of ionized metals. Figure 10 shows a definite correlation between the numbers of lines of *Fe* II and of *Fe* I measured on various plates. Since the lines of *Fe* I are considerably weaker than those of *Fe* II, none at all were measured when the number of *Fe* II lines fell below 35, but, after they begin to appear, their intensity increases more or less in proportion to that of the *Fe* II lines.

The measured displacements of various *Fe* I lines on the same plate agree well, nor is there much range from plate to plate (Table 5). Lines of *Fe* I, *Si* I, *Al* I, and *Mg* I yield nearly the same displacements. Mean residuals with respect to *Fe* I are: *Si* I, −0.1 km/sec (14 plates); *Al* I, −0.2 km/sec (2 plates); *Mg* I, −2.2 km/sec (10 plates). Moreover, the displacements of these M I lines are closely similar to those of M II lines. In

fact, the general behavior of lines of neutral metals closely resembles that of lines of ionized metals.

FORBIDDEN LINES

Lines of [*Fe* II] have been weak since 1924; only a few of the strongest have been measured on the recent series of spectrograms. The line λ 4658 of [*Fe* III] likewise has recently been weak or absent. The red lines of [*N* II] λ 6548 and λ 6583 were present in low intensity on three plates; λ 5755 has not been observed.

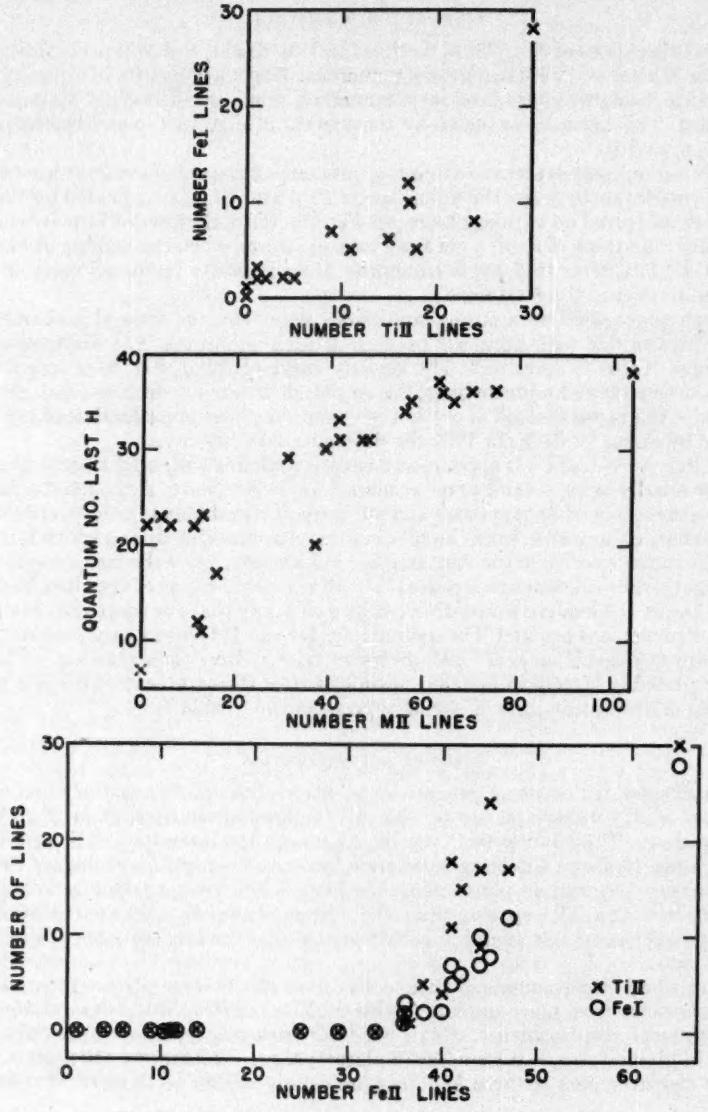

FIG. 10.—Correlations between numbers of lines measured

The nebular lines of [*O* III] λ 4959 and λ 5007 were recognized for the first time in 1943 as weak diffuse lines (Table 4). They were visible also in 1944 and 1945 but disappeared throughout 1946, 1947, and 1948. During 1949 and 1950 they have been well-marked lines, their intensities greater than ever before. They are very wide, their profiles (Fig. 9) corresponding to a velocity spread of 220 km/sec. The [*O* III] line λ 4363 and the [*Ne* III] line λ 3869 were also present during 1949 and 1950. The λ 4363 line was not definitely seen in earlier years. A very weak diffuse line had been regularly observed near the posi-

TABLE 5

RADIAL VELOCITIES DERIVED FROM METALLIC EMISSION LINES AND INTERSTELLAR *Ca* II ABSORPTION
(Km/Sec)

Plate No.	Emission								Interstellar	
	Fe I	No.	*Si* I	No.	*Fe* II	No.	*Ti* II	No.	*Ca* II	No.
γ 24221	.....		−23.5	(1)	−14.4	(11)	.....		.....	
γ 24657	.....		.....		−10.1	(8)	.....		.....	
Ce 3082	.....		−18.5	(1)	−19.7	(11)	.....		− 8.9	(2)
3503	−17.0	(28)	−17.5	(2)	−16.7	(65)	−17.4	(29)	−10.5	(1)
3531	−16.9	(10)	−17.0	(2)	−15.2	(44)	−15.8	(17)	−10.5	(2)
3567	−15.2	(8)	−18.0	(2)	−14.5	(45)	−15.0	(24)	−10.4	(2)
3606	−16.3	(6)	−21.2	(2)	−15.6	(42)	−13.8	(15)	−11.9	(1)
3989	.....		−19.7	(1)	−16.5	(11)	.....		−10.0	(2)
4323	−20.7	(7)	−18.9	(2)	−17.1	(41)	−18.1	(18)	− 7.9	(1)
4419	−18.4	(12)	−18.9	(2)	−16.6	(47)	−15.4	(17)	−12.8	(1)
4459	−19.3	(5)	−21.2	(2)	−16.4	(41)	−17.3	(11)	−14.5	(2)
4737	.....		−19.9	(1)	−20.0	(9)	.....		− 8.5	(1)
4807	.....		.....		−18.5	(4)	.....		− 8.2	(1)
4810	.....		.....		−16.2	(6)	.....		− 7.3	(1)
4932	.....		.....		−18.8	(1)	.....		− 8.3	(1)
5208	−20.4	(2)	−18.9	(2)	−23.0	(40)	−21.4	(4)	− 8.7	(1)
5312	−17.5	(7)	−18.8	(2)	−17.3	(44)	−16.8	(9)	−10.0	(1)
5681	.....		−18.6	(2)	−15.6	(29)	.....		−10.1	(1)
5808	.....		−19.4	(1)	−15.8	(14)	.....		− 9.7	(2)
6024	.....		.....		.....		.....		− 9.0	(1)
6245	.....		−21.3	(1)	−22.9	(11)	.....		− 5.7	(2)
6337	−18.1	(1)	−18.4	(1)	−21.4	(33)	.....		− 6.6	(2)
6355	.....		−21.3	(1)	−19.3	(25)	.....		− 8.2	(1)
6429	−18.9	(2)	−16.8	(1)	−18.2	(36)	−22.4	(1)	− 7.5	(1)
6435	−16.9	(2)	−16.2	(2)	−18.8	(38)	−17.5	(5)	− 8.5	(1)
6444	−18.9	(2)	−14.1	(2)	−19.5	(36)	−18.4	(2)	− 9.6	(2)
6540	−14.9	(3)	−14.6	(2)	−15.9	(36)	−11.9	(1)	.....	

tion of the [*Ne* III] line, but before 1949 it may have been the *He* I line λ 3868.54. The measured velocities of the centers of the nebular lines on a few plates are recorded in Table 6.

WIDTHS OF EMISSION LINES

The apparent widths of the hydrogen lines increase enormously with increasing intensity from the ultraviolet longward. Moreover, the widths, especially those of lines toward the limit of the series, depend upon the phase in the 800-day cycle, being smallest near the midpoint of the rising branch of the velocity-curve. The narrowest lines in the ultraviolet, *H* 34–*H* 36, are about 0.5 A wide, while *Hβ* is at least 8 A wide. The intense central portion of *Hα* is about 10 A wide, while the wings extend more than 5 A on either side, the total width exceeding 20 A.

The weaker lines of *He* I measure about 3 A in width, the stronger ones 4–5 A. The *He* II line λ 4686 is about 3.5 A wide. Most of the lines of *N* II, *N* III, *N* IV, *Si* III, and *Si* IV are from 3 to 5 A wide.

The apparent widths of lines of *Fe* I, *Si* I, *Mg* I, *Fe* II, *Mg* II, *Si* II, *Ti* II, *Cr* II, and *Ni* II range from 0.4 to 1.0 A, depending largely on their intensities. The narrowest lines are those of *Fe* I and *Si* I; their intrinsic widths probably do not exceed 0.2 or 0.3 A.

The forbidden lines [*O* III] and [*Ne* III] have widths that correspond to a velocity spread of 220 km/sec.

THE M-TYPE SPECTRUM

Traces of an M-type spectrum are seen longward from *Hγ* on most of the coudé spectrograms. In the yellow and red the M-type spectrum is somewhat stronger relative to the superposed early-type spectrum, and a number of dark lines of neutral metals are measurable. Even in the red, however, the lines are not strong, and the list in Table 2 is

TABLE 6

RADIAL VELOCITIES DERIVED FROM FORBIDDEN LINES
(Km/Sec)

PLATE NO. (CE)	JD 243+	[*Ne* III] λ 3868.77	[*O* III]	
			λ 4363.22	λ 5006.85
6024	3233	.....	−30	.....
6245	3427	.....	−55	−15
6337	3462	.....	−49	−17
6355	3465	.....	−54	.....
6429	3498	.....	−61	−18
6435	3499	−56	−59	−18
6444	3501	−48	−62	−23
6445	3501	.....	.....	−15
6540	3549	−72	−50	−14

incomplete. The displacements (Table 7) yield a mean value of −14.0 km/sec, with little evidence of variation.

DISCUSSION

The persistent 800-day period probably corresponds to some kind of an oscillation in the star's extended atmosphere. Nevertheless, the wide emission lines and the displaced absorption components give evidence of a rapidly expanding atmosphere. How the two types of motion can coexist is a problem. All the observed spectroscopic phenomena can scarcely arise in the same atmospheric stratum but must be localized in various strata. The localization probably depends chiefly on physical conditions rather than on the relative abundances of various chemical atoms, but a partial sorting of various kinds of atoms and ions may occur.

If the velocity-curve derived from hydrogen lines represents a volume pulsation, then various emission lines are strongest and narrowest when the atmosphere is largest and most tenuous. This is quite reasonable and tends to substantiate the pulsation hypothesis.

Parameters which are important in determining the observed spectroscopic phenomena are (1) the radius of effective zone of spectroscopic action and (2) the velocity of outflow above the photosphere. Both of these appear to differ for various kinds of atoms and ions and to vary with time.

Interesting facts concerning the 800-day cycle in line displacements are brought out by comparing the recent data with those obtained in the 1920's. Table 8 shows that the phases of curves for helium, metals, and other elements now precede the corresponding phase for hydrogen by considerably smaller intervals than they did in 1926. A formal explanation might lie in the assumption of longer periods for these elements than for hydrogen, but it probably has more physical significance to say—and data for intermediate dates seem to bear this out—that immediately after the outburst in 1920 the phases differed greatly but since then have tended to become coincident.

TABLE 7

RADIAL VELOCITIES DERIVED FROM LINES IN THE RED REGION
(Km/Sec)

Plate (Ce)	Emission						Absorption	No.
	H Curve	*Hα*	*He* I λ 5876	*He* I λ 6678	M II	No.		
4034	−23	.....	−16	−29	−20.0	(2)	−13.5	(12)
4038	−23	−27	−11	−23	−20.0	(3)	−11.0	(10)
5202	−24	−20	−23	−15	−23.6	(9)	−14.1	(15)
5318	−17	−12	− 4	.....	−15.2	(7)	−15.2	(7)
6027	+ 4	−14	− 3	.....	.....	.....	−20.1	(4)
6445	−26	− 9	− 6	.....	−20.3	(14)	−13.6	(23)

TABLE 8

PHASES IN THE 800-DAY CYCLE

Lines	1926 JD 242+	1946 JD 243+
H	4860	2100
He I	4700	2050
N II	4660	.....
Al III	4680	.....
He II	.....	2070
N III	.....	2060
Si IV	.....	2060
M II	4540	2010
Quant. no. last *H*	.....	1880
No. M II	.....	1880

The mean velocities of lines of various elements differ considerably (Table 9). For *H*, *He* I and II, and *Si* IV the mean velocity is now about −7 km/sec; that of metals, neutral and once ionized, *N* II and *N* III about −20 km/sec. Elements *H*, *He* I, *N* II, and perhaps *N* III have shown a decided decrease (algebraic) since 1926. Thus there is now a smaller difference between *H*, *He* I, and M II than in earlier years. The line λ 5007 [*O* III] yields the same mean velocity as M II, *N* II and III; but λ 3968 [*Ne* III] and λ 4363 [*O* III] have a much greater negative velocity. The great width of the lines is probably produced by an expanding atmosphere. The λ 3968 and λ 4363 lines have larger transition probabilities

than λ 5007 and thus may be produced at a higher density. Occultation may therefore cut off more of the longward end of the line than for λ 5007 and thus give a shortward shift of the center. For broad permitted lines the shortward range absorbed can just balance the longward range occulted, allowing the center of the line to yield the true radial velocity of the star as a whole. Lines of M II apparently have much smaller outward velocities.

The semiamplitudes (Table 10) yielded by all elements with broad lines are about 20 km/sec; the value for *H* has varied somewhat but has now about the same value as in

TABLE 9

MEAN VELOCITIES
(Km/Sec)

Lines	1926	1939	1946
H	+12	− 4	− 8
He I	+ 6	+ 1	− 8
He II	.....	−13	− 6
Si IV	.....	+ 1	− 7
M II	−22	−14	−18
N II	+ 6	−12	−20
N III	.....	(− 8)	−20
Al III	−20	.....	.....
[*Ne* III]	.....	.....	−59
λ 4363 [*O* III]	.....	.....	−54
λ 5007 [*O* III]	.....	.....	−17

TABLE 10

SEMIAMPLITUDES IN THE 800-DAY CYCLE
(Km/Sec)

Lines	1926	1939	1946
H	20	12	20
He I	16	14	18
He II	.....	15	16
N II	17	14	.....
N III	.....	14	26
Al III	18	.....	.....
Si IV	.....	18	23
M II	8	5	3
[*Fe* II]	7	.....	.....

1926. Other elements with broad lines have shown no progressive changes. The narrow metallic lines have shown much smaller semiamplitudes, about 8 km/sec in 1926, decreasing to 3 km/sec in 1946.

Certain *progressive* changes have been intensified in 1949 and 1950. Bright lines of *He* II, *N* III, *N* IV, [*Ne* III], and [*O* III] are now more intense than in previous years.

The wide emission lines and the displaced absorption components indicate an atmosphere expanding with an outward velocity that has been increasing since 1915 until in 1950, for certain elements, it exceeds 200 km/sec (see Fig. 11). The outward velocity for atoms emitting lines of [*O* III] and [*Ne* III] appears to be slightly greater than 110 km/sec.

The fact that velocities seem to increase with increasing electric charge (successive stages of ionization) and to decrease with increasing atomic weight suggests the possibility that electric forces play some part in the complex periodic phenomena.

The resemblance to symbiotic spectra noted in 1941 can be traced in many details of the behavior of various lines. It has recently become more pronounced through the increased intensity of *He* II λ 4686 and the appearance of forbidden lines of [*O* III] and [*Ne* III]. If the development of those features characteristic of symbiotic stars should continue, it will not be many years before BD+11°4673 has a full-fledged combination

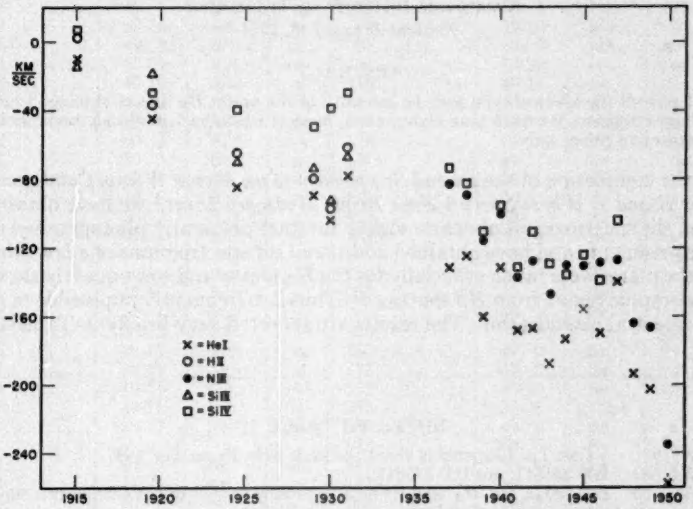

FIG. 11.—Displacements of absorption lines, 1915–1950

spectrum. The light-curve should be closely followed. According to Cecilia Payne-Gaposchkin[11] and Balfour S. Whitney[12] the photographic magnitude has gradually declined from 6.9 in 1900 to 8.5 in 1950.

Although the transformation of a Be spectrum into a combination spectrum in a few decades is extraordinary, it is not entirely unique. On one occasion Z Andromedae did somewhat the same thing in a few months. Symbiotic stars, as well as Be stars with symbiotic tendencies, should be closely watched by spectroscopic and photometric observers.

[11] *Harvard Ann.*, **115**, 233, No. 22, 1950.

[12] Unpublished data.

SPECTROSCOPIC OBSERVATIONS OF Be STARS

WILLIAM C. MILLER AND PAUL W. MERRILL
MOUNT WILSON AND PALOMAR OBSERVATORIES
CARNEGIE INSTITUTION OF WASHINGTON
CALIFORNIA INSTITUTE OF TECHNOLOGY
Received January 16, 1951

ABSTRACT

Table 1 records the spectral type and the intensity of the bright $H\alpha$ line as obtained from low-dispersion slit spectrograms for more than eighty stars, most of which had previously been photographed with the objective prism only.

Since the completion of the *Second Supplement to the Mount Wilson Catalogue of Stars of Classes B and A Whose Spectra Have Bright Hydrogen Lines*,[1] we have obtained low-dispersion slit spectrograms of nearly eighty Be stars previously photographed with the objective prism only and have obtained additional slit spectrograms of a few other stars. Most of the plates were taken especially for the $H\alpha$ region and consequently show poorly the photographic region from $H\beta$ shortward. Thus it is frequently impossible to make an accurate spectral classification. The results are reported very briefly in Table 1.

NOTES TO TABLE 1

MWC 9	γ Cas. The spectrum is about the same as in November, 1947.
MWC 683	HD 236611, not HD 237011.
MWC 760	HD 36376. $H\beta$, $H\gamma$, and $H\delta$ have unusually narrow bright components superposed on wide dark lines.
MWC 789	HD 250550. The spectrum is about the same as in January, 1946.
MWC 803	HD 44351. Now a well-developed shell spectrum, the narrow dark lines of ionized metals are much stronger than in October, 1946.
MWC 1009	HD 228707. Possibly a shell star.
AS 42	Probably BD+60°341. In NGC 663.
AS 43	BD+60°343. In NGC 663.
AS 126	BD−21°1449. Bright $H\alpha$ is very strong and seems to have a wing shortward.
AS 335	MHα 308-17. $H\alpha$ is a well-marked bright line on plates taken on May 5 and October 28, 1950. It is not seen on plates taken on September 24, 1949, and July 28, 1950; these plates may possibly be of a brighter star 2!5 north preceding.
AS 336	Probably BD+0°4080. The K-type lines appear weak, and the spectrum may be composite. $H\beta$ is bright.
AS 366	Not HD 333003 but a fainter star slightly north. The spectrum appears to resemble that of AS 357.
AS 372	HD 351123. Possibly a shell star.
AS 520	HD 251050. BD+13°1094. Not in original list. 1900 R.A. $5^h58^m.4$; Dec. +13°34′; mag. 9.1.
AS 521	MHα 255-77. Not in original list. 1900 R.A. $21^h25^m.7$; Dec. +54°27′; mag. (10.8).

[1] Merrill and Burwell, *Mt. W. and P. Obs. Reprints*, No. 8; *Ap. J.*, **110**, 387, 1949.

TABLE 1

SLIT SPECTROGRAMS OF Be STARS

Star	Date (Yr.-Mo.)	Spect.	Int. of Bright $H\alpha$†
MWC*			
9	49-10	B0e	w
493	49-11	B8e	m
558	50- 3	B8e	m
683	49- 8	Ae	w
706	49- 8	B5e	w
732	50- 1	B9e	w
743	49-10	A0e	w
755	49-12	A0e	w
760	49-11	A2e	s
762	50- 3	A2e	m
771	50- 3	B0e	m
774	49-11	Ae	w
784	49-10	B5e	s
786	50- 2	B2e	w
787	49-11	B8e	w
789	50-10	Aep	s
803	49-11	Bep	.....
807	49-11	B5e	s
810	50- 1	B5e	m
812	50- 2	B8e	w
816	49-11	A0e	m
817	49-11	Ae	m
824	49-11	B9e	w
837	49-11	Be	m
1009	50- 7	Ae	m
AS‡			
2	49- 9	Be	m
3	49- 9	Be	m
5	50- 1	Be	s
6	49-10	Be	s
9	49-10	Be	s
15	49- 8	B(2)e	w
16	49- 8	B(3)e	s
18	49- 8	Be	m
19	49- 9	Be	s
20	49- 9	Be	m
27	49-11	Be	s
36	49- 9	Ae	w
37	50-10	Be	w
39	49- 9	Be	s!
41	49- 8	B(0)e	m
42	49- 8	Be	s
43	49-11	Be	m
48	49- 9	B(8)e	w
AS‡			
49	49- 9	Be	m
52	50- 1	Ae	m
78	50- 1	Beq	s!
90	49-10	B9e	m
95	49- 9	A0e	w
101	49-12	Be	m
116	49-11	Be	s
117	50- 1	Ae	m
124	50- 1	B(8)e	s
126	50-10	Be	s
127	49-11	Be	m
138	49-11	A0e	w
145	50- 3	Be	s
157	50- 4	Ae	m
162	50- 4	Be	s
189	50- 4	.....	m
199	50- 4	Be	m
233	49- 7	Be	m
242	49- 7	Be	m
258	49- 8	Be	m
286	49- 9	Be	s
332	49- 7	Be	m
335	50-10	Be	m
336	50- 6	gK0pe	.....
339	49- 8	Be	s
343	50- 5	Be	m
347	50- 6	Be	m
357	50- 6	.....	s!
366	50- 7	.....	s!
367	49- 8	B5e	m
368	50- 6	Be	m
372	50- 6	B8e	m
384	49- 9	B8e	w
437	49- 7	B(5)e	m
442	49- 8	B(8)e	s
443	49- 9	Be	s
444	49- 9	Be	s
485	49- 9	Be	m
504	49- 7	B3e	w
516	49- 7	Be	s
518	49- 9	Be	m
520§	50- 3	B8e	m
521§	49-11	B(5)e	s

* MWC. Mount Wilson Catalogue: *Mount Wilson Contributions*, Nos. 471 and 682; *Mount Wilson and Palomar Observatories Reprints*, No. 8; *Ap. J.*, **78**, 87, 1933; **98**, 153, 1943; **110**, 387, 1949.

† Estimated intensity of the bright $H\alpha$ line on the following scale: w = weak; m = medium; s = strong; s! = very strong.

‡ AS. Additional Stars: *Mount Wilson and Palomar Observatories Reprints*, No. 24; *Ap. J.*, **112**, 72, 1950.

§ Not in the original list.

ABSORPTION LINES AND BANDS IN THE SPECTRUM OF CHI CYGNI

YOSHIO FUJITA*
Lick Observatory
Received December 21, 1950

ABSTRACT

This paper gives results from five spectrograms of χ Cygni obtained with spectrographs attached to the 36-inch refractor of the Lick Observatory. The mean radial velocity of this star near its light-maximum was found to be +2.4 km/sec from atomic absorption lines, from heads of absorption bands of *TiO* and *ZrO*, and from rotational lines of *TiO*. The existence of *AlO*, *MgH*, *AlH*, *CH*, etc., molecules in the star's atmosphere appears to be probable from the identification of corresponding lines. The intensity distribution of vibrational bands of *TiO* was calculated and compared with observation. The vibrational-band temperature of this star was found to be 2200° K.

Although a comprehensive study of the spectrum of the long-period variable star χ Cygni has been made by P. W. Merrill,[1] it was thought worth while to re-examine the spectrum with the aim of obtaining more detailed information about the molecular lines. For this purpose five spectrograms of this star near its light-maximum were obtained with the Mills spectrograph, which has a dispersion of 10 A/mm at 4500 A, and with the two-prism, 6-inch camera spectrograph of dispersion 75 A/mm at $H\gamma$, both attached to the 36-inch refractor of the Lick Observatory. The investigation deals mainly with the Mills spectrograms, with the others serving as check plates. The region of the spectrum studied with the Mills spectrograph is reproduced in Figure 1. The observational data are given in the accompanying tabulation.

No. Plates	Date (1950)	Spectrograph	Emulsion
2.....	October 10, 19	Mills	Eastman II*a*-O
3.....	October 8, 10	Two-prism, 6-inch	Eastman II*a*-O

Measurements for wave lengths of about 660 absorption lines in the region between 4324 A and 4875 A have been made, and their intensities have been estimated visually. Many of these lines are blended with others because of too small dispersion; it would have been much better if a dispersion of 2–3 A/mm had been available. For this reason, some blends undoubtedly were measured as one line, although they might be separated into two or more lines on a spectrogram of higher dispersion. But some of the lines are quite free from blending, and there are no other conspicuous lines in their neighborhood to cause confusion. These lines were selected for determining the radial velocity of the star, with the results shown in Table 1.

If the radial velocity derived from each line is plotted against the corresponding lower excitation potential, the results are as shown in Figure 2. It seems probable, from this figure, that greater velocities of recession correspond to higher excitation potentials. This result agrees with measurements of *Fe* I lines made by Merrill, who found that "iron lines at excitation potential 1.0 volt are displaced longward 2 km/sec with respect to the ultimate lines."

* Martin Kellogg Fellow, Lick Observatory, September 15–December 15, 1950. On leave from the Department of Astronomy, University of Tokyo, Japan.

[1] *Ap. J.*, 106, 274, 1947.

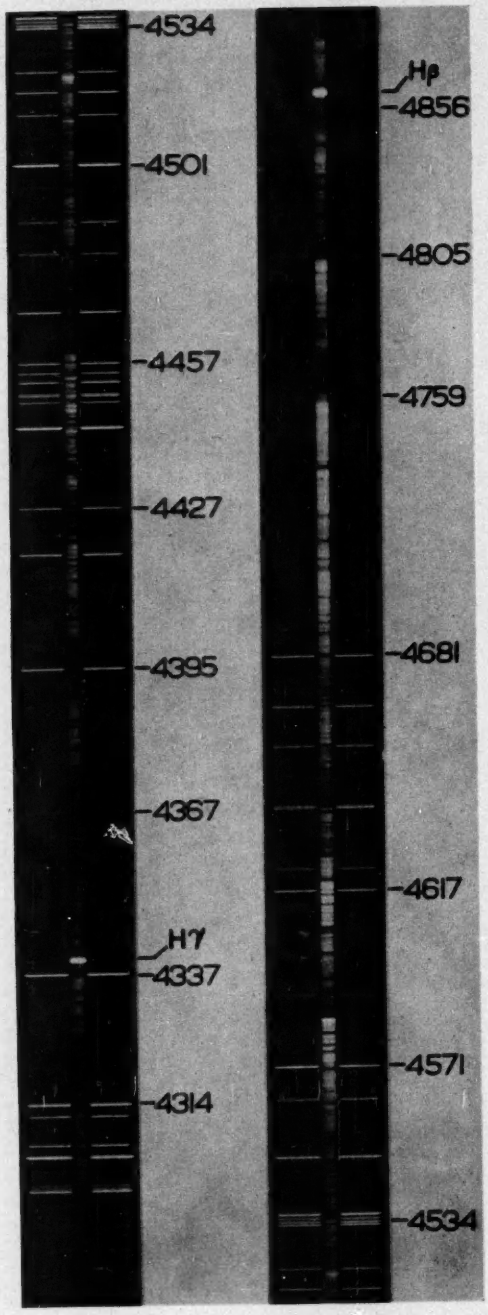

FIG. 1.—The spectrum of χ Cygni on October 10, 1950

It is well known that both *TiO* and *ZrO* molecules coexist in this star. This fact sometimes leads to confusion in the identification of lines, since lines of both molecules in some cases are coincident in wave length not only with each other but occasionally with lines of other elements. For this reason, the same procedure was followed as for the atomic lines, and only those molecular lines were used that are clearly distinguishable from other lines. Thus the radial velocity of this star was determined from band heads of *TiO* and *ZrO* and from any rotational lines in *TiO* bands. The results are shown in Table 2.

TABLE 1

RADIAL VELOCITIES FROM UNBLENDED ATOMIC LINES*

Element	No. Lines	Mean Lower E.P.	Radial Velocity (Km/Sec) Oct. 10	Oct. 19	Element	No. Lines	Mean Lower E.P.	Radial Velocity (Km/Sec) Oct. 10	Oct. 19
Ca I.....	1	1.89	+4.0	−1.3	*Cr* I.....	11	0.98	−1.3	−2.9
	1	2.51	+1.3	+2.0		1	2.53	+2.6	−4.6
Sc I.....	1	1.44	+1.9	−1.9		3	3.14	−0.4	+1.0
	3	0.02	−2.2	−2.8		2	0.05	−3.5	−3.4
Ti I.....	7	0.87	+1.6	0.0	*Fe* I.....	2	0.98	+3.3	+6.3
	2	1.43	+3.0	+5.8		7	1.52	+1.4	+0.6
	8	1.80	+1.7	−0.2		2	2.20	+7.0	+8.7
Ti II.....	2	1.23	+3.0	+7.7		3	3.63	+8.4	+8.5
V I.....	4	0.03	−4.1	−3.8	*Zr* I.....	1	0.07	0.0	+1.4
	8	0.28	+4.1	+3.1		3	0.61	+1.4	−2.4
						1	1.39	−0.7	+4.2

* Laboratory data are from Miss C. E. Moore's *Revised Multiplet Table, Contr. Princeton U. Obs.*, No. 20, 1945.

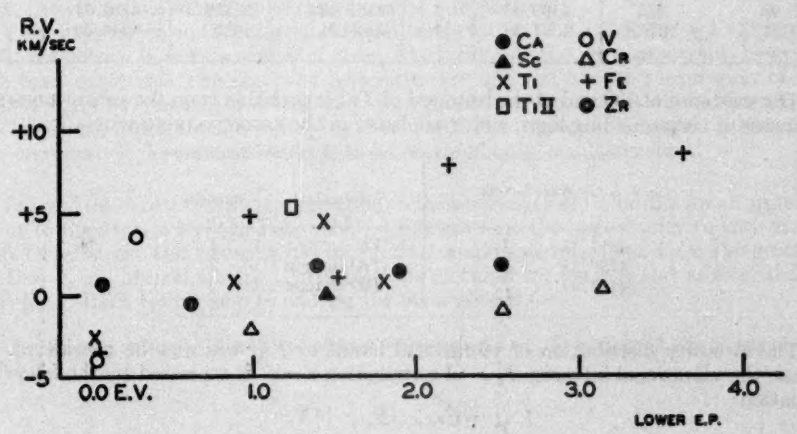

FIG. 2.—Radial velocity plotted against lower excitation potential for unblended lines

The mean radial velocity derived from atomic and molecular absorption lines is +2.4 km/sec, which is in good agreement with Merrill's determination. This result is consistent with the idea that both molecular and atomic absorption lines are formed in nearly the same layer of this star's atmosphere.

In regard to other molecules, such as *AlO*, *MgH*, *AlH*, and *CH*, most of their lines are coincident in wave length with *TiO* or *ZrO* features or with atomic lines, so that it is difficult to establish the existence of these compounds in the usual way. But the lines listed in Table 3, which are quite distinct in wave length from any lines of other sources, may indicate the existence of these compounds in the atmosphere of χ Cygni.

TABLE 2

RADIAL VELOCITIES FROM MOLECULAR FEATURES*

Spectral Feature	No.	Radial Velocity (Km/Sec)	
		Oct. 10	Oct. 19
TiO band heads	20	+2.8	+5.0
ZrO band heads	12	+1.0	+3.2
Rotational lines of *TiO*	78	+2.2	+2.9

* Laboratory data are from A. Christy, *Phys. Rev.*, **33**, 701, 1929; F. Lowater, *Phil. Trans. R. Soc. London, A*, **234**, 355, 1935.

TABLE 3

MOLECULES PROBABLY PRESENT IN χ CYGNI

Laboratory Wave Length (A)	Molecule	χ Cygni		Laboratory Wave Length (A)	Molecule	χ Cygni	
		Wave Length	Intensity			Wave Length	Intensity
4842.74	*AlO*	4842.7	4*b*	4396.93	*CH*	4396.87	2
4398.98	*AlH*	4399.05	1	4362.02	*AlH*	4362.11	2
4397.51	*CH*	4397.53	1	4348.31	*CH*	4348.36	2

The existence of *YO* and of the isotopes[2] of *TiO* is probable from the conspicuous appearance of corresponding lines, which are listed in the accompanying tabulation.

Wave Length (A)	Molecule	Intensity
4817.33	*YO*	4
4788.25	*TiO* isotope	2
4787.01	*TiO* isotope	2

The intensity distribution of vibrational bands of *TiO* will now be considered. As usual, the vibrational intensity $I_{v'v''}$ of a transition $v'-v''$ is expressed by the following equation:

$$I_{v'v''} = C\nu_{v'v''}|R_{v'v''}|^2 N_{v''},$$

[2] G. H. Herbig, *Pub. A.S.P.*, **60**, 378, 1948.

in which $|R_{v'v''}|^2$ is proportional to the transition probability. If a Maxwell-Boltzmann distribution is assumed, $N_{v''}$ can be replaced by $e^{-E_{v''}/kT}$. In the case of a symmetrical molecule, Hutchisson's theory may be applied for the calculation of $R_{v'v''}$. But in the case of an unsymmetrical molecule, such as *TiO*, this theory is only approximate, and the computations to follow are uncertain to this extent. The quantity $R_{v'v''}$ was computed in this way with the molecular constants[3] for *TiO*, and the calculations were carried out with six values of the temperature: 1500°, 1700°, 2000°, 2300°, 2500°, and 2800° K. To take account of a possible error affecting visual estimates that extend over a wide range of wave lengths, it was desirable to consider the intensity distribution separately for two regions; one from 4400 to 4600 A and the other from 4600 to 4880 A. The calculation shows that the intensity distribution of two heads in the shorter-wave-length region is quite the same throughout the temperature range considered. That is to say, the (3, 0) head at 4584 A is always stronger than the (4, 0) head at 4422 A, which is in agreement with observation. But in the longer-wave-length region where bands arising from different lower vibrational levels are well seen, some interesting features occur that are given in Table 4.

TABLE 4

VALUES OF LOG *I* FOR DIFFERENT TEMPERATURES

λ (v', v'')	T(° K)					
	1500	1700	2000	2300	2500	2800
4847 (4, 2)	3.015	3.110	3.215	3.294	3.334	3.386
4804 (3, 1)	3.153	3.228	3.310	3.371	3.402	3.443
4761 (2, 0)	3.204	3.257	3.316	3.360	3.383	3.412
4668 (5, 2)	2.708	2.824	2.951	3.047	3.096	3.160
4626 (4, 1)	2.775	2.870	2.974	3.053	3.093	3.143

Comparison of the calculated intensities for temperatures of 2000° and 2300° K for the (2, 0) and (3, 1) band heads at 4761 A and 4804 A, respectively, shows that they reverse their relative intensities. Since observation shows them to be of nearly equal intensity, the vibrational-band temperature can be interpolated.

This observation indicates a vibrational temperature of 2200° K for χ Cygni at its light-maximum. A certain source of error, which can become very important, however, has been neglected. The observed intensities are affected by the suppression of the λ 4804 band by the tail of λ 4761 and, to a much lesser extent, by the suppression of λ 4761 by the structure of bands lying shortward. The neglect of this effect means that the temperature determined above is to be regarded only as a lower limit.

I should like to express my appreciation to the University of California for an appointment to the Martin Kellogg Fellowship, which gave me the opportunity to stay at the Lick Observatory and to use the 36-inch refractor and spectrographs. I am also grateful to Drs. P. W. Merrill and G. H. Herbig for their kind suggestions and advice, and to Mr. R. A. Rach for his help in making the observations.

[3] G. Herzberg, *Molecular Spectra and Molecular Structure* (2d ed.; New York: D. Van Nostrand Co., 1950).

ON THE COLOR-MAGNITUDE DIAGRAM FOR M 15*

HAROLD L. JOHNSON† AND MARTIN SCHWARZSCHILD‡
Washburn Observatory, University of Wisconsin, and Princeton University Observatory
Received January 10, 1951

ABSTRACT

Magnitudes and colors have been determined for 251 nonvariable stars in the globular cluster M 15. The resulting color-magnitude diagram indicates that the brighter stars in M 15 may belong to two sequences. The first sequence consists of red giants and supergiants and may possibly be the bright end of the subdwarf sequence. The second sequence consists of the horizontal branch characteristic of globular clusters. This branch appears to bend downward at its blue end and may thus possibly be the bright continuation of the regular main sequence.

I. INTRODUCTION

Recent investigations, mainly by Olin Eggen,[1] indicate that the Hertzsprung-Russell diagram may be occupied by stars not in broad strips and areas but rather along sharply defined curves. Because of their important implications for the theory of the stellar interior and of stellar development, it seems worth while to try to extend the data on which the present conclusions rest. As a small step in such an extension, a limited program of photometric measurements in the globular cluster M 15 is here reported.

To obtain results of high accuracy, it is, of course, a great advantage if all the measurements for a color-magnitude diagram can be made photoelectrically. In a globular cluster, however, the crowding of stars presents an appreciable difficulty to the photoelectric method. The diaphragm in a photoelectric photometer must be at least as large as the seeing disk and is usually chosen several times this size so as to avoid guiding difficulties. Correspondingly, to use a diaphragm smaller than 0.5 mm in diameter at the Newtonian focus of the 100-inch telescope (8″ angular diameter) would at present seem very difficult. On the other hand, if a photographic plate is measured with an iris-diaphragm photometer, the effective diaphragm diameter usually chosen is smaller than the seeing disk and will generally be less than 0.1 mm for the fainter images on plates taken with the 100-inch telescope. Thus the chance of including a faint neighbor in the measurement is reduced by more than a factor of 25.

Accordingly, in the present program the bulk of measurements were made photographically. For a sequence of stars in the outer parts of the cluster, however, magnitudes and colors were determined photoelectrically. Thus the system of colors and magnitudes could be based entirely on photoelectric measurements, and the photographic measurements had only to be used in an interpolative manner.

The following two sections contain the photoelectric and photographic measurements, respectively. In the last section the results are described in terms of the color-magnitude diagram for M 15.

II. THE PHOTOELECTRIC MEASUREMENTS

The photoelectric measurements were made at both the 100-inch and the 60-inch telescopes with the photoelectric photometer developed at the Washburn Observatory.

* This investigation is based on observations obtained by the authors as guest investigators at the Mount Wilson and Palomar Observatories.

† Now at the Yerkes and McDonald Observatories.

‡ This research was supported in part by funds of the Eugene Higgins Trust allocated to Princeton University.

[1] *Ap. J.*, 112, 141, 1950.

The photometer, filters, and reductions are described by Johnson[2] and by Stebbins, Whitford, and Johnson.[3] The standard North Polar Sequence stars and the colors and magnitudes adopted for them are given by Stebbins, Whitford, and Johnson.[3]

The 60-inch telescope was used for the comparisons with the North Polar Sequence and observations of some of the brighter stars in M 15, while the 100-inch telescope was used for observations on all the stars listed in Table 1. The diaphragm used for all these observations is 0.7 mm in diameter, corresponding to a diameter of 11″ at the 100-inch telescope and 18″ at the 60-inch telescope.

The values of Pg_p and C_p, given in Table 1, represent the means of two or more accordant observations on each star. The probable errors, from internal consistency, are as follows:

$$C_p\text{: p.e.} = \pm 0.015 \text{ mag.}\ ; \qquad Pg_p\text{: p.e.} = \pm 0.02 \text{ mag.}$$

Stars in the list with Nos. 28, 32, 1130, and 1134 were used as standards calibrated from the North Polar Sequence, and, since these stars were observed much more than the other stars in the list, the values given in Table 1 for these four standard stars are more accurate than those given for the other stars.

TABLE 1

PHOTOELECTRIC MEASUREMENTS

Star	Pg_p	C_p	Star	Pg_p	C_p
1	14.92	+0.46	307	14.01	+0.40
7	13.54	+ .68	1114	16.68	+0.54
9	14.74	+ .65	1124	16.99	+1.28
17	15.54	+ .54	1130	13.76	+0.71
23	14.07	+ .60	1132	17.15	+0.66
28	14.60	+ .88	1134	13.89	+0.09
32	12.72	+ .54	1137	13.98	+0.75
33	14.51	+ .44			
51	16.74	+ .86			
54	16.75	+0.56			

III. THE PHOTOGRAPHIC MEASUREMENTS

The photographic data are based on four blue plates and four yellow plates, all taken at the Newtonian focus of the 100-inch telescope on November 22, 1949, within a 2-hour interval. The 58-inch diaphragm was used in the telescope to reduce the coma. The blue exposures were made on 103*a*-O Eastman plates through a Schott GG 1 filter, with exposure times of 7 minutes. The yellow exposures were made on 103*a*-D Eastman plates through a Schott GG 11 filter, with exposure times of 10 minutes. On all plates the cluster was centered on the optical axis.

Two hundred and fifty-one stars, including the 17 sequence stars of Table 1, were selected from Kuestner's catalogue[4] for the measurements on the plates. All these stars fall within a square 1100″ wide and centered on the cluster. Excluded were the stars less than 190″ from the center of the cluster. Similarly excluded were all known variables. Finally excluded were all those stars having a disturbing close neighbor. All the selected stars are brighter than approximately photographic magnitude 17.2.

[2] *Ap. J.*, 112, 240, 1950.

[3] *Ap. J.*, 112, 472, 1950.

[4] *Bonn Veröff.*, No. 15, p. 47, 1921.

All the measurements of the selected stars on the eight plates were made by Mrs. U. B. Knight with the iris-diaphragm photometer of the Warner and Swasey Observatory. The photometer readings were transformed into magnitudes with the help of calibration-curves derived from the photoelectrically measured sequence stars. The calibration-curves do not seem entirely secure at their faint ends (below 17.0 for the blue plates and 16.3 for the yellow plates). Systematic errors of as much as a tenth of a magnitude may therefore be expected in the colors and magnitudes of the faintest stars.

The results for each star from the four blue plates were averaged to give the final photographic magnitude. Similarly, the results for each star from the four yellow plates were averaged to give the final photovisual magnitude. The photographic magnitudes and the color indices thus obtained are listed in Table 2.

The internal accuracy of the photographic measurements can be estimated from the interagreement between the four blue plates and the four yellow plates. In this way the following probable errors were found:

p.e. of m_{pg} from one plate:	$\pm 0^m032$	for $m_{pg} < 17^m0$;
p.e. of final m_{pg}:	$\pm 0^m016$	
p.e. of m_{pv} from one plate:	$\pm 0^m036$	for $m_{pv} < 16^m3$;
p.e. of final m_{pv}:	$\pm 0^m018$	
p.e. of final CI:	$\pm 0^m024$.	

The data for the faintest stars are less accurate, since here the calibration-curves are less certain and since some of these stars could not be measured on all eight plates.

IV. COLOR-MAGNITUDE DIAGRAM

Figure 1 gives the color-magnitude diagram for all the stars contained in Tables 1 and 2. The stars less than 300″ from the center are marked with dots. They have a higher probability of being cluster members than do the more distant stars, which are marked with crosses.

Considering, first, the yellow and red stars brighter than $m_{pg} = 16.0$, the present data confirm the recent result of A. Brown: a well-defined sequence of red supergiants.[5] The intrinsic sharpness of this sequence may be estimated by comparing the scatter found among the red supergiants in the color-magnitude diagram with the scatter to be expected from the observational uncertainties. For this purpose the 40 stars brighter than $m_{pg} = 16.0$ that fall into the strip outlined on Figure 1 may be used. The half-width of this strip was chosen to be four times the probable error of a color index, so that virtually all members of the supergiant sequence should be within this strip. Forming for each of these stars the residual in color index from the center line of this strip and computing the probable error from these residuals, one obtains ± 0.024 mag. Comparing this value with the observational probable error for a color index of ± 0.024 mag., one may conclude that the intrinsic dispersion in color index in the supergiant sequence is most likely less than ± 0.01 mag.

In addition to the red supergiants, there are, in Figure 1, 42 additional stars brighter than $m_{pg} = 15.6$. That the majority of these stars are foreground stars is made likely by their colors, since most of the foreground stars for the apparent magnitudes in question should be G dwarfs, in accordance with the colors observed. Furthermore, as enumerated in Table 3, one should expect approximately 30 foreground stars brighter than $m_{pg} = 15.6$ among the stars measured. Whether the statistically very uncertain excess of 12 stars found really indicates the existence of some bright yellow-cluster members can only be decided with the help of the proper motions which have recently been determined by A. Brown.

[5] *A.J.*, **55**, 165, 1950.

TABLE 2

PHOTOGRAPHIC MEASUREMENTS

No.	m_{pg}	CI	No.	m_{pg}	CI	No.	m_{pg}	CI
2.....	14.95	+0.60	79.....	15.65	+0.25	270.....	16.47	−0.14
3.....	15.98	−0.17	80.....	16.98	+0.53	295.....	15.34	+0.98
4.....	16.71	+0.82	81.....	16.08	+0.36	297.....	17.02	+0.23
5.....	14.84	+0.62	82.....	16.00	−0.02	320.....	17.06	+0.51
8.....	15.14	+0.84	83.....	16.74	+0.59	337.....	15.53	+0.78
10.....	16.54	−0.31	84.....	16.96	+0.54	356.....	14.64	+0.57
12.....	15.64	+0.51	85.....	16.87	+0.53	367.....	17.16	+0.13
13.....	16.73	+0.65	86.....	15.57	+0.53	374.....	16.90	+0.59
14.....	16.91	+0.62	88.....	15.92	−0.06	377.....	16.22	+0.56
16.....	16.42	+0.51	89.....	15.17	+0.79	400.....	16.68	−0.21
18.....	16.84	+0.91	90.....	16.63	−0.23	416.....	16.54	−0.20
19.....	17.00	−0.11	92.....	15.90	+0.58	448.....	16.86	+0.51
20.....	16.44	−0.27	93.....	16.98	+0.51	456.....	16.45	+0.59
21.....	15.57	+0.57	94.....	15.99	−0.08	466.....	16.81	−0.17
22.....	15.23	+0.84	95.....	15.52	+0.74	476.....	15.32	+0.78
24.....	17.04	+0.86	96.....	17.00	+0.50	477.....	16.76	+0.46
25.....	16.18	−0.20	97.....	15.85	+0.67	486.....	16.18	+0.60
26.....	15.76	+0.67	99.....	16.68	+0.60	544.....	16.28	+0.38
27.....	15.72	+0.55	100.....	16.64	+0.74	553.....	15.61	+0.70
31.....	15.90	+0.59	104.....	16.98	−0.05	571.....	16.84	+0.70
34.....	16.26	+0.53	107.....	17.24	+0.49	580.....	15.98	−0.02
35.....	13.44	+0.29	109.....	16.31	+0.63	581.....	15.70	−0.02
36.....	16.90	+0.53	111.....	16.40	+0.55	609.....	15.54	+0.72
37.....	16.96	+0.49	113.....	14.83	+0.45	628.....	16.70	+1.03
39.....	17.11	+0.49	115.....	16.82	+0.52	658.....	15.91	−0.01
41.....	16.75	−0.18	125.....	17.02	+0.39	676.....	15.00	+0.58
42.....	15.85	+0.59	126.....	15.87	−0.17	677.....	15.54	+0.52
43.....	15.98	0.00	127.....	15.28	+0.82	714.....	15.66	+0.46
44.....	16.26	+0.80	131.....	17.21	+0.68	717.....	15.69	−0.10
45.....	14.16	+0.62	142.....	15.83	−0.14	740.....	16.71	+1.30
46.....	17.12	+0.42	145.....	15.98	+0.54	763.....	17.16	+0.49
47.....	14.92	+0.92	149.....	16.96	−0.13	793.....	16.45	+0.67
49.....	15.20	+0.57	150.....	16.08	+0.55	802.....	14.07	+0.42
50.....	16.90	+0.48	152.....	15.92	+0.58	813.....	15.57	+0.52
52.....	16.41	+0.59	153.....	16.15	+0.61	829.....	16.88	+0.54
53.....	17.14	+0.43	157.....	17.11	+0.48	836.....	15.89	−0.07
56.....	16.07	+0.58	160.....	13.52	+0.60	846.....	14.87	+0.96
57.....	15.24	+0.81	161.....	17.04	+0.49	857	17.04	+0.05
59.....	16.05	+0.04	168.....	16.92	+0.45	875.....	14.86	+0.86
62.....	16.34	+0.59	172.....	14.58	+0.62	879.....	15.06	+0.92
64.....	15.89	+0.58	182.....	16.78	+0.57	890.....	16.57	+0.63
65.....	16.08	+0.58	196.....	16.27	+0.55	900.....	16.32	+0.50
67.....	16.89	+1.03	208.....	16.32	+0.54	904.....	16.83	−0.04
68.....	17.04	+0.51	209.....	17.03	+0.37	924.....	16.32	−0.26
69.....	15.20	+0.83	221.....	16.42	+0.54	944.....	16.15	+0.30
70.....	15.10	+0.88	233.....	16.00	+0.20	947.....	15.06	+0.86
75.....	17.20	−0.02	234.....	16.21	+0.55	953.....	16.06	+0.58
76.....	16.96	+0.57	245.....	17.04	+0.41	955.....	16.98	+0.41
77.....	14.74	+0.97	253.....	16.86	+0.51	957.....	14.78	+0.98
78.....	17.00	+0.58	269.....	15.42	+1.11	962.....	16.51	−0.19

TABLE 2—*Continued*

No.	m_{pg}	*CI*	No.	m_{pg}	*CI*	No.	m_{pg}	*CI*
967.....	14.81	+1.33	1068.....	16.50	+0.56	1105.....	15.78	+0.37
969.....	14.43	+1.01	1069.....	15.32	+ .81	1106.....	15.49	+ .86
978.....	15.50	+0.34	1070.....	15.98	+ .58	1107.....	16.12	+ .65
984.....	16.89	+0.58	1071.....	16.18	+ .58	1108.....	15.84	+ .40
997.....	16.90	+0.48	1072.....	17.02	+ .04	1109.....	17.06	+ .29
1001.....	15.10	+0.35	1073.....	15.03	+ .93	1110.....	17.17	+ .51
1003.....	16.36	+0.44	1074.....	15.89	+ .61	1111.....	17.06	+ .53
1004.....	15.92	−0.04	1076.....	16.08	+ .48	1112.....	15.95	− .15
1006.....	15.02	+0.92	1077.....	16.94	+ .61	1113.....	17.13	+ .44
1009.....	15.91	−0.12	1078.....	15.91	+ .59	1115.....	13.88	+ .48
1013.....	15.85	−0.11	1079.....	14.97	+ .95	1116.....	16.42	+ .53
1021.....	16.87	+0.50	1081.....	16.55	+ .46	1117.....	14.96	+ .70
1028.....	16.44	−0.31	1082.....	14.98	− .05	1119.....	15.91	− .15
1030.....	15.00	+0.97	1083.....	16.12	+ .60	1121.....	17.03	+ .05
1031.....	15.97	−0.05	1084.....	15.20	+ .87	1123.....	16.71	+ .52
1032.....	16.82	−0.09	1085.....	16.21	+ .63	1125.....	17.02	+ .76
1044.....	15.75	−0.09	1086.....	16.82	+ .53	1126.....	16.06	+ .18
1045.....	17.01	+0.66	1087.....	16.90	+ .48	1127.....	16.00	− .15
1046.....	16.86	+0.52	1088.....	16.90	+ .45	1128.....	16.64	+ .71
1049.....	15.38	+0.82	1089.....	13.94	+ .68	1129.....	15.87	− .08
1050.....	16.73	+0.54	1090.....	16.81	+ .52	1131.....	16.17	+ .32
1051.....	15.96	−0.06	1094.....	15.35	+ .59	1133.....	15.48	+ .40
1056.....	15.50	+0.78	1096.....	14.44	+ .50	1135.....	15.16	+ .40
1057.....	17.10	+0.49	1097.....	16.08	+ .61	1136.....	15.54	+0.74
1058.....	16.22	+0.57	1098.....	16.58	+ .79			
1060.....	16.72	+0.62	1099.....	14.95	+ .35			
1061.....	16.68	+0.57	1100.....	16.80	+ .45			
1063.....	17.08	+0.47	1101.....	16.10	+ .25			
1064.....	15.95	−0.09	1102.....	16.81	+ .36			
1067.....	16.54	+0.64	1103.....	16.94	+0.37			

Considering, next, the stars of intermediate brightness, one finds in Figure 1 the horizontal sequence characteristic of color-magnitude diagrams for globular clusters.[6] The gap in this sequence at color index +0.1 is probably not real, since the variables which are excluded from the present material would most likely fill this gap. It cannot be decided from the present observations whether the horizontal sequence stops before it reaches the red-giant sequence or whether it joins this sequence or whether it might even cross the red-giant sequence.

Considering, finally, the faint stars below $m_{pg} = 16.5$, one finds that two groups of faint stars seem to exist in M 15. The main group has a color index of about +0.5 and thus appears to be a continuation of the red-giant sequence toward fainter magnitudes. The second group of faint stars has negative color indices and may possibly be connected with the blue end of the horizontal sequence.[7] This connection, however, does not seem entirely certain, since there is a gap in blue stars at $m_{pg} = 16.2$.

Among the 152 intermediate and fainter stars (between $m_{pg} = 15.6$ and $m_{pg} = 17.0$) Figure 1 shows 26 stars outside the outlined sequences. These 26 stars may well be all

[6] H. Shapley, *Star Clusters* (New York, 1930), p. 26; W. Baade, *Ap. J.*, **100**, 137, 1944.

[7] A bending-down at the blue end of the horizontal branch had already been found in M 92 by O. Hachenberg, *Zs. f. Ap.*, **18**, 49, 1939.

foreground stars, since, from the general star counts,[8] 37 such stars could be expected among those measured—as enumerated in Table 3. The difference of 11 stars, which is statistically quite uncertain, may be made up by G dwarf foreground stars, which cannot be separated in the color-magnitude diagram from the fainter G giant cluster members.

In Figure 2 a composite color-magnitude diagram is drawn, containing in the upper portion the sequences indicated by Figure 1 and in the lower portion the sequences found by O. Eggen from the near-by stars. His sequences have been transformed to the color system of this paper by the transformation given by Johnson.[9] It is tempting to connect in this composite diagram the red-giant sequence of M 15 with the subdwarf sequence of the near-by stars and to connect the horizontal sequence of M 15 with its bending around at the blue end with the main sequence of the near-by stars. These two connections are indicated in Figure 2 by dotted lines. At present, however, they should be considered as entirely speculative.

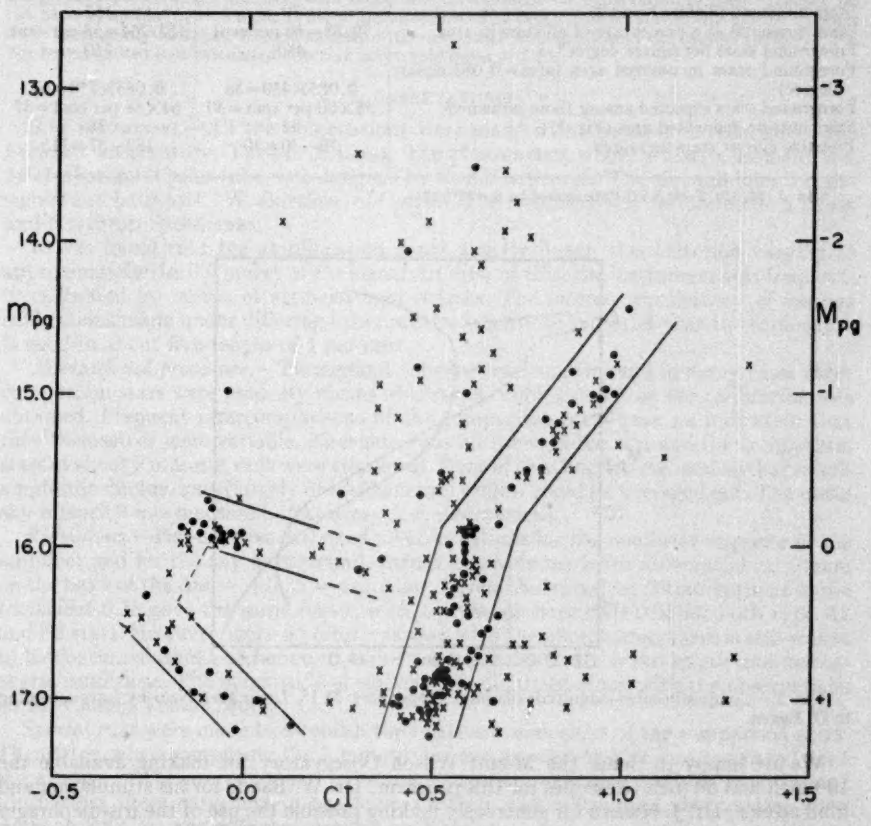

FIG. 1.—Color-magnitude diagram for M 15. Dots represent stars less than 300″ from the center. Crosses represent stars more than 300″ from the center. The absolute-magnitude scale on the right-hand side is only very approximate.

[8] Seares *et al.*, *Ap. J.*, **62**, 320, 1925 (Table XVII, interpolated for $\beta = 28°$).

[9] *Ap. J.*, **112**, 240, 1950.

One may summarize the above results as follows: The stars of M 15 brighter than $m_{pg} = 17.2$ seem to represent two sequences. The first sequence contains red giants and supergiants. This sequence may be the bright end of the subdwarf sequence. The second sequence in M 15 starts with the horizontal branch, which contains, among other stars, the cluster-type variables. This sequence may be the bright end of the main sequence.

TABLE 3

NUMBER OF FOREGROUND STARS

	Magnitude Range	
	$m_{pg}<15.60$	$15.60<m_{pg}<17.00$
All stars in covered area (approximate count)	88	264
Stars measured (Tables 1 and 2)	70	152
Stars measured as a percentage of all stars in area	70/88=80 per cent	152/264=58 per cent
Foreground stars per square degree*	450	750
Foreground stars in covered area (area=0.085 square degree)	0.085×450=38	0.085×750=64
Foreground stars expected among those measured	38×80 per cent=30	64×58 per cent=37
Stars outside delineated area (Fig. 1)	42	26
Probable cluster stars measured	70−30=40	152−37=115

* *Ap. J.*, **62**, 320, Table XVII (interpolated for $\beta = 28°$), 1925.

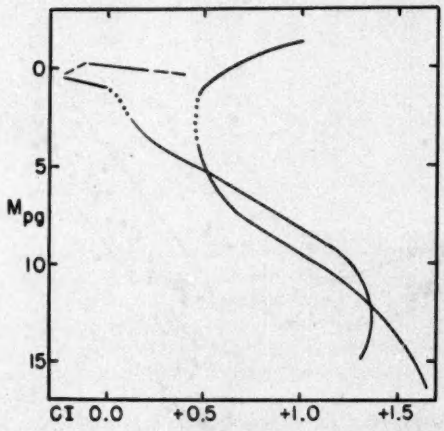

FIG. 2.—Composite color-magnitude diagram. *Upper part:* M 15. *Lower part:* Near-by stars according to O. Eggen.

We are happy to thank the Mount Wilson Observatory for making available the 100-inch and 60-inch telescopes for this program; Dr. W. Baade for his stimulation and kind advice; Dr. J. Nassau for generously making possible the use of the iris-diaphragm photometer of the Warner and Swasey Observatory; Mrs. U. B. Knight for her thorough measurements of all the plates; and Mr. J. Schopp for assisting with the reductions. The development of the photoelectric photometer used to obtain the photoelectric calibrations was supported in part by the Office of Naval Research.

A PHOTOELECTRIC STUDY OF THE ECLIPSING STARS RS CANUM VENATICORUM AND YY SAGITTARII

G. KELLER AND D. N. LIMBER*
Perkins Observatory†
Received January 2, 1951

ABSTRACT

Photometric investigations of the eclipsing binary systems RS Canum Venaticorum and YY Sagittarii have been carried out, and light-curves have been obtained. Photometric elements have been calculated by means of Merrill's tables. The surmise of Sitterly that there are cyclic fluctuations in the primary period of RS CVn has been substantiated, although the explanation of their existence on the basis of apsidal motion alone is found questionable. The larger, fainter star of this system appears to be intrinsically variable. Determinations of the photometric elements and the apsidal period of YY Sgr have resulted in a calculated effective polytropic index of 3.55.

I. OBSERVATIONS

The instrument.—All the observations were made with the 36-inch reflector of the Steward Observatory, Tucson, Arizona. The photometer, whose sensitive element is a 1P21 photomultiplier tube, was designed by E. F. Carpenter.[1] The a.c. amplifier was designed and built by C. W. Gartlein, of Cornell. The recording was performed on a Leeds and Northrup Speedomax.

It was found that the amplification is not strictly linear, the deflection varying as approximately the 0.9 power of the signal. In view of this, the instrument was frequently calibrated by means of artificial light-sources. The internal consistency of various calibrations made under differing experimental conditions indicates that the calibration is good to about five-tenths of 1 per cent.

Observational procedure.—Throughout the observations, two and in many cases three comparison stars were used. By means of these, a running check on the calibration was obtained. Frequent intercomparisons of the comparison stars gave no indication that they themselves were variable. Alternate runs on the variable star and the comparison stars of about 2 minutes each were employed. Runs of this length were used so that small-amplitude fluctuations (largely of instrumental origin) could be averaged out. The mean sky intensity was measured after every few observations.

Reductions.—Having first corrected all observations for the nonlinear response of the amplifier and for the sky background, corrections were made for differential extinction on the basis of the $\Delta m = +0.35$ secant ζ law. Several independent determinations of the coefficient 0.35 gave the same result, with a probable error of ± 0.02 for both type A2 and F5 stars. However, since no filter was used with the photometer, there is still reason to be concerned about a change in extinction coefficient with wave-length and atmospheric conditions. The magnitude of this effect is discussed along with the observations on RS Canum Venaticorum.

Special runs were made to establish the relative luminosities of the comparison stars. Thereafter, when computing the luminosity of the variable star, it was compared with the average of the preceding and following comparison-star observations, regardless of which stars these happened to be. Approximately twelve hundred observations were made on RS CVn and 480 observations on YY Sgr.

* Now at Yerkes Observatory.

† This research was aided by an Office of Naval Research contract.

[1] *A.J.*, **54**, 182, 186, 1949.

II. RS CANUM VENATICORUM

(BD+36°2344; 13^h08^m3, +36°12′ [1950]; F4n, G8)

The variability of this star was first detected by Mme Ceraski[2] in 1914. The first estimate of the orbital period was given by Hoffmeister[3] as approximately 4.797 days. In a later paper,[4] he suggests that the period may be variable and refutes a suggestion by Maggini[5] that the period should be only 2.4 days. Baker and Cummings[6] made a more accurate period determination and also noted for the first time the existence of an interval of constant light during the primary minimum. The first analysis of the light-curve (based on the 4.8-day period) was published by Schneller.[7] His ephemeris,

$$\text{Primary minimum: } 2423579.344 + 4.797944E\,, \qquad (1)$$

is the one which has been used in reducing the present observations. Schneller's observations further indicated the existence of a secondary minimum and of flat maxima of equal heights separating the minima.

Sitterly[8] has published two light-curves, one making use of Harvard patrol-plate estimates while the other is based on observations with the Princeton visual polarizing photometer. His analysis of the observed times of minima shows a definite nonlinear relationship between the phases of observed primary minimum (with reference to his own ephemeris) and the epoch of observation. He suggests that there may be a 26-year sinusoidal variation in the orbital period. He further observes that the primary minimum of his visual light-curve is asymmetrical and that there is a pronounced asymmetry outside eclipse. He notes that the maximum following primary minimum averages about 0.07 mag. brighter than the other maximum. Attempting to explain this phenomenon by the simultaneous existence of a tidal lag and a difference in brightness of the advancing and following sides of the brighter component, he was unable to obtain a reasonable fit with the observational data and was obliged to leave the asymmetry unexplained. Sitterly's photographic light-curve, on the other hand, does not reveal the asymmetry and has constant amplitude outside primary minimum. However, this difference between the two light-curves is due, at least in part, to the lower accuracy of the photographic estimates.

Magnitude estimates from the Harvard plates were also made by Miss Pilsworth, and a light-curve based on these is given by Mrs. Payne-Gaposchkin.[9] The times of primary minimum were also redetermined, strengthening the evidence in favor of a variation in the orbital period. The photographic light-curve derived by these workers exhibits a secondary minimum of about the same depth as that of Sitterly's visual curve.

Mrs. Payne-Gaposchkin believes that there is evidence that during the epoch of Sitterly's observations the photographic light-curve may have shown an inequality in the heights of maxima and in the same direction Sitterly found visually. She suggests that there may even be a fluctuation in the heights of maxima which is correlated with the fluctuation in the orbital period. As she points out, however, the accuracy of her data is such that the support which they give to this hypothesis is only of "possible significance."

[2] *A.N.*, **197**, 256, 1914.

[3] *A.N.*, **200**, 178, 1914.

[4] *Ibid.*, **208**, 249, 1918.

[5] *Arcetri Pub.*, **34**, 64, 1916.

[6] *Bull. Laws Obs.*, **2**, 150, 1916.

[7] *A.N.*, **233**, 361, 1928.

[8] *Contr. Princeton U. Obs.*, **11**, 21, 1930.

[9] *Proc. Amer. Phil. Soc.*, **81**, 189, 1939; *Harvard Reprint*, No. 170.

A spectroscopic investigation of the system has been carried out by Joy,[10] who finds that the radial-velocity-curve shows no measurable eccentricity. The spectral type of the smaller, brighter component is F4n, while that of the larger, fainter star is dG8. Joy remarks on the fact that, although the absolute magnitude and spectrum would place the fainter component among the dwarfs, its size and mass would lead to its identification as a subgiant.

Hiltner[11] has observed the H and K lines of *Ca* II in emission. Moreover, the emission approaches invisibility at secondary minimum when only a small fraction of the secondary star is eclipsed by the primary component. The emission is strong at primary minimum and at maximum light. He concludes from a study of RS CVn and similar eclipsing systems that the *Ca* II emission is confined to restricted areas of the fainter star, such as the ends of the tidal bulges.

Observations and light-curve.—The comparison stars used in the investigation of this system are among those used by Schneller[7] and are given in the accompanying tabulation.

COMPARISON STARS FOR RS CVn

No. of Star	BD	Schneller's Photographic Magnitude	Spectrum	Relative Photoelectric Luminosity
1.....	+35°2421	7.96	F5	1.560±0.020
5.....	+35 2422	8.81	G0	1.000
6.....	+35 2418	9.22	G0	0.556±0.010

Individual observations in the neighborhoods of the minima are given in Table 1 and have been plotted in Figures 1 and 2. Times of observation are heliocentric. Luminosities have been referred to comparison star 5. Examination discloses an apparent systematic difference between the luminosities near the bottom of primary minimum as measured on different nights. While this result might be due to intrinsic variations in the luminosity of the fainter star, it is also possible that these discordant measures are the result of systematic observational errors.[12]

One possible source of systematic night error might be variable humidity of the air. This is particularly true, since the same coefficient of atmospheric extinction (0^{m}35) has been used for both variable star (spectrum G8 at primary minimum) and comparison star (spectrum G0). However, a difference between the minimum brightness at phases 1965.97 and 1976.97 of about 0.10 mag. must be accounted for, and humidity variations do not seem likely to account for more than 0.01 mag. It is also possible that the difference between nights is due to a difference between the mean hour angles at which observations on different nights were made. One should have

$$\log_{10} L_a = (0.4)\,(C_c - C_v)\,\sec \zeta + \log_{10} L\,,$$

where L is the relative luminosity of the variable as seen outside the earth's atmosphere, L_a is the apparent relative luminosity at the telescope, ζ is the zenith distance, and C_c C_v are the extinction coefficients for the comparison and variable stars, respectively. If one plots $\log L_a$ versus $\sec \zeta$ for the several discordant nights, then all points should lie on a straight line, provided that the value of $\log L$ is the same for all nights, that is, that the variable has constant luminosity during totality and the same luminosity at all times

[10] *Ap. J.*, **72**, 41, 1930.

[11] *Ap. J.*, **106**, 481, 1947.

[12] The writers are indebted to Dr. John Irwin for a discussion on this point.

TABLE 1

RS CANUM VENATICORUM

Primary Minimum

Epoch-Phase	Luminosity	Epoch-Phase	Luminosity	Epoch-Phase	Luminosity	Epoch-Phase	Luminosity
1965.92008	1.497	1966.97142	.404	1970.94204	1.172	1973.03504	1.524
.92309	1.526	.97292	.394	.94280	1.149	.03694	1.553
.92598	1.486:	.97495	.401	.94416	1.079	.03804	1.596
.92978	1.431	.98177	.396	.94503	1.034	.03888	1.508
.93082	1.457	.98298	.390	.94568	1.008	.04062	1.638
.93156	1.406	.98567	.420	.94635	1.006	.04146	1.534
.93386	1.397	.98653	.400	.94719	0.969	.04263	1.552
.93444	1.358	.98844	.410	.94799	.940	.04480	1.541
.93507	1.324	.98971	.385	.94878	.904	.04575	1.590
.93552	1.316	.99368	.396	.94952	.889		
.93600	1.313	.99516	.408	.95033	.848	1974.04055	1.618
.93668	1.338:	.99589	.405	.95117	.808	.04233	1.545
.95233	0.728	.99673	.402	.95186	.786	.04418	1.466
.95314	.718	.99746	.403	.95338	.732	.04582	1.499
.95425	.667	.99824	.402	.95408	.718		
.95490	.646	.99889	.429	.95499	.682	1975.93533	1.386
.95554	.621	.99976	.403	.95571	.670	.93651	1.274
.95632	.601			.95667	.629	.93730	1.256
.95684	.585	1967.00044	.409	.95741	.615	.93853	1.302
.95807	.552:	.00115	.414	.95825	.577	.93963	1.248
.95862	.545	.00310	.452	.95987	.534	.94041	1.191
.95929	.519	.00388	.485	.96081	.526	.94117	1.174
.95981	.511	.00461	.473	.96163	.486	.94228	1.153
.96052	.516	.00547	.494	.96252	.474	.94351	1.079
.96111	.476	.00607	.515	.96324	.469	.94416	1.030
.96182	.452	.00669	.533	.96418	.424		
.96234	.452	.00759	.551	.96518	.424	1976.96161	0.516
.96304	.429	.00824	.577	.96596	.441:	.96261	.482
.96354	.424	.00935	.610	.96786	.415	.96371	.469
.96433	.423	.01022	.628	.96883	.421	.96449	.468
.96489	.407	.01138	.670	.96970	.439	.96715	.430
.96554	.399	.01209	.699			.96812	.433
.96602	.389	.01300	.732	1972.99515	0.397	.96892	.416
.96667	.394	.01370	.761	.99595	.403	.96998	.438
.96719	.395	.01458	.790	.99689	.392	.97109	.417
.96786	.397	.01526	.818	.99769	.408	.97300	.428
.96838	.397	.01595	.853	.99870	.414	.97423	.433
.96910	.391	.01682	.875	.99941	.410	.97595	.426
.96972	.389	.01773	.919			.97695	.431
.97051	.392	.01862	.933	1973.00073	.404	.98038	.436
.97113	.399	.01967	.986	.00163	.436	.98148	.424
.97191	.388	.02050	1.003:	.00272	.436	.98245	.431
.97247	.400			.00346	.466	.98392	.428
.97323	.392	1969.92126	1.463	.00449	.492	.98475	.447
.97381	.409	.93052	1.443	.00808	.578	.98775	.438
.97464	.413	.93407	1.389	.00883	.610:	.98911	.419
.97517	.413	.93488	1.368	.01011	.605:	.99024	.469
.97589	.402	.93576	1.345	.01090	.635	.99541	.435
.97644	.396			.01190	.625	.99641	.444
.97726	.397	1970.92083	1.431	.01275	.681		
.97786	.407	.92212	1.466	.01536	.806	1978.00446	.497
		.92426	1.453	.01749	.886	.00528	.534
1966.96004	.522	.92677	1.484	.01870	.911	.00653	.576
.96095	.504	.92766	1.464	.01985	.991	.00728	.540
.96165	.494	.92900	1.434	.02140	1.053	.00841	.626
.96236	.474	.92986	1.437	.02216	1.144	.00916	.633
.96323	.451	.93079	1.420	.02335	1.190	.01028	.627
.96386	.437	.93215	1.466	.02413	1.183	.01109	.653
.96460	.410:	.93321	1.411	.02523	1.213	.01226	.718
.96538	.424	.93526	1.359	.02603	1.231	.01304	.722
.96606	.413	.93644	1.332	.02713	1.279	.01415	.798
.96683	.407	.93741	1.301	.02795	1.288	.01497	.815
.96751	.404	.93853	1.274	.02986	1.375	.01599	.869
.96842	.404	.93932	1.224	.03075	1.495	.01679	.902
.96910	.400	.94011	1.165	.03195	1.459	.01796	.940
.97059	.398	.94102	1.177	.03428	1.490	.01889	.964

TABLE 1 (Continued)

RS CANUM VENATICORUM

Primary Minimum

Epoch-Phase	Luminosity	Epoch-Phase	Luminosity	Epoch-Phase	Luminosity	Epoch-Phase	Luminosity
1978.02012	.993	1968.46278	1.477	1969.50848	1.444	1975.51913	1.479
.02087	1.003	.46360	1.446	.51207	1.466	.52026	1.440
.02193	1.019	.46443	1.462	.51291	1.469	.52158	1.419
.02268	1.113	.46525	1.462	.51394	1.445	.52237	1.512
.02371	1.159			.51476	1.469	.52331	1.484
.02447	1.206:	1969.44828	1.441	.51578	1.460		
.02530	1.256:	.44918	1.488	.51650	1.498:	1978.43424	1.477
.02610	1.186	.45015	1.475	.51748	1.459	.43536	1.523
.02686	1.259	.45101	1.575	.51821	1.468	.43639	1.594
.02845	1.326	.45213	1.537			.43761	1.504
.02919	1.343	.45294	1.496	1971.53143	1.540	.43842	1.546
.03029	1.392	.45399	1.494	.53218	1.535	.43950	1.551
.03107	1.418:	.45474	1.499	.53350	1.501	.44062	1.467
.03288	1.434	.45588	1.495	.53428	1.544	.44160	1.539
.03372	1.425:	.45669	1.464	.53545	1.526	.44285	1.560
.03644	1.506:	.45785	1.476	.53619	1.548	.44389	1.539
.03746	1.500	.45944	1.508	.53706	1.565	.44486	1.511:
.03864	1.549:	.46004	1.446:	.53780	1.511	.45586	1.485:
.03960	1.526	.46106	1.466	.53870	1.479	.45664	1.490
.04038	1.507	.46198	1.488			.45773	1.488
.04173	1.536	.46441	1.482:	1973.43753	1.564	.45859	1.473
.04278	1.523	.46675	1.438	.43846	1.463	.45959	1.508
.04357	1.523	.46768	1.447	.43985	1.556		
.04468	1.537	.46845	1.460:	.44201	1.484	1980.49730	1.430:
		.47001	1.452:	.44303	1.438	.49851	1.409
Secondary Minimum		.48005	1.419	.44416	1.504	.50101	1.417
		.48085	1.414	.44623	1.510	.50253	1.463:
1968.44056	1.499	.48181	1.412:	.44722	1.548	.50440	1.424
.44175	1.514	.48337	1.432	.44819	1.543	.50715	1.400:
.44584	1.520:	.48427	1.416	.45011	1.483	.50806	1.449:
.44678	1.514	.48511	1.421	.45124	1.480	.50935	1.441
.44746	1.511	.48606	1.402			.51080	1.488
.44853	1.522	.48689	1.414	1974.46534	1.514	.51252	1.509
.44930	1.516	.49127	1.414:	.46933	1.417:	.51398	1.462
.45020	1.506	.49223	1.425	.47113	1.478	.51524	1.489
.45104	1.494	.49298	1.438	.47298	1.471	.51738	1.524
.45195	1.517	.49412	1.412	.47521	1.499	.51947	1.511
.45269	1.501	.49548	1.398	.47783	1.492	.52148	1.508
.45359	1.490	.49634	1.407			.52378	1.542
.45434	1.500	.49787	1.422	1975.49958	1.470	.52536	1.572
.45528	1.479	.49951	1.420	.50059	1.514	.52733	1.461
.45621	1.484	.50048	1.418	.50189	1.477	.53051	1.613
.45690	1.486	.50150	1.434	.51227	1.501:	.53160	1.577
.45781	1.477	.50268	1.444	.51308	1.498	.53293	1.532
.45855	1.473	.50341	1.455	.51404	1.458	.53436	1.586
.45948	1.470	.50431	1.447	.51501	1.442	.53569	1.589
.46022	1.455	.50598	1.454	.51569	1.439	.53717	1.495
.46110	1.467	.50679	1.436	.51696	1.485		
.46187	1.460	.50774	1.460	.51789	1.485		

of totality. Figure 3 is a plot of this kind, in which data from the three nights for which most information was available are plotted. The slope of the dashed line corresponds to a value of $C_c - C_v$ of $0^m.06$.

Two comments may be made concerning the figure: (1) there may be an hour-angle effect for each night corresponding to $C_c - C_v$ of the order of $0^m.06$; (2) there is a vertical shift between the run of points for different nights, which is not correlated with the hour angle. It is simplest to attribute the shift to intrinsic variability, i.e., to changes in log L.

No attempt has been made to allow for the quantity $(0.4) \times (C_c - C_v) \sec \zeta$ in the reduction of measurements. It is not possible to determine it accurately from Figure 3

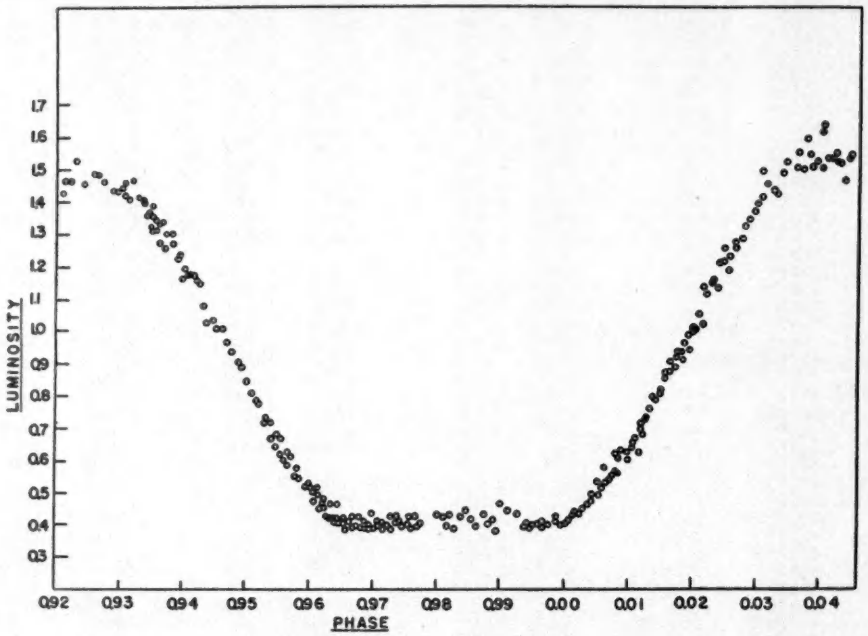

FIG. 1.—Primary minimum of RS Canum Venaticorum

(or to be quite sure that it is appreciably different from zero). Moreover, the value of $C_c - C_v$ changes constantly during partial phases as the net color of the variable changes. The quantity $C_c - C_v$ will be much smaller well outside the primary totality, because there the colors of the variable and comparison stars more nearly correspond. Since the majority of observations were made for values of secant ζ between 1.0 and 1.4, it is reasonable to suppose that systematic shifts due to hour-angle effects will not average more than 0.01 mag. for a particular night. At any point where the run of the mean light-curve is based on the averages of several nights' observations, the hour-angle error in the mean light-curve will usually be further reduced.

Normal points lying between minima, combining ten observations each, have been calculated and are given in Table 2. The entire light-curve, with selected points during the minima, is given in Figure 4. It will be noted that the maximum following primary minimum is unmistakably higher than the other maximum, confirming the observations

of both Sitterly and Mrs. Payne-Gaposchkin. The amplitude of the difference is about 0.06 intensity units or 0.04 mag. It may be compared with the difference of 0.07 mag. measured in the visual region by Sitterly. Mergentaler[13] has recently suggested that the increase of the difference with increasing wave length is associated with the absorptive properties of gaseous clouds streaming around the fainter component.

The solution.—The major function of any rectification is the rigorous and systematic adjustment of the light-curve toward a more idealized behavior, i.e., the behavior it would have if the physical circumstances which cause the light to vary between eclipses were not present. This adjustment, however, should be made on the basis of a definite physical theory of the mechanisms which are responsible for that variation. The correct

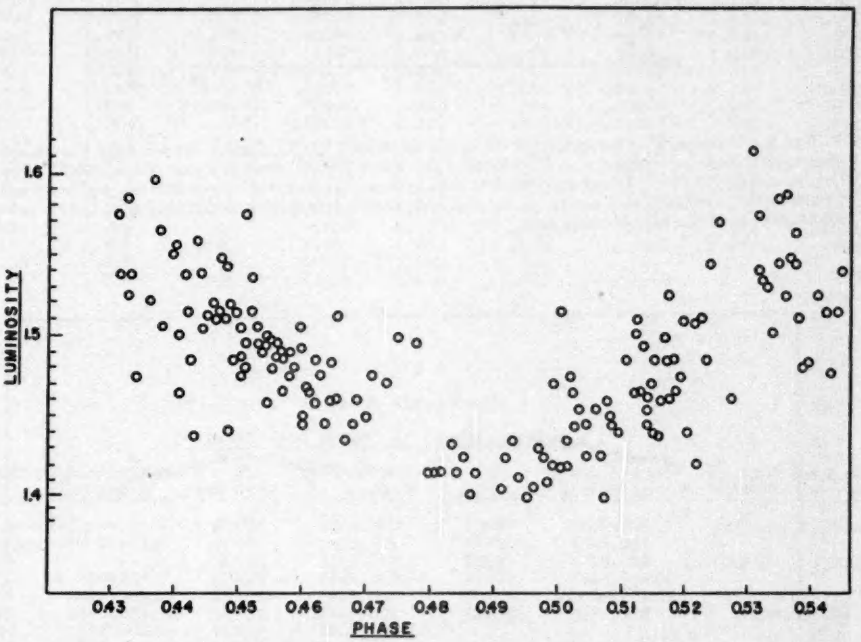

FIG. 2.—Secondary minimum of RS Canum Venaticorum

method of rectification depends upon the particular effect being dealt with. It is because of this point that the rectification for asymmetrical terms is unsatisfactory at best in the absence of any physical explanation for the asymmetry.

In the light-curve of the system being discussed, asymmetry is quite pronounced, and the attempt, even formally, to fit the light-curve outside an eclipse with a Fourier expansion which includes $\sin 2\theta$ and $\cos 2\theta$ terms has been found quite unsatisfactory. However, by disregarding observations lying less than 15° beyond the actual ends of the minima, a satisfactory fit has been obtained by means of the following expression:

$$L(\theta) = 1.552 - 0.0257 \cos\theta - 0.0355 \cos 2\theta + 0.0290 \sin\theta - 0.0133 \sin 2\theta . \quad (a)$$

[13] *Wroclaw Contr.*, No. 4, 1950.

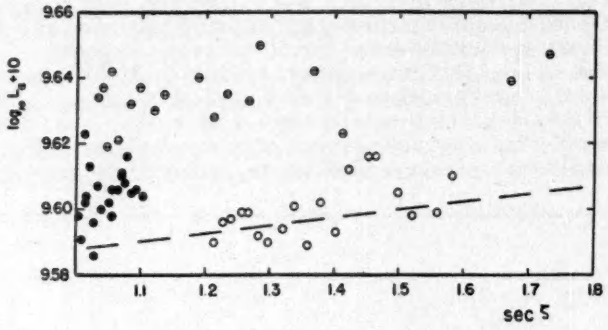

FIG. 3.—Luminosity as a function of the zenith distance ζ for RS Canum Venaticorum. Circles are observations during the period of primary totality near epoch 1965.97, small dots near epoch 1966.97, large dots near epoch 1976.97. The general vertical shift between the observations for different nights cannot be attributed to differences in zenith distance (or hour angle). It is suggested that they arise from intrinsic variability of the fainter component.

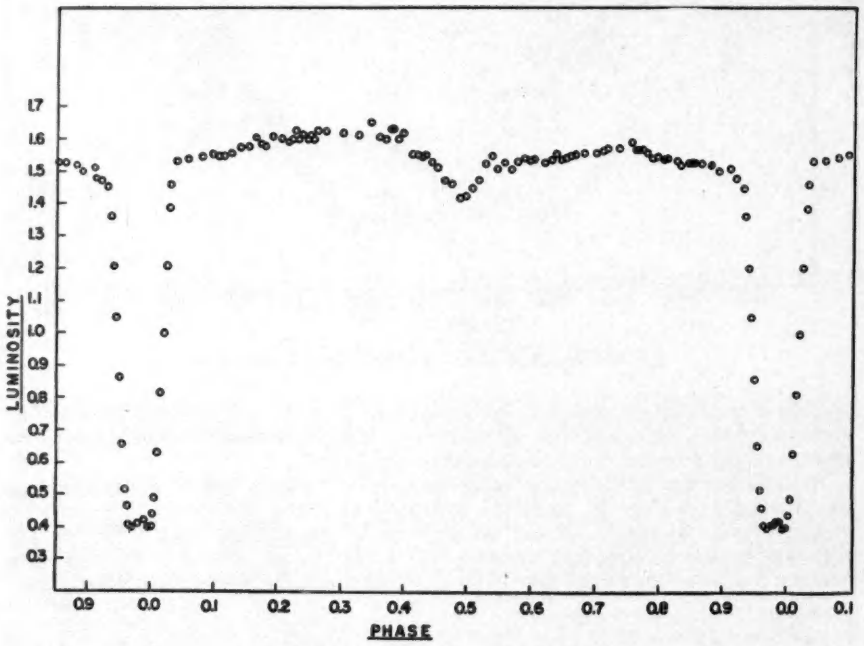

FIG. 4.—Light-curve of RS Canum Venaticorum

TABLE 2

RS CANUM VENATICORUM

Normal Points

Phase	Luminosity	Probable Error	Phase	Luminosity	Probable Error	Phase	Luminosity	Probable Error
.05779	1.535	.006	.32514	1.608	.004	.67945	1.557	.003
.07797	1.544	.006	.34469	1.649	.006	.69977	1.555	.003
.09575	1.551	.006	.35787	1.601	.003	.70856	1.561	.004
.10495	1.543	.005	.36872	1.596	.002	.71745	1.569	.006
.11423	1.546	.005	.37623	1.625	.005	.73388	1.569	.007
.12570	1.553	.004	.38182	1.628	.006	.75405	1.588	.006
.13849	1.570	.007	.38865	1.596	.006	.76011	1.568	.008
.15294	1.573	.006	.39492	1.613	.012	.76470	1.567	.005
.16309	1.602	.011	.41107	1.549	.004	.76983	1.564	.008
.17206	1.580	.004	.41993	1.548	.005	.77859	1.559	.007
.17866	1.578	.003	.42496	1.542	.005	.78668	1.539	.002
.18465	1.609	.005	.43059	1.545	.006	.79519	1.545	.003
.19019	1.603	.006	.54403	1.505	.005	.80362	1.536	.006
.20277	1.598	.005	.55492	1.522	.008	.81129	1.537	.004
.21164	1.590	.005	.56577	1.501	.005	.82647	1.532	.005
.21668	1.589	.004	.57505	1.526	.005	.83612	1.519	.003
.22190	1.596	.008	.58665	1.536	.006	.84313	1.524	.006
.22584	1.623	.005	.59636	1.531	.004	.84732	1.528	.008
.23212	1.595	.005	.60246	1.535	.006	.85210	1.529	.005
.23817	1.608	.005	.61794	1.526	.002	.86469	1.522	.004
.24509	1.597	.008	.62949	1.534	.004	.88014	1.519	.004
.24999	1.605	.004	.63734	1.553	.003	.89129	1.500	.009
.25629	1.596	.006	.64403	1.537	.007	.91046	1.508	.006
.26177	1.622	.009	.65233	1.538	.005	.91766	1.477	.004
.27314	1.619	.006	.65856	1.547	.004			
.30071	1.616	.005	.66723	1.550	.002			

TABLE 3

RS CANUM VENATICORUM

Epochs and Phases of Primary Minima

JD -2400000	Epoch + 3000 and Phase
Sitterly From Harvard Plates	
12270	643.036
12679	728.049
15552	1327.031
15778	1374.028
15787	1376.026
15879	1395.032
16181	1458.026
16622	1550.028
16901	1608.021
16977	1624.025
17208	1672.018
17285	1688.016
17995	1836.020
18057	1849.019
18489	1939.015
19837	2220.007
19938	2241.010
20144	2284.005
20192	2294.007
20245	2305.008
20269	2310.008
20902	2442.016
20960	2454.001
20964	2455.006
21574	2582.003
21948	2659.999
22020	2674.999
23071	2893.995
23090	2898.003
Hoffmeister	
20298	2315.996
20302	2316.995
20346	2326.003
20370	2331.002
20423	2341.992
20489	2356.004
20566	2372.007
20653	2389.993
20681	2369.021
21267	2518.002
21607	2588.004
21982	2666.998
21986	2667.998
Sitterly, Visual Obs.	
22792	2835.998
22807	2838.998
22816	2840.999
22831	2843.998
22840	2845.999
23095	2898.997
23100	2099.999
23162	2912.999
23167	2913.997
Nijland & Godomski	
23579	3000.001
Schneller	
25249	3347.000
Himpel	
27873.524	3895.004
Keller & Limber	
33016.81924	4966.9832 ±.0003
Lause	
28636.377	4054.000
28948.230	4118.997

Requiring the rectification to remove the inequalities in the shoulders of the minima necessitates the following expression:

$$L(\theta) = 1.5542 - 0.0184 \cos\theta - 0.0347 \cos 2\theta + 0.0510 \sin\theta - 0.0133 \sin 2\theta\,. \quad \text{(b)}$$

Since this latter expression fits only the shoulders and deviates appreciably from the light-curve near quadrature, it has been felt that expression (*a*), while by no means completely satisfactory, provides the better over-all representation. In the absence of any better criterion it has been assumed that the cos θ term is due entirely to the reflection effect. Using Joy's spectral classifications[10] and Sitterly's value for the inclination,[8] it follows that that part of the cos 2θ coefficient due to reflection is $C_2 = +0.01316$, while that part of the constant coefficient due to reflection[14] is $C_0 = +0.0538$. Assuming, again in the absence of any more satisfactory assumption, that the constant and the cos 2θ terms, when corrected for the reflection effect, are affected only by the ellipticity, one finds, following Russell, that $z = \epsilon^2 \sin^2 i = +0.0478$, where $1/N$ has been taken as 0.38. Finally, it has been assumed that the sin θ and sin 2θ terms are to be applied with no diminution through the minima. Under these tentative assumptions, the following expression has been subtracted from the observed light-curve to effect rectification:

$$A_1 \cos\theta + (A_2 - C_2)L_b(1 - \alpha_b)\cos 2\theta + (A_2 - C_2)L_f(1 - \alpha_f)\cos 2\theta + C_2 \cos 2\theta + B_1 \sin\theta + B_2 \sin 2\theta\,, \quad \text{(c)}$$

where L_b and L_f are the relative luminosities of the components, α_b and α_f are the fractions of the light of the brighter and fainter component obscured at a given instant, and the constants have the following values:

$$A_1 = -0.0257,\ A_2 = -0.0355,\ B_1 = +0.0290,\ B_2 = -0.0133,\ (A_2 - C_2) = -0.0487\,.$$

Rectification for ellipticity has customarily been performed by division by the factor $(1 - z\cos^2\theta)^{1/2}$. However, when $z \ll 1$, as in the present case, one may set

$$(1 - z\cos^2\theta)^{1/2} = \left(1 - \frac{z}{4}\right) - \frac{z}{4}\cos 2\theta$$

and thence show that the subtraction of the second and third terms in expression (*c*) has the same effect as the usual division procedure would have had. Following this rectification, the light-curve was phase-rectified and then plotted.

Owing to the uncertainty in secondary minimum, the analysis has been based entirely upon the primary minimum.[15] In the present case the spectrum of the star eclipsed during primary (F4n) and the photometer's wave-length response have indicated the use of 0.8 as the limb-darkening coefficient.[16] In view of the wide spectral response of the instrument, this darkening coefficient represents an average.

The determination of k, the ratio of the radius of the smaller component to that of the larger, has been carried out by means of the ψ-functions. It should be noted that, owing to the asymmetry remaining in the primary minimum, the values of θ corresponding to a given loss of light have been taken as the averages of the values obtained from the descending and ascending branches. These derived elements are the following:

$$L_b = 0.726, \qquad k = 0.365, \qquad i = 82^\circ.5 \pm 0^\circ.5\,,$$
$$L_f = 0.274, \qquad r_f = 0.265, \qquad p_0 = -1.35 \pm 0.05,$$

where the inclination, i, has not been corrected for any possible polar flattening.

[14] Russell, *Ap. J.*, **108**, 388, 1948.

[15] The writers are indebted to Dr. John Merrill for the loan, prior to publication, of *Contr. Princeton U. Obs.*, No. 23, 1950.

[16] Münch and Chandrasekhar, *Harvard Circ.*, No. 453, 1949.

These elements lead to a satisfactory fit at secondary minimum, though the uncertainties in the observations of the latter prevent any really accurate check. About 14 per cent of the light of the fainter star is obscured at the center of secondary minimum, and thus on a rectified light-curve the depth of secondary minimum should be 0.0384 times the maximum light. Combining the photometric elements with Joy's spectrographic elements,[10] one obtains

$$a_b = 6{,}090{,}000 \text{ km}, \qquad r_f = 3{,}360{,}000 = 4.83R_\odot,$$
$$a_f = 6{,}590{,}000 \text{ km}, \qquad m_b = 1.84\odot,$$
$$r_b = 1{,}230{,}000 = 1.77R_\odot, \qquad m_f = 1.70\odot.$$

All elements given in this section should be regarded as quite tentative. No great effort was made to reduce the discrepancies between the computed and the observed light-curves to an absolute minimum. In view of the possible night errors or intrinsic variation of the fainter star and the possible existence of a gaseous envelope (see the section on "General Comments"), a definitive calculation of the photometric elements did not seem worth while. All observations in Tables 1 and 2 are original in the sense that they contain no correction for night errors.

Apsidal motion.—The observed phases of primary minimum have been collected in Table 3, most of these having been taken directly from Sitterly's paper after conversion to Schneller's ephemeris (eq. [1]). Points due to Himple,[17] Lause,[18] and the present investigation have also been included. This same material, with a further group of points from Mrs. Payne-Gaposchkin's paper, has been plotted in Figure 5. Since the latter author does not give her initial epoch but implies that her curve agrees substantially with Sitterly's, the writers have taken the liberty of assuming an epoch, so that both curves agree in all but the first few points. The resulting plot suggests that Sitterly's surmise concerning a cyclic fluctuation in the period has been substantiated. The cycle has a period of 35 years or more and an amplitude of roughly 0.009 of the orbital period.

It is not possible to obtain the phase of the secondary minimum with very much precision; however, by considering only the bottom portion of that minimum, the following estimate has been made:

$$\text{Phase of secondary minimum near JD } 2433017: 0.489 \pm 0.002 .$$

It follows that the displacement of secondary minimum from a position midway between primary minima is

$$1.489 - 0.983 - 0.500 = 0.006 \pm 0.002 \text{ periods} .$$

Whether this represents a sufficient displacement to allow the cyclic changes in the primary periods to be explained on the basis of apsidal motion is not readily calculable, since neither the time of secondary nor the present displacement in phase of the primary from the zero phase of the mean ephemeris is sufficiently well known. However, a tentative calculation of the effective polytropic index has been made, using Sterne's method.[19] The above elements were used, the period was assumed to be 36 years, and the motion of the apse was attributed entirely to the tidal distortion of the fainter component. The result, which applies only to the larger star, is $n = 2.95$.

General comments.—Using the total luminosities and radii of the components which were derived from the photometric orbit, the ratio of the mean surface intensities is 20. Since the photometer responds to a whole range of wave lengths, this figure reflects not

[17] *A.N.*, **261**, 233, 1936.

[18] *A.N.*, **277**, 40, 1949.

[19] *M.N.*, **99**, 451, 1939.

only the spectral-energy distributions of the stars but also the relative response of the telescope and photometer to different wave lengths. Let us assume that the brighter component is an F4 main-sequence star with an effective temperature of 6700° and that the fainter star is a G8 subgiant with an effective temperature of 4870°. After correcting the corresponding Planck emission-curves for the effect of the Balmer discontinuity, for the estimated effects of atmospheric transmission, and for the response-curve of the instrument, the expected ratio of surface intensities (as measured on the photometer) was computed. This value came out to be 5.5. While the latter figure may be in error by 50 per cent, it seems difficult to account for the difference between it and the larger ratio of surface intensities which was obtained from elements of the light-curve.

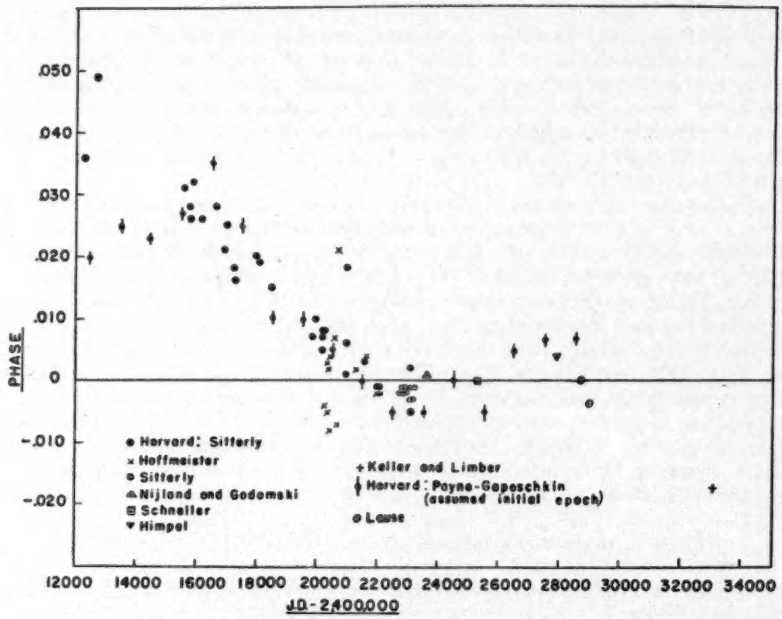

FIG. 5.—Phases of the primary minima of RS Canum Venaticorum. They have been computed, using the ephemeris (1), from the observed times of minimum.

There are a number of observed similarities between RS CVn and the system U Cephei which suggest that the two binaries may be physically similar. Both systems contain small early-type and larger later-type companions (B8 and G2 in the case of U Cephei). The principal minima are asymmetrical in both cases, and the maxima are unequal in height.[20] The orbital periods of both systems are subject to slow variations. Struve[21] has presented convincing spectroscopic evidence that U Cephei is surrounded by streams of gas, and it is not unlikely that the streams affect the light-curve of that star and perhaps its dynamical behavior as well. It will be recalled that Mergentaler[13] bases his explanation of the difference of the heights of maxima upon the assumption of the existence of gas streams. Hiltner's[11] observations of *Ca* II emission are also suggestive of the presence

[20] Recent light-curves in two colors for U Cephei are given by Walter, *A.N.*, **276**, 225, 1948.

[21] *Ap. J.*, **99**, 222, 1944.

of some sort of gaseous shell. It would be of interest to study RS CVn spectroscopically during the partial phases of primary eclipses to determine whether it, too, may not show evidence of sharp absorption lines having anomalous velocities.

III. YY SAGITTARII

(BD−19°5148; 18^h41^m7, −19°27′ [1950]; A0)

Historical.—This star was first discovered to be variable by Miss Cannon[22] and was first observed visually by Zinner,[23] who obtained a 1.31-day period. The first published light-curve was due to Kordylewski,[24] who found not only that Zinner's period should be doubled but also that the secondary minimum was markedly displaced, both results being subsequently confirmed by Zinner.[25] Shapley and Keller[26] and later Shapley and Miss Swope[27] published results based upon estimates of Harvard patrol plates and have suggested the following ephemeris for primary minimum, which has been employed throughout in the present investigation:

$$\text{Primary minimum: } 2419467.0871 + 2.6284841E\,. \qquad (2)$$

Shapley and Swope found that the depths of primary and secondary minima were 0.55 and 0.53 mag., respectively, and they further estimated the orbital eccentricity to be greater than 0.15 and the apsidal period to be greater than 300 years, their data indicating no difference in the widths of minima. Russell[28] estimated that the orbital eccentricity was 0.17 and the apsidal period 350 years, basing these estimates partly upon the near-equality of the widths of the minima. Sterne[29] later computed the period of apsidal motion and effective polytropic index on the basis of estimates by Miss Swope, employing the elements $r_1/A = r_2/A = 0.127$ due to Mrs. Shapley. His results, based on a least-squares fitting to the data, are $e = 0.140 \pm 0.010$, $P' = 282 \pm 49$ years, and $n = 2.83 \pm 0.20$.

Observations and light-curve.—In the present investigation the comparison stars given in the accompanying tabulation were used. The individual observations in the neighborhoods of the minima are given in Table 4 and are plotted in Figures 6 and 7, luminosities in the table and in the figures being referred to comparison star E as 1.000. The probable error per observation has been found to be approximately 1.3 per cent. Normal

COMPARISON STARS FOR YY Sgr

Comp. Star	BD	Harvard Photographic Magnitude	Spectrum	Relative Photoelectric Luminosity
D.....	−19° 5140	9.55	A0	1.201±0.007
E.....	−20 5243	9.80	F5	1.000
F.....	−19 5147	10.09	A2	0.657±0.005

[22] Pickering, *Harvard Circ.*, No. 137, 1908.

[23] *A.N.*, **190**, 377, 1912; **195**, 460, 1913; *Astr. Abh.*, Vol. **4**, No. 3, 1922.

[24] *Acta Astr.*, Ser. c, **1**, 95, 1930.

[25] *A.N.*, **239**, 60, 1930.

[26] *Harvard Bull.*, No. 893, p. 6, 1933.

[27] *Harvard Bull.*, No. 909, p. 9, 1938.

[28] *Ap. J.*, **90**, 647, 1939.

[29] *M.N.*, **99**, 662, 1939.

TABLE 4

YY SAGITTARII

Primary Minimum

Epoch-Phase	Luminosity	Epoch-Phase	Luminosity	Epoch-Phase	Luminosity	Epoch-Phase	Luminosity
5170.96116	.891	5181.97945	.786	5185.01546	.545	5169.46907	.908
.96322	.887	.98114	.776	.01744	.568		
.96546	.891	.98296	.761	.01945	.574	5171.36056	.933
.96731	.890	.98545	.691	.02085	.585	.36222	.927
.96935	.866	.98709	.696	.02281	.627	.36436	.906
.97088	.854	.98901	.653	.02788	.675	.36592	.892
.97334	.836	.99102	.621	.03018	.747	.36816	.883
.97516	.828	.99364	.621	.03298	.781	.36999	.862
.97722	.800	.99779	.564	.03443	.775	.37173	.876
.97902	.772			.03644	.779	.37382	.851
.97976	.724	5182.00122	.511	.03890	.811	.37561	.840
.98224	.760	.00354	.499	.04056	.823		
.98735	.728	.00571	.474	.04265	.854	5177.38564	.691
.98663	.694	.00804	.459	.04468	.847	.39162	.706
.98879	.669	.01023	.463	.04624	.860	.39438	.624
.99022	.655	.01205	.486	.04825	.876	.39665	.607
.99223	.634	.01409	.516	.05026	.888	.39885	.594
.99360	.608	.01673	.546	.05197	.882	.40112	.554
.99558	.598	.01871	.567	.05401	.884	.40374	.551
		.02053	.587			.40680	.499
5177.01304	.492	.02257	.612	Secondary Minimum		.40913	.534
.01574	.561					.41140	.528
.03190	.788	5184.97757	.762	5166.42171	.600		
.03397	.764	.98061	.731	.42325	.642	5180.42064	.571
.04773	.885	.98191	.743	.42840	.656	.42326	.568
.05000	.911	.98418	.711	.42977	.688	.42566	.613
.05241	.897	.98558	.678	.43167	.728	.42867	.655
.05489	.884	.98806	.661			.43612	.735
		.99004	.634	5169.42186	.571		
5180.04354	.805	.99139	.619	.42852	.653	5183.46477	.822
.04618	.806	.99388	.593	.43058	.666	.46686	.892
.04872	.830	.99541	.578	.43710	.723	.46937	.917
.05083	.869	.99734	.533	.44054	.761		
.05315	.875	.99948	.531	.44363	.794	5185.36224	.909
.05482	.904			.44682	.834	.36398	.898
		5185.00093	.502	.44875	.825	.37624	.805
5181.96056	.892	.00296	.473	.45081	.854	.37880	.787
.96304	.896	.00436	.479	.45221	.877	.38187	.761
.96569	.889	.00582	.479	.45462	.877	.39476	.644
.96833	.836	.00756	.455	.45808	.886	.39838	.594
.97089	.844	.00901	.489	.46006	.893	.39999	.605
.97332	.839	.01041	.489	.46302	.894	.40118	.618
.97506	.798	.01213	.493	.46511	.902	.40324	.560
.97723	.803	.01406	.496	.46690	.911	.41280	.497
						.41473	.512

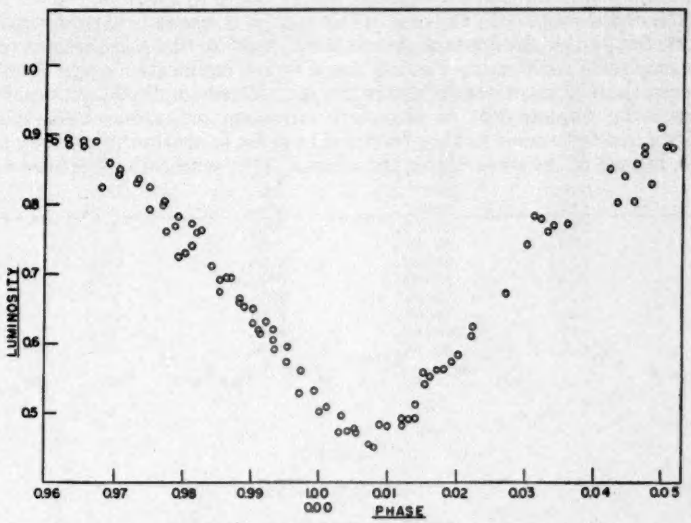

FIG. 6.—Primary minimum of YY Sagittarii

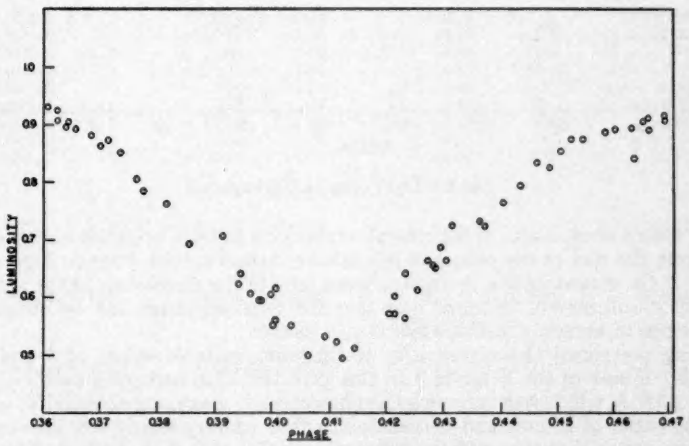

FIG. 7.—Secondary minimum of YY Sagittarii

points combining ten observations each are given in Table 5, while the entire light-curve, using selected points through the minima, is reproduced in Figure 8.

Analysis and elements.—In the case of this system it was felt that the maxima were sufficiently flat (within the limits of observational error) so that there seemed to be little need for amplitude rectification. Fearing that a formal rectification might distort rather than correct the minima, it was decided to proceed without amplitude rectification. However, since the displacement of secondary minimum indicates considerable orbital eccentricity, the light-curve has been rectified in phase to obtain the intensity as a function of θ, instead of the time, during the minima. This rectification has been made pos-

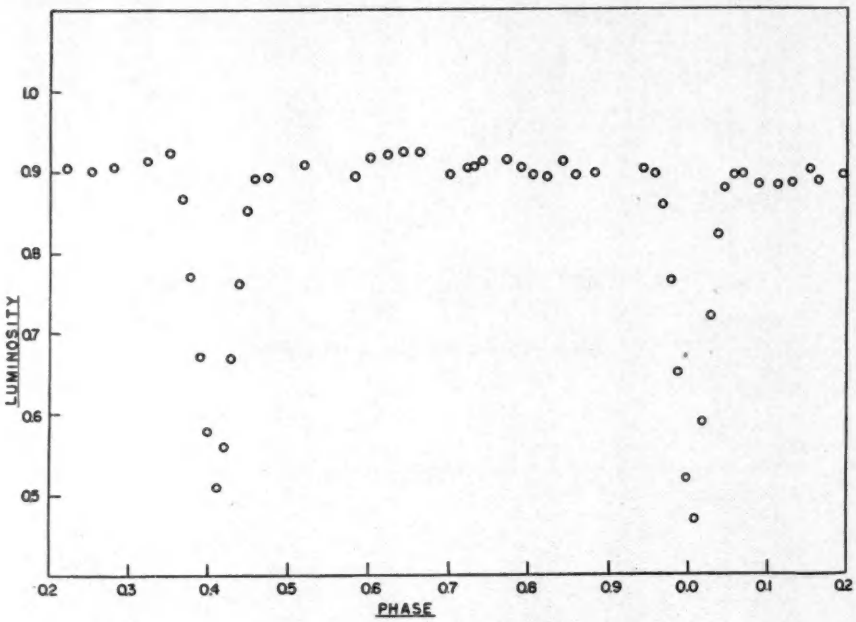

FIG. 8.—Light-curve of YY Sagittarii

sible by means of estimates of the orbital eccentricity and the longitude of the periastron made from the plot of the phases of minima at various epochs given in Figure 9. This figure and the estimates will be treated more fully in the discussions of the apsidal motion, and it will merely be noted here that the required values can be obtained with a fair degree of accuracy in this way.

Having performed this eccentricity rectification, suitable values of k and a_0 were sought by means of the χ tables.[15] In this case the limb-darkening coefficient for A0 stars at 4000 A, which was very near the photometer's maximum sensitivity, was found from the paper of Münch and Chandrasekhar[16] to be very nearly 0.8. However, their paper also shows that this coefficient drops to a value of 0.35 at 3647– A. The problem of the photometer's relative response to the various wave lengths was then investigated. The necessary corrections were made for atmospheric absorption, deviation from the Planck law due to the Balmer discontinuity at 3646 A, reflection at the mirror, transmission and reflection in the glass parts, and the tube response. The study has shown that

TABLE 5

YY SAGITTARII

Normal Points

Phase	Luminosity	Probable Error	Phase	Luminosity	Probable Error
0.05941	0.895	0.008	.60569	.919	.008
.06981	.896	.002	.62449	.920	.002
.08935	.884	.003	.64555	.926	.003
.11259	.888	.004	.66666	.922	.003
.13365	.887	.002	.70333	.898	.003
.15326	.900	.003	.72090	.904	.005
.16711	.889	.006	.73278	.908	.006
.19733	.898	.002	.74523	.911	.004
.22241	.908	.003	.77490	.913	.004
.25563	.900	.001	.79095	.904	.004
.28105	.906	.008	.80649	.897	.003
.32599	.917	.005	.82315	.891	.003
.35061	.922	.003	.84440	.911	.010
.47900	.893	.004	.86047	.896	.004
.52232	.909	.004	.88556	.899	.003
.58096	.895	.003	.94753	.903	.004

TABLE 6

YY SAGITTARII

Epochs and Phases of Minima

Epoch		Primary		Secondary		e cos ω	
Shapley and Swope							
1893.5 ±	3	-0.004 ±	0.005	0.479 ±	0.015	-0.027 ±	0.025
1902.0	2	+ .002	.003	.471	.003	- .049	.007
1908.5	1.5	+ .004	.002	.459	.004	- .071	.007
1913.0	1.3	- .001	.003	.453	.004	- .072	.008
1917.5	1.5	.000	.003	.446	.003	- .085	.007
1922.5	1.5	+ .002	.005	.443	.005	- .093	.011
1927.5	1.5	+ .004	.002	.433	.002	- .112	.004
1932.0	1.3	+ .005	.002	.429	.002	- .119	.004
1936.0	1.3	+ .003	.004	.419	.003	- .132	.008
Kordylewski							
1927.5 ±	1.5	+0.010 ±	0.003			-0.123 ±	0.010
Zinner							
1913.0 ±	1.5	+0.005 ±	0.002	0.449 ±	0.002	-0.088 ±	0.005
Keller and Limber							
1949.44±	0.03	0.0075±	0.0005	0.4110±	0.0005	-0.1516±	0.0011

the instrument's relative response to all radiation below 3646 A was only one-tenth its response to longer wave lengths, and it is felt that this justifies the use of the 0.8 darkening coefficient.

The solution by means of the χ tables was found to be somewhat indeterminate from the primary eclipse alone; and, unfortunately, there was quite a little uncertainty in the depth of secondary, limiting its usefulness as a check. In view of this uncertainty, three solutions were carried out, giving the following elements:

Solution I: Primary as Transit

$a_0 = 1.00$, $i = 88°56'$,
$k = 0.90$, $L_1 = 0.5602$,
$r_1 = 0.171$, $L_2 = 0.4398$.

Solution II: Primary as Occultation

$a_0 = 1.00$, $i = 89°48'$,
$k = 0.98$, $L_1 = 0.5070$,
$r_1 = 0.163$, $L_2 = 0.4930$.

Solution III: Primary as Transit

$a_0 = 1.00$, $i = 89°29'$
$k = 0.95$, $L_1 = 0.5189$,
$r_1 = 0.169$, $L_2 = 0.4811$.

Here the r_1 values have been corrected for the orbital eccentricity, while L_1 and L_2 refer to the larger and the smaller stars, respectively. Solution I gives rise to a slightly more satisfactory fit at secondary, though it does not fit the deeper portion of primary quite so well as do Solutions II and III.

Apsidal motion.—The phases of minima at various epochs, referred to ephemeris (2), are presented in Table 6. Dr. Shapley and Miss Swope have kindly permitted the presentation of their results in greater detail than heretofore. Since $e \cos \omega$ is approximately equal to $(\pi/2)(P_s - P_p - \frac{1}{2})$ for small eccentricity, e (where P_s and P_p are the phases of secondary and primary minima, respectively, for a given epoch and ω is the longitude of the periastron), it is possible to compute $e \cos \omega$ as a function of the epoch. Such a plot is given in Figure 9, each point on the plot being surrounded by a box indicating the extent of the probable error. The point at 1893.5 is quite uncertain, depending upon only two observations of subnormal brightness near secondary minimum, and it is not known whether these observations lie on the ascending or the descending sides of that minimum. The top and bottom of the shaded box correspond to the two possibilities.

It is clear that any attempt at fitting a cosine-curve to Figure 9 is at best an uncertain process, and it is not impossible that the apsidal period is very long. However, curves which bound the region in which the true solution is likely to lie have been investigated and the following two estimates have been decided upon:

Estimate A: $e = 0.163$,
$t_0 = 1890$, $\omega = 158°.4$ at 1949.4.

Estimate B: $e = 0.163$,
$t_0 = 1883$, $\omega = 158°.4$ at 1949.4.

It is felt that, while these values are not so accurately determined as might be desired, some weight can be attached to them. Since both estimates give $\omega = 158°.4$, that quantity was used in the phase rectification. Estimate A leads to an apsidal period of 312 years, while B leads to the higher value of 360 years.

Effective polytropic index calculations have been carried out following Sterne[19] for both apsidal periods and for each of the three orbital solutions. The mass ratios have been

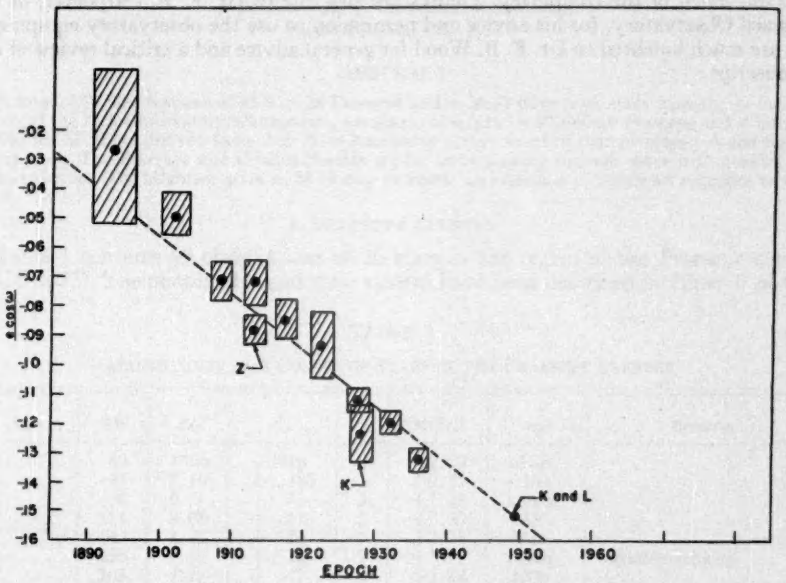

FIG. 9.—The displacement of the secondary minimum of YY Sagittarii. It is measured in units of phase multiplied by $\pi/2$, and is approximately equal to $e \cos \omega$. The point labeled *Z* is due to Zinner, the point *K* is due to Kordylewski, that labeled *K and L* is due to the authors. All others are from Shapley and Swope. Shaded boxes indicate the estimated range of probable errors.

obtained on the assumption that they are equal to the fourth root of the luminosity ratio. The results are given in the accompanying tabulation. It is seen at once that the

	312-Year Period	350-Year Period
Solution I	3.52	3.57
Solution II	3.51	3.56
Solution III	3.55	3.59

effective polytropic index is relatively insensitive to uncertainties in the elements and to the apsidal period uncertainty. A mean of the above values is $n = 3.55$. The effect of the possible ellipticities of the components upon these results has been investigated, and it

is found that, even assuming the greatest possible effect in keeping with the light-curve, the changes in the effective polytropic indices are of the order of ± 0.02. It is felt that the present result is likely to be more nearly correct than Sterne's value of 2.83, inasmuch as it is based on more accurate photometric elements.

The authors are indebted to Messrs. Donald Arveson, Angus Gillis, and Paul Orth, who assisted with the observing, and to Miss Mary Beck and Mrs. Constance Slettebak, who did much of the computing. Thanks are also due to Dr. E. F. Carpenter, of the Steward Observatory, for his advice and permission to use the observatory equipment. We are much indebted to Dr. F. B. Wood for general advice and a critical review of our manuscript.

PHOTOELECTRIC STUDIES. VI. COLOR-LUMINOSITY ARRAYS FOR STARS IN PRAESEPE AND IN M 39*

OLIN J. EGGEN
Lick Observatory, University of California
Received January 10, 1951

ABSTRACT

A total of 92 observations of 43 stars in Praesepe and in M 39 have been made with the 12-inch refractor at the Lick Observatory. Photometric parallaxes of π (ptm) = 0".0080 for Praesepe and π (ptm) = 0".0045 for M 39 are derived from their color-luminosity arrays fitted to that previously found for the nearer stars. The Praesepe and Hyades clusters appear to be moving through space with parallel and equal velocities. The brightest stars in M 39 may represent an extension of the dwarf sequence to $M = -0.5$.

I. PRAESEPE CLUSTER

Table 1 contains 49 observations of 26 stars in the region of the Praesepe cluster (NGC 2632). The photometer and color system have been described in Paper I[1] of this

TABLE 1

MAGNITUDES AND COLORS OF STARS IN THE PRAESEPE CLUSTER

VI	KW	P_{gp}	C_p	n	$M(P_{gp})$	Sp.	Remarks
467	40	7^m.68	+0^m.16	2	+2.20	dF2p	
483	45	8.19	+ .185	1	+2.71	dA6n	
501	50	6.77	+ .12	3	+1.29	sgA7n	
659	114	8.08	+ .17	1	+2.60	dA8	
747	143	8.23	+ .20	1	+2.75	dA6	
761	150	7.39	+ .20	2	+1.91	dA6n	Variable velocity
877	203	7.77	+ .17	2	+2.29	dF0n	
880	204	6.75	+ .19	2	+1.27	sgA7n	
889	207	7.56	+ .155	2	+2.08	A4	
899	212	7.28	+ .88	2	+1.80	gG8	
947	244	10.32	+ .55	2	+4.84	.....	Eclipsing var. at maximum light, TX Cnc
958	253	7.24	+ .88	2	+1.76	(G7)	
979	265	6.46	− .03	3	+0.98	(A2s)	
997	276	7.40	+ .145	2	+1.92	sgA6n	
1009	283	7.16	+ .935	2	+1.68	(G7)	Visual binary; companion 14^m, distant 13"
1005	284	6.87	+ .185	2	+1.39	sgA5n	
1012	286	7.90	+ .15	1	+2.42	dA9	
1022	292	8.21	+ .24	1	+2.73	dA5n	Variable velocity
1031	300	6.31	+ .12	3	+0.83	gA6n	ϵ Cnc, double lines
1079	328	6.88	+ .15	2	+1.40	gA8n	
1098	340	8.46	+ .22	1	+2.98	.....	
1114	348	6.79	+ .11	3	+1.31	sgA5n	
1180	385	7.85	+ .195	2	+2.37	dA5n	Visual binary; brighter star also spectroscopic binary
1263	429	8.54	+ .26	1	+3.06	.....	
1300	445	7.88	+ .15	2	+2.40	dA5	
1304	449	7.82	+0.16	2	+2.34	.....	

* *Contributions from the Lick Observatory*, Ser. II, No. 35.

[1] *Ap. J.*, 111, 68, 1950.

series. The radial velocities and proper motions of all 26 stars indicate that they are cluster members. The numbers assigned in the first two columns of Table 1 are those given the stars in the catalogues of Vanderlinden[2] (Vl) and of Klein Wassink[3] (KW). The spectral types in Table 1 are those given by Wilson and Joy;[4] the few values in parentheses are earlier Mount Wilson determinations.[5] The colors and magnitudes are best fitted to the color-luminosity array given in Paper IV of this series[6] if we assume (1) an apparent distance modulus of $m - M = +5^{m}.53$ for the cluster and (2) that the observed colors are affected by 0.01 mag. selective absorption. The resulting color-luminosity array for the Praesepe stars is shown in Figure 1, in which the several lines represent the sequences established from observations of stars in other clusters and the

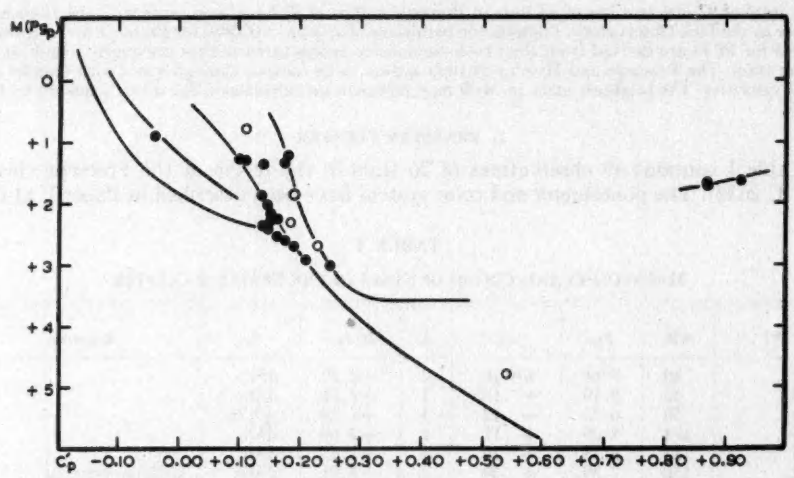

FIG. 1.—Color-luminosity array for the stars in the Praesepe cluster. The open circles indicate known binary stars. The color-luminosity array determined from the cluster stars discussed in previous papers of this series is also indicated in the figure by the solid lines. The colors have been corrected for $0^{m}.01$ selective absorption: $C'_p = C_p - 0^{m}.01$.

open circles represent known binaries. For any reasonable value of the ratio of total to selective absorption, the total absorption will amount to only 0.04 or 0.05 mag., and $m - M = +5^{m}.48$ or π (ptm) $= 0''.0080$. From a discussion of all the previous determinations of the parallax of this cluster, J. M. Ramberg[7] has obtained $\pi = 0''.0077$.

In 1937 Haffner and Heckmann[8] published magnitudes, obtained photographically in two wave-length regions, λ 4270 and λ 6450, for 180 cluster stars. A comparison of Pg_p

[2] *Étude de l'amas de Praesepe* (Gembloux: J. Duculot, 1933).

[3] *Groningen Pub.*, Vol. **41**, 1927.

[4] *Ap. J.*, **111**, 221, 1950.

[5] Adams *et al.*, *Ap. J.*, **53**, 13, 1921.

[6] *Ap. J.*, **112**, 429, 1950.

[7] *Stockholm Obs. Ann.*, **13**, 130, 1941.

[8] *Veröff. U. Sternw. Göttingen*, Nos. 53, 54, 55, 1937.

and C_p for the stars in Table 1 with the values of Pg (λ 4270) and $C(H) = Pg$ (λ 6450) $-$ Pg (λ 4270) results in the following relationships:

$$Pg_p(H) = Pg(\lambda 4270) - 0^m.074 - 0.136C(H),$$
$$C_p(H) = +0^m.134 + 0.575C(H). \quad (1)$$

Table 2 contains a comparison of $Pg_p(H)$ and $C_p(H)$, the magnitudes and colors determined from expressions (1), with the values of Pg_p and C_p given in Table 1.

TABLE 2

COMPARISON OF VALUES OF Pg_p AND C_p DETERMINED PHOTOELECTRICALLY WITH THOSE DERIVED FROM PHOTOGRAPHIC MAGNITUDES AND COLORS DETERMINED BY HAFFNER AND HECKMANN

KW	Pg_p	$Pg_p(H)$	$Pg_p - Pg_p(H)$	C_p	$C_p(H)$	$C_p - C_p(H)$
40	7^m.68	7^m.75	−0^m.07	+0^m.16	+0^m.16	0^m.00
45	8.19	8.24	− .05	+ .185	+ .19	.00
50	6.77	6.75	+ .02	+ .12	+ .16	− .04
114	8.08	8.13	− .05	+ .17	+ .18	− .01
143	8.23	8.30	− .07	+ .20	+ .18	+ .02
150	7.39	7.42	− .03	+ .20	+ .20	.00
203	7.77	7.68	+ .09	+ .17	+ .16	+ .01
204	6.75	6.69	+ .06	+ .19	+ .20	− .01
207	7.56	7.60	− .04	+ .155	+ .13	+ .03
212	7.28	7.31	− .03	+ .88	+ .87	+ .01
244	10.22	10.27	− .05	+ .55	+ .55	.00
253	7.24	7.16	+ .08	+ .88	+ .93	− .05
265	6.46	6.42	+ .04	− .03	− .02	− .01
276	7.40	7.47	− .07	+ .145	+ .11	+ .03
283	7.16	7.19	− .03	+ .935	+ .935	.00
284	6.87	6.78	+ .09	+ .185	+ .19	.00
286	7.90	7.98	− .08	+ .15	+ .15	.00
292	8.21	8.21	.00	+ .24	+ .245	.00
300	6.31	6.29	+ .02	+ .12	+ .15	− .03
328	6.88	6.82	+ .06	+ .15	+ .15	.00
340	8.46	8.45	+ .01	+ .22	+ .21	+ .01
348	6.79	6.74	+ .05	+ .11	+ .13	− .02
385	7.85	7.86	− .01	+ .195	+ .17	+ .03
429	8.54	8.54	.00	+ .26	+ .24	+ .02
445	7.88	7.91	− .03	+ .15	+ .14	+ .01
449	7.82	7.86	−0.04	+0.16	+0.15	+0.01
$\overline{O-C}$			±0.045 (A.D.)			±0.013 (A.D.)

With a dozen or so exceptions, for which cluster membership is uncertain, the magnitudes and colors given by Haffner and Heckmann have been converted to $Pg_p(H)$ and $C_p(H)$ by expressions (1), adjusted for a distance modulus, uncorrected for absorption, of +5.53 mag. and a selective absorption of 0.01 mag., and plotted on the color-luminosity array in Figure 2. As was pointed out by Haffner and Heckmann, the sprinkling of stars above the dwarf sequence indicates that some 20 per cent of the cluster stars probably are double or multiple. Known double stars are indicated by open circles in Figures 1 and 2. The manner in which the remaining 80 per cent of the stars fall on the various sequences of the color-luminosity array attests to the excellence of these photographic magnitudes.

The star Vl No. 947, TX Cancri, in Table 1 is of particular interest, since Haffner

found it to be an eclipsing binary of the W Ursae Majoris type.[9] The proper motion and radial velocity of this star make it quite certain that it belongs to the cluster. The period is given by Haffner as 0.38 day, and the two minima are of nearly equal depth, 0.3 mag. The observed values of Pg_p and C_p, 10.32 mag. and +0.55 mag., respectively, made at maximum light, agree very well with the values of $Pg_p(H)$ and $C_p(H)$. If we apply the modulus of +5.53 mag., we obtain +4.79 mag. for the luminosity, which places the system 0.72 mag. above the dwarf sequence. The position in the color-luminosity array, therefore, confirms the equality in brightness of the components indicated by the nearly equal depths of the two eclipses.

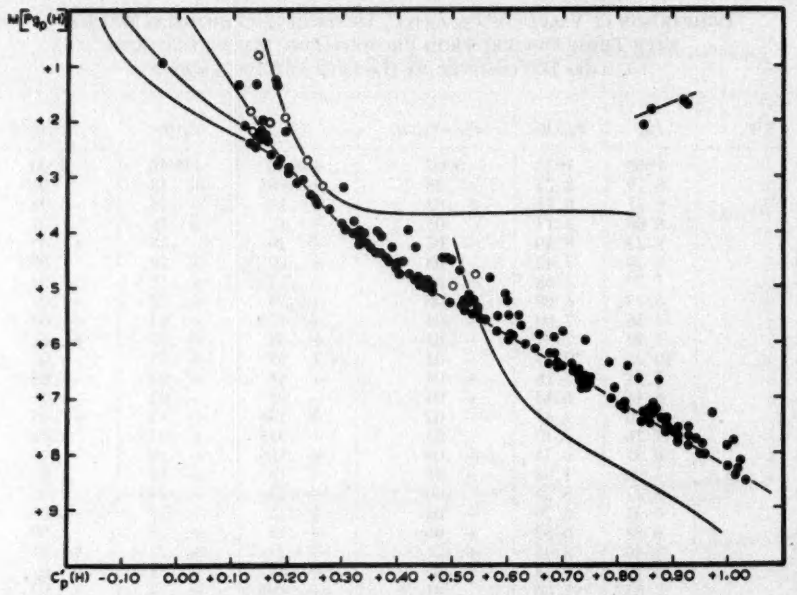

FIG. 2.—The color-luminosity array for the members of the Praesepe cluster derived from colors and magnitudes determined photographically by Haffner and Heckmann converted to the scales of Pg_p and C_p. The open circles indicate known binary stars. The colors have been corrected for 0^m01 selective absorption: $C'_p(H) = C_p - 0^m01$.

D. M. Popper[10] has determined the spectroscopic orbit of TX Cancri. He finds $m_1 \sin^3 i = 0.95$ and $m_2 \sin^3 i = 0.48$, or a mass ratio of 1.9. A mass ratio of nearly 2 between components of equal luminosity is obviously a contradiction of the mass-luminosity relation; this contradiction is known to exist in all W Ursae Majoris stars for which spectroscopic data are available.[11] It should be noted that the combined color of the components of TX Cancri, 0.54 mag., places these stars at the intersection of the dwarf and subdwarf sequences, and it is possible that the more massive star is a dwarf and the other component a subdwarf. It may be recalled that the color and luminosity[12] of 85 Pegasi A also places that star near the intersection of the two sequences, a fact suggesting that its relatively small mass, 0.6, may be characteristic of subdwarfs.

[9] *Veröff. U. Sternw. Göttingen*, No. 56, 1938.

[10] *Ap. J.*, **108**, 493, 1948.

[11] Eggen, *Ap. J.*, **108**, 15, 1948.

[12] Eggen, *Pub. A.S.P.*, **61**, 258, 1949.

The Algol-type eclipsing binary S Cancri also is in the region of the Praesepe cluster, but it was excluded from consideration as a cluster member by Haffner and Heckmann because of its proper motion. This star was observed at maximum light on the present program, with a resulting magnitude and color in agreement with the values of $Pg_p(H)$ and $C_p(H)$:

$$Pg_p = 8^m.13\,, \quad C_p = +0^m.045\,,$$

$$Pg_p(H) = 8^m.13\,, \quad C_p(H) = +0^m.04\,.$$

The assumption that the star is a nonmember of the cluster is supported by its position in the color-luminosity array.

Several previous investigators have suggested that the Hyades and Praesepe clusters are moving toward the same convergent point with the same space velocity. In Paper I

TABLE 3

COLORS AND MAGNITUDES OF STARS IN THE CLUSTER M 39 (NGC 7092)

STAR	Pg_p	C_p	n	$M(Pg_p)$	Sp.(T)	CLASS	
						μ	ρ
1.....	$7^m.20$	$-0^m.075$	3	$+0^m.45$	A0	1	*
3.....	8.92	+0.07	3	+2.17	A1n	1	×
4.....	9.08	+0.12	2	+2.33	A3n	1	*
5.....	7.61	−0.03	3	+0.86	A1n	1	SB
9.....	9.03	+0.64	2	+2.28	G7	3	o
17.....	7.77	−0.015	3	+1.02	A1n	1	*
19.....	8.78	+0.05	3	+2.03	A2	1	*
20.....	9.48	+0.19	3	+2.73	A3n	1	*
22.....	8.81	+0.11	1	+2.06	A3s	1	×
23.....	7.41	−0.06	1	+0.66	A1	1	*
26.....	6.67	−0.06	3	−0.08	A0s	2	*
30.....	8.28	−0.035	2	+1.53	A1	3	*
31.....	8.50	−0.01	3	+1.75	A2n	1	×
33.....	6.43	−0.05	3	−0.32	A0	1	×
35.....	8.89	+0.055	2	+2.14	A2	1	*
38.....	8.01	−0.015	3	+1.26	A0	2	o
40a.....	6.67	−0.07	3	−0.08	A0s	1	*
46.....	9.97	+1.43	1	+3.22	.....	1	.....

we quoted R. E. Wilson's recent determination of the convergent point of the Hyades cluster, $A = 94°.0$ and $D = +7°.6$ (1950). From Wilson's data we also found 45.3 km/sec as the space velocity of the cluster. From the assumption that the space velocities and convergents are the same for the two clusters, we find for Praesepe a parallax of

$$\pi = \frac{4.738\mu}{V \sin \lambda} = 0''.0077\,, \tag{2}$$

if we adopt $\alpha = 8^h37^m.5$ and $\delta = +19°45'$ (1950) for the center of the Praesepe cluster as given by Heckmann and Kruse,[13] and $\mu = 0''.0424$ derived by the same authors from 19 cluster stars contained in the *General Catalogue*. If we take the mean radial velocity of the cluster stars, $\rho = +33.0 \pm 0.6$ km/sec, as determined by Adams and Kohlschütter,[14] we find

$$\pi = \frac{4.738\mu}{\rho \tan \lambda} = 0''.0083\,. \tag{3}$$

[13] *A.N.*, **275**, 73, 1947.

[14] *Ann. Rept. Director Mt. W. Obs., Carnegie Yearbook*, **50**, 200, 1923.

The mean of determinations (2) and (3) gives $\pi = 0''.0080$, the same value derived above photometrically. Also, from our assumption that the convergent points of the two clusters are the same, we can compute the expected position angle of the mean proper motion of the Praesepe stars to be 255°, as compared with the observed value of 250°. Within the uncertainties of the observational quantities, then, we can conclude that the two clusters are apparently moving parallel, with the same speed, in space.

II. MESSIER 39 (NGC 7092)

The only published catalogue of stars in M 39 is one by E. G. Ebbighausen.[15] A total of 43 observations of 18 stars has been made during the present program; the small separation of stars Nos. 22 and 23 made it necessary to observe these two stars with the Crossley reflector. The resulting magnitudes and colors are listed in Table 3, together with the spectral types assigned by R. Trumpler and quoted by Ebbighausen,

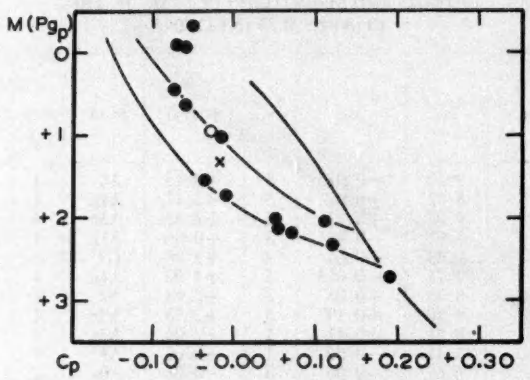

FIG. 3.—The color-luminosity array for stars in the cluster M 39(NGC 7092). The open circle indicates a known spectroscopic binary, and the cross represents a probable nonmember (star No. 38 in Table 3).

Sp. (T), and a measure of probability, based upon proper motion and radial velocity, that a star is a cluster member. Stars of class 1 probably are cluster members; those of class 2 are uncertain members; and those of class 3 most probably are field stars, as judged by their proper motions. Dr. Trumpler has kindly supplied the classification given in the last column of Table 3, where an asterisk signifies that the stellar velocity differs from the mean cluster velocity by less than 2 km/sec; and a cross that it differs by less than 4 but greater than 2 km/sec. Nonmembers are indicated by open circles. Star No. 5 is a spectroscopic binary, SB.

The stars in Table 3 are best fitted to the color-luminosity array if $m - M = +6^m.75$ or if $\pi = 0''.0045$. The resulting luminosities for the stars are plotted in Figure 3; the spectroscopic binary, No. 5, is indicated by an open circle, and star No. 38 is plotted as a cross. Two stars, Nos. 9 and 46, are not plotted in the figure, since apparently they are nonmembers of the cluster. Star No. 30 appears to be a cluster member despite its class 3 rating. If the stars of highest luminosity, Nos. 26, 33, and 40*a*, are cluster members, either they are binaries, or they represent an extension of the dwarf sequence to brighter absolute magnitudes than have been hitherto discussed.

[15] *Ap. J.*, 92, 434, 1940.

PHOTOELECTRIC STUDIES. VII. COLOR AND MAGNITUDE SYSTEMS FOR BRIGHTER STARS AND THE COLOR–SPECTRAL-TYPE RELATION*

OLIN J. EGGEN
Lick Observatory, University of California
Received January 10, 1951

ABSTRACT

The values of Pg_p and C_p, discussed in previous papers of this series, are compared with (1) Hertzsprung's effective color temperatures; (2) Greenwich gradients; (3) the six-color photometry of Stebbins and Whitford; (4) the visual magnitudes given in *Harvard Mimeograms*, Series 3, Nos. 1 and 2; (5) photographic magnitudes by de Vaucouleurs; and (6) photoelectrically determined colors and magnitudes by Miss Güssow. It is demonstrated that a close relation between color and spectral type exists for the various luminosity classes included in the Yerkes spectral atlas.

In previous papers of this series,[1] colors and magnitudes of a number of bright stars have been presented. Eventually, accurate photoelectric colors and magnitudes will be available for most of the stars in the *Yale Catalogue of Bright Stars*,[2] but, since the completion of this program is some years distant and it may be desirable to have the colors and magnitudes of many of the brighter stars on a homogeneous system, we shall examine the material now available in the literature.

I. HERTZSPRUNG'S CATALOGUE OF COLOR EQUIVALENTS

E. Hertzsprung[3] has given mean color equivalents, C_2'/T, for 834 bright stars compiled from the various series, photographic and photoelectric, of color measurements available in 1940, reduced to a common system. Values of C_p are available for 110 stars contained in Hertzsprung's catalogue, and the correlation between the two color systems is shown in Figure 1. The straight line shown in the figure is represented by

$$C_p = -1^m.00 + 0^m.57\,\frac{C_2'}{T}. \qquad (1)$$

There is some suggestion that the stars with $C_p = -0^m.15$ to $-0^m.20$ deviate from the linear relationship (1) in the sense that they are bluer in C_p than they are in C_2'/T. Since the stars in this color range are of spectral types B5–B8, the small departure from linearity between the two scales probably is a result of Balmer absorption in these stars. Heavily reddened B stars have been omitted from Figure 1.

II. GREENWICH GRADIENTS

Relative spectroscopic gradients of 250 stars have been determined at the Greenwich Observatory.[4] Values of C_p are available for 43 of these stars. Figure 2 is the correlation diagram between C_p and the gradients G; the five filled circles represent stars whose gradients were given in an earlier Greenwich publication.[5] Since the difference between

* *Contributions from the Lick Observatory*, Ser. II, No. 36.

[1] *Ap. J.*, **111**, 65, 81, 414; **112**, 141, 1950; **113**, 367, 1951.

[2] Yale University, 1940. [3] *B.A.N.*, **9**, 101, 1940. [4] *M.N.*, **100**, 189, 1940.

[5] *Observations of Colour Temperatures of Stars* (London: H.M. Stationery Office, 1932).

the gradients G and the colors C_p is that the former are measured in the continuous spectra while the latter are measured over integrated sections of the spectra including both absorption lines and continuum, we would not expect to find a linear relationship between the two values. Moreover, Figure 2 should give an indication of the effect of line absorption on the colors C_p, and the fact that the relationship between the two systems is not linear probably results from a combination of the effects of the Balmer absorption in the blue stars and a shifting, with color, of the effective wave lengths that define C_p. Very few red stars were measured by the Greenwich observers. As previously pointed out by the Greenwich observers,[5] except for the effect of line absorption on the colors, the values of C_p and G should differ in scale only by the factor $\Delta(1/\lambda)/0.92$, where $\Delta(1/\lambda)$ refers to

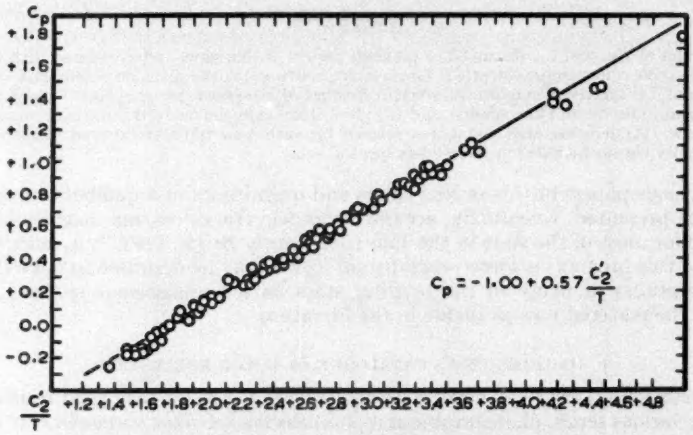

FIG. 1.—Relationship between values of C_2'/T (Hertzsprung) and C_p

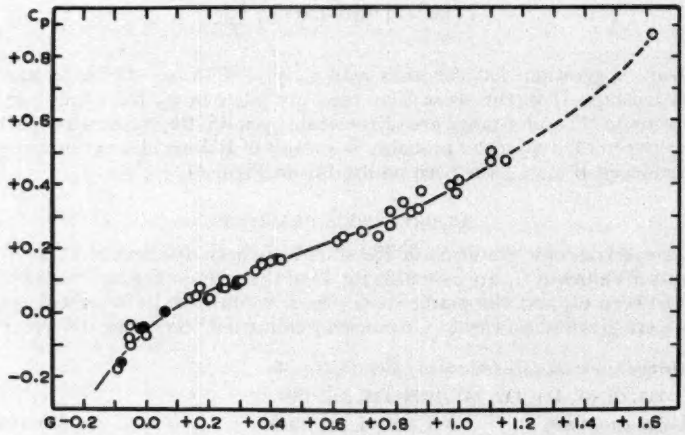

FIG. 2.—Relationship between the Greenwich gradients, G, and the values of C_p

the difference in the reciprocals of the two effective wave lengths used in determining C_p. In Figure 2, for stars with $G = +0.25$ to $+1.1$, the total line absorption has relatively little effect upon C_p, and the linear relationship,

$$C_p = -0^m04 + 0.475G\,, \qquad (2)$$

determined by least squares, satisfies the observations fairly well. If we take the mean effective wave lengths of Pg_p and Pv_p as 4400 A and 5450 A, respectively, as given in Paper I, Table 2, then $\Delta(1/\lambda)/0.92 = 0.48$, which is in excellent agreement with $\Delta C_p/\Delta G = 0.475$ given by expression (2). Table 1 shows the mean relation between C_p and G for $G = -0.1$ to $+1.15$. Heavily reddened B stars have been omitted from this discussion.

TABLE 1

MEAN RELATIONSHIP BETWEEN THE COLORS, C_p, AND THE GREENWICH GRADIENTS, G

G	C_p	G	C_p	G	C_p
−0.10	−0m16	+0.35	+0m13	+0.80	+0m30
− .05	− .10	+ .40	+ .15	+0.85	+ .32
.00	− .06	+ .45	+ .175	+0.90	+ .35
+ .05	− .01	+ .50	+ .19	+0.95	+ .38
+ .10	+ .02	+ .55	+ .205	+1.00	+ .41
+ .15	+ .04	+ .60	+ .22	+1.05	+ .44
+ .20	+ .065	+ .65	+ .24	+1.10	+ .47
+ .25	+ .09	+ .70	+ .26	+1.15	+0.50
+0.30	+0.11	+0.75	+0.28		

III. SIX-COLOR PHOTOMETRY

Forty stars for which values of C_p are available also were observed by Stebbins and Whitford[6] in their program of six-color photometry. Figure 3 shows the correlation between the values of C_p and $V - \frac{1}{2}(B+G)$, interpolated from the six-color data. Since the effective wave length of the blue photoelectric magnitudes, used in determining C_p, is somewhat to the violet of the V-magnitudes in the six-color results, Figure 3 contains only stars with $C_p > +0^m10$, in order to avoid difficulty with the Balmer absorption in the bluer stars. Heavily reddened B stars have been omitted from the comparison. The linear relationship in Figure 3 is represented by

$$C'_p = +0^m61 + 0.96\,[\,V - \tfrac{1}{2}\,(B+G)\,]\,. \qquad (3)$$

Data for the individual stars that define this relationship are given in Table 2, where the values of C'_p are those derived from the six-color results and from relationship (3). Figure 4 shows how the 14 stars with $C_p < +0^m10$ fall with reference to the straight line extrapolated from relationship (3). Observed and computed values of colors of these bluest stars are tabulated in Table 3, where C'_p is again computed from relationship (3). If the bluest star, β Cephei, is neglected, the stars in Table 3 can be divided roughly into two groups, one containing the seven Pleiades stars and the other the six stars α Lyrae, λ Bootes, and NPS 1, 2, 4, and 5. Stars in the latter group are similar, in that the six-color observations show them to be affected by heavy Balmer absorption; the U-magnitudes are all fainter than the V-magnitudes. On the other hand, the Pleiades stars are brighter in the U-magnitudes than they are in the V-magnitudes, and they show little

[6] *Ap. J.*, **102**, 318, 1945.

effect of Balmer absorption. The mean deviation of the Pleiades group from relationship (3) is -0.07 mag. in $C_p - C'_p$; the average deviation for the stars affected by Balmer absorption is -0.04 mag.; the mean is -0.06 mag. for all stars contained in Table 3.

IV. HARVARD REVISED PHOTOMETRY

For 42,000 stars Mrs. Gaposchkin[7] has given visual magnitudes reduced to a photovisual system; the system is that "given by the 10-inch Metcalf refractor, the Iso-presto

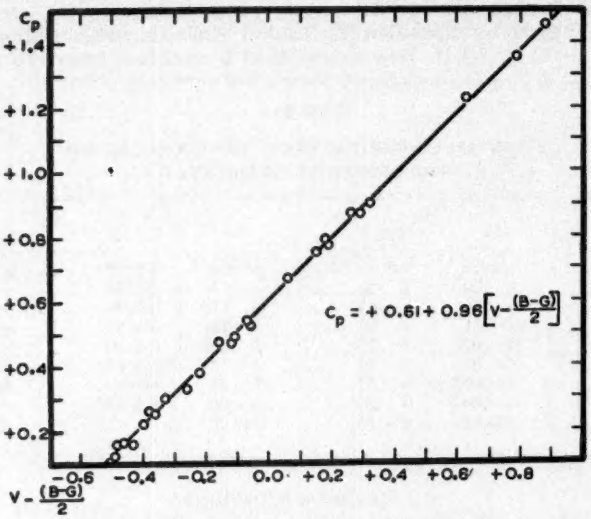

FIG. 3.—Relationship between values of $[V - \frac{1}{2}(B + G)]$ interpolated from the six-color photometry of Stebbins and Whitford, and the values of C_p larger than $+0^m1$. In the diagram, for $(B - G)/2$ read $(B + G)/2$.

TABLE 2

COMPARISON BETWEEN OBSERVED VALUES OF C_p AND THOSE COMPUTED FROM THE SIX-COLOR RESULTS, C'_p

Star	C_p	C'_p	O−C	Star	C_p	C'_p	O−C
NPS 6	$+0^m12$	$+0^m13$	-0^m01	βCVn	$+0^m49$	$+0^m49$	0^m00
γ Boo	+ .16	+ .15	+ .01	31 Com	+0.53	+0.55	− .02
NPS 3	+ .16	+ .18	− .02	45 Dra	+0.54	+0.54	.00
α Cep	+ .165	+ .17	.00	HD 152391	+0.68	+0.67	+ .01
α Aql	+ .165	+ .17	.00	β Aqr	+0.75	+0.75	.00
ϵ Cep	+ .22	+ .23	− .01	β Aql	+0.77	+0.78	− .01
β Cas	+ .25	+ .26	− .01	HD 166620	+0.79	+0.77	+ .02
NPS 2s	+ .26	+ .25	+ .01	β Dra	+0.87	+0.86	+ .01
78 UMa	+ .30	+ .29	+ .01	δ Boo	+0.87	+0.88	− .01
NPS 3s	+ .33	+ .34	− .01	α Aqr	+0.90	+0.92	− .02
α Per	+ .38	+ .40	− .02	HD 151288	+1.23	+1.23	.00
χ Her	+ .47	+ .46	+ .01	β UMi	+1.36	+1.36	.00
β Com	+0.47	+0.49	−0.02	α Tau	+1.46	+1.48	−0.02
$\overline{O-C}$							-0.004 ± 0.010 (A.D.)

[7] *Harvard Mimeograms*, Ser. 3, Nos. 1 and 2.

plate, and the 'Rapid Filter Yellow' filter."[7] The visual catalogues used were Volumes **24, 34, 44, 45, 46, 64, 70, 72,** and **74** of the *Harvard Annals*, together with the *Potsdam Generalkatalog*, and the *Yerkes Actinometry*. A large number of stars for which values of Pg_p and C_p are available is included in Mrs. Gaposchkin's catalogue. The differences between $Pv_p = Pg_p - C_p$ and the magnitudes taken from her compilation, Pv, for a representative sample of 180 stars are plotted against Pv_p in Figure 5 and against C_p in Figure 6. Although there is a suggestion of a small color equation in Figure 6, it is apparent that a value of Pv taken directly from the catalogue has a high probability of being within, say, 0.15 mag. of the value of Pv_p. The Harvard catalogue, then, provides a source for a large number of visual magnitudes with an accuracy sufficient for many purposes. Of the sample of 180 stars plotted in Figures 5 and 6, only 5 stars have residuals

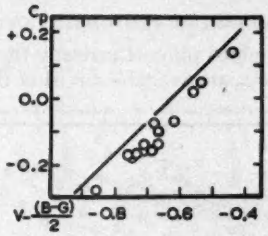

FIG. 4.—Relationship between $[V - \frac{1}{2}(B + G)]$ and C_p for stars with C_p less than +0.1. The linear relationship shown in the figure is extrapolated from that shown in Figure 3. In the diagram, for $(B - G)/2$ read $(B + G)/2$.

TABLE 3

COMPARISON BETWEEN C'_p COMPUTED FROM SIX-COLOR OBSERVATIONS AND C_p FOR BLUEST STARS

Star	C_p	C'_p	O−C	Star	C_p	C'_p	O−C
β Cep.....	−0.28	−0.22	−0.06	NPS 2....	−0.09	−0.03	−0.06
19 Tau....	− .18	− .11	− .07	α Lyr.....	− .08	− .03	− .05
η Tau.....	− .18	− .11	− .07	NPS 1....	− .07	− .03	− .04
17 Tau....	− .17	− .12	− .05	NPS 5....	+ .02	+ .07	− .05
27 Tau....	− .17	− .10	− .07	λ Boo.....	+ .05	+ .09	− .04
20 Tau....	− .16	− .07	− .09	NPS 4....	+0.14	+0.19	−0.05
21 Tau....	− .14	− .03	− .11				
23 Tau....	−0.14	−0.07	−0.07	O−C...	.....	.....	−0.06±0.01 (A.D.)

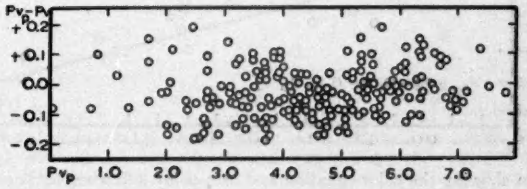

FIG. 5.—Correlation diagram between values of Pv, given by Mrs. Gaposchkin, and $Pg_p - C_p = Pv_p$ for 180 representative stars.

in $Pv_p - Pv$ larger than 0.2 mag.; these 5 stars are listed in Table 4. The value of $Pv = 5^m01$ in the catalogue for HD 27429 may be a misprint for 6^m01. The red star 119 Tauri is not plotted in Figures 5 and 6, but the values of $Pv_p = 4^m31$, $Pv = 4^m36$, and $C_p = -1^m79$ give further evidence that there is very little color difference between the two magnitude systems.

V. PHOTOMETRY OF DE VAUCOULEURS

G. de Vaucouleurs[8] has determined the photographic magnitude of 76 bright stars by extra-focal photometry. Values of C_p and Pg_p are available for 30 of these stars, and the differences, $Pg_p - Pg$, are plotted against C_p in Figure 7. The straight line in the figure is represented by

$$Pg_p = Pg - 0^m14 - 0.25C_p. \qquad (4)$$

VI. PHOTOELECTRIC PHOTOMETRY OF GÜSSOW

Miss M. Güssow[9] has determined photoelectrically the magnitudes and colors of 94 bright stars. Values of C_p and Pg_p are available for 31 of these stars. Figure 8 shows the

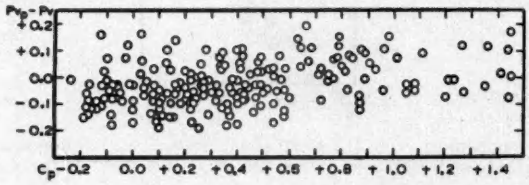

FIG. 6.—Diagram showing the color-equation and zero-point difference between values of Pv_p and Pv (Gaposchkin) for the same 180 stars as in Figure 5.

TABLE 4

STARS IN *Harvard Mimeograms** WITH $Pv_p - Pv > 0.2$ MAG.

HD	Pv_p	Pv	$Pv_p - Pv$	C_p	HD	Pv_p	Pv	$Pv_p - Pv$	C_p
88230....	6^m73	6^m38	$+0^m35$	$+1^m23$	154363....	7^m87	7^m41	$+0^m46$	$+1^m07$
95735....	7.46	7.23	+ .23	+1.32	209750....	2.85	3.08	−0.23	+0.89
102647....	2.03	2.43	−0.40	+0.08					

* Ser. 3, Nos. 1 and 2.

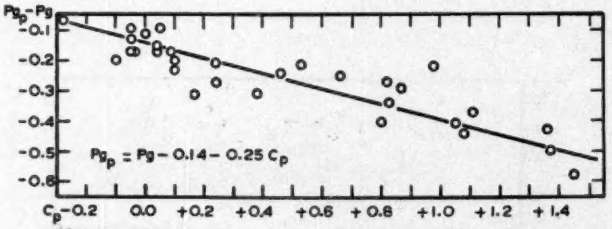

FIG. 7.—Diagram showing the color-equation and zero-point difference between values of Pg_p and the photographic magnitudes determined by de Vaucouleurs.

[8] *Ann. d'ap.*, **10**, 107, 1947. [9] *Zs. f. Ap.*, **10**, 25, 1940.

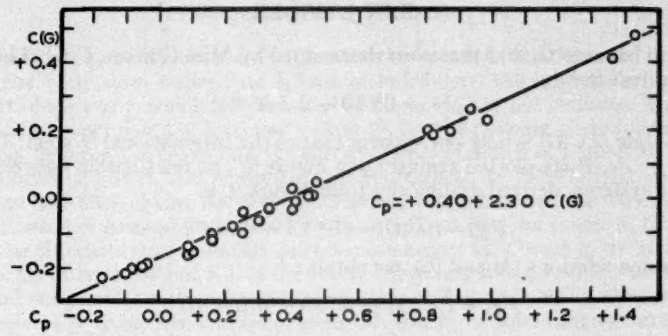

FIG. 8.—Relationship between the colors determined photoelectrically by Miss Güssow, $C(G)$, and values of C_p.

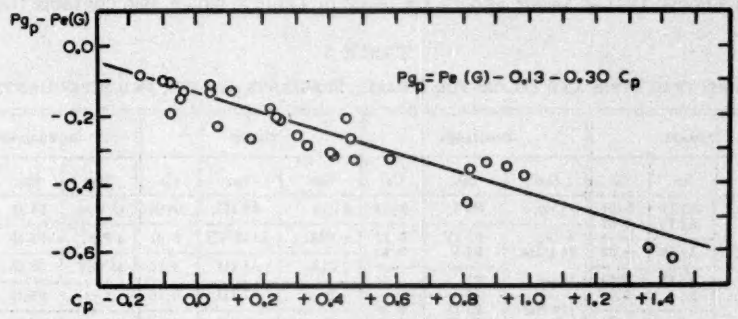

FIG. 9.—Diagram showing the color-equation and zero-point difference between values of Pg_p and the photoelectric magnitudes determined by Miss Güssow, $Pe(G)$.

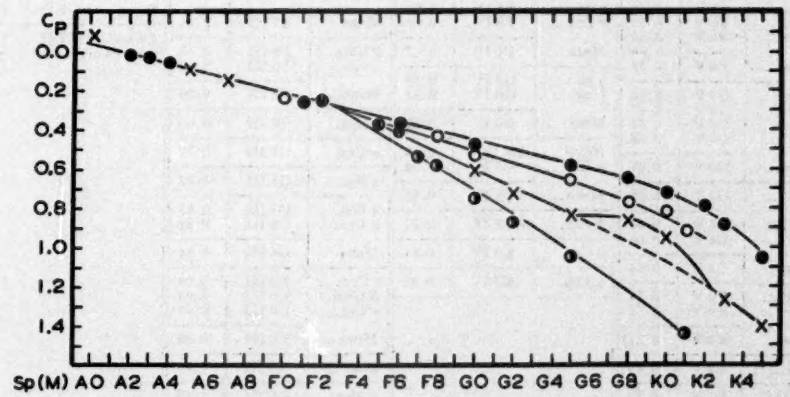

FIG. 10.—Relationship between color, C_p, and spectral type (Morgan). The filled circles represent dwarfs, the open circles subgiants, the crosses giants, and the half-filled circles supergiants of luminosity class I*b*.

relationship between C_p and the colors determined by Miss Güssow, $C(G)$. The straight line in Figure 8 is

$$C_p = +0^m40 + 2.30C\,(G)\,; \tag{5}$$

hence the scale of $C(G)$ is only one-quarter that of the International System. The differences $Pg_p - Pe(G)$ are plotted against C_p in Figure 9. The relationship between the two magnitude systems, derived graphically from Figure 9, is

$$Pg_p = Pe\,(G) - 0^m13 - 0.30C_p\,. \tag{6}$$

If we combine relations (5) and (6), we obtain:

$$Pg_p = Pe\,(G) - 0^m25 - 0.69C\,(G)\,. \tag{7}$$

VII. THE RELATIONSHIP BETWEEN COLOR AND SPECTRAL TYPE

The stars mentioned in the previous papers of this series that are known to populate the dwarf and subgiant sequences of the color-luminosity array and that are contained in the Yerkes *Atlas of Stellar Spectra* are listed in Table 5, which also contains the stars

TABLE 5

SPECTRAL TYPES AND COLORS FOR DWARFS, SUBGIANTS, GIANTS, AND SUPERGIANTS

Dwarfs			Subgiants			Giants			Supergiants		
Star	Sp.	C_p	Star	Sp.	C_p	Star	Sp.	C_p	Star	Sp.	C_p
β Aur	A2 IV	0m01	ε Cep	F0 V	0m22	δ Cyg	A0 III	0m08	41 Cyg	F4 Ib	0m33
β Ser	A2 IV	0.03	δ Gem	F2 IV	0.22	γ UMi	A3 II–III	0.04	α Per	F5 Ib	0.38
Mean	A2 IV	0.02	78 UMa	F2 V	0.30	α Oph	A5 III	0.10	45 Dra	F7 Ib	0.54
δ Her	A3 IV	0.03	Mean	F2	0.26	γ Boo	A7 III	0.16	γ Cyg	F8 Ib	0.58
α Lib	A5 V	0.08	110 Her	F5 IV	0.37	β Cas	F2 III	0.25	β Aqr	G0 Ib	0.75
Mean	A4	0.06	τ Boo	F6 IV	0.38	υ UMa	F2 III	0.23	α Aqr	G2 Ib	0.89
γ Vir	F0 V	0.25	σ² UMa	F6 IV	0.40	Mean	F2 III	0.24	β Dra	G2 Ib	0.87
σ Boo	F2 V	0.27	γ Ser	F6 IV	0.40	α Tri	F5 III	0.37	Mean	G2 Ib	0.88
Mean	F1 V	0.26	θ Boo	F6 IV	0.41	β Del	F5 III	0.34	9 Peg	G5 Ib	1.04
ι Peg	F5 V	0.34	Mean	F6 IV	0.40	Mean	F5 III	0.36	ζ Cep	K1 Ib	1.44
π³ Ori	F6 V	0.34	υ And	F8 IV	0.41	θ UMa	F6 III	0.40			
χ Dra	F6 V	0.40	θ Dra	F8 IV	0.45	ι Vir	F6 III	0.40			
Mean	F6 V	0.37	Mean	F8 IV	0.43	Mean	F6 III	0.40			
η Cas	G0 V	0.46	η Boo	G0 IV	0.52	ε Hya	G0 III	0.60			
χ¹ Ori	G0 V	0.47	ζ Her	G0 IV	0.53	π Cep	G2 III	0.72			
β Com	G0 V	0.47	Mean	G0 IV	0.525	η Her	G5 III	0.83			
β CVn	G0 V	0.48	70 Vir	G5 IV–V	0.64	δ Boo	G8 III	0.87			
Mean	G0 V	0.47	μ Her	G5 IV	0.66	η Dra	G8 III	0.82			
κ Cet	G5 V	0.58	Mean	G5 IV	0.65	Mean	G8 III	0.84			
61 UMa	G8 V	0.63	β Aql	G8 IV	0.77	ι Cep	K0 III	0.99			
ξ Boo	G8 V	0.66	η Cep	K0 IV	0.81	β Gem	K0 III	0.93			
Mean	G8 V	0.64	γ Cep	K1 IV	0.92	ε Cyg	K0 III	0.95			
107 Psc	K0 V	0.71				Mean	K0 III	0.96			
σ Dra	K0 V	0.72				α Sct	K3 III	1.16			
Mean	K0 V	0.715				α Tau	K5 III	1.43			
ε Eri	K2 V	0.79				β UMi	K5 III	1.36			
HR 8832	K3 V	0.88				Mean	K5 III	1.40			
61 CygA	K5 V	1.05									

that are known to populate the giant sequences; these stars will be discussed in Paper IX of this series. Only stars earlier than K5 are included here; the subdwarfs, blue-dwarfs, and bright blue-dwarfs, which are discussed in Paper IV, are not included. Table 5 also contains a few supergiants of luminosity class I*b*, for the purpose of completeness. The relationship between the colors and the spectral types is shown in Figure 10, where the dwarfs, subgiants, giants, and supergiants are represented by filled circles, open circles, crosses, and half-filled circles, respectively. The separation between the various luminosity classes becomes marked for spectral types near F6 or F8. The course of the relationships for the different types of stars is quite smooth except for a break in the giant branch between stars of type G6 and K3. If the run of the giants is to be similar to that of the dwarfs and subgiants, we would expect such stars as δ Bootes and η Draconis, which now are called G8, to be classified G6 or even G5, and those stars that now are classified K0 would be nearer G8.

VARIATIONS IN THE STELLAR LUMINOSITY FUNCTION IV. A REGION IN CEPHEUS-LACERTA

S. W. McCuskey
Warner and Swasey Observatory, Case Institute of Technology
Received January 17, 1951

ABSTRACT

Spectral types, red color indices, and photographic magnitudes have been observed in an area of 16.9 square degrees centered at R.A. 22^h22^m; Dec. $+53°.8'$ (1945). A distribution of 4256 spectral types according to magnitude is summarized in Table 1. Analysis of the data to $m_{pg} = 12.5$ indicates a considerable excess of early-type stars at about 500 parsecs from the sun. Space densities are given for several spectral groups in Table 6. The absorption in this region is quite moderate, 1 mag. at 2000 parsecs.

Construction of a luminosity function at distances 100, 200, 400, and 600 parsecs has given results shown in Figure 3. The function does not change appreciably within this distance range. An excess in stars of $-1 < M < 1$ over the van Rhijn function (*Groningen Pub.*, Vol. **47**, 1936) is found. This amounts to about 0.3 in log $\phi(M)$.

INTRODUCTION

The Milky Way in Cepheus and Lacerta presents two markedly different aspects. On the north the absorbing clouds and resulting irregularities in stellar population are predominant. On the south the surface distribution of the stars smoothes out, with little indication of patches of nebulosity. The region LF4, which forms the subject of this paper, lies in the relatively smooth area south of the galactic circle at $l = 70°$ and $b = -3°$ [R.A. 22^h22^m; Dec. $+53°.8'$ (1945)]. Its center is about 2° north of β Lacertae, and it covers a circular area of 16.9 square degrees. LF4 is one of the twelve Milky Way regions under investigation at the Warner and Swasey Observatory for purposes of extending our knowledge of the stellar luminosity function near the galactic plane. Similar studies for LF1, 2, 3b, 7, and 8 have already been published.[1]

Although region LF4 contains many interesting objects, such as faint galactic clusters and early-type stars, these will not be discussed in the present paper. The detailed catalogue of spectral types, colors, and photographic magnitudes will be published in the near future.

OBSERVATIONAL DATA

Table 1 presents a summary of the spectral-type distributions in LF4 as a function of apparent photographic magnitude. The spectra were taken with the 4° and the 2° prisms attached to the 24–36-inch Burrell telescope of this observatory. In general, an adopted spectral class for the brighter stars depends upon estimates made on three to six plates. For the fainter stars, three plates were used.

Detailed luminosity classes were assigned to all stars F0 and later and brighter than $m_{pg} = 11.0$. For the fainter stars only classes III (giant) and V (dwarf) could be recognized with reasonable certainty. The nomenclature of Morgan, Keenan, and Kellman[2] was used for the luminosity classification, while criteria for this work have been published by Nassau and van Albada.[3] In many cases, particularly for the fainter stars, overlapping spectra made the assignment of a luminosity class impossible. As shown in the next to last column of Table 1, the number of completely unclassified objects does not become seriously large until the interval 12.00–12.50 in apparent magnitude is reached.

[1] *Ap. J.*, **106**, 1, 1947; **109**, 139 and 414, 1949; **110**, 40, 1949.

[2] *An Atlas of Stellar Spectra* (Chicago: University of Chicago Press, 1943).

[3] *Ap. J.*, **106**, 20, 1947.

TABLE 1

DISTRIBUTION OF OBSERVED SPECTRAL TYPES IN LF4
(Area 16.9 Sq. Deg.)

m_{pg}*	B0, 1†	B2	B3	B5	B8	B9	A0	A2, 3	A5	F0‡			F2			F5		
										III	IV	V	III	IV	V	III	IV	V
⩽ 6.00	0	0	0	0	0	0	0	0	0	0	0	0	0	0	0	0	0	0
6.25	0	0	0	1	0	0	0	0	0	0	0	0	0	0	0	0	0	0
6.75	0	1	0	0	1	0	0	0	0	0	0	0	0	0	0	0	0	0
7.25	0	0	0	0	2	1	1	0	1	0	1	1	0	0	0	0	0	1
7.75	0	1	0	1	2	1	1	1	1	0	0	1	0	0	0	0	0	0
8.25	0	0	1	0	4	5	4	2	1	0	1	1	0	0	1	0	0	0
8.75	3	1	0	2	6	11	4	3	1	2	1	1	0	0	1	0	0	1
9.25	2	3	0	2	7	7	6	5	3	1	0	2	0	0	1	0	2	0
9.75	1	4	2	4	15	16	11	5	2	0	2	2	0	0	2	0	0	0
10.25	3	3	3	13	32	19	14	16	3	3	1	11	0	0	0	0	0	0
10.75	3	6	2	19	44	24	32	16	4	1	6	9	1	1	7	1	0	3
11.25	4	3	4	22	46	45	54	29	12	3	2(1)	15	0	2	4	0	2(2)	4
11.75	2	4	5	40	66	51	108	59	24	...	45	....	...	5	....	....	8	...
12.25	6	5	4	54	109	92	230	99	29	...	90	....	...	21	....	....	15	...
12.75	5	5	6	53	93	87	228	102	20	...	50	....	...	10	....	....	5	...
Total	29	36	27	211	427	359	693	337	101	...	253	....	...	56	....	....	44	...

* The entries under m_{pg} refer to intervals of a half-magnitude, e.g., 7.01–7.5, 7.51–8.0, etc.

† A major fraction of the stars B0–B3 and m_{pg} 7.75–10.25 inclusive are supergiants.

‡ Parentheses around entries for the fainter stars of late spectral class indicate those for which no luminosity class could be assigned.

TABLE 1—*Continued*

m_{pg}*	F8			G0			G2			G5			G8			K0		
	III	IV	V	III	IV	V	III	IV	V	III	IV	V	III	IV	V	III	IV	V
⩽ 6.00	0	0	0	0	0	0	0	0	0	1	0	0	0	0	0	0	0	0
6.25	0	0	0	0	0	0	0	0	0	0	0	0	0	0	0	0	0	0
6.75	0	0	0	0	0	0	0	0	0	0	0	0	0	0	0	1	0	0
7.25	0	0	0	0	0	0	0	0	0	1	0	0	1	0	0	0	0	0
7.75	0	0	0	0	0	0	0	0	0	0	0	0	0	0	0	0	0	1
8.25	0	0	0	0	2	0	1	0	0	0	0	0	1	0	0	0	0	0
8.75	0	0	0	1	1	1	0	0	2	2	0	1	0	0	1	1	0	0
9.25	0	2	0	0	1	0	0	0	0	1	1	0	0	0	0	2	4	0
9.75	0	0	3	0	0	1	1	0	0	1	1	1	2	1	0	0	1	0
10.25	0	2	5	2	1	4	1	0	1	8	1	1	1	5	0	0	1	0
10.75	1	(1)	9	4	0	7	1	2	2	9	8(1)	5	3	2	0	7	4(1)	2
11.25	1	0	7	6	1(3)	12	0	(1)	4	13	8	5	10	3	1	8	4(1)	3
11.75	...	17	....	....	47	....	2	1(1)	8	21	7(1)	13	17	7(1)	8	22	4(3)	2
12.25	....	38	....	....	190	....	....	32	....	48	7(19)	32	42	8(10)	18	43	4(13)	7
12.75	....	11	....	....	88	....	....	24	....	29	1(25)	10	26	(18)	0	27	2(19)	3
Total	....	97	....	....	372	....	....	84	....	....	282	....	....	186	....	....	190	....

TABLE 1—*Continued*

m_{pg}*	K2, 3			K5		M0, 2		M5, 8‡		Unclassified§	All Stars
	III	IV	V	III	V	III	V	III	V		
⩽ 6.00	0	0	0	0	0	0	0	0	0	0	1
6.25	0	0	0	0	0	0	0	0	0	0	1
6.75	0	0	0	0	0	0	0	0	0	0	3
7.25	0	0	0	0	0	0	0	0	0	0	10
7.75	3	0	0	0	0	0	0	0	0	1	14
8.25	1	0	0	0	0	0	0	0	0	0	25
8.75	1	1	0	1	0	0	0	0	0	0	50
9.25	0	0	0	1	0	0	0	0	0	1	54
9.75	1	0	0	0	0	1	0	1	0	0	81
10.25	3	1	0	0	0	3	0	0	0	4	165
10.75	8	0	0	3	0	2	0	0	0	13	274
11.25	10	1	1	2	1	2	0	1	1	13	377
11.75	8	(1)	3	1	0	4	0	(1)	0	27	644
12.25	16	(10)	4	2(1)	0	5(1)	1	1	0	104	1410
12.75	9	1(10)	0	2(1)	0	1(3)	0	0	0	173	1147
Total	.....	93	.....	15		23		5		336	4256

§ Included under the heading "Unclassified" are: double stars too close together to show separate spectra; stars showing composite or peculiar spectra; stars unclassifiable owing to overlapping spectra.

Photographic magnitudes have been determined from four Eastman II*a*-O plates. They are based upon a sequence established by fourteen comparisons with the NPS, SA39, and another sequence set up here for region LF3b. The measures were made with the Eichner astrophotometer of this observatory for 1728 stars on two of the plates and with a graduated scale of stellar images for 4476 stars on the other two. A comparison of the two sets of measures indicated that the internal accuracy for the astrophotometer measures was twice that for the measures made with the scale, the probable error of a single observation in these two cases being ± 0.05 and ± 0.10 mag., respectively. There was some systematic difference between the two sets, but remeasurement of 100 stars with the astrophotometer on one of the plates which had been measured with the scale indicated that this difference could not be ascribed to the method of measurement. The finally adopted blue magnitudes were obtained by weighting the photometer measures 4 and the scale measures 1 for the 1728 stars for which colors were to be obtained. For the balance of the stars the scale measures were corrected to the astrophotometer system by applying the weighted average systematic difference between the two sets of measures. Thus, for statistical purposes, the final magnitudes may be considered to have a probable error of ± 0.07 mag.; for the stars used in the color analysis the p.e. of a final photographic magnitude is ± 0.04 mag.

Photored magnitudes of 1764 stars in LF4 were determined in order to study the interstellar reddening. As in the previous investigations, Eastman 103*a*-E plates and a No. 22 Wratten filter were used for this work. The effective wave length of the combination is about λ 6200. A sequence for this work was established in LF4 by intercomparison with the NPS, SA39, and SA65. Red magnitudes for this calibration were taken from a paper by Nassau and Burger[4] and from unpublished later work by these authors. Two plates were measured in the astrophotometer to obtain the magnitudes of the field stars, the probable error of a final determination being ± 0.03 mag.

To supplement the data provided by the spectral-type distributions, counts of faint stars to $m_{pg} = 18.0$ have been made in four regions situated symmetrically about the

[4] *Ap. J.*, **103**, 25, 1946.

center of LF4. They encompass a total area of 1.15 square degrees. A calibration sequence for this work was established by intercomparison with the NPS and SA39. The total number of stars counted was 12,476.

Table 2 provides data for strengthening the statistical analysis for the brighter stars. Counts in an area of 100 square degrees surrounding LF4 have been made in the *Henry Draper Catalogue*. The distribution of spectral types in broad groupings is sufficient here, since the data of Table 1 will be recombined for analysis.

The average red color indices as a function of photographic magnitude and of spectral type for the early-type stars are shown in Table 3. Normal red indices and mean absolute magnitudes required in analyzing these colors are listed in the second and third columns. Data for a few late-type stars are provided, in order to check the zero point of the color system. Numbers in parentheses indicate the number of colors entering into the mean.

TABLE 2

DISTRIBUTION OF SPECTRAL TYPES FROM THE *Henry Draper Catalogue* FOR THE REGION SURROUNDING LF4
(Area 100 Sq. Deg.)

m_{pg}	Spectral Type									All Stars
	B0–B2	B5	B8–A0	A2–A5	F0–F5	F8–G0	G5	K0–K2	K5–M	
6.51–7.00.....	1	1	4	1	1	0	0	2	1	11
7.01–7.50.....	1	0	14	3	4	1	2	5	0	30
7.51–8.00.....	1	2	34	9	11	4	1	8	2	72
8.01–8.50.....	4	0	38	15	12	5	0	6	3	83
8.51–9.00.....	1	0	79	35	14	7	7	21	11	175

INTERSTELLAR ABSORPTION IN LF4

An inspection of the average red indices in Table 3 for the late-type dwarf stars and of the graph in Figure 1 shows them to be nearly normal for their spectral class, with no appreciable dependence upon magnitude. Since these stars are near by, the negligible color excesses imply that the system of red indices has no serious zero-point error. From the entries of Table 3, therefore, we may derive the interstellar absorption as a function of the distance. The normal red indices and mean absolute magnitudes used here are those published recently by Nassau and MacRae.[5]

Figure 1 shows the average red color excesses, E_R, for given ranges in $m-M$ plotted against the distance modulus uncorrected for absorption. Numbers after a plotted point indicate the number of entries in each average. Large circles near $m - M = 7.0$ are average red excesses for the dwarf F8, G0, G2, and G5 stars.

The curve in Figure 1 has been converted into a relation between total photographic absorption, A_{pg}, and corrected distance in parsecs, with the result shown in Figure 2. A ratio $A_{pg}/E_R = 2.6$ has been used for the conversion. This is the same ratio used in analyses of the other LF regions. LF4 appears to be a remarkably clear region on the whole, the absorption at 2000 parsecs being only 1 mag. Thereafter, the value of A_{pg} increases at a rate of 0.32 mag. per kiloparsec.

A comparison of these results with the total absorption deduced from photoelectric color indices measured by Stebbins, Huffer, and Whitford[6] for the region immediately

[5] *Op. cit.*, p. 45.

[6] *Ap. J.*, 91, 20, 1940.

TABLE 3

AVERAGE RED INDICES OBSERVED IN LF4

SPECTRUM	NORM.	$\mathfrak{M}_{pg}$	m_{pg}									
			<8.0	8.01–9	9.01–10	10.01–10.5	10.51–11	11.01–11.5	11.51–12	12.01–12.5	12.51–13	13.01–13.5
B0	−0.62	−4.0	.....	−0.14(2)	−0.14(2)	+0.03(3)	+0.12(2)	+0.18(2)	+0.12(2)	+0.18(6)	+0.29(6)	.....
B2	−0.61	−2.8	+0.08(2)	− .03(1)	− .17(5)	− .34(1)	− .13(6)	−0.30(2)	−0.05(2)	+0.07(4)	+ .10(3)	.....
B3	−0.57	−2.2	.....	− .34(2)	.00(1)	− .21(4)	− .11(2)	−0.15(3)	−0.01(4)	0.00(6)	+ .06(6)	.....
B5	−0.50	−1.4	− .20(2)	.....	− .16(5)	− .21(11)	− .13(13)	−0.23(10)	−0.07(28)	+0.04(35)	+ .19(30)	+0.21(7)
B8	−0.40	−0.4	− .13(2)	− .12(5)	− .14(15)	− .16(24)	− .09(32)	−0.08(34)	−0.02(41)	+0.05(67)	+ .12(66)	+ .19(10)
B9	−0.33	0.0	− .57(1)	− .16(15)	− .13(17)	− .04(11)	− .05(15)	−0.07(31)	−0.01(38)	+0.09(60)	+ .12(64)	+ .30(16)
A0	−0.20	+0.4	.00(1)	− .03(4)	− .03(12)	− .02(8)	+ .01(21)	+0.04(37)	+0.07(78)	+0.10(161)	+ .17(161)	+ .22(45)
A2	−0.08	+1.0	− .13(1)	+ .06(1)	+ .03(7)	+ .07(5)	+ .09(7)	+0.12(11)	+0.17(28)	+0.19(42)	+ .26(43)	+ .27(10)
A3	−0.05	+1.2	.....	+ .08(3)	+ .33(3)	+ .22(6)	+ .21(4)	+0.16(13)	+0.22(16)	+0.27(23)	+ .23(20)	+ .31(3)
A5	0.00	+1.7	+ .02(1)	+ .40(1)	+ .18(4)	+ .27(2)	+ .21(4)	+0.27(9)	+0.29(14)	+0.36(21)	+0.27(10)	+0.27(6)
F8V	+0.40	+3.9	.....	.....	+0.44(1)	+ .50(2)	+ .51(2)	+0.38(5)	+0.44(2)	.....	.....	.....
G0V	+0.46	+4.3	.....	.....	.....	+ .50(2)	+ .48(2)	+0.48(6)	+0.56(5)	.....	.....	.....
G2V	+0.60	+4.6	.....	+ .40(1)	.....	.....	+ .52(1)	+0.62(2)	+0.55(1)	.....	.....	.....
G5V	+0.84	+5.2	.....	+ .92(1)	.....	+0.79(1)	+0.96(4)	+0.88(4)	+1.16(3)	.....	.....	.....
G8V	+1.04	+5.9	.....	+0.88(1)	.....	.....	.....	+1.44(1)	+1.53(1)	.....	.....	.....
K0V	+1.13	+6.4	+0.85(1)	.....	.....	.....	.....	+1.56(1)	+1.02(2)	+1.10(1)	.....	.....
K2V	+1.21	+6.8	.....	.....	.....	.....	.....	.....	+1.29(1)	+1.08(2)	.....	.....

surrounding LF4 can be made. Color excesses E_1 on the photoelectric scale have been converted into A_{pg} by use of the ratio $A_{pg}/E_1 = 9.0$. Resulting values of A_{pg} for 9 stars are plotted in Figure 2. Six of these determinations in the range from 0 to 1500 parsecs bracket the curve for LF4. Three, however, deviate by a magnitude or more. These are HD 210809, 210628, and 212455, with color excesses $E_1 = +0.17$, $+0.13$, and $+0.28$, respectively. The spectral types given for these by Stebbins, Huffer, and Whitford are O8, B5s, and cB3, and it is immediately apparent that they are highly luminous stars. This is confirmed by the recent work of Morgan and Nassau, described at the symposium on galactic structure held at the University of Michigan in June, 1950. Their survey showed a high concentration of very luminous B stars in this area. Dr. Morgan has kindly communicated to me in advance of publication new distance moduli and absorptions for HD 210809 and 212455. These data are shown in Figure 2 by crosses and indicate the considerable corrections required for the original assignments of spectral type and luminosity class. Both stars are classed as supergiants (I*b*).

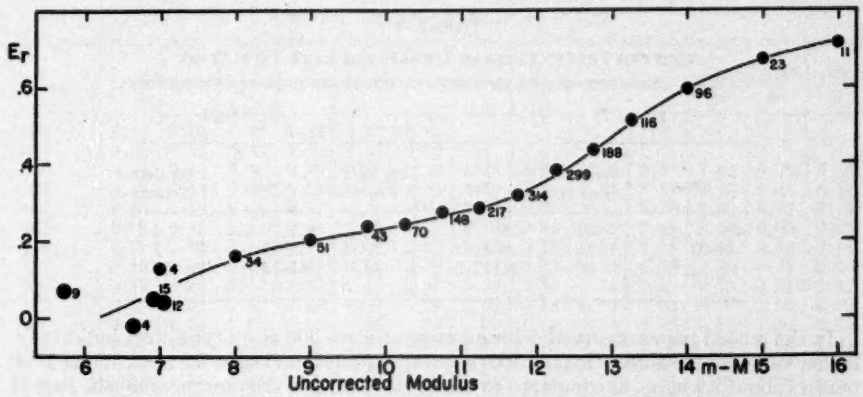

FIG. 1.—The average red color excess (*ordinate*) is plotted against an uncorrected distance modulus $m-M$ (*abscissa*). Numbers indicate the number of colors entering each average. The large dots near the origin represent the observed color excesses for late-type dwarfs. Presumably these are free of interstellar reddening.

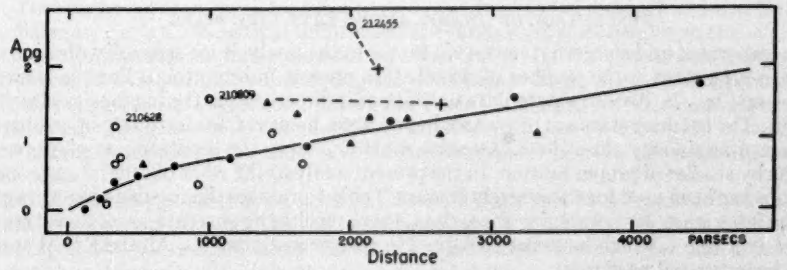

FIG. 2.—Total photographic absorption, A_{pg}, is plotted against corrected distance in parsecs. Dots are from our color data by way of Fig. 1; open circles are from photoelectric color excesses published by Stebbins, Huffer, and Whitford; triangles refer to a small area surrounding HD 212455 (see text).

HD 212455 still appears much too red for its spectral class, an effect possibly due to a local spot of high interstellar reddening. An examination of the red color indices, however, for eight stars immediately surrounding and within 8′ of HD 212455 does not confirm such a local red spot. The total photographic absorption for these stars is plotted in Figure 2 as triangles. Only two stars show unusual absorption, and they are no closer to HD 212455 than others which have color excesses in agreement with the average.

Two investigations by Risley[7] of the Milky Way in Cepheus and, in particular, of the bright core of the Cepheus star cloud at $l = 70°$ and $b = -3°$ furnish a source of comparison with the present results. These papers, by the way, give full references, which will not be repeated here, to the work by Schalén, Wernberg, Vanäs, and others. By means of all available published data on photoelectric colors, nebular counts, and photographically determined color indices, Risley came to the conclusion that the absorption in region *M* was 0.5 mag. at 1000 parsecs and 0.7 mag. at 2000 parsecs. It is apparent that these results point to an even greater clarity for the region than do our data, the agreement being good for this kind of analysis.

TABLE 4

ADOPTED PERCENTAGES OF DWARFS FOR LATE-TYPE STARS

F8–G2		G5		G8–K3	
m_{pg}	Per Cent Dwarfs	m_{pg}	Per Cent Dwarfs	m_{pg}	Per Cent Dwarfs
<8.....	30	<8.....	20	<8.....	4
8–10.....	55	8–11.....	20	8–11.....	7
10–12.5.....	80	11–12.5....	30	11–12.5....	15

In the second paper observed color excesses of some 200 early-type stars indicated a higher value for the absorption. At 500 parsecs, A_{pg} was found to be 0.8 mag. and at 1000 parsecs about 1.4 mag., as compared to 0.4 and 0.7 found in the present analysis. Part of this discrepancy may be due to the use by Risley of mean absolute magnitudes 0.5 mag. fainter than those shown in Table 3. Allowance for this difference, however, will not entirely remove the discordance. In view of the fact that seven nebulae have been observed by Hubble[8] in this region, it seems unlikely that the absorption can be as high as 1.0–1.5 mag. per kiloparsec. The density analyses that follow will be based on the assumption that the absorption in LF4 is that shown in Figure 2.

PERCENTAGE OF DWARFS AMONG LATE-TYPE STARS

An important and somewhat uncertain factor in the analysis for space distribution of the late-type stars is the number of dwarf stars present in any group. For the fainter stars—say, $m_{pg} > 10$—we obtain data on this point directly from the luminosity classifications. The brighter stars are too scarce in any area, however, for us to rely upon observations of luminosity class alone. Recourse must be had to the separation of giants and dwarfs by studies of proper motion. In the present analysis the work of others[9] on proper motions has been used for these brighter stars. Table 1 provides the requisite percentages for the faint stars By combining these data, there results the percentages of dwarf stars shown in Table 4, which have been adopted in the present analysis. All the K5–M stars have been treated as giants.

[7] *Ap. J.*, **97**, 277, 1943, and **109**, 314, 1949. [8] *Ap. J.*, **79**, 8, 1934; *Mt. W. Contr.*, No. 485.

[9] See *Ap. J.*, **106**, 1, 1947, for detailed mention of these.

ADOPTED VALUES OF LOG $A'(m)$ FOR ANALYSIS

The material in Table 1 has been regrouped for analysis to embrace broader intervals of spectral type. Furthermore, our data have been supplemented for the stars brighter than $m_{pg} = 7.0$ by the counts of stars in the *Henry Draper Catalogue* published by Seydl.[10] In the case of these bright stars, values of log $A'(m)$ have been computed[11] for the galactic-latitude zones 0° to ±10°. The visual magnitudes were corrected to photographic before the data were combined with those for the fainter stars.

In the magnitude range from 6.5 to 9.0, the data in Table 1 have been supplemented by the count data exhibited in Table 2, that is, the stellar distributions for an area of 100 square degrees surrounding LF4 as obtained from the *Henry Draper Catalogue*.

The adopted values of log $A'(m)$ for the magnitude range 4.0–12.5, obtained from these sources and smoothed graphically, are shown in Table 5. They form the basis for our space-density analysis.

TABLE 5

ADOPTED VALUES OF LOG $A'(m)$ IN LF4

m_{pg}	B0, 1	B2, 3	B5	B8–A0	A2–A5	F0–F5	dF8–G2	gF8–G2	dG5	gG5	dG8–K3	gG8–K3	gK5–M
4.0	8.82	9.40	9.17	9.20	9.22	8.83	.....	.....	.....	.....	.....	.....	.....
4.5	9.00	9.58	9.33	9.53	9.47	9.10	.....	.....	.....	.....	.....	.....	.....
5.0	9.20	9.74	9.50	9.90	9.70	9.38	8.48	8.75	7.95	8.53	7.82	9.19	8.58
5.5	9.40	9.93	9.69	0.23	9.92	9.63	8.70	8.98	8.23	8.84	8.10	9.48	8.88
6.0	9.58	0.10	9.86	0.57	0.15	9.90	8.91	9.20	8.52	9.15	8.38	9.72	9.18
6.5	9.78	0.30	0.02	0.90	0.39	0.17	9.18	9.48	8.82	9.45	8.66	0.00	9.48
7.0	9.97	0.50	0.20	1.19	0.61	0.42	9.48	9.79	9.13	9.75	8.93	0.30	9.78
7.5	0.16	0.68	0.40	1.45	0.85	0.70	9.82	0.13	9.43	0.05	9.20	0.55	0.09
8.0	0.35	0.85	0.60	1.70	1.10	0.97	0.20	0.50	9.73	0.36	9.50	0.81	0.39
8.5	0.55	1.00	0.86	1.93	1.32	1.24	0.64	0.78	0.04	0.66	9.79	1.09	0.60
9.0	0.73	1.16	1.10	2.11	1.51	1.49	1.09	1.04	0.34	0.95	0.10	1.30	0.82
9.5	0.91	1.30	1.32	2.30	1.70	1.70	1.37	1.20	0.65	1.23	0.42	1.53	1.00
10.0	1.10	1.44	1.57	2.49	1.90	1.89	1.60	1.35	0.95	1.50	0.75	1.77	1.20
10.5	1.25	1.57	1.80	2.68	2.10	2.10	1.91	1.46	1.26	1.79	1.07	1.98	1.36
11.0	1.30	1.67	2.03	2.85	2.30	2.29	2.20	1.63	1.56	2.05	1.38	2.20	1.50
11.5	1.38	1.71	2.27	3.03	2.52	2.49	2.48	2.00	1.88	2.30	1.62	2.41	1.62
12.0	1.42	1.76	2.50	3.22	2.73	2.68	2.80	2.32	2.14	2.56	1.86	2.64	1.74
12.5	1.50	1.80	2.75	3.40	2.93	2.88	3.10	2.63	2.40	2.80	2.10	2.88	1.85

SPACE-DENSITY FUNCTIONS IN LF4

The number of stars per 1000 cubic parsecs as a function of distance and spectral type is shown in Table 6. Numerical solutions of the fundamental integral equation were employed, the assumption being that for any spectral group the absolute-magnitude distribution of stars per unit volume of space is Gaussian. Mean absolute magnitudes and dispersions required for this computation have been published by Nassau and MacRae.[5] The density functions have been corrected for absorption according to the curve shown in Figure 2. Several features of the galactic structure as revealed by these functions are as follows:

a) The density of early-type stars B2, 3, and 5 decreases by a factor of 5 in the first 1000 parsecs from the sun. On the other hand, the B8–A0 stars increase rapidly to a density at 400 parsecs, 2.3 times that in the solar neighborhood. Then the density decreases to a value comparable to that near the sun and remains nearly constant from 1000

[10] *Pub. Obs. Nat. Prague*, No. 6, 1929.

[11] $A'(m)$ is the number of stars per 100 square degrees with magnitude $m - \frac{1}{4}$ to $m + \frac{1}{4}$.

parsecs to 2000 parsecs. The density of A2–A5 stars decreases rapidly in the first 500 parsecs from the sun, then slowly to a minimum at 1200 parsecs, followed by an indication of an increase beyond.

b) As in all the other LF regions analyzed thus far, the F0–F5 stars diminish rapidly in number, by a factor of 4, in the first kiloparsec from the sun.

c) The marked increase in density of the gG5 stars is particularly striking. Furthermore, the dwarfs of this spectral group increase rapidly in the region within 500 parsecs of the sun.

d) Both the giants and the dwarfs of the F8–G2 group show a peculiar distribution in space. Among the former there is a distinct maximum of density at 300 parsecs and a

TABLE 6

SPACE-DENSITY FUNCTIONS IN LF4
(Number of Stars per 1000 Cubic Parsecs)

DISTANCE (PARSECS)	SPECTRAL GROUP											
	B2, 3*	B5	B8–A0	A2–A5	F0–F5	dF8–G2	dG5	dG8–K3	gF8–G2	gG5	gG8–K3	gK5–M
25	.....	.....	0.104	1.040	2.38	1.04	3.12	10.4	0.091	0.041	0.205	0.048
50	.....	0.0196	.109	0.680	1.96	0.55	3.27	12.0	.084	.045	.214	.050
75	.....	.0207	.115	0.575	1.84	0.89	3.45	13.8	.055	.048	.212	.053
100	0.0072	.0192	.125	0.480	1.70	1.85	3.65	13.2	.048	.051	.181	.055
200	.0066	.0099	.228	0.354	1.46	2.52	4.52	8.9	.089	.066	.186	.080
300	.0046	.0060	.239	0.284	1.05	1.40	4.44	8.4	.119	.073	.175	.052
400	.0035	.0046	.236	0.219	0.87	3.59	4.92	.....	.081	.077	.151	.043
500	.0029	.0041	.218	0.184	0.75	4.28	5.56	.....	.015	.081	.146	.036
600	.0024	.0037	.197	0.158	0.66	3.78	.....	.....	.015	.086	.135	.030
800	.0015	.0030	.127	0.114	0.50	1.32	.....	.....	.036	.083	.101	.016
1000	.0015	.0031	.102	0.090	0.48	.....	.....	.....	.066	.086	.098	.011
1200	.0014	.0031	.082	0.072	0.44	.....	.....	.....	.081	.082	.099	.007
1400	.0012	.0029	.080	0.141	0.42	.....	.....	.....	.051	.084	.105	.007
1600	.0010	.0030	.083	0.227	0.39	.....	.....	.....	.055	.096	.119	.006
1800	.0009	.0032	.088	0.325	.....	.....	.....	.....	.057	.110	.135	.006
2000	.0008	.0034	.090	.....	.....	.....	.....	.....	0.056	0.124	0.152	0.006
2500	.0006	.0040	.061	.....	.....	.....	.....	.....	.....	.....	.....	.....
3000	0.0006	0.0052	0.042	.....	.....	.....	.....	.....	.....	.....	.....	.....

* These are subject to considerable uncertainty because of the clustering of highly luminous B stars in this area.

minimum at 600. In the region from 1000 to 2000 parsecs the density remains about 0.6 of that in the solar neighborhood. The dwarfs increase in number, on the average, in the first 600 parsecs from the sun. There are, however, distinct fluctuations, with maxima occurring at 200 and 500 parsecs and a minimum at 300 parsecs. Part of this behavior may be due to the assumed variation of the percentage of dwarfs with magnitude. One must therefore accept such wide fluctuations with some reservation.

e) The late-type giants, G8–M, appear to decrease with the distance as far as the limit of the survey, 2000 parsecs.

Others[12] have shown that the surface density and also the space density of A stars within 500 parsecs of the sun is high in this area of Cepheus. A comparison of the densities

[12] Pannekoek, *Amsterdam Pub.*, Vol. 2, 1929; Malmquist and Hufnagel, *Stockholm Obs. Ann.*, Vol. 11, No. 9, 1933; Fr. Tibor, *Acta della Pontifica accad. delle sci.*, 1, 85, 1937; Schalén, *Upsala Medd.*, No. 37, 1928, and No. 55, 1932.

found by Risley[13] in her recent analysis of the bright Cepheus region with those of Table 6 indicates good *relative* agreement, as may be seen in the accompanying tabulation for the

	r (Parsecs)				
	100	200	300	500	1000
Risley	0.12	0.16	0.15	0.13	0.06
McCuskey	0.13	0.23	0.24	0.22	0.10

B8–A0 stars. The rigid restriction of our data to the bright cloud accounts for the larger absolute densities exhibited in the third line. Risley's data cover 80 square degrees, ours only 17 square degrees at the center of the cloud area. There seems to be little doubt of the high concentration of early A stars in this area. On the other hand, Table 6 shows no indication of a clustering of A2–A5 stars.

RELATIVE DENSITIES FROM GENERAL STAR COUNTS

In spite of the lower precision obtainable by use of general star-count data, it seems worth while to present briefly the results of an analysis of faint star counts in LF4. Of course, for $m_{pg} < 12.5$, the totals shown in the last column of Table 1 suffice for the data.

TABLE 7

FAINT-STAR COUNTS IN LF4

m_{pg}	log $N(m)$			m_{pg}	log $N(m)$		
	LF4	Van Rhijn	Risley (M)		LF4	Van Rhijn	Risley (M)
9	0.75	0.55	0.80	14	2.81	2.59	2.65
10	1.16	1.03	1.25	15	3.18	2.95	3.05
11	1.58	1.45	1.63	16	3.50	3.31	.....
12	2.00	1.84	2.03	17	3.85	3.67	.....
13	2.41	2.22	2.36	18	4.20	4.03	.....

For the stars with $12 < m_{pg} < 18$, counts were made as already indicated in four sample areas symmetrically situated with respect to the center of LF4. Two plates were counted, the average absolute difference between the values of log $N(m)$ being 0.02 over the magnitude range 12–18.

Table 7 shows the values of log $N(m)$, where $N(m)$ is the number of stars brighter than or equal to m per square degree. For comparative purposes the counts published by Risley for region M are also shown, together with the values of log $N(m)$ from *Groningen Pub.*, No. 43, Table 10, by van Rhijn. The excess of stars in this core of the Cepheus cloud is quite marked even among the fainter stars.

By means of an $(m, \log \pi)$ tabular analysis employing the luminosity function of van Rhijn,[14] the density distribution of the fainter stars has been computed. Modification of the luminosity function has been made to take into account the decrease in the number of highly luminous stars with distance from the galactic plane. Corrections for absorption

[13] *Ap. J.*, **109**, 319, 1949.

[14] *Groningen Pub.*, No. 47, 1936.

according to the curve of Figure 2 were applied. The resulting values of relative space density as a function of distance are given in Table 8. The third column gives a relative density function computed from our data in Table 6. The excess in density indicated when the usual luminosity function is used for analysis clearly shows that this stellar cloud, within 400 parsecs of the sun, has a population about 2.2 times that of the solar neighborhood. As a consequence of the lower absorption used by Risley in computing the density function for her region *M*, the densities obtained by her and shown in the fourth column of Table 8 are somewhat smaller than those found in LF4.

TABLE 8

RELATIVE DENSITY FUNCTIONS FROM GENERAL STAR COUNTS

Distance (*r*) (Parsecs)	*D*(*r*)			Distance (*r*) (Parsecs)	*D*(*r*)		
	Counts	Spectra	Risley (*M*)		Counts	Spectra	Risley (*M*)
100	1.80	1.00	1.00	600	1.35	.....	1.10
200	1.74	0.86	1.20	1000	1.20	.....	0.55
300	1.53	0.76	1.20	1500	1.18	.....	0.25
400	1.44	0.48	1.20	2000	1.13	.....	0.15
500	1.37	0.53	1.20				

TABLE 9

LUMINOSITY FUNCTIONS IN LF4
(log $\varphi[M] + 10$)

M_{pg}	Distance (Parsecs)				Standard
	100	200	400	600	
−2	4.89	4.76	4.56	4.41	4.75
−1	5.38	5.43	5.38	5.30	5.07
0	5.88	6.06	6.05	5.97	5.68
+1	6.39	6.44	6.36	6.26	6.34
+2	6.76	6.73	6.60	6.48	6.77
+3	7.02	7.00	6.90	6.84	6.86
+4	7.18	7.23	7.28	7.28	7.19
+5	7.25	7.34	7.42	7.45	7.35
+6	7.57	7.58	7.61	7.65	7.50
+7	7.76	7.64	7.63	7.64	7.53

VARIATIONS IN THE LUMINOSITY FUNCTION

It is very apparent from the relative density functions exhibited in Table 8 that there must be in LF4 an excess of the intrinsically bright stars over the number predicted on the basis of the standard luminosity function of van Rhijn. This effect has been found in all the LF regions studied thus far. LF4 is situated in an area of marked clustering of highly luminous (OB) stars studied by Nassau and Morgan[15] in an extensive survey of the

[15] Unpublished data. A report of the survey was made at the symposium on galactic structure, at the University of Michigan, June, 1950.

galactic belt. In the 16.9 square degrees of LF4 there are eighteen of these objects, while in the surrounding area of 100 square degrees the total number is three times as great. These, however, show a tendency to cluster at a distance much greater than we are considering in the construction of the luminosity function.

We can compute from the density functions of Table 6 a luminosity function at those distances for which the spectral data can be considered relatively complete. Table 9 shows the values of log $\varphi(M)$[16] so computed for distances of 100, 200, 400, and 600 parsecs. The assumption is that the absolute magnitudes of the stars of each spectral group are distributed in a Gaussian fashion about the same mean M_0 per unit volume and with the same σ_0 as were used in computing the densities.

In Table 9 the right-hand column gives the standard van Rhijn luminosity function for comparison. All these functions are plotted in Figure 3. One sees at a glance that for M

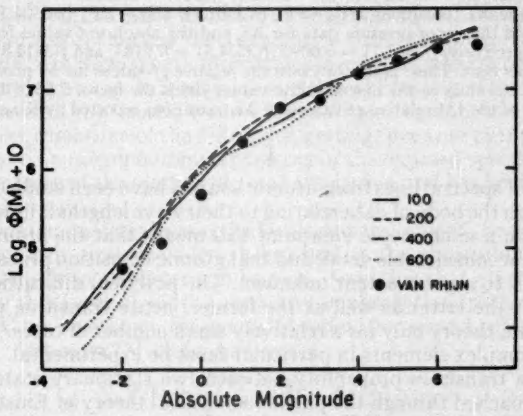

FIG. 3.—Observed luminosity functions in LF4. The large dots represent the standard van Rhijn function. The curves represent log $\varphi(M)$ at 100, 200, 400, and 600 parsecs.

between -2 and $+1$ the values of log $\varphi(M)$, on the average, exceed those of the standard function by about 0.3. Furthermore, there appears to be very little over-all difference between the functions computed at the various distances. It should be noted that, in making the computation for 400 and 600 parsecs, the density of dG8–K3 stars was assumed to be 8.4 stars per 1000 cubic parsecs, the value at 300 parsecs. The density of the dG5 stars at 600 parsecs was taken to be the same as at 400 parsecs.

No attempt has been made to allow for the above-mentioned cluster of luminous B stars in the luminosity function for LF4. At present their absolute magnitudes and colors are being studied, and ultimately they may be used to strengthen the conclusions reached in this area. We leave for future discussion also a detailed comparison of these luminosity functions with those found in the analyses of the other LF regions. It is sufficient to say here that the core of the Cepheus bright cloud appears to be a region rich in stars of all spectral types, but particularly of the early A stars.

[16] $\varphi(M)$ is the number of stars per cubic parsec with absolute magnitude $M - \frac{1}{2}$ to $M + \frac{1}{2}$.

ABSOLUTE OSCILLATOR STRENGTHS OF CHROMIUM AND NICKEL

FRANK B. ESTABROOK*
California Institute of Technology, Pasadena, California
Received November 2, 1950

ABSTRACT

By the method of total absorption, absolute *nf*-values have been obtained for the resonance triplet of *Cr* $a^7S_3-z^7P^\circ_{2,3,4}$, respectively λλ 4290, 4275, and 4254. These do not agree with existing vapor-pressure data for *Cr*, but, using the best of such data available, the tentative assignment of absolute *f*-values for these transitions is: $f(4290) = 0.0068$, $f(4275) = 0.0097$, $f(4254) = 0.0122$.

Similar work on the *Ni* transitions $a^3D_3-z^3F^\circ_4$ (λ 3461.7), $a^3D_3-z^3P^\circ_4$ (λ 3524.5), and $a^3D_3-z^3F^\circ_4$ (λ 3414.8) corroborated the vapor-pressure data for *Ni*, and the absolute *f*-values for these transitions were found to be, respectively, $f(3461.7) = 0.0093$, $f(3524.5) = 0.0183$, and $f(3414.8) = 0.0171$, with a probable error of 10 per cent. These agree well with the relative *gf*-values for *Ni* previously reported by R. B. King. A fit of his values to the new absolute values yields the factor 2.55×10^{-8}, multiplication by which reduces any of the 134 relative *gf*-values for *Ni* transitions reported by King to the corresponding absolute *gf*-value.

I

The intensities of spectral lines from atomic sources have been studied occasionally in recent years, though the body of data relating to their wave lengths is much more detailed and accurate. From a microscopic viewpoint this means that the atomic energy-levels have been located in considerable detail and that atomic transition probabilities between these levels remain to a great extent unknown. The practical difficulties of theoretical computation beset the latter as well as the former; hence transition probabilities are reliably known from theory only for a relatively small number of cases.[1] The determinations for heavy, complex elements in particular must be experimental.

The notion of a transition probability between two stationary states of an atom is perhaps best approached through the phenomenological theory of Einstein. Briefly, if u refers to the level of higher energy and l to that of lower energy, we let A_{lu} be the probability per unit time that an atom in the upper state will spontaneously "jump" to the lower, emitting a quantum $h\nu$. If u_ν is the electromagnetic energy density per unit frequency range present at the frequency ν, the probability per unit time of absorption of a quantum by an atom in the lower state is proportional to u_ν and will be denoted by $u_\nu B_{ul}$. The probability per unit time that an atom in the upper state will be induced to jump to the lower (and emit a photon) will be denoted by $u_\nu B_{lu}$. Postulating detailed balance in the equilibrium of atoms and radiation at temperature T then leads to

$$g_l B_{ul} = g_u B_{lu} = \frac{g_u A_{lu} c^3}{8\pi h \nu^3},$$

where the g's are the statistical weights of the states.

Anomalous dispersion and line absorption are classically regarded as being due to resonance effects of the bound electrons in a medium traversed by light. If there be $\mathfrak{N}$ such induced dipoles per unit volume, one can then obtain[2] the classical formulae of normal and anomalous dispersion. It was shown in 1927 by Schrödinger and Heisenberg that these formulae may all be taken over in a modern formulation by recognizing that $\mathfrak{N}$ is *not* equal to the number of excited atoms per unit volume N; rather, we must set $\mathfrak{N} = Nf$,

* Now at Miami University, Oxford, Ohio.

[1] D. R. Bates and A. Damgaard, *Phil. Trans. R. Soc. London, A*, **242**, 101, 1949.

[2] See, e.g., R. Becker, *Theorie der Elektrizität*, Vol. 2 (Berlin: Teubner, 1933).

where f is called the *oscillator strength* of the transition. The expression for f in terms of the matrix elements for the transition is given in the *Handbuch* article of H. Bethe.[3] If white light is passed through a rarefied medium, on the basis of the classical theory the power absorbed per unit volume may be shown to be $\pi \mathfrak{N} e^2 u_\nu / m$. The phenomenological theory gives the same quantity to be $N u_\nu B_{ul} h\nu$. Equating these, we obtain the relationship between the Einstein coefficients and the oscillator strength:

$$f = \frac{m h\nu}{\pi e^2} B_{ul} = \frac{m c^3}{8\pi^2 e^2 \nu^2} \frac{g_u}{g_l} A_{iu}.$$

The results of this work will be reported as oscillator strengths, or f-values, for the transitions investigated.

II

The experimental method used was that of determining A_λ, the *equivalent width* or *total absorption* of an absorption line. This quantity is customarily expressed in Angstrom units and is the effective wave-length interval removed from a beam of continuous light by a layer of absorbing atoms. It is easily shown that the folding of the natural shape of the absorption line with the "window curve" of the spectrograph (due to the finite slit-width and imperfect resolution of the diffraction grating) does not change the equivalent width as measured on a microphotometer tracing of the exposed spectrogram. This is a very convenient feature of the method of total absorption and has been verified experimentally by R. Minkowski.[4]

If the incident continuous light be practically plane-parallel, let S_λ be the incident power per unit cross-section in unit wave-length interval at the absorption frequency. The resonant energy density in the layer will be S_λ / c. Assuming that all the excited atoms Nl in the optically thin layer of width l are active in absorption (picturesquely, none of them are shadowed by the others), the energy absorbed per second per unit cross-section will be $h\nu N l u_\nu B_{ul}$. Also $u_\nu = (\lambda^2/c^2) S_\lambda$. And hence

$$A_\lambda = \frac{h\nu N l B_{ul} (\lambda^2/c^2) S_\lambda}{S_\lambda} = \frac{\pi e^2 \lambda^2}{m c^2} N l f.$$

This is, of course, a linear approximation based on the assumption of optical thinness. The exact functional dependence of A_λ on Nlf is the so-called "curve of growth."[5] With larger equivalent widths, the absorbing layer is no longer optically thin for wave lengths near the center of the line, and the "growth" of the line with increasing Nlf becomes dependent on the line shape, especially in the wings. The method of total absorption is applicable with accuracy only on the linear and lower Doppler regions of the curve of growth, where pressure and natural damping effects are absent. If care is taken to maintain thermal equilibrium in the vapor comprising the absorbing layer, $N = N_0 (g_l/g_0) \exp(-E_l/kT)$; here N_0 is the population of the ground state and is, in turn, calculable if the total population $n = P/kT = \sum_l N_0 (g_l/g_0) \exp(-E_l/kT)$ can be determined. In the present investigation the vapor was confined in equilibrium with the solid. The weakest link in the entire calculation was P, as reliable measurements of the vapor pressures of solids exist for surprisingly few substances.[6] Hence the results of this work will be reported first as the product nf and then as f, where this latter is calculated using the best obtainable values of P from the work of other investigators.

[3] *Handbuch der Physik*, Vol. **24**, Part I (Berlin: J. Springer, 1933).

[4] *Zs. f. Phys.*, **36**, 839, 1926.

[5] See, e.g., A. Unsöld, *Physik der Sternatmosphären* (Berlin: J. Springer, 1938).

[6] Ditchburn and Gilmour, *Rev. Mod. Phys.*, **13**, 310, 1941.

III

The elements to be studied were introduced into small quartz absorption cells, 1 inch in diameter and approximately ½ inch long. This last dimension, *l*, the length of the column of absorbing vapor, was obtained by micrometering the end-plates of the absorption cell before they were welded onto the cylindrical side wall and by subtracting their thickness from the over-all depth of the completed cell. The cells were then baked out and sealed under a pressure of less than 1 μ.

The doubly wire-wound electric resistance furnace in which the cells were heated has been described by King and Stockbarger,[7] and the operating techniques were essentially those used by them.

The continuous light-source used for the *Cr* investigation was a 1-kv, 30-ampere, 4-coil projection lamp, overloaded to 33 amperes. About 15 minutes' exposure of the photographic plate was required to record a continuum of proper density at λ 4200. For the *Ni* investigation (at around λ 3400) a quartz, water-cooled, super-high-pressure *Hg* arc lamp was used. This lamp is similar in type to the Bol lamp made by Philips[8] and was constructed by the Huggins Laboratories, Menlo Park, California. In the spectral region used, 10 minutes' exposure gave a continuum of proper density. This continuum was crossed at the *Hg* lines by regions of greater intensity, which fortunately did not occur close to the *Ni* lines being investigated.

The spectrograph used was the 15-foot vertical Rowland spectrograph of the Mount Wilson Observatory. In the second order it has a dispersion of 1.86 A/mm. Fine-grain, high-contrast plates were used, both Eastman IV-O and Cramer Contrast, the Cramer plates being ultimately adopted because of slightly higher speed and greater uniformity of emulsion. These plates, 3 × 10 inches, were cut lengthwise, one half being used for the exposure, the other half for a calibration plate. The two halves were then developed simultaneously in D-19 developer.

IV

Experimental work has been done on the vapor pressure of *Cr* by Baur and Brunner,[9] and an extensive catalogue of relative *f*-values for *Cr* transitions has been obtained by Dr. Armin Hill[10] at the California Institute of Technology. Therefore, absolute determination of oscillator strengths for a few *Cr* transitions should be possible, and these would be of value in reducing Hill's catalogue to absolute values.

Cr has a strong resonance triplet in the visible, which was easily observable in absorption at temperatures around 1150° C. These three transitions are $a^7S_3 - z^7P^o_{2,3,4}$, respectively $\lambda\lambda$ 4290, 4275, and 4254. The results to be reported were derived from one plate taken during one furnace run. This plate carries five exposures, at temperatures ranging from 1137½° to 1164° C. Each line on each exposure was microphotometered five times. The relative *f*-values, computed at each temperature, had about a 3 per cent average deviation from exposure to exposure. Their averages were in the ratio 0.56 : 0.79 : 1.00, which is within 2 per cent of the 5 : 7 : 9 ratio of their statistical weights. This ratio has also been confirmed by Hill.

The ground state of *Cr* is single and is well separated from the first excited state. Hence for these transitions $N = n$, and values of nf were obtained directly from the measured equivalent widths and the curve of growth. These are given in Table 1 and are plotted against T in Figure 1. The general trend of the curves for the three lines shows the increase of vapor pressure with temperature, and the scatter is indicative of the random errors. If the vapor-pressure equation of Baur and Brunner is used to reduce

[7] *Ap. J.*, **91**, 488, 1940.

[8] C. Bol. *Das Licht*, **5**, 84, 1935; *Ingénieur*, **50**, 91, 1935.

[9] *Helvet. chim. acta*, **17**, 958, 1934.

[10] Thesis, California Institute of Technology, 1950 (in press).

these results to absolute *f*-values, the *f*-values appear to increase with *T*. On the other hand, if the equation arrived at from free-energy considerations by K. K. Kelley[11] is used, the *f*-values appear to decrease with *T*. There is, furthermore, a large difference in the order of magnitude of *n* as computed from these two sources: at 1150° C Baur and Brunner measured a pressure corresponding to *n* of the order of 10^{15} atom/cc, while calculations based on Kelley's work give *n* to be of the order of 10^{12} atom/cc. Thus, if Baur and Brunner's data were adopted, the *f*-values for these strong resonance transitions would be of the order of 10^{-5}, which is incredibly small.

It was concluded that the data of Baur and Brunner are incorrect, and, for lack of better, the absolute *f*-values for the three transitions were tentatively calculated with the

TABLE 1

EXPERIMENTAL *nf*-VALUES FOR *Cr*

λ	1410°5 K	1425° K	1423° K	1436° K	1437° K
4290.....	2.42×10^{10}	2.84×10^{10}	2.74×10^{10}	4.05×10^{10}	3.86×10^{10}
4275.....	3.53	4.02	4.14	5.67	4.93
4254.....	4.47	5.40	5.26	6.55	6.28

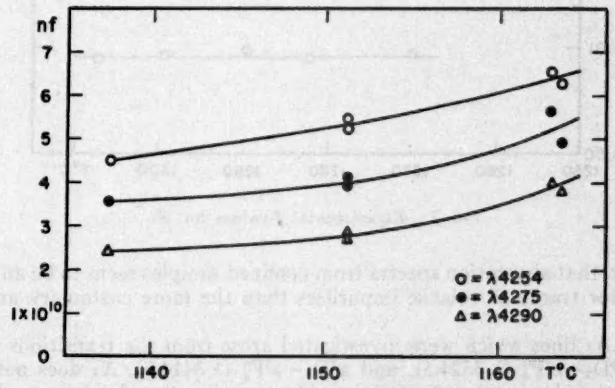

FIG. 1.—Experimental *nf*-values for *Cr*

vapor-pressure expressions given by Kelley. Systematic deviations of these *f*-values at the lowest temperature again emphasize that the trend of the present *nf*-values is not in good agreement with Kelley's curve. Recognizing this provisional validity, the averaged absolute *f*-values so calculated may be reported: $f(4290) = 0.0068$, $f(4275) = 0.0097$, $f(4254) = 0.0122$. The values of *nf*, which are good to a probable error of around 7 per cent, can again be reduced to absolute *f*-values when further work is done on the vapor pressure of *Cr*.

V

The relative *gf*-values for some 134 lines in the near ultraviolet spectrum of *Ni* have been reported by R. B. King,[12] who also includes for comparison on the same relative

[11] *Contributions to the Data on Theoretical Metallurgy III* (Bull. 383, U.S. Bureau of Mines, 1935).

[12] *Ap. J.*, **108**, 87, 1948.

scale some 50 measurements of arc emission intensities by H. van Driel.[13] The vapor pressure of *Ni* has been calculated by Kelley, principally on the basis of work by Jones, Langmuir, and Mackay.[14] More recently, the vapor pressure has been redetermined by Johnston and Marshall,[15] whose values of n (near 1300° C) are about two-fifths those of Kelley. The work of Johnston and Marshall, done in the General Electric laboratories, agrees well with the original data of Jones, Langmuir, and Mackay and appears very reliable. They estimate their error at no more than 5 per cent.

The *Ni* used was electrolytically purified and showed no traces of impurities in an arc spectrum. In the absorption spectrum, however, where the metal was confined in a quartz cell, the resonance absorption lines of both *Na* and *Ag* were detectable. The vapor pressures of both these elements are quite high relative to *Ni*, and the fairly weak absorption lines which they gave at around 1300° C showed that they were present in amounts which would not influence the vapor pressure of the *Ni*. It is of interest to

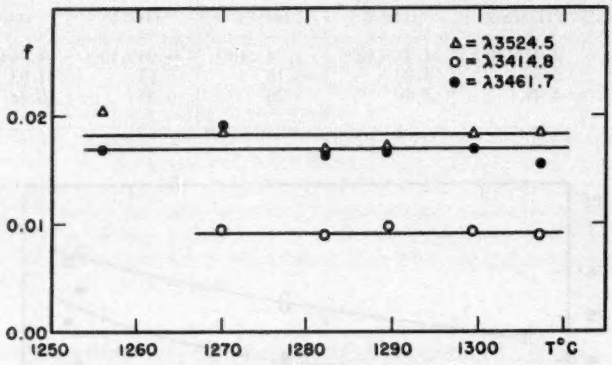

FIG. 2.—Experimental f-values for *Ni*

note, however, that absorption spectra from confined samples seem to be an even more delicate test for traces of volatile impurities than the more customary arc emission spectra.

The three *Ni* lines which were investigated arose from the transitions $a^3D_3 - z^5F_4^\circ$ (λ 3461.7), $a^3D_3 - z^3P_2^\circ$ (λ 3524.5), and $a^3D_3 - z^3F_4^\circ$ (λ 3414.8). *Ni* does not possess a single, well-isolated ground state. It has, rather, some seven closely spaced low levels with excitation energies ranging up to 3410 cm^{-1}, over which a summation must be taken at a given temperature to compute the fractional population of any one of them.

The *Ni* data that were obtained agreed with the vapor-pressure curve given by Johnston and Marshall. The results from one plate are shown in Figure 2, in which f is plotted against T for the three observed lines. The horizontal lines shown in this figure represent the average f-values derived. These are: $f(3461.7) = 0.0093$, $f(3524.5) = 0.0183$, and $f(3414.8) = 0.0171$. The over-all probable error for these f-values, considering the 5 per cent probable error reported by Johnston and Marshall for their vapor-pressure data, is probably about 10 per cent.

King reports relative gf-values for these three lines of 2400, 5500, and 4500, respectively, while he gives the relative gf-values of van Driel on the same arbitrary scale to be

[13] Thesis, University of Utrecht, 1935.

[14] *Phys. Rev.*, **30**, 201, 1927.

[15] *J. Amer. Chem. Soc.*, **62**, 1382, 1946.

3560, 5810, and 5270. A fit of the new absolute values to the relative values of King for these three lines results in the conversion factor 2.55×10^{-5}. This number, multiplied by any one of the relative *gf*-values of King's table, should then give the corresponding absolute *gf*-value.

The three experimental absolute *f*-values derived in the present work, multiplied by 7 (*g* for a^3D_3), and divided by 2.55×10^{-5}, give, respectively, 2550, 5020, and 4690 as the new relative *gf*-values on King's arbitrary scale. These compare well with King's previous results and differ considerably and systematically from those of van Driel.

I would like to record my gratitude to Professor Robert B. King for his continued encouragement, guidance, and aid. The experimental work was done in the laboratory of the Mount Wilson Observatory, all of whose facilities were most generously made available to me.

THE USE OF CALCULATED AND OBSERVED ENERGIES IN THE COMPUTATION OF OSCILLATOR STRENGTHS AND THE *f*-SUM RULE*

LOUIS C. GREEN, NANCY E. WEBER, AND ELEANOR KRAWITZ
Strawbridge Observatory, Haverford College
and
Watson Scientific Computing Laboratory, Columbia University
Received December 19, 1950

ABSTRACT

The oscillator strengths or *f*-values for all transitions of importance from the 3d state of *Ca* II have been computed, using wave functions with and without exchange. Each value has been determined by the use of the calculated as well as the observed energies. The *f*-sum rule is well satisfied by the results with and without exchange if calculated energies are employed. However, the *f*-values for particular transitions differ considerably. The meaning of the results is considered. The size of the total *f*-value for the 3d−f continuum appears to be even larger than was suggested by earlier work.

Values of the oscillator strengths for all transitions of importance from the 3d state of *Ca* II have been determined. The calculations are based on numerical wave functions from Hartree self-consistent fields both with and without exchange. This work was undertaken primarily for three reasons: In the first place, earlier results[1, 2] had indicated that the total oscillator strength or *f*-value for the 3d−f continuum of *Ca* II is distinctly larger than would be expected on the basis of a comparison with hydrogen. None of the earlier sets of wave functions included exchange in a systematic way, and it seemed probable that better values for $df/d\epsilon$ could be obtained without undue effort by the inclusion of exchange. Since *f*-values for transitions between excited states have often been assumed to be hydrogen-like, it appeared to be worth while to investigate with some care the present case of a probable deviation. Second, previous work[3] had suggested that more meaningful *f*-values were obtained by the use of calculated, rather than observed, energies, and it seemed wise to test this suggestion, in so far as possible, by determining to what extent the *f*-sum rule was satisfied in each case. Satisfaction of the sum rule could not be taken as establishing the physical reality of the *f*-values obtained, but a failure to satisfy the rule would indicate inferior values. Third, in view of the physical reliability which has occasionally been attributed to *f*-values which do satisfy the *f*-sum rule, it appeared to be desirable to place side by side for the same transitions two rather different sets of *f*-values, both satisfying the *f*-sum rule.

With these objectives in view, it was decided to find *f*-values for all important transitions from the 3d state to discrete f states and the f continuum and to discrete p states and the p continuum. The *f*-values were found both from wave functions with exchange and from wave functions without, and in each case two values were obtained, one with the calculated energy and one with the observed.

* This work was supported in part by the Office of Naval Research, Contract No. N8 onr-570 Project No. NR 010-016 administered by Yale University, and Contract No. N onr-04300 Project No. NR 010-022 administered by the University of Pennsylvania.

[1] L. C. Green, *Ap. J.*, **109**, 289, 1949.

[2] L. C. Green and N. E. Weber, *Ap. J.*, **111**, 587, 1950.

[3] *Ibid.*, p. 582.

WAVE FUNCTIONS

The wave functions with exchange for the core electrons and for the 4s, 4p, and 3d electrons have been given by Hartree.[4] The wave functions without exchange for the core electrons have also been given by Hartree.[5] The other wave functions were derived by numerical integration of the radial part of the Schrödinger equation with the self-consistent field without exchange given by Hartree. The actual integrations were carried out by a rapid method on the relay calculators of the Watson Scientific Computing Laboratory of the International Business Machines Corporation at Columbia University.[6]

Convenient forms have already been given for the dipole moment, momentum, and acceleration expressions for the f-value for transitions between discrete states and for the $df/d\epsilon$-value for transitions to the continuum.[2, 3]

RESULTS

The results of the calculations are presented in the accompanying tables. Table 1 contains the $df/d\epsilon$-values as found from the expression involving the dipole moment for the 3d—f continuum. The columns contain the following information: the first column gives

TABLE 1

VALUES OF $df/d\epsilon$ FOR THE 3d—f CONTINUUM OF *Ca* II

ϵ	Without Exchange		With Exchange		ϵ	Without Exchange		With Exchange	
	Obs.	Calc.	Obs.	Calc.		Obs.	Calc.	Obs.	Calc.
0.00.....	1.499	1.017	1.182	1.053	2.00.....	0.032	0.029	0.141	0.137
0.20.....	0.605	0.452	0.777	0.710	3.00.....	0.016	0.015	0.083	0.082
0.50.....	0.243	0.196	0.486	0.454					
1.00.....	0.093	0.080	0.291	0.277	Total f.	0.470	0.377	0.975	0.925

the energy of the free electron in units of the ionization energy of H; the second and third give $df/d\epsilon$ calculated from wave functions without exchange, using the observed and the calculated energy differences, respectively (these values are taken from an earlier paper[2]). Throughout the present paper the expression "calculated energies," when used in connection with results obtained without exchange, will be taken to refer to ϵ-values. Since the derivation of the sum rule for a single electron is based on a fixed field, the ϵ-values rather than the quantities obtained by the customary procedure from Slater integrals are identified with the energy. This identification is supported by the fact that the energy for the 3d electron is made more negative by 0.166 by the inclusion of the Slater integrals, while the energies of the f electron cannot be much varied, as shown below. These changes result in energy differences which lead to a much poorer value for the f-sum. The fourth and fifth columns give $df/d\epsilon$, using observed and calculated energy differences, respectively, when the 3d wave function includes exchange but the f continuum wave functions do not. It is felt that the fourth and fifth columns contain almost the same results as would be found if exchange were included in the f continuum wave functions. Two arguments uphold this view: first, the eigen-value for the 4f electron for the field without exchange was only 0.002 units in ϵ higher than the observed energy, and therefore the 4f wave function cannot differ greatly from the true wave function and should differ even

[4] D. R. Hartree and W. Hartree, *Proc. R. Soc. London*, *A*, **164**, 167, 1938.

[5] *Ibid.*, **149**, 210, 1935.

[6] L. C. Green, *A.J.*, **54**, 186, 1949 (to be described more fully elsewhere).

less from the wave function with exchange. Second, three different f continuum wave functions for $\epsilon = 0.000$, one function without exchange from a field without exchange, one without exchange from a field with, and one with exchange from a field without, showed no difference as great as 0.4 per cent in the magnitude or positions of the maxima or the positions of the zeroes over the range of interest. The final line in Table 1 gives the total f-value for the continuum as found from the $df/d\epsilon$-values.

Table 2 contains the f-values as found from the expression involving the dipole moment for the 3d—nf series in *Ca* II. The first column gives the value of n for the series electron. In the third line from the bottom the symbol "13–∞" indicates that the following columns contain the estimates of the sum of the f-values for all transitions from 3d—13f to the series limit. The second line from the bottom gives the total f for the continuum taken from Table 1. The final line gives the sum of all f-values for transitions from the 3d state to all f states. The second and third columns give the f-values calculated with a 3d wave function without exchange, using the observed and calculated energy differences, respectively. The fourth and fifth columns give the analogous information when

TABLE 2

f-VALUES FOR THE 3d—nf SERIES IN *Ca* II

n	WITHOUT EXCHANGE		WITH EXCHANGE		n	WITHOUT EXCHANGE		WITH EXCHANGE	
	Obs.	Calc.	Obs.	Calc.		Obs.	Calc.	Obs.	Calc.
4.....	1.254	0.651	0.267	0.226	11.....	0.011	0.007	0.008	0.007
5.....	0.275	.162	.108	.093	12.....	.008	.005	.006	.006
6.....	0.110	.068	.059	.051	13–∞.....	.041	.028	.029	.026
7.....	0.057	.036	.034	.030	Cont.....	0.470	0.377	0.975	0.925
8.....	0.034	.022	.022	.019					
9.....	0.022	.014	.015	.013	Total f.	2.297	1.380	1.533	1.405
10.....	0.015	0.010	0.010	0.009					

the 3d wave function includes exchange. In view of the similarity mentioned above of the f wave functions with and without exchange, a 4f function was obtained by numerical integration from a field without exchange and used for both cases. The 5f, 6f, and 7f wave functions were taken to be identical with the hydrogen wave functions for these same electrons. This procedure was thought to be acceptable for two reasons: first, the eigen-value found for the 4f electron was only 0.0002 more negative than the corresponding eigen-value for hydrogen. This difference should decrease for increasing n. Second, the result of a calculation of the f-value for the 3d--4f transition using the 3d wave function with exchange and the hydrogen wave function for 4f differed by only 0.001 from the result of a similar calculation, using the numerically determined 4f wave function. Here also the difference should decrease for increasing n. The f-values for the 3d—nf transitions from $n = 8$ to $n = 12$ were found in the following way: the ratio of the square of the radial integral for the dipole moment for *Ca* II to the corresponding integral for hydrogen for $n = 4, 5, 6, 7$, and ∞ was plotted as a function of $1/n^2$. The ratio for $n = \infty$ was found from the $df/d\epsilon$-value at $\epsilon = 0$ for *Ca* II and from the asymptotic formula for the square of the dipole moment for the discrete transitions for H.[7] A smooth curve was drawn through these five points, and the values of the ratio for $n = 8$ to $n = 12$ were read off. The f-values for *Ca* II were then obtained from the known values for the square of the dipole moment for H. The sum of the f-values for all transitions from 3d—13f to the series limit was obtained, using an average value for both the ratio and the energy

[7] H. Bethe, *Handbuch der Physik*, 2. Aufl., **24**, Part 1 (Berlin: J. Springer, 1933), 442.

difference and the known value for the sum of the squares of the corresponding dipole moments for H.

Table 3 contains the f-values as found from the expression involving the dipole moment for the 3d—np series in *Ca* II. The arrangement of the table is similar to that of Table 2. For the case without exchange, the 2p wave function was taken directly from Hartree[5] (he gives the same function for both *Ca* and Ca^{++}), and the 3p was found from his values by an interpolation on the basis of the energy. The energies for the 2p and 3p of Ca^{+}, when the single valence electron is 3d, were taken as the mean of the values found by first-order perturbation calculations from *Ca* and Ca^{++}, $\epsilon_{2p} = -25.97$ and $\epsilon_{3p} = -2.543$, with a difference between the two calculations of 0.C6 and 0.043, respectively. As pointed out below, these are not precisely the correct wave functions or energies for the present purpose, but it is thought that the differences are small. The 4p, 5p, and 6p wave functions were found by numerical integration. Since for the Hartree field

TABLE 3

f-VALUES FOR THE 3d—np SERIES IN *Ca* II

n	Without Exchange		With Exchange	
	Obs.	Calc.	Obs.	Calc.
2	−0.011	−0.011	−0.037	−0.039
3	− .263	− .268	− .377	− .402
4	+ .236	− .139	+ .098	+ .043
5	+ .054	+ .025	+ .003	+ .008
6	+ .007	+ .004	+ .001	+ .001
7	+ .002	+ .002	.000	.000
8	+ .001	+ .001	.000	.000
9–∞	.000	.000	.000	.000
Cont.	+0.003	+0.003	+0.003	+0.003
Total f for 3d—np series and continuum	+0.029	−0.383	−0.309	−0.386
Total f for 3d—np and 3d—nf series and continua	+2.326	+0.997	+1.224	+1.019

without exchange the order in regard to energy of the 3d and 4p electrons is reversed from the experimental order, the f-value for this transition appears with a negative sign in the third column. For n = 7, 8, and 9 up to ∞ the same procedure was followed as for Table 2, using a plot of the known values of the ratio of the square of the radial integral for the dipole moment of *Ca* II to that of H. The total f-value for the continuum was taken from earlier work.[1] For the case of exchange, Hartree[4] gives the 2p and 3p wave functions only for Ca^{++}, but these functions were used in view of the small change from *Ca* to Ca^{++} for the case without exchange. The energies were again found by perturbation calculations, $\epsilon_{2p} = -27.28$ and $\epsilon_{3p} = -2.802$. The 4p wave function with exchange is given by Hartree. For n = 5, 6, 7, 8, and 9 up to ∞, it seemed adequate to use a plot as above by drawing a curve of similar shape to that for the case without exchange through the points of known ratio at n = 4 and n = ∞. The total f-value for the continuum was estimated from earlier work,[1] in which only the bound-state wave function included exchange and from the difference between the previously used continuous wave function and that given by Bates and Massey[8] for $\epsilon = 0$, which includes exchange. To obtain "observed

[8] *Proc. R. Soc. London, A*, **177**, 329, 1941.

energies" for the 2p and 3p electrons, it was assumed that each of these levels lies as far below the ground state of *Ca* II as the $2p^{-1}$ and $3p^{-1}$ states of the X-ray spectrum lie above, 25.58 and 1.87 units in ϵ, respectively.[9] The observed energy differences between 3d and 2p and 3p are then -25.70 and -2.00, respectively. As is pointed out below, this choice would appear to yield quantities comparable to the predictions of the *f*-sum rules for the "one-electron" spectrum of *Ca* II, for which the 2p and 3p energies should be those from a field which takes account of the charge distribution of six 2p and six 3p electrons.[10]

DISCUSSION

The results collected in Tables 2 and 3 can be discussed with the aid of the *f*-sum rules. Of these, the "total *f*-sum rule" gives the sum of the *f*-values for all transitions from a state, and the "partial *f*-sum rule" gives the sum for transitions for which ΔL is $+1$ or for transitions for which ΔL is -1. These two sum rules have an experimental, as well as a theoretical, basis. However, the experimental material is very limited,[11, 12] and, unfortunately, experimental values are lacking for the series in *Ca* II considered here. On the theoretical side the total-sum rule states that, for one electron moving in a fixed but arbitrary field, the sum of the *f*-values for all transitions from a given state is 1 and that, for N electrons moving in such a field, the sum of the *f*-values for all transitions from a given state is N if the interactions of all the electrons are considered. For a single electron in an arbitrary fixed field, the partial-sum rule gives the sum of the *f*-values for the transitions from a d state to all f states, both discrete and continuous, as 1.400 and from a d state to all p states as -0.400.[13]

For the total *f*-sum for all transitions from a d state, the present computations yield 1.019 and 0.997, using calculated energies, for the fields with and without exchange, respectively, and 1.224 and 2.326, using observed energies. Since no experimental values are available for comparison, the proper theoretical sum is the only recourse. *Ca* I is a "one-electron" spectrum, and it is reasonable to expect the *f*-sum, therefore, to be 1.000. With this criterion, the calculated energies clearly give superior results. Again the partial *f*-sums given in the last line of Table 2 and in the next to last line of Table 3 are in at least moderate agreement with the theoretical partial sum for a single electron wherever the calculated energies have been used and are in poorer agreement or in distinct disagreement wherever the observed energies have been employed.

These results might have arisen from the particular expression used to determine the *f*-values, namely, the radial integral for the dipole moment. To determine whether or not this was the case, the partial *f*-sum for the 3d—nf series for wave functions without exchange was computed, using the dipole momentum and acceleration expressions and the observed energy. Since it is known that the *f*-values given by the three expressions must be identical when wave functions without exchange and calculated energies are used,[2,3] the values of the necessary radial integrals were found from the *f*-values already available. The results of these computations gave the *f*-sum as 0.901 when the dipole momentum form for *f* was used and as 0.343 when the dipole acceleration form was employed. These values strengthen the case for the calculated energies.

The partial *f*-sum for the 3d—nf series for wave functions with exchange and the calculated energies is very close to 1.400. However, this result depends on an extrapolation for the continuum. The question arises as to why the other partial *f*-sums with calculated energies are not closer to the values given by the rule. In the case of the 3d—np

[9] Y. Cauchois and H. Hulubei, *Longeurs d'onde des émissions X et des discontinuités d'absorption X* (Paris: Herman, 1947).

[10] A. Unsöld, *Physik der Sternatmosphären* (Berlin: Julius Springer, 1938),p. 191.

[11] S. A. Korff and G. Breit, *Rev. Mod. Phys.*, **4**, 471, 1932.

[12] Unsöld, *ibid.*, pp. 205–7.

[13] Bethe, *op. cit.*, p. 435.

series the procedure would appear to have involved a sufficient number of approximations of various kinds to account for the discrepancy. For the 3d−nf series without exchange, the difference seemed more surprising; and for this reason the four largest contributions to the sum were completely recomputed by one of the other expressions for the *f*-value. The remaining *f*-values were checked for numerical errors. No significant change was indicated. When the sum of the squares of dipole moments for the series was compared with the value given by the sum rule for this quantity,[14] agreement to better than 1.0 per cent was obtained.

Several other comments seem to be in order. To treat Ca^+ as a problem of one electron moving in a fixed field means strictly that the 2p and 3p wave functions and energies should be derived from the same field as that used for the outer electron, that is, from a field which takes account of the charge distribution of six 2p and six 3p electrons.[10] It is also interesting to note that the procedure involved in including exchange, even when the exchange effects of the outer electron on the core electrons are neglected, is such that the outer electron cannot then be considered as moving in a strictly fixed field because the radial integrals which enter the problem and make the set of differential equations for the exchange case nonhomogeneous are different for each state. The present results would suggest that the differences in these additional terms are not large as compared with that part of the field which is held fixed, namely, the field for Ca^{++}.

The question arises as to why the calculated energies give superior results when the observed energies are, in fact, the true energies. The matter may be looked at in the following way: The two treatments of Ca^+ by the Hartree method with and without exchange represent two levels of approximation, and, although neither corresponds exactly to reality, both are consistent in the sense that the resulting calculated wave functions and energies are logically related. In a very rough way it may be thought of as a matter of "scale factor" in the energy. All the experimentally observed states, except those associated with spin, are present in the theory at these two levels, and a wave function and an energy consistent with it are available for each state. In a general way both schemes give a consistent picture not unlike reality but differing from it in "scale." If one then takes the observed energies and combines these with approximate wave functions, one is using together quantities of different "scale," and it is not surprising that the values obtained are inferior. The results presented above suggest that it is better to use consistent sets of wave functions and energies.

If we now concentrate our attention on the two sets of *f*-values computed with the calculated energies, we note that they satisfy the *f*-sum rules almost equally well. Indeed, since the *f*-values as found from the various expressions involving the dipole moment, momentum, and acceleration integrals would probably differ for the exchange case but would be identical for the case without exchange, the present slight superiority of the exchange results might not be present if another formula had been used. If the satisfaction of the *f*-sum rule or rules is made the only basis of decision, there is not much to choose between the results calculated with and without exchange. Of course, there are other reasons for choosing the results obtained with exchange—for example, the fact that the determinant form for the wave function is more satisfactory theoretically and that, in general, exchange calculations give results in closer agreement with experiment (diamagnetic susceptibilities, etc.). In particular, in the present case the energies for *Ca* II found with exchange give the observed order for the 4s, 4p, and 3d states, whereas the ϵ-values found without exchange do not.

It is also interesting to note that, in spite of the approximate equality of the *f*-sums, the individual *f*-values are very different. Occasionally in the past physical reliability has been assumed for a set of *f*-values because they satisfied the sum rule. This would not be possible here, where the individual *f*-values are so discordant. It is clear that the close

[14] *Ibid.*, p. 436.

approximate satisfaction of the sum rule by a set of f-values is no guaranty of the physical reliability of the f-values.

As pointed out above, there is reason to consider the exchange results as superior and therefore the large size of the 3d—f continuum as given by these calculations as the best estimate of this quantity. In any case there seems to be no doubt that the continuum is very large and not like hydrogen, $f_H = 0.098$. The question at once arises as to why the inclusion of exchange should make so great a difference. An examination of the radial integrals shows that the inward movement of the maximum for the 3d wave function when exchange is introduced is such as to bring this maximum more exactly in phase with the first maximum for the f wave functions and to reduce cancellation from the first negative loop of the f wave function.

SUMMARY AND CONCLUSIONS

The f-values for all transitions of importance from the 3d state of *Ca* II have been computed, using wave functions with and without exchange and both calculated and observed energy differences. Comparison of the sums of these values with the predictions of the f-sum rules strongly suggests that the calculated, rather than the observed, energy differences should be used in computing oscillator strengths.

The two sets of f-values calculated for the 3d—nf series, using wave functions with and without exchange and the calculated energy differences, satisfy the partial f-sum rule equally well. In spite of this approximate equality of the f-sums, the individual f-values are very different. This result makes it very clear that the fact that a given set of f-values satisfies the f-sum rules does not establish the physical reliability of those values.

Probably the most reliable of the sets of f-values computed here are those found from wave functions including exchange and the calculated energy differences. On this basis the total f-value for the 3d—f continuum is found to be even larger than earlier work had indicated. In any case it seems certain that this continuum is considerably stronger than one would predict on the basis of a comparison with hydrogen.

We wish to thank Dr. W. J. Eckert, of the Watson Scientific Computing Laboratory of the International Business Machines Corporation, for having made available the facilities of the laboratory. We must also thank Mr. Robert T. Mertz, of the laboratory staff, and Miss Marjorie M. Mulder, of the Strawbridge Observatory, for their extensive help.

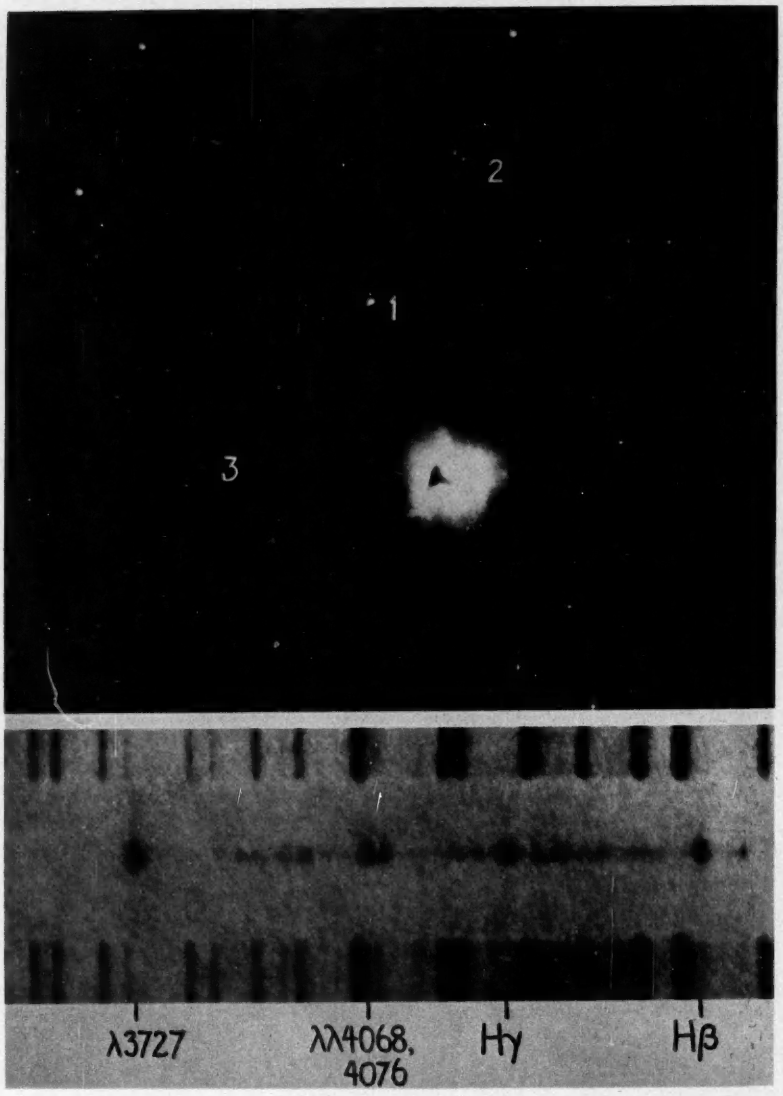

FIG. 1.—*Above:* The region of NGC 1999, with objects Nos. 1, 2, and 3 marked. The negative was obtained with the Crossley reflector on January 20, 1947. The dimensions of the field are 9′.2 by 10′.5. South is at the top and east to the right.

Below: The spectrum of object No. 1, photographed with an exposure of 2.5 hours on November 12, 1950. $H\beta$, $H\gamma$, and λ 3727 are in emission all along the slit, due to faint nebulosity over the entire field. A few night-sky lines also are present.

NOTES

THE SPECTRA OF TWO NEBULOUS OBJECTS NEAR NGC 1999

On a series of direct photographs taken with the Crossley reflector in 1946 and 1947 and centered on the diffuse nebula NGC 1999, there appear several peculiar nebulous objects (Fig. 1). The brighter of these (referred to hereafter as "No. 1") resembles, on the best plates, a slightly diffuse star with a very short, curved, nebulous "tail" extending for 5″ in p.a. 52°. Its visual magnitude was estimated at the telescope to be near 16. It lies 1.′0 west and 2.′2 south of BD−6°1253, the illuminating star of NGC 1999. Object No. 2, which is 0.′1 east and 4.′1 south of BD−6°1253, is composed of two faint stars 9″ apart, one much fainter star, and three closely associated semistellar clots of nebulosity; the entire object would be contained in a circle 20″ in diameter. It is superimposed on much fainter nebulosity in the form of a ring, and slit spectrograms indicate that still

TABLE 1

EMISSION LINES MEASURED IN SPECTRA OF OBJECTS NOS. 1 AND 2 NEAR NGC 1999

Wave Length	Identification	Estimated Intensity	Wave Length	Identification	Estimated Intensity
6727*.....	[*S* II] λ 6717, λ 6731	50	4359.....	[*Fe* II]	2
6562.....	*Hα*	100	4340.....	*Hγ*	8
6363.....	[*O* I]	20	4287.....	[*Fe* II]	2
6300.....	[*O* I]	60	4249*.....	[*Fe* II]+?	2
5006.....	[*O* III]	3	4101.....	*Hδ*	4
4958.....	[*O* III]	1	4070.....	[*S* II] λ 4068, λ 4076	10
4861.....	*Hβ*	15	3970.....	*Ca* II, *Hε*, [*Ne* III]	5
4657†.....	[*Fe* III]?	1	3933.....	*Ca* II	2
4571†.....	*Mg* I?	1	3888.....	*H8*	1
4452.....	[*Fe* II]	1	3868†.....	[*Ne* III]	1
4416*.....	[*Fe* II] λ 4413, λ 4416	2	3727.....	[*O* II] λ 3726, λ 3729	15

* Measured wave length of unresolved pair or blend.

† Measured wave length; the line was seen only on the most strongly exposed plate.

feebler emission nebulosity is present over the entire field. The two brighter stars in object No. 2 were estimated to be about visual magnitude 17.5. It is the purpose of this note to describe the spectra of objects Nos. 1 and 2 and to draw some conclusions from them.

The spectrograms were obtained with the Crossley nebular spectrograph (dispersion 430 A/mm at *Hγ*) with exposure times up to 2.5 hours. They show spectra composed of strong bright lines on a weak continuous background (the spectrum of object No. 1 in the photographic region is shown in Fig. 1). The strongest lines are the lower members of the Balmer series, the [*O* I] lines at λ 6300, λ 6363, the [*O* II] doublet at λ 3727 and the [*S* II] pairs at λ 4068, λ 4076 and at λ 6717, λ 6731. A list of emission lines is given in Table 1, which is based on three plates of object No. 1 and one of object No. 2. The line spectra of the two are quite similar. In the case of No. 2 the slit passed through the southwest star of the pair and the clot of nebulosity immediately to the south of it, but star and nebulosity are too close together to be separately distinguishable on this plate.

These spectra are remarkable for several reasons: (*a*) the great strength of [*S* II]; (*b*) the large range in excitation energy (as represented by ionization plus excitation potentials) between such lines as those of [*O* I] (2 e.v.) to [*O* III] and [*Ne* III] (51 and 65 e.v.); and (*c*) their striking dissimilarity to the spectra of ordinary T Tauri-like stars in the same dark nebula[1] and in the Taurus-Auriga dark clouds. The explanation of reason *b* undoubtedly is that we are observing the integrated radiation from nebulous envelopes in which there exist very large variations of density.

The only object known to the writer that possesses a spectrum like that of the objects near NGC 1999 is the nebulosity close to T Tauri discovered by Burnham and by Baade.[2] In that case, owing to the proximity of T Tauri, only the lines of *H*, [*S* II], and [*O* II] could be directly observed in the nebula, but it is possible that the [*O* I] and [*Fe* II] lines found in the spectrum of the star actually originate in the surrounding nebulosity. If the source of the continuum—presumably a star—in object No. 1 were several magnitudes brighter, we should find the nebulosity near it to appear, spectroscopically, very much as does that near T Tauri, since then the weaker emission lines would be observable only with difficulty.

The generally accepted mechanism for the production of the emission lines in the gaseous nebulae involves the photoelectric ionization of the abundant lighter elements by the intense ultraviolet radiation of the very hot exciting star. The permitted lines then result from recombination or fluorescent excitation by recombination lines, while the forbidden lines are due to collisional excitation of metastable levels by the free electrons. There is no indication of the presence of a blue star, which is a vital part of this mechanism, at T Tauri. No statement can be made at the present time regarding the energy distribution or spectral type of the continuous spectra in the objects near NGC 1999, on account of both the weakness of the spectra and the interference of the numerous bright lines on the Lick plates. The absolute magnitudes inferred from the apparent distance modulus of the Orion Nebula are, however, about those to be expected for late K- or early M-type dwarfs.

One is faced with the alternative of postulating either (1) the existence of a faint blue companion near T Tauri and the presence of similar low-luminosity, high-temperature stars in the NGC 1999 objects or (2) the operation of an excitation mechanism involving the interaction of a late-type dwarf star with the nebular material. The latter seems more plausible to the writer. Certainly, at face value there is no lack of energy available to such an interaction process: the kinetic energy of, for example, a hydrogen atom falling from infinity is 1200 e.v. at the surface of a K-type dwarf, if radiation pressure is not important. The problem is to discover a mechanism involving such infalling material that explains the observed spectrum and whose operation is demanded by the properties of the star and its environment. The relative rarity of objects such as those near NGC 1999 suggests that some special condition, not of frequent occurrence, is required for the production of this type of spectrum. Apparently, the absolute magnitude of the associated star is not critical: the distance modulus of the Taurus clouds indicates an $M_v \sim +4$ for T Tauri, while the sources of continuous spectra in the objects near NGC 1999 have $M_v \sim +9$.

The possibility should be kept in mind, in considering this situation, that the T Tauri "stars" and kindred objects in nebulae may not be normal stars. Although what can be seen of the absorption spectra resembles, with low dispersion, the spectra of late-type dwarfs, it is not certain that one can correctly infer all the physical properties of the objects from this resemblance. There is strong evidence that, in the case of the absolute magnitude, one cannot so infer in every case.

[1] This remark is based on Lick observations of the spectra of a number of the faint *Hα* emission stars found in this region by G. Haro (*A.J.*, **55**, 72, 1950) on objective-prism plates. In the course of that work Haro noted the bright *Hα* in the two objects discussed here.

[2] G. H. Herbig, *Ap. J.*, **111**, 11, 1950.

In addition to objects Nos. 1 and 2, the Crossley plates show a number of other semi-stellar features near NGC 1999. Most of these are very faint. The brightest, after Nos. 1 and 2, lies 3'.3 west and 0'.1 south of BD−6°1253 and resembles a very faint diffuse star with a nebulous wisp extending about 14″ in p.a. 21°. It is indicated as No. 3 in Figure 1. It has not been observed with a slit spectrograph, but an objective-prism plate of the field, kindly loaned by Dr. Haro, shows a bright *Hα* line.

These objects define another type in the growing list of peculiar objects that occur where stars and nebular material are intimately associated.

GEORGE H. HERBIG

LICK OBSERVATORY
January 22, 1951

CIRCUMSTELLAR LINES OF *Ca* II IN THE SPECTRUM OF EPSILON AURIGAE

On a coudé spectrogram (dispersion 2.8 A/mm; emulsion Eastman III-O) obtained at the 100-inch telescope of the Mount Wilson Observatory on September 24, 1950, the strong absorption lines H and K show narrow absorption cores displaced shortward of the stellar lines, which at this phase of the 27.1-year cycle are displaced redward of the gamma velocity. The radial velocities of the two sharp *Ca* II lines, corrected to the sun, are as follows: *Ca* II K, λ 3933.66, −28.6 km/sec; *Ca* II H, λ 3968.47, −26.6 km/sec; with a mean of −27.6 km/sec. The projected solar motion is +8 km/sec, and the interstellar velocities measured by W. S. Adams[1] in several O and B stars in the region of Auriga agree closely with this value. It is therefore improbable that the sharp lines in ε Aurigae are of interstellar origin. Perhaps they are circumstellar, being produced in an expanding cloud surrounding the F-component.[2]

Another possible explanation would be the spectrum of the second component, which is usually invisible. But the light of the F-component passing through the outer layers of the I-component produces strong absorption lines of *Ti* II, *Fe* II, etc. Hence, we should expect the *Ca* II lines of the I star to be strong. Moreover, the chances of observing the spectrum of the I star outside eclipse are remote: it must be too faint in the photographic region.[3]

The sharp *Ca* II lines are much narrower than any of the normal stellar lines of the F-component; hence they are also much narrower than the lines of the I star. Both stellar components are famous for the amount of turbulence in their atmospheres. K. O. Wright[4] found that in the F star the turbulent velocities vary with the excitation potential, reaching a value of 20 km/sec for *Fe* I lines of low excitation potential but of only 2 km/sec for those of high excitation potential. This may indicate an increase of turbulent velocity with height in the atmosphere.[5] If so, the small widths of the violet *Ca* II cores would indicate that at very great heights the turbulent velocities are again much smaller.

OTTO STRUVE

BERKELEY ASTRONOMICAL DEPARTMENT
UNIVERSITY OF CALIFORNIA
December 21, 1950

[1] *Ap. J.*, **109**, 354, 1949.

[2] Dr. W. S. Adams has recently informed me that he measured in 1940 a component of the ionized calcium lines of ε Aurigae in precisely this same position at −27 km/sec.

[3] G. P. Kuiper, O. Struve, and B. Strömgren, *Ap. J.*, **86**, 570, 1937.

[4] *Contr. Dom. Ap. Obs. Victoria*, No. 17, 1949; *J.R.A.S., Canada*, **43**, 15, 1949.

[5] A. Unsöld and O. Struve, *Ap. J.*, **110**, 455, 1949; O. Struve, *Ap. J.*, **104**, 138, 1946.

HD 26—AN UNUSUAL HIGH-VELOCITY STAR*

A radial velocity of −213 km/sec was found for the star HD 26 (BD+7°5128, $m_v = 8.2$) by R. E. Wilson and Joy,[1] who classified the spectrum as sgG2p, noting that the *Sr* II lines 4077 and 4215 were unusually strong. Consequently, the star was placed upon the Perkins spectrographic program for high-velocity stars.

A spectrogram of the blue region taken on October 16, 1950, with the *f*/1.0 camera (scale, 104 A/mm at $H\gamma$) is reproduced as the central strip in the upper part of Figure 1. If the spectrum of HD 26 is compared to the normal G5 III spectrum shown just above it, it can be seen that the G band of *CH* near λ 4300 is greatly strengthened in HD 26, while most of the atomic lines usually seen in the λλ 4000–4300 region (excepting 4077 and 4215) are much weakened. The case of *Ca* 4226 is particularly striking. In HD 26 this line is reduced to approximate equality with the line which has come up just to the violet, near λ 4223.5. The position of the latter, along with those of a number of other lines, which are strengthened in HD 26 and appear also in the carbon star HD 156074, are marked by dots under the figure. These absorption features agree in position with the stronger isolated bands of the open *CH* systems, of which the concentrated *Q* branches of the $\Delta v = 0$ system of the $^2\Delta - {}^2\Pi$ transition forms the G band. The general appearance of the spectrum of HD 26 suggests that in this star the general absorption by the *CH* molecule partially obliterates the metallic lines. On the other hand, the *CN* band extending to the violet of λ 4215 is scarcely stronger in HD 26 than in ordinary G-type giants and does not show the great strength that is characteristic of even the earliest of the typical carbon stars.

The stars which most resemble HD 26 in the enhancement of *CH* relative to *CN* are the few high-velocity carbon stars known; in fact, every carbon star which has a high space velocity and has been examined in the blue region of its spectrum can be termed a *CH* star in this sense.[2, 3] This fact led to a search for the Swan bands of C_2 in HD 26. The strongest of these are the $\Delta v = 0$ sequence degrading shortward from λ 5165 and the $\Delta v = 1$ sequence with its strongest head at λ 4737.

Spectrograms of this region, taken with the $P\beta$ camera giving a scale of 90 A/mm at $H\beta$, are shown in the lower part of Figure 1. Here a slightly later giant, of type G8, was chosen for the upper comparison spectrum, in order to bring out the metallic lines clearly. It is the close coincidence of the *Mg* triplet, λλ 5167, 5172, and 5183, with the strongest C_2 head at λ 5165 which makes the identification of weak C_2 bands difficult without high dispersion. On the spectra shown here, however, the Swan bands can be seen slightly displaced to the violet of the *Mg* lines in both HD 26 and the carbon star below it, and the presence of the fainter C_2 heads at λλ 5129, 4737, and 4715 in HD 26 is also evident.

Thus HD 26 is one of the high-velocity carbon stars, but its spectrum represents an extreme case, in that both *CN* and C_2 are much weaker than in any of the other *CH* stars yet observed. It is possible that this difference is at least partly due to a slightly higher temperature in the atmosphere of HD 26. The temperature class of HD 26 can be estimated roughly as g5 on the scale for giants, on the basis of the relative exposures required for the blue, yellow, and infrared spectral regions. Most of the other *CH* stars appear to lie in the range g7 to k0,[2] although no accurate color temperatures are available for any of them. That HD 26 is not so hot as a G0 star is suggested by the lack of any strong feature at the position of the group of lines of neutral carbon near λ 4762, which

* *Contributions from the Perkins Observatory*, No. 30.

[1] *Ap. J.*, 111, 221, 1950.

[2] P. C. Keenan and W. W. Morgan, *Ap. J.*, 94, 501, 1941.

[3] Keenan, *Ap. J.*, 96, 101, 1942.

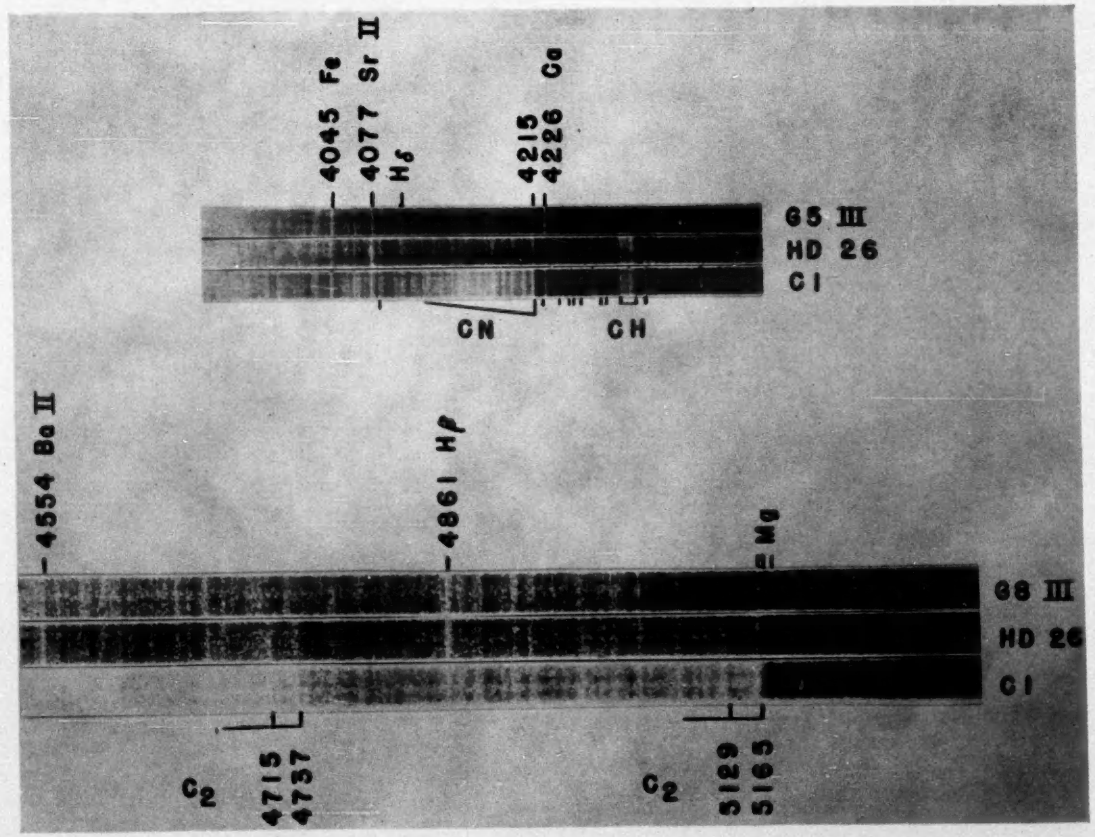

FIG. 1.—*Upper:* top spectrum, β Boo; bottom spectrum, HD 156074. *Lower:* top spectrum, o Tau; bottom spectrum, HD 156074

show strongly on our plates of R CBr, although luminosity differences may affect this comparison.

The fact that the molecular absorption by *CN* and C_2 is not so great in HD 26 as in the other *CH* stars makes this a favorable one in which to look for peculiarities in the atomic lines—aside from the weakening of those lying in the *CH*-band region. The strengthening of the *Sr* II lines 4077 and 4215, remarked by the Mount Wilson observers, is conspicuous in the upper part of Figure 1 and is particularly striking when it is noticed that they both lie in regions of *CH* absorption. The only other line in the regions photographed here which is much enhanced in HD 26 is λ 4554 of *Ba* II (Fig. 1, lower).

Whether the hydrogen lines are considered as having abnormal intensity depends upon the precise temperature assigned to HD 26, but when allowance is made for the *CH* absorption in the region of $H\gamma$ and $H\delta$, it can be said that they are at least as strong as in a normal G5 giant and are probably somewhat stronger.

The enhancement of the lines of *Sr* II and *Ba* II is more noticeable in HD 26 than in any of the other known *CH* stars. In this respect it is similar to a small group of peculiar G and K stars to which Bidelman has called attention.[4] These stars have spectra in which these same lines, particularly λ 4554, are so strongly enhanced that it is convenient to refer to them as "*Ba* II" stars. The possible connection of this group with the *CH* stars has been suggested by Bidelman,[5] who noted strengthening of the G band and found the C_2 bands present, though very weak, in the spectra of several of them. Bidelman's suggestion is confirmed by the spectrum of HD 26, which appears to stand intermediate between the other *CH* stars and the *Ba* II stars.

PHILIP C. KEENAN
GEOFFREY KELLER

PERKINS OBSERVATORY
January 20, 1951

APPARENT MAGNITUDES AND COLOR INDICES FOR SOME FURTHER WHITE DWARFS AND DEGENERATE STARS

Among the white dwarfs for which the writer published colors and magnitudes recently,[1] there were several stars for which the values given were uncertain, largely because these stars are not observable in Tucson during the periods that the writer was usually there (in March) and consequently too few plates were available. When permission was granted the writer to work as a guest investigator at the Mount Wilson and Palomar Observatories during the summer of 1950, a number of plates were taken in the Newtonian focus of the 60-inch telescope to remedy this situation. The same emulsions and filters (103*a*-O and 103*a*-G with a No. 12 filter) were used as in Tucson, as well as the same magnitudes in the same Selected Areas; since both telescopes in question have aluminized mirrors and the Ross corrector used in Tucson is thin and very transparent, while no corrector was used on the 60-inch, color differences between the two sets of magnitudes may be expected to be small.

The data obtained are shown in Table 1, in which the first three columns give the

[4] *Ap. J.*, **112**, 219, 1950 (final paragraph).

[5] Private communication.

[1] *Ap. J.*, **112**, 212, 1950.

star's designation and its right ascension and declination for 1950; the fourth column the number of pairs of blue and yellow plates on which these determinations rest; the next three columns the photographic and photovisual magnitudes as well as the color indices as determined at Mount Wilson; and the last three columns the corresponding quantities as determined at Tucson.

The star L 994-27 was originally announced as a possible white dwarf,[2] since it appears much whiter than the background stars, even though it is a seventeenth-magnitude star with a proper motion of 0".4 annually, situated in low galactic latitude. It was noticed at the time, however, that the background appeared obscured and that insufficient allowance might have been made for the extra reddening. Unfortunately, this has proved to be

TABLE 1

ADDITIONAL WHITE DWARFS AND DEGENERATE STARS

Star	1950		No. Pls.	Mt. Wilson			Tucson		
	R.A.	Dec.		m_{pg}	m_{pv}	I.C.	m_{pg}	m_{pv}	I.C.
LDS 1 A	0^h08^m7	−21°00′	3	12.10	11.80	+0.30	12.29	.....	+0.2:
LDS 1 B	08.7	−21 00	3	14.24	13.55	+0.69	14.03	.....	+0.5:
W 1	11.1	+ 0 03	2	15.41	14.96	+0.45	15.40	14.94	+0.46
L 870-2	1 35.5	− 5 16	4	12.96	12.93	+0.03	12.98	12.75	+0.23
M 57*	18 51.7	+32 58	1	15.06	15.51	−0.45	15.12	15.50	−0.38
L 994-27	18 57.6	− 1 30	3	16.98	15.29	+1.69	16.83	.....	.....
LDS 683 A	19 32.9	−13 36	3	14.96	13.44	+1.52	14.8:	13.55	+1.3
LDS 683 B	32.9	−13 36	3	15.38	15.47	−0.09	15.04:	15.34	−0.30
L 997-21	54.0	− 1 09	3	13.70	13.74	−0.04	13.62	13.62	0.00
L 930-80	21 45.0	− 7 58	4	14.22	14.52	−0.30	14.23	14.73	−0.50
L 1512-34	23 41.4	+32 15	5	12.72	12.90	−0.18	13.04	12.84	+0.20
L 1512-35	41.4	+32 18	5	13.17	11.74	+1.43	13.31	11.42	+1.89

* Central star, ring nebula.

correct, one faint star just north preceding the proper-motion star having a photographic magnitude of 17.4, a photovisual magnitude of 14.8, and a color index of +2.6. The proper-motion star therefore appears to be a normal red dwarf and should be removed from the published lists of possible white dwarfs.

It should be borne in mind that LDS 1 A, L 870-2, and L 1512-34/35 are so bright that exposures had to be so short that it was very difficult to control their lengths exactly, thus involving greater inaccuracies in the determination of the magnitudes. Taking this into consideration, the two sets of magnitudes determined at Mount Wilson and Tucson would seem to agree well enough, though there is some suggestion that the Mount Wilson magnitudes are brighter for the bright stars and fainter for the faint stars than those at Tucson.

WILLEM J. LUYTEN

DEPARTMENT OF ASTRONOMY
UNIVERSITY OF MINNESOTA
December 18, 1950

[2] *Harvard Announcement Card*, No. 648, 1943.

THE SPECTRUM OF HD 217050

The shell spectrum of HD 217050[1] was described a few years ago by R. B. Baldwin,[2] and later by O. Struve,[3] who determined radial velocities from fifty-nine Yerkes spectrograms obtained mainly between 1941 and 1944.

Nine spectrograms were obtained by the authors in 1949 between July 26 and August 6, at the Haute Provence Observatory, with the 80-cm reflector and small four-prism spectrograph (dispersion, 53 A/mm at $H\gamma$). Radial velocities have been determined from these spectra and are shown in Table 1. They are based upon the lines $H\gamma$, $H\delta$, $H\epsilon$, $H\zeta$, H 9, H 10, H 11, *Ca* II K, and the strongest *Fe* II lines.

It will be seen that these radial velocities, when compared with those of O. Struve, do not support the suggestion[2] that there may be a periodicity of at least 19 years, with a

TABLE 1

RADIAL VELOCITIES OF HD 217050

No.	Date 1949	U.T.	Radial Velocity (Km/Sec)	Quality*
1.....	July 26	2^h28^m	−18.3	g
2.....	27	2 35	−24.4	g
3.....	28	23 28	−28.6	f
4.....	29	0 44	−22.2	f
5.....	29	2 43	−21.0	g
6.....	31	1 46	−23.8	g
7.....	Aug. 3	2 12	−24.8	g
8.....	3	3 14	− 9.9	p
9.....	6	2 33	−21.4	g

* g = good; f = fairly good; p = poor.

range of velocity of at least 22 km/sec. There may, however, be real variations in velocity, but the evidence so far is not conclusive. Individual elements do not show significant differences in radial velocity, although it is suspected that the photospheric lines of *He* I may show smaller negative radial velocities than do the shell lines.

In view of O. Struve's suggestion[3] that there may be fairly rapid changes in the intensities of the α Cygni lines taking place within a few days, the plates have been carefully examined, and microphotometer tracings have been made. However, because of the faintness of these lines, it was not possible to be certain whether or not the intensities varied, but the *Fe* II lines did appear slightly stronger than average on Nos. 1 and 6.

In this series of spectra, the elements detected in the shell, in addition to hydrogen, were as follows, in order of decreasing strength: *Ca* II (λ 3968, λ 3934); *Fe* II (λλ 4385, 4352, 4303, 4233, 4179, 4173); *Sc* II (λλ 4374, 4325, 4321, 4314, 4247); *Si* II (λλ 4131, 4128, 3856); *Sr* II (λ 4216, λ 4078); *Ca* I (λ 4227); *Mg* I (λ 3838, λ 3832); *O* I (λ 4368); *Ni* II (λ 4067). The general appearance of the spectrum was similar to the 1940 spectrum as described by R. B. Baldwin.[2] An underexposed spectrum, obtained on August 13, 1949, with the 120-cm reflector and large four-prism spectrograph, shows both $H\alpha$ and $H\beta$ in emission, $H\alpha$ being very strong and $H\beta$ weak.

E. MARGARET BURBIDGE
G. R. BURBIDGE

UNIVERSITY OF LONDON OBSERVATORY
December 16, 1950

[1] HR 8731 = MWC 394 = BD+47°3985; $\alpha = 22^h52^m7$; $\delta = +48°9'$ (1900); Sp. B3ne; mag. 5.2.

[2] *Ap. J.*, **93**, 388, 1943.

[3] *Ap. J.*, **99**, 205, 1944.

NOTE ON THE DOUBLY EXCITED STATE OF THE NEGATIVE HYDROGEN ION

It has been pointed out by H. M. James[1] that the energy value $E = -0.27123Rh$ of the doubly excited $(2s)(2p)^3P$ state[2] of H^- cannot be considered an upper limit to the true energy as long as the orthogonality of the state with respect to the whole $(1s)(np)^3P$ system of states, including the continuous spectrum and with energies below $-0.25Rh$, has not been insured.

It appears difficult to take into account such an infinite number of states, even though their influence must be small. However, the continuous, as well as the discrete, energy wave functions of hydrogen can be expressed in terms of the modified hydrogen functions where the arguments r/n in the Laguerre functions have been replaced by r, as has already been done by the correction of the s-function in $(2s)(2p)^3P$. We have thus to express generally the radial part of the wave function by product functions, $f_n(r_1)g_m(r_2)$, $n = 1, 2, \ldots, m = 2, 3, \ldots$. Of these, only $m = 2$ was used in my first paper, the function $n = 1$ raising, and all functions above $n = 2$ tending to lower, the calculated energy value. To get a measure of the total raising of the energy, only the functions $n = 1$,

TABLE 1

Approx.	Energy/Rh	k
3.....	−0.26675	0.377
4.....	− .26662	.373
5.....	−0.26673	0.380

$m = 2, 3, \ldots$, besides the first approximation $n = 2$, $m = 2$, have been considered. Besides the first and second approximations as given in my first paper, we get in this way the values given in Table 1, where k is the scale constant referred to earlier.

The total raising of the energy from the second approximation is 29×10^{-5} as compared to 263×10^{-5} as caused by $n = 1, m = 2$, and to the approximate electron affinity 2123×10^{-5} of the excited H atom.

This moderate raising of the calculated energy—which is certainly more than counterbalanced by other states, as, for instance, $n = 2, m = 3$, which have not been taken into account—can therefore be neglected within the degree of accuracy which so far has been obtained.

It should also be noticed, as pointed out to me by D. R. Bates,[3] that the $(2s)(2p)^3P$ state is subject to auto-ionization and should therefore be termed a *closed* but not a *stable* state.

EGIL HYLLERAAS

INSTITUTE FOR THEORETICAL PHYSICS
UNIVERSITY OF OSLO
August 16, 1950

[1] Private communication.

[2] E. Hylleraas, *Ap. J.*, **111**, 209, 1950.

[3] Private communication.

NOTICE CONCERNING LATE-TYPE EMISSION-LINE STARS

The writer is preparing for early publication a catalogue of all known emission-line stars of types later than A, together with a bibliography of the spectroscopic observations of these stars. In order to make this catalogue as complete and accurate as possible, he requests observers to send to him, before October 1, 1951, any unpublished data which they would care to have incorporated in the catalogue.

WILLIAM P. BIDELMAN

YERKES OBSERVATORY
WILLIAMS BAY, WISCONSIN

ERRATA

In *Ap. J.*, **107**, 151, 1948 (*Contr. McDonald Obs.*, No. 145), the constant in equation (20) should be -2.62 instead of -2.92. As a consequence, all values of Γ/γ_{el} in Table 7 should be multiplied by 2; the value of Γ/γ_{el} for the sun is 8.6. This correction somewhat reduces the difference between the damping constants obtained from curves of growth based on the Milne-Eddington and Schuster-Schwarzschild theories of line formation.

JESSE L. GREENSTEIN

In the paper on the Ursa Major Group (*Ap. J.*, **110**, 205, 1949), the notes to Table 19 were inadvertently omitted. They should read as follows:

185. (45 Leo) A spectrum variable. The line at λ 4077 and the blends near λ 4171 and λ 4130 are strong. The K line becomes almost invisible at times, while at other times it reaches the strength that it has in an A1 star.
204. (HD 108134) The spectrum of this star indicates that it is somewhat below the main sequence. *Sr* II λ 4215 and λ 4077 are definitely weaker than in χ^1 Ori (G0 V). The cyanogen break is completely absent. The velocity is a mean of the value -46.7 ± 1.3 km/sec found by Wilson for this star (*Pub. A.S.P.*, **57**, 311, 1945) and the value -37.8 ± 0.7 km/sec found from plates taken by Dr. A. Blaauw with the Cassegrain quartz spectrograph of the McDonald Observatory.
330. (δ Del) This star is similar to υ UMa (F2 III), but the K line has the intensity of one in an A7 star. The small parallax and proper motion indicate that this star is brighter than the metallic-line stars.

NANCY GRACE ROMAN

In *Ap. J.*, **111**, 631, 1950, Table 2, the value of $(\mu/kT)_0$ for A-type chemical composition and $L/L_\odot = 10^{-2}$ should read 15.0 instead of 51.0.

T. D. LEE

Professor Martin Schwarzschild has kindly pointed out a numerical error that appeared in the paper, "The Apsidal Motion of Giant Binary Stars" (*Ap. J.*, **112**, 434, 1950). In substituting the value $\eta(R) = 2.98475$ (eq. [37]) in equation (2), an incorrect value 0.003059 was obtained for k_2 instead of the correct value 0.001530.

If one uses this value of k_2 for the noise-zone model, one obtains the value 3.96 for the effective polytropic index, instead of 3.70. This result is consistent with the value 4.01 found for the second model and removes the rather puzzling discrepancy that appeared to exist between the apsidal motions of the two models. Because of the identical atmospheres of the two models, one would expect them to behave nearly identically in regard to apsidal motions.

Professor Schwarzschild has pointed out two other features of interest. If we compare these giant models with the main-sequence model calculated by Keller (*Ap. J.*, **108**, 373, 1948), we find a difference of about 0.5 in the effective polytropic index. This may be accounted for by supposing that it does not represent a real difference in the polytropic index between giant models and main-sequence models but that it arises rather from the fact that the giant models have lower densities and therefore imitate stars of higher polytropic indices in their apsidal motion.

The discrepancy of about 0.3 between the calculated value in the effective polytropic index and the observed value for TX UMa need not be of too great concern. Schwarzschild has pointed out to me that the interpolation power laws which he and his collaborators used are not very representative for the law densities of giants. If one uses a constant guillotine factor for giants, one lowers the polytropic indices in all the envelopes by about 0.4, and this would bring the theoretical values in line with the observed value.

LLOYD MOTZ

In *Ap. J.*, **113**, 18, 1951, in the list of final elements, for $a = 1\overset{\prime}{.}217 \pm 0\overset{\prime}{.}002$ (p.e.) read $a = 1\overset{\prime}{.}217 \pm 0\overset{\prime}{.}015$ (p.e.).

K. AA. STRAND

In Figure 2 of my article, "Displaced Calcium Lines in the Spectrum of HD 190073," *Mt. W. and P. Reprint* No. 30‡ *Ap. J.*, **113**, 55, 1951, the line marked *Sc* II 4246 is actually *Cr* II 4242. The *Sc* II line is the weak dark line with bright edges slightly shortward from the iron comparison line λ 4247. In Figure 3 the marker for *Fe* I 4383 is displaced about 2 mm to the right in the second strip from the top; it is correctly placed in the third strip. I am indebted to Dr. R. F. Sanford for calling my attention to these errors.

PAUL W. MERRILL

In *Ap. J.*, **113**, 209, 1951, equation (65) should read:

$$(\nu + 5)\frac{\psi}{\phi} + 2 = 0 .$$

ZDENĚK KOPAL

In the article "Spectral Classification of Stars Listed in Miss Payne's Catalogue of c Stars," *Ap. J.*, **113**, 304, 1951, the spectral type of 61 Ursae Majoris should have been given as G8 V, rather than B8 V.

WILLIAM P. BIDELMAN